DESIGN STUDY OF AN MGR DIRECT BRAYTON-CYCLE POWER PLANT

VOL 1

by

James E. Staudt

B.S.M.E., United States Naval Academy, 1979
M.S.M.E., Massachusetts Institute of Technology, 1986

SUBMITTED IN PARTIAL FULFILLMENT
OF THE REQUIREMENTS FOR THE
DEGREE OF

DOCTOR OF PHILOSOPHY
IN MECHANICAL ENGINEERING

at the

MASSACHUSETTS INSTITUTE OF TECHNOLOGY
May 1987

Signature of Author _

Certified by __

Professor Lawrence M. Lidsky
Thesis Supervisor
Department of Nuclear Engineering

Certified by _____

Professor David Gordon Wilson
Committee Chairman
Department of Mechanical Engineering

Accepted by _____

Professor Ain A. Sonin
Chairman, Department Graduate Committee
Department of Mechanical Engineering

DESIGN STUDY OF AN MGR DIRECT BRAYTON-CYCLE POWER PLANT

by

James E. Staudt

Submitted to the Department of Mechanical Engineering on May 18, 1987, in partial fulfillment of the requirements for the degree of Doctor of Philosophy in Mechanical Engineering

ABSTRACT

A conceptual design of a direct Brayton-cycle power plant for a Modular Gas Reactor is presented. The system is intended for commercial electricity production. The power plant, called the MGR-GT, uses a 200-MWth pebble-bed nuclear reactor with an outlet temperature of 850°C for the heat source. The power system maintains passive safety and achieves high performance while utilizing only currently available technologies.

The MGR-GT has the following features:

- A highly-recuperated plate-fin recuperator,
- Active-magnetic bearings,
- A passively-safe, helium-cooled, graphite-moderated nuclear reactor heat source,
- A high-speed, high-pressure-helium cooled generator, and
- A load commutated inverter system for electrical frequency conversion.

Through the employment of a highly-recuperated cycle, busbar efficiencies in excess of 45% are possible. Operation at high system pressure enables component size to be kept small, resulting in a low-cost, totally-modular nuclear power-generating system. The high performance, economic potential, and current technological state-of-the-art support near-term development of this power system.

Thesis Supervisor: Dr. Lawrence M. Lidsky
Title: Professor of Nuclear Engineering

AKNOWLEDGEMENTS

At this time I would like to aknowledge those individuals and organizations who in some way contributed to this work.

First I wish to thank those members of the MIT faculty and staff who assisted me during this research project, particularly the members of my thesis committee - Professors Lawrence M. Lidsky, David Gordon Wilson, Warren M. Rohsenhow, Michael J. Driscoll, and David D. Lanning - for their careful review of my work and helpful guidance during the course of my research. I am especially grateful for the enthusiasm demonstrated throughout the project by my thesis supervisor - Professor Lawrence M. Lidsky - that made the project very enjoyable to work on. I would also like to thank Professor A. Douglas Charmichael for his assistance early in the study, and Dr. Hideo Kaburaki, visiting scientist from JAERI, whose preliminary analysis got the program off to a good start.

I cannot possibly give individual "thank yous" to all of the individuals and organizations in industry who provided assistance on this thesis. However, I would like to single out those who gave a particularly large part of their time and resources. First, I wish to express my gratitude to Gas-Cooled Reactor Associates, Northeast Utilities Service Company, and the Southern California Edison Company for their financial support. Northeast Utilities Service Company deserves special credit for initiating this program of research. Many thanks are owed to Rick Saker and the other engineers at Toshiba Corporation for all of their help on the generator and electrical system. Ken Parker and John McDonald of AiResearch Manufacturing Company deserve thanks for all of the information they provided on the

heat exchangers. Finally, I would like to thank Colin McDonald, of GA Technologies, for his interest, advice, and insight.

To the friends that I have made here at MIT - including those from the Combustion Research Facility, the Mechanical Engineering Department, and the Nuclear Engineering Department - I express my gratitude for helping to make my experience at MIT an enjoyable one.

Most of all, I would like to thank my family, especially my parents - Henry and Teresa Staudt - to whom I am grateful for much more than I can express here, and to whom this work is dedicated.

For my parents

Table of Contents

List of Figures

List of Tables

CHAPTER ONE

INTRODUCTION AND BACKGROUND

1.1 Introduction.

The development of the open-cycle gas-turbine was made possible by the availability of relatively inexpensive clean-burning fuel. As these fuels become more scarce, the need to develop new technologies that produce power from other energy sources will increase. The Closed-Cycle Gas-Turbine (CCGT) is one such technology. It is capable of using either a nuclear reactor or a furnace that burns unclean fuel such as coal. The use of a Modular Gas Reactor (MGR) is one especially promising application of this technology. With its graphite core, the MGR is capable of delivering high-temperature helium at temperatures up to 950°C. Fossil-fuel systems, on the other hand, are limited to a helium temperature of only about 750°C by the materials of their heater [B1,M1]. High temperatures are necessary for the achievement of high thermal efficiencies in the CCGT. Hence, the MGR takes greater advantage of the high thermal-efficiency potential of the closed Brayton-cycle.

The MGR also offers several advantages over previous nuclear-reactor-plant designs. By limiting the size of the core and the power density to about 250-MWth and 4-W/cc respectively, it is possible to design a reactor plant that can transfer its decay heat to the environment by totally passive means. This ensures both the retention of fission products and plant survival even in the event of a severe reactor accident. In this way, safety is insured and risk to the investor is reduced. Therefore, systems exclusively for the

purpose of decay-heat removal are not needed. The elimination of the need for these safety systems greatly simplifies the reactor system. The small size and simple design of the MGR also permit easier construction than large Light Water Reactor (LWR) plants. The MGR lends itself very well to factory construction with monolithic on-site emplacement. Quality assurance and construction time are expected to be improved signifcantly over LWR's. There are also implications to potential streamlining of licensing procedures for the MGR [I1, M3]; however, this topic is beyond the scope of this study.

All MGR power-plant designs to date have used a steam-generating system and Rankine cycle. For reasons already discussed, an MGR in a direct Brayton-cycle could more fully utilize the high efficiency potential of this cycle than fossil-fuel systems. It is also believed that a direct Brayton-cycle could more effectively utilize the modularity of the MGR than a steam-plant Rankine-cycle MGR (MGR-SC) because convenient gas-turbine sizes are a better match to the MGR rating than are conventional steam-turbines. The current MGR concepts become economically competitive only when arranged in multiple-modules supplying a common steam-plant of roughly 400-600 MWe [A4, C8, E1, L3]. Therefore, most proposed MGR-SC plants use a number of MGR's to provide for a common steam-plant. The MGR with a direct-cycle Gas Turbine (MGR-GT), on the other hand, may be built in individual systems of roughly 100 MWe each, or in multimodule plants that parallel at the busbar. A commitment to a multi-module system is not necessary. In this way, the MGR-GT has a greater stand-alone capability than the MGR-SC, permitting an electric utility more flexibility in capacity expansion. An MGR-GT is simpler, with fewer

components than an MGR-SC. The simplicity of the MGR-GT may result in lower capital costs and lower operating costs resulting from easier automation of plant.

1.2 The History of Gas-Cooled Reactors and the MGR.

The MGR is a product of thirty years of gas-cooled reactor evolution. In the following section a brief history of gas-cooled reactors will be given. Emphasis will be placed on key developments that distinguish each of the following designs.

1.2.1 MAGNOX Reactors:

Gas-cooled nuclear reactors have been in existence since the early days of the nuclear industry. The world's first commercial reactor was a 40 MWe, CO_2-cooled, graphite-moderated reactor completed in 1956 at Calder Hall, England. These MAGNOX reactors, by 1972, totaled 37 in number and were located in Great Britain (26), France (8), Italy (1), Japan (1) and Spain (1). Some of these reactors used on-line refueling and a Prestressed Concrete Reactor Vessel (PCRV). Proper operation of on-line refueling equipment could significantly improve plant availability over plants that must shutdown to refuel [M12]. The PCRV elimates limitations on reactor size imposed by shipping limitations of steel pressure vessels. A PCRV also eliminates the possibility of a catastrophic failure of the pressure vessel. A PCRV is shown in Fig. 1.1. Eleven of the Magnox reactors use PCRVs. Despite its "first-of-a-kind" status, small size and low efficiency, the MAGNOX has been a success, as demonstrated by its wide acceptance and high capacity factor [M12].

1.2.2 Advanced Gas Reactors (AGR):

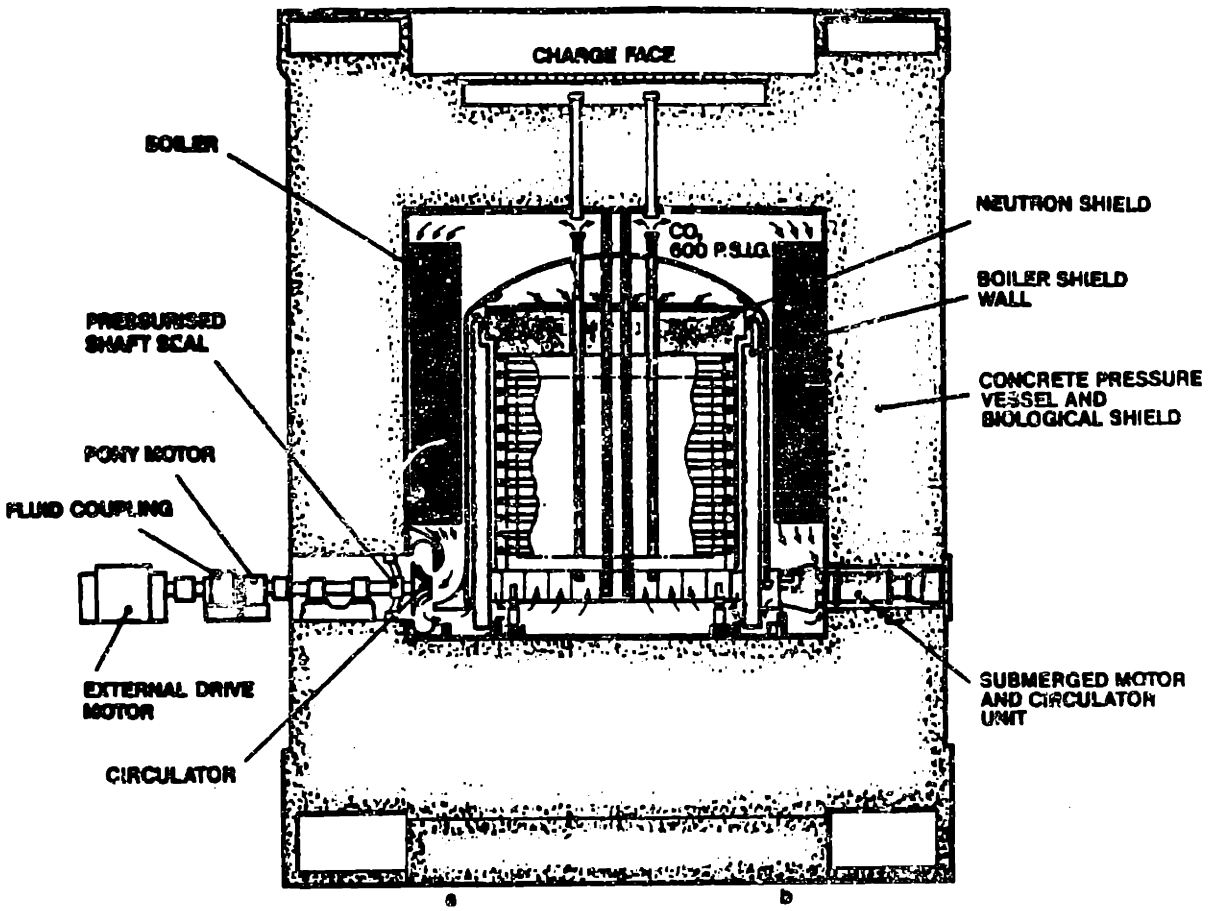

Figure 1.1. An AGR, showing PCRV and gas flowpath (S10).

An improvement in fuel permitted a large increase in coolant temperature over the MAGNOX reactors. This resulted in improved thermodynamic efficiency in AGR power plants over the MAGNOX plants. The AGR's were designed for 600-MWe at a net efficiency of about 41% [M12] Like the MAGNOX reactors, the AGR reactors used CO_2 as a coolant. Experience with the MAGNOX and AGR reactors showed that flow vibrations were pronounced. It is believed that if helium were used as a coolant, designing the gas circulation system to avoid these flow vibrations would have been less difficult [M12]. Additionally, corrosion of steel components is an area of serious concern in high-temperature CO_2 environments. Although fairly unreactive at low temperatures, CO_2 promotes oxidation at high temperatures. CO_2 coolant, therefore, limits the maximum temperature possible in these reactors. Helium, an inert gas, was recognized early in the gas-cooled reactor program for its excellent neutronic behavior, high specific heat and high heat-transfer coefficient as the preferred coolant. However, it was not readily available at that time for a reasonable cost.

The AGR circulators are of the submerged-gas type [S10]. The entire motor and impeller operate in a high-pressure CO_2 atmosphere. This design lowers the pressure difference across the rotating-shaft seal and greatly simplifies its design [S10]. This was a significant improvement over earlier designs with externally mounted motors requiring a shaft seal to prevent leakage of CO_2 across a high pressure-difference. Figure 1.1 shows circulator orientation in the AGR and Figs. 1.2 a and b show details of the installations. Since the shaft seals were generally of the oil-buffered type, the risk of oil

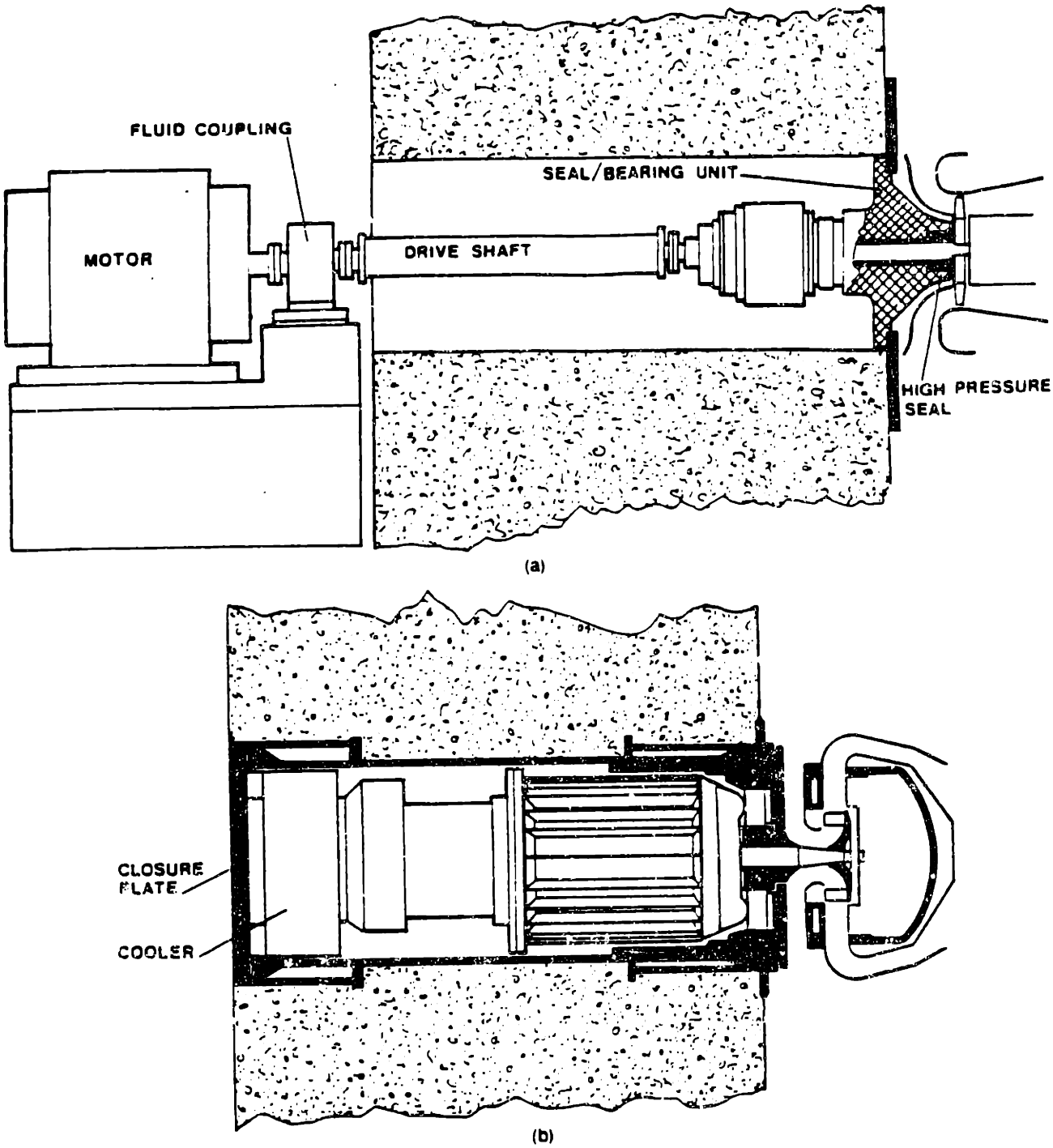

Figure 1.2. AGR gas circulators (F).
(a) not submerged type.
(b) submerged type.

ingress into the CO_2 heat-transfer medium was possible. Design of such seals to minimize gas leakage and avoid lubricant ingress under all plant transients is a difficult task. By totally submerging the unit in high-pressure gas, the large pressure-difference across the shaft seal is elimated and the bearing-seal design is much simpler. Although the new submerged-gas circulators accounted for a large portion of the plant unavailability shortly after installation, the problems were not associated with the seals but with vibration of the unit foundation [S10]. The problems with the circulators were eventually corrected, and no problems have since been experienced [S9, S10].

1.2.3 The High-Temperature Gas-Cooled Reactor (HTGR):

By using an all ceramic-graphite core and helium as a coolant, it is possible to operate the reactor at coolant- exit temperatures that are much higher than attainable in the MAGNOX and AGR reactors. Such a design would be capable of efficiencies considerably improved over previous gas-cooled reactor designs. Development of HTGR (High Temperature Reactor-HTR-in Europe) designs has been in progress in the United States, Europe and Japan. Although some effort has been expended on designs for gas-turbine variant HTGR's, the only commercial HTGR's that have been built to date have employed steam-Rankine cycles.

The American and Japanese HTGR programs have headed in a different direction than the German HTGR program. Several HTGR fuel geometries have been considered in the past. Today, however, prismatic-element and pebble-type fuel geometries are the only fuel geometries being considered for use in HTGR's. In the U.S. and Japan, emphasis has been placed on prismatic-graphite fuel-elements. In

Germany, emphasis is on the pebble-type fuel. In the pebble-bed reactor design, thousands of 6-cm diameter graphite pebbles are loaded into a reactor. Pebble bed reactors offer the advantage of on-line refueling, while prismatic-element fueled cores must be shut down during refueling. The fundamental fuel particle contained within these two types of fuel geometries, however, is the same. Thousands of tiny (about 400 μm diameter) fuel kernels are dispersed in a graphite matrix within each fuel-pebble or prismatic-element. Figure 1.3 shows a fuel-particle, a pebble and a prismatic fuel element. Each TRISO fuel particle has a protective coating composed of a Silicon-Carbide layer sandwiched between two Pyrolytic-Carbon layers that prevents the release of fission products at temperatures below 1600°C. Although early HTGR reactors did not have the TRISO fuel, TRISO fuel is the only fuel that is considered for use in HTGR's today because it is such an improvement over other HTGR fuels.

HTGR technology has been proven over the years in a number of commercial and test HTGR plants. In the United States, two HTGR units have been built, Peach Bottom and Fort St. Vrain. In Europe, the Dragon Project HTGR, the AVR and the Thorium High-Temperature Reactor (THTR) have demonstrated HTGR technology. A brief discussion of each will follow.

1.2.3a Dragon.

The Dragon Project HTR was a joint project sponsored by several European nations with the test reactor located in Great Britain. This helium-cooled, 20-MWth reactor was the first HTGR to be built. It passed its heat to a low-pressure secondary circuit of steam and water, which passed its heat to a tertiary water-loop. Finally, the

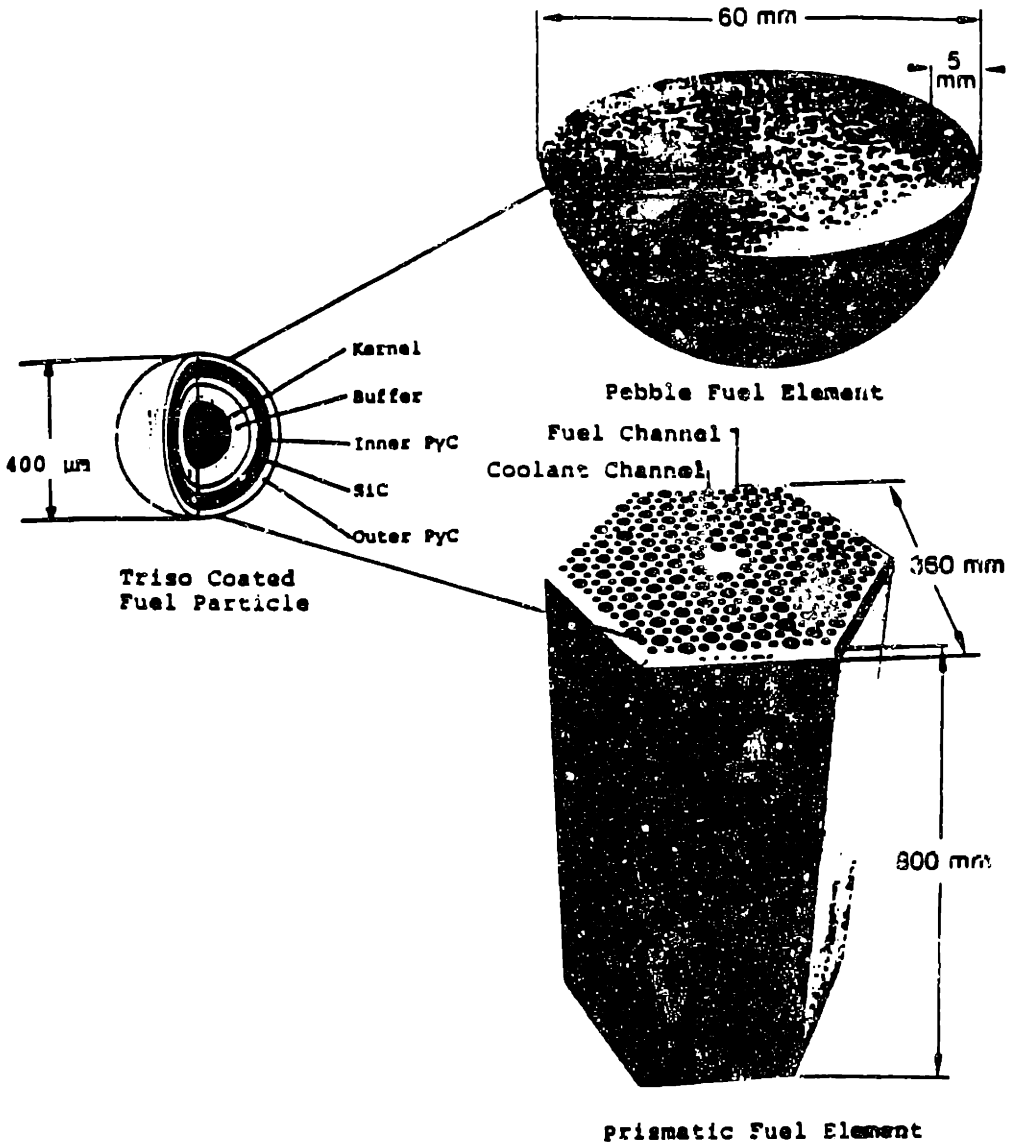

Figure 1.3. TRISO fuel particle, and Pebble and Prismatic fuel elements (11)

water loop rejected heat to the atmosphere by air-blast coolers. The active core had 37 hexagonal fuel-moderator assemblies with highly-enriched uranium and thorium fuel regions. The primary purpose of the Dragon experiment was to test fuels and examine the behavior of graphite under fast neutron irradiation. Studies conducted in the Dragon reactor laid the groundwork for later HTGR designs.

1.2.3b Peach Bottom.

The Peach Bottom reactor plant was built in Philadelphia as an HTGR steam-Rankine cycle demonstration plant. The Peach Bottom reactor plant produced 40 MWe at 35% efficiency. The cylindrical core of the reactor was contained within a steel pressure-vessel.

Although the first core loading of cylindrical fuel elements demonstrated significant fuel failure, the second core, using BISO fuel (two Py-C layers), performed very well. Excluding losses resulting from the first core and scheduled shutdowns for demonstration or experiments, the gross lifetime plant capacity factor was 74%. In addition to an impressive capacity factor, after final shutdown, examination of the Peach Bottom reactor system found low activity levels and proved satisfactory performance of the fuel.

1.2.3c AVR.

The AVR reactor is a small, 15 MWe, pebble-bed test reactor built at Julich, West Germany. It was built for the purpose of demonstrating the feasibility of the pebble-type fuel. The pebble-type fuel is expected to be less expensive to manufacture than prismatic-element fuels and offers the potential for on-line refueling. Pebble-bed reactors with on-line refueling also offer improved neutronic behavior due to the lower excess reactivity required. Fast control rod

insertion is difficult in large pebble-bed reactor cores. However, in smaller cores, up to about three meters in diameter, control rods may be located in the radial reflector. Figure 1.4 shows the AVR reactor.

The AVR reactor was initially operated at a helium-outlet temperature of 750°C from initial electricity production in 1967, until 1972, when the helium-outlet temperature was raised to 850°C. However, in 1974 the AVR reactor helium-outlet temperature was again raised to 950°C, and has been operating at this temperature ever since. In this time, the AVR reactor has proven the high-temperature capability of its fuel. It has also demonstrated safe response to a loss of coolant-flow from full power with the rods fully withdrawn. The fuel did not exceed its maximum-allowed temperature, and the reactor remained shutdown for about 24 hours, after which power was regained at a level low enough (1% of full power) for heat to be removed passively through the reactor and pressure-vessel structure [M20].

The introduction of water or lubricants into the primary-coolant circuit causes concern over the possibility of the foreign matter reacting with core graphite or other surfaces in the reactor plant. Damage to the reactor or plant components will reduce plant availability. This foreign material could also scrub off deposited fission products to later permit release in the event of a leak. Moisture or lubricants may be introduced through the heat exchangers or the machinery bearing-lubrication system. Steam-plant HTGR (HTR) designs operate with a steam pressure that is higher than the helium pressure in the primary. In the event of a steam-generator leak, the potential for a major ingress of moisture into the primary coolant

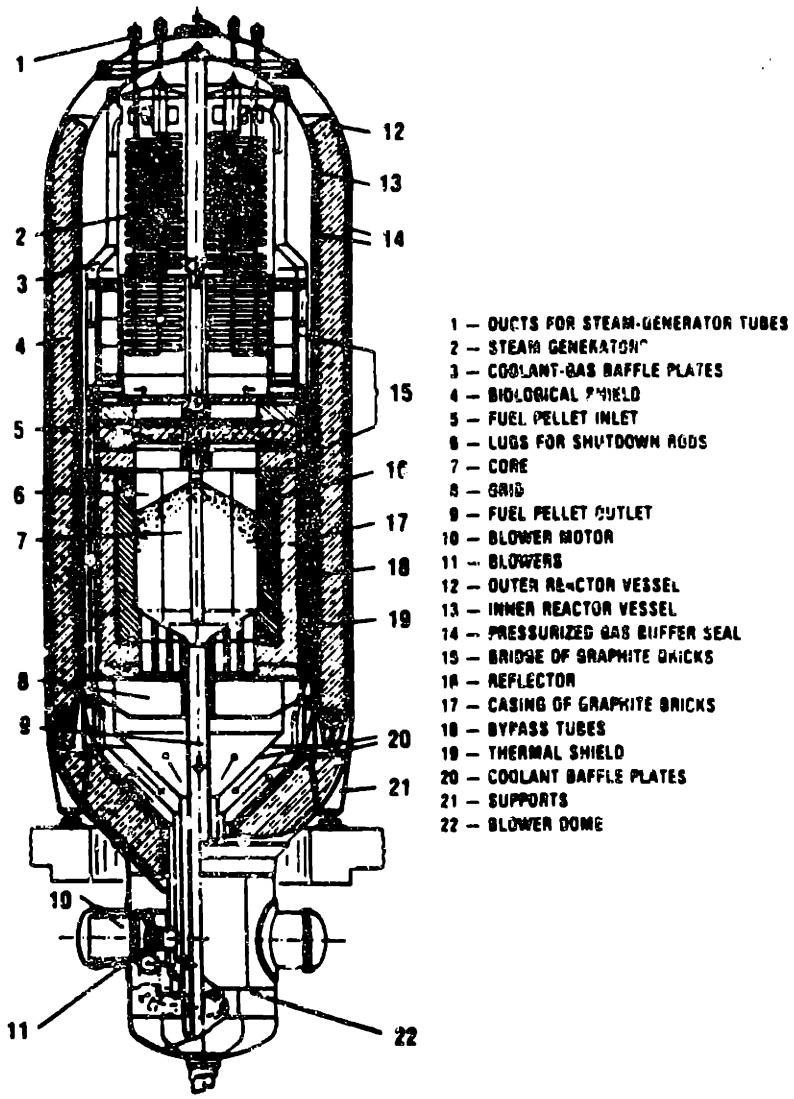

Figure 1.4. The AVR reactor [from M12].

circuit is great. The AVR reactor experienced such a leak in a superheater pipe of its steam-generator, permitting 30-m^2 of water into the primary circuit. In the course of repairing the steam-generator, clearing the moisture from the primary circuit, and inspecting and testing the repairs, the AVR reactor was unavailable for electricity production for the roughly fifteen months between May 1978 and August 1979 [M20].

1.2.3d Fort Saint Vrain.

The 330-MWe Fort Saint Vrain (FSV) nuclear-power station in Colorado is the only commercial gas reactor in the United States. The core is made of hexagonal-prismatic fuel elements and the primary-coolant circuit of the FSV plant is entirely contained within a PCRV.

The FSV plant has been plagued by numerous problems that have produced a capacity factor of only 20.79% and an availability factor of only 42.16% for the years 1979-1983. A major reason for the large difference between the capacity factor and the availability factor of the FSV plant is that the reactor has been limited to 70% power due to observed outlet-temperature oscillations at high power levels. A significant portion of the loss in availability has been a result of high moisture levels in the primary coolant circuit. The primary source of this moisture has been the water-lubricated bearings of the helium circulators. The helium circulators are driven by steam turbines, thereby requiring a water-lubricated shaft-penetration seal. During a plant transient affecting the circulators, the bearing-water pressure-control system frequently will not control pressure properly, causing bearing-water to leak into the primary circuit. This problem

is aggravated by the fact that the Plant Protective System (PPS) trips the circulators as a corrective action. Spurious PPS trips and PPS logic trip failures have caused a number of circulator trips and a bearing-water accumulator firing, and consequent large ingresses of moisture. Table 1.1 identifies the moisture contributions to lost output. The numbers are very high. Moisture accounts for a loss in availability of nearly 25% and a loss in capacity of nearly 32%. Losses in output identified as originating from specific circulator trips appear to contribute only about half as much as moisture not identified as originating from specific trips (non-trip moisture on Table 1.1). It is important to note that the losses to output from non-trip moisture result primarily from moisture introduced to the primary coolant circuit by a ar earlier circulator trip. This moisture remains in the system to cause some plant difficulty, such as corrosion. Additional maintenance is thereby required, increasing the losses in output from other maintenance procedures such as refueling [A5].

1.2.3e Thorium High Temperature Reactor (THTR).

THTR is a 300-MWe pebble-bed reactor built in Schehrusen, West Germany. As in all large gas-cooled reactors, the entire helium primary coolant circuit is contained within a PCRV. During normal operation, reactivity control is achieved by motion of 36 absorber rods in the graphite reflector. For long shutdowns, 42 in-core rods are slowly inserted into the pebble bed with pneumatic drives. The reactor first went critical in September 1983 and started generating electricity in 1986. Therefore, there is little experience to date with the THTR.

Table 1.1. Fort St. Vrain loss-of-output due to moisture [A5].

Category	Historical CF Loss%				Historical AF Loss%			
	Total	Non-trip Moisture	Trip Moisture	Total Moisture	Total	Non-trip Moisture	Trip Moisture	Total Moisture
Refueling	9.68	2.89	--	2.89	9.49	2.93	--	2.93
Circ Loop Split	8.20	2.63	--	2.63	8.19	2.62	--	2.62
Moisture Unknown	7.93	7.93	--	7.93	6.15	6.15	--	6.15
70% Power Limit	5.63	--	--	--	--	--	--	--
Circ Buffer He/Dryer	5.28	3.08	1.60	4.68	2.83	1.57	.76	2.33
Plant Protect System	4.19	--	3.44	3.44	3.60	--	3.22	3.22
Reactor Bldg/Seismic	3.66	1.65	--	1.65	3.31	1.60	--	1.60
Feedwater Chemistry	3.60	--	--	--	2.91	--	--	--
Install Core Constrnt	3.33	--	--	--	3.32	--	--	--
Feedwater Control	2.40	--	0.75	0.75	0.54	--	0.28	0.28
Circ Static Seal	2.14	--	--	--	2.14	--	--	--
Electrical System	2.01	--	1.38	1.38	1.67	--	1.18	1.18
Feedwater Pumps	1.96	--	--	--	0.08	--	--	--
Circ Bearing Water	1.92	--	1.88	1.88	0.72	--	0.72	0.72
Penetration He Leak	1.91	--	--	--	1.85	--	--	--
Steam Generators	1.87	1.62	--	1.62	1.74	1.57	--	1.57
Circ Other	1.67	--	0.77	0.77	1.36	--	0.55	0.55
Turbine I&C	1.42	--	--	--	1.21	--	--	--
Main Steam System	1.41	0.14	--	0.14	1.23	0.08	--	0.08
Turbine Valves	1.10	--	1.09	1.09	0.79	--	0.78	0.78
Turbine Vib. & Test	1.06	--	--	--	0.91	--	--	--
Control & Orif Assem	0.79	--	--	--	0.75	--	--	--
Circ Speed Control	0.71	--	--	--	0.30	--	--	--
Unknown	0.71	--	--	--	0.31	--	--	--
Miscellaneous System	0.65	0.32	--	0.32	0.58	0.25	--	0.25
Circulating Water	0.65	--	--	--	0.28	--	--	--
Operator Training	0.53	--	--	--	0.53	--	--	--
Feedwater Other	0.49	--	--	--	0.16	--	--	--
Fluctuations & Tests	0.48	--	--	--	--	--	--	--
Feedwater Valves	0.47	0.14	--	0.14	0.16	0.08	--	0.08
Main Generator	0.37	--	--	--	0.32	--	--	--
He Purification System	0.33	0.26	--	0.26	0.07	0.07	--	0.07
Fires	0.30	--	--	--	0.25	--	--	--
Grid/System Demand	0.14	--	--	--	0.02	--	--	--
Moisture Monitors	0.12	--	--	--	0.12	--	--	--
Condenser	0.10	--	--	--	0.06	--	--	--
TOTAL	78.21	20.95	10.91	31.86	57.85	17.15	7.49	24.64

1.2.4 The Modular Gas Reactor (MGR).

By incorporating the technology of the HTGR into a reactor that is small enough to transfer all of its decay heat to the environment by totally passive means and prevent any plant damage or release of fission products, a "passively safe" reactor will result. The Modular HTGR (MGR) was developed for this purpose. Several modular concept designs have been developed in the United States, Germany, and Japan. Table 1.2 lists the salient features of three MGR-concept steam power-plant designs.

The principal difference between the MGR cores is in the fuel geometry, pebble versus prismatic. Pebble cores offer the advantage of on-line refueling, but at the penalty of an increased pressure-drop. Prismatic cores offer a higher power and lower pressure drop, but must be shut down for refueling. The United States Department of Energy (DOE) has selected the prismatic-core design with a side-by-side vessel arrangement as its reference design for the MGR.

Another feature of the modular concept designs is installation of the Nuclear Steam Supply System (NSSS) in a below-grade silo as in Figs. 1.5a and b. Figure 1.5a shows a side-by-side arrangement and Fig. 1.5b shows a vertical-in-line arrangement for an MGR steam power plant. The below-grade silo offers many safety and economic advantages. The walls of the silo are maintained cool by the Reactor Cavity Cooling System (RCCS), also called the Reactor Enclosure Cooling System (RECS). Two RCCS designs have been proposed, one incorporating air cooling by natural convection as in Fig. 1.5a and the other incorporating water cooling by natural circulation as in Fig. 1.5b. The reactor vessel of the MGR must be manufactured from

Table 1.2. Typical MHTGR Concept Design Parameters

from (M3)

Parameter	IL 250 MWt	SBS 250 MWt	SBS 350 MWt
Core:			
Type	Pebble	Pebble	Prismatic (Annular)
MHR Configuration*	ILV	SBS	SBS
Power Level (MWt)	256	250	350
Power Density (W/cc)	4.2	4.8	5.9
Diameter, (m) outer	3.5	3.0	3.5
inner	NA+	NA	1.6
Height, (m)	8.7	10.8	8.0
Estimated LOFC fuel T_{max} (°C)	1800	<1600	<1600
Graphite Elements (% of core)	90	90	NA
Reactivity Control and Shutdown	Top mounted side reflector rods; RLSR absorber balls in reflector buttresses	Top mounted side reflector rods and four rods in buttresses	Top mounted rods in prism elements and reflector
Fuel Elements:			
Cycle	LEU/Th	LEU/Th	LEU/Th
Coating	TRISO	TRISO	TRISO
HM Loading, (g/element)	16.0	14.0	7.0
Burnup (MWd/t)	95,000	82,000	82,460
Helium Coolant:			
Flow Direction	Upflow	Downflow	Downflow
Temperature, (°C) Inlet/Outlet	260/730	263/493	258/687
Flowrate, kg/s)	120	110	160
Pressure, (MPa)	7.0	7.1	7.0
Core ΔP, (bar)	1.3	2.0	0.34
Core Coolant Volume Fraction	(Not available)	0.39	0.19
Helium Inventory, (kg)	3740	2632	(Not available)

*ILV: In-Line Vertical configuration
+SBS: Side-By-Side configuration
+NA: Not Applicable

steel so that, in all perceived accidents, it may transfer enough heat by passive means to the RCCS such that damage to the plant is avoided. A PCRV cannot transfer enough heat to the environment to ensure passive safety and, therefore, cannot be used in an MGR.

Although the coolant exit temperature of the MGR is much higher than the maximum temperature covered by the normal guidlines for construction of nuclear structural components, Section 3, Division 1 of the ASME Boiler and Pressure Vessel Code, the pressure vessels of the MGR designs are, in fact, designed within the guidelines of this section of the pressure-vessel code. This is made possible by circulating the cooler return-gas from the steam-generator or process heat-exchanger around the inner surface of the pressure-vessel as in Fig. 1.6 so that the vessel temperature is kept within the temperature limitations of Section 3, Division 1. Coaxial piping is used in the side-by-side arrangement so that the high-temperature duct is not a pressure-retaining surface. For higher vessel temperatures, between 800°F and 1500°F, it is necessary to use the high-temperature version of the ASME Boiler and Pressure Vessel Code, Case N-47 [A1]. It will be shown in Chapter Three that the pressure vessel imposes serious limitations on the design of the MGR-GT.

1.3 The Closed-Cycle Gas-Turbine (CCGT).

Since J. Ackeret and C. Keller first proposed the CCGT in 1939, the concept of a large CCGT power plant has primarily been a subject of study. Although a number of commercial CCGT plants have been operated with success in Europe and Japan, the largest is only 50-MWe in rated capacity, with most others much smaller. This is largely due

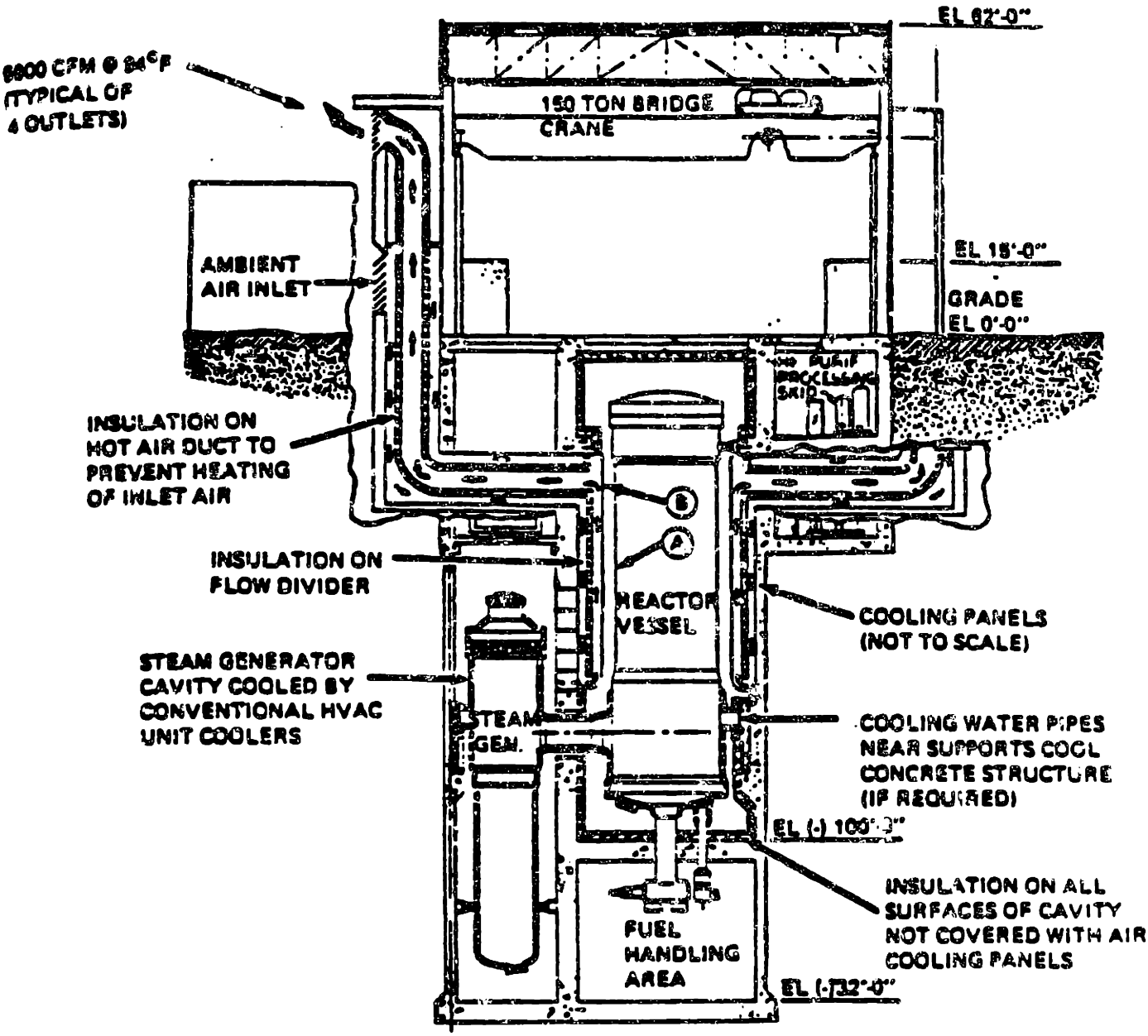

Figure 1.5a. Side-by-Side vessel arrangement with air RCCS [from A4].

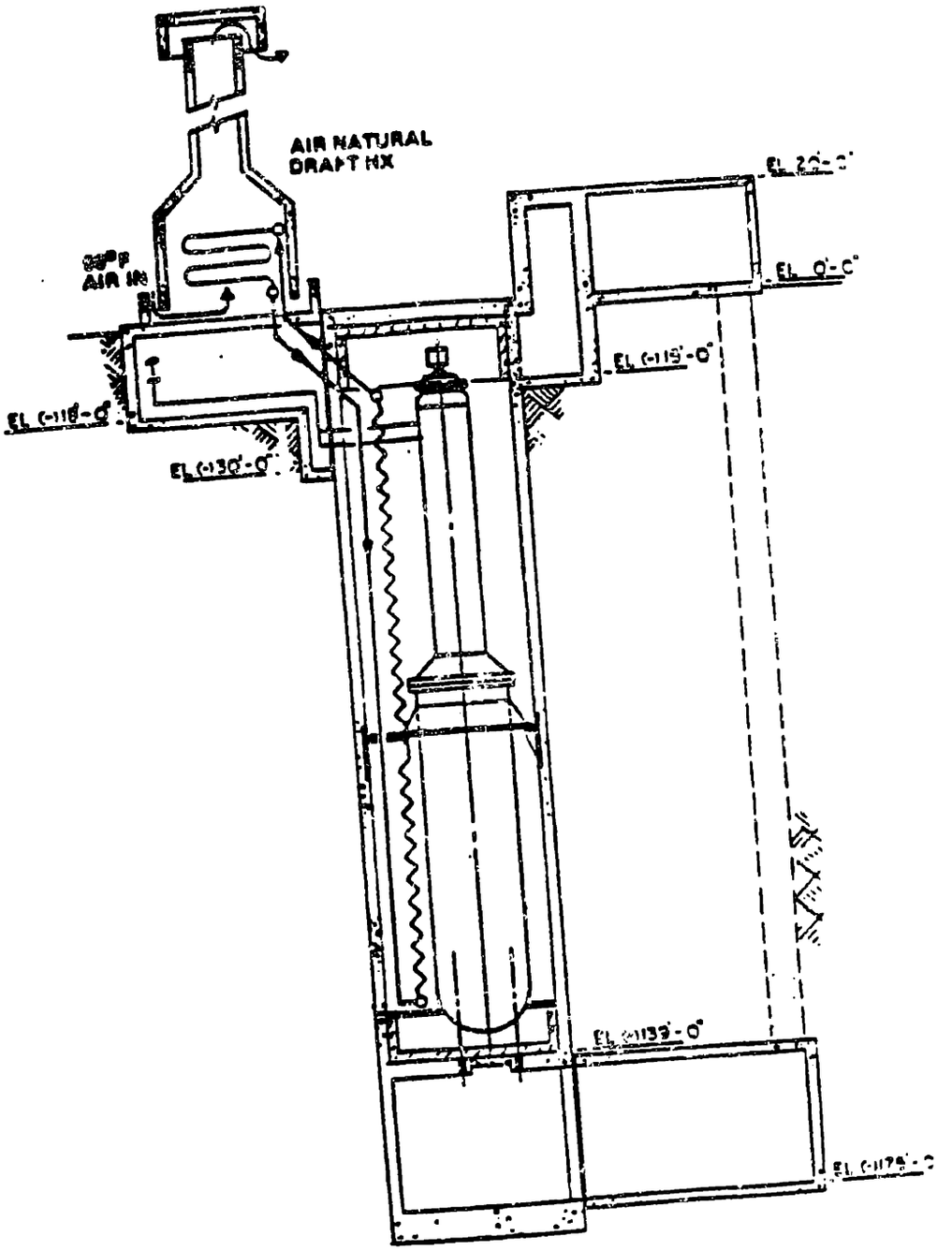

PASSIVE WATER COOLING CONCEPT.

Figure 1.5b. In-Line-Vertical vessel configuration with passive water RCCS [from B19].

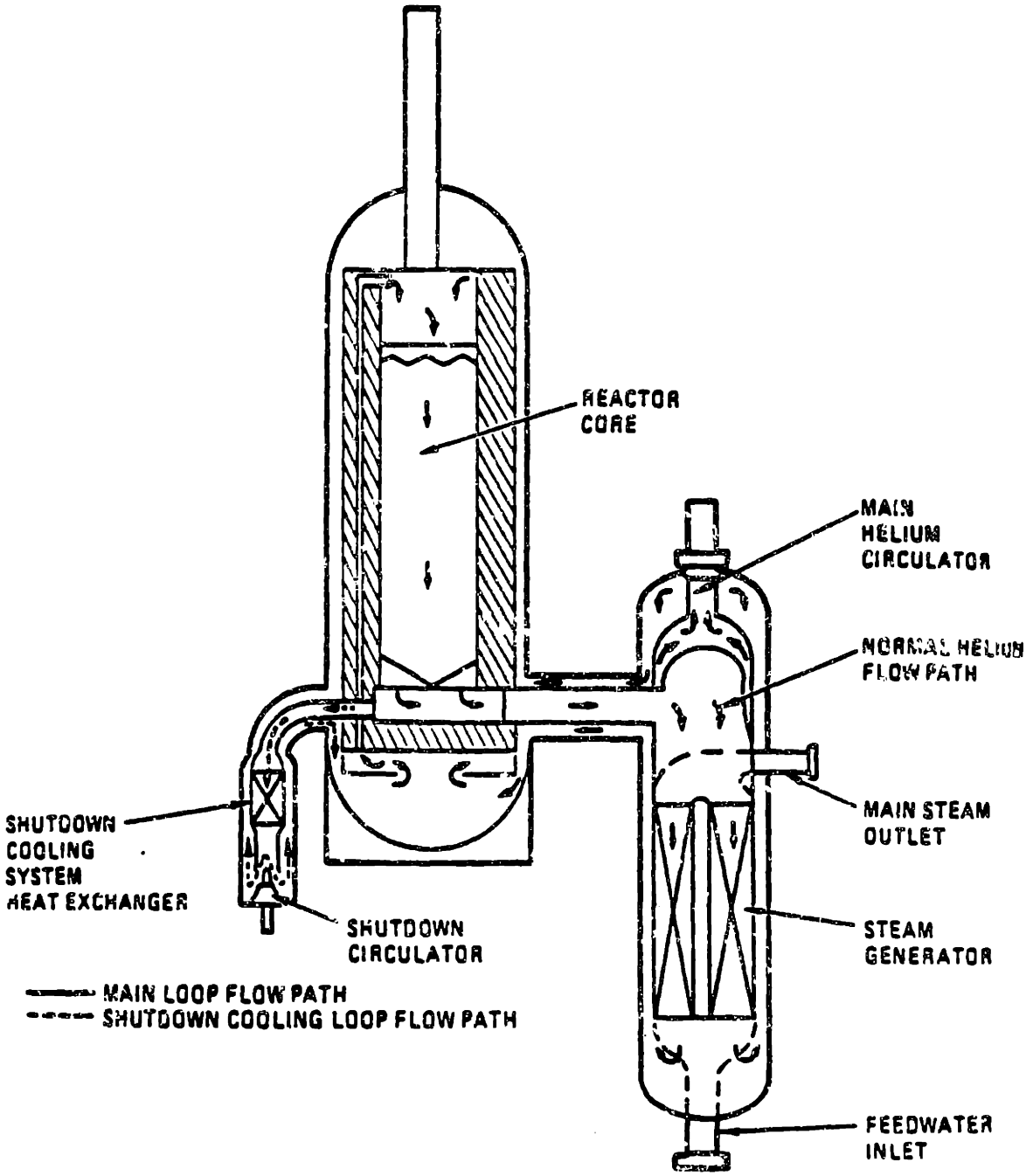

Figure 1.6. Gas flowpath in the Side-by-Side vessel configuration [from B31].

to the advanced nature of the CCGT. Despite attractive theoretical performance, until this time a number of technical difficulties have diminished the attractiveness, if not the feasibility, of large, commercial, CCGT power-plants. Many of the technical problems associated with the CCGT have been identified as a result of operating experience with these plants. Other difficulties have been discovered in design studies. Table 1.3 shows a list of operating experience with CCGT power plants. Not on this list is a roughly 10-MWe CCGT-Rankine combined-cycle power- plant recently completed by the GWF Power Systems. Its heater is a fluidized-bed coal/coke furnace. A recuperator is not used. Rather, turbine-exhaust gas is used for steam generation and furnace-exhaust gas preheats the compressor-discharge gas prior to heating in the furnace. All CCGT power plants to date have used fossil-fuel heat sources. Except for Oberhausen-2, all plants have used air as their working fluid. Oberhausen-2 was built as a test plant to gain experience for the design of a CCGT with an HTGR heat source.

There have been several design studies concerning the nuclear CCGT. The two most rigorous studies were conducted in the United States (the HTGR-GT by General Atomic Co.) and in Germany and Switzerland (the High Temperature Helium Turbine-HHT). A CCGT design study was performed as part of the Dragon project also; however, this study was not as extensive as either the HTGR-GT or the HHT. The HHT project was very extensive and incorporated several major projects and design studies. Two facilities were actually built as part of the HHT project, the Oberhausen-2 CCGT plant and the high-temperature-helium test loop (HHV). Although only a conceptual design study, the HTGR-GT

Operating closed-cycle gas turbine experience

Plant	Pioneer CCGT	Ravensburg	Oberhausen 1	Coburg	Haus Aden	Gelsenkirchen	Oberhausen 2
Country	Switzerland	Germany	Germany	Germany	Germany	Germany	Germany
Manufacturer	Escher Wyss	GHH	GHH	GHH	GHH	GHH	GHH
Fuel	Oil	Coal	Coal/coke oven gas	Coal	Coal/mine gas	Furnace gas	Coke oven gas
Working fluid	Air	Air	Air	Air	Air	Air	Helium
Electrical output, MW(e)	2.0	1.3	13.75	6.6	6.4	17 25	50*
Heat output, MW(t)	--	2.3 – 4.1	18.5 – 28	8 – 16	7.8	20 – 29	53.5
Efficiency at terminal, %	32.6	25.0	29.5	28.9	29.5	30.8	31.3
Fuel utilization, %	--	--	65.6	64.5	65.4	65.9	65.0
Turbine inlet temperature, C (F)	650 (1202)	660 (1220)	710 (1310)	680 (1256)	680 (1256)	711 (1312)	750 (1382)
Turbine inlet pressure, MPa (psia)	2.5 (363)	2.7 (392)	3.2 (464)	2.75 (399)	3.1 (450)	3.8 (551)	2.8 (406)
Commissioning date	1939	1956	1959	1961	1963	1967	Started 1975
Running time, hours to March 1977	6,000	120,000	102,000	107,000	101,000	75,000	**
Plant availability, %	Plant operated during the second World War	87	73	83	91	75	--

*Physical dimensions of turbomachinery and heat exchangers equivalent to a nuclear helium gas turbine of about 300 MW(e).

**Plant not yet at full load. Nearly 10,000 hours of operation up to Spring of 1978 at electrical power outputs up to 30 MW(e). Full heat load of 53.5 MW(t) delivered during winter operation to city of Oberhausen district heating system.

Table 1.3. Closed Cycle Gas Turbine power plant operational experience (M4).

was a rigorous project and addressed many of the important issues of closed-cycle gas-turbine design. Additionally, information is plentiful and readily available on the HTGR-GT in the United States. The HHT and HTGR-GT projects will therefore be described in the following sections.

1.3.1 The HHT Project.

The HHT project was part of the European High Temperature Reactor (HTR) program and encompassed several projects within the total HHT project. The HHT project was intended to develop a large, nuclear CCGT power-plant. The development plan was in steps, the first of which was to design and build a small HTR gas-turbine plant. This was to be the 25-MWe Schleswig-Holstein Nuclear Power Plant (KSH).

1.3.1a The Schleswig-Holstein Nuclear Power Plant (KSH).

To demonstrate the feasibility of a direct-cycle gas-turbine for a commercial, central-station nuclear power plant, the Federal Republic of Germany planned to build the 25-MWe KSH plant near Geesthacht in Schleswig-Holstein. The reactor to be used was an HTGR quite similar in design to the Peach Bottom HTGR except in power level. Both reactors used similar cylindrical-geometry fuel elements and were enclosed in a steel pressure-vessel. The reactor was to be connected to the rest of the system through a concentric pipe with the high-temperature turbine-supply helium within the inner pipe and the low-temperature reactor-return helium in the outer pipe. This was to ensure that the walls of the very high-temperature pipe were not subjected to a large pressure difference.

The KSH power cycle is shown in Fig. 1.7 and cycle parameters are listed in Table 1.4. Compression occurred in three stages requiring

two intercoolers. It will be seen that this is the only proposed nuclear gas-turbine variant that used three stages of compression. A higher pressure ratio and improved cycle efficiency is possible with intercooling. The turbine pressure ratio was 2.55, which is small in comparison to simple-cycle, combustion-turbine pressure ratios. Turbomachine speed was 8000-rpm and was reduced through a reduction gear to 3000-rpm for synchronous generator speed. All four turbomachines were on a single shaft. The number of stages of the turbomachines was 12 for the turbine and 9 for each of the compressors. Figure 1.8 shows the complexity of this turbogroup.

Control of the KSH plant was by inventory and bypass control. For most power-level changes between 50% and 100%, inventory control was to be used [K10]. Plant inventory, hence massflow, is changed by simply changing the pressure level of the plant. Temperatures remain the same during this form of power level control. Efficiencies remain high over the range of power levels between about 40% and 100% with this method of control. Inventory control, however, is usually slow, only about 3% per minute for the KSH plant [B27]. For rapid changes in power and for loads less than 50%, bypass control is used. Figure 1.9a shows the combined inventory and bypass control systems. Valves V-1 through V-4 are part of the inventory-control system. The inventory-control vessel is (k), where excess helium is stored at lower powers. The transfer compressor is (l). Figure 1.9b shows the pressures in the control-vessel, the HP-compressor outlet and the precooler inlet. The difficulty produced by using only one control vessel is seen. As plant inventory is reduced, control-vessel pressure rises until at some point, in this case 80% plant inventory,

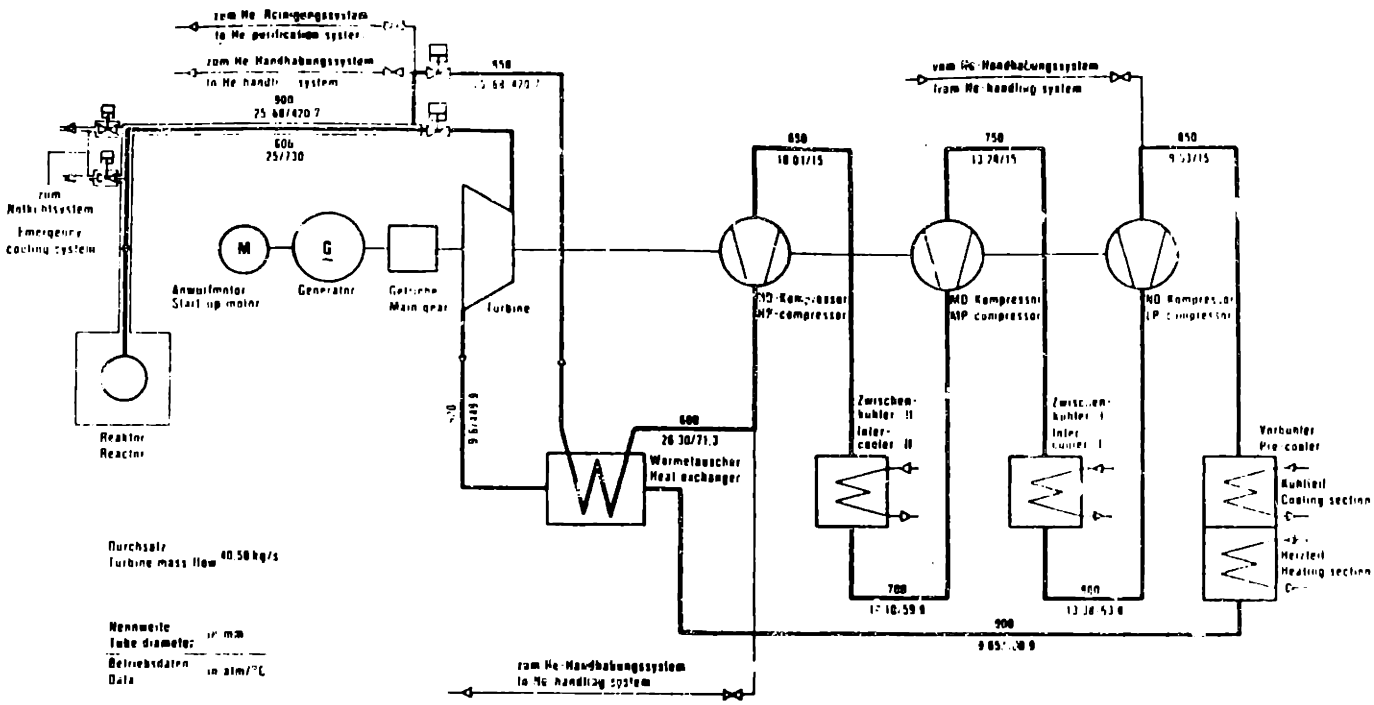

Figure 1.7. Cycle diagram of the KSH nuclear powered CCGT (B8).

Table 1.4

KSH Plant Cycle Parameters [B8]

Location	T (^{o}C)	P (MPa)	$\dot{m}$ (kg/s)
Turbine Inlet	730	2.500	40.58
Rec. Inlet (LP)	450	0.980	40.77
Precooler Inlet	101	0.965	41.26
LP Comp. Inlet	15	0.953	41.35
Intercooler Inlet	64	1.338	41.22
MP Comp. Inlet	15	1.328	41.10
Intercooler Inlet	60	1.810	41.10
HP Comp. Inlet	15	1.801	40.88
Rec. Inlet (HP)	71	2.630	40.71
Reactor Inlet	421	2.568	40.58

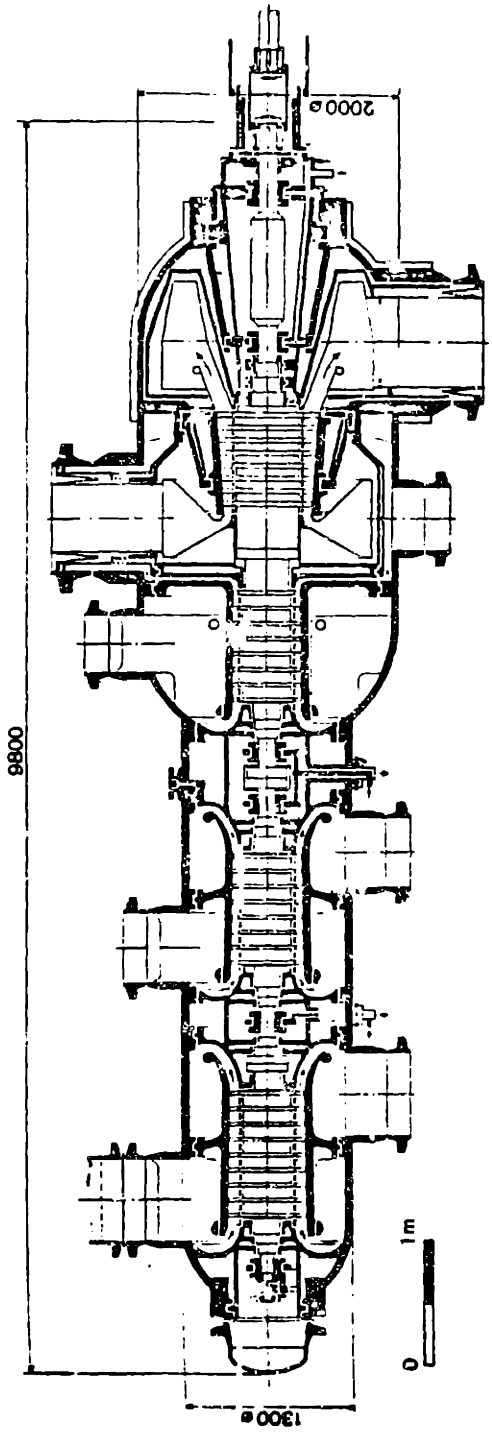

Figure 1.8. Cross section of the KSH turbogroup (B8).

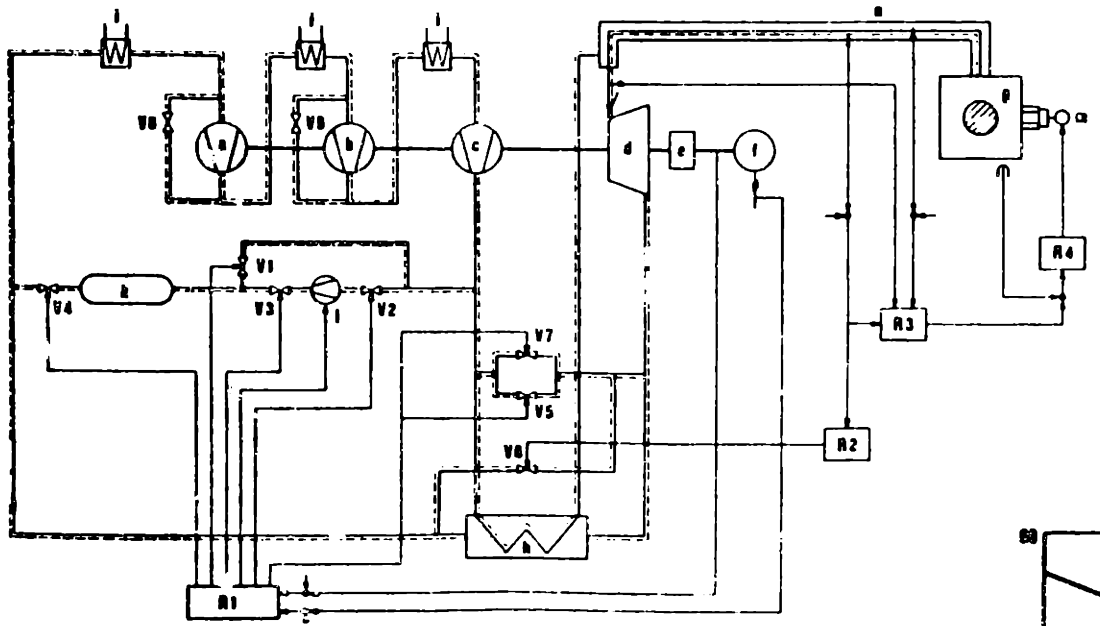

Figure 1.9a. The control system of the KSH nuclear CCGT (B8).

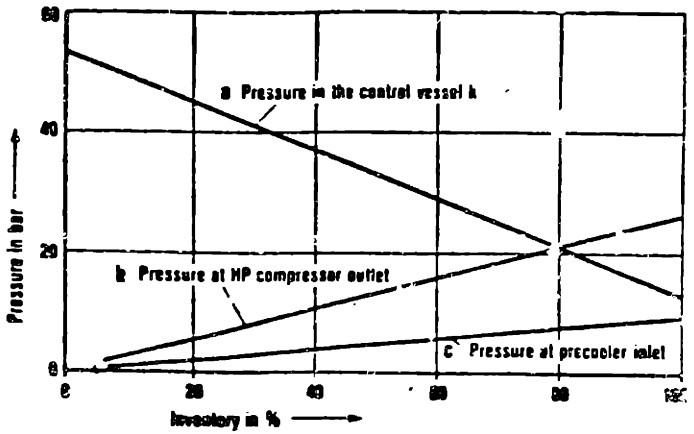

Figure 1.9b. KSH inventory control behavior (B8).

control-vessel pressure equals HP-compressor-outlet pressure. At this point, it becomes necessary to use the transfer compressor to further reduce plant inventory. This problem is diminished if the number of the control-vessels is increased. By using several control-vessels, a broader power range may be controlled with the same control-vessel volume. Alternatively, the same load range may be controlled with several small vessels with less total volume.

For most load changes, bypass control is used. Valve V-5 is the control-bypass valve. It permits part of the HP-compressor discharge to be released to the low-pressure part of the system, bypassing the recuperator and turbine. Maximum load allowed for the level of inventory is possible if no flow is bypassed. Bypassing 36% of the total helium mass flow is sufficient to operate the plant at no load. Bypass control, however, is very inefficient and requires a reactor output of 92% for an electrical output of 50%. On the other hand, inventory control requires a reactor output of only 51% for an electrical output of 50%. Because of the high reactor-inlet temperature, it is necessary to divide the bypass flow such that part of it passes through valve V-6 (up to 1/5 of the total bypass quantity) to the recuperator inlet. This cools the turbine exhaust, which is at a higher temperature when bypassed due to the reduction in turbine pressure-ratio, and prevents an increase in reactor-inlet temperature. Normal operating reactor-inlet temperature is very high, 421 C (790 F), and is pushing the limits of the pressure-vessel code even at the low operating pressures of the KSH plant. In the event of a sudden loss in electrical load, valve V-7 bypasses the recuperator and turbine such that the turbine is fully unloaded in one second.

Overspeed of the turbine is limited to less than 6% for this accident. R1 through R4 are the controllers. R1 controls the valves for bypass and pressure-level control. R2 controls the reactor-outlet temperature. Reactor power is controlled in proportion to turbine-inlet pressure; which jointly, with the reactor-outlet temperature being controlled and the reactor-inlet temperature acting as the disturbance variable, acts upon the output controller R3. R3 calculates an ideal reactor power which is compared to the actual reactor power. R4 corrects reactor power based upon the error in the ideal and actual reactor powers [B24, B27].

Although detailed designs were performed, the KSH plant was never constructed because it was believed that the state-of-the-art was sufficiently developed that work could proceed toward development of the HHT without the expense of building an intermediate nuclear plant. Turbomachine and cycle development would proceed with the high-temperature-helium test loop (HHV) and a fossil-fueled COGT.

1.3.1b HHV.

The HHV was intended to be a full-scale prototype of a turbogroup for a large COGT as part of the HHT and HTGR-GT programs. The system incorporated a two-stage 45-MW turbine and an eight-stage 86-MW compressor in a system as shown in Fig. 1.10. The turbogroup is shown in Fig. 1.11. The difference in turbine and compressor power is made up by a large 45-MW synchronous motor. The pressures and temperatures, 50-bar and 850-1000°C, respectively, were selected such that the turbomachine components could be tested under anticipated conditions for the large turbogroup of an HTGR-COGT [H5]. The bearings of the HHV are oil lubricated and require a complex sealing system because of the

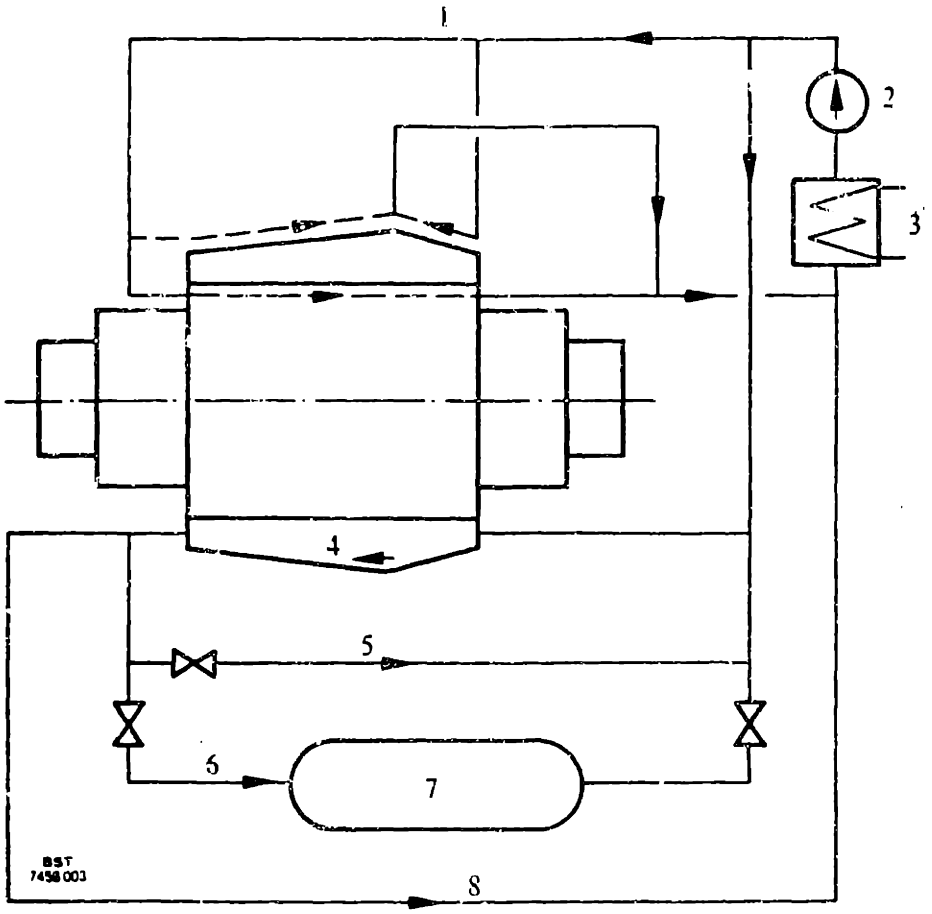

Figure 1.10. Schematic diagram of the HHV test loop (H5).

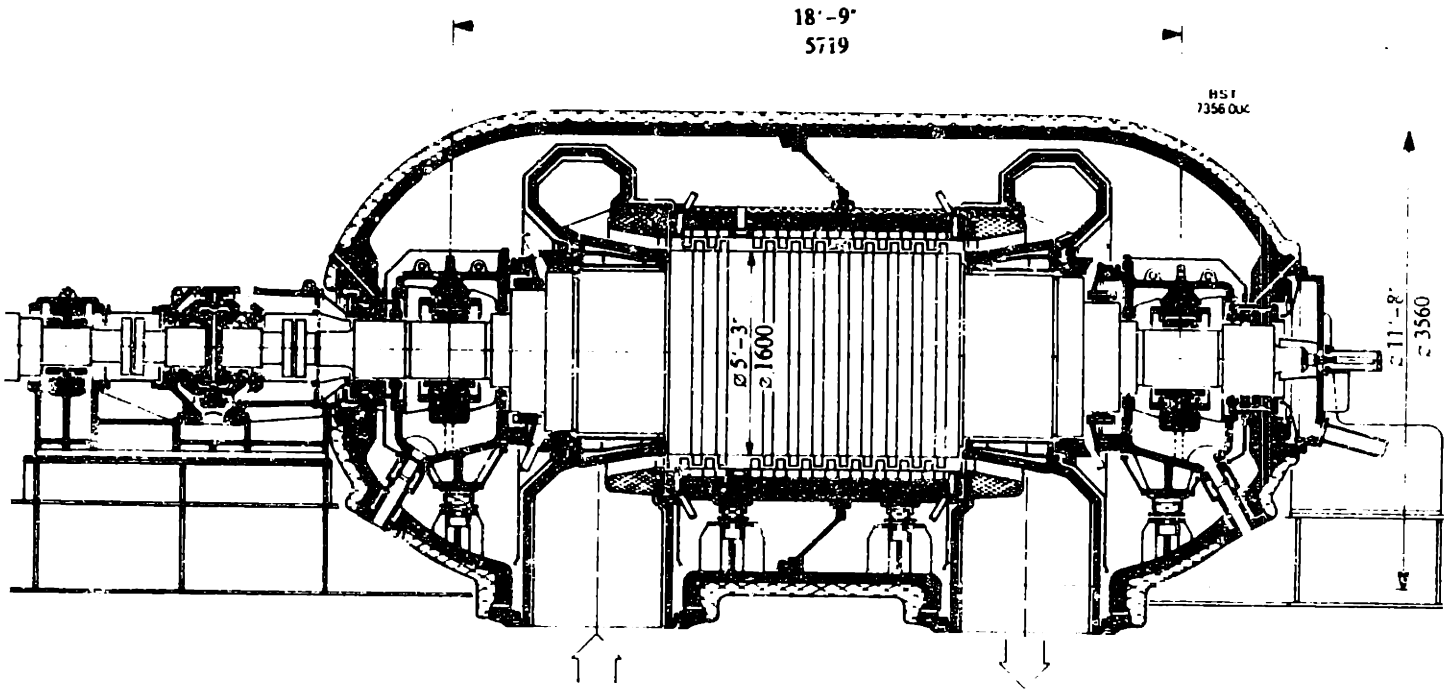

Figure 1.11. The HHV turbogroup (H5).

high pressure of the HHV. The floating seal-ring must sustain full operating pressure (50-bar) over a very large diameter. No previous floating seal-ring system had ever been designed for such a high pressure difference and large diameter [H5]. Shortly after the HHV was placed into operation, a major oil leak from the sealing system resulted in an extensive cleanup because of oil leakage into the thermal liner [Z2]. In this respect the HHV drew early attention to what is a serious problem in large CCGT design, that of the shaft-sealing system.

1.3.1c Oberhausen-2.

The Oberhausen-2 CCGT was designed primarily as a test facility to gain experience with helium CCGT plants for the purpose of obtaining operating data for nuclear gas-turbine (HHT) development. It was also built as an electric-power and district-heating plant. The novelty of the plant is that all previously constructed closed-cycle power plants used air as a working fluid and therefore Oberhausen-2 provided the first experience with helium turbomachinery in an operational CCGT power plant.

1.3.1c.1 Oberhausen-2 Plant Design:

Oberhausen-2 was designed to supply 50-MW of electricity and 53.5-MW of district-heating load [B3,B4,B5,B18]. Since Oberhausen-2 was built primarily as an exercise in constructing a helium CCGT for a nuclear Brayton-cycle, the turbine was scaled to be approximately the same size as the anticipated nuclear Brayton-cycle gas-turbine. HP-turbine-inlet pressure was selected at only 2.7-MPa, resulting in the turbine to be roughly the same size as a 300-MW unit for the HHT. The cycle diagram of the Oberhausen-2 plant is shown in Fig. 1.12 with

cycle parameters and system-design parameters listed in Tables 1.5a and b. Two-stage compression and expansion was used with an intercooler between the two compressors. Reheat was not expected to be used in the HHT and therefore was not employed between the two expansion stages. Because the output shaft was limited to the rotational speed of the generator, seperate high and low pressure turbines were employed. This enabled proper matching of turbomachine speed for the compressor. By connecting the high-pressure and low-pressure turbines with gearing, it was possible to have a machine that behaved similarly to a single-shaft machine on a loss of electrical load. Because of the aerodynamic load and increased inertia of the compressor, a single-shaft machine will exhibit less overspeed on a loss of electrical load than a split-shaft machine [B4,B5]. Intercooling was used to improve system efficiency. Because European designs incorporate district heating into their closed-cycle designs, intercooling is generally a feature of their plants. Intercooling results in higher pressure ratios and therefore, lower turbine exit temperatures. Unlike dry cooling, district heating does not require high-temperature rejection heat; and therefore, the improved cycle efficiency makes intercooling a more attractive option for the Europeans.

Each machine is contained within its own pressure-vessel as in Fig. 1.13. Since a closed-cycle system is entirely at high pressure, unlike open-cycle turbine plants, the entire system must be contained within a pressure-retaining boundary. Separate vessels for each component allow for improved access to equipment, but can result in high system pressure-drops in the piping. The turbomachinery was

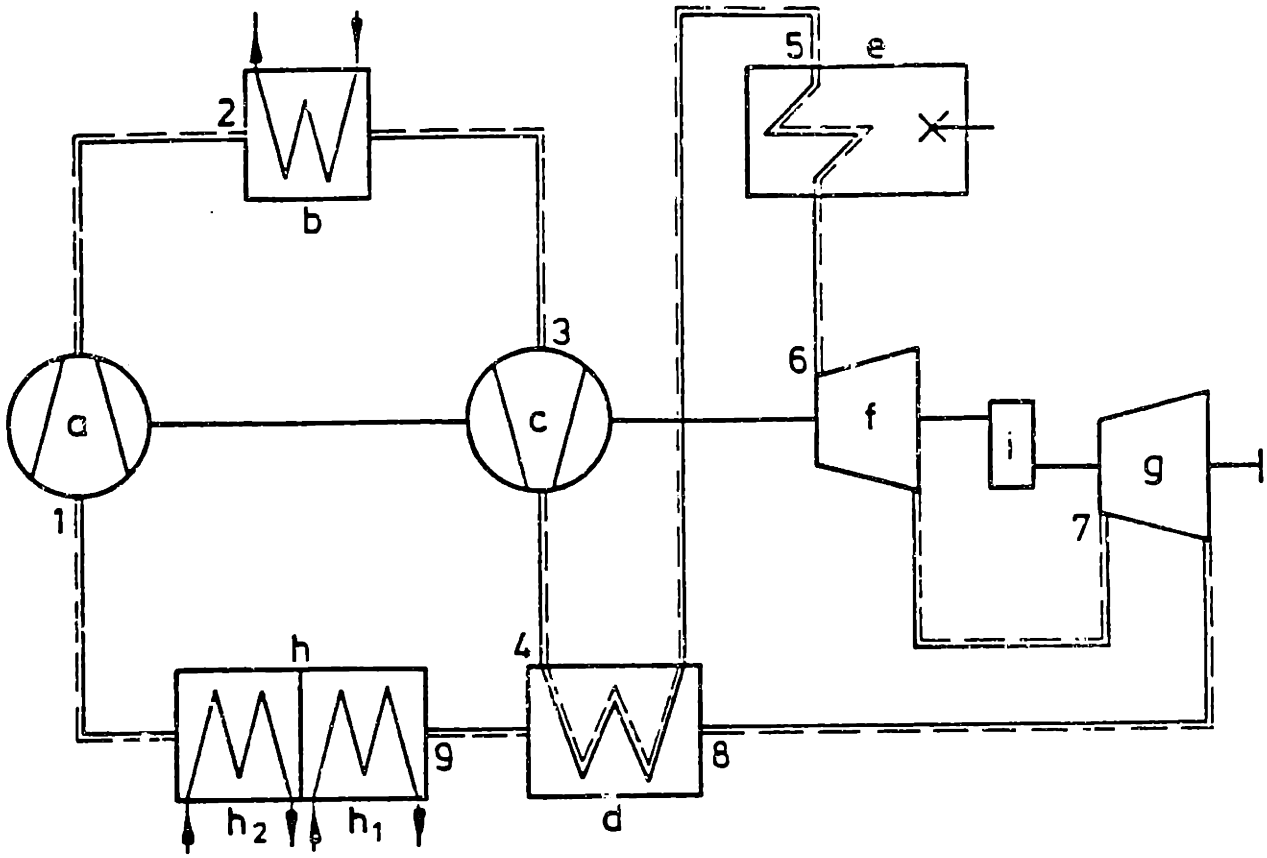

Circuit diagram of the 50 MWe helium turbine power plant

a	LP compressor	g	LP turbine
b	intercooler	h	Precooler
c	HP compressor	h_1	Heating part
d	Recuperator	h_2	Cooling part
e	Heater	i	Gear box
f	HP turbine		

Figure 1.12. The Oberhausen 2 CCGT cycle diagram (B21).

No.	Component	Temperature °C	Pressure bar
1	Low-pressure compressor	25	10.5
2	Intercooler	83	15.5
3	High-pressure compressor	25	15.4
4	Heat exchanger, HP side	125	28.7
5	Heater	417	28.2
6	High-pressure turbine	750	27.0
7	Low-pressure turbine	580	16.5
8	Heat exchanger, LP side	460	10.8
9	Precooler	169	10.6

Table 1.5a. The Oberhausen 2 cycle design gas state points (B21).

Net electric output	50.0 MW
Heating output	53.5 MW
Rejected heat of cooler	37.5 MW
Fuel heat input	159.6 MW
Net electrical efficiency	31.3 %
Overall efficiency (electricity + district heating)	65.0 %
Heater efficiency	92.2 %
Helium mass flow rate at HP turbine inlet	84.4 kg/s
Heat exchanger temperature difference	40.0 K
Total pressure losses	10.4 %

Table 1.5b The Oberhausen 2 system design parameters (B21).

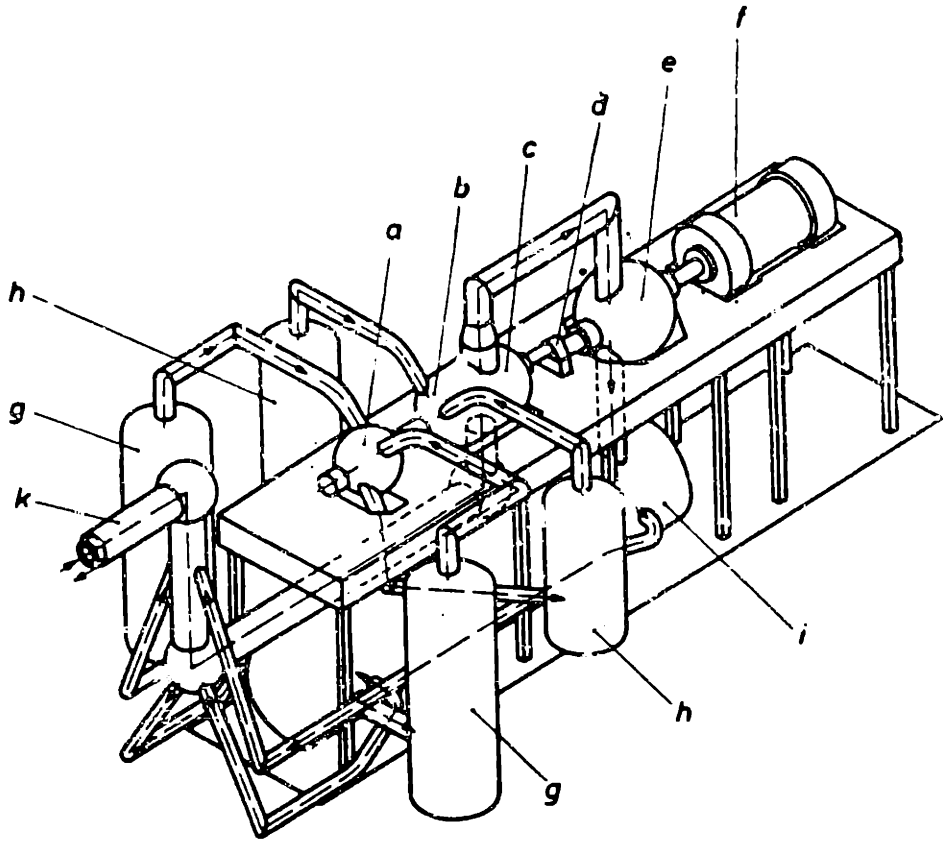

a LP compressor
b HP compressor
c HP turbine
d Gear
e LP turbine
f Generator
g Precooler
h Intercooler
i Heat exchanger
k Concentric double duct

Figure 1.13. Isometric view of the Oberhausen 2 CCGT plant (B4).

contained within spherical vessels as shown in Fig. 1.14a. The internal surface of each vessel is swept with the low temperature gas from the component, or components, in order to maintain metal strength. It was therefore necessary to install another component, the HP-compressor, in the same vessel as the HP-turbine because both HP-turbine supply and exhaust are at temperatures that are too high to sweep the walls of a pressure vessel.

Oberhausen-2 turbine-inlet temperature is limited to 750°C. This is a result of the limitations of the heater materials. The maximum heater temperature is 800°C. A 50°C difference is needed to allow for heat transfer. The heater is powered by a coke-oven-gas furnace [B3]. The recuperator is an annular, multiple-pass, cross-counterflow, straight-tube, tube-and-shell heat-exchanger as pictured in Fig. 1.14b. Although not the most compact of heat-exchanger geometries, this configuration was selected for its ruggedness. At the time of the construction of Oberhausen-2, tube-and-shell heat-exchangers were considered the only type of industrial heat-exchanger suitable for high-pressure service.

1.3.1c.2 Oberhausen-2 Control:

Control of the Oberhausen-2 plant is performed three ways: pressure-level control, bypass control and safety-bypass control. For steady operation, the power is maintained by regulating the pressure, hence the massflow, of the system. All temperatures and turbomachine velocities remain essentially the same at all pressure levels. Specific pressure drops will change only slightly as pressure is altered. Hence, efficiency of the system changes very little from one power level to another with this method of power-level control. Figure

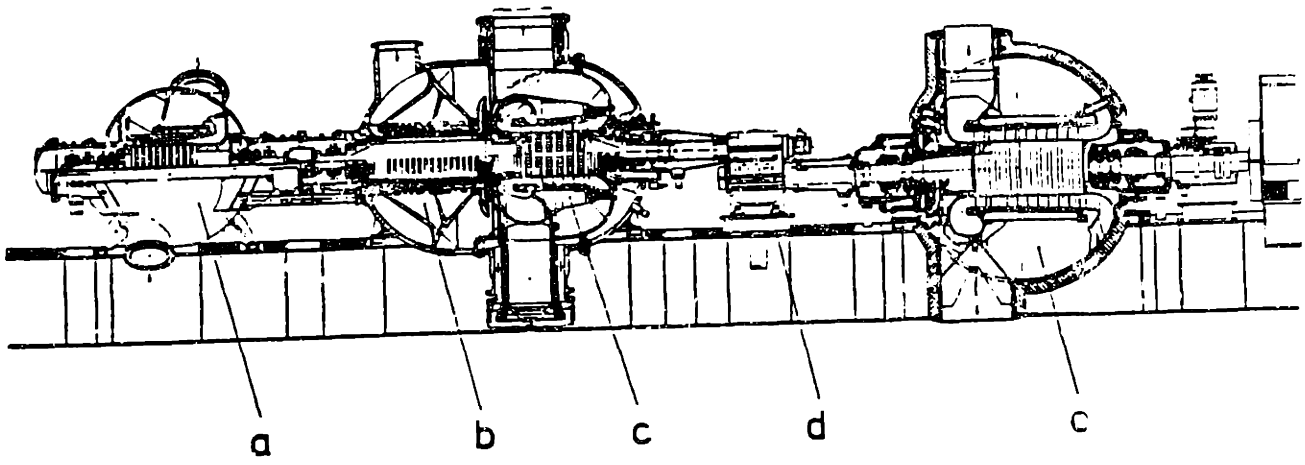

Figure 1.14a. Cross section of the 50 MWe helium turbine plant [from B4]

a LP compressor
b HP compressor
c HP turbine
d Gear unit
e LP turbine
Design: MAN/GHH

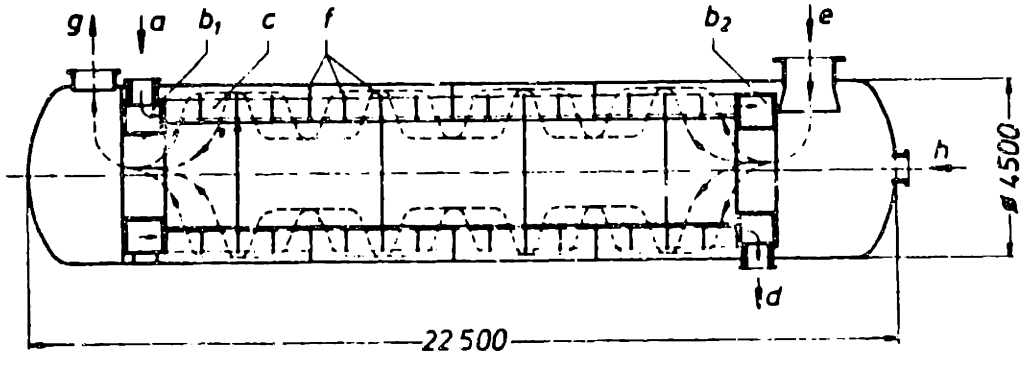

Figure 1.14b. Longitudinal section of the heat exchanger [from B4]

a HP gas inlet
b_1, b_2 Ring collector
c Tube bundle
d HP gas outlet
e LP gas outlet
f Guide baffles
g LP gas outlet
h Bypass connection

Dimensions in mm

1.15 shows the Oberhausen-2 pressure-control system. Helium inventory is removed from the HP-compressor exhaust, and inventory is added upstream of the precooler. Three 120-m^3 control-reservoirs are used during normal operation and two storage reservoirs are available for long-term helium storage [B5]. With this arrangement it is not necessary to use the helium-transfer compressors during normal operation. This method of power-level control is capable of power-level changes at a rate of 20% per minute with a 40-cm diameter control valve [Z1].

As shown in Fig. 1.15, two bypasses branch off downstream of the high-pressure compressor. The control-bypass valve (o) may be throttled to control the plant during isolated operation or after a load release. Figure 1.16 shows electrical-power output and shaft-power consumed as functions of control-valve mass-flow. Idling is attained at 37.2% mass-flow through the control valve. By lowering the pressure head across the turbine, turbine power can be reduced. Turbine-exhaust temperature experiences a resulting temperature increase. Therefore, the cooler helium from the compressor exit is discharged through the bypass into the low-pressure inlet of the recuperator to reduce the temperature of the hot turbine-exhaust and prevent thermal shock to the recuperator. Figure 1.17a shows the response of the plant to a sudden loss of electrical load from 100% at time t = 0 and sudden reconnecting of 50% load at time t = 17.5 seconds. The power at the gear shaft equals the power of the LP-turbine less the shaft power consumed by the generator, and therefore jumps rapidly upon unloading of the generator. Only 7% overspeed occurs on control bypass alone. The low overspeed is largely

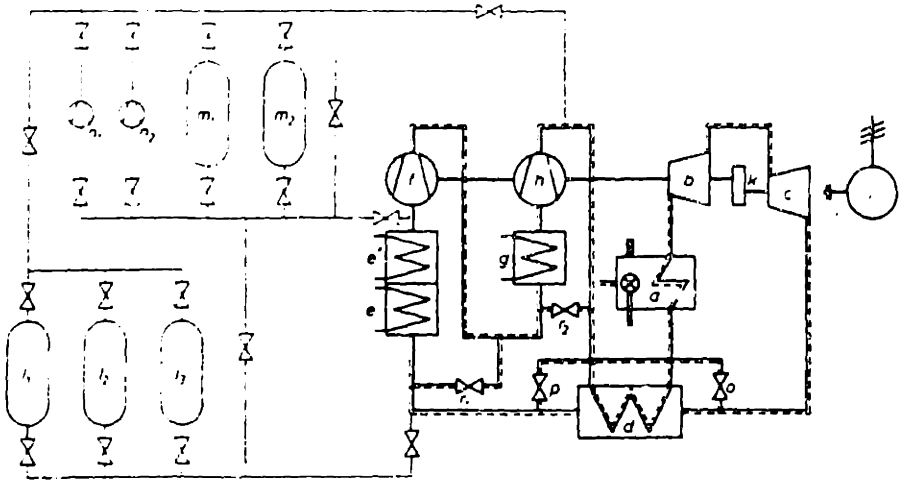

a - heater
b - HP turbine
c - LP turbine
d - heat exchanger
e' - heating part of precooler
e" - cooling part of precooler
f - LP compressor
g - intercooler
h - HP compressor
i - alternator (starter motor)
k - gear
$l_1 \ldots l_3$ - regulating reservoirs
m_1, m_2 - storage reservoirs
n_1, n_2 - transfer compressors
o - control valve
p - shutdown valve
r_1, r_2 - recirculating valves

Figure 1.15. The Oberhausen 2 CCGT control system (B5).

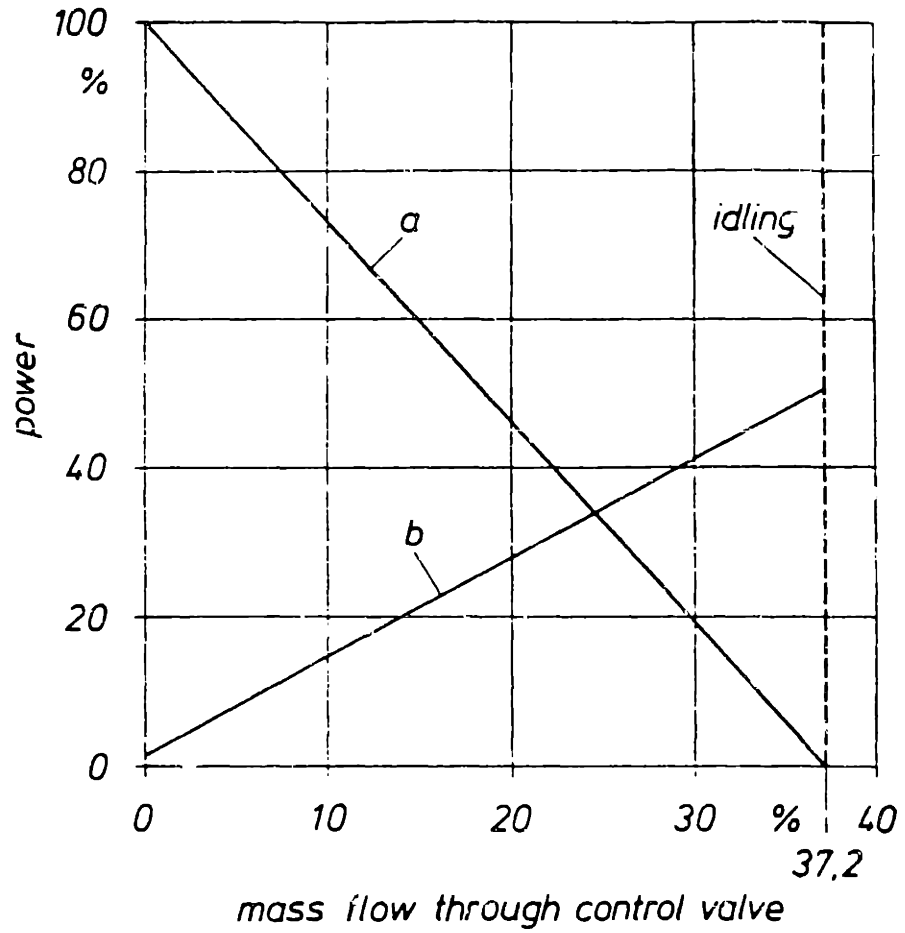

Figure 1.16. The effect of control valve bypass massflow on plant steady-state electrical power and shaft power (B5).

Figure 1.17. Oberhausen 2 plant response to a sudden loss of electrical load (B5).
(a) Control bypass response only.
(b) Safety shutdown system response.

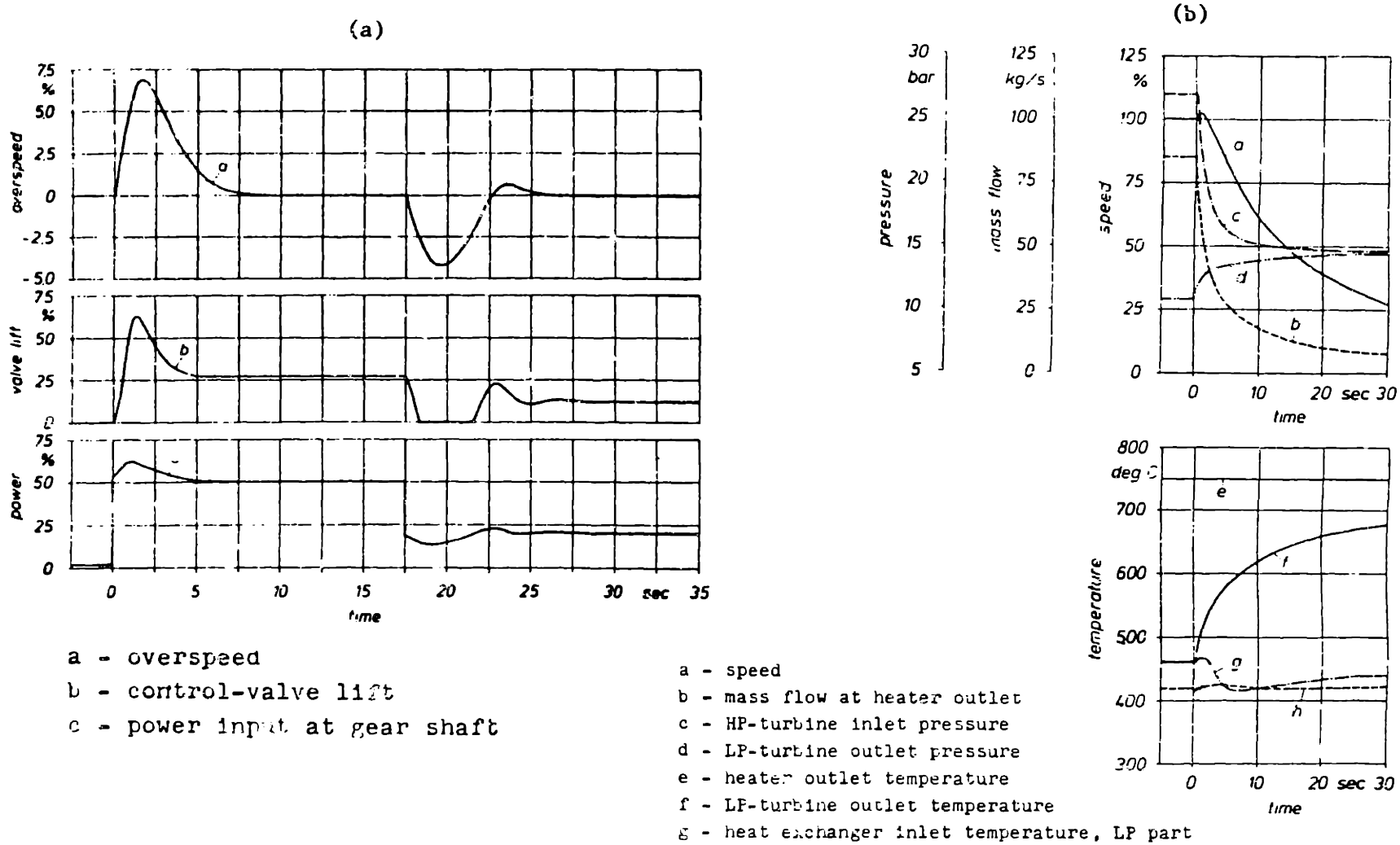

a result of the high inertia and aerodynamic loading of the coupled turbomachinery.

The primary control system to prevent turbomachine overspeed from full load is the safety shutdown system. For this accident the control bypass is considered a backup system. In the case of sudden loss-of-load, or any other potential overspeed situation, the shutdown valve (p) opens to vent HP-compressor exhaust to the precooler inlet. The bypass-control valve (o) opens slightly to allow cooler helium to the low-pressure recuperator inlet and prevent thermal shock of the recuperator due to the high turbine-exhaust temperature. Figure 1.17b shows the plant response to a loss in electrical load from 100% rated power and shutdown by the safety-shutdown system. A slight overspeed occurs followed by a rapid drop in speed. LP-Turbine-exhaust temperature rises rapidly upon the rapid drop in turbine pressure-ratio. Most other temperatures in the cycle remain relatively constant.

1.3.1c.3 Operating Experience with Oberhausen-2.

Operating experience with the Oberhausen helium CCGT has been a mixture of both good and bad results. Although the electrical output of the turbine has fallen far short of the design values and there has been difficulty with turbomachine failure, the systems that were considered new to the Oberhausen plant and vital to HHT development generally performed successfully [Z2].

1.3.1c.3a Shaft-Sealing System.

The shaft-sealing system of the Oberhausen turbine has operated successfully over the plant life. Figure 1.18 shows the principle of operation of this system that seals the main circuit from the

bearing-oil system and the bearing-oil system from the atmosphere. The left side of Fig. 1.18 is the last stage of the HP turbine. There are three labyrinths divided by two chambers between the last turbine stage and the bearing. Sealing helium introduced into the left chamber (2) is at a pressure slightly higher than the turbine-exhaust pressure. Thus, helium bleeds continuously into the primary helium system and also bleeds to the right chamber, where it is taken to feed the corresponding system of the LP turbine. The mixture of bearing oil and helium is sent to a filtration system where the helium and oil are separated. A sealing-oil bearing provides leaktightness to the atmosphere. Some of the discharging sealing-oil mixes with some of the discharging bearing-oil and is sent to a closed low-pressure tank. The sealing oil that comes into contact with the atmosphere is returned to the sealing-oil tank. It is essential that the pressure differences indicated are maintained under all circuit conditions or major leakage could result. The auxiliary-circuit pressure-control system must therefore track quickly and accurately in all transients. This system is similar to that of the HHV which experienced a major oil leak into the hot-gas-duct insulation. The potential availability problems resulting from a poorly operating control system are great. It will be shown that this system was a major problem in the HTGR-GT design. Therefore, the successful operation of this system at Oberhausen is a significant accomplishment.

1.3.1c.3b Helium Leakage

It is necessary to minimize helium leakage, or plant efficiency will suffer severely. Additionally, the helium from a nuclear plant may contain radioactive species which should not be released to the

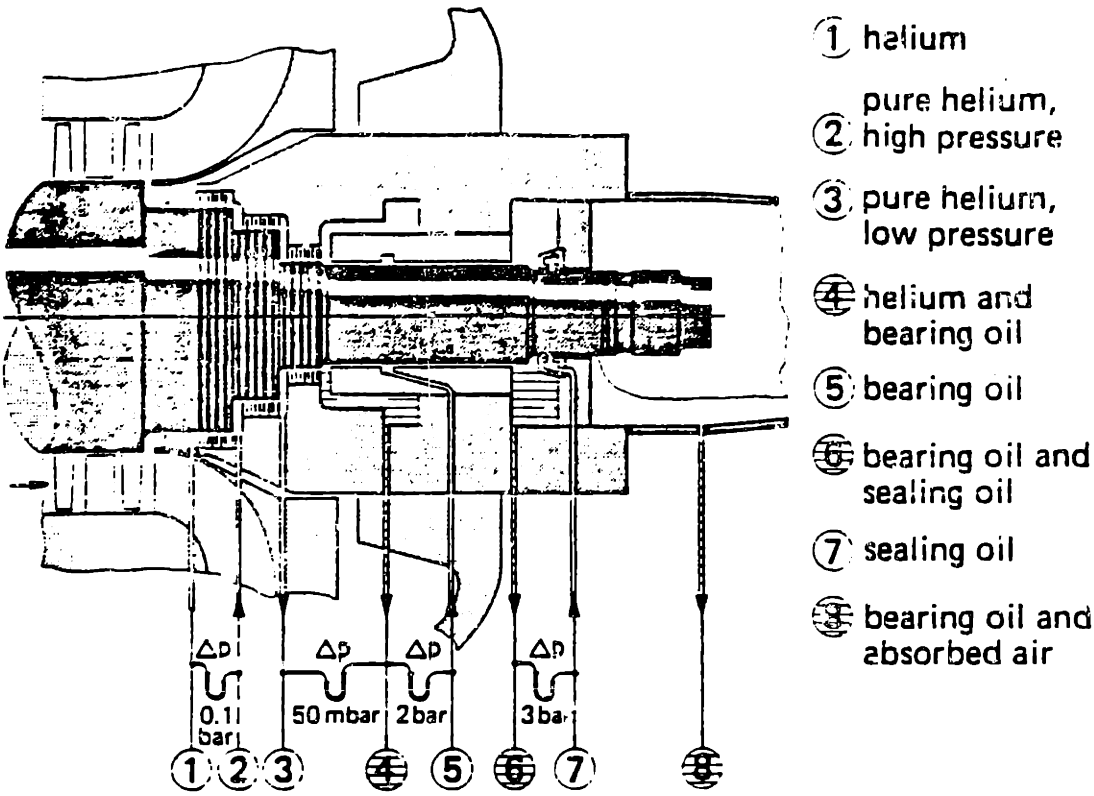

Figure 1.16. The Oberhausen 2 shaft sealing system (Z2).

atmosphere. Oberhausen helium leakage was initially 40-kg per day, but was reduced to 5-10 kg per day. Helium-leakage rates from Oberhausen 2, AVR and Dragon are listed in Table 1.6. Also on Table 1.6 are the estimated daily costs of the helium that leaks from these plants. The helium costs are clearly not the major cause of concern for reducing the helium-leakage rates. In nuclear systems, the primary concern is in regard to release of activity from the plant. The Oberhausen leakage rates, though a seemingly low percentage of the total inventory, produce total leakage rates that are still too high for a nuclear system. A nuclear CCGT must do better.

1.3.1c.3c Thermal Barrier Integrity.

The construction of the concentric hot-gas-duct is shown in figure 1.19. The inner duct carries high-temperature turbine-inlet helium and the outer duct carries lower-temperature helium to the furnace. The pressure drop across the inner duct surface equals only the pressure drop across the heater. The thermal barrier is used to protect the surface of the inner duct from the high-temperature helium. A metal liner is used to maintain the integrity of the fibrous KAO-wool insulation. There was much concern over the ability of the insulation to maintain its integrity in the high-temperature and high acoustic-pressure-level environment. The insulation was therefore heavily instrumented with thermocouples for the purpose of monitoring its performance. In 11,000 hours of electricity production, the insulation maintained its integrity very well, as indicated by a stable temperature profile that was maintained over this time [Z2].

1.3.1c.3d Tribology Problems.

In a helium environment metals do not form oxide layers and tend

Table 1.6

Helium Leakage Rates [Z2]

Plant	Inventory	Leakage Rate		He Cost*
	kg	kg/day	%/day	$/day
Oberhausen 2	1,400	5.0-10	0.3-0.7	6.50-13.00
Dragon	180	0.2-2.0	0.1-1.0	0.26-2.60
AVR	240	1.0-3.0	0.4-1.2	1.30-3.90

* Based upon $ 0.22/scf ($ 1.30/kg) [N2]

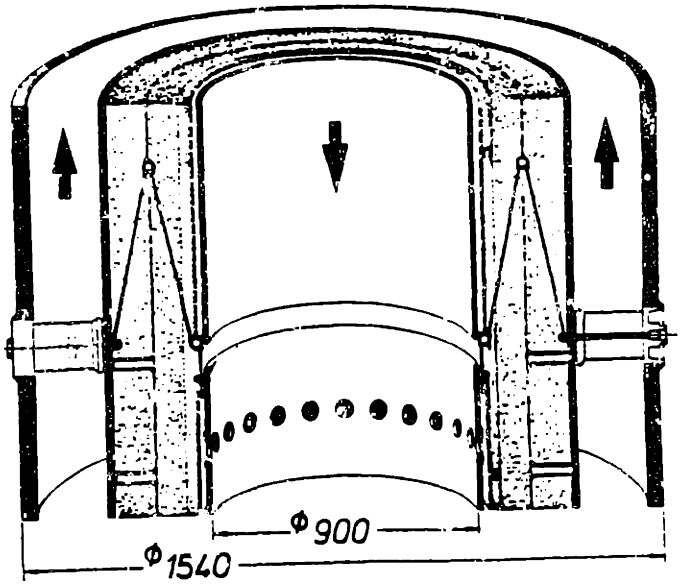

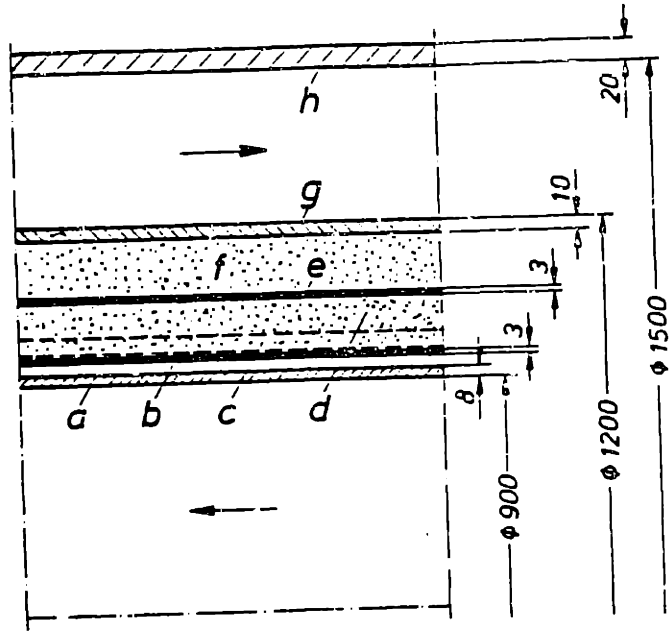

Hot-gas piping of the 50 MWe helium turbine plant

a Inner liner (core pipe)
b Perforated inner pipe
c Insulation (KAO mats)
d Insulation (KAO wool)
e Perforated pipe
f Insulation (KAO wool)
g Inner wall of annular duct
h Outer wall of annular duct

← from heater to turbine
→ from HP compresssor to recuperator, and from recuperator to heater

Dimensions in mm

Figure 1.19. The Oberhausen 2 concentric gas duct and thermal barrier construction (upper from Z2, lower from B21).

to experience problems with wear and welding of mating surfaces. The following methods proved successful in preventing these problems [Z2]:

In the concentric pipe, the inside pipe support may rub the outer surface of the inside pipe due to vibrations or thermal expansion/contraction. Molybdenum-disulphide solid lubricant was applied at this surface.

Where an inner-liner guide-tube of the concentric duct meets the next guide-tube, abrasion may result. At these locations chromium-carbide was deposited by electro-deposition.

Loaded stationary-contact surfaces were protected against surface welding by a boronitrite coating.

Fretting was prevented by placing plates coated with titanium-carbide between parts that moved relative to each other.

1.3.1.d The High Temperature Helium Turbine (HHT).

The German HHT-Project was directed toward the construction of a nuclear helium-turbine of large output to be carried out within the framework of the fourth atomic program of the Federal Republic of Germany. Designs were made for a plant of 3000-MWth and 1000-MWe capacity. A single recuperated turbine loop would be used. The loop would incorporate two stages of compression with intercooling. The entire plant would be contained within a PCRV. Figure 1.20 shows the HHT design.

In 1981 the HHT program was terminated because it was not felt that a large HTR with a helium turbine could be built and operated to generate electricity at costs that were competitive with LWR's. The German Ministry of Research and Development was also heavily burdened with the THTR and breeder-reactor projects and could not afford

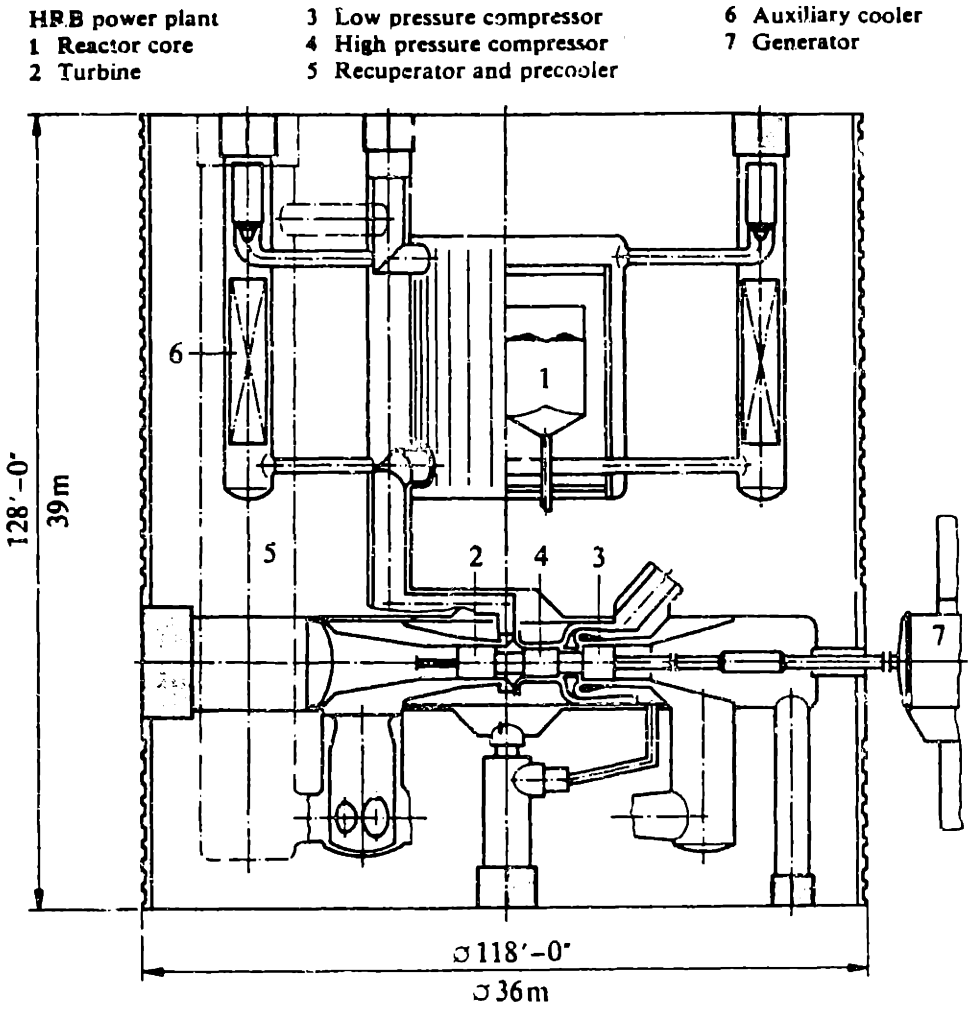

Figure 1.20. The High Temperature Helium Turbine (HHT) (H5).

another major nuclear project [Z3].

1.3.2 HTGR-GT.

In the United States, the General Atomic Company conducted a design study of a large direct Brayton-cycle plant for use with an HTGR. Several design variants were generated in the study as optimum arrangements and operating parameters were determined. A number of technical problems became clear in the study. Many of them resulted from the large size and advanced nature of the system planned. As already noted, small closed cycle plants had been successfully operated in Europe for years. The large size of the HTGR-GT plant and the safety criticality of the nuclear systems could not be extrapolated from the modest systems that engineers had previous experience with to such a large and advanced system.

1.3.2a HTGR-GT Design Configurations.

HTGR-GT variants ranged from 800-MWe to 1200-MWe with as many as four and as few as two Power Conversion Loops (PCL's) arranged within a PCRV. Figure 1.21 shows the general arrangement of the two PCL, HTGR-GT reference design plant and Fig. 1.22 shows a PCL cycle diagram. The turbomachines are mounted horizontally with either end accessible from outside of the PCRV. However, some variants incorporated vertical turbomachine designs. Vertical machines are easily removed, but are not space effective in the PCRV [M13]. In all variants the 60-hz. generator is mounted externally to the system, requiring a shaft-penetrating seal. Heat exchangers were mounted vertically in all variants. The use of a PCRV requires the use of a thermal-barrier system which consists of insulation and a carbon-steel liner. The insulation protects the PCRV from high temperatures, and

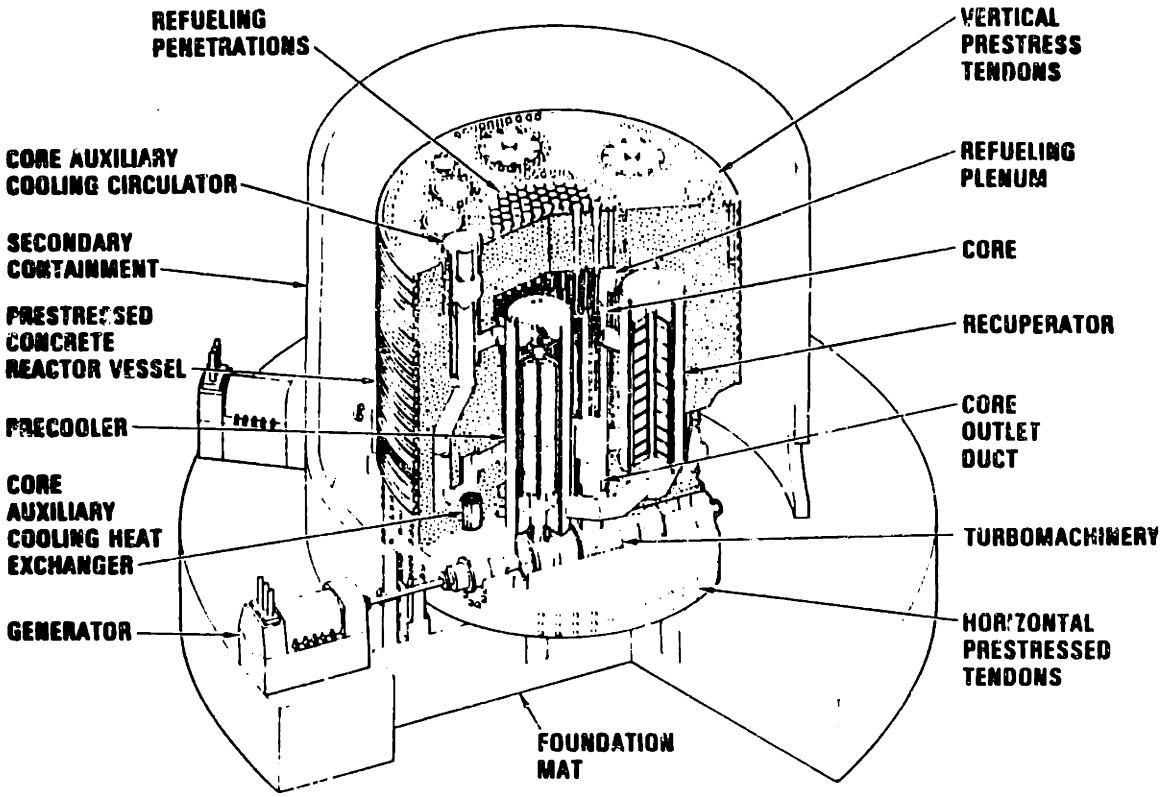

Figure 1.21. The two-PCL HTGR-GT power plant (G6).

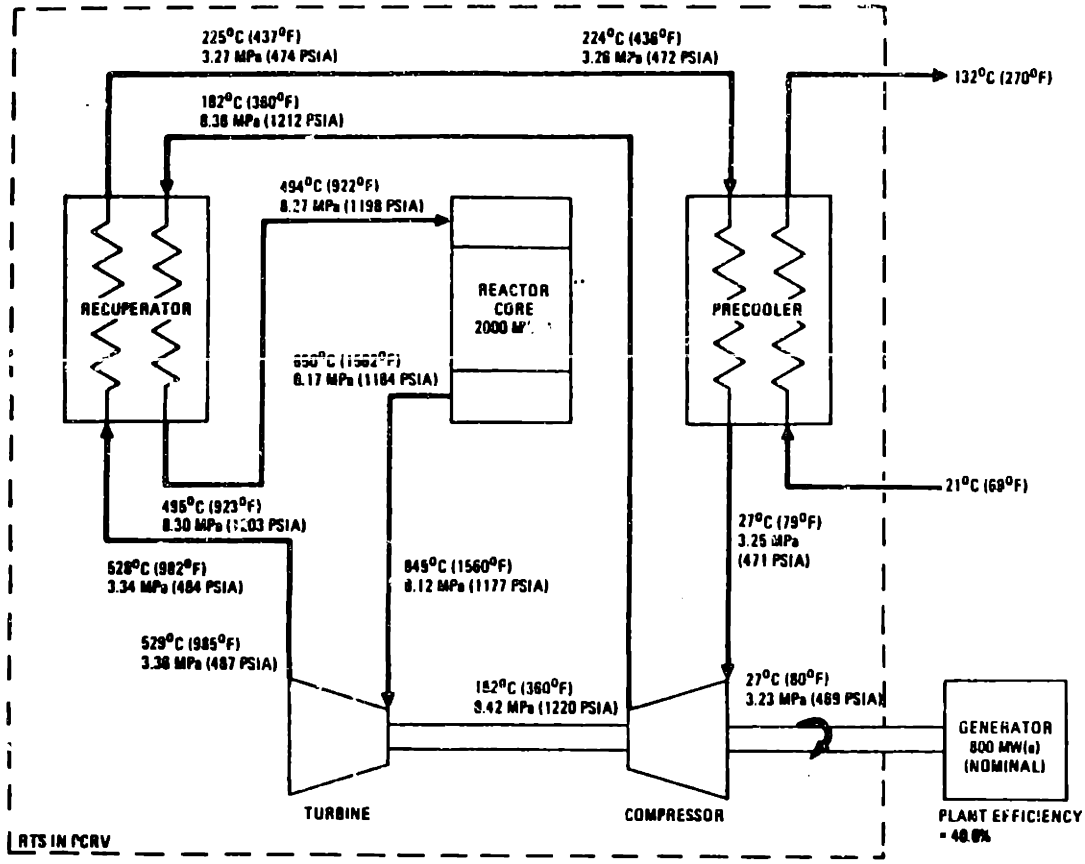

Figure 1.22. The HTGR-GT PCL cycle diagram (G6).

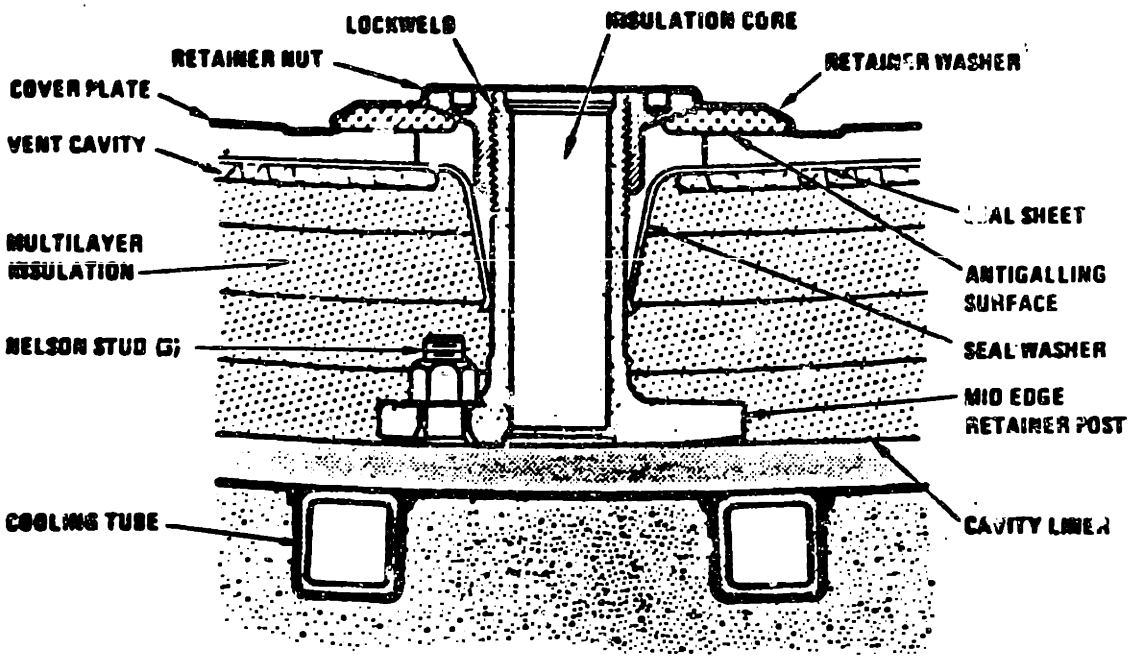

Figure 1.23. HTGR-GT Thermal Barrier construction [from M4].

the liner seals the helium coolant inside the PCRV. Additionally, cooling water is circulated through tubes in the concrete wall of the barrier as in Fig. 1.23. A PCRV was chosen since it enabled incorporation of the entire system into one structure, eliminated vessel transportation restrictions, and virtually eliminated the possibility of a catastrophic failure. The variants were evaluated on the basis of minimizing overall size and cost of the system as compared to other arrangements considered. The turbine-inlet temperature was selected at 850°C for all variants so that blade cooling was not needed for conventional turbine-blade alloys. Turbine-inlet pressure varied between about 7.5-MPa and about 8.5-MPa. Pressures resulted from optimization studies that considered material capabilities, equipment sizing and PCRV limitations [K4,M13].

1.3.2b Heat Exchangers.

All variants of the HTGR-GT utilized vertically-mounted tube-and-shell heat exchangers throughout. At the time of the HTGR-GT study, tube-and-shell heat exchangers were the only geometry heat exchangers that were believed to have the reliability necessary to be put into a nuclear system [M11]. The heat exchangers were all mounted in a vertical manner so that they could be removed easily for maintenance and to simplify incorporation into the PCRV. In all cases the precooler was an annular, multiple-pass, cross-counterflow heat-exchanger with helically-wound, finned, circular-tubes. Water circulated within the tubes and helium flowed over the finned tubes. This arrangement offered relatively small size with the potential for dry-cooling due to the high water-outlet temperature possible. It is shown in Fig. 1.24. Although all of the tube-and-shell counterflow

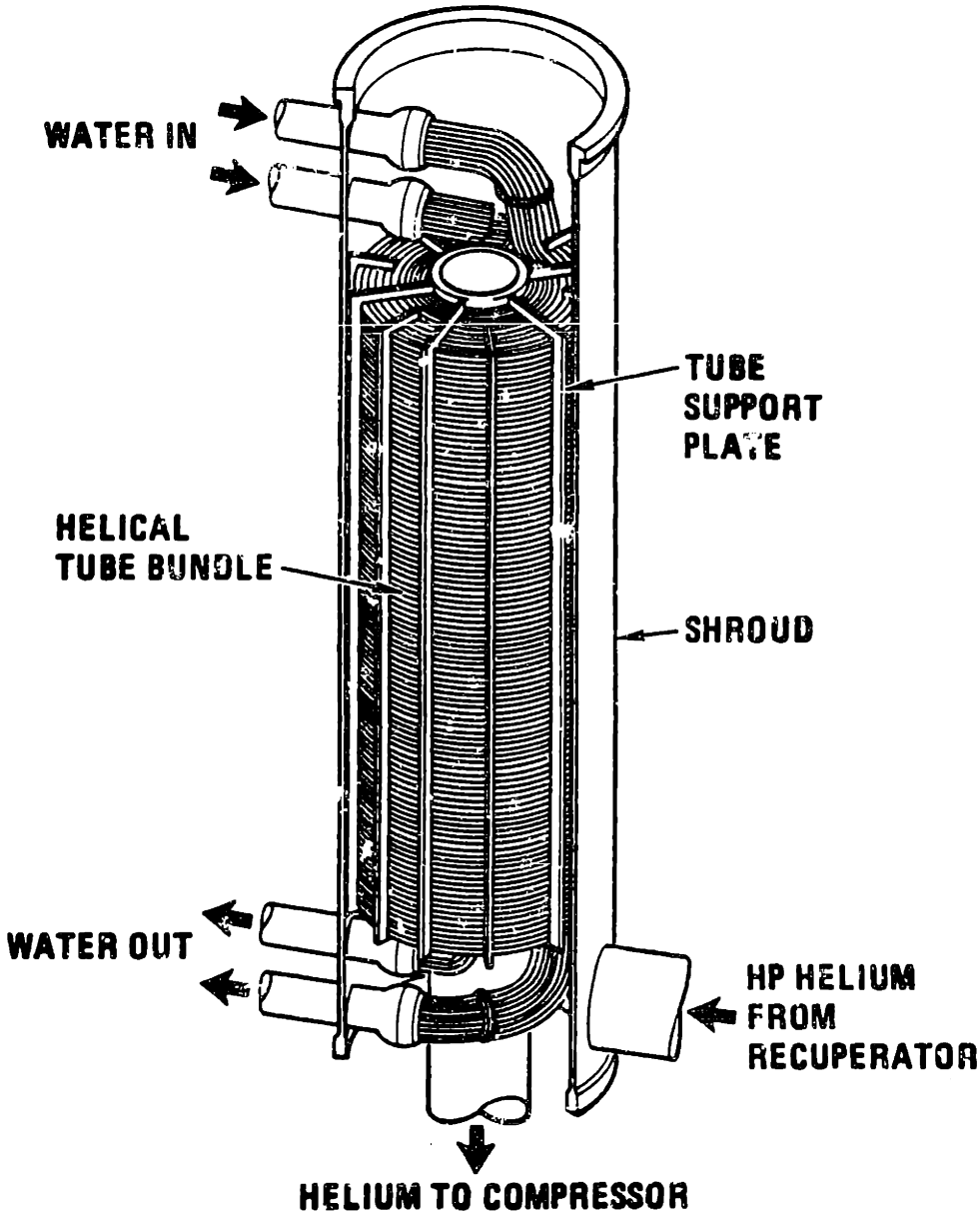

Figure 1.24. The HTGR-GT Precooler (G6).

Figure 1.25. Two HTGR-GT recuperator designs.
(a) Tube and Shell Counterflow (G6).
(b) A less conventional Tube and Shell counterflow design (M12).

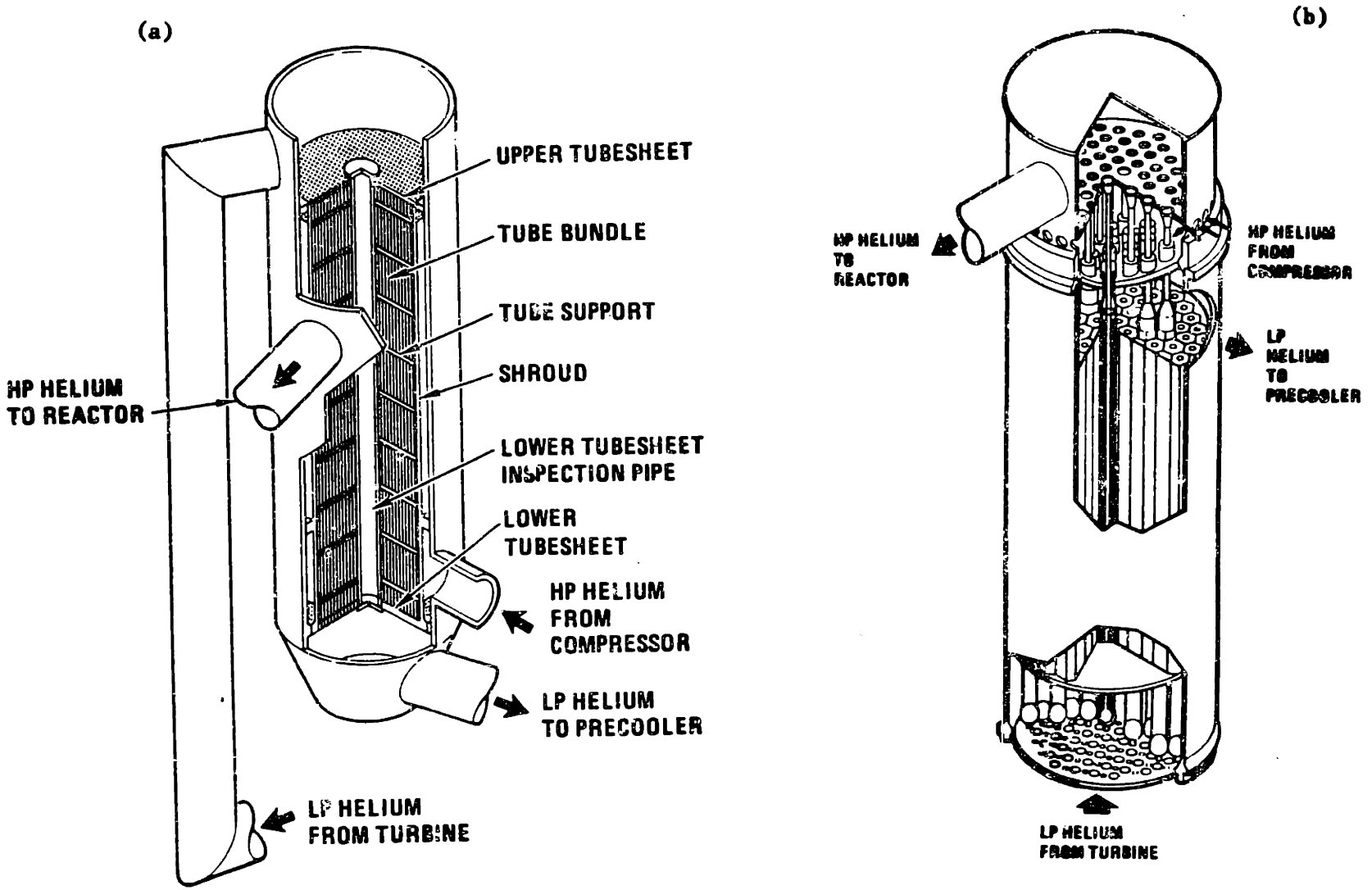

design, the recuperators varied widely in the way they achieved a counterflow arrangement. Figure 1.25a shows a conventional straight-tube arrangement for one of the HTGR-GT variant recuperator designs. Figure 1.25b, however, shows a more novel arrangement in one of the other variants. The use of different counterflow arrangements in the recuperator was a result of attempts to minimize the recuperator size by fitting the most heat-transfer surface area into the minimum volume. Ferritic and austenitic stainless-steels were used for construction of all heat exchangers since these materials are easily formed into heat-exchanger surfaces and provide ample strength at the temperatures being considered [M11].

1.3.2c Machinery Design.

The turbomachinery designs varied widely from one HTGR-GT variant to another. Since the turbomachinery is the heart of the direct Brayton-cycle plant, its arrangement dictates the design of the remainder of the plant. The HTGR-GT variants included systems with and without intercooling, and systems with and without split shafts. Most the reference designs incorporated a single compressor and a single shaft for turbine and compressor in each PCL. Despite its roughly 3% efficiency advantage, intercooling was disregarded because of the complexity it added to the plant [A2,M2]. Since intercooling frequently requires a split-shaft arrangement for proper turbomachine speed matching, two additional turbomachines are usually needed along with an additional heat exchanger and ducting. Placing all of this into an already crowded PCRV was untenable.

Because the turbine is limited to the maximum synchronous speed of the generator, it could not operate above 3600-rpm. Aerodynamic

design of the turbomachine, especially the compressor, becomes difficult when limited to this low rotational speed. In a split-shaft arrangement it is possible to have one turbine driving the generator at synchronous speed and a second turbine driving the compressor at a higher rotational speed. Figure 1.26 shows one such cycle arrangement considered for the HTGR-GT [G1]. Besides creating the additional complexity of the second turbine, the split-shaft arrangement proves to be difficult to control upon a sudden loss of electrical load. In a single-shaft arrangement, the aerodynamic loading and inertia of the compressor significantly reduce turbine overspeed during such an accident.

The oil-lubricated bearings and shaft-penetration seals create the difficult problem of preventing the ingress of lubricant into the primary coolant and the leakage of primary coolant into the lubrication system. Lubricants that leak into the primary coolant may react with the hot graphite or deposit on equipment surfaces with deleterious effects on plant performance. Although the helium coolant itself does not become radioactive under a neutron flux, it may carry with it entrained radioactive particles. If the helium coolant were to leak to the lubrication system, the lubrication system would become potentially contaminated. Maintaining these two fluids separate while meeting all plant operating requirements is a difficult task.

In the HTGR-GT, the bearing compartments were contained within the coolant-pressure boundary. The shaft to the generator necessarily penetrated the pressure boundary through a sealing system. An oil-buffered sealing system was used for both bearing and penetration seals to keep lubricant separate from coolant. Such a sealing system

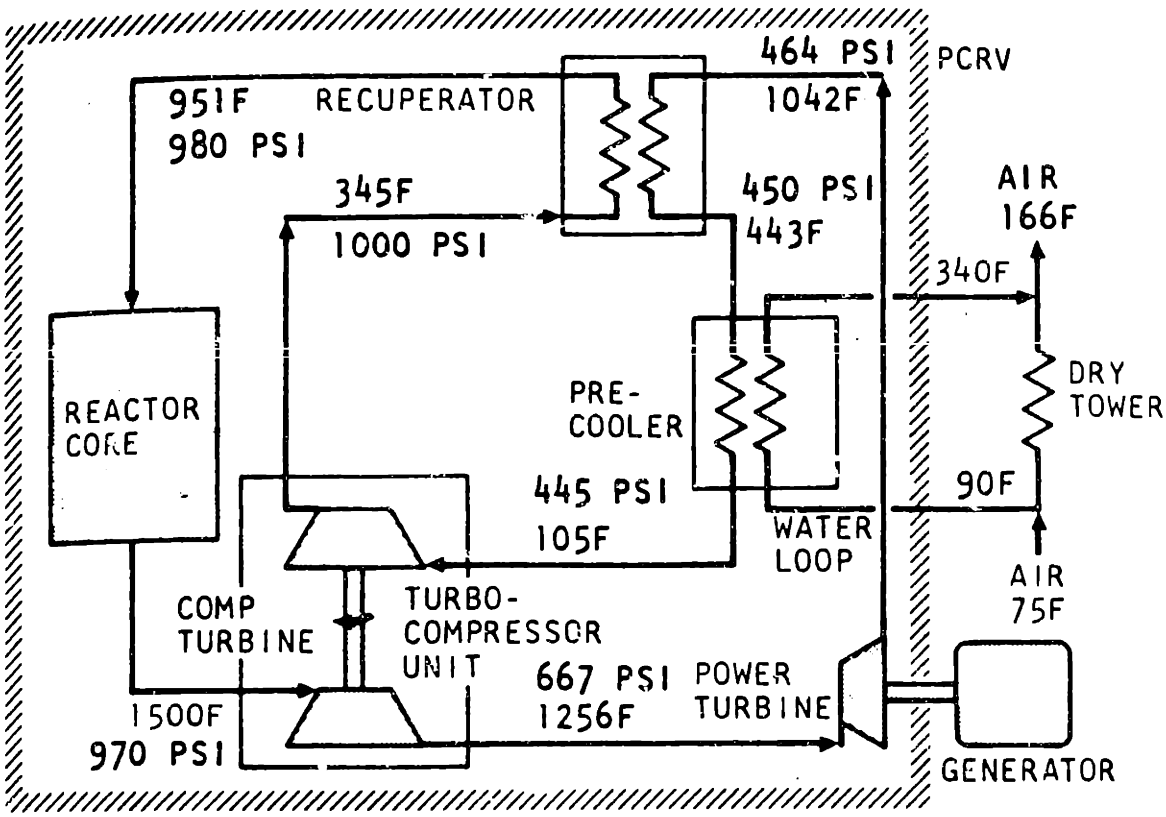

Figure 1.26. HTGR-GT split shaft turbomachine PCL cycle diagram (G1).

is pictured in Fig. 1.27 along with a bearing cavity that is to be sealed from contact with the primary coolant. A gland for venting of helium and lubricant leakby is located between the bearing cavity and the buffering-helium cavity. The buffering-helium cavity is located between the gland and the primary system. Labyrinth seals separate the cavities. During normal operation, the buffering helium, which is at a pressure slightly higher than the primary, leaks into the primary and into the gland, keeping the lubricant separate from the coolant. In the HTGR-GT, the primary system experiences very rapid pressure transients even during normal operations such as start up and shutdown. Pressure of the buffering helium must be closely controlled during system transients so that it does not drop below primary-coolant or lubrication-system pressures. If that were to happen, the lubrication system would come into contact with the coolant. If buffering-helium pressure were maintained above any possible coolant pressure at all times, separation of the lubrication system and coolant system would be assured; however, this arrangement would not be economical. If the pressure-control system for the buffering helium is designed so that separation of coolant and lubricant is assured under all possible conditions, an extremely complex control system results. Such a system would probably be beyond the capabilities of present control-system technology. If the requirements are relaxed slightly to allow some leakage under certain conditions, the problem is not impossible, but still very difficult [A3].

1.3.2d Control of the HTGR-GT.

The HTGR-GT Plant Control System (PCS) is designed to

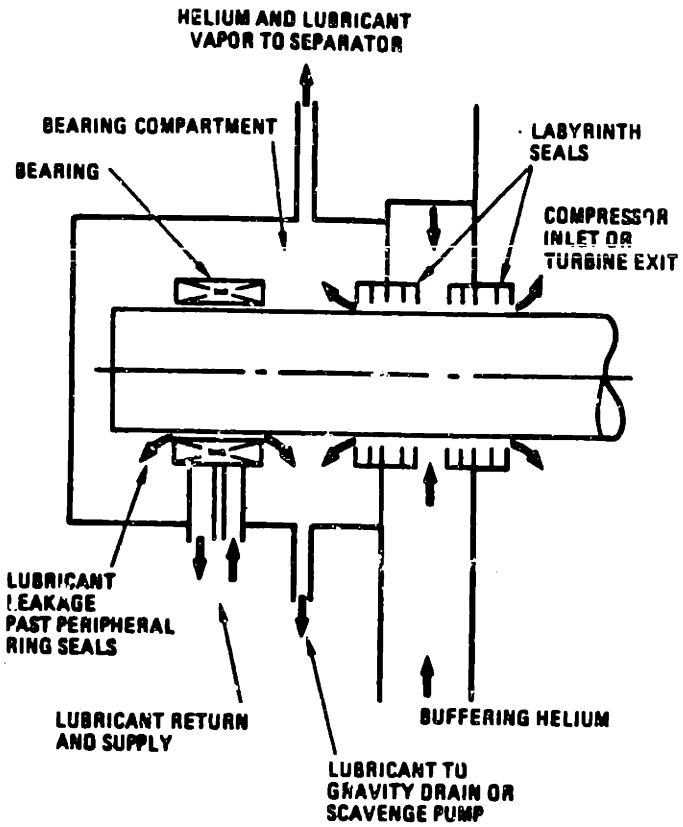

Figure 1.27. Bearing compartment sealing system for the HTGR-GT machinery (A3).

automatically perform the following three functions:

1. control load and speed;
2. control thermal transients; and
3. control reactor power and temperature.

The PCS additionally limits system-induced transients that could lead to Plant Protection System (PPS) actions. The PPS provides all reactor-protective systems and a turbine-overspeed protective system.

Load and speed control are accomplished by bypass control, reactor-outlet temperature control and helium-inventory control. Because of its size, the HTGR-GT presents a control problem. Inventory control offers high efficiency over a broad power range and is the accepted method of control for small CCGT power-plants. In the HTGR-GT, an inventory-control system that could meet normal design transients would be too large to be economically feasible. The response of the inventory-control system incorporated into the HTGR-GT design was, therefore, much too slow (on the order of hours) for normal use and was intended only for extended periods of low-power operations. Temperature control uses control rods to vary reactor power and to control turbine-inlet temperature. This control function is performed in concert by the Turbine Inlet Temperature Controller and the Flux Controller. Temperature control does not offer the broad range of high efficiency that inventory control offers; however, its efficiency performance is still better than bypass control (see Fig. 1.28). The high thermal inertia of the core makes reactor-outlet temperature control fairly slow, on the order of minutes. It is therefore used only in concert with bypass control for control of load changes of moderate rate. Bypass control was chosen as the primary

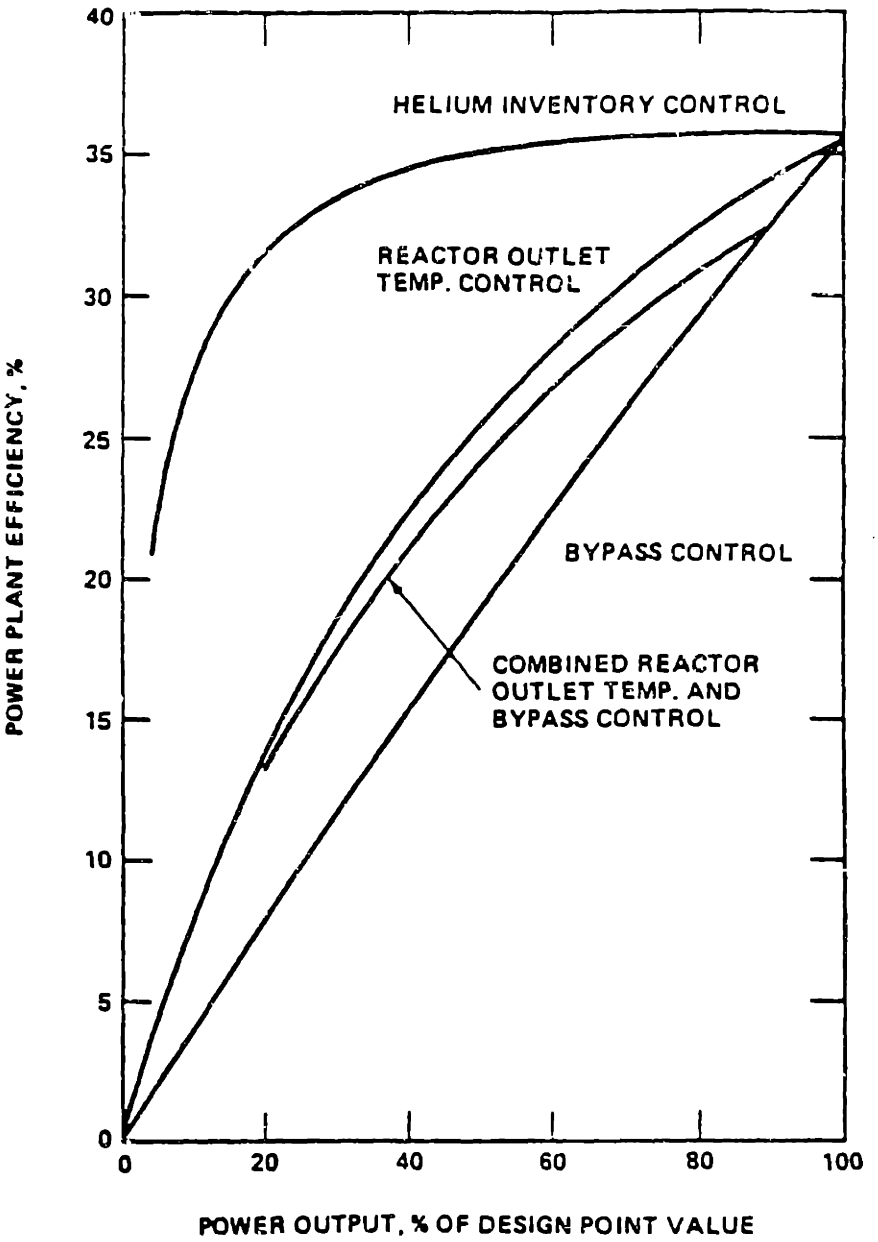

Figure 1.28. The effects of different control methods on CCGT steady-state system efficiency (G6).

fast method of load control.

For rapid power transients of the HTGR-GT, bypass control is the only method of control that can match plant power to electric load demand. Also, it is the only method of control that acts rapidly enough to prevent turbine overspeed and potentially serious damage to the plant on a loss of electric load. The bypass arrangement considered for the HTGR-GT is shown in Fig. 1.29. Except for the Safety and Trim valves, these bypass valves are controlled by the five controllers on the PCS, which is schematically described by the block diagram of Fig. 1.30.

The Turbine Inlet Temperature Controller of the PCS provides the command signal to the Reactor Neutron-Flux Controller, which regulates control rod position and reactor flux. The heat input to the helium and the turbine-inlet temperature are thus regulated.

The Load/Speed Controller regulates the power delivered to the turbomachine such that the shaft power delivered to the generator matches the turbomachine shaft equivalent of the electrical power throughout the normal load range. By regulating the Primary Bypass Valve (PBV), the Load/Speed Controller partially diverts flow from the turbine such that turbine pressure-ratio and turbine power are reduced from the full-mass-flow pressure ratio and power until load and speed are matched to required load and speed. Load and speed errors are the input to this controller. Proportional-plus-integral action is used to regulate load and speed. Integral control ensures that PBV position is brought to the correct position for accurate matching of load and speed. A term proportional to speed error is summed with integrated error such that the response is properly damped for a sufficiently

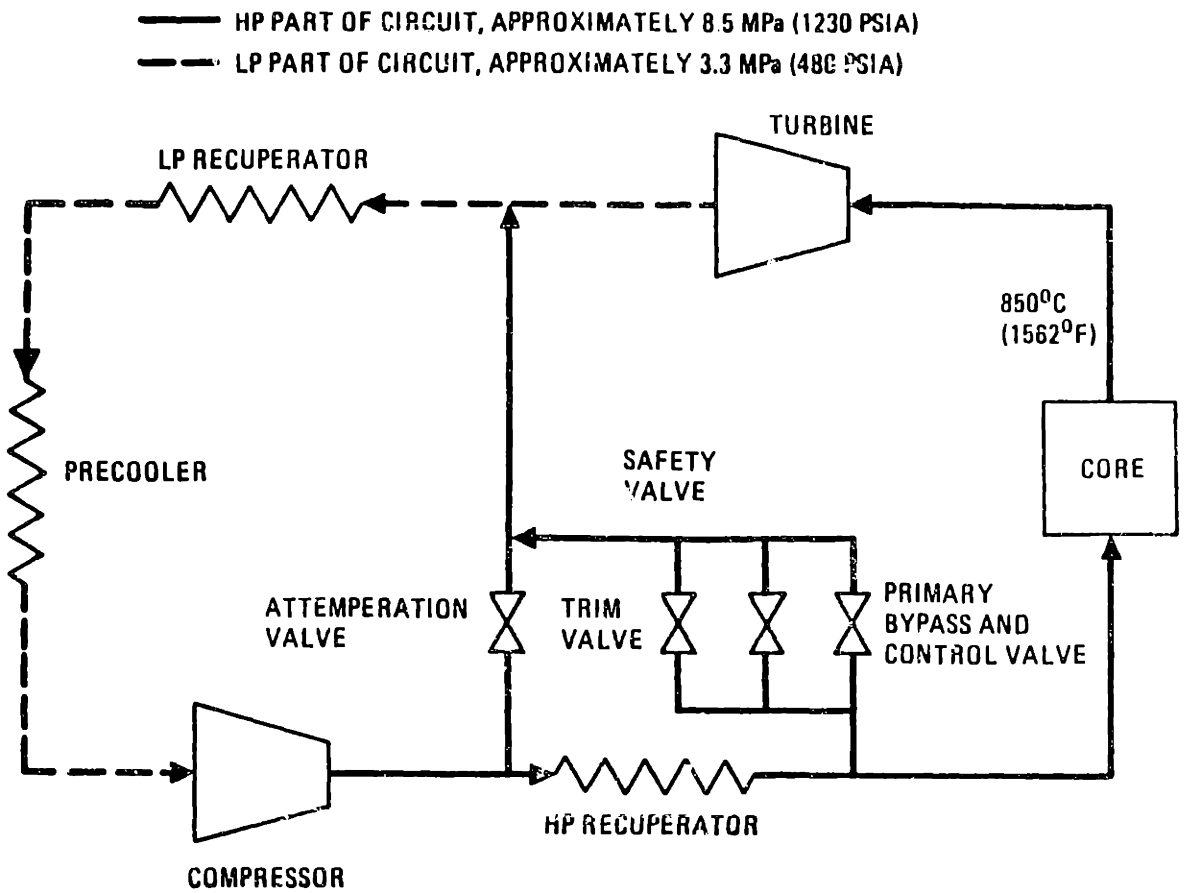

Figure 1.29. Bypass valve arrangement in the HTGR-GT (G6).

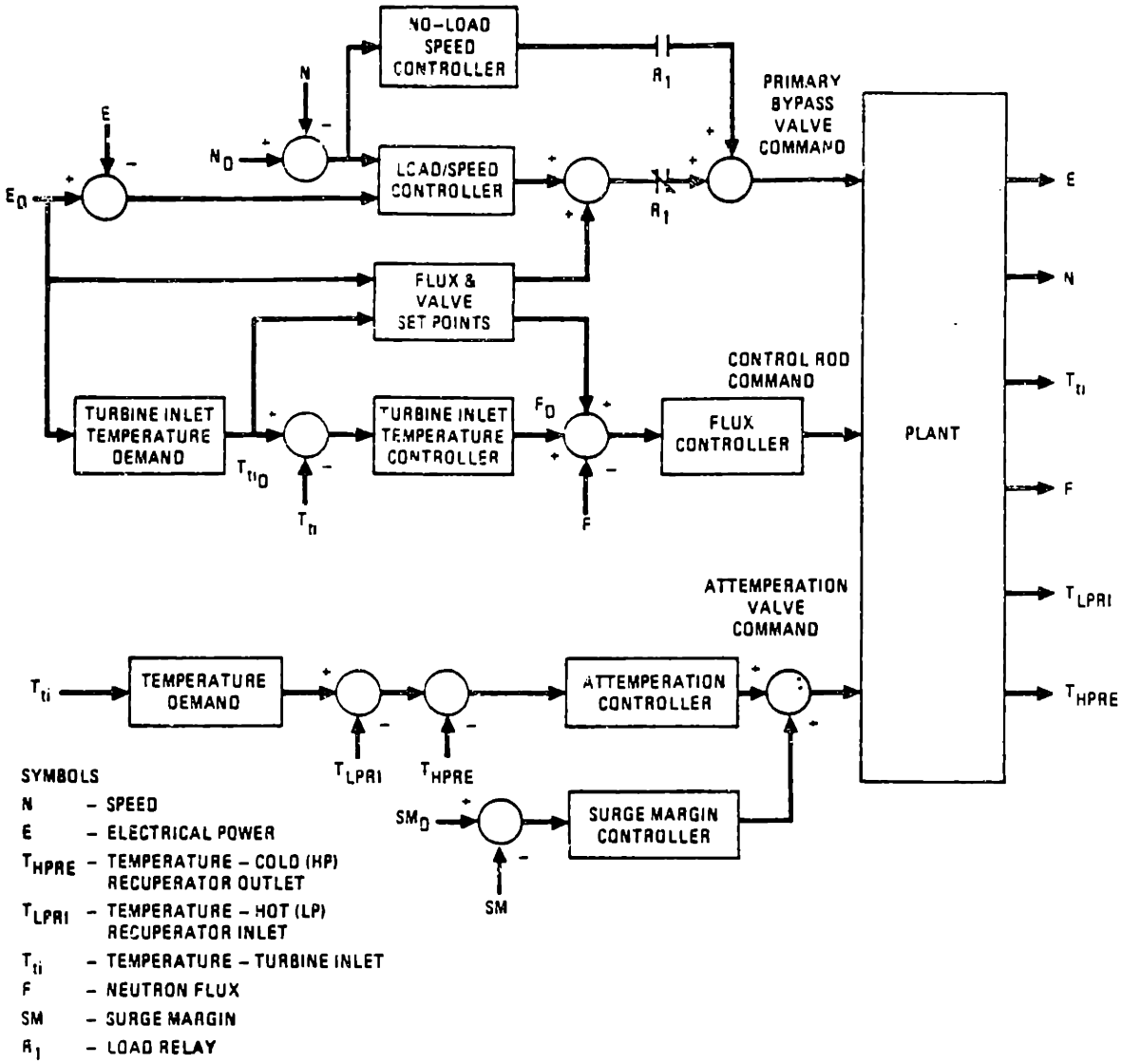

Figure 1.30. Block diagram of the HTGR-GT Plant Control System (G6).

short settling time.

The No-Load/Speed Controller provides manual control of the turbomachine during periods of plant idling with no electric load, or for plant evolutions such as shutdown, startup, or synchronization. It also provides control of the PBV in the event of a loss of electric load. Upon a loss of electric load deenergization of relay R1 closes contacts between the the No-Load/Speed Controller and PBV operator and opens contacts between the Load/Speed Controller and the PBV operator. The No-Load/Speed Controller, through proportional-plus-integral action, then rapidly opens the PBV fully.

When the PBV opens, turbine-exhaust temperature rises as a result of the reduced turbine pressure-ratio. This can cause high reactor-inlet temperatures and excessive thermal stresses on the recuperator and reactor components. The Attemperation Controller acts to prevent excessive thermal transients of the PCL and reactor components. Low-pressure recuperator-inlet and high-pressure recuperator-outlet temperatures are manipulated to a demanded value that is a programmed value of the turbine-inlet temperature. Control is accomplished by the Attemperation valve which bleeds compressor-discharge helium to the turbine-exhaust plenum. The turbine exhaust is thus cooled, reducing the thermal transients on the heat exchangers and reactor components.

The Surge-Margin Controller acts to open the Attemperation valve to maintain compressor surge-margin. If compressor surge-margin becomes sufficiently low, as indicated by the compressor-inlet pressure and temperature, and the compressor-exit pressure, the Surge-Margin Controller orders the Attemperation Valve open to reduce

compresser pressure-ratio.

The control functions of the PCS are clearly demonstrated in Figs. 1.31a-d, which show the plant response to a sudden loss of the electric load of a single loop. Initially, turbomachine speed rises rapidly. The No-Load/Speed Controller orders the PBV (valve 1) fully open upon the loss of electric load. Turbine speed turns down and rapidly falls. Turbine pressure-ratio drops and turbine-exhaust temperature increases rapidly causing the Attemperation Controller to open the Attemperation Valve. LP-recuperator outlet-temperature, which initially rises, quickly peaks and falls as a result of the attemperation valve opening. Backflow in the loop causes precooler-inlet temperature to drop rapidly. Turbine-inlet temperature drops rapidly due to the backflow. The Attemperation Valve closes due to the dropping temperatures. During this entire time the core-outlet temperature is fairly constant due to the high thermal inertia of the core.

Studies were performed to determine optimum control methods for turbine overspeed for a loss of electrical load. Sensitivity studies showed that the amount of turbine overspeed was strongly governed by the following variables: bypass-valve size, turbomachine moment-of-inertia and volumes of primary plenums. Increased bypass-valve size tended to reduce the overspeed, but increased the thermal transients on the plant. Increased turbomachine moment-of-inertia also reduced overspeed but without inducing greater thermal transients. The plenum volumes affected how long it took the pressure ratio to drop and therefore how rapidly the turbine power dropped. In all cases it was possible to provide adequate overspeed protection.

Figure 1.3la-d. HTGR-GT response and plant transient resulting from sudden loss of electric load in one PCL (02).

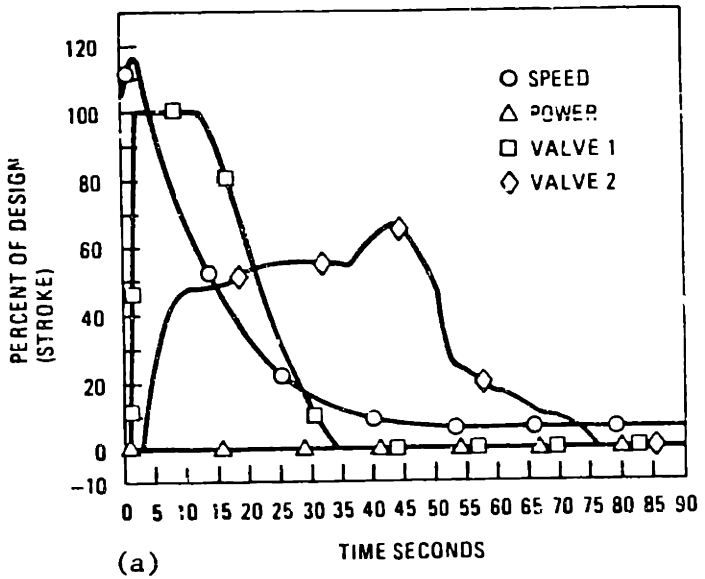

(a)

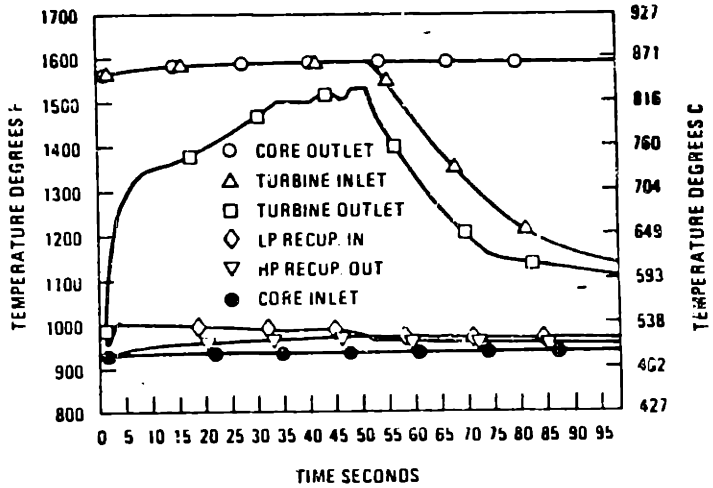

(b)

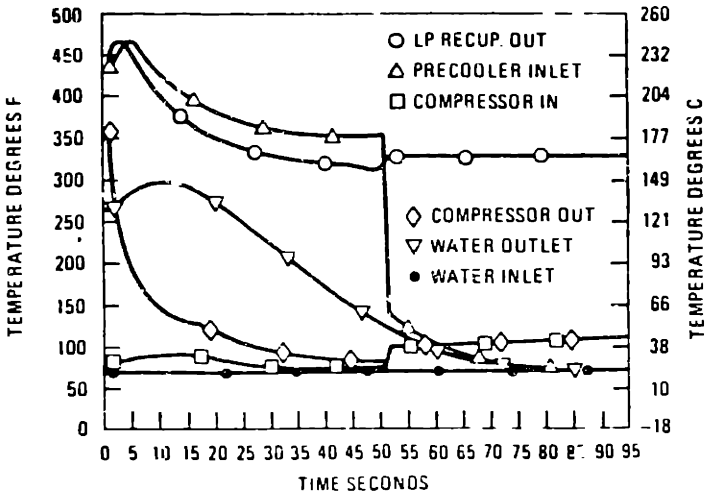

(c)

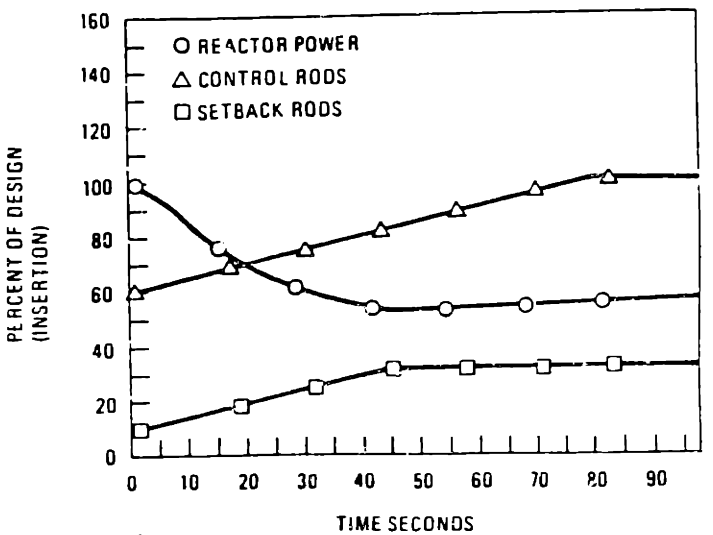

(d)

1.3.2e Turbine Deblading Accident.

The existence of large pressure differences in the direct-cycle gas-turbine plant during normal operation introduces concern over the consequences of an accident that would allow rapid pressure equilibration. If one of the turbomachines were to suddenly deblade, rapid primary-pressure transients would ensue, and the reactor plant could potentially suffer damage. Of most concern is that the core geometry or structural supports could be damaged in such a way as to prevent the removal of decay heat [C2]. Of additional concern is the integrity of the thermal liner of the PCRV during such a pressure transient [L1].

Because of its high operating temperature, the turbine is the most likely of the two turbomachines to deblade. The accident scenario that was assumed for most analyses was the deblading of one stage of the turbine for each rotation. This corresponds to a situation where the debris from a previous stage deblades a downstream stage. For a nine-stage machine at 3600 rpm, total deblading would occur in 150-ms. Figures 1.32a-e show plant transients that would occur in such an accident. Additionally, complete deblading in one revolution was considered. The flow in the turbine may be modelled as a linear decrease in flow resistance over the deblading time or a linear decrease in pressure drop coefficient with time. Both methods yield similar results. Turbine mass-flow will increase rapidly until it chokes (Fig. 1.32b). The sudden drop in momentum as the flow chokes causes partial repressurization of the turbine-inlet plenum. A rarefaction wave is sent from the turbine-inlet plenum to the reactor-outlet plenum during this flow transient. The rapidity of the

Figure 1.32a-d. HTGR-GT plant transient resulting from postulated turbine deblading (C2).

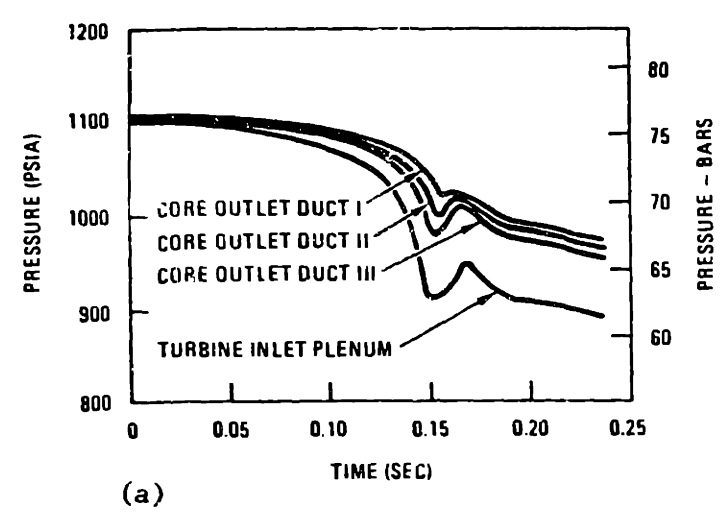

(a)

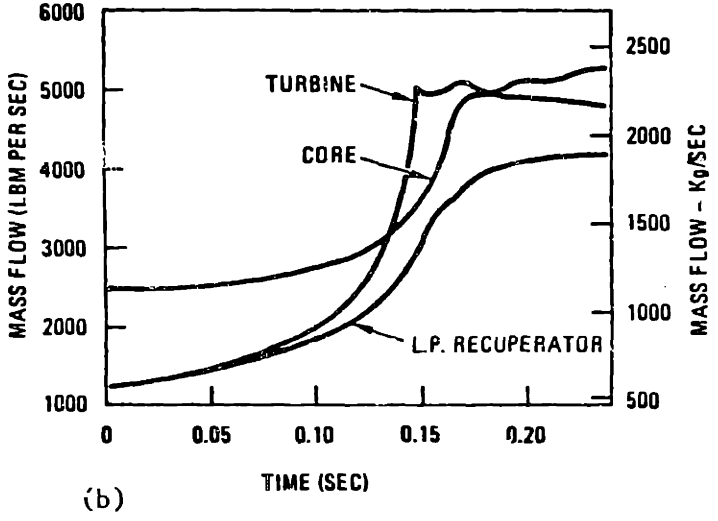

(b)

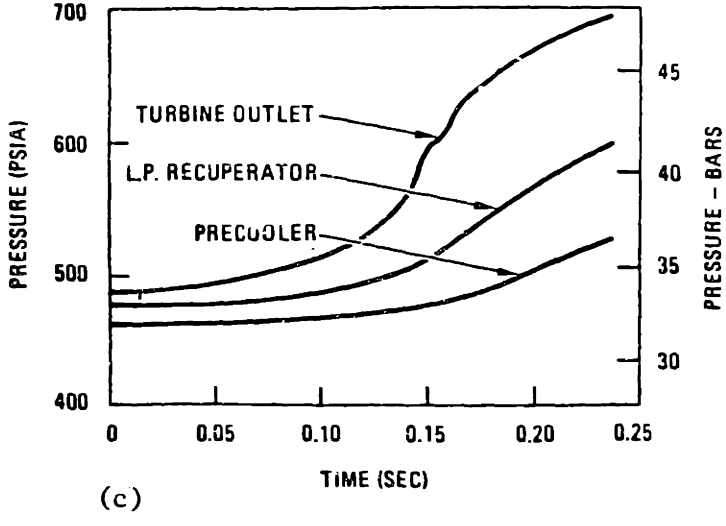

(c)

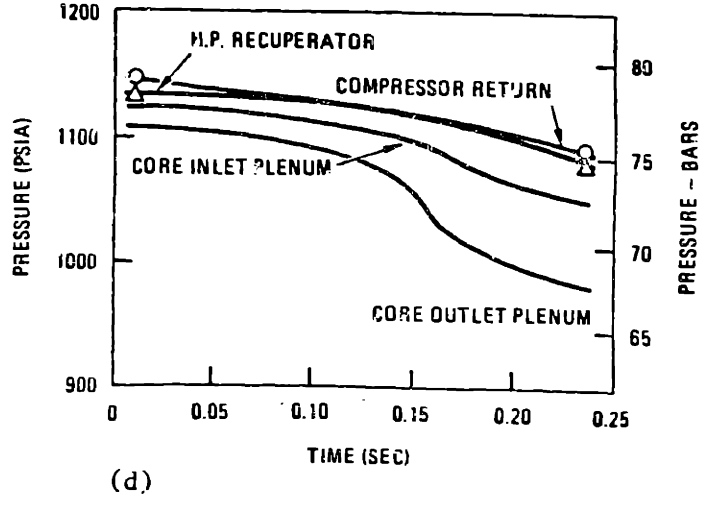

(d)

pressure transient in the core-outlet plenum is of major concern as it most severely affects the design of structural components in the reactor, especially the thermal-barrier coverplates [C2].

If the turbine geometry leaves a minimum flow area, such that choking occurs, the effect of the accident is somewhat diminished. The designed turbine-inlet annulus is of such an area that, if left intact, core-outlet depressurization rate is reduced by 1/3 of the depressurization rate were choking not to occur. Other effects that could reduce the severity of the pressure transient are if first-stage guide vanes remain intact and if the deblading occurs over a longer period of time [02, 03]. The HTGR-GT was, in fact, shown to be able to withstand the imposed transients. However, by this time it had been decided to terminate the HTGR-GT program [M17].

1.3.2f Termination of the HTGR-GT Program.

The HTGR-GT program was finally terminated for economic rather than technical reasons. Although many of the previously discussed technical problems were eventually addressed sufficiently, the HTGR-GT was shown not to be economically advantageous when compared to the steam-plant HTGR (HTGR-SC). The original incentive for development of the HTGR-GT was to take advantage of dry cooling and a potential for greater efficiencies than the HTGR-SC. The HTGR-GT in a dry-cooling or wet/dry-cooling mode, however, was not significantly more efficient than the HTGR-SC with wet cooling (40% vs. 38%). Although the dry cooling of the HTGR-GT was a real advantage, it was not seen as being sufficiently advantageous to offset the higher capital and development costs of the plant. Although the capital cost of the HTGR-GT was originally projected to be lower than the capital cost of the HTGR-SC,

later studies found the contrary to be true. This is attributed to the larger PCRV needed and the additional turbine-maintenance building needed for the HTGR-GT. Making the economics even more difficult was the the additional development cost of the HTGR-GT. GCRA therefore recommended in 1980 that the HTGR-GT not be pursued as a lead project [G6].

1.4 FOCUS OF THE PRESENT WORK.

It is the objective of this dissertation to apply present "state-of-the-art" technology to develop a self-consistent MGR-GT design while avoiding many of the weaknesses of earlier nuclear-CCGT designs. The previous section discussed the evolution of gas-cooled reactors and the MGR, and identified some of the important technical developments that occurred along the way. Previous nuclear-CCGT designs were examined with emphasis on system and component design considerations. Technical difficulties and specific technical developments that governed plant design were identified in the discussion. These issues and their specific relevance to design of the MGR-GT are as follows:

1.4.1 Development of the MGR.

The evolution of gas-cooled reactors resulted in the use of all-graphite core material and the exclusive use of helium as the coolant. Although most operating CCGT's use air as the working fluid, and helium mixtures with other gases have been recommended by some as a preferred working fluid for some nuclear CCGT's [B10, M14], helium remains the only acceptable coolant for the HTGR. It is therefore the only working fluid that can be used in the direct-cycle MGR-GT.

Development of the modular concept and "passive safety" have resulted in the need for a smaller plant design and the use of steel pressure-vessels. It was shown that smaller plants are more capable of utilizing inventory control. Large CCGT plants require a more complicated and less efficient bypass-control system for all operations. Additionally, it will be shown that the use of steel pressure-vessels will require a complicated flow path for the MGR-GT

in order to meet pressure-vessel design-code requirements.

1.4.2 Moisture and Lubricant Ingress, and Seal Design.

Moisture and lubricant ingress is a major contributor to gas-cooled reactor and CCGT losses in availability. For a gas-cooled-reactor equipped with a steam-plant, the steam-generator is a potential source for large ingresses of moisture. This source of moisture is not of concern for a gas-cooled-reactor equipped with a direct Brayton-cycle. Operations at the Fort St. Vrain HTGR steam power plant demonstrate that the circulator bearing-lubrication and shaft-sealing systems cannot be overlooked as a source of moisture ingress. The bearing-lubrication and shaft-sealing systems are the primary sources of moisture or lubricant ingress for the CCGT. The number and complexity of the bearings, and the shaft connection to the generator, make this problem more difficult to solve for a CCGT than for the HTGR-SC gas circulators. By submerging the circulator in the gas, steam-plant gas-cooled reactor designers were able to eliminate the more difficult of these two sources: the shaft-penetration seals. In CCGT designs, totally submerging the machinery requires that the generator also be submerged. Previous CCGT's designed for commercial electric-power generation required oil or water lubricated bearings. In these cases the difficulty resulting from the inaccessability of the generator outweighed the limited advantage of totally submerging the machinery. Although Oberhausen-2 experienced some success with its seals, HHV and Ft. St. Vrain did not. Major ingresses of moisture and lubricants into these plants resulted in great expense, proving that the problem of lubricant ingress from the shaft-penetration and bearing seals is not yet fully solved. Furthermore, helium leakage

past the shaft-penetration seal results in loss of efficiency in the CCGT. For nuclear systems, helium leakage must be maintained low to minimize the release of activity to the atmosphere. It will be shown in the remainder of this thesis how newly developed technologies might be incorporated into an MGR-GT design to alleviate these problems.

1.4.3 Efficiency and Economy of the MGR-GT.

The MGR-GT must be proven to be economically advantageous over other power-generating systems in order to justify a major development effort. The HTGR-GT was found to be lacking in economic potential compared to other power systems. The advantages of dry cooling and the slightly better thermal efficiency of the dry-cooled HTGR-GT over the wet-cooled HTGR-SC were not sufficient to offset additional capital costs. It will be shown that the use of a high-effectiveness recuperator will significantly increase the thermal efficiency of the MGR-GT and that recuperators of high surface compactness are currently available for industrial gas-turbines. Such recuperators make high-effectiveness designs much more economically attractive. Additionally, because of its size, an MGR-GT plant will not require many of the additional facilities that were required of the HTGR-GT over the HTGR-SC. Most equipment is small enough to be transported easily to a central maintenance facility, eliminating the need for large, on-site maintenance facilities. Since steel pressure-vessels will be used rather than a PCRV, this capital-cost-affecting aspect of the economics problem is different for the MGR-GT than for the HTGR-GT. Although a detailed economic analysis will not be performed in this dissertation, it is believed by this author that the high efficiency and potentially low capital cost of an MGR-GT plant may

make it attractive for the production of electric power.

1.4.4 Methods of Analysis.

Chapters Two through Six will discuss methods of analysis for each component or system of the MGR-GT. Each of of these chapters will be concluded with its own list of nomenclature to be used when reading that chapter.

Chapter Two will discuss the methods for analysis of the thermodynamic cycle and the effects of the operating variables on cycle performance. Results of calculations will be presented. Considerations for optimizing cycle performance will be discussed.

Material and design-code considerations will be presented in Chapter Three. A brief description of the MGR to be used as the cycle heat-source will also be given. Of principal concern in this chapter will be the effect of the pressure-vessel design limitations in determining the plant configuration and flowpath.

Chapter Four will discuss the machinery and electric-plant design methods. Included in this chapter will be a discussion of turbomachine design considerations and theory, a discussion of active-magnetic-bearing technology, electrical-generator design principles, and methods of frequency conversion.

Chapter Five will present the methods and considerations for heat-exchanger design. Recuperator, precooler, and dry-cooler designs will be discussed.

Chapter Six will discuss the control systems to be used in the MGR-GT. Background on CCGT control methods was presented in Chapter One. This chapter will attempt to consolidate the ideas of the previous chapters and develop a method of control. Methods of control

analysis for the MGR-GT will be presented.

1.4.5 Plant Design and Conclusions.

The first six chapters should provide background on the design considerations and design methods for the MGR-GT. Chapter Seven will present a proposed plant design based upon the results of the previous chapters. A general plant description will be given. Specific component and system designs will be discussed individually. In this final chapter, issues regarding safety and investment-risk will be considered. The cost of MGR-GT components will be estimated. In this final chapter, the conclusions of this study will be summarized, and recommendations for future work will be suggested.

CHAPTER TWO

BRAYTON CYCLE ANALYSIS

2.1 Brayton Cycle Analysis.

The net power produced by a Brayton cycle is the difference between two large quantities, the power produced by expanding gas in a turbine minus the power consumed by compressing gas in a compressor. The ability of the Brayton cycle to produce power results from the fact that the power produced by expanding a gas at a high temperature is greater than the power it takes to compress a gas between the same pressures at a low temperature. Temperature is defined as:

$$T = \left.\frac{\partial h}{\partial s}\right]_p \tag{2.1}$$

and for a perfect gas:

$$\frac{T}{C_p} = \left.\frac{\partial T}{\partial s}\right]_p \tag{2.2}$$

Figure 2.1 shows the enthalpy of helium over a broad temperature and pressure range. Specific heats remain almost constant, with a maximum change of 0.02% over the temperature range of 100 - 1500^{o}K at pressures up to 10-MPa. Therefore, in this analysis helium can be treated as a perfect gas with virtually no error.

Figure 2.2a shows an H-S diagram (or a T-S diagram for a perfect gas) for the simple Brayton cycle of Fig. 2.2b. It is clear from Eqs. 2.1 and 2.2 why the isobars on Fig. 2.2a curve upward. The isobars are curved in such a way that, at any given temperature, the tangents of all of the isobars are parallel. It is the curvature of the isobars that causes the work extracted by expansion from point 4 to point 5 to exceed the work absorbed by compression from point 1 to point 2. Assuming constant specific heats, the compressor work per unit mass

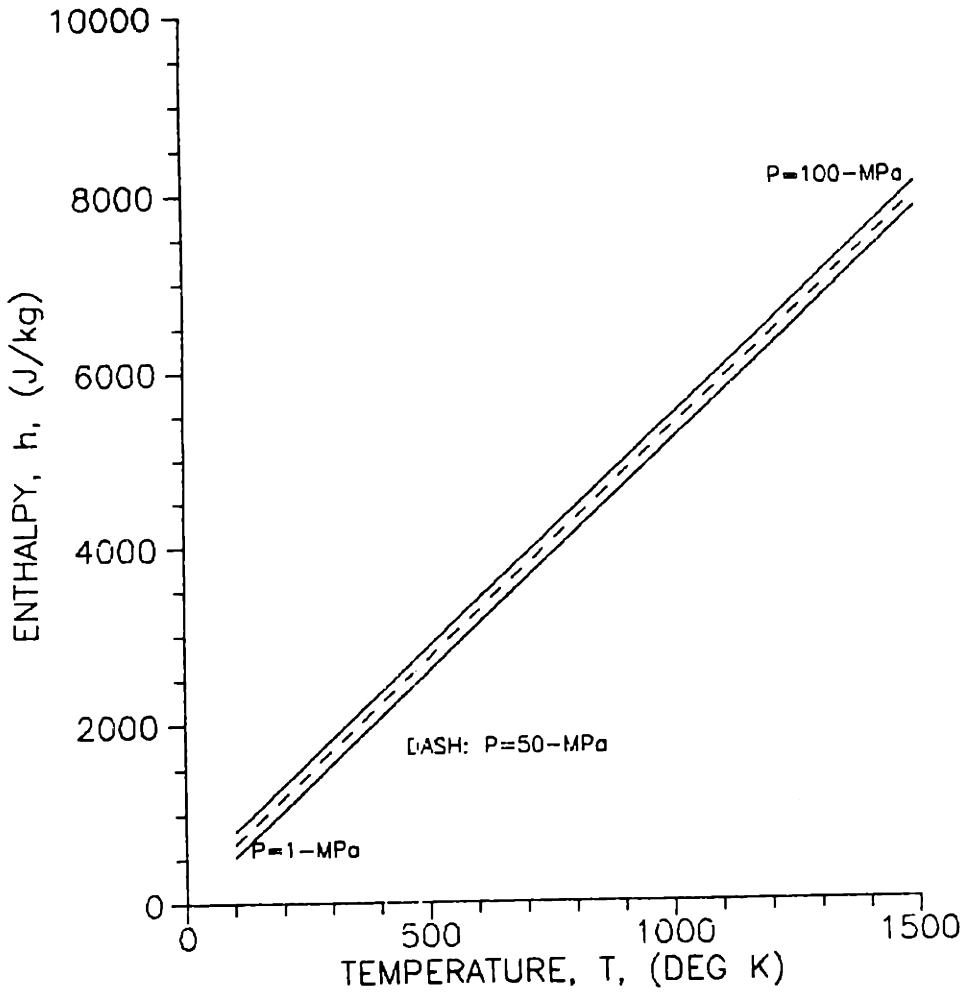

Figure 2.1 **Enthalpy of helium as a function of temperature and pressure.**

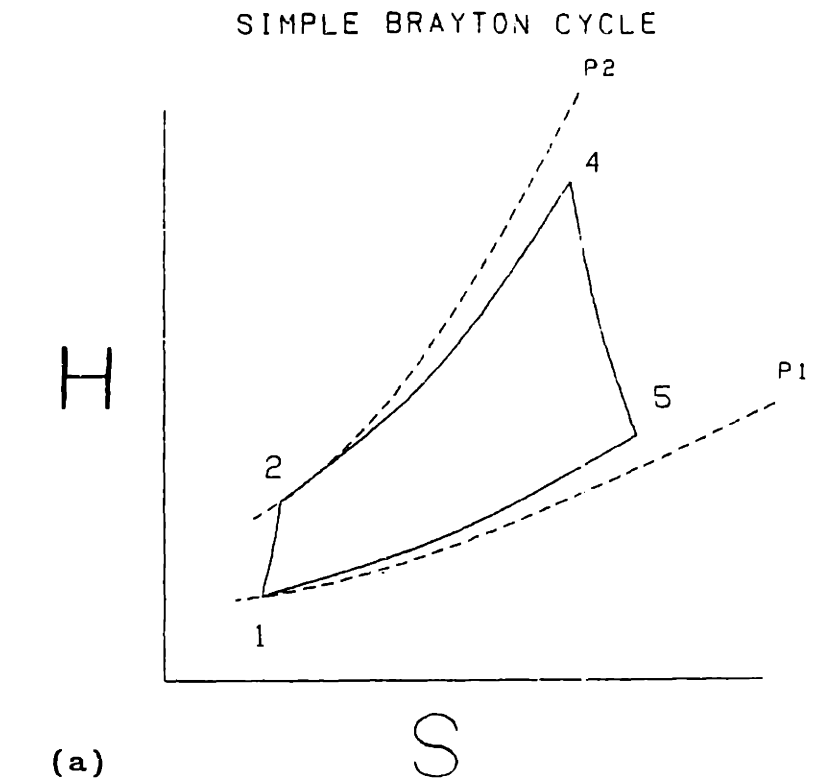

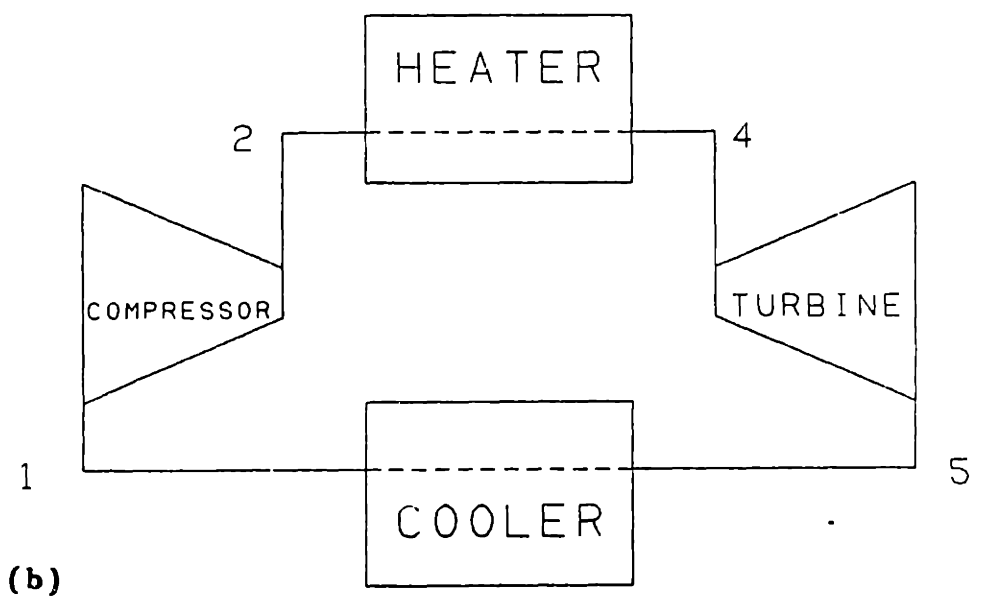

Figure 2.2. A simple Brayton cycle.
(a) H-S Diagram
(b) Cycle Diagram

flow of working fluid is

$$W_c = C_p(T_{o2} - T_{o1}) \tag{2.3}$$

Stagnation temperatures are used because the kinetic energy of the gas cannot be neglected in turbomachinery design and therefore, for consistency, stagnation temperature will be distinguished from static temperature in the following analysis. Similarly, turbine work per unit mass flow of the working fluid is equal to

$$W_t = C_p(T_{o4} - T_{o5}) \tag{2.4}$$

The heat added in the heater is equal to

$$Q_h = C_p(T_{o4} - T_{o2}) \tag{2.5}$$

For equal massflows of perfect gas in all cycle components, plant efficiency can be expressed as

$$\eta_{th} = \frac{(T_{o4} - T_{o5}) - (T_{o2} - T_{o1})}{(T_{o4} - T_{o2})} \tag{2.6}$$

or

$$\eta_{th} = \frac{T'E_1 - C}{T' - C - 1} \tag{2.7}$$

with

$$T' = \frac{T_{o4}}{T_{o1}} \; ; \quad E_1 = \frac{T_{o4} - T_{o5}}{T_{o4}} \; ; \quad C = \frac{T_{o2} - T_{o1}}{T_{o1}} \tag{2.8}$$

The effect of turbine efficiency and system pressure-losses can be determined. Turbine work is equal to:

$$W_t = \dot{m}\,\eta_t C_p(T_{o4} - T_{o5s}) = \dot{m}\,\eta_t C_p T_{o4}\left[1 - \left[\frac{P_{o5}}{P_{o4}}\right]\left[\frac{R}{C_p}\right]\right] \tag{2.9}$$

Since

$$P_{o5} = P_{o1} + \Delta P_{o1} \tag{2.10}$$

$$P_{o4} = P_{o2} - \Delta P_{o2} \tag{2.11}$$

and
$$E_1 = \eta_t \left[\frac{T_{o4}-T_{o5s}}{T_{o4}}\right] \tag{2.12}$$

where ΔP_{o1} and ΔP_{o2} are pressure losses in the system. It can be shown that

$$\left[\frac{E_1}{\eta_t}\right] = \frac{W_t}{\dot{m}\,\eta_t C_p T_{o4}} = 1 - \left[\frac{P_{o1} + \Delta P_{o1}}{P_{o2} - \Delta P_{o2}}\right]\left[\frac{R}{C_p}\right] \tag{2.13}$$

Moving terms outside of the parentheses:

$$\left[\frac{E_1}{\eta_t}\right] =$$

$$1 - \left[\frac{P_{o1}}{P_{o2}}\right]\left[\frac{R}{C_p}\right]\left[\frac{1 + \left[\frac{\Delta P_{o1}}{P_{o1}}\right]}{1 - \left[\frac{\Delta P_{o2}}{P_{o2}}\right]}\right]\left[\frac{R}{C_p}\right] \tag{2.14}$$

Since $\frac{\Delta P}{P} < 1.0$, the term inside the brackets on the far right of Eq. 2.14 can be expressed as the sum of two power series,

$$\frac{1}{1 - \left[\frac{\Delta P_{o2}}{P_{o2}}\right]} =$$

$$1 + \frac{\Delta P_{o2}}{P_{o2}} + \left[\frac{\Delta P_{o2}}{P_{o2}}\right]^2 + \left[\frac{\Delta P_{o2}}{P_{o2}}\right]^3 + \ldots. \tag{2.15}$$

and

$$\frac{\left[\frac{\Delta P_{o1}}{P_{o1}}\right]}{1 - \left[\frac{\Delta P_{o2}}{P_{o2}}\right]} =$$

$$\left[\frac{\Delta P_{o1}}{P_{o1}}\right]\left[1 + \left[\frac{\Delta P_{o2}}{P_{o2}}\right] + \left[\frac{\Delta P_{o2}}{P_{o2}}\right]^2 + \left[\frac{\Delta P_{o2}}{P_{o2}}\right]^3 + \ldots\right]. \tag{2.16}$$

If $\left[\frac{\Delta P_{o1}}{P_{o1}}\right]$ and $\left[\frac{\Delta P_{o2}}{P_{o2}}\right]$ are both much less than one, say below 0.1, second order and above terms can be neglected. This will yield:

$$E_1 = \eta_t \left[1 - r^{-\left[\frac{R}{C_p}\right]} \left[1 + \frac{\Delta P_{o1}}{P_{o1}} + \frac{\Delta P_{o2}}{P_{o2}}\right]^{\left[\frac{R}{C_p}\right]}\right] \qquad (2.17)$$

where r is the compressor pressure ratio, $\left[\frac{P_{o2}}{P_{o1}}\right]$.

The turbine specific work is therefore diminished by the sum of all the *specific* pressure losses, and it makes no difference where in the cycle these pressure losses occur.

Isentropic efficiency can be expressed in terms of polytropic efficiency (see Chapter Four). For the turbine:

$$\eta_t = \frac{1 - \left[\frac{P_{o5}}{P_{o4}}\right]^{\left[\frac{\eta_{pe} R}{C_p}\right]}}{1 - \left[\frac{P_{o5}}{P_{o4}}\right]^{\left[\frac{R}{C_p}\right]}} \qquad (2.18)$$

For the compressor:

$$\eta_c = \frac{\left[\frac{P_{o2}}{P_{o1}}\right]^{\left[\frac{R}{C_p}\right]} - 1}{\left[\frac{P_{o2}}{P_{o1}}\right]^{\left[\frac{R}{\eta_{pc} C_p}\right]} - 1} \qquad (2.19)$$

Combination of Eqs. 2.10, 2.11, 2.17 and 2.18 results in

$$E_1 = 1 - r^{-\left[\frac{\eta_{pe} R}{C_p}\right]} \left[1 + \frac{\Delta P_{o1}}{P_{o1}} + \frac{\Delta P_{o2}}{P_{o2}}\right]^{\left[\frac{\eta_{pe} R}{C_p}\right]}$$

$$= 1 - r^{-\left[\frac{\eta_{pe} R}{C_p}\right]} \left[1 + \sum \frac{\Delta P_o}{P_o}\right]^{\left[\frac{\eta_{pe} R}{C_p}\right]}$$

$$= 1 - r^{-\left[\frac{\eta_{pe} R}{C_p}\right]} \left[\frac{1}{1 + \sum \frac{\Delta P_o}{P_o}}\right]^{-\left[\frac{\eta_{pe} R}{C_p}\right]}$$

$$= 1 - r^{-\left[\frac{\eta_{pe}R}{C_p}\right]} \left[\frac{1 - \sum \frac{\Delta P_o}{P_o}}{\left[1 - \sum \frac{\Delta P_o}{P_o}\right]\left[1 + \sum \frac{\Delta P_o}{P_o}\right]}\right]^{-\left[\frac{\eta_{pe}R}{C_p}\right]}$$

$$= 1 - r^{-\left[\frac{\eta_{pe}R}{C_p}\right]} \left[\frac{1 - \sum \frac{\Delta P_o}{P_o}}{1 + \sum \frac{\Delta P_o}{P_o} - \sum \frac{\Delta P_o}{P_o} + \left[\sum \frac{\Delta P_o}{P_o}\right]^2}\right]^{-\left[\frac{\eta_{pe}R}{C_p}\right]}$$

If $\sum \frac{\Delta P_o}{P_o} << 1.0$, say below 0.10, then the second order term can be neglected to yield:

$$E_1 = 1 - \left[\left[1 - \sum \frac{\Delta P_o}{P_o}\right] r\right]^{-\left[\frac{\eta_{pe}R}{C_p}\right]} \tag{2.20}$$

For a compressor, the specific work can be shown to be equal to

$$C = \left[\frac{T_{o2s} - T_{o1}}{\eta_c \, T_{o1}}\right] = \frac{r^{\left[\frac{R}{C_p}\right]} - 1}{\eta_c} \tag{2.21}$$

Combining Eqs. 2.19 and 2.21 yields:

$$C = \left[r^{(R/C_p)/\eta_{pc}} - 1\right] \tag{2.22}$$

Using these equations, it is possible to quantify the effects of different parameters on cycle thermal-efficiency. It can be seen from Eqs. 2.7 and 2.8 that increasing the ratio of turbine-inlet temperature to compressor-inlet temperature (T') will raise cycle thermal-efficiency. This can be physically explained by stating that if heat addition is greater, the state 4 to state 5 line on Fig. 2.2a is pushed farther to the right, increasing the effect of the curvature in the isobars. Also, if pressure ratio is increased, the difference between the expansion work and the compression work again increases, while heat addition is reduced. This has the effect of raising cycle efficiency.

In a simple Brayton-cycle, all of the available energy in the

turbine exhaust is lost to the environment. At low pressure ratios, the turbine-exhaust temperature is often higher than the compressor-outlet temperature. In these situations it is beneficial to place a heat exchanger in the system to recover some of the sensible heat of the turbine exhaust and utilize this energy to heat the working fluid prior to entering the heater (in this case, the heater being an MGR). This will reduce the amount of energy needed to be supplied by the heater and improve cycle efficiency. This type of heat exchanger is called a recuperator (Or, sometimes a regenerator.) and Figs. 2.3a and b show a recuperated Brayton cycle.

ϵ_x, the effectiveness of the recuperator, is defined as:

$$\epsilon_x = \frac{\text{heat actually transferred}}{\text{maximum heat transfer possible}} \qquad (2.23)$$

In the case of a helium-CCGT recuperator, the mass flowrates and specific heats are essentially the same on either side of the heat exchanger. Effectiveness can be shown to equal

$$\epsilon_x = \frac{T_{o5} - T_{o6}}{T_{o5} - T_{o2}} = \frac{T_{o3} - T_{o2}}{T_{o5} - T_{o2}} \qquad (2.24)$$

With a recuperator

$$\eta_{th} = \frac{(T_{o4} - T_{o5}) - (T_{o2} - T_{o1})}{T_{o4} - T_{o3}}$$

Divide numerator and denominator by T_{o4} to yield

$$\frac{E_1 - (1/T_{o4})(T_{o2} - T_{o1})}{(1/T_{o4})(T_{o4} - T_{o3})}$$

Multiplying numerator and denominator by T_{o4} and dividing numerator and denominator by T_{o1} will result in

$$\eta_{th} = \frac{E_1 T' - C}{T' - (T_{o3}/T_{o1})}$$

Reducing the denominator:

$$T' - \left[\frac{T_{o3}}{T_{o1}}\right] = T' - \frac{(T_{o3} - T_{o2} + T_{o2})(T_{o5} - T_{o2})}{T_{o1}(T_{o5} - T_{o2})}$$

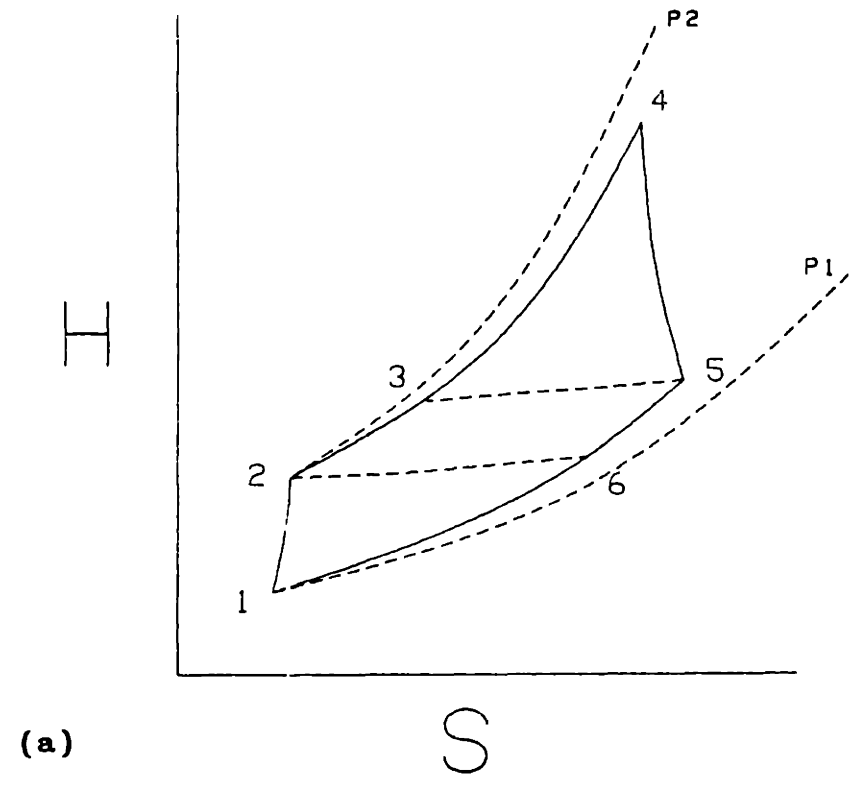

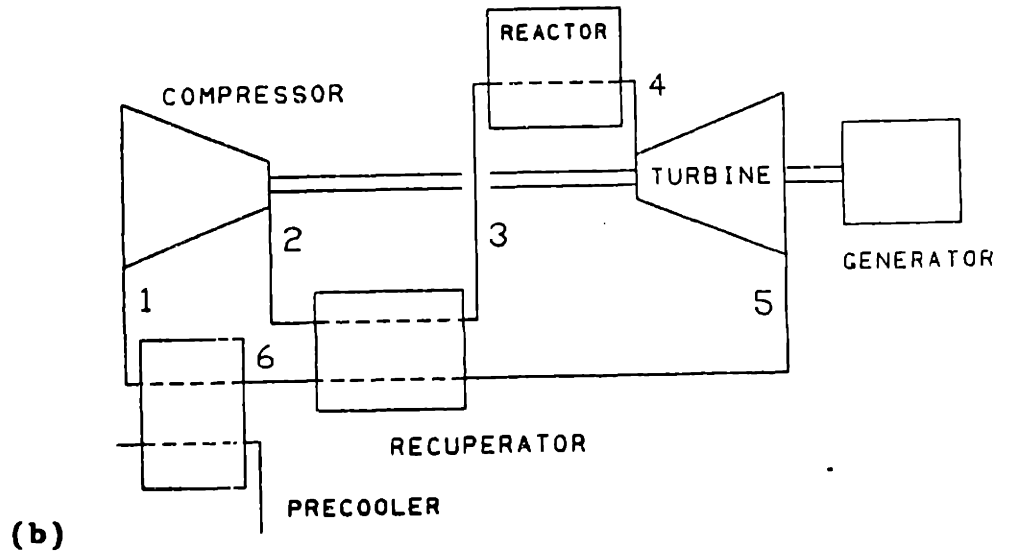

Figure 2.3 A recuperated Brayton cycle.
(a) H-S Diagram
(b) Cycle Diagram

$$= T' - \frac{(T_{o3} - T_{o2})(T_{o5} - T_{o2})}{T_{o1}(T_{o5} - T_{o2})} - \frac{T_{o2}}{T_{o1}}$$

$$= T' - \epsilon_x\left[\frac{T_{o5} - T_{o2}}{T_{o1}}\right] - \frac{T_{o2} - T_{o1} + T_{o1}}{T_{o1}}$$

$$= T' - C - 1 - \epsilon_x\left[\frac{T_{o5} - T_{o2} + T_{o1} - T_{o1}}{T_{o1}}\right]$$

$$= T' - C - 1 - \epsilon_x\left[\frac{T_{o5}}{T_{o1}} - C - 1\right]$$

$$= T' - C - 1 + \epsilon_x C + \epsilon_x - \epsilon_x\left[\frac{T_{o5} - T_{o4} + T_{o4}}{T_{o1}}\right]$$

$$= T' - C - 1 + \epsilon_x C + \epsilon_x + \epsilon_x E_1 T' - T'\epsilon_x$$

$$= T'(1 + \epsilon_x(E_1 - 1)) - (1 + C)(1 - \epsilon_x)$$

Therefore, for a recuperated Brayton cycle,

$$\eta_{th} = \frac{E_1 T' - C}{T'(1 - \epsilon_x(1 - E_1)) - (1 + C)(1 - \epsilon_x)} \qquad (2.25)$$

The curvature of the isobars on the T-S diagram can be further taken advantage of by the addition of intercooling or reheat. Intercooling allows compression to occur in stages, at lower temperatures, demanding less total compression work. Reheat allows expansion in stages, at higher temperatures, permitting more total work to be extracted by the turbines. Therefore, a system utilizing intercooling requires more than one compressor and additional heat exchangers and a system that utilizes reheat requires more than one turbine and additional heaters. Fig. 2.4a shows the H-S diagram of an intercooled Brayton cycle. Figure 2.4b shows an H-S diagram of a Brayton cycle with reheat. In an intercooled cycle, the compressor-inlet temperatures to all of the compressors are about the same. In this case, it can be shown that for an intercooled cycle with n intercooled stages of compression,

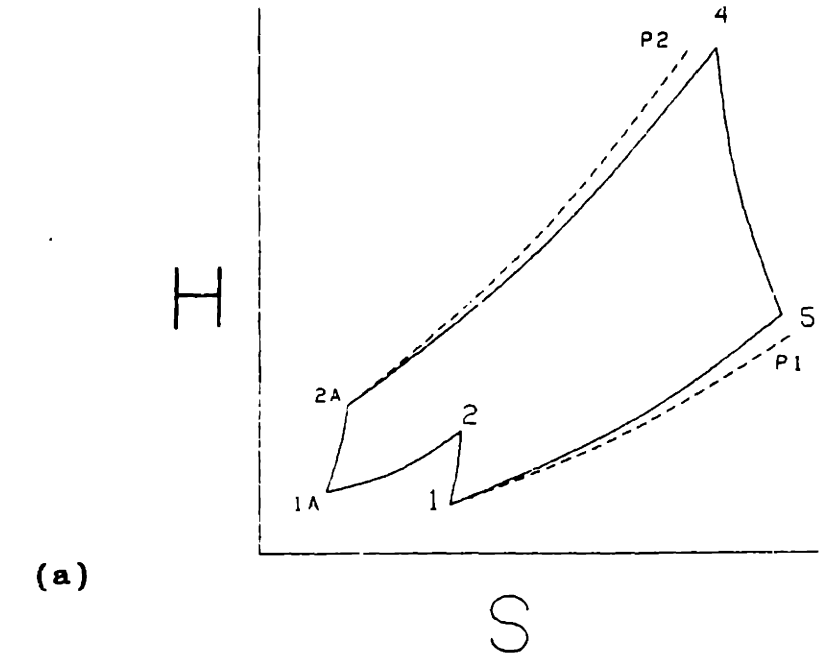

(a)

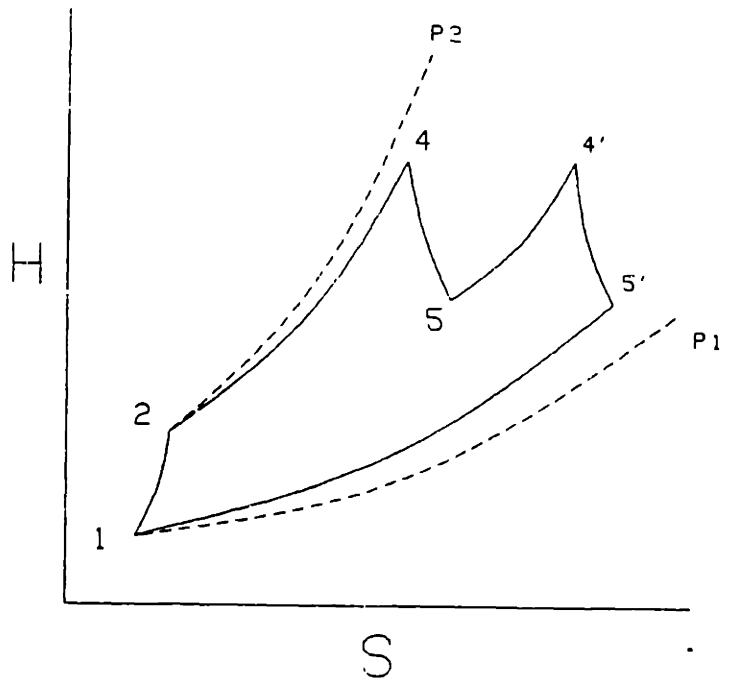

(b)

Figure 2.4. H-S Diagrams for
(a) An intercooled Brayton cycle
(b) A Brayton cycle with reheat

$$\eta_{th} = \frac{E_1 T' - (C_1 + C_2 + \ldots + C_n)}{T' \left[1 - \epsilon_x (1 - E_1)\right] - (1 + C_n)(1 - \epsilon_x)} \qquad (2.26)$$

The reactor flowpath for a Brayton cycle with reheat would be very complicated, and would pose difficult questions regarding the safe operation of the reactor and the additional capital cost of the plant. Therefore, reheat is not considered a viable possibility for the MGR-GT, and will not be quantitatively evaluated.

2.2 Results of Analysis.

By incorporating the equations developed in the previous section into computer programs, it is possible to evaluate the performance of gas-turbine cycles for different configurations and operating parameters. Two computer programs were developed, CYCLE and INTCLD. More information on these programs is found in Appendix A. Kaburaki and Lidsky [K1] performed cycle analyses using a computer program very similar to CYCLE with many of the same parameters of this study. In all cases the results of CYCLE agreed with the results of Kaburaki and Lidsky. The results were also in agreement with the results of calculations with the BRAY code, another Brayton-cycle analysis code used by GA Technologies [S13, S14]. By comparing the results of CYCLE and INTCLD, it was possible to compare the peak efficiencies possible from each cycle and quantify the advantages of intercooling.

In order to determine the important efficiency-affecting parameters in the gas-turbine cycle, a series of sensitivity analyses were performed. The variable parameters were:

- Compressor Pressure-Ratio

- Recuperator Effectiveness
- Total Specific Pressure Drop
- Turbine-Inlet Temperature
- Compressor-Inlet Temperature
- Turbine Polytropic Efficiency
- Compressor Polytropic Efficiency

2.2.1 Pressure Ratio.

Figure 2.5 shows the effect of pressure ratio and recuperator effectiveness on the cycle efficiency. The cycle efficiency rises to a peak and then falls off as pressure ratio is increased. The initial increase in efficiency is a result of the increased effect of the curvature of the isobars on the H-S diagram at higher pressure ratios. This effect will cause turbine work to rise at a more rapid rate than compressor work. However, as pressure ratio increases, the beneficial effects of the recuperator decrease because the difference between turbine-exhaust temperature and compressor-exhaust temperature decreases. For pressure ratios above the Pressure Ratio for Peak Efficiency (PRPE), at about 2.0 to 2.4 on Fig. 2.5, the beneficial effects of the recuperator tend to be reduced at a rate that is more rapid than the beneficial effects of raising pressure ratio. For sufficiently high pressure ratios, the turbine-exhaust temperature, in fact, is lower than the compressor-exhaust temperature, and the presence of a recuperator in the cycle will actually reduce the cycle efficiency. This effect is further discused in Section 2.2.2.

2.2.2 Recuperator Effectiveness.

The effect of the recuperator in reducing the PRPE of the cycle is seen in the progression to the left of the peak efficiency points

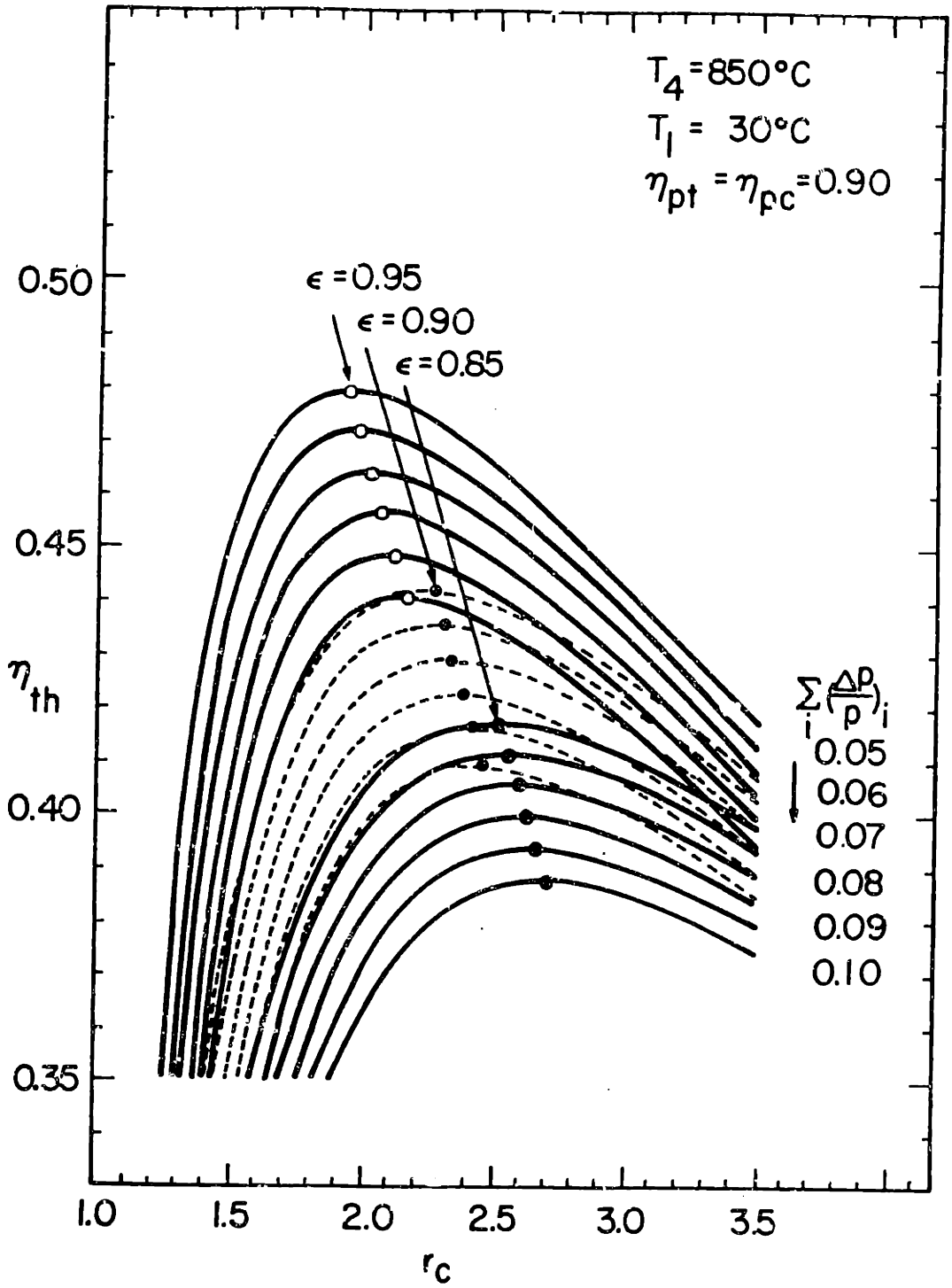

Figure 2.5. **Brayton-cycle efficiency as a function of pressure ratio, recuperator effectiveness, and pressure loss. [from K1]**

on Fig. 2.5, but is possibly best explained by Fig. 2.6. Figure 2.6 shows the calculated efficiencies of otherwise ideal cycles (100% efficient machines, and no pressure losses) with recuperator effectivenesses ranging from 0 to 100%. At the one extreme, the efficiency of a non-recuperated cycle ($\epsilon_x = 0$) increases continuously with pressure ratio. This is a result of the increased effect of the curvature of the isobars on the cycle H-S diagram. At the other extreme, a cycle with a 100% effective recuperator will have its highest efficiency at a pressure ratio approaching 1.0 (this, of course, is an unrealistic situation because no work is performed) and efficiency will decrease as pressure ratio is increased. For cycles with "real" recuperators, the behavior lies between the two extremes. Initially, cycle efficiency increases as pressure ratio is increased, rising to a peak efficiency. For these pressure ratios, the turbine work increases at a faster rate than the compressor work increases, improving cycle efficiency. For pressure ratios greater than the PRPE, the efficiency drops off. This is a result of reduced turbine-exhaust temperature and increased compressor-exit temperature at high pressure-ratios, both of which reduce the beneficial effects of the recuperator. Cycles with recuperators of high effectiveness will behave more like the 100% recuperator case, and their PRPE will be low. Cycles with recuperators of low effectiveness will behave more like the unrecuperated system, and their PRPE will be high. For turbine-inlet temperatures of 850°C, compressor-inlet temperatures of 30°C and pressure ratio greater than about 5.3, the presence of a recuperator in the cycle will always reduce helium Brayton-cycle efficiency. Above this pressure ratio, turbine-exhaust temperature is,

in fact, lower than compressor-exhaust temperature (see Fig. 2.6). Recuperated cycles are therefore most efficient at low pressure-ratios.

Figure 2.6 demonstrates that the most efficient recuperated cycles operate with a recuperator of high effectiveness at low pressure-ratios. Figure 2.7 demonstrates the effect of recuperator effectiveness on the peak efficiency at PRPE of real cycles. As recuperator effectiveness is increased while all other cycle parameters are kept the same, the cycle efficiency at PRPE rises rapidly. The sensitivity of cycle efficiency to recuperator effectiveness is greater with increased recuperator effectiveness, as demonstrated by the concave upward shape of the curves on Fig. 2.7. However, as will be discussed in Chapter Five, the marginal benefits of increased recuperator effectiveness come at the marginal price of greatly increased heat-exchanger size, particularly in these regions of high recuperator effectiveness. Additionally, for cycles of equal reactor thermal-output, helium mass-flow increases as recuperator effectiveness is increased, making it more difficult to design cycles with high-effectiveness recuperators and low pressure drops. Therefore, if it is desired to design a system for high cycle efficiency by using a recuperator of high effectiveness, it is necessary to recognize that the helium mass-flow will be high. In these situations, methods for reducing system pressure drop should be considered so that the benefits of a high-effectiveness recuperator may be fully realized. Some of these methods will be discussed in the next section.

2.2.3 Effects of System Specific Pressure Drop.

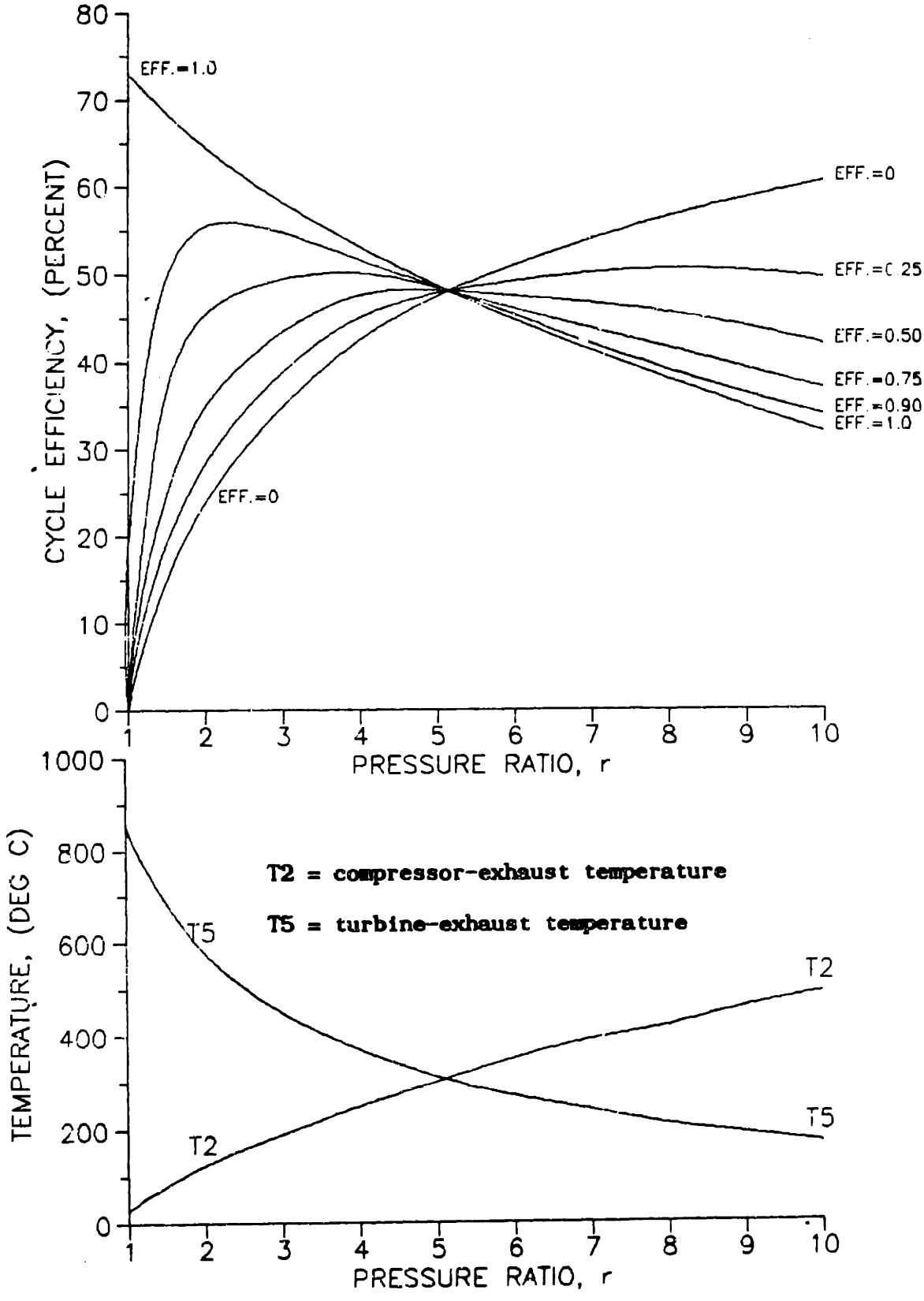

Figure 2.6. **The relationships between pressure ratio, recuperator effectiveness, turbine and compressor exhaust temperatures and cycle efficiency for an otherwise ideal cycle.**

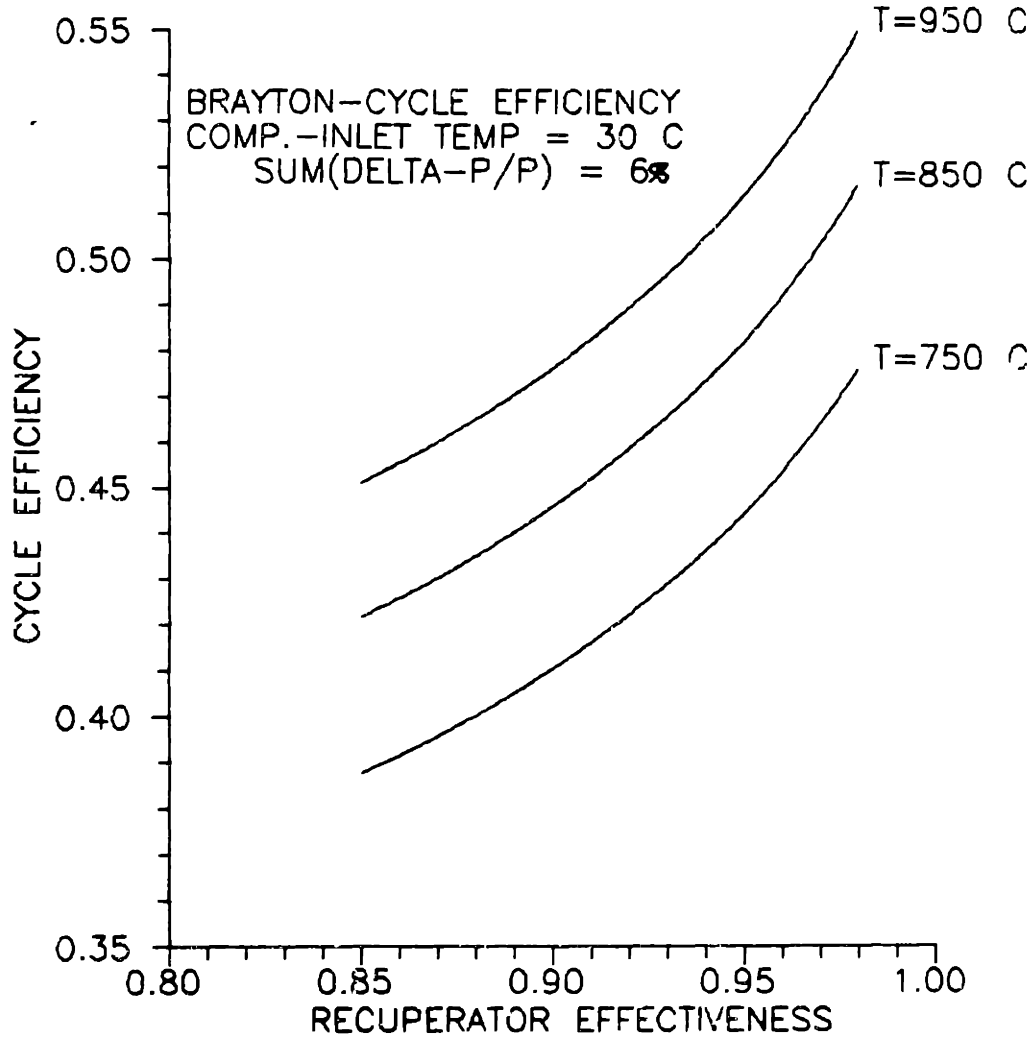

Figure 2.7. **Brayton cycle efficiency as a function of recuperator effectiveness and turbine-inlet temperature.**

The system pressure-drops act to reduce the pressure ratio across the turbine, thereby reducing the work that can be extracted in the turbine expansion process. Figure 2.8 shows calculated efficiencies at PRPE for CCGT systems as a function of specific pressure-drop for selected cycle parameters and recuperator effectivenesses. The curves fall off almost linearly in this region. Efficiencies are actually dropping at a rate that slowly increases as pressure losses increase. Kaburaki and Lidsky calculated the heat rejected at PRPE over a broad range of pressure drops at different recuperator effectivenesses. Figure 2.9 shows their results. Specific pressure-drops greater than 10% showed significant increases in heat rejection. For specific pressure-drops significantly greater than 10%, the heat rejection is actually greater than the results of these calculations suggest because higher order terms that were neglected in the analysis become significant and cannot be left out of Eqs. 2.14 and 2.20. Hence, the rapid rise in losses for total specific pressure-drop greater than 10% makes it important to consider a total specific pressure-drop of 10% as an upper bound for design considerations.

Pressure losses are generated primarily by fluid friction in ducting and heat-exchange equipment, and irreversible losses in dynamic head during sudden flow-area changes. Both of these pressure losses are proportional to dynamic head and can be represented by Eq. 2.27.

$$\frac{\Delta P}{P} = f \frac{L}{D} \frac{G^2}{2 \rho P} \qquad (2.27)$$

f is strictly a function of Reynolds number and duct surface-roughness, both of which remain constant in a fixed system for all operating pressures if mass flow is maintained. The

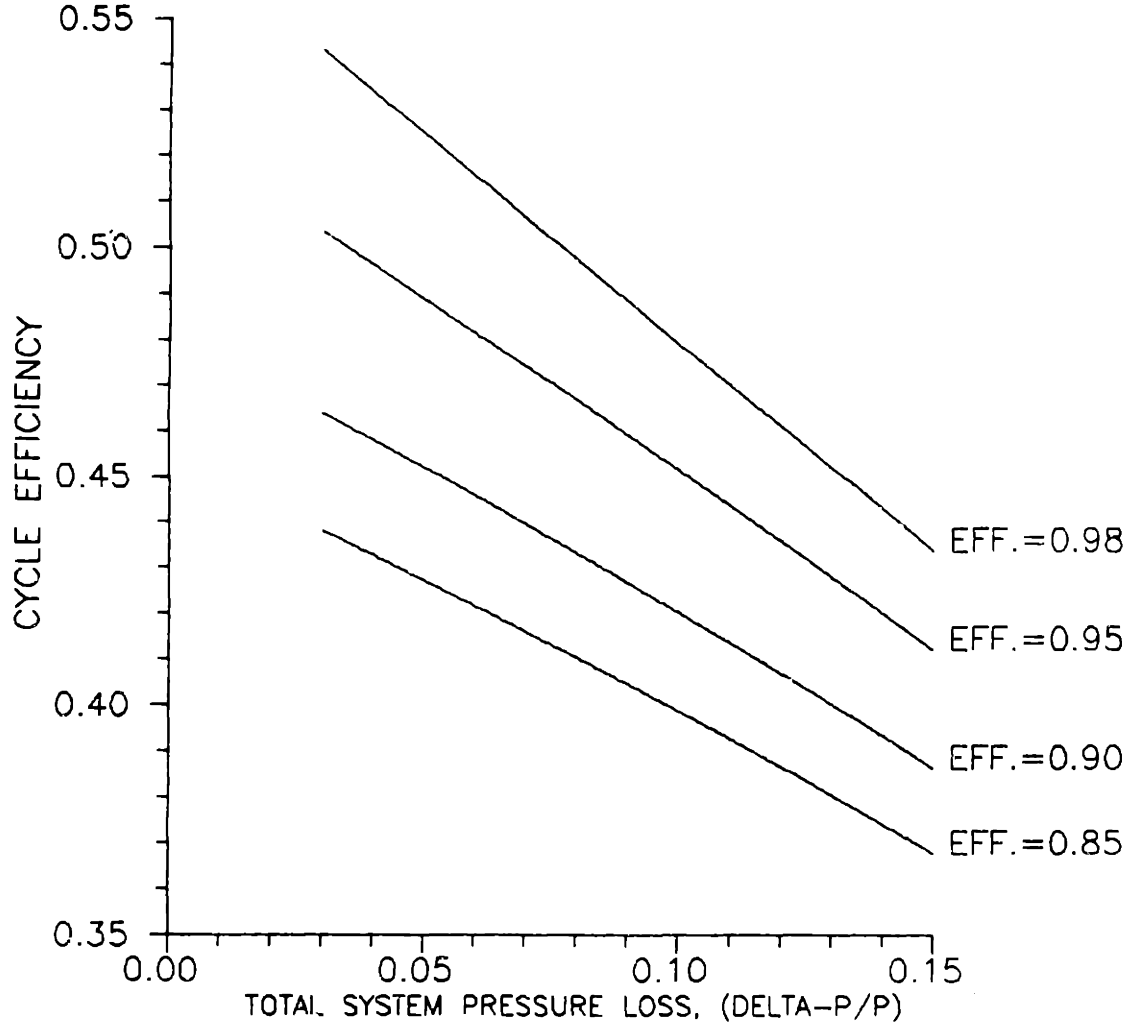

Figure 2.8. **Cycle efficiency as a function of pressure loss and recuperator effectiveness.**

Turb.-inlet temp. = 850°C

Comp.-Inlet temp. = 30°C

$\eta_{pc} = 0.91$

$\eta_{pt} = 0.91$

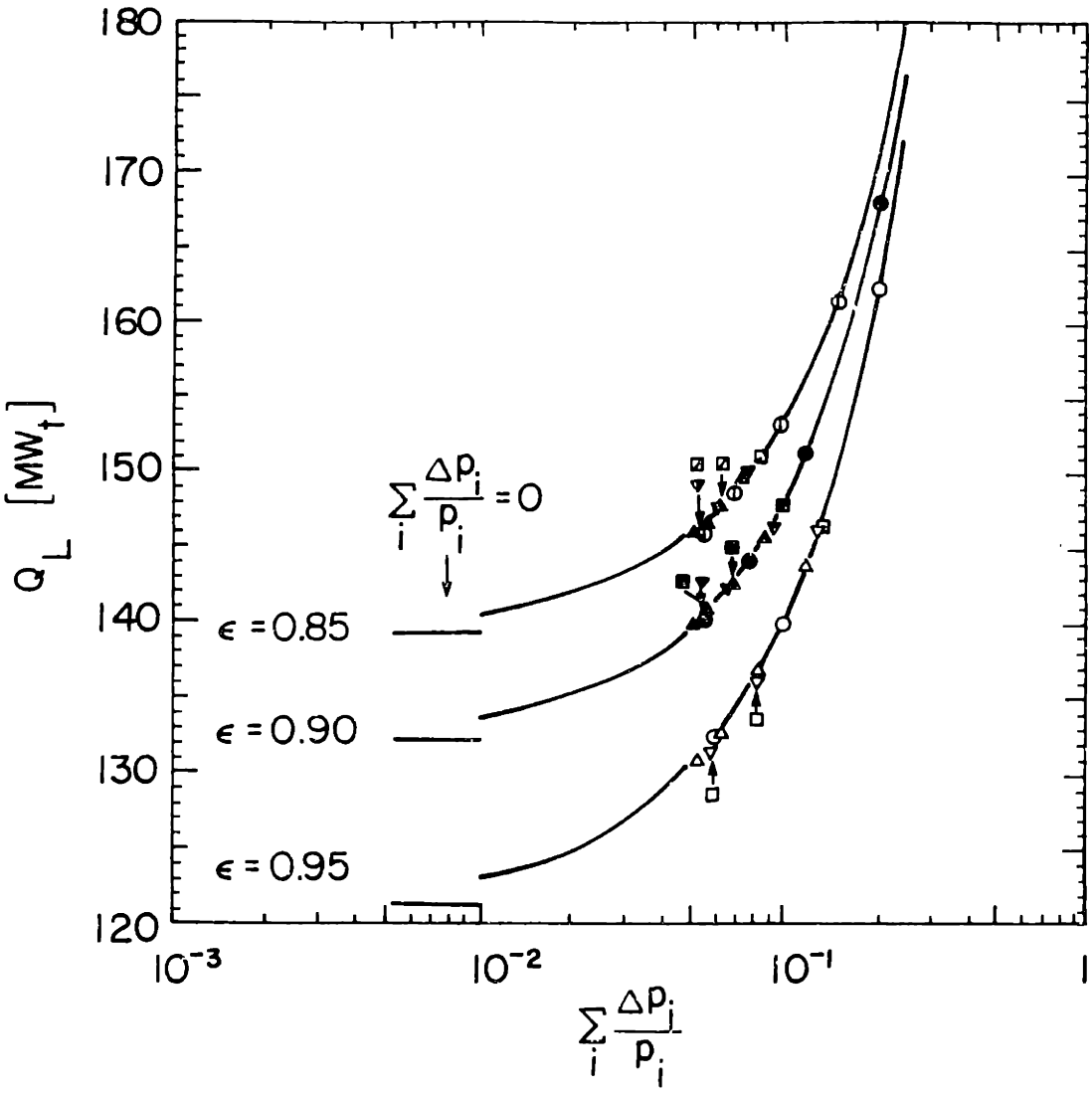

Figure 2.9. The rejected heat as a function of the specific pressure-loss and recuperator effectiveness. [from K1]

length-to-diameter ratio $\left[\frac{L}{D}\right]$ is a geometric characteristic of the system and for a fixed system remains constant for all pressures. Pipe bends and valves have an equivalent $\frac{L}{D}$, and sudden expansions and contractions have loss coefficients, K, that represent the fraction of the dynamic head lost. Both $\frac{L}{D}$ and K remain constant as pressure and mass flow change. For a system of fixed size, geometry, and reactor thermal-output; as system pressure is changed, the specific pressure-drop varies as

$$\left[\frac{\Delta P}{P}\right] = \left[\frac{\Delta P}{P}\right]^{*} \left[\frac{P^{*}}{P}\right]^{2} \qquad (2.28)$$

From this equation it is clearly seen that a high pressure-level is extremely beneficial for minimizing system pressure-drop and improving cycle efficiency. This is especially true when using a recuperator of high effectiveness because of the higher mass flows. It is therefore advantageous to operate at the highest system pressure that design limits will allow. Otherwise, the system must be made much larger in size or smaller in output in order to reduce mass velocity (G) and the pressure drop.

2.2.4 Turbine-Inlet and Compressor-Inlet Temperatures.

From Fig. 2.2 and Eqs. 2.1 and 2.2, it is seen that more work can be extracted by expanding the gas between two pressures if the gas is initially at a high temperature. Similarly, less work is consumed when the gas is compressed at a low temperature than when the gas is at a high temperature. According to Eq. 2.25, the ratio of the turbine-inlet temperature to compressor-inlet temperature (T'), not their individual values, determines the effect of these temperatures on the cycle efficiency. Figure 2.10 shows the effect of T' on cycle efficiency at PRPE. Figure 2.11 demonstrates the effect of

turbine-inlet temperature on cycle efficiency at PRPE. There are clearly strong reasons to operate at the highest turbine-inlet temperature and lowest compressor-inlet temperature possible. The upper limit of the allowed turbine-inlet temperature is primarily determined by the highest temperature that the reactor may be safely operated at while still maintaining the objective of "passive safety". In the event of an accident, maximum core temperature must stay below 1600°C and the pressure vessel must stay below an upper temperature limit determined by the pressure-vessel material. For temperatures above these limits, fission products may be released or the steel of the pressure vessel may be weakened. Another issue to consider in determining the upper limit of the turbine-inlet temperature, is the need to cool the turbine blades at sufficiently high temperatures. Cycle efficiency suffers a large penalty when blade cooling is used. In combustion turbines, temperatures are high enough that the performance benefits of high turbine-inlet temperatures outweigh the penalties of blade cooling. However, in the MGR-GT the reactor-safety considerations become limiting before temperatures become high enough such that it is necessary to employ blade cooling. Calculations by Izenson [I3] showed that a 200-MWth pebble bed reactor, operating at conditions similar to those of a CCGT plant with a turbine-inlet temperature of 850°C, maintained peak-core temperature just below 1600°C during a depressurized cooldown. This temperature of 850°C is also sufficiently cool that turbine blading of conventional turbomachine-blade alloys (IN-100) will not require blade cooling. Hence, 850°C will be used as the nominal turbine-inlet temperature in this study.

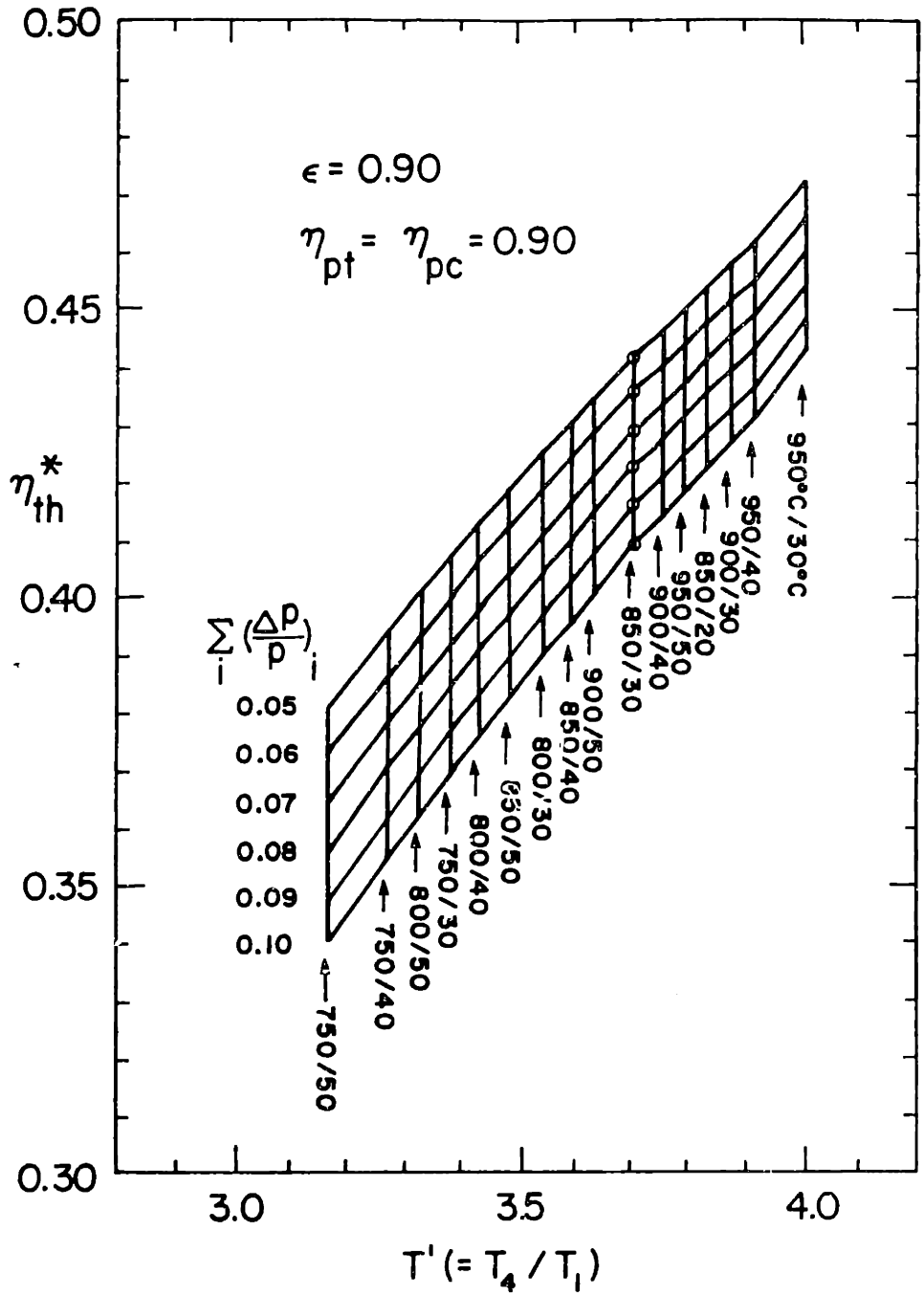

Figure 2.10. Effect of $T' = \frac{T_4}{T_1}$ on cycle efficiency. [from K1]

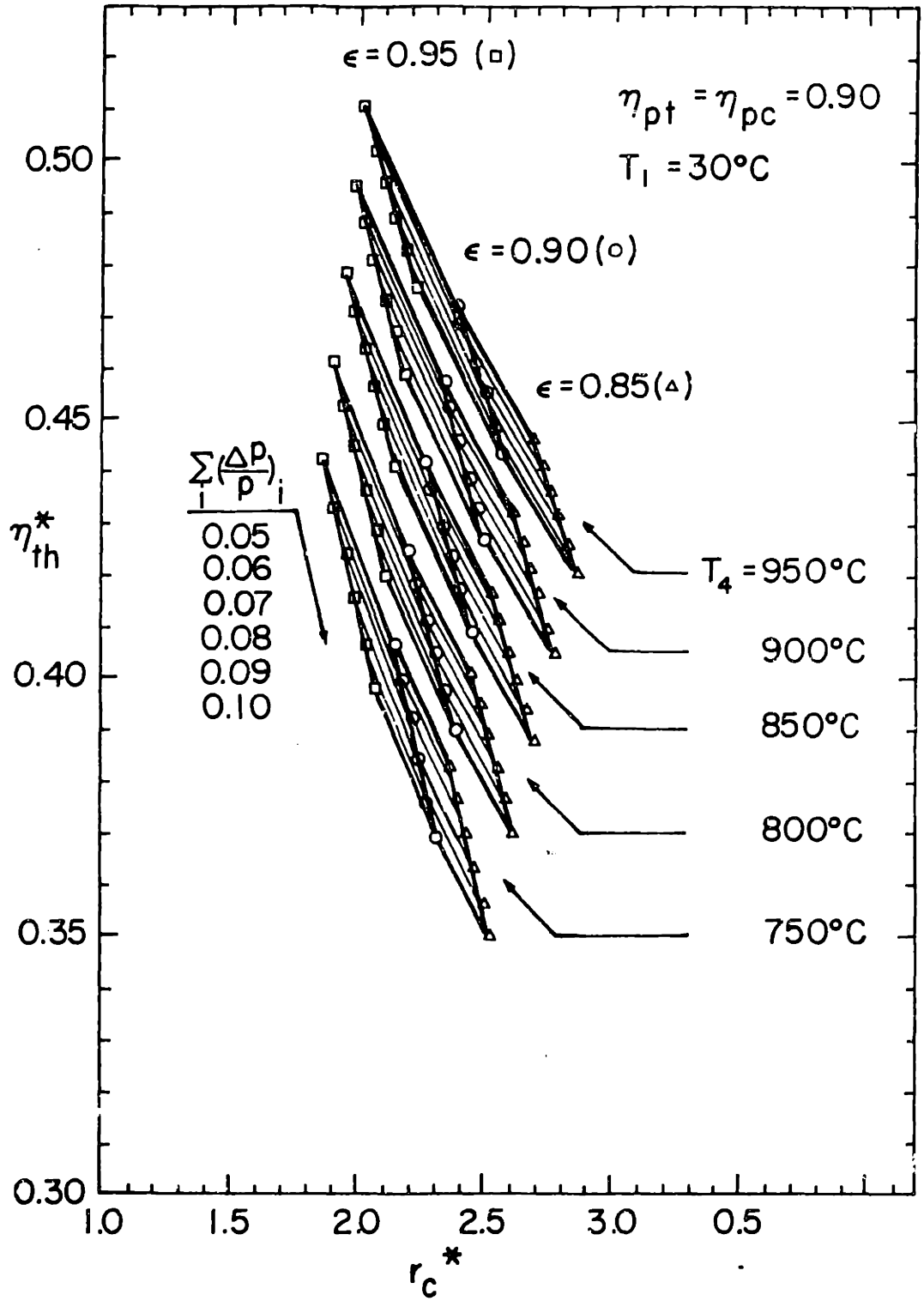

Figure 2.11. Effect of Turbine-inlet temperature (T_4), ϵ_x, $\sum \frac{\Delta P}{P}$, and pressure-ratio on cycle efficiency. [from K1]

Compressor-inlet temperature has a lower limit that is primarily determined by the temperature of the heat sink being used and also by the method of heat rejection. This study will consider wet and dry methods of heat rejection. The nominal compressor-inlet temperature was selected to be 30°C. This temperature is consistent with previous studies as a nominal point for design. Lower temperatures might be expected in cold climates and higher temperatures can be expected in hot weather while using dry cooling. The effects of compressor-inlet temperatures other than 30°C on cycle performance and heat-exchanger design will be discussed in Chapter Five.

2.2.5 Turbine and Compressor Polytropic Efficiencies.

Turbine and compressor polytropic efficiencies are limited by the state-of-the-art in turbomachine design. Present-day, industrial, axial-flow turbomachines are capable of polytropic efficiencies slightly over 90%. For this reason a nominal polytropic efficiency value of 91% for both the turbine and compressor were selected as first estimates for the analyses in this chapter. Actual machine efficiencies may be as much as a few percent different from these values. They will be evaluated in Chapter Four.

Figures 2.12 and 2.13 show the results of calculations to determine the effect of turbomachine polytropic efficiency on the cycle efficiency. Both turbine and compressor polytropic efficiencies significantly effect the cycle efficiency. Increasing the compressor efficiency results in an increase in the PRPE while an increase in the turbine efficiency has little impact on the PRPE. The compressor polytropic-efficiency has, in fact, a greater effect on cycle efficiency at PRPE than turbine polytropic efficiency. This result may

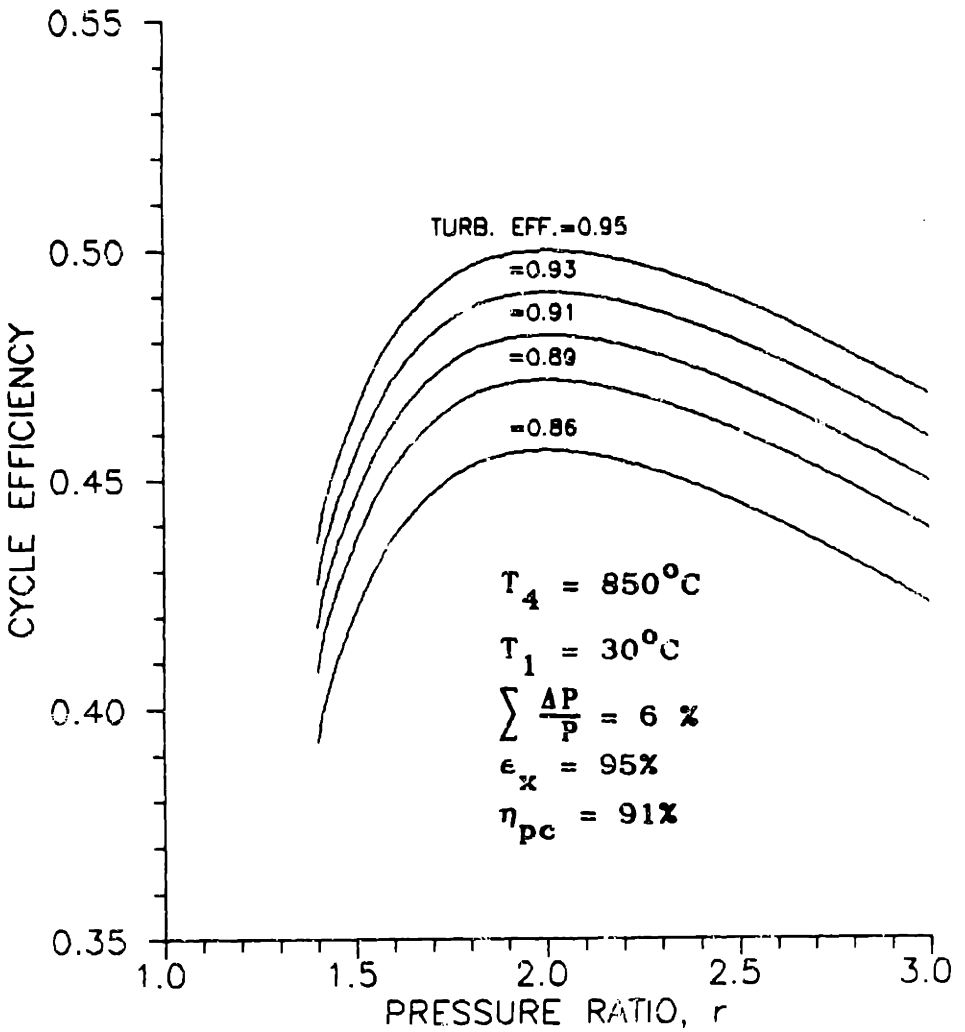

Figure 2.12 **Effect of turbine polytropic-efficiency on cycle efficiency.**

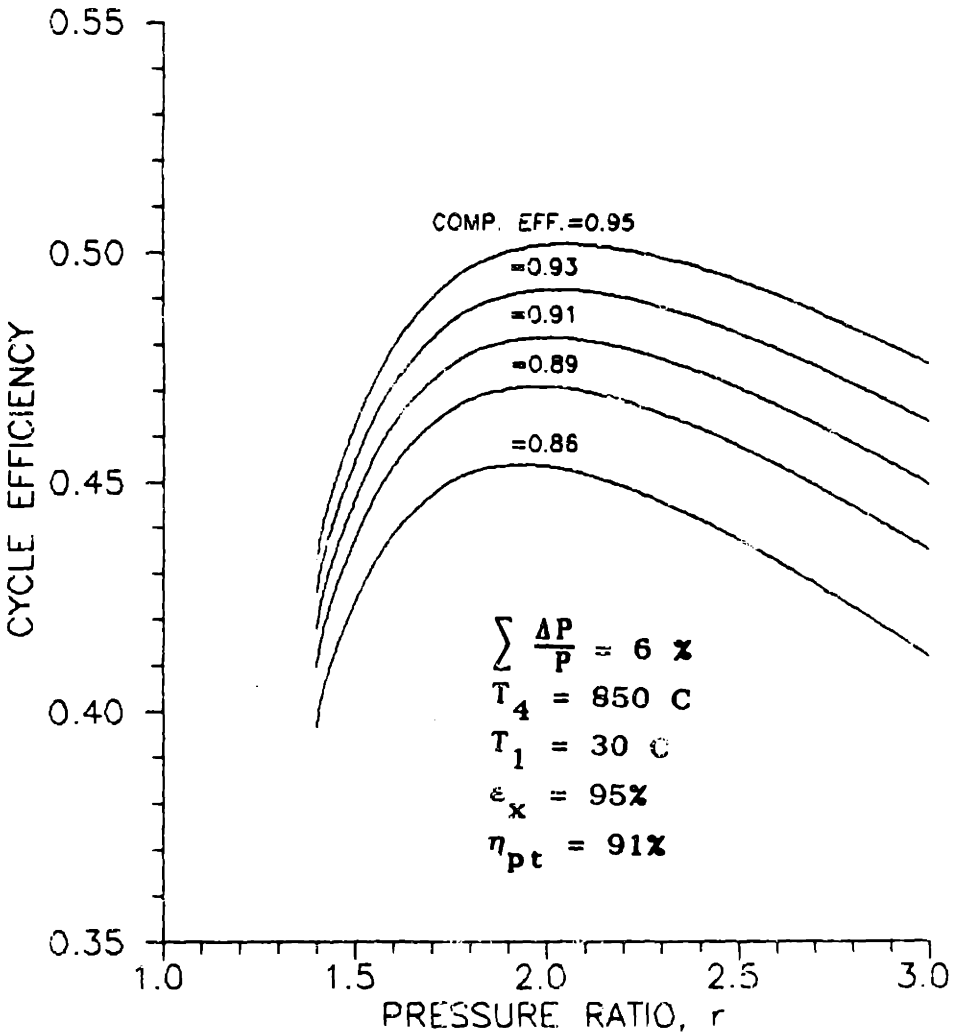

Figure 2.13 **Effect of compressor polytropic-efficiency on cycle efficiency.**

seem surprising at first because the turbine power is greater than the compressor power; however, component location in the cycle plays an important role in determining the net effects of machine efficiency on cycle efficiency and PRPE. Performance of a particular component will not only affect the component, but the other components in the cycle as well. Machine performance will affect heat transfer in the heat exchangers of the cycle. The net effect of machine efficiency on cycle efficiency and PRPE is, therefore, a result of several interacting effects.

2.2.6 Intercooling.

Higher cycle efficiencies are available with intercooling. The price of the higher efficiency is a more complicated system with at least one more turbomachine, one more heat exchanger, and additional ducting. The results of INTCLD were compared to those of CYCLE to quantify the efficiency advantage of intercooling. Figure 2.14 shows the results of calculations for two-stage compression with intercooling, compared to calculations for one-stage compression. The intercooled cycle has roughly a 3% efficiency advantage over the non-intercooled cycle at the PRPE. The PRPE of the intercooled cycle was higher than that of the non-intercooled cycle. This is because intercooled cycles have a lower compressor-outlet temperature for the same total pressure-ratio than non-intercooled cycles. Therefore, in an intercooled cycle, the pressure ratio at which the compressor-outlet temperature will equal the turbine-outlet temperature is greater than that of a non-intercooled cycle operating between the same compressor-inlet and turbine-inlet temperatures. This will tend to increase the PRPE of intercooled cycles relative to

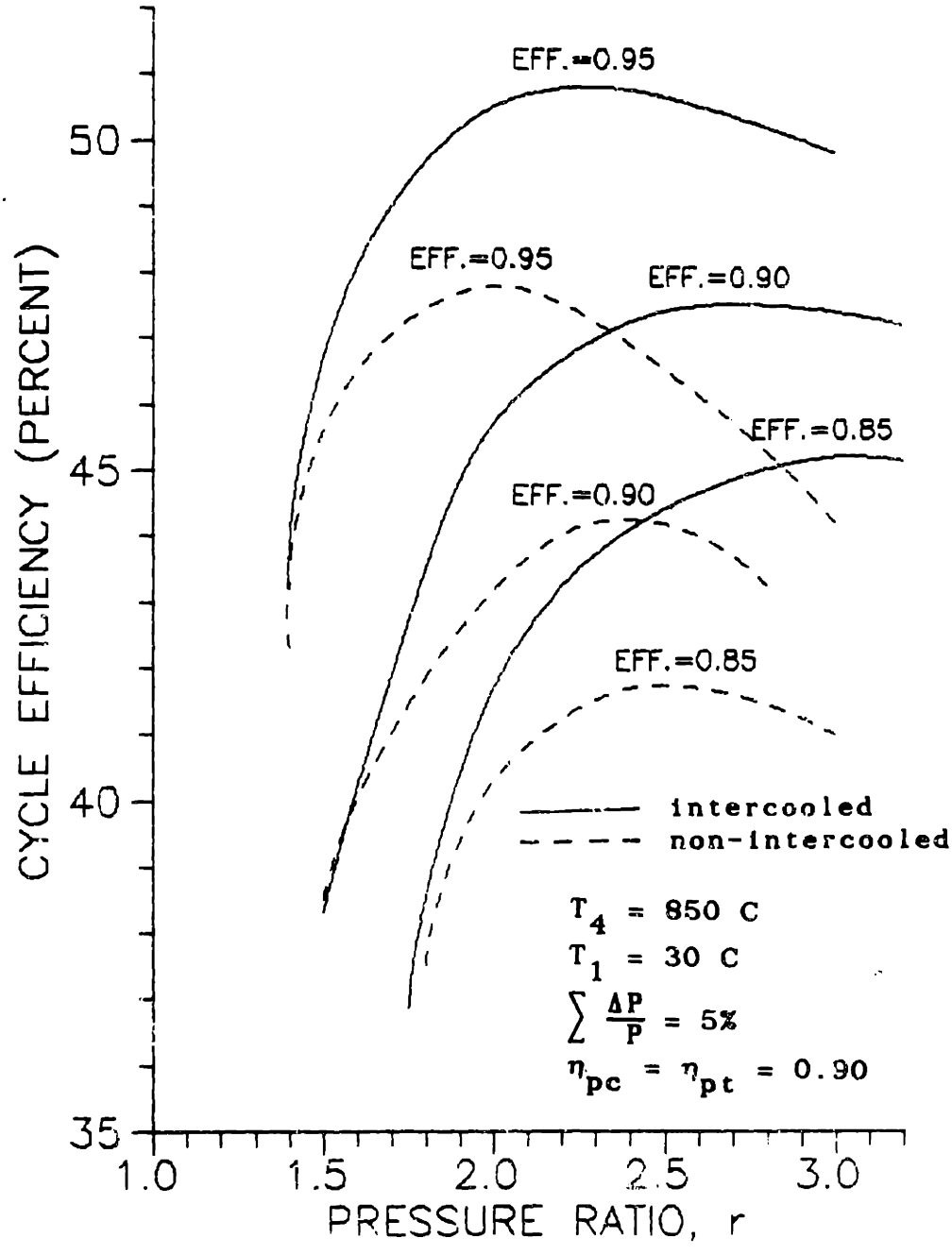

Figure 2.14. The effect of intercooling (two stage compression) on cycle efficiency.

non-intercooled cycles.

Although the additional 3% efficiency offered by intercooling is attractive, the additional complexity of the intercooled cycle is not in keeping with the general philosophy of the MGR plant, which emphasizes safety and economy through simplicity. Intercooling might be considered as a feature for future MGR-GT variants; however, the complexity added by intercooling is judged as too great to incorporate into a first-of-its-kind design.

2.2.7 Sensitivity Analysis.

The sensitivity of plant efficiency to each of these parameters on a non-intercooled cycle was determined. Sensitivity is defined as:

$$\sigma = \frac{\partial \eta}{\partial \Pi} \tag{2.29}$$

The numerator being the change in cycle efficiency in percentage points, and the denominator being percent change in the parameter from the base case parameter value. Since all cycle parameters except turbine-inlet and compressor-inlet temperatures are measured in percentage, the effect of turbine-inlet and compressor-inlet temperatures will be determined such that:

$$\partial \Pi \ (\%) = 100 \left[\frac{T - T^*}{T^*}\right] \% \tag{2.30}$$

Since all other parameters can be measured in percent, the numerical difference in their value (measured in percent) from the base case will be used as the value for $\partial \Pi$.

$$\partial \Pi \ (\%) = \Pi \ (\%) - \Pi^* (\%) \tag{2.31}$$

The sensitivity of the cycle efficiency is also affected by the selection of the base parameters. Hence, it is important to select base parameters that are in a region of operation that is of interest. For this reason, the base case parameters of Table 2.1 were selected.

The results of the sensitivity analysis are presented in Fig. 2.15. Each line on the figure shows the value of efficiency at PRPE resulting in a change from the base case in only the parameter for that line. All other cycle parameters are at the base case value. Cycle efficiency at PRPE is fairly sensitive to all of the parameters studied. The order of sensitivity, from most sensitive to least sensitive is:

1. Recuperator Effectiveness
2. Specific Pressure-Loss
3. Compressor Polytropic-Efficiency
4. Turbine Polytropic-Efficiency
5. Turbine-Inlet Temperature[#] [*]
5. Compressor-Inlet Temperature[#] [*]

[#] These two parameters are not normally measured in percent.

[*] These two parameters have equal, but opposite, effects.

The effects of turbine-inlet and compressor-inlet temperatures are equal, and opposite, because the ratio of these two temperatures to one another, not their actual values, are what affects cycle efficiency.

The above list only considers the numerical differences in efficiency obtained for the changes in parameters as defined. It does not consider the expense, nor the design difficulty incurred in such parameter changes. Such considerations will be the subjects of Chapters Three through Five of this dissertation. This analysis also does not consider any dependence of one parameter on the other, such as the interrelationship between recuperator effectiveness and

Table 2.1

Nominal Parameters for

MGR-GT Cycle Analysis Sensitivity Study

Parameter	Value
Turbine-Inlet Temp.	850°C
Compressor-Inlet Temp.	30°C
Recuperator Effectiveness	0.95
$\sum \frac{\Delta P}{P}$	0.06
Compressor Poly. Efficiency	0.91
Turbine Poly. Efficiency	0.91

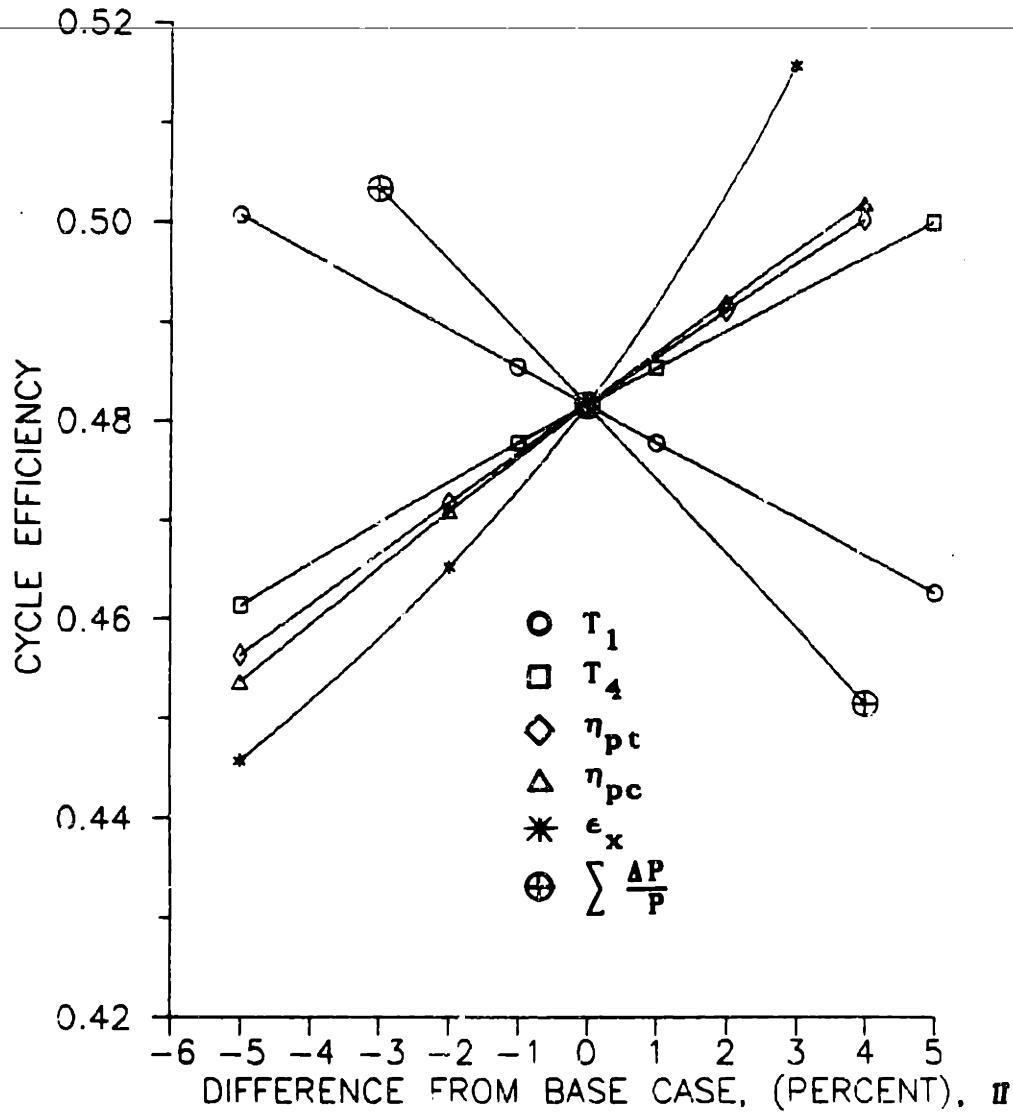

Figure 2.15 Sensitivity-Analysis Results.

Base case:

T_1 = 30 C $\quad \eta_{pc} = 0.91$

T_4 = 850 C $\quad \eta_{pt} = 0.91$

$\epsilon_x = 0.95 \quad \sum \frac{\Delta P}{P} = 0.06$

pressure drop that was discussed in Section 2.2.2. Figure 2.15 shows, however, that all of the parameters considered have a strong influence on the performance of the closed Brayton-cycle and that none should be overlooked when considering parameter selection for optimum design.

2.3 Limitations of this Analysis.

It is important to note that the results of the preceding section are based upon a simplified analysis. Certain losses exist that were not considered in the equations developed for the analysis. Since the purpose of this chapter was simply to identify and quantify the important efficiency-affecting parameters, a simple approach is appropriate. However, for a detailed plant design, several additional losses must be taken into account. Other losses to consider are discussed briefly below and are addressed in more detail in other chapters of this dissertation.

2.3.1 Gas Bleed and Leakage.

In a real gas-turbine cycle some of the gas is bled from the compressor discharge for turbine-blade and rotor cooling and for shaft sealing. Additionally, some of the gas leaks through shaft seals and any other possible leak locations. Most of the gas that is lost from the power cycle in these ways is not available to perform work in the turbine, thereby reducing the efficiency of the cycle by as much as a few percent. Fortunately, as will be further discussed in Chapter Four, none of the above losses is expected to be significant for the MGR-GT design that will be proposed.

2.3.2 Heat Losses to the Environment.

A certain amount of heat will be lost to the environment due to

heat transfer. Some of the heat will be lost through the reactor vessel because thermal insulation cannot be put on the MGR reactor pressure-vessel due to reliance on this path of heat rejection as a passive-safety feature. As will be shown in Chapter Seven, heat will also be lost due to reactor-vessel cooling. Heat lost to the environment from the vessels of the power-conversion system components will be negligible because this equipment will be well insulated from the environment. The effect of heat losses on cycle thermal-efficiency will be evaluated in Chapter Seven.

2.3.3 Electrical System Losses.

The analysis of this chapter does not consider the losses in the generator or associated electrical equipment. Although usually highly efficient, generator and electrical systems have losses that can be significant. These will be considered in Chapters Four and Seven.

2.3.4 Auxiliary Loads.

Other losses will be those associated with operation of auxiliary equipment. Power demands of equipment such as cooling water pumps, electrical control and instrumentation systems, and plant lighting must all be taken into consideration in a detailed design.

2.4 Summary of Conclusions.

The results presented in this chapter provide insight into the governing parameters of CCGT performance. It can be concluded that all of the parameters discussed in this chapter play a significant role in determining the performance of a CCGT cycle. The quantitative results of cycle analysis presented in Section 2.2 provide guidance for parameter selection in a CCGT design. The following paragraphs will

highlight the conclusions of this chapter.

2.4.1 Pressure Ratio, Recuperator Effectiveness, System Pressure and Pressure Drop.

These four parameters are so dependent upon one another, they will be discussed together. The addition of a recuperator to a CCGT cycle totally changes the cycle behavior. First, it has the effect of creating a pressure ratio where maximum efficiency occurs (called PRPE). The efficiency of an unrecuperated cycle, on the other hand, increases with pressure ratio. The pressure ratio where maximum efficiency occurs becomes lower as recuperator effectiveness is increased and cycle behavior approaches that of the perfectly recuperated cycle. As will be discussed in Chapter Four, the turbomachine design generally becomes easier as pressure ratio is reduced. Thus, the highly-recuperated cycle offers the advantage of high cycle efficiency at low pressure ratios.

The gain in efficiency from using a recuperator of high effectiveness is reduced somewhat by the increased pressure drop generated by the higher mass flow. This is not a reason to avoid using high effectiveness recuperators, but a reason to be wary of this problem in the design process. High-effectiveness recuperators have the ability to dramatically raise the cycle efficiency. Therefore, in this study, recuperators of high effectiveness ($\geq$ 90%) will be used.

Pressure drop and cycle efficiency were shown to be strongly dependent upon system pressure. It appears that efficiency of a fixed-size system benefits the most by operation at the highest possible pressure level. It will be seen in Chapters Four and Five that pressure has additional advantages in reducing component size.

Strength limitations in the pressure-vessel and component design affect the magnitude of the allowable system pressure. System pressure must be determined by consideration of all of these effects.

2.4.2 Turbine-Inlet and Compressor-Inlet Temperatures.

It is beneficial to operate at the highest turbine-inlet temperature and lowest compressor-inlet temperature possible, within the constraints of other limitations. Because of concern over the safety of the reactor and turbine design considerations, the turbine-inlet temperature has been selected to have a nominal value of 850°C.

The compressor-inlet temperature is affected by the temperature of the environment and the method of heat rejection employed. The ability to use dry cooling as well as wet cooling will be incorporated into the design, and the impact of these will be discussed in Chapter Five. Consideration of the above effects resulted in a nominal compressor inlet temperature of 30°C.

2.4.3 Turbine and Compressor Polytropic Efficiencies.

Turbomachine polytropic efficiencies are largely dependent upon the state-of-the-art of the technology. Well-designed, industrial, axial-flow turbomachines are capable of efficiencies slightly over 90%. Hence, 91% was selected as the preliminary estimate of both turbine and compressor polytropic efficiencies. More accurate estimates of turbine and compressor efficiencies will be made in Chapter Four.

Calculations showed that cycle efficiency at PRPE is slightly more sensitive to compressor efficiency than turbine efficiency.

2.4.4 Intercooling.

Intercooled cycles were determined to have roughly a 3% advantage

in cycle efficiency over non-intercooled cycles. However, because a principle design feature of the MGR is simplicity, the complexity of the intercooled cycle, as compared to the non-intercooled cycle, makes the intercooled cycle less attractive for the MGR-GT. It has therefore been decided that intercooling will not be considered in this study.

Brayton Cycle Analysis Nomenclature

Symbol	Meaning	Units
C	Specific compressor work	
C_p	Constant pressure specific heat	J/kg^oK
D	Hydraulic diameter	m
E_1	Specific turbine work	
G	Mass velocity	kg/m^2sec
h	Specific enthalpy	J/kg
L	Length of duct	m
$\dot{m}$	Mass flow rate	kg/sec
n	Indicating an integer	
p or P	Pressure	Pa
Q	Heat-transfer per unit mass-flow	J/kg
r	Compressor pressure ratio	
R	Ideal gas constant	J/kg^oK
s	Specific entropy	J/kg^oK
S	Entropy	$J/^oK$
T	Temperature	^oK, or ^oC
T'	$\frac{\text{Turbine inlet temperature}}{\text{Compressor inlet temperature}}$	
W	Specific work	J/kg

Greek

∂	Partial derivative	
ϵ_x	Recuperator effectiveness	
τ	Ratio of specific heats	
η_{pc}	Compressor polytropic efficiency	

η_{pe}	Turbine polytropic efficiency	
η_t	Turbine isentropic efficiency	
η_{th}	Cycle thermal efficiency	
Π	A system parameter	
ρ	Density	kg/m^3
σ	Sensitivity	

Italics

f	Friction factor	
i	An integer	

Superscripts

$\dot{}$	Time derivative of	sec^{-1}
$*$	Base case	

Subscripts

c	Of the compressor
exh	At the turbomachine exhaust
h	Of the heater
in	At the turbomachine inlet
n	An integer
o	Indicating at stagnation conditions
s	Property resulting from an isentropic process

Cycle Locations

1	At the compressor inlet

2	At the compressor outlet
3	At the heater (or reactor) inlet
4	At the turbine inlet
5	At the turbine exhaust
6	At the LP recuperator outlet

CHAPTER THREE

MATERIALS, DESIGN CODE REQUIREMENTS, AND HEAT SOURCE

3.1 Material and Design Code Applicability.

Chapter One briefly raised the issue of pressure-vessel design for the MGR-GT and its role in determining the gas flowpath in the helium-coolant circuit. The high helium temperatures in the MGR-GT cause the structural design of the MGR-GT components to be a major concern. As metal temperature is raised, the failure mechanisms of metals become time dependent. At the high temperatures being considered for the HTGR, time-dependent material behavior is a serious concern. Case N-47 of the ASME Boiler and Pressure Vessel Code considers time-dependent material behavior. It has a temperature coverage of 800-1500°F, or 427-816°C, for 304 and 316 Stainless Steels, and 800-1400°F (427-760°C) for Alloy 800H. Figure 3.1 shows the range of operating temperatures for various nuclear power plant types, and the temperature range of present structural design-code coverage. The figure demonstrates that plant designs have outpaced the materials and design-code developments. Hence, high-temperature-reactor designs are very limited by the design codes, and some work in the area of high-temperature materials must be performed before the high-temperature-reactor design concepts can be fully exploited.

Much of the ongoing work toward a design code for very-high-temperature materials is directed toward the immediate goal of developing a high-temperature heat exchanger for the process-heat

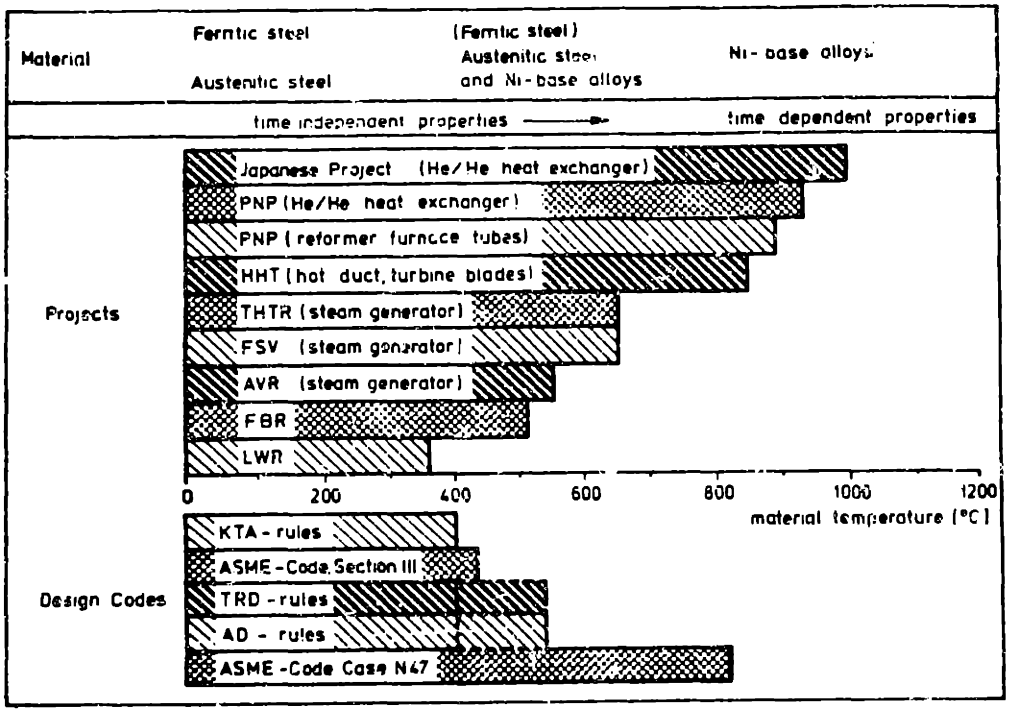

Figure 3.1. Material temperatures and design codes for metallic components in nuclear applications (from N1).

MGR. This heat exchanger has pressure-retaining surfaces at a temperature of 950°C. Fortunately, turbine and heat-exchanger high-temperature-material performance are beyond the applications of this study, especially in light of the non-corrosive helium environment. Turbine-inlet temperatures for the MGR-GT are well within the capabilities of present turbine materials such as IN-100 and TZM. 304 and 316 stainless steels meet or surpasses requirements imposed by all anticipated MGR-GT heat-exchanger operating conditions. Thus, attention will be focused on the primary-pressure boundary, especially that of the reactor, as the principal area of material concern.

Helium flowing to the reactor from the MGR-GT recuperator is at a temperature of roughly 500-600°C. Helium-coolant temperature at the reactor inlet is a function of turbine-inlet temperature, pressure ratio, and recuperator effectiveness. High turbine-inlet temperature, low-pressure ratio and high recuperator-effectiveness are all characteristics of a high-efficiency CCGT design, and all contribute to a high reactor-inlet temperature. If reactor-pressure-vessel temperature is to be maintained at reactor-inlet temperature, the part of the ASME Boiler and Pressure Vessel Code normally used for nuclear components, Section 3, Division 1, cannot be used. At these high temperatures, it is necessary to consider time-dependent failure mechanisms that are addressed in the high-temperature part of the ASME code, Case N-47.

3.1.1 Mechanisms of Failure at Elevated Temperature.

Plastic deformation at low temperatures (below about 1/2 the metal melting temperature) is normally dependent only upon the applied stress and not the time duration of the load. At low temperatures, a

material will deform elastically until its yield stress is exceeded. When a material is loaded beyond its yield stress, plastic deformation results. Dislocations in the crystal lattice move and multiply, and their interactions cause strain hardening, which eventually stops the plastic flow. The yield stress of a material is strongly dependent upon microstructure and sometimes temperature. For example, the yield stress of a face-centered-cubic metal is generally low with respect to its elastic modulus, but insensitive to changes in temperature. Body-centered-cubic metals, on the other hand, have relatively high yield stresses with respect to their elastic modulus, but a strong temperature dependence is exhibited.

At elevated temperatures (above about 1/2 the metal melting temperature), the criteria for material failure are different than the criteria at lower temperatures. This is due to time-dependent plasticity. If a load is applied to a metal specimen at high temperatures, the metal will deform plastically, regardless of the stress level. In this regard, the term yield stress has no meaning at elevated temperatures. The rate of plastic deformation, or creep, is dependent upon stress level and temperature. Figure 3.2 is a generalized creep curve and it shows total deformation of a specimen under constant tensile load as a function of time. Initial elastic-strain and initial plastic-strain occur immediately upon loading. These are followed by primary creep, which is characterized by a strain rate that steadily decreases due to the effects of strain hardening. As creep-rate drops, the softening effects of strain recovery (dislocation annihilation and rearrangement) grow until they exactly compensate for the effects of strain hardening. At this point

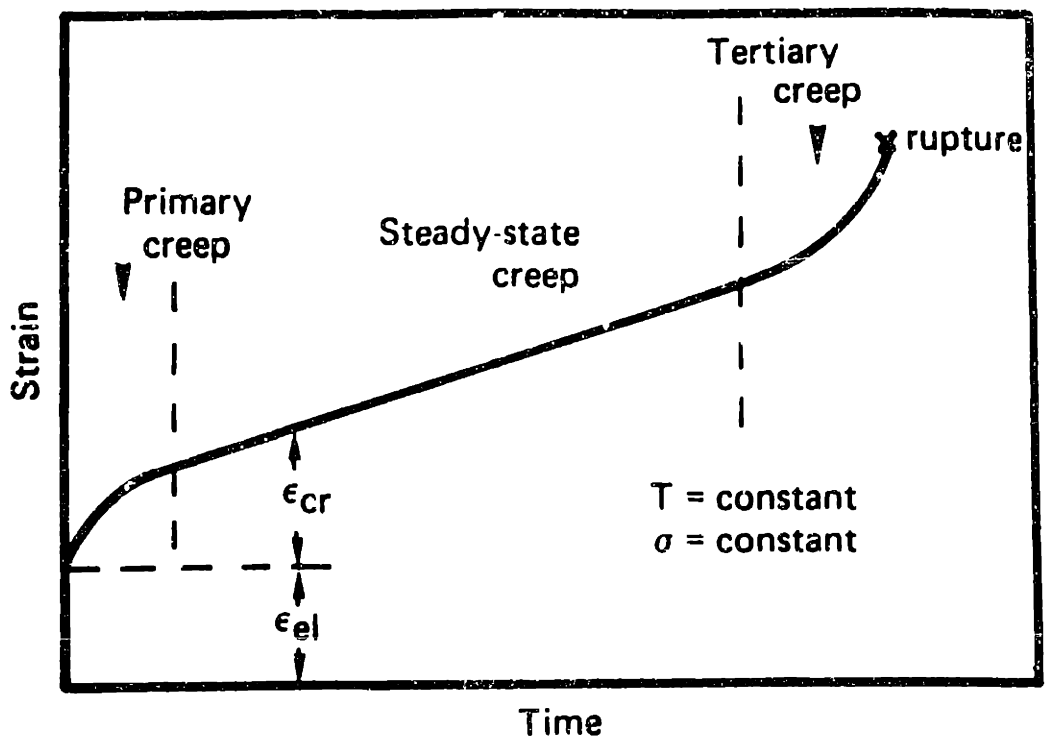

Figure 3.2. Generalized creep curve (from P7).

a steady strain-rate is achieved. The period of almost constant strain-rate accounts for most of the total deformation that will occur, and is termed secondary, or steady-state creep. The very rapid deformation that occurs immediately before rupture is termed tertiary creep. In this stage, the effects of strain recovery dominate. Necking of the specimen causes stresses to increase rapidly during a constant load test in this final stage of creep.

Numerous investigators have characterized secondary-creep rate for a variety of metals and have developed expressions to predict the creep rate of their material of interest. Creep is a thermally-activated, stress-dependent process and it is of general agreement that creep rate at high temperatures can be given by a stress-related activation-energy expression of a form similar to the following [B30]:

$$\dot{\epsilon} = B \left[\frac{\sigma}{E}\right]^n D_o \, e^{-\left[\frac{\Delta E_D}{RT}\right]} \qquad (3.1)$$

The part of the expression to the right and including D_o is the temperature-dependent self-diffusion coefficient, a parameter that influences recovery rate. The remainder of the expression results from the effects of both recovery rate and strain-hardening rate. Plastic-deformation rate is thus a strong function of stress level and temperature. It is clear from this expression that as temperature is increased, creep rate increases rapidly. At a very-high temperature, then, a limiting deformation will be reached much sooner than at a lower temperature for the same stress level.

3.1.2 Failure Criteria at High Temperatures.

Two criteria generally exist to evaluate failure of a component

by creep. The first is stress to rupture at a given temperature and time. The second is stress to result in excessive deformation for a given temperature and time. A third, that is sometimes used, is stress to reach tertiary creep; however, this might be considered a special case of the first criteria since tertiary creep immediately precedes rupture.

Figure 3.3 shows creep rupture data for IN-617. One set of plots shows stress to rupture for several times and temperatures, the longest time being 10^5 hours and the highest temperature being $1000^{o}C$. The other plots similarly show the stress for 1% total deformation of IN-617 for various times and temperatures. However, in order to use this data to design a component for a forty-year lifetime (280,000 hours at 80% availability), an appropriate transformation must be made.

Several parameters have been developed to characterize the time and temperature effects of stress on the creep-failure modes. Most commonly used of these is a parameter developed by Larson and Miller. It is of the form:

$$P_{LM} = T\ (\log\ t + C)\ (10)^{-3} \qquad (3.2)$$

Temperature (T) is most often taken in ^{o}R, and time (t) in hours. For a large number of materials, C = 20. However, C may vary somewhat from 20 for some materials. If experimental data is available, it is possible to estimate C. Since equal Larson-Miller parameters suggest equal material stress limits, C can be determined by solving the following expression for C:

$$T_1\left[C + \log(t_1)\right] = T_2\left[C + \log(t_2)\right] \qquad (3.3)$$

This will result in:

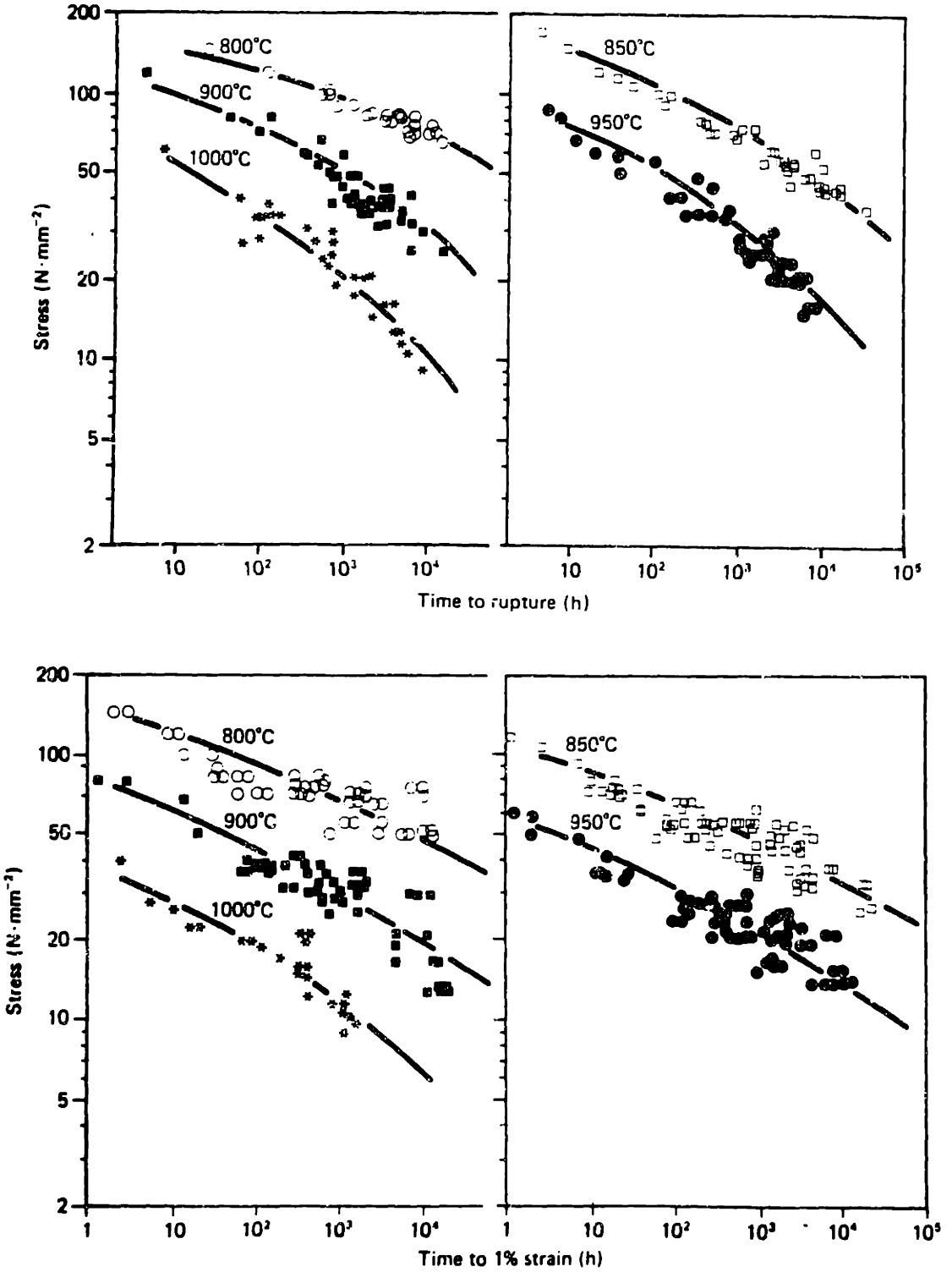

Figure 3.3. Creep-rupture data for IN-617 (from S1).

$$C = \frac{T_2 \log(t_2) - T_1 \log(t_1)}{T_1 - T_2} \qquad (3.4)$$

where the stress-to-rupture at state 1 equals the stress-to-rupture of the material at state 2.

The creep-rupture data of Fig. 3.3 was transformed in terms of the Larson-Miller parameter and plotted on Fig. 3.4. It was estimated that $C \cong 21$ from the data of Fig. 3.3. Figure 3.4 shows evidence of a strong correlation between P_{LM} and the limiting stresses. From this plot, stress limits can be estimated for component lifetimes in excess of the test duration. For example, a specimen to be operated at 280,000 hrs. at 850°C has $P_{LM} = 53.5$. This corresponds to a stress for 1% deformation of 17 MPa. and a stress-to-rupture of 24 MPa.

The limits of Code Case N-47 of the ASME Boiler and Pressure Vessel Code are based on such data for 304 and 316 stainless steels and Alloy 800H. S_t, the time dependent stress-intensity limit, is equal to the least of:

1. 100% of the stress to 1% total strain.
2. 2/3 of the stress to rupture.
3. 80% of the stress to reach tertiary creep.

To demonstrate the use of time and temperature parameters in predicting material failure, predicted stress-to-rupture data from Case N-47 of the ASME Boiler and Pressure Vessel Code was plotted by the author against the Larson-Miller parameter in Fig. 3.5. It was estimated from the predicted stress-to-rupture data that $C \cong 13$. Correlation is excellent. The correlation of predicted stress-to-rupture to Larson-Miller parameter in Fig. 3.5 demonstrates how failure of materials at elevated temperatures and extended

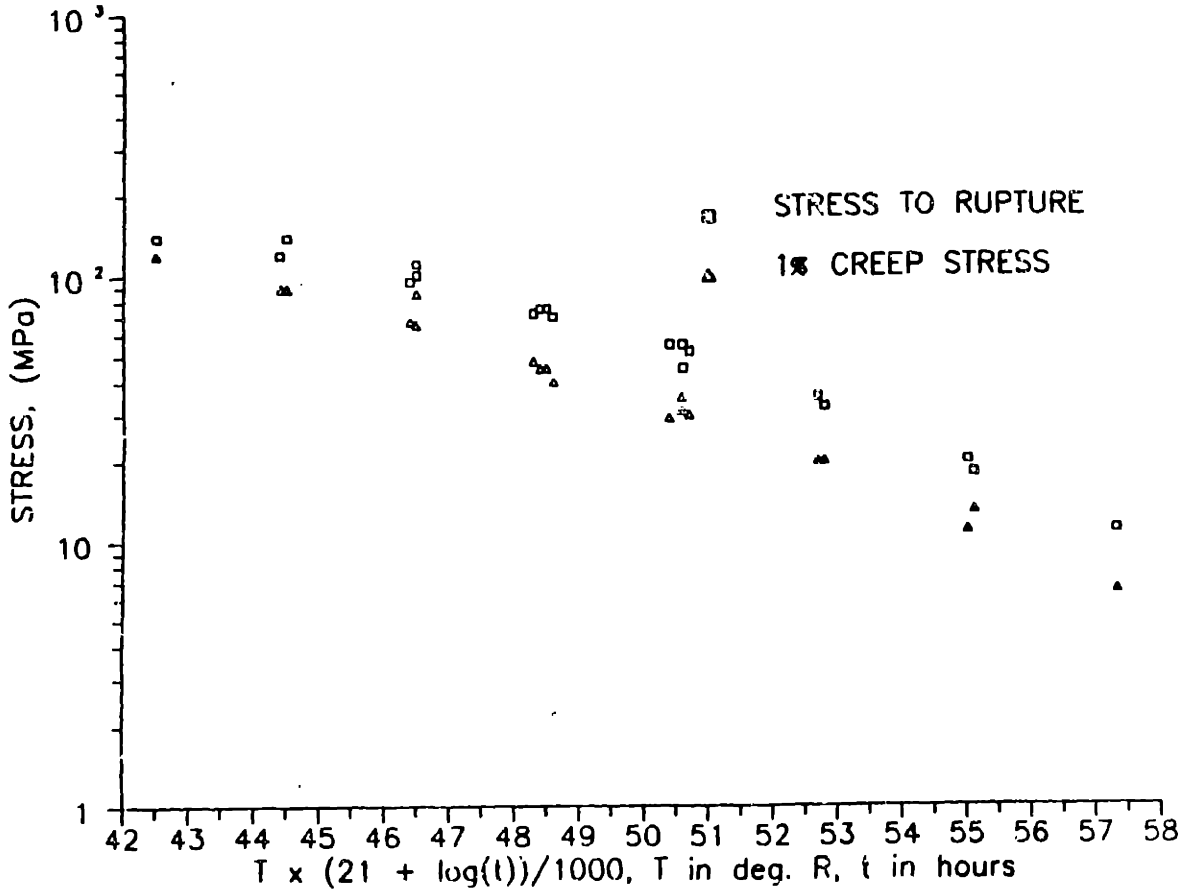

Figure 3.4. Creep-rupture data for IN-617 correlated to Larson-Miller parameter. Reduced from data in S1.

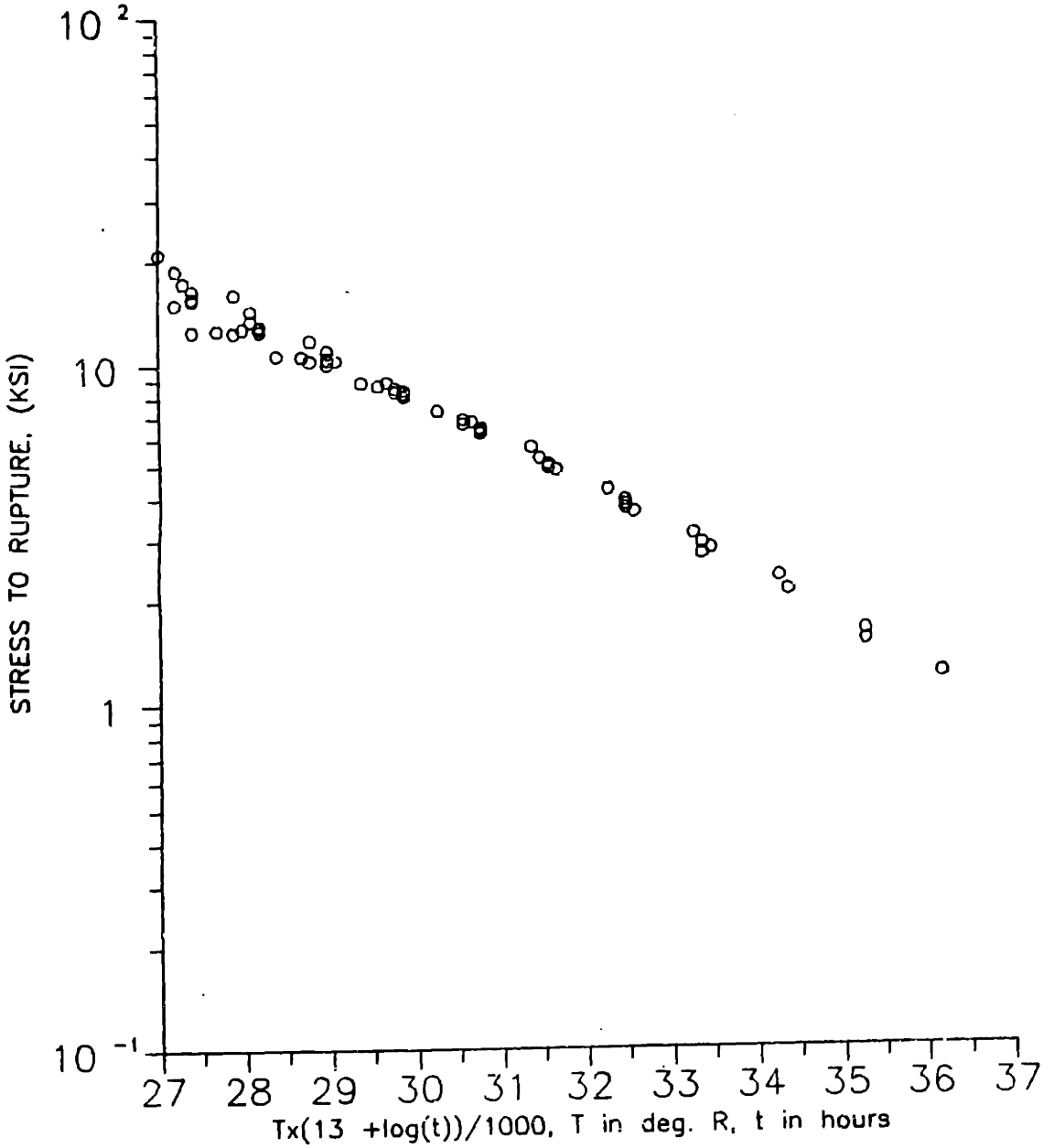

Figure 3.5. **Stress-to-rupture data of 316 stainless steel, from the ASME Boiler and Pressure Vessel Code, Case N-47, correlated to Larson-Miller parameter.**

lifetimes is normally predicted by time-and-temperature parameter correlation with experimental data, such as with the Larson-Miller parameter.

3.1.3 A Design Code for Very-High-Temperature Materials.

It was recognized early in the HTGR program that the present design codes were inadequate in the very-high-temperature regions of potential HTGR operation. Previous HTGR designs operated within the present design-code limits. Those using PCRV's used the limits of Section 3, Division 2 of the ASME Boiler and Pressure Vessel Code for their pressure-vessel design. The steam generators of the Fort St. Vrain and THTR reactor plants were designed and licensed by the rules of ASME Code Case 1592 (now called Case N-47). The reactor vessels of present steam-cycle-MGR and process-steam-MGR concept designs can be designed within the guidelines of Section 3, Division 1 of the ASME Code because of the low helium return-gas temperature (about 200°C). However, the advanced MGR designs, such as the direct-cycle gas-turbine MGR, and the process-heat MGR, are very limited by the present design code because they can have pressure retaining surfaces at very-high temperatures. For this reason, by 1983, work was underway in the Federal Republic of Germany, Japan and the United States to develop a design code for Very High Temperature Gas Cooled Reactors (VHTR) [N1]. Although such a design code would have applications to the gas-turbine MGR, the immediate goal of this design-code work is development of a high-temperature heat exchanger for process-heat applications.

There are some additional concerns regarding material failure at very-high temperatures, especially in regard to the effects of

impurities. However, the reactor-inlet temperature of the MGR-GT is below the temperature region where chemical effects due to impurities become important.

By piping reactor-outlet helium through the insulation-lined inner duct of two concentric ducts, exposure of pressure surfaces to the very-high-temperature reactor-outlet helium can be prevented. But even if the reactor vessel is swept by the reactor-inlet helium, failure by creep mechanisms is still of primary concern for an MGR-GT reactor vessel. The creep-failure criteria of Case N-47 of the ASME Boiler and Pressure Vessel Code may then be applied to estimate limits that would be imposed by a design code for very-high-temperature materials used for the MGR-GT reactor vessel. IN-617 is the most promising metal for use as a basis of a very-high-temperature design code because of its high strength at elevated temperatures, good workability, and because it is relatively well understood as compared to other candidate very-high-temperature metals. Other candidate materials are Hasteloy X and Alloy 800H [R3]. If the data of Fig. 3.4 were to be translated into a set of limits using the criteria of Code Case N-47, the limits for the time-dependent stress-intensity limit, S_t, listed in Table 3.1 would result. At the long lifetimes for which these limits are being evaluated, S_t is more limiting than the temperature-dependent stress intensity limit, S_m. Therefore, the limits of Table 3.1 will be used in the next section to estimate the advantages IN-617 might have in the design of the MGR-GT pressure vessel over the materials presently covered in Case N-47 of the ASME Boiler and Pressure Vessel Code.

Table 3.1

S_t Limits for IN-617

t = 300,000 hrs

temperature F, (C)	S_t ksi, (MPa)
1150, (621)	14.5, (100)
1200, (649)	13.1, (90)
1250, (677)	10.4, (72)
1300, (704)	8.3, (57)
1350, (732)	7.0, (48)
1400, (760)	5.5, (38)
1450, (788)	4.6, (32)
1500, (816)	3.5, (24)
1550, (844)	2.5, (17)
1600, (872)	1.7, (12)

based on creep-rupture data of ref. 51 and criteria of ASME Boiler and Pressure Vessel Code, Case N-47.

3.2 Pressure Vessel Design.

It is the intent of this section to identify the possible flowpaths and operating temperatures and pressures of the plant such that the pressure vessel can be designed within current ASME design codes. For the simple side-by-side vessel arrangement of Fig. 3.6, coaxial ducts are used for the flows to and from the reactor. The inner duct contains the high-temperature helium from the reactor. The low-temperature helium flowing to the reactor is in the outer duct. It is also required that insulation not be used on the reactor pressure-vessel. This is because of the need to permit decay-heat to transfer to the environment through the pressure-vessel in the event of an accident where normal means of decay-heat removal are lost. Although the gas within the inner duct is at a temperature in excess of the design codes, a thermal barrier helps to maintain the temperature of the inner tube close to the temperature of the cooler gas in the outer tube. Also, during normal operation, the inner tube has only the core pressure drop across its surface. Hence, it normally experiences very low stress levels.

3.2.1 Pressure Vessel Thickness.

Pressure vessel thickness will be evaluated by Level A loading requirements as specified in the ASME Boiler and Pressure Vessel Code. The Level A requirements will be based upon normal operating temperatures and pressures for a design lifetime of 300,000 hours (280,000 hours is 40 years at 80% availability; however, the closest time specified in the code is 300,000 hours). The effects of accident transients will be considered in Chapter Seven. Since pressure-vessel cost is largely governed by thickness (thickness determines mass and

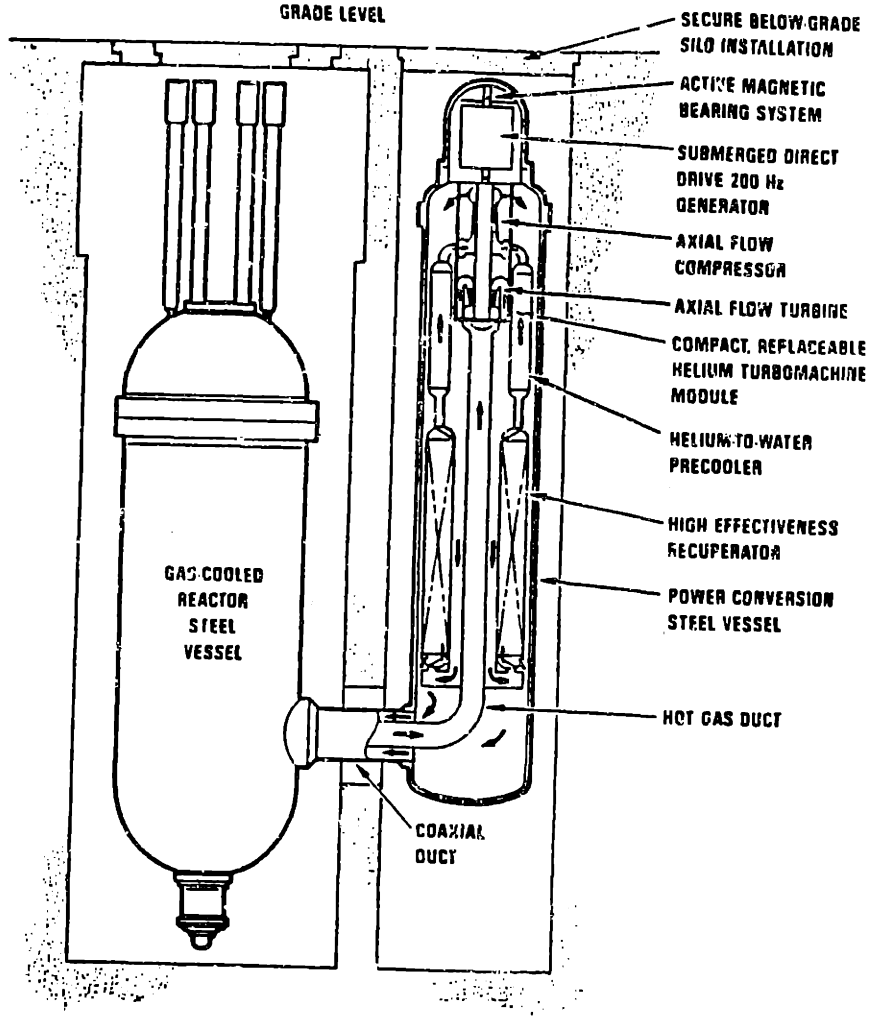

Figure 3.6. Simple side-by-side vessel arrangement for advanced Modular HTGR Gas Turbine (from M21).

difficulty of manufacture as well as workability and availability of the plate), vessel-wall thickness will be determined for evaluation of pressure-vessel designs. The vessel thickness will be less than one tenth the radius of the vessel. Accordingly, local and bending stresses will not be important in evaluating the vessel thickness; only average primary-membrane stresses will be evaluated.

The pressure-vessel thickness will be determined by maintaining stress intensity below S_{mt}, which is the lower of the time-dependent and time-independent stress-intensity limits for a given temperature. Because these limits are based upon ductile failure, maximum shear-stress theory is used for determining stress-intensity [A1]. Maximum shear-stress theory states that the maximum shear-stress at a point is equal to one half the largest algebraic difference between two primary-membrane stresses, tensile stresses being positive and compressive stresses being negative. The code requires that double the maximum shear-stress be less than the stress-intensity limit. For example:

$$S_{12} = \sigma_1 - \sigma_2 \tag{3.5}$$

$$S_{13} = \sigma_1 - \sigma_3 \tag{3.6}$$

$$S_{23} = \sigma_2 - \sigma_3 \tag{3.7}$$

The stress intensity, S, equals twice the maximum shear-stress, and is the largest absolute value of S_{12}, S_{13} and S_{23}.

For this case, the three primary-membrane stresses are circumferential stress, longitudinal stress and radial stress. Neglecting the effect of weight as small, the average primary-membrane stresses can be determined from the thin-walled-pressure-vessel stress equations.

$$\sigma_c = \frac{P\,R}{t} \qquad (3.8)$$

$$\sigma_l = \frac{P\,R}{2\,t} \qquad (3.9)$$

$$\sigma_r \cong -\frac{P}{2} \qquad (3.10)$$

Therefore

$$S_{cl} = \frac{P\,R}{2\,t} \qquad (3.11)$$

$$S_{cr} = P\left[\frac{R}{t} + \frac{1}{2}\right] \cong \frac{P\,R}{t} \qquad (3.12)$$

$$S_{lr} = P\left[\frac{R}{2t} + \frac{1}{2}\right] \cong \frac{P\,R}{2\,t} \qquad (3.13)$$

S_{cr} is clearly the largest of the three stress intensities. Therefore, S_{cr} must be maintained less than S_{mt} in accordance with the pressure-vessel-design code.

Required vessel thickness may be determined by using the above equations and the stress-intensity limits given in the ASME pressure-vessel code. Alloy 800H and 316 stainless steel were selected as candidate pressure-vessel materials because of their exhibited strength in the temperature range of interest. Alloy 800H exhibits a strength advantage over 316 stainless steel; however, 316 stainless steel is more available than alloy 800H. 304 stainless steel has strength and temperature dependence similar to 316 stainless steel. Figures 3.7 and 3.8 show minimum pressure-vessel thickness as a function of pressure-vessel temperature and pressure for standard MGR pressure vessels of 5.90 meters inner diameter. Since these materials are limited by manufacturing considerations to plate thicknesses of three inches or less [M22], it is impossible to construct an MGR pressure vessel for reasonable pressure levels at these high pressure-vessel temperatures. Even if a vessel of these thicknesses could be manufactured, the cost would probably be prohibitive. If an advanced material like IN-617 is used, the pressure-vessel is still

too thick (see Fig. 3.9). IN-617 has a temperature advantage over the stainless steels and alloy 800H, but does not have a strength advantage over them. Like stainless steel and alloy 800H, IN-617 is not available in plate thicknesses greater than three inches. In a very advanced, future plant, new high-temperature materials may permit the configuration of Fig. 3.6; however, current pressure-vessel materials do not.

3.2.2 The MGR-GT Reactor Pressure Vessel.

The proposed solution to this dilemma is to sweep the inside of the reactor pressure vessel with gas from the compressor discharge, as in Fig. 3.10. Compressor-discharge-gas temperature is in the range of 130-160°C for anticipated MGR-GT design parameters. Although a somewhat complicated flowpath with possibly higher pressure losses results from this arrangement, the advantages of such an arrangement are that the pressure vessel can be designed within the limitations of Section 3, Division 1 of the ASME Boiler and Pressure Vessel Code. Low-alloy steels that offer greater strength at these low temperatures than the more expensive high-temperature alloys can thereby be used. The material chosen for the MGR-GT pressure vessel is SA-533 low-alloy steel. This is the same material used in current MGR-concept designs [R4]. At these low temperatures, time-dependent effects are unimportant and the temperature-dependent stress-intensity limit, S_m, is the only stress-intensity limit that need be applied. Reference A1 specifies a stress-intensity limit of S_m= 26.7 ksi for class 1 components manufactured of SA-533 at the temperature of interest. Figure 3.11 shows the reactor-pressure-vessel thickness for different plant pressures. For a compressor-discharge pressure of 8-MPa, an MGR

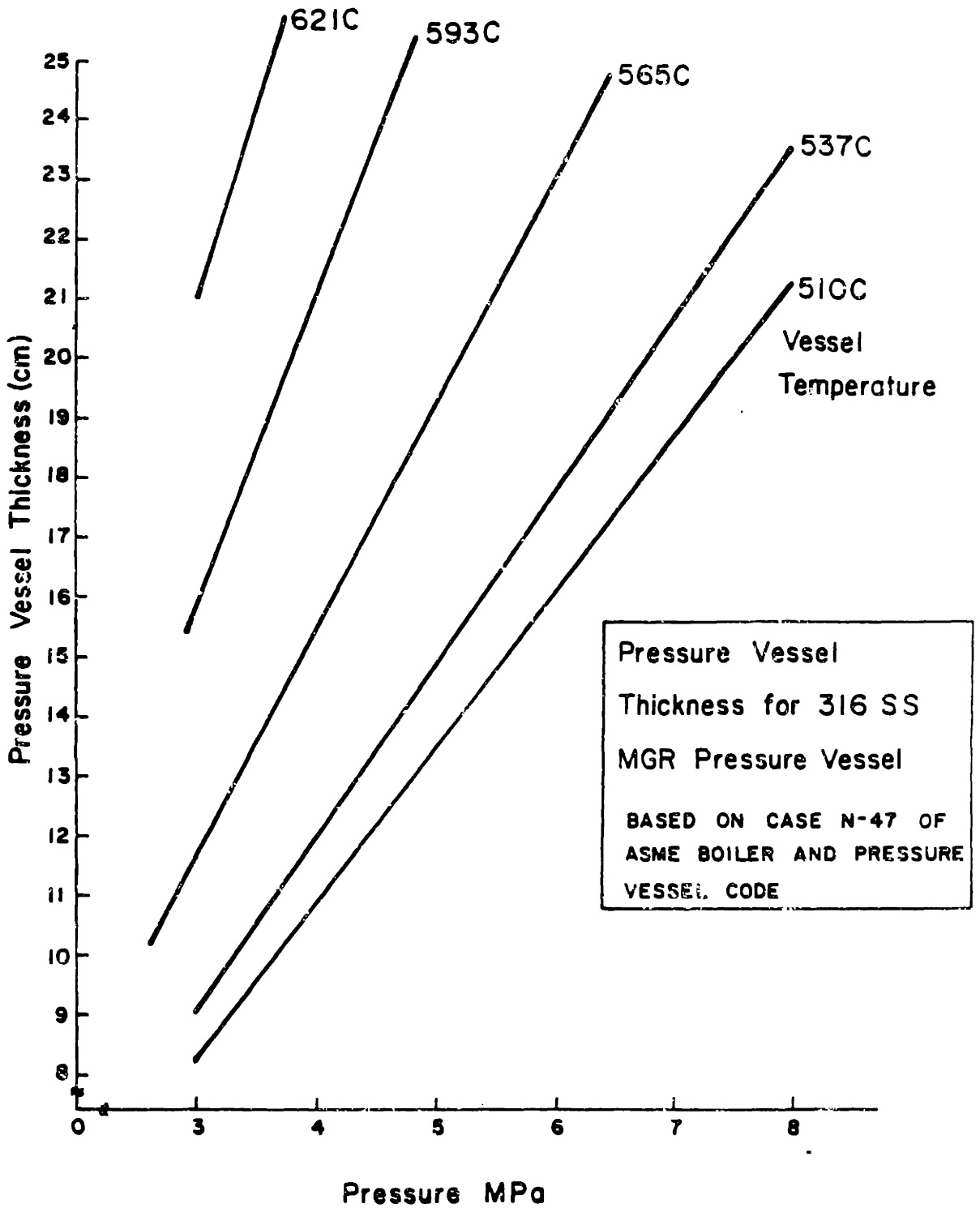

Figure 3.7. Minimum MGR reactor-vessel thickness for simple side-by-side vessels made of 316 stainless steel.

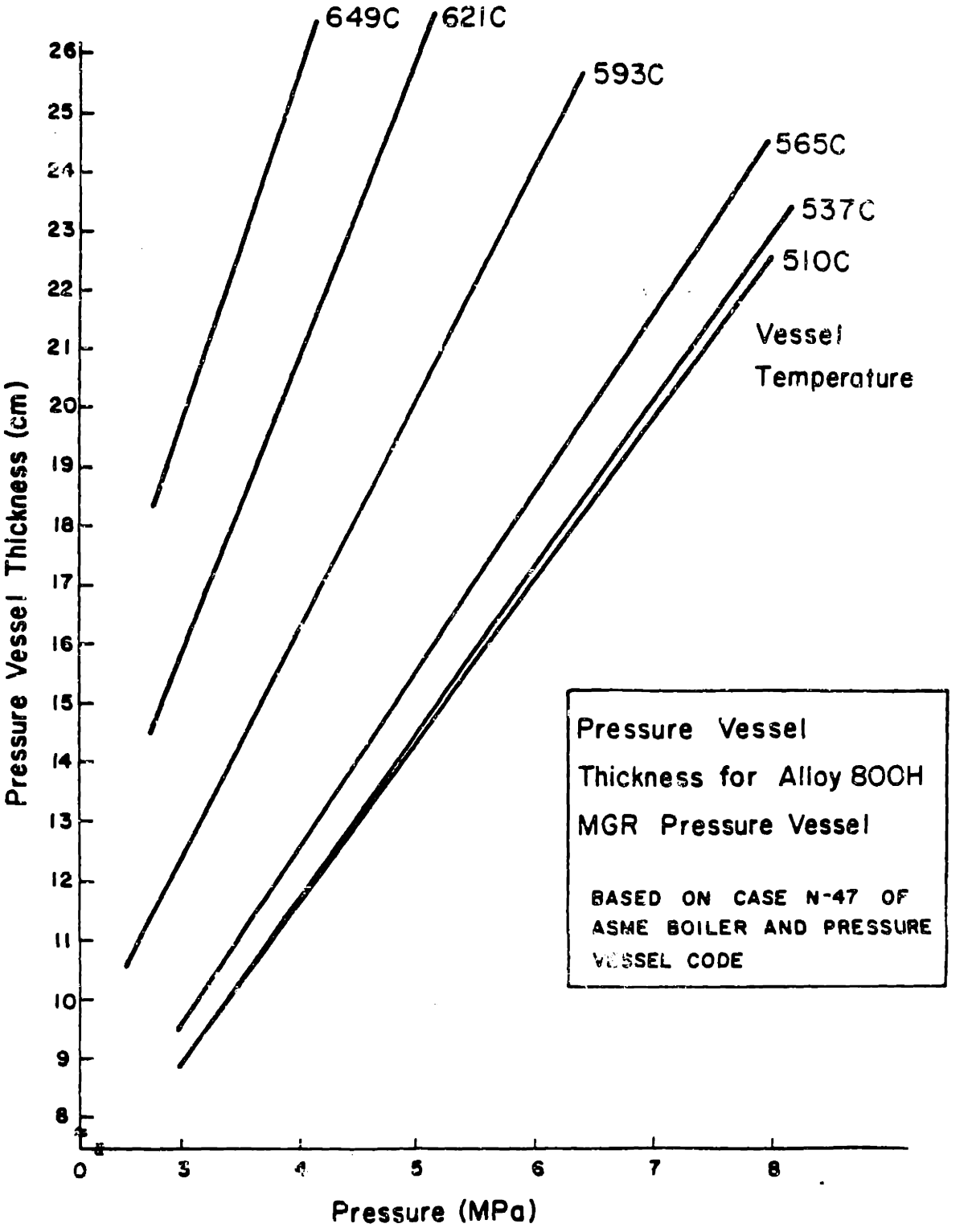

Figure 3.8. Minimum MGR reactor-vessel thickness for simple side-by-side vessels made of Alloy 800H.

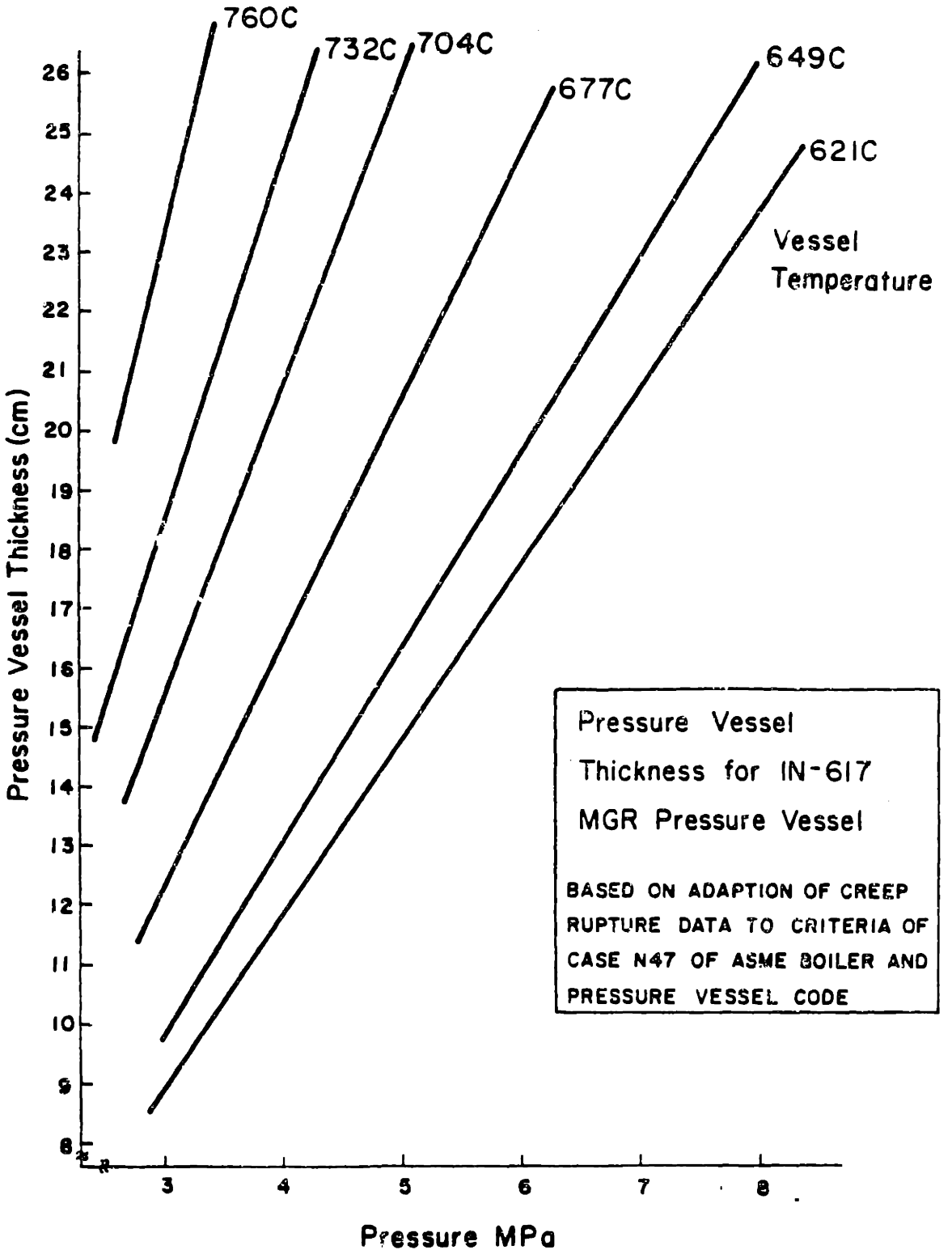

Figure 3.9. Estimated minimum MGR reactor-vessel thickness for simple side-by-side vessels made of IN-617. IN-617 creep-rupture data of ref. S1 was adapted to criteria of Case N-47 of ASME Boiler and Pressure Vessel Code.

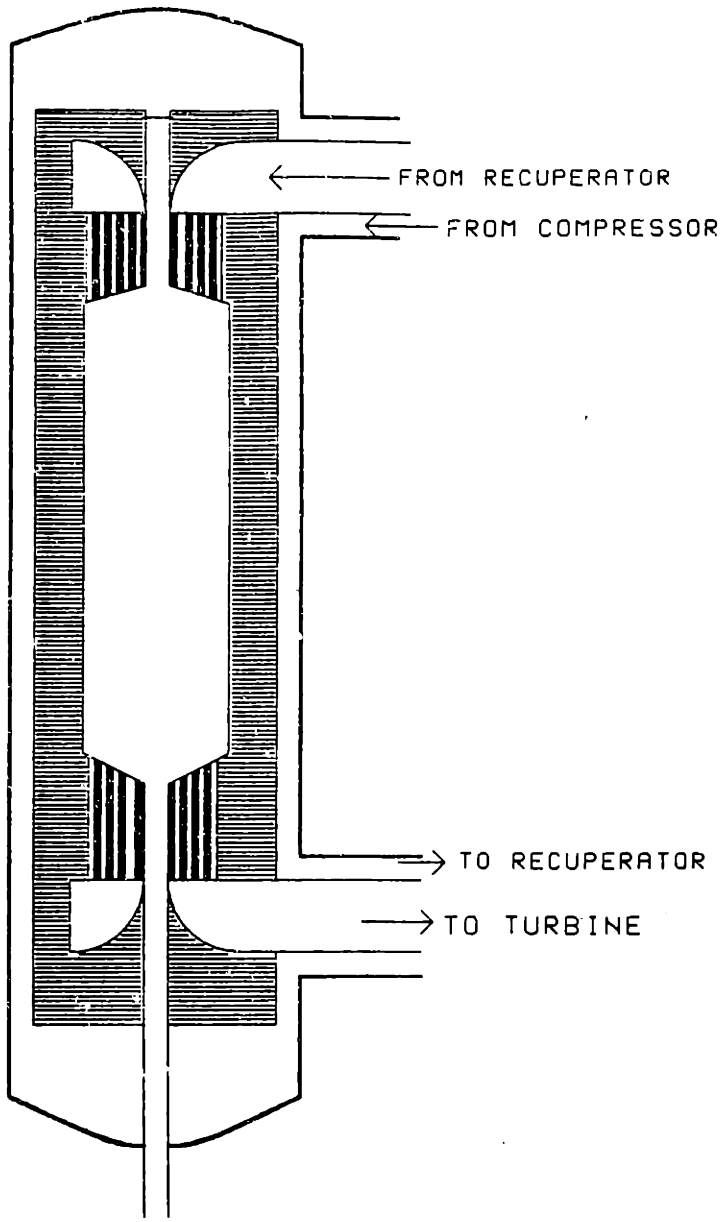

Figure 3.10. MGR-GT reactor-vessel flowpath with compressor-discharge gas sweeping the reactor-vessel wall.

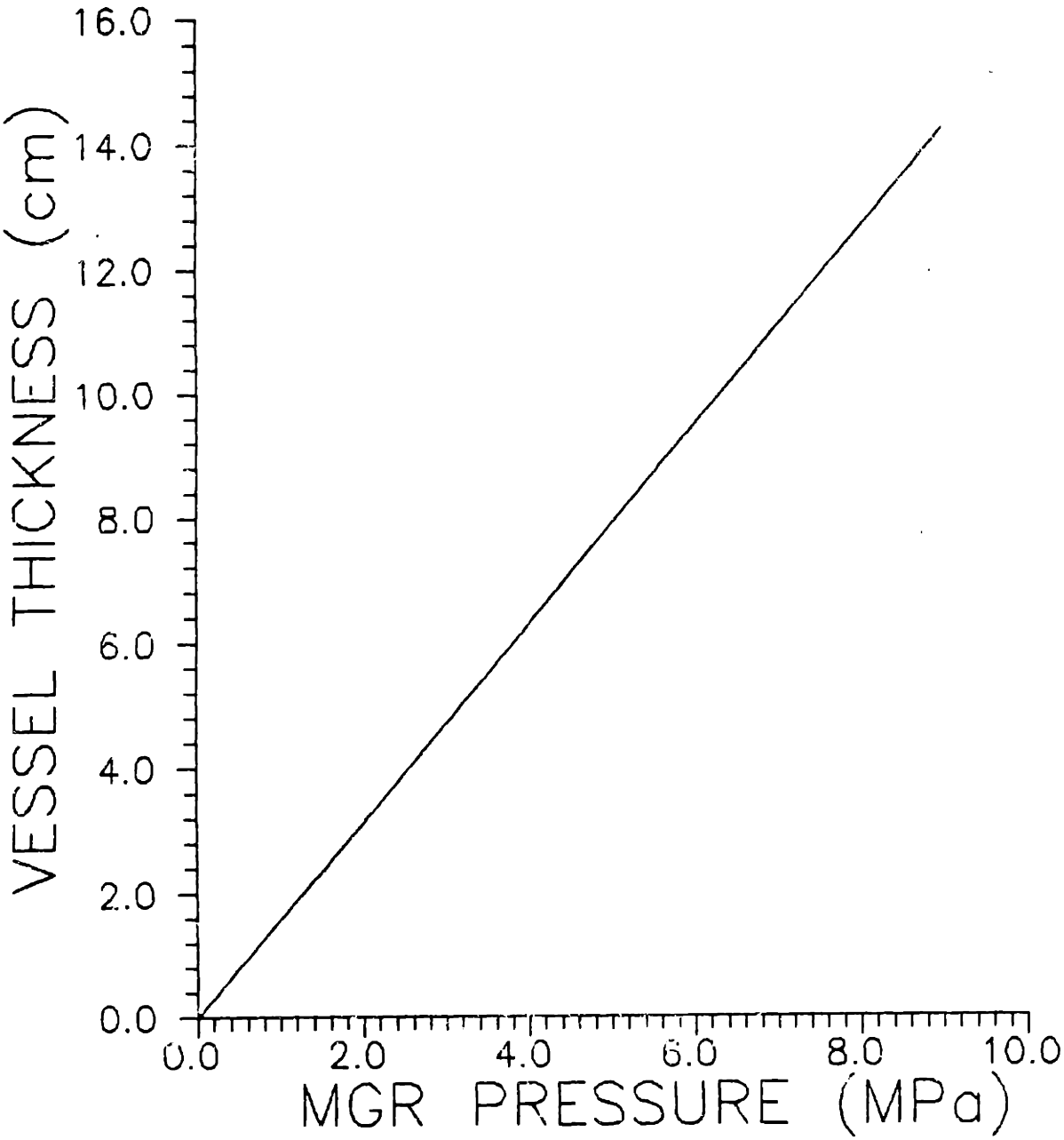

Figure 3.11. Minimum MGR reactor-vessel thickness for vessel swept with compressor-discharge gas. Vessel material is SA-533 low-alloy steel.

reactor-vessel thickness of about five inches is required. Vessels as thick as eight inches are commonly constructed from SA-533 [C5]. In this way, it is possible to construct a pressure vessel of conventional materials and still operate with system parameters that permit high performance.

3.3 The Heat Source.

The nuclear reactor that will be used to power the MGR-GT will be selected from the MGR designs presently available. There are essentially two types, categorized by fuel type: prismatic, and pebble-bed. These will be briefly described below.

3.3.1 The Prismatic Core.

The prismatic-core-MGR concept designs are capable of either 250-MWth or 350-MWth [I1]. The active-core region of the 250-MWth prismatic core is composed of prismatic-fuel elements arranged in a cylinder no greater than 3 meters in diameter. Graphite reflector surrounds the core. Because of the small size of the core, the control rods may be located in the reflector. The 350-MWth version has an active-core region composed of prismatic-type fuel elements arranged in an annulus. The reactor is controlled with 30 control rods located in the active-core region. Graphite reflector is within, and around the periphery of the annular, active-core region. The use of prismatic fuel requires that the reactor be shutdown for refueling. Figure 3.12 shows a cross section of the annular-prismatic core for the DOE reference plant.

3.3.2 The Pebble-Bed Reactor.

The pebble-bed MGR has an active core region consisting of

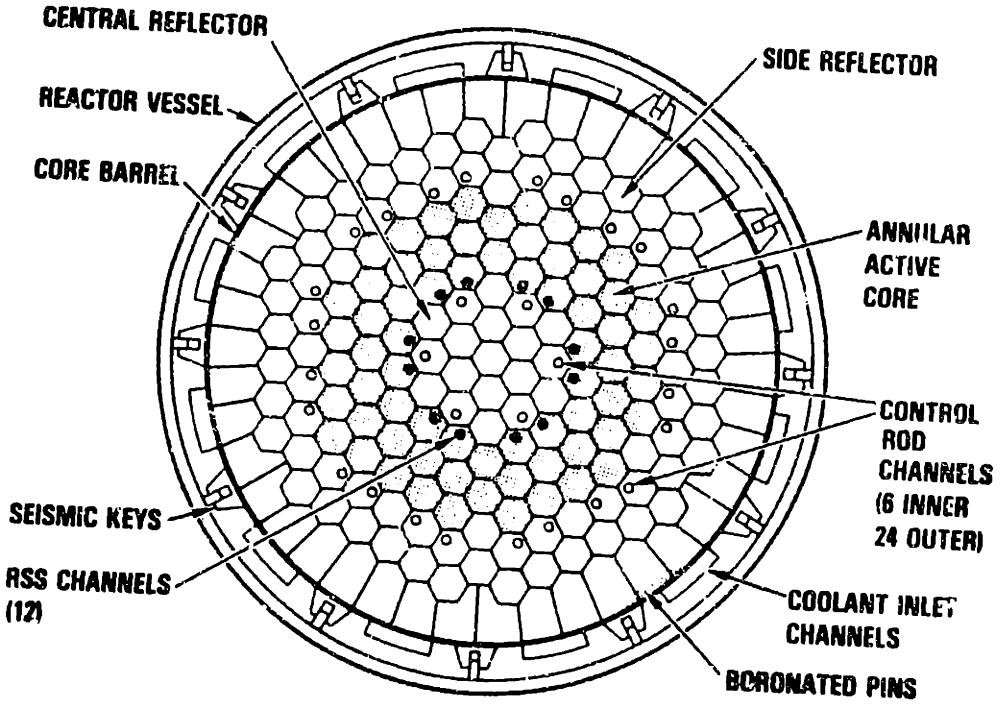

Figure 3.12. Cross section of the annular-prismatic MGR reactor core (from D5).

thousands of 6 cm diameter fuel pebbles contained within an annular-graphite reflector [F5]. The pebble-type fuel elements are continuously cycled through the core. A fuel burnup machine determines if a removed pebble should be returned to the core. Pebble-type fuel elements that are not expended, are returned to the reactor. The remaining pebble-type elements are disposed of. As fuel elements are disposed of, new pebble-type fuel elements are added to the core to replace the old fuel elements. On-line refueling permits a very low amount of excess reactivity to remain in the core. The low excess reactivity permits the reactor to be controlled with only six control rods located in the reflector. For cold shutdowns, eighteen channels located in the side reflector can be filled with boronated spheres [R5]. The diameter of the active-core region is limited to a maximum of 3 meters. A diameter larger than this would require that control rods be driven into the active core.

3.3.3 The MGR-GT Reactor Core.

The selection of reactor type for the MGR-GT will partly be determined by a consideration of the effects of the higher pressure drop of the pebble-bed core, and the loss in availability from refueling the prismatic core, on the economics of plant operations. The higher pressure drop across the pebble-bed-reactor core is a major concern for the MGR-GT because the pressure drop has such a strong effect in degrading the performance of the gas-turbine cycle. Section 3.3.3a will discuss pebble-bed core pressure drop in more detail.

Also of great importance in the determination of the preferred reactor type, is the gas flowpath for the MGR-GT, as this determines the feasibility of the design. As stated in Section 3.2.2, the

limitations of the pressure-vessel design make it necessary to route the helium through the plant differently than in the proposed MGR-SC designs. Figure 3.10 shows the proposed flowpath for the MGR-GT reactor vessel of a pebble-bed reactor. This arrangement makes the pebble-type fuel appear more attractive because the control rods of the prismatic core may interfere with the helium flowpath. Because the pebble-bed reactor requires fewer control rods, the helium ducting can be designed such that control-rod interference with the helium flow is avoided. A flowpath that might work for either the pebble-bed or prismatic core MGR-GT is shown in Fig. 3.13. There are two difficulties with this flowpath. One problem is that the control rods of the annular-prismatic core create a path for helium gas leakage that would cause the recuperator to be bypassed by part of the flow. The other problem is that this flowpath could require that more complex ducting be used, or the reactor vessel be significantly lengthened to accomodate the gas-turbine-plant equipment.

Finally, passive safety is a key feature of the MGR-concept designs. It is essential, therefore, that the MGR-GT be passively safe, even at the elevated operating temperatures that are anticipated. As will be discussed in Chapter Seven, Izenson [I3] found that a 200-MWth MGR, operating at core inlet and outlet temperatures representative of anticipated MGR-GT temperatures, maintained peak core temperatures below 1600^{o}C during a depressurized cooldown. Additionally, operations of the pebble-bed type AVR reactor have proven the pebble-bed reactor's ability to shut itself down in the event of an accident, even without inserting the control rods.

Considering the first-of-its-kind nature of this plant, it is

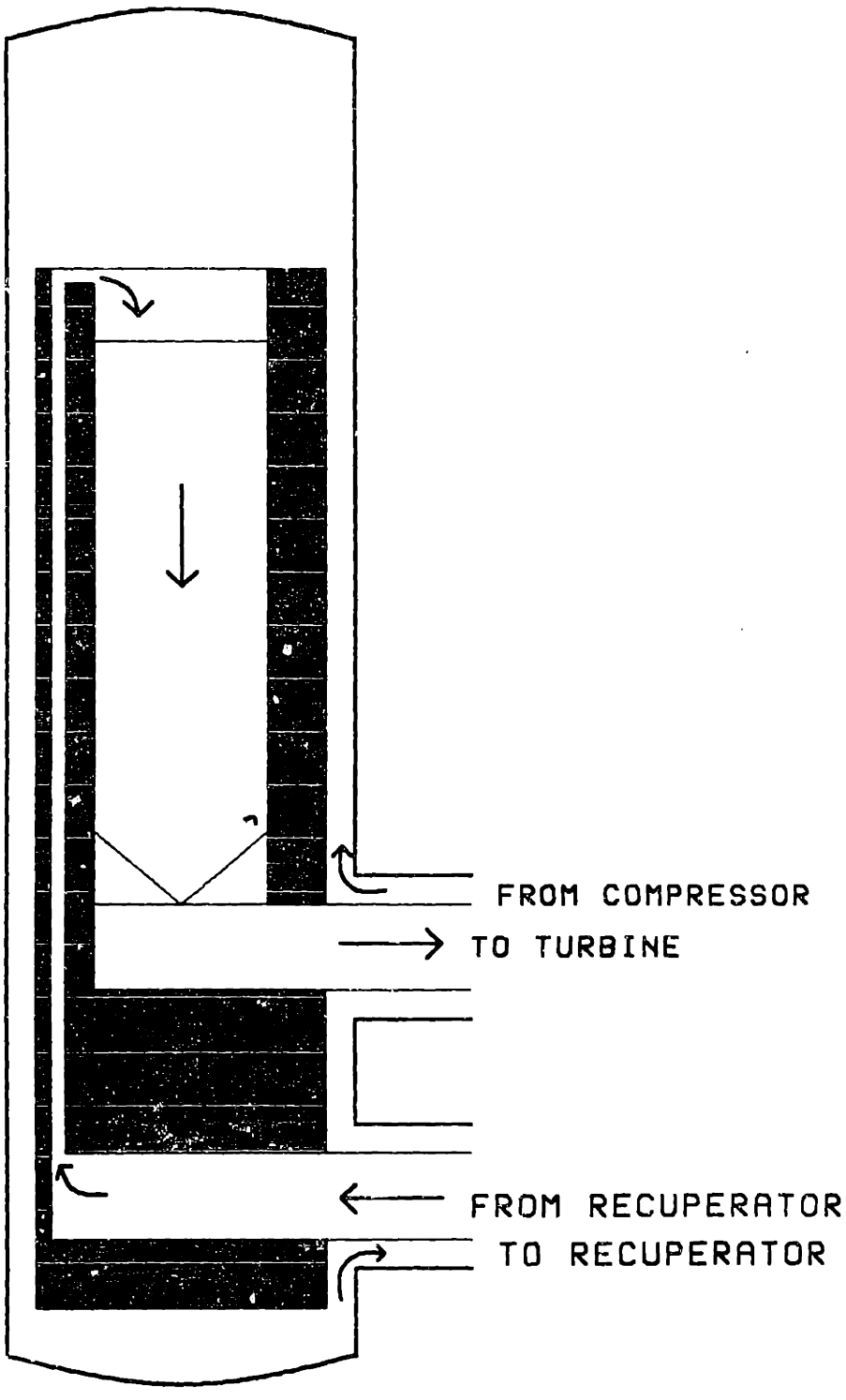

Figure 3.13. Flowpath for prismatic or pebble-bed reactor core. The distance between the two concentric ducts is determined by the plant configuration.

wise to use the technology that is most proven and has the lowest potential for error. The abundance of information available on the pebble-bed reactor made it the prefered type of MGR reactor for this study. Additionally, the flowpath for the pebble-bed core is more attractive than the flowpath for the prismatic cores. No flowpath has been determined that permits the use of the annular-prismatic core. Additionally, the 200-MWth pebble-bed core has been proven to maintain core temperatures sufficiently low to achieve passive safety, and has also demonstrated a passive-shutdown capability. For these reasons, a 200-MWt pebble-bed reactor has been chosen for the MGR-GT heat source.

The principal advantages of the pebble-bed reactor are summarized below.

- On line refueling.
- Demonstrated passive-shutdown capability.
- Permits flowpath which maintains a low reactor-vessel temperature.
- Passive-safety (ie. decay-heat removal) at gas-turbine plant temperatures.

3.3.3a Pebble-Bed Core Pressure Drop.

The primary disadvantage of the pebble-bed reactor core is its high pressure drop. The pressure drop across the prismatic MGR core is about one-fifth that of the pebble-bed MGR core. The pebble-bed MGR core pressure drop is equal to [V3]:

$$\Delta P = \Psi \frac{\rho v^2}{2 d_h} =$$

$$\frac{9}{8}\left[133.3 + 3.663\ Re^{0.905}\right] \frac{(1-\phi)^2}{\phi^3} \frac{\mu H \bar{G}}{\rho d_k^2} \qquad (3.14)$$

where $$Re = \frac{G d_h}{\mu} = \frac{2}{3}\left[\frac{1}{1-\phi}\right]\left[\frac{\bar{G} d_k}{\mu}\right] \qquad (3.15)$$

and the parameters involved are defined in the nomenclature section that concludes this chapter.

Figure 3.14 shows how $\frac{\Delta P}{P}$ of a 200-MWth pebble-bed-MGR core operating with a reactor-inlet temperature of 600°C and a reactor-outlet temperature of 850°C varies with system pressure. These temperatures are close to those expected for the MGR-GT. The figure shows that $\frac{\Delta P}{P}$ drops rapidly as system pressure is increased. The only term in Eq. 3.12 that is affected by a change in pressure alone is density, ρ, which is directly proportional to pressure. Thus, $\frac{\Delta P}{P}$ behaves as $\left[\frac{1}{P}\right]^2$ when all other parameters are held constant. As discussed in Chapter Two, operating at a high system pressure reduces the pressure drop, making it possible to achieve much higher efficiencies than if system pressure were kept low. The flowpath that is proposed permits construction of a pressure vessel that allows operation of the plant at system pressures much higher than otherwise permitted. In this way, the pressure-drop penalty incurred by using the pebble-bed core can be reduced.

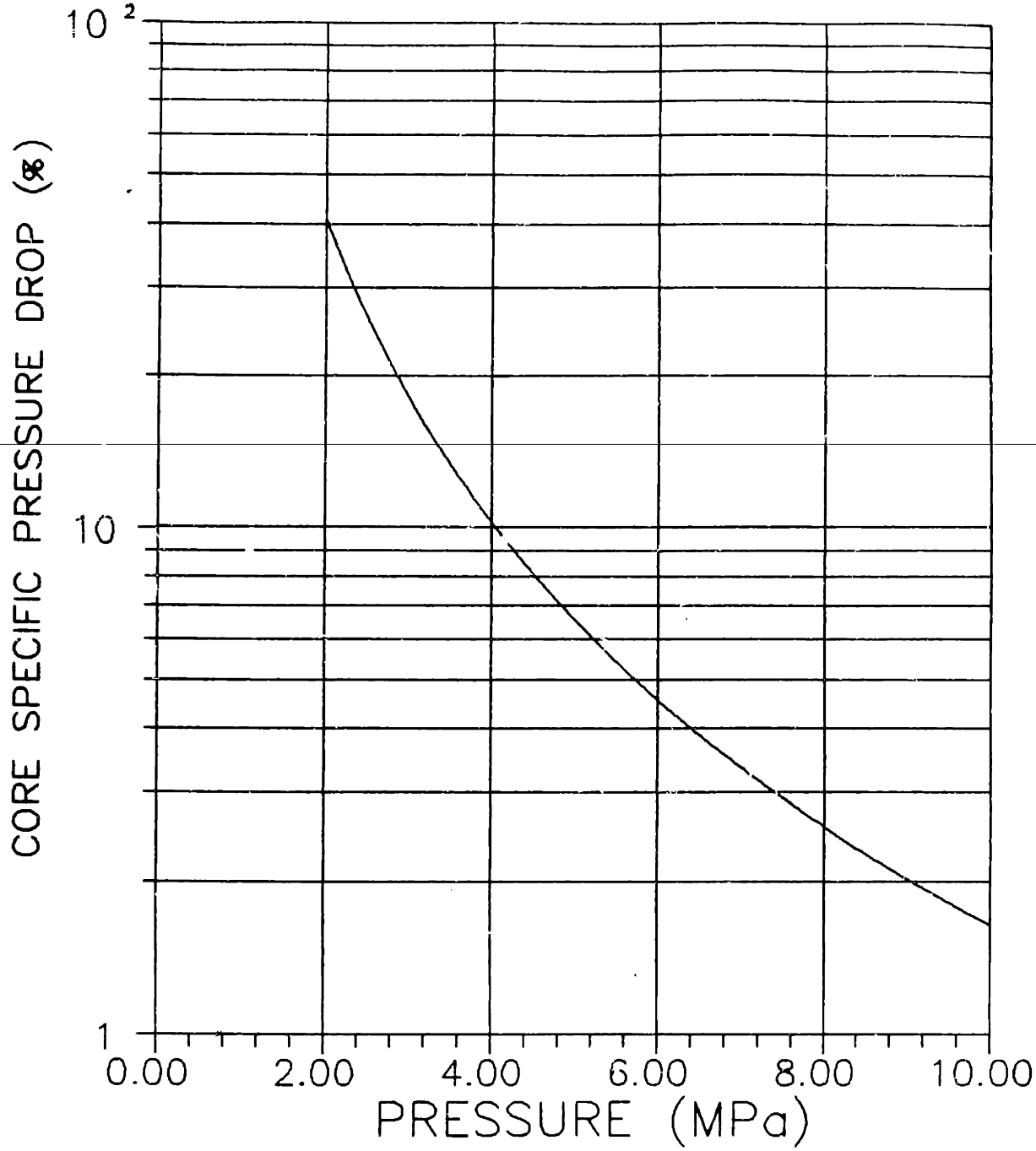

Figure 3.14. **Specific pressure drop across a 200-MWth pebble-bed MGR core as a function of plant pressure. Reactor-inlet temperature of 600 C, reactor-outlet temperature of 850 C, pebble-bed height of 9.43 meters, and core diameter of 3 meters.**

Nomenclature for Chapter Three

Symbol	Meaning	Units
B	Strain-recovery/strain-hardening equilibration constant	m^{-2}
C	Constant for P_{LM} equation	
d_h	Hydraulic diameter	m
d_k	Fuel-pebble diameter	m
D_o	Reference-state self-diffusion coefficient	m^2/s
E	Modulus of Elasticity	Pa
ΔE_D	Activation energy of self diffusion	J/mole
G	Mass velocity (flow area basis)	kg/m^2s
$\bar{G}$	Average mass velocity (frontal area basis)	kg/m^2s
H	Pebble-bed core height	m
P	Pressure	Pa
ΔP	Pressure drop	Pa
P_{LM}	Larson-Miller Parameter	
R	Vessel inner radius	m
R	Boltzman constant / Avogadro's number (Ideal Gas Constant)	$J/mole^oK$
Re	Reynolds' number	
S	Stress intensity	Pa
S_T	Temperature-dependent stress-intensity limit	Pa

S_t	Time-dependent stress-intensity limit	Pa
t	Vessel thickness	m
t	Time	hours
T	Temperature	^oK, or ^oR
v	Gas velocity through core	m/s

Greek

ϵ	Deformation	
$\dot{\epsilon}$	Deformation rate or creep rate	s^{-1}
μ	Dynamic viscosity	Pa•sec.
ρ	Density	kg/m^3
σ	Stress	Pa
ϕ	Core-void volume fraction	
Ψ	Core-friction coefficient	

Subscripts

1, 2, 3	Orthogonal components
c	Circumferential
l	Longitudinal
r	Radial

CHAPTER FOUR

MACHINERY DESIGN

4.1 Machinery Design.

The machinery of the MGR-GT is composed of the turbomachinery, the turbine and compressor, and the electrical generator. What follows will be a discussion of turbomachine aerodynamic and mechanical design. Active-magnetic bearings will then be described. Next, generator design and background on frequency conversion methods will be discussed. Finally, a list of nomenclature used in this chapter can be found at the end of the chapter.

4.2 Turbomachine Aerodynamic Design.

A turbomachine is a machine that transforms the energy of a working fluid into power, and vice-versa, through a transfer of momentum between the working fluid and a row of rotating blades. Although there is a wide variety of turbomachinery types, the two types of turbomachines that will be specifically addressed here are axial compressors and axial turbines. However, much of the discussion of general turbomachine theory will be applicable to all types of turbomachinery.

A turbomachine may transform the energy of a working fluid into shaft power, or it may make use of shaft power to add to the energy of a working fluid. The former application is a turbine, and the latter application is a pump or compressor. The energy of the working fluid is the sum of the enthalpy and the kinetic energy of the fluid. The combination of these two energies is called the stagnation enthalpy.

$$h_o = h + \frac{C^2}{2} \tag{4.1}$$

For a perfect gas

$$C_p T_o = C_p T + \frac{C^2}{2} \tag{4.2}$$

Helium behaves very much like a perfect gas (see Chapter Two). Therefore, the perfect gas approximation will result in virtually no error in this analysis.

4.2.1 Euler's Pump/Turbine Equation.

Torque is equal to the rate of change of angular momemtum.

$$\bar{T} = m \frac{d}{dt}(rC_\theta) \tag{4.3}$$

Applying this to the control volume of Fig. 4.1, we get for two-dimensional steady flow

$$\bar{T} = \dot{m} (r_2 C_{\theta 2} - r_1 C_{\theta 1}) \tag{4.4}$$

For a pump or compressor operating at a rotational speed ω, the blading power consumed is equal to

$$\bar{T}\,\omega = \dot{m} (U_2 C_{\theta 2} - U_1 C_{\theta 1}), \tag{4.5}$$

or

$$\frac{\bar{P}}{\dot{m}} = (U_2 C_{\theta 2} - U_1 C_{\theta 1}) \tag{4.6}$$

This is known as Euler's pump equation. For a turbine, the power produced is simply the negative of the above expression, and is Euler's turbine equation.

$$\frac{\bar{P}}{\dot{m}} = (U_1 C_{\theta 1} - U_2 C_{\theta 2}) \tag{4.7}$$

This work is equal to the change in stagnation enthalpy of the working fluid. If the working fluid is a perfect gas,

$$C_p (T_{o1} - T_{o2}) = (U_1 C_{\theta 1} - U_2 C_{\theta 2}) \tag{4.8}$$

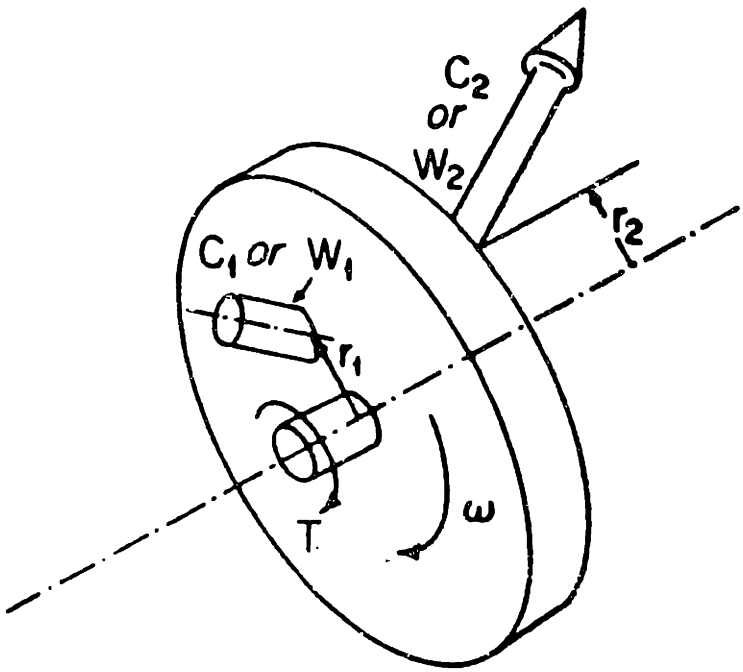

Figure 4.1. Control volume for a turbomachine rotor [from W1].

Euler's pump and turbine equation applies to all turbomachinery, regardless of whether or not the flow is compressible.

4.2.2 Velocity Triangles.

The velocity vectors specify the magnitude and direction of fluid flow at some diameter, often the mean diameter, of a turbomachine stage. The mean diameter is the diameter within which half of the mass flows. Or, to a close approximation,

$$D_m^2 - D_h^2 = D_t^2 - D_m^2 \qquad (4.9)$$

In preliminary design, mean radius of a stage is usually held constant as a simplifying assumption. This practice will be used in this analysis for the entire turbine. At the low pressure ratios used in the MGR-GT, constant-hub-diameter, constant-mean-diameter, and constant-tip-diameter turbomachine designs will be of similar size and performance.

Absolute and relative velocities are specified in a velocity triangle. Machine performance is governed by the fluid velocities. It is therefore essential that the designer carefully select the velocity triangles. Figure 4.2 shows the velocity triangles of an axial-turbine stage. All angles are measured with respect to the direction of axial flow.

For axial machines, several non-dimensional parameters have been developed that together characterize the velocity triangles. Certain assumptions and design constraints are applicable for these parameters. It is assumed that the axial machine is designed such that C_x is constant through the stage. Considering continuity, this means that

$$C_{x1} = C_{x2} = C_x \qquad (4.10)$$

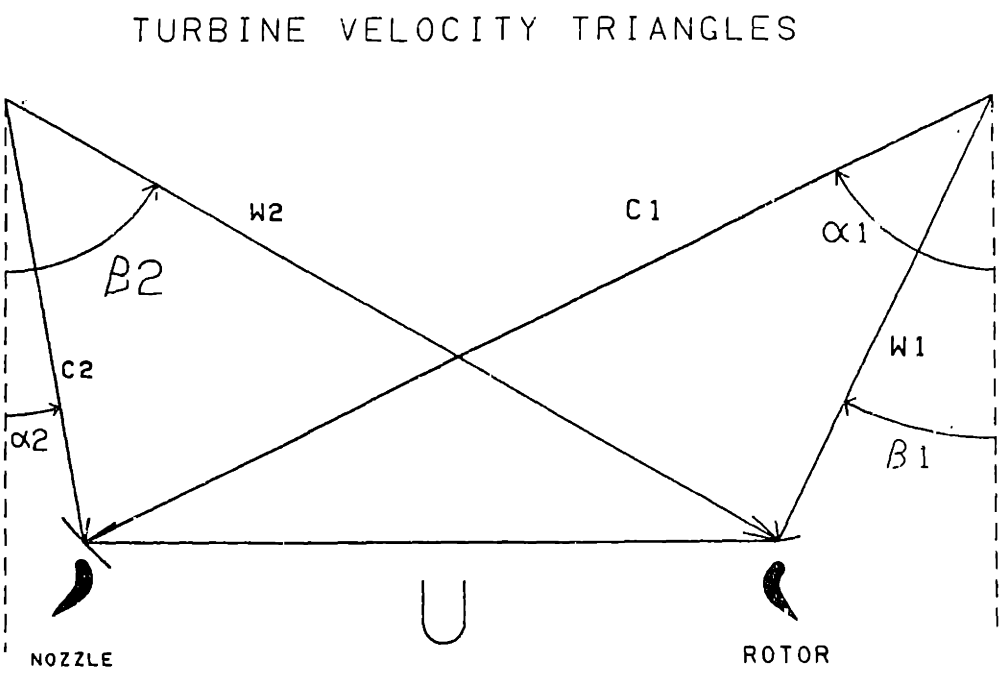

Figure 4.2. Velocity triangles of an axial-turbine stage.

and

$$\rho A = \text{constant.} \tag{4.11}$$

Therefore, turbine-stage flow area must increase, while the flow area of a compressor stage must decrease. Furthermore, it is approximated that the fluid streamlines maintain the same radial position through a stage in an axial-flow machine such that

$$r_1 = r_2 \tag{4.12}$$

and

$$U_1 = U_2 \tag{4.13}$$

4.2.2a Flow Coefficient.

Flow coefficient is defined as

$$\phi = \frac{C_x}{U} \tag{4.14}$$

4.2.2b Loading Coefficient.

The stage-loading coefficient is defined as

$$\psi = \frac{\Delta h_o}{U^2} \tag{4.15}$$

which equals

$$\psi = \frac{U_1 C_{\theta 1} - U_2 C_{\theta 2}}{U^2} \tag{4.16}$$

Since $U_1 = U_2 = U$

$$\psi = \frac{C_{\theta 1} - C_{\theta 2}}{U} = \frac{C_x(\tan \alpha_1 - \tan \alpha_2)}{U}$$

$$= \phi \left[\tan \alpha_1 - \tan \alpha_2\right] \tag{4.17}$$

For turbines, stage loading coefficients range from about 1.0 for lightly loaded stages, to over 1.5 for heavily loaded stages [W1]. For compressors, stage loading coefficients have a negative value, with magnitudes ranging from less than 0.3 (lightly loaded) to greater than 0.5 (heavily loaded) [W1].

4.2.2b.1 Determination of Stages from Loading Coefficient.

If a turbomachine is designed such that all stages have the same

stagnation-enthalpy change, it is possible to determine the number of stages from the stage loading coefficient and the mean blade speed. If n equals the number of stages,

$$\left[\Delta h_o\right]_{total} = n\,\psi\,U^2 \qquad (4.18)$$

In helium turbomachines, blade velocity is only limited by centrifugal stresses because the very high sonic velocities eliminate concern for Mach-number limitations. If blade speed and the loading coefficient are known, the number of stages can be determined with the above equation.

4.2.2c Reaction.

Stage reaction coefficient is defined as

$$Rn = \left[\frac{\Delta h}{\Delta h_o}\right]_{rotor} \qquad (4.19)$$

Since

$$\Delta h = \Delta h_o + \frac{C_1^2}{2} - \frac{C_2^2}{2} \qquad (4.20)$$

and

$$C_1^2 = C_x^2 + C_{\theta 1}^2 \qquad (4.21)$$
$$C_2^2 = C_x^2 + C_{\theta 2}^2$$

it can be shown that

$$Rn = 1 - \frac{C_{\theta 1} + C_{\theta 2}}{2U} \qquad (4.22)$$

or

$$Rn = 1 - \frac{C_x(\tan \alpha_1 + \tan \alpha_2)}{2\,U}$$
$$= 1 - \frac{\phi\,(\tan \alpha_1 + \tan \alpha_2)}{2} \qquad (4.23)$$

For gas turbines, it is quite common to use a stage reaction of 0.5 or less at the mean diameter. For compressors, mean-diameter stage reaction is normally 0.5 or greater, and as high as 1.2. The camber line of a low-reaction blade has a pronounced curvature, while the

camber line of a high-reaction blade has little curvature. In any case, for both turbines and compressors, stage reaction is always kept greater than or equal to zero at all radial locations. A negative reaction will cause static enthalpy across the rotor to change in a direction opposite the stagnation enthalpy change. Significant losses could result. Often, stage reaction is defined in a similar way as above, except that pressures are substituted for enthalpies. This is commonly done because pressure will behave much as enthalpy across a rotor. For example, a zero reaction turbine (or, impulse turbine) has zero static-pressure change across the rotor. Therefore, if reaction across a turbine stage is negative, the flow is against a positive static-pressure gradient, causing the potential for boundary layer separation. If reaction is too low in a compressor, separation will result from excessive turning of the flow.

The velocity triangles for the MGR-GT will be selected with the goal of high efficiency in mind. Figure 4.3 shows lines of constant efficiency plotted against flow coefficient and load coefficient for 50% reaction (at the mean diameter) turbines. It was assembled by plotting the reported performace data for a large number of turbines. Figure 4.3 can be used as a guide for turbine velocity-triangle selection. Compressors are generally designed for 50% reaction in the United States and Great Britain, and for 100% or more in continental Europe [W1]. 50% reaction turbomachines generally have the highest peak-design efficiency [H1, H11, W1]; however, high-reaction compressors normally have a broad operating band for peak efficiency and permit easier starting of high pressure-ratio machines [K17, W1]. Because the MGR-GT will have a fairly narrow operating band and a low

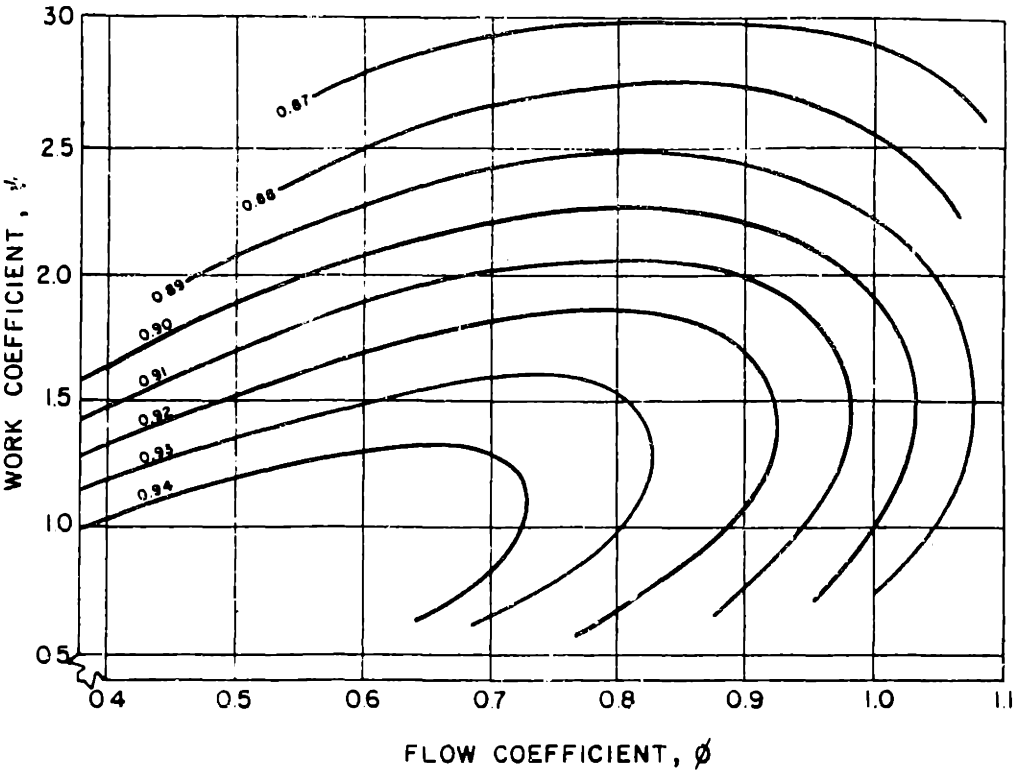

Figure 4.3. Constant efficiency lines plotted against flow coefficient and load coefficient for 50% reaction turbines [from W1].

pressure ratio, 50% reaction (at the mean diameter) blading will be used for both turbine and compressor.

4.2.4 The Three Dimensional Velocity Field.

The curvature of the tangential components of fluid velocity within a turbomachine generates a radial pressure gradient. In most cases, this radial pressure gradient is moderate. In such cases it is desirable to design the turbine stages such that constant work is performed across the stage at every radial location. If the governing equations for this case are solved with the assumptions that

$$\frac{\partial h_o}{\partial r} = 0$$

$$\frac{\partial s_{st}}{\partial r} = 0$$

$$\frac{\partial p_o}{\partial r} = 0$$

and $C_r = 0$ at the entrance and exit of a blade row, what is commonly known as the Simple Radial Equilibrium (SRE) equation will result.

$$\frac{1}{r^2}\frac{\partial}{\partial r}\left[r^2 C_\theta^2\right] + \frac{\partial}{\partial r} C_x^2 = 0 \qquad (4.24)$$

One general solution of this equation is of the form [H1, W1]:

$$C_{\theta 1} = a' r^n - \frac{b'}{r} \qquad (4.25)$$

$$C_{\theta 2} = a' r^n + \frac{b'}{r} \qquad (4.26)$$

with n=an integer

A commonly used solution of the SRE is for a constant C_x at all radial locations. In this case, the solution is a free vortex.

$$C_\theta \, r = \text{constant} \qquad (4.27)$$

This solution of the SRE is most often used for the velocity field of a turbine. For a compressor, a free vortex flow will often make it difficult to avoid excessive diffusion and losses at the hub. One velocity distribution commmonly used in compressors is [H1]:

$$C_{\theta 1} = a' - \frac{b'}{r} \tag{4.28}$$

$$C_{\theta 2} = a' + \frac{b'}{r} \tag{4.29}$$

$$Rn = 1 - \frac{a'}{U} \tag{4.30}$$

This velocity distribution results in a slightly increasing reaction over the length of the blade. In this study, free-vortex flow was assumed in the turbine, and Eqs. 4.28 through 4.30 characterized the compressor velocities.

4.2.5 Turbine Design:

Once the velocity triangles are selected, the blade heights can be determined by application of conservation-of-mass to calculate annulus areas and hub-to-tip diameter ratios of the stages. Hub-to-tip diameter ratios should be roughly between 0.7 and 0.9 for most industrial axial-flow turbomachines [W1]. For hub-to-tip ratios below 0.7, it is usually difficult to design for satisfactory velocity triangles at the hub. The upper limit is to minimize boundary-layer and tip-leakage effects.

Next, it is necessary to select the number of blades. The number of blades will determine the length of the machine and is therefore governed by size limits and critical speed limits. Many blades per stage will result in a short machine, as in aircraft applications, and few blades will result in a large machine, as in industrial applications.

Zwiefel's rule suggests that a lift coefficient of 0.8 is optimum. However, current design practice is to consider a lift coefficient of close to 1.0 as optimum [W1]. For this case:
For rotors,

$$b = s\ |2.0\ \cos^2\beta_2[\tan\beta_1 - \tan\beta_2]| \tag{4.31}$$

For stators, substitute α_2 for β_1, and α_1 for β_2.

Figure 4.4 shows a turbine blade, and the characteristic blade parameters.

At low Mach numbers, throat (O) may be determined by the following [W1]:

For rotors:

$$|\beta_2| = \left[\frac{7}{6}\left[\left|\cos^{-1}\left[\frac{O}{s}\right]\right| - 10^{o}\right] + 4^{o}\left[\frac{s}{e}\right]\right] \qquad (4.32)$$

where: $$0.25 < \left[\frac{s}{e}\right] < 0.625$$

For stators, substitute α_1 for β_2.

It is possible to obtain a rough sketch of the blades at this point, keeping in mind that

$$\cos\lambda = \frac{b}{c} \qquad (4.33)$$

This procedure is usually iterated several times using different design values until the preferred design is selected. Considerations include: 1) desired machine efficiency, 2) desired machine size, and 3) results of vibration analysis.

4.2.6 Compressor Design.

Compressors are generally more restrictive in their design than turbines because the flow is moving in a direction of increasing pressure. The compressor must obey certain restrictions to prevent excessive boundary-layer separation and the resulting high losses. Most important of these restrictions is that the diffusion factor must be kept below a value of 0.5. This may be performed by maintaining the relative-velocity ratio above the limit,

$$\frac{W_2}{W_1} > 0.707 \qquad (4.34)$$

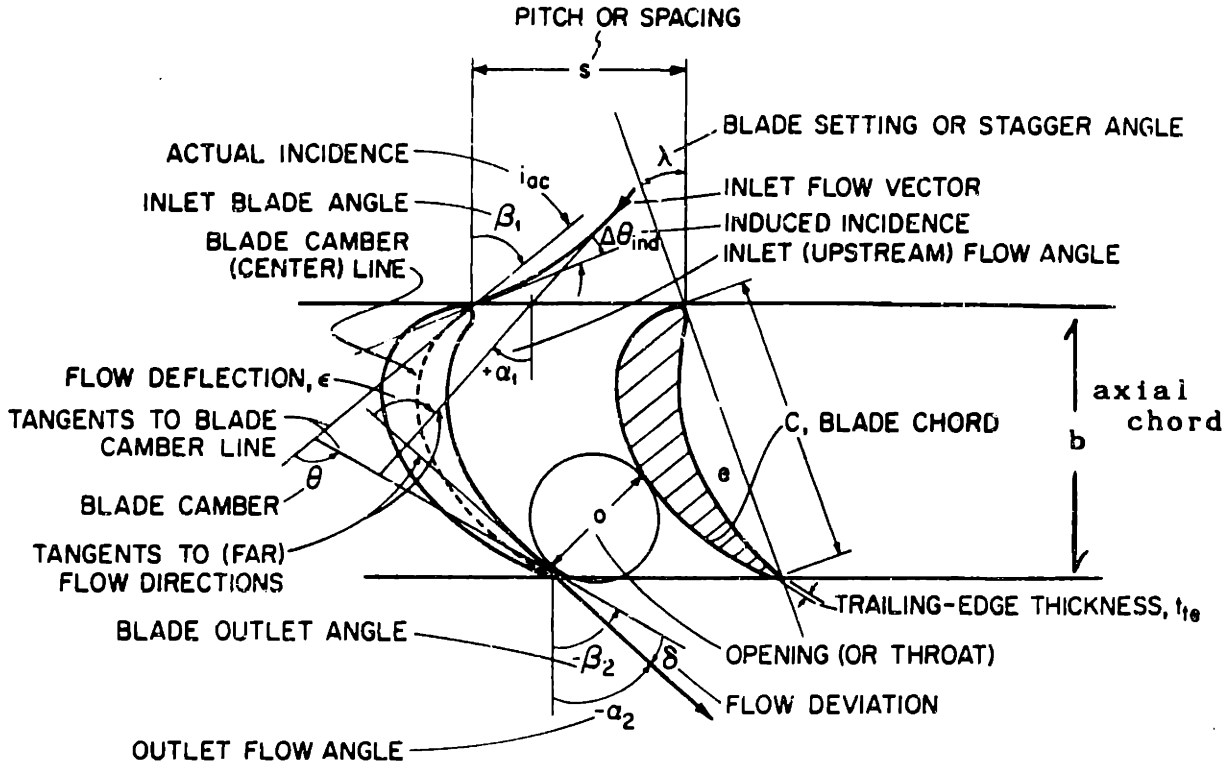

Figure 4.4. An axial-flow-turbine blade [from W1]. (Note that in this figure β is blade angle, not relative-flow angle. α is relative-flow angle in this figure.)

and $$\frac{C_1}{C_2} > 0.707 \qquad (4.35)$$

These numbers should be increased in dirty or corrosive systems [W1]. However, in a very clean system, such as a gas-cooled nuclear reactor, the limits of Eqs. 4.34 and 3.35 can be used with confidence.

For axial-flow compressors, blade heights are determined in the same manner as for turbines; however, the blade shapes are not normally designed, but are selected from blades for which cascade-test results are available. Blades were selected from the NACA-65 series for this study. The method is discussed in numerous references [H1, W1, among others]. Therefore, it will not be discussed here.

4.2.7 Turbomachine Efficiency.

Efficiency is one means of measuring the "goodness" of a design. A high-efficiency machine will achieve the desired result with less expenditure of energy than a low-efficiency machine. Therefore, it is always desirable to operate a machine at the maximum efficiency possible because the cost of saved shaft energy will greatly exceed the amortized cost of reasonable modifications to a design. There are, however, several definitions of efficiency that may be used in reference to a turbomachine, making efficiency a sometimes confusing measure of the "goodness" of a design. The efficiency definition to be used depends upon the application. The following briefly describes the important measures of turbomachine efficiency that are referred to in this dissertation.

4.2.7a Isentropic Efficiency.

Isentropic efficiency of a machine is the most common efficiency definition. It is the one that most engineers think of when the term efficiency is used to describe a machine. For a turbine, isentropic

efficiency is defined as the ratio of the actual expansion work to the expansion work that would occur between the same stagnation pressures in a reversible, adiabatic process.

$$\eta_t = \frac{h_{oin} - h_{oexh}}{h_{oin} - h_{oexh_s}} = \frac{T_{oin} - T_{oexh}}{T_{oin} - T_{oexh_s}} \qquad (4.36)$$

or

$$\eta_t = \frac{1 - \frac{T_{oexh}}{T_{oin}}}{1 - \left[\frac{P_{oexh}}{P_{oin}}\right]^{\left[\frac{R}{C_p}\right]}} \qquad (4.37)$$

For a compressor, the isentropic efficiency is equal to the reversible, adiabatic work necessary to compress the fluid between two stagnation pressures, divided by the actual work consumed in performing the compression. It can be shown to be equal to:

$$\eta_c = \frac{1 - \left[\frac{P_{oexh}}{P_{oin}}\right]^{\left[-\frac{R}{C_p}\right]}}{1 - \frac{T_{oexh}}{T_{oin}}} \qquad (4.38)$$

4.2.7b Polytropic Efficiency.

Because the isobars on an H-S diagram are curved, isentropic efficiency is a function of pressure ratio. It is, therefore, not proper to use isentropic efficiency as a measure of the merit of the aerodynamic design of a turbomachine, especially when comparing turbomachines designed for different pressure ratios. If it were possible to divide a turbine into an infinite number of stages, each stage having a pressure ratio very close to one, it would be possible to compare the stages of different turbines with an equal measure. The isentropic efficiency of such a turbine stage is

$$\eta_{pt} = \frac{\partial h}{\partial h_s} = \frac{C_p \partial T_o}{v \partial P_o} = \frac{C_p P \partial T_o}{R T_o \partial P_o} \qquad (4.39)$$

$$\frac{dT_o}{T_o} = \left[\frac{R\,\eta_{pt}}{C_p}\right] \frac{dP_o}{P_o} \tag{4.40}$$

For an entire turbine,

$$\left[\frac{T_{oexh}}{T_{oin}}\right] = \left[\frac{P_{oexh}}{P_{oin}}\right]^{\left[\frac{R\,\eta_{pt}}{C_p}\right]} \tag{4.41}$$

Combining this with Eq. 4.37, polytropic efficiency can be related to isentropic efficiency for a turbine.

$$\eta_t = \frac{1 - \left[\frac{P_{oexh}}{P_{oin}}\right]^{\left[\frac{\eta_{pt}\,R}{C_p}\right]}}{1 - \left[\frac{P_{oexh}}{P_{oin}}\right]^{\left[\frac{R}{C_p}\right]}} \tag{4.42}$$

Similarly, for a compressor:

$$\eta_c = \frac{\left[\frac{P_{oexh}}{P_{oin}}\right]^{\left[\frac{R}{C_p}\right]} - 1}{\left[\frac{P_{oexh}}{P_{oin}}\right]^{\left[\frac{R}{\eta_{pc} C_p}\right]} - 1} \tag{4.43}$$

It is possible to approximate the expansion process of a turbine or the compression process in a compressor by a polytropic process. For a turbine

$$\frac{T_{o2}}{T_{o1}} = \left[\frac{P_{o2}}{P_{o1}}\right]^{\left[\frac{R}{C_p}\right] \eta_{pt}} \tag{4.44}$$

For a compressor,

$$\frac{T_{o2}}{T_{o1}} = \left[\frac{P_{o2}}{P_{o1}}\right]^{\left[\frac{R}{C_p}\right] \frac{1}{\eta_{pc}}} \tag{4.45}$$

where 1 and 2 are two points along an adiabatic, polytropic expansion or compression process line.

4.2.7c Total-to-Total Efficiency.

When discussing the isentropic efficiency of a single stage that is not the last stage of a multistage turbomachine, the total-to-total efficiency is normally used. Total-to-total efficiency is simply equal to the isentropic efficiency across the stage.

For a turbine:

$$\eta_{tt,t} = \frac{h_{o1} - h_{o2}}{h_{o1} - h_{o2s}} \tag{4.46}$$

For a compressor:

$$\eta_{tt,c} = \frac{h_{o1} - h_{o2s}}{h_{o1} - h_{o2}} \tag{4.47}$$

These equations can also be applied to determine the total-to-total efficiency of a machine if 1 represents the inlet and 2 represents the exhaust.

4.2.7d Total-to-Static Efficiency.

In single-stage turbomachines, or the last stage of a multistage turbomachine, much of the kinetic energy of the exiting fluid is lost as the gas exits the turbomachine to the exhaust plenum. The stagnation pressure of the exhaust plenum will roughly equal the static pressure at the last stage exit because of the resulting stagnation-pressure loss. Total-to-total efficiency does not account for the exit kinetic energy losses. For this reason total-to-static efficiency is often used to evaluate these situations. For a turbine, total-to-static efficiency is defined as

$$\eta_{ts,t} = \frac{h_{o1} - h_{o2}}{h_{o1} - h_{2s}} \tag{4.48}$$

For a compressor,

$$\eta_{ts,c} = \frac{h_{o1} - h_{2s}}{h_{o1} - h_{o2}} \tag{4.49}$$

These account for losses in kinetic energy. As with the

total-to-total efficiency equations, these can be used to describe machine efficiency if 1 represents inlet conditions and 2 represents exhaust conditions. In cycle calculations, turbomachine-exhaust kinetic-energy losses can be accounted for by using total-to-static turbomachine efficiency in the calculations, or by using total-to-total turbomachine efficiency and accounting for the kinetic-energy loss as an additional system-pressure drop. Both methods will yield the same results. In the cycle calculations of Chapter Two, the latter method was used. The turbomachine efficiency values used reflect total-to-total polytropic efficiencies.

4.2.8 Turbomachine Losses.

Turbomachine losses are often categorized into three groups:

- Group One.
  Pressure losses in the fluid, including: profile losses, secondary losses, annulus losses, diffuser losses, and dynamic pressure losses.

- Group Two.
  Losses that produce enthalpy addition to the fluid by adding heat generated from mechanical friction.

- Group Three.
  Mechanical friction losses that absorb work produced by a turbine to reduce shaft output work, or require that additional work be expended in a compressor.

Group Three losses are considered external to the turbomachine, and are therefore evaluated separately from the other losses. The methods for evaluating Group One and Group Two losses are discussed in the next section.

4.2.8a Turbomachine Loss Estimation Methods.

The two most widely accepted methods for estimating turbine losses are the method of Craig and Cox [C6], and the method of Ainley and Mathieson [A7]. Kacker and Okapuu [K3] reviewed and updated the

method of Ainley and Mathieson in 1981. In this dissertation, the method of Craig and Cox will be used as the method of turbine-loss estimation. Wilson [W1] gives a summary of this method for design point calculations. Wilson also describes the methods of Koch and Smith [K17], and Lieblein [L5] for axial-compressor loss estimation. The method of Koch and Smith will be used in this dissertation. These turbomachine-loss-estimation methods are applied in Appendix B to estimate turbomachine efficiencies. They will not be described here.

4.3 Turbomachine Mechanical Design.

The mechanical design of the turbomachine includes consideration of blade and rotor stress analysis, and machine dynamic behavior. The following sections will briefly address these topics and how they affect the machine design.

4.3.1 Turbomachine Blade Materials.

The turbine blades must withstand high stresses at high temperatures. At these temperatures, time-dependent failure mechanisms that reduce blade lifetime must be considered. It is possible to improve blade mechanical performance by cooling. Combustion turbines often use cooled blades; however, combustion turbines operate at temperatures much higher than are possible with a passively-safe MGR. The high temperatures in a combustion turbine offer performance advantages that outweigh the performance penalties incurred by cooling the blades. This is not the case with the MGR-GT. Blade cooling incurs greater penalties than advantages.

The temperatures in the compressor are sufficiently cool that the compressor-blade material selection is is not a limiting problem.

Thus, the emphasis of this section will be on the turbine-blade materials.

The following are material requirements for the turbine blading:

- Creep Strength. Failure by creep mechanisms can occur at the high temperatures in the MGR-GT turbine. Material lifetimes are severely shortened by the high temperatures, high stresses, and stringent design criteria in a high-performance turbomachine.

- Fatigue Strength Toughness. The cyclic loading of the blades resulting from aerodynamic forces (high number of cycles), and machine transients (low number of cycles), generates a need for materials exhibiting good cycle-fatigue strength at high temperatures.

- Corrosion Resistance. Although the MGR-GT coolant is relatively inert, some impurities may exist in the coolant, such as methane, that can react with component materials at high temperatures. The resulting corrosion can lead to stress-corrosion cracking. These impurities usually exist in very small concentrations. Nonetheless, carburization has been identified as a potential area of concern for high-temperature reactors [J2].

- Aging Resistance. At elevated temperatures, the structure of a crystalline material may change over time, changing the material properties. It is important that materials are selected that do not experience changes that reduce their performance over the desired lifetime of the machine.

- Non-Activating. In order to permit decontamination of the turbine for maintenance and repair, the turbine-blade material should contain low amounts of activating elements, such as cobalt.

In the HTGR-GT study, IN-100 was identified as an acceptable turbine-blade material. The European HHT project used turbine blades of Nimonic-80; however, they required cooling. Molybdenum-TZM and Alloy-713LC have also been identified as possible turbine-blade materials. Figure 4.5 shows creep-rupture strength of IN-100 and some other turbine alloys plotted against Larson-Miller parameter. A creep-rupture strength of 30-ksi (200-MPa) for IN-100 corresponds to a

lifetime of only about 5000-hrs at 850°C, but corresponds to a lifetime of over 10^6 hrs at 750°C. Because of its high melting temperature, molybdenum-TZM has a very high creep resistance as compared to the other materials under consideration (see Fig. 4.6); however, it is highly susceptable to corrosion in an oxidizing environment, and it is more difficult to manufacture turbine blades from TZM than most other turbine-blade alloys. Although oxidation is a very serious problem in combustion turbines, in the MGR-GT helium, oxidation of TZM is not a problem [J2]. The excellent creep resistance of TZM makes uncooled turbine-blade lifetimes of over 100,000 hours possible for turbine blades at 850°C [J2]. In the MGR-GT, TZM should be considered for use as the turbine-blade material of the first one or two turbine stages. However, the turbine blades for most stages should be manufactured from IN-100 because it is well understood and more easily formed than TZM.

4.3.2 Stresses in Turbomachine Blades.

Turbomachine-blade stresses result from the centrifugal forces on the rotating blades, bending induced by fluid forces, and shear stresses induced by fluid forces. In general, the centrifugal stresses are much greater than the other stresses, making them the limiting stresses. These three stresses are briefly discussed below.

4.3.2a Centrifugal Blade Stress.

The rotating blades of a turbomachine travel at great angular speeds. Additionally, most turbomachine blading is made of dense metals, such as steels and nickel alloys. The centrifugal stresses in these blades can easily approach material limits, particularly in high-temperature environments where failure by creep mechanisms is

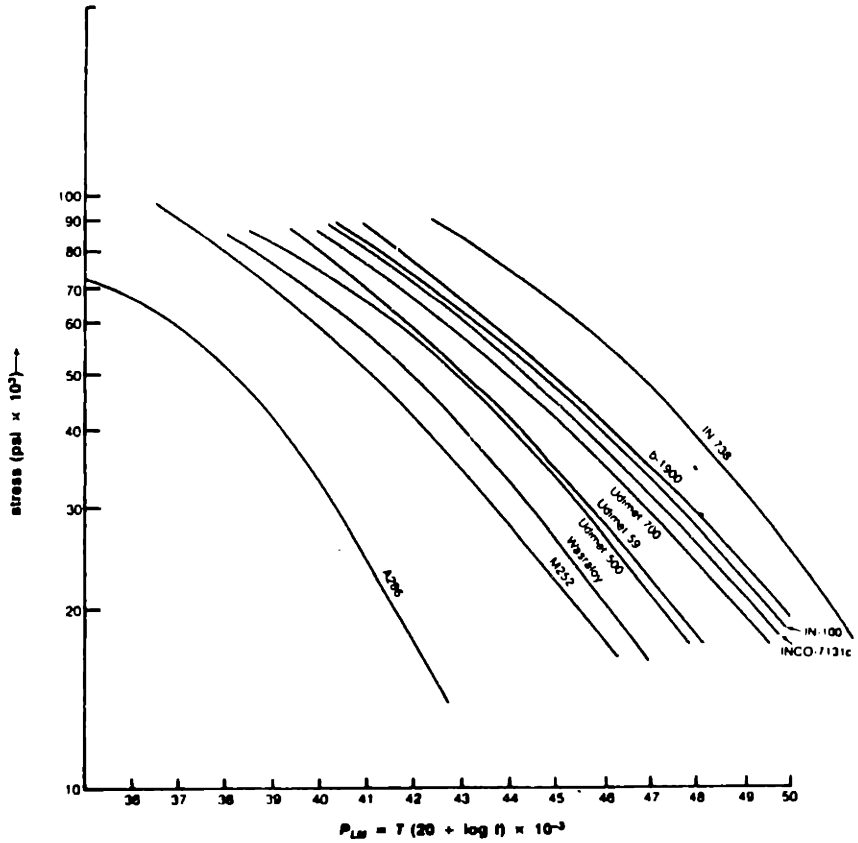

Figure 4.5. Creep-rupture stress for turbine-blade alloys correlated to Larson-Miller parameter [from B11].

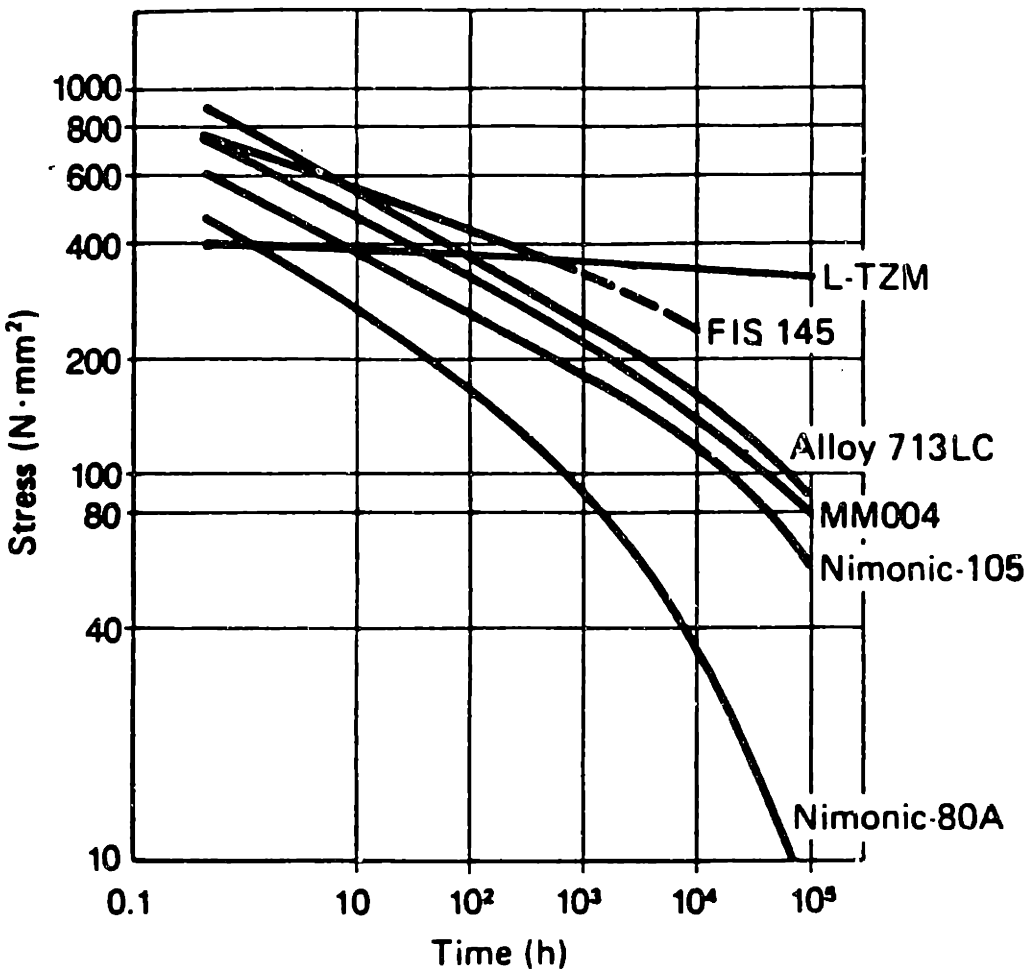

Figure 4.6. Creep-rupture stress for turbine alloys in helium at 850°C [from J2].

more likely. The centrifugal stress due to the rotation of an incremental piece of blade is equal to:

$$d\sigma_c = \left[\frac{N\,\pi}{60}\right]^2 \rho_m\, r\, dr \qquad (4.50)$$

The highest centrifugal stress in the blade will, therefore, occur at the hub. Integrating over the length of a blade of uniform cross sectional area, the stress at the hub can be determined. Since most turbine blades are not of uniform cross sectional area, the integral of Eq. 4.50 is multiplied by a taper factor to produce:

$$\sigma_h = tf \left[\frac{N\,\pi}{60}\right]^2 (1/2)(r_t^2 - r_h^2) \qquad (4.51)$$

It is necessary to know the blade shapes and sizes over the entire length of the blade to accurately determine shape factor. This is known only after detailed design of the blades, which will not be performed in this study. In this study, a taper factor of 0.5 was assumed.

4.3.2b Blade Bending Stress

Fluid forces tend to bend a turbomachine blade as a cantilever beam, resulting in bending stresses within the blade. Bending stresses are experienced by both stator and rotor blades. The greatest bending stresses are experienced at the fixed end of the blade. The stresses are equal to:

$$\sigma_b = \frac{c^* M}{I} \qquad (4.52)$$

Rotor blades are the more limiting blades because they experience centrifugal stress as well as bending stress. For a rotor blade, the moment can be estimated by dividing the power of a stage by its number of blades and rotational speed. (c^*/I) can be estimated as $2x(10)^4\ m^{-3}$ for most low-reaction blades [B17], the condition that generally

exists at turbine-rotor hubs. In any case, bending stresses are usually much less than centrifugal stresses. Centrifugal stresses will, therefore, be of primary concern.

4.3.2c Shear Stresses.

Shear stresses at a point in the blade equal the net tangential force acting on the blade between the point of interest and the free end of the blade, divided by the blade cross-sectional area at the point of interest. Highest shear stresses occur at the hub, but they are still insignificant in comparison to the other stresses.

4.3.3 Turbomachine Blade Vibration.

Although in preliminary design the flow approaching a blade row is treated as uniform, it is, in fact, quite non-uniform, containing wakes and other flow disturbances from upstream blade rows. The resulting aerodynamic forces induce vibration of the blades. Analysis of this phenomenon is very involved and beyond the scope of preliminary design. It will not be considered in this dissertation.

4.3.4 Turbomachine Rotor Construction.

Several methods of turbomachine-rotor construction exist. The merits of the designs are strongly affected by the stresses encountered in the rotor, and the rotor's inspectability for material defects.

4.3.4a Rotor Stresses.

A turbine rotor is usually modeled as a rotating disk. The principal-stress components are in the radial and tangential directions. The axial component of stress, even for a vertically mounted machine, is much less than the radial and tangential components, and is therefore not considered in this analysis. The

radial and tangential components of stress are equal to

$$\sigma_r = \frac{\rho\,\omega^2(3+\upsilon)}{8}\left[r_1^2 + r_2^2 - \frac{r_1^2\,r_2^2}{r^2} - r^2\right] \qquad (4.53)$$

$$\sigma_t = \frac{\rho\,\omega^2(3+\upsilon)}{8}\left[r_1^2 + r_2^2 + \frac{r_1^2\,r_2^2}{r^2} - \frac{1+3\upsilon}{3+\upsilon}\,r^2\right] \qquad (4.54)$$

r is the radial location of interest

r_2 is the c ıter radius

r_1 is the inner radius (= 0 for solid disks)

If these equations are normalized with respect to the stress at the center of a solid disk, Fig. 4.7 results. S_v is equal to the von Mises stress, as determined by distortion-energy theory, normalized in the same way as the other stresses.

$$\sigma_v = \left[\sigma_r^2 + \sigma_t^2 - \sigma_r\sigma_t\right]^{1/2} \qquad (4.55)$$

The results show that the limiting stress, σ_v, is greatest at r_1. As r_1 is reduced to zero, the peak stress in the rotating disk drops rapidly. Hence, a centerbore should be avoided, if possible.

4.3.4b Methods of Turbomachine Rotor Construction.

Three methods of multistage-turbomachine rotor construction exist; built-up rotor, solid rotor, and welded rotor. Aircraft gas-turbines are often constructed of separate splined-disks that are joined by a single bolt. However, this method of construction is not useful for longer, industrial machines. Built-up steam-turbine rotor disks are fitted or bolted onto the rotor shaft as in Fig. 4.8a. Keys are often used to increase the ridgidity of the disk-shaft connection. Built-up rotor construction permits ease of construction, inspection of individual parts, and stress compensation through prestressing of components. On the other hand, built-up-rotor construction results in

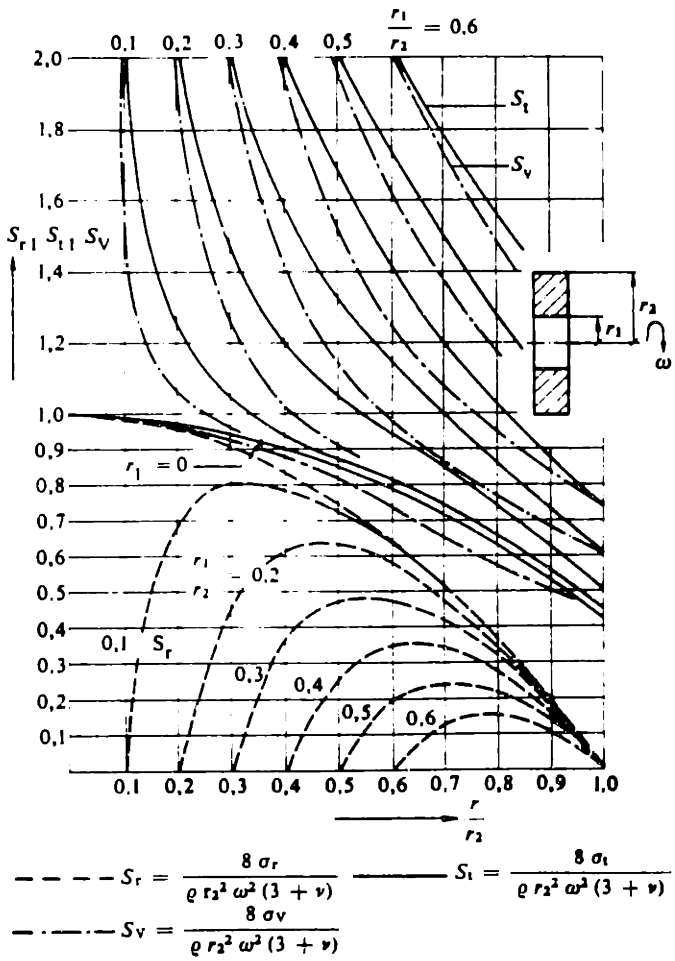

Figure 4.7. **Stresses in a rotating disk normalized to stress at the center of a solid disk [from H8].**

high stress concentrations in the regions of shrink-fits and keyways. Also, the stresses in the disk are much higher than if the rotor were solid, because of the shrink-fit and the large inner diameter of the disk. The shaft of a built-up rotor is usually bored. This removes the ingot-core material, which may contain defects. The bore also provides a passage for rotor cooling. However, bored shafts have high local stresses at the shaft inner radius, increased local stresses at the shaft outer radius, and increased local stresses at the shrink-fit and disk inner-radius, which compounds the stress problems that already exist with this rotor-construction method. Maximum allowed flaw size (measured in flaw area) for a shaft with a centerbore can be 50 times smaller than for a solid shaft of the same diameter [M16]. This is complicated by the reduced ability to detect flaws in bored shafts by ultrasonic testing because of the reflections at the bore [M16].

By eliminating the shrink-fit and keyways, and their resulting stress concentrations, solid-rotor construction provides some solution to some of the problems of built-up rotors. However, this method of construction, shown in Fig. 4.8b, has two problems. First, it is difficult to manufacture large forgings because of the sheer mass of the forging needed. Also, it is more difficult to inspect solid- rotor forgings for material defects than the individual pieces of a built-up rotor. It is possible to improve access for inspection by boring the shaft; however, this results in increased stress and the ultrasonic-testing difficulties discussed earlier.

In the welded-rotor method, rotor drums are welded together at their periphery, as shown in Fig. 4.8c. The welded-rotor method has several advantages over the other methods of construction. Each rotor

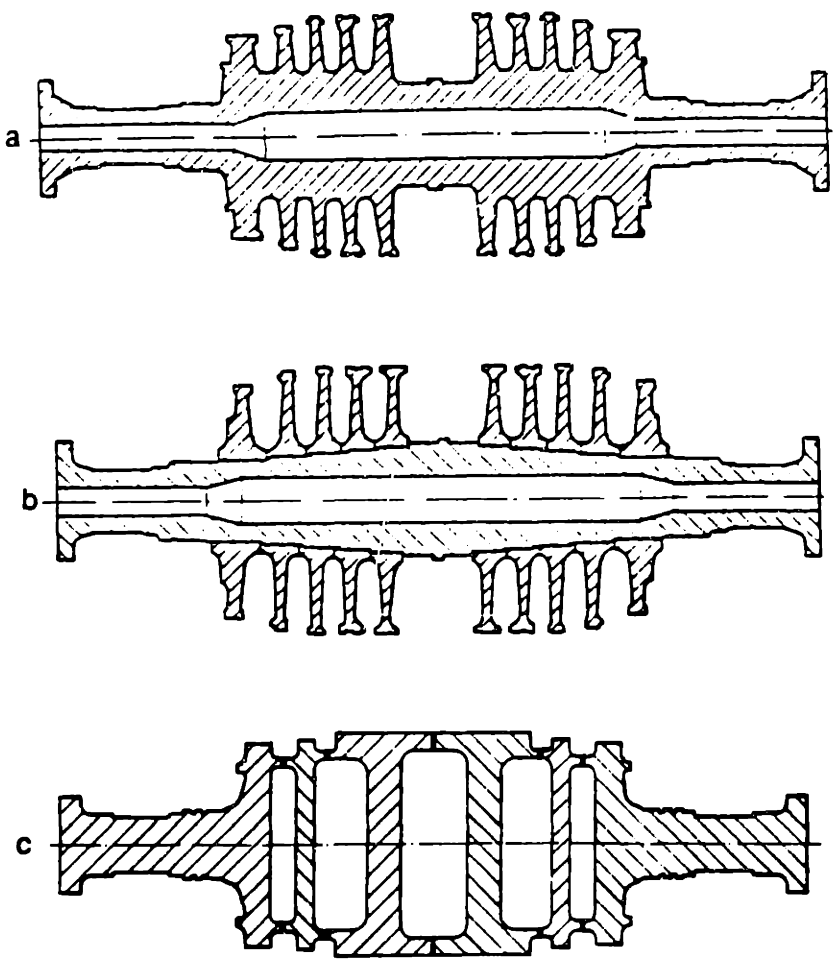

a: Solid rotor
b: Rotor with shrunk-on discs
c: Welded rotor according to BBC design

Figure 4.8. **Methods of turbomachine-rotor construction [from B26].**

disk may be individually inspected, so that defects are easier to find. Rotor welds are easily accessible for inspection on a welded rotor. Also, stress concentrations and general stresses are reduced through the lack of shrink fits, keyways, or the centerbore; however, thermal stresses cannot be compensated for by prestressing, as in the built-up method of construction. Nonetheless, Brown Boveri Company (BBC) claims that thermal stresses are lower in their welded rotors than in rotors of other construction [B26]. The lower stresses in welded-rotor designs permit the use of low yield-strength materials, which are less susceptable to crack propagation. Figure 4.9 shows stress-corrosion-crack-propagation rate in steam-turbine rotors as a fuction of material yield stress. Although stress corrosion is of less concern in helium turbomachinery than in steam turbomachinery, the propagation of cracks initiated by defects, wear, or corrosion is still of concern as a major cause of rotor failure.

BBC has had much success with welded-rotor designs. Of the over 4000 gas and steam turbomachines that they have constructed by the welded-rotor method, no disk or shaft failures have been experienced. Furthermore, of the 79 BBC low-pressure rotors installed in U.S. nuclear power plants, none have demonstrated signs of stress-corrosion cracking in over five million turbine-hours of operation. In contrast to this, 75% of the nuclear power plants in the United States with shrunk-on steam-turbine rotor disks have experienced some difficulty with stress-corrosion cracking [B25]. This is attributable to the lower stresses in welded rotors that render all forms of crack-propagation and failure less critical [B25, B26].

It is essential that the rotor of a nuclear direct-cycle

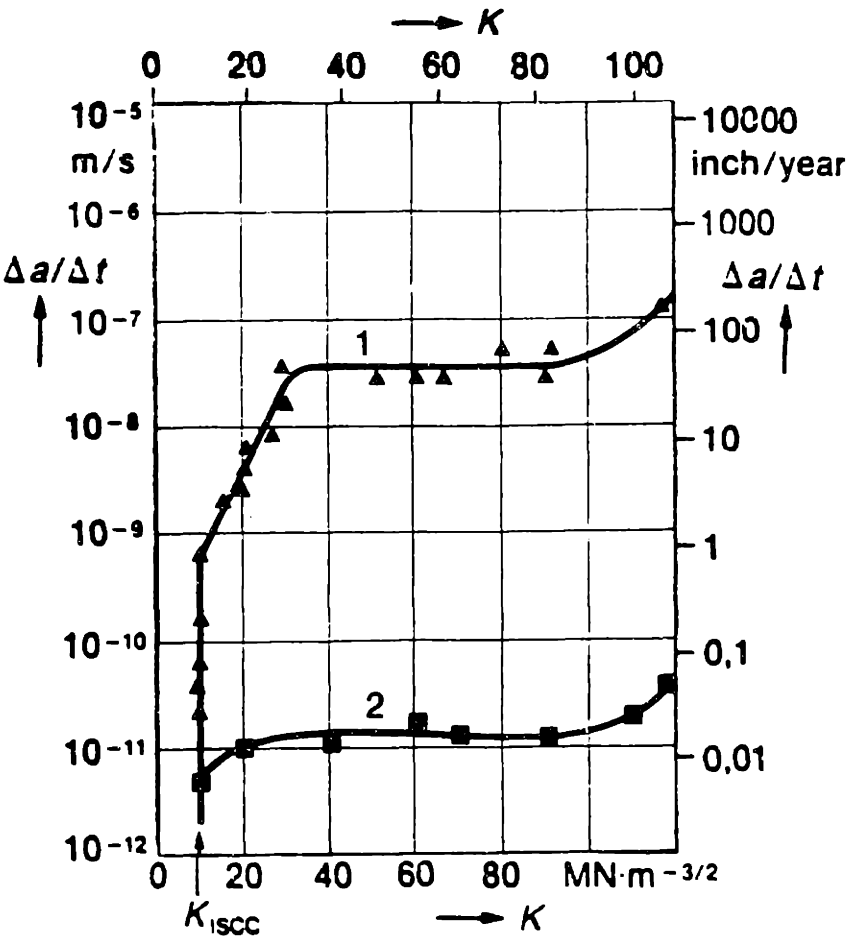

Intergranular stress corrosion cracking in deionised water at 100 °C

$\frac{\Delta a}{\Delta t}$ = Propagation rate of stress corrosion cracks
a = Crack depth
t = Time
K = Stress intensity
Re = Yield strength
K_{Iscc} = Threshold value
1 = Steel 26 NiCrMoV 12 7 (471)
Re = 1220 MN/m² = 177 ksi
2 = Steel 26 NiCrMoV 12 7 (471)
Re = 760 MN/m² = 110 ksi

Figure 4.9. Stress-corrosion-crack-propagation rates for turbine rotors [from H8].

gas-turbine maintain its integrity to avoid costly damage to the plant. The high degree of reliability demonstrated by welded-rotor construction is impressive. For this reason, welded-rotor construction was used in the HTT and HTGR-GT concept designs. It is anticipated that welded-rotor construction will be employed for the MGR-GT.

4.3.4c Rotor Cooling.

It is recognized that some rotor cooling may be required for the turbine rotor of the MGR-GT. The precise amount of rotor cooling that will be required depends on many specific design details that will not be considered in this dissertation. However, the inlet-temperature to the MGR-GT turbine is substantially less than the inlet-temperatures to combustion turbines, which do not require excessive rotor cooling. It is anticpated that the effect of rotor cooling on the system design and performance is, therefore, small, and can be neglected without significant loss in accuracy of the analysis.

4.3.5 Shaft Critical Speed.

Rotating shafts become dynamically unstable at certain rotating speeds, known as critical speeds. This phenomenum occurs when the shaft rotational speed, in revolutions per second, equals the natural frequency for shaft lateral vibration.

If Rayleigh's energy method is applied to a multi-mass system with weights W_1, W_2, W_3, . . . W_n, the first critical speed will be equal to

$$\omega_{cr1} = \left[\frac{g \sum_{i=1}^{i=n} W_i y_{oi}}{\sum_{i=1}^{i=n} W_i y_{oi}^2} \right]^{1/2} \qquad (4.56)$$

$$y_{oi} = \frac{W_i}{k} \tag{4.57}$$

where W_i is the weight of the shaft or disks mounted on the shaft, y_{oi} is the static beam displacement resulting from W_i, and k is the combined stiffness of the shaft and the supports (to include the bearings). Eq. 4.56 will provide only the first harmonic. Several harmonics will exist at higher shaft speeds. Analysis of these harmonics requires highly sophisticated methods. However, as a simple example, the first critical speed of a solid, uniform, circular rotating shaft on rigid bearings is equal to

$$\omega_{cr1} = 2 \frac{D}{l^2} \left[\frac{g\ 6\ E}{5\ \rho}\right]^{1/2} \tag{4.58}$$

where: D = shaft diameter

l = shaft length

E = Modulus of elasticity of shaft material

ρ = Density of shaft material

Critical speed is strongly dependent upon the dimensions of the shaft. In particular, it is best to use a short, thick shaft because its first critical speed will be higher, and the rotating shaft will have fewer harmonics to pass through when it speeds up to full speed. Aircraft gas turbines often have several harmonics in their operating range. Nonetheless, it is preferred to avoid operation at or near a critical-speed harmonic because of the potential for excessive shaft vibration. For this reason, the length-to-diameter ratio of rotating machinery is often limited in the design process by critical-speed considerations. The MGR-GT rotating machinery will operate at the same speed during all full-power and part-power operations, except during plant shutdown, startup, and upset conditions. Furthermore, the use of

active magnetic bearings (disussed in Section 4.6) may significantly ease this design difficulty. Hence, shaft critical-speed considerations exist, but may be much less than what is encountered in many existing engineering systems.

4.4 Turbomachine Design Programs and Scaling Relationships.

Simple computer programs were written to aid in the design of the turbomachinery. TURBINE and COMPRES were written to perform turbine and compressor mean-line design calculations. Turbomachine dimensions, including number of stages, hub and tip diameters, velocity-triangle data, and blade stresses are among the results calculated. All of the assumptions of the analysis techniques discussed in Sections 4.2 and 4.3 were used in these programs. A more specific description with listings and sample input and output are given in Appendix B. TURBINE and COMPRES, and the simple scaling relationships to be developed below, were used in a parametric study to estimate the effects of various parameters on the turbomachinery design. The scaling relationships also serve the purpose of providing a verification of the computer program results. Agreement between the scaling relationships and the computer programs was found to be excellent.

4.4.1 Scaling Relationships.

In the process of the MGR-GT design, it is advantageous to estimate the effects of various turbomachine and plant parameters on the turbomachine design. The following paragraghs will discuss the relationships between system pressure, number of machine stages, and turbomachine rotational speed on the turbomachine design.

The following scaling rules will assume the same perfect-gas

working fluid and constant inlet and exhaust temperatures. Working-fluid mass flow will be held constant for scaling of turbines of equal power. Other assumptions will be geometric similarity of velocity triangles in all cases, and equal velocity triangles in cases where the number of stages are being held constant. Hub-to-tip-diameter ratio will be held constant for all cases as well. At the low Mach numbers expected in the helium turbomachines, compressibility effects can be neglected when necessary with very little error. An asterisk (*) used in an equation indicates the parameter value at a base-case condition.

4.4.1a Effect of System Pressure and Power Level on Machine Size and Speed.

One of the significant advantages of closed-cycle gas-turbine cycles is the ability to operate the system at high pressures. At high pressures, the size of a turbomachine is reduced from that of a machine of comparable power operating at lower pressures. The operation of the closed-cycle plant at high pressures may offer benefits in capital cost because of its reduced size.

Blade annulus area equals:

$$A = \frac{\pi}{4} D_t^2 \left[1 - \Phi^2\right] \tag{4.59}$$

Also,

$$\sigma_c \approx N^2 A \tag{4.60}$$

and

$$U_m = \frac{N \pi D_m}{60} \tag{4.61}$$

U_m is held constant for a constant number of stages, velocity triangles remain the same, and C_x is kept constant. Therefore, annulus area is a function of density and mass flow. For the same power output, the mass flow must not change. Hence, pressure will vary

inversely with annulus area. If hub-to-tip diameter ratio is held constant, then some simple algebra will result in

$$D_t = D_t^* \left[\frac{P^*}{P}\right]^{1/2} \tag{4.62}$$

and

$$N = N^* \left[\frac{P}{P^*}\right]^{1/2} \tag{4.63}$$

Thus, designing the system to operate at a high pressure will result in a smaller turbomachine that operates at a higher rpm for the same power output than a machine designed to operate at a lower pressure. Additionally, from these relationships it is seen that centrifugal blade stress remains constant for different system-design pressures when velocity triangles and hub-to-tip diameter ratio are held constant (ie., constant # of stages). This is because as system-design pressure is changed, the effect of the change in rotational speed on stress is exactly offset by the effects of the change in annulus area.

On the other hand, if system-design pressure level is kept constant while massflow is changed, thereby changing power level, the following equations result:

$$D_t = D_t^* \cdot \left[\frac{\dot{m}}{\dot{m}^*}\right]^{1/2} \tag{4.64}$$

and

$$N = N^* \cdot \left[\frac{\dot{m}^*}{\dot{m}}\right]^{1/2} \tag{4.65}$$

A turbomachine for a low-power plant will operate at a higher speed and be smaller than a turbomachine for a high-power plant with the same velocity triangles, same hub-to-tip ratio, and same operating pressure. Centrifugal blade stresses, however, will again remain constant, for the same reasons as discussed above regarding the effects of changing the system design-pressure.

A unique feature of CCGT plants is the ability to control power output by pressure, or mass flow. Turbomachine inlet and outlet temperatures are maintained constant with this control method. In this case it is easy to show that because the massflow changes in proportion to the density, the volumetric flow will be constant at all times when controlling CCGT plant power in this manner. The required turbomachine size, speed, and number of stages all remain constant over all power levels for this method of control.

4.4.1b Number-of-Stages and Rotational Speed.

When operating under the same pressure, turbine parameters may be varied within the limitations of design constraints or stress limits. The best design resulting from varying the parameters is selected. The relationship between rotational speed, number of stages, and tip diameter is an important consideration in the turbomachine design.

If the velocity triangles are kept geometrically similar, but are permitted to change in magnitude only, the number of required stages will change. In this situation, if hub-to-tip diameter ratio is held constant, the effect of number of stages on rotational speed and tip diameter can be determined.

Recall: $$\Delta h_o = n \psi U_m^2$$

Keeping in mind that Δh_o and ψ are constant, and because velocity triangles are kept geometrically similar,

$$C_x \approx U_m$$

and for a constant Φ,

$$C_x D_t^2 = C_x^* D_t^{*2}$$

it can be shown that

$$D_t = D_t^* \left[\frac{N^*}{N}\right]^{1/3} = D_t^* \left[\frac{n}{n^*}\right]^{1/4} \qquad (4.66)$$

also

$$U_m = U_m^* \left[\frac{N}{N^*}\right]^{2/3} = U_m^* \left[\frac{n^*}{n}\right]^{1/2} \tag{4.67}$$

and

$$N = N^* \left[\frac{n^*}{n}\right]^{3/4} \tag{4.68}$$

also

$$\sigma = \sigma^* \left[\frac{n^*}{n}\right]^{1/3} \tag{4.69}$$

Thus, a machine with fewer stages will operate at a higher rpm with higher blade stresses.

4.5 Results of Turbomachine Design Calculations.

Calculations with the computer programs discussed in Section 4.4 were performed to develop designs for the turbomachinery at cycle conditions that were based upon the results of Chapters Two and Three. The cycle conditions that characterize the base-case design conditions are listed in Table 4.1. These conditions are considered to be constant for the results of all calculations presented, except for system-pressure levels and reactor-power levels (mass flows). The computer programs and the scaling relationships discussed in the previous sections were used to determine the effect of changes in plant parameters, such as pressure level and power level, and turbomachine parameters, such as number-of-stages and rotational speed, on the turbomachine design.

4.5.1 The 200-MWth MGR-GT Turbomachines.

Figures 4.10 and 4.11 show the size of the turbine and the compressor, respectively, as a function of system pressure for the MGR-GT with a 200-MWth reactor. The turbomachinery is characterized by

the parameters listed on Table 4.2, chosen as being characteristic of machines of high efficiency. Figures 4.10 and 4.11 demonstrate, quite clearly, the advantages of a CCGT in reducing the size of the machinery. By increasing system pressure to 8-MPa, it is possible to build a turbine with a last-stage-tip diameter of less than one meter. Such a machine designed for exhaust to atmospheric pressures would be of colossal size. Furthermore, it is identified from this figure that a machine that would operate at a synchronous electrical speed and a system-design pressure of about 8-MPa would require a high number of stages (over 20 turbine stages, and many more compressor stages), or require an operating pressure that is much lower than desirable. This is largely a result of the high enthalpy drop across the turbomachinery and the low volumetric flow rate. In previous designs of small helium CCGT systems, Oberhausen-2 and KSH in particular, this problem was resolved in two ways. First, by compressing in multiple compressors and expanding in multiple turbines, the enthalpy drop across any individual turbomachine was reduced. Second, by operating at a lower system pressure, only 2.7-MPa, the volumetric flow of helium was increased. The first solution is not considered attractive for the MGR-GT because it introduces additional complexity which is contrary to the basic design philosphy of the MGR-GT, that is, safety and economy through simplicity. Lowering system pressure in order to reduce the number of required turbomachine stages is not an attractive solution because it will result in much larger components and/or higher system pressure losses. Reduced component size is a key economic advantage of the CCGT, especially in regard to a modular plant that requires transportability. High system pressure losses

Table 4.1

Cycle Parameters for MGR-GT

station	temperature (C)	pressure (MPa)
compressor inlet	30.0	3.97
compressor outlet	145.3	8.14
reactor inlet	593.2	8.02
turbine inlet	850.0	7.80
turbine exhaust	616.7	4.11
precooler inlet	168.9	3.99

helium mass flow = 150 kg/s

Table 4.2

MGR-GT Turbomachinery Characteristics

Turbine Characteristics

• Mean dia. flow coefficient	0.65
• Mean dia. load coefficient	1.26
• Mean dia. reaction coefficient	0.50
• Last stage hub-to-tip diameter	0.75
• Pressure ratio	1.90

Compressor Characteristics

• Mean dia. flow coefficient	0.48
• Mean dia. loading coefficient	-0.326
• Mean dia. reaction coefficient	0.50
• W_2/W_1	0.717
• C_1/C_2	0.717
• Last-stage hub-to-tip diameter	0.86
• Pressure ratio	2.05

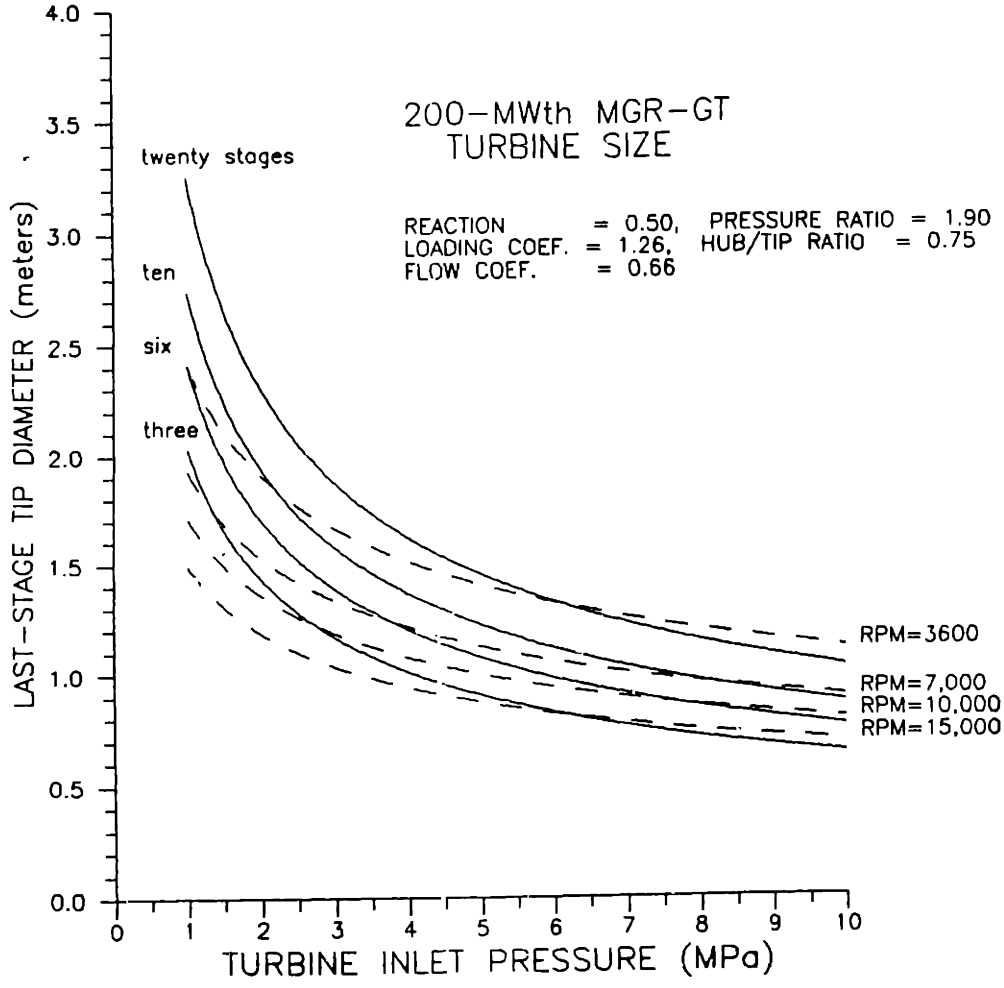

Figure 4.10. 200-MWth MGR-GT turbine size and speed.

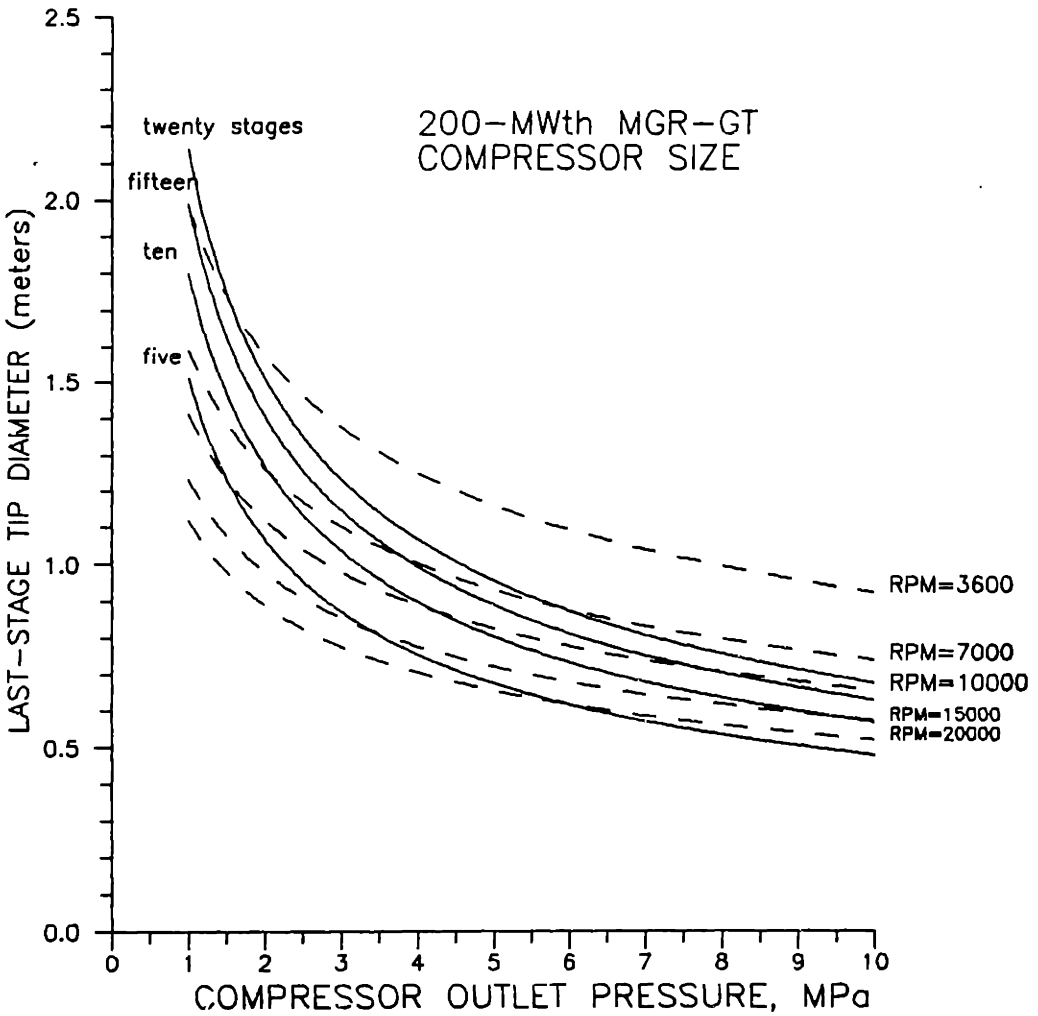

Figure 4.11. 200-MWth MGR-GT compressor size and speed.

would incur an unacceptable penalty in efficiency.

Therefore, if a machine of reasonable size is to be used in the 200-MWth MGR-GT, it is essential that it operate at a rotational speed well above 3600-rpm. This will require that additional consideration be given to the electric-plant design. Section 4.7 will discuss the MGR-GT electric-plant design. If the turbomachine is to be designed without consideration to the electrical system, with the primary objective being reducing the number of stages while maintaining within blade-stress limitations, Fig. 4.12 may be used as a guide in selecting the number of stages and rotational speed. Figure 4.12 shows the rotational speed for turbines of various numbers of stages designed for an inlet pressure of 7.8-MPa. Centrifugal blade stress of the first stage is shown beside the data point. Although last-stage centrifugal blade stress is higher than first-stage centrifugal blade stress, the first-stage blade stress is more limiting because of the high temperatures of the first-stage blades. If turbine first-stage blade stress is limited to 30-ksi (207-MPa), a four-stage, 13,550-rpm turbine can be designed. This will correspond to a ten-stage compressor. If the limiting turbine first-stage blade-stress is around 20-ksi (138-MPa), a six-stage, 10,000-rpm turbine can be designed, which will correspond to a fifteen-stage compressor. Fifteen-stages was taken as the upper limit for the number of stages that a practical machine should be designed for. Increasing turbomachine stages beyond fifteen would result in a machine that is too awkward and expensive.

Turbomachine length is a function of the number of blades as well as the number of stages. For blade-aspect ratios that are typical of industrial machines, the 10,000-rpm design discussed in the previous

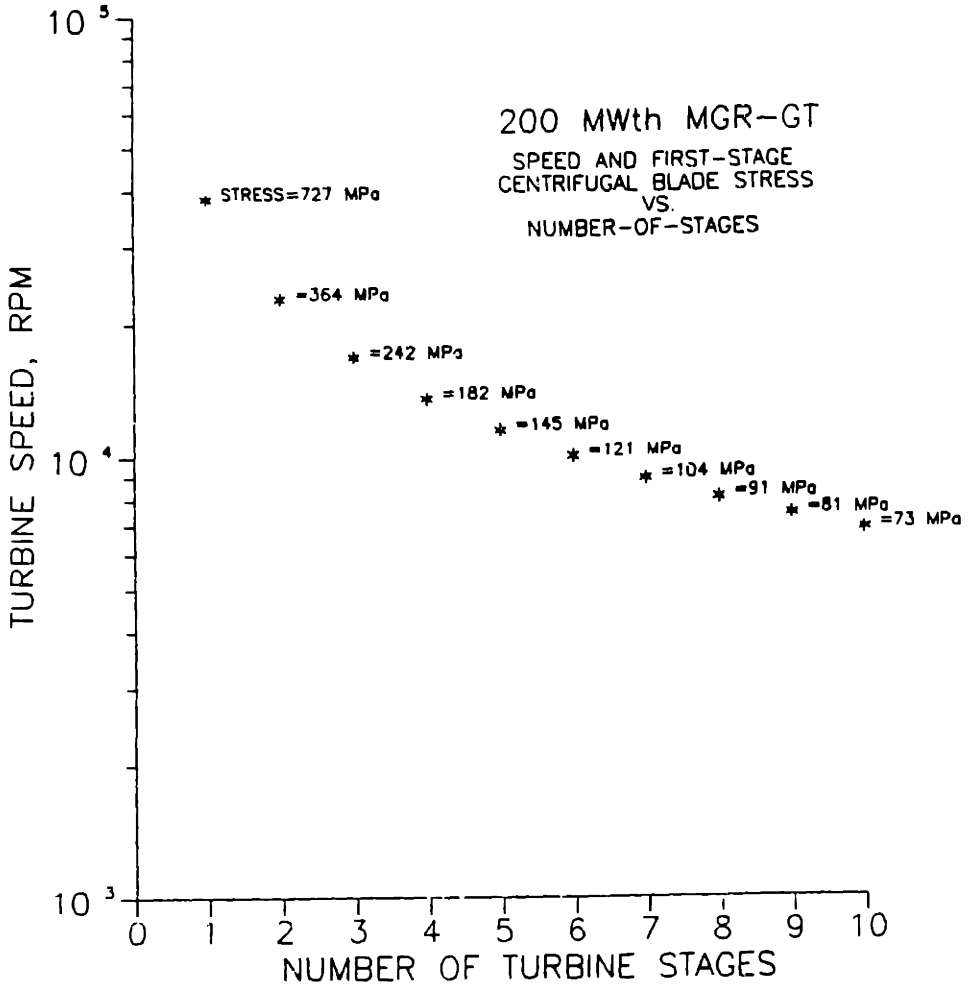

Figure 4.12. Rotational speed and first-stage centrifugal blade stress for 200-MWth MGR-GT turbines.

paragragh would have a turbine length of about 0.630-meters and a compressor length of about 1.30-meters, not including inlet and exhaust ducting (see Appendix B).

Calculations in Appendix B show that both of these machines are capable of polytropic efficiencies of over 93%. The combined effects of low Mach numbers, high Reynolds numbers, low molecular weight, and efficient velocity triangles result in low blade-profile losses. Because of the unusually clean environment in which the turbomachines will be operating, it is not expected that the performance of these machines will deteriorate significantly over life. Hence, a polytropic efficiency of 91% for both turbomachines can be considered a very conservative assumption, with higher efficiencies expected.

4.5.2 Turbomachines for an MGR-GT Prototype.

It is likely that before a full-scale MGR-GT would be built, a part-scale prototype would be constructed in order to provide experience in design and construction, and to identify areas that may require design alteration in a full-scale MGR-GT design. This section will present the results of calculations similar to those of the previous section for MGR-GT plants of 100-MWth and 50-MWth capacity. The machine characteristics are the same as for the machines of the previous section, except that helium mass flow is reduced as necessary to match the reactor thermal rating.

Figures 4.13a and b and Figs. 4.14a and b show the same general trends as Figs. 4.10 and 4.11. High operating pressures enable machines of small diameter to be constructed; however, they must operate at high speeds. A six-stage turbine for the 100-MWth plant at a maximum pressure of 8-MPa must operate at 14,140-rpm. A six-stage

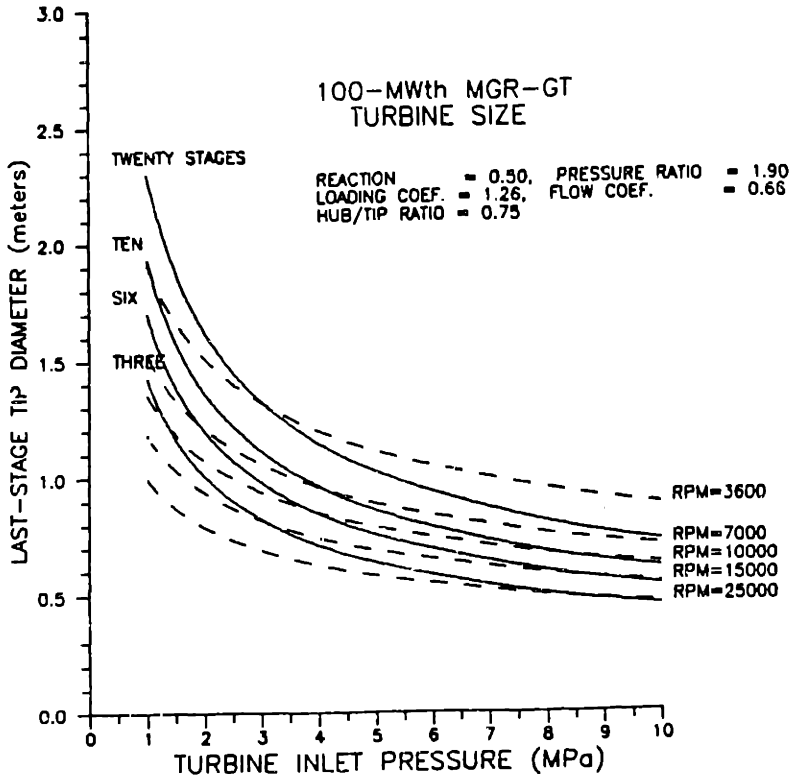

Figure 4.13a. 100-MWth MGR-GT turbine size and speed.

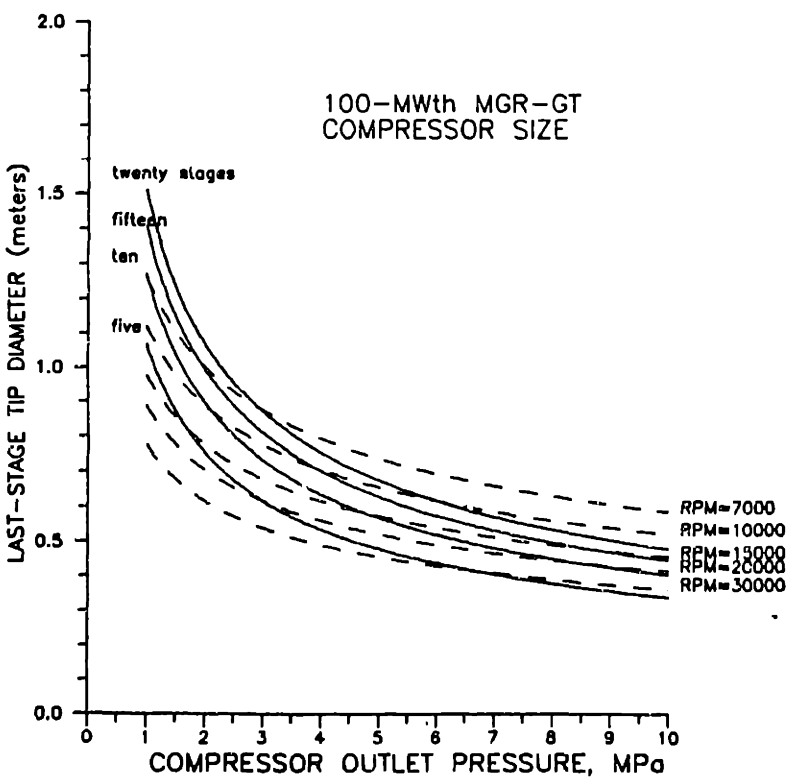

Figure 4.13b. 100-MWth MGR-GT compressor size and speed.

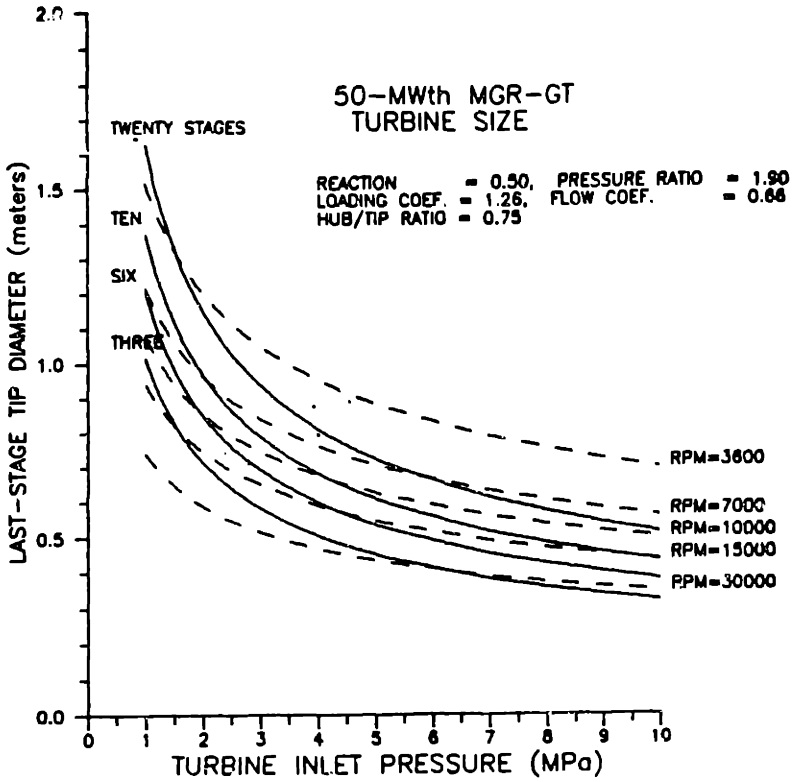

Figure 4.14a. 50-MWth MGR-GT turbine size and speed.

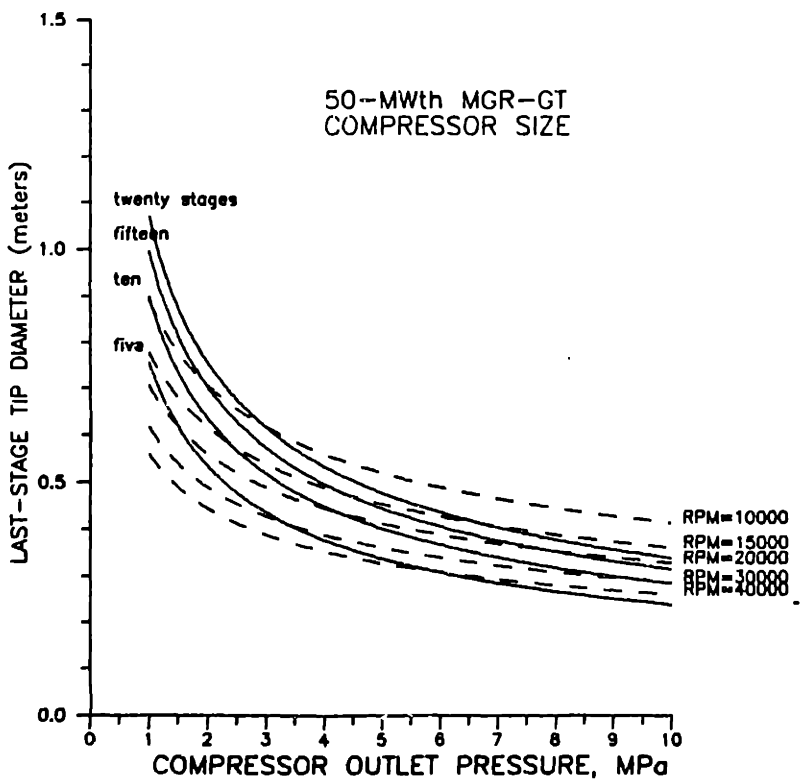

Figure 4.14b. 50-MWth MGR-GT compressor size and speed.

machine for the 50-MWth plant at a turbine-inlet pressure of about 8-MPa must operate at 20,000-rpm. At these speeds, additional consideration must be given to shaft critical speeds and to design of the electrical system. The frequency produced by a two-pole synchronous generator at 20,000-rpm is 333-hz, versus 167-hz for a 10,000-rpm machine. As will be discussed in Section 4.7, this frequency difference is not expected to substantially change the technology of the electrical system; however, it may produce difficulty in the electrical-generator mechanical design. Also, it may nonetheless be preferable to test the prototype electrical system at the same frequency as the full-scale system. For these reasons it may be advantageous to operate the prototype at lower pressures in order to enable the turbomachines to operate at speeds that are similar to those expected of the full-scale plant. On the other hand, if the prototypes are operated at lower pressures, their size will be increased, and their performance will be degraded. The increased size of the plant would increase the cost of power-conversion components. However, since most of the cost of the plant is in the reactor, the cost of a reduced-scale, low-pressure prototype would still be less. One alternative is to reduce plant pressure in proportion to reactor thermal rating such that the helium volume flowrate of the prototype is the same as that anticipated of the full-scale plant. In this situation, the turbomachinery size and speed of the reduced-scale prototype would be the same size and speed as the full-scale plant. These are issues that must be considered in detail should a small-scale MGR-GT prototype actually be built.

The efficiencies of the turbomachines of a reduced-scale MGR-GT

prototype would not be as high as those expected for the full-scale MGR-GT because of their lower Reynolds numbers. Although detailed efficiency calculations were not performed for the smaller machines, one might expect a drop in efficiency of a few percentage points for the smallest of the machines expected.

The results of Figs. 4.10, 4.13, and 4.14 may all be correlated to volume flow in Fig. 4.15. In so doing, it is observed that the quantity

$$n^{3/4} \cdot N \cdot Q^{1/2} = \text{constant} \tag{4.70}$$

Figure 4.15 enables scaling of all MGR-GT turbines with the same inlet and exhaust temperatures and pressure ratios as those listed on Table 4.1, regardless of power level. Equation 4.70 is similar to specific speed. Specific speed is defined as:

$$N_s = \frac{N \cdot Q^{1/2}}{60 \cdot (\Delta h_o)^{3/4}} \tag{4.71}$$

Δh_o refers to the stagnation-enthalpy drop of the stage. If we consider a turbine of total stagnation-enthalpy drop equal to Δh_o, with n stages of equal stagnation-enthalpy drop, Eq. 4.70 will result from Eq. 4.71. Specific speed is a measure of turbomachine geometry, and equal specific speeds indicate geometric similarity. Geometric similarity of the velocity triangles, and an equal hub-to-tip diameter ratios, ensure geometric similarity for turbomachine stages. Figure 4.15 results for a turbine with a specific speed at the exhaust equal to 0.143. As a rule of thumb, a specific speed of about 0.15, as determined by exhaust conditions, is close to optimum for axial-flow turbine stages [C4].

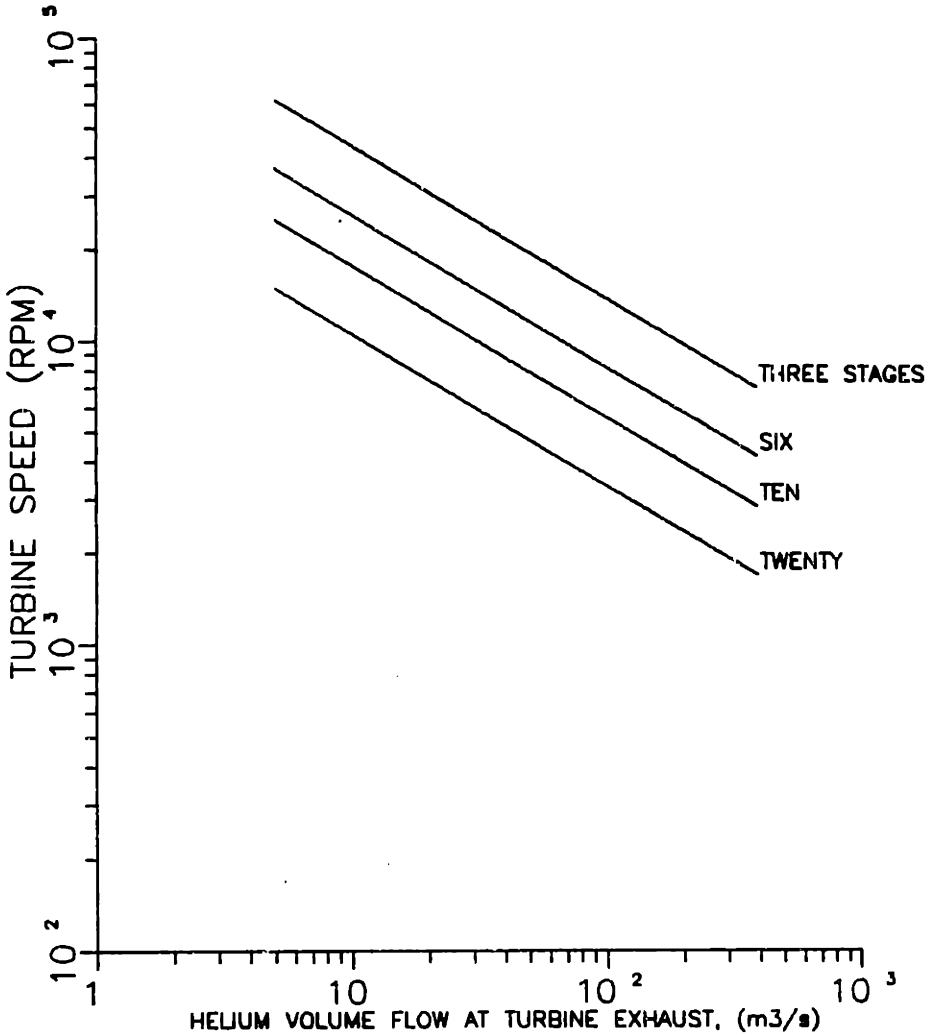

Figure 4.15. **MGR-GT turbine speed versus turbine-exhaust volume-flow rate.**

4.6 Magnetic Bearings.

Chapter One discussed the difficulties resulting from the use of water-lubricated and oil-lubricated bearings and seals in gas-cooled reactors and CCGT plants. The use of water or oil lubricated bearings should clearly be avoided if possible. Because of the size and configuration of the machine, gas-lubricated bearings cannot be used. It is fortunate that in the past few years active-magnetic bearings have been developed to a level where they appear as promising-candidates for the MGR-GT machinery bearing system. A brief description of active-magnetic bearings and their operational limitations follows.

4.6.1 Principles of Operation.

There are two methods of magnetically suspending an object, as shown in Fig. 4.16. The object may be suspended by a repulsive magnetic force, in which case the object suspended will tend to some equilibrium position. This method is inherently stable and requires no control system. It is therefore called a passive-magnetic-suspension system. The other method of magnetic suspension is by attractive forces, in which case the system is inherently unstable. Alternating attractive forces must be applied in this case to maintain the position of the object. Such a suspension system requires a control system and is therefore called an active-magnetic-suspension system.

Passive-magnetic-suspension systems do not have the stiffness or the damping characteristics necessary to suspend a dynamically loaded rotating machine, such as a turbine or a generator, and are, therefore, of limited use. The controller of an active-magnetic-suspension system can be used to vary the stiffness

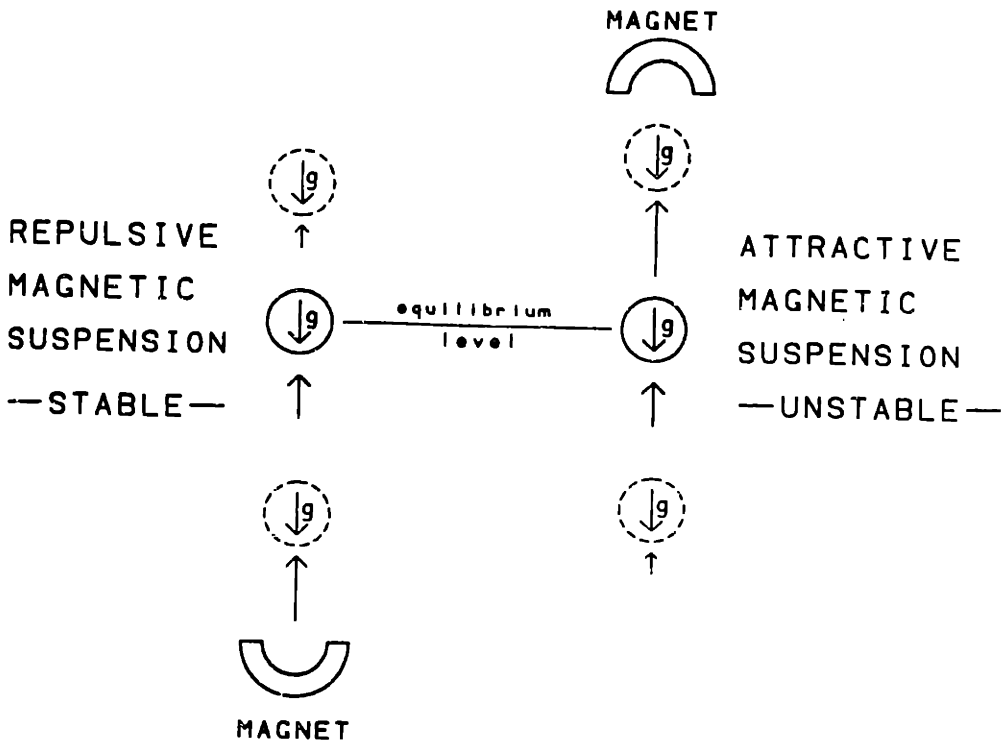

Figure 4.16. Attractive and repulsive methods of magnetic suspension.

and damping of the suspension system. Thus, active systems have much greater potential as rotating-machinery bearing systems.

A radial active-magnetic bearing, such as shown in Figs. 4.17 and 4.18a, requires four electromagnets set in two orthogonal, radial, opposed pairs. Position sensors measure the shaft position in each radial direction and feed the position back to the control system. To reduce eddy-current losses in the rotor of a radial magnetic bearing, the rotor is made of a stack of circular laminations. The laminations are pressed onto a bearing sleeve which is fitted onto the shaft. The stator of a radial magnetic bearing is a slotted lamination stack with wound coils. An axial magnetic bearing, such as in Fig. 4.18b, requires two electromagnets and a shaft axial-position sensor. Its rotor does not experience changes in magnetization during rotation and, therefore, is made of a solid disk. An axial-magnetic-bearing stator consists of a solid-steel toroid with annular grooves machined for the electromagnet coils. Radial slots with laminations reduce eddy-current losses and improve magnet response.

4.6.2 Magnetic-Bearing Control.

The control system of the active-magnetic bearing maintains shaft position at the desired location and also controls shaft dynamic behavior. An active-magnetic-bearing control system is schematically shown in Fig. 4.19. The shaft position, measured by inductance, capacitance, or electro-optical methods, is compared to a reference-position signal. The error generated is processed in a Proportional plus Integral plus Derivative (PID) controller, the signal processor, which provides the bearing damping and stiffness. The bearing damping and stiffness can be controlled to optimize the

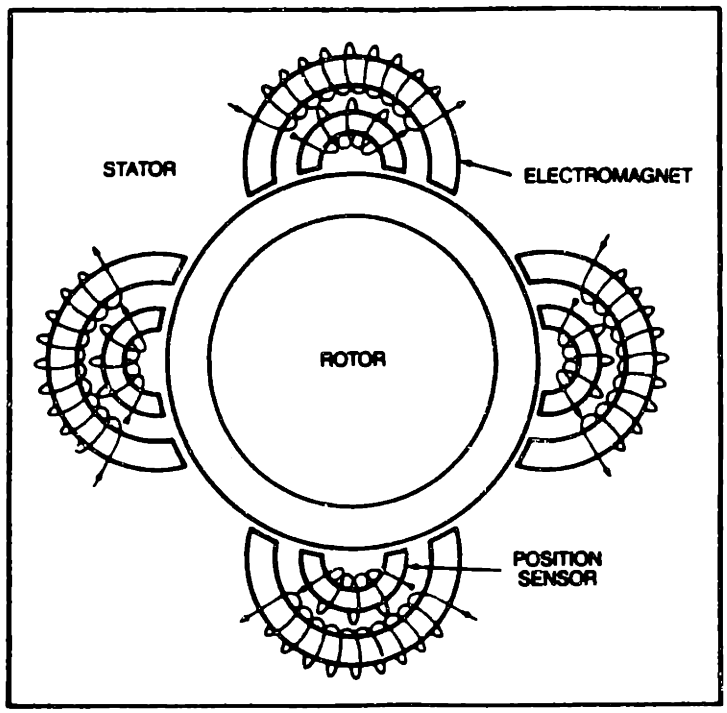

Basic diagram of an active magnetic bearing.

Figure 4.17. A radial active-magnetic bearing [from I2].

(a)

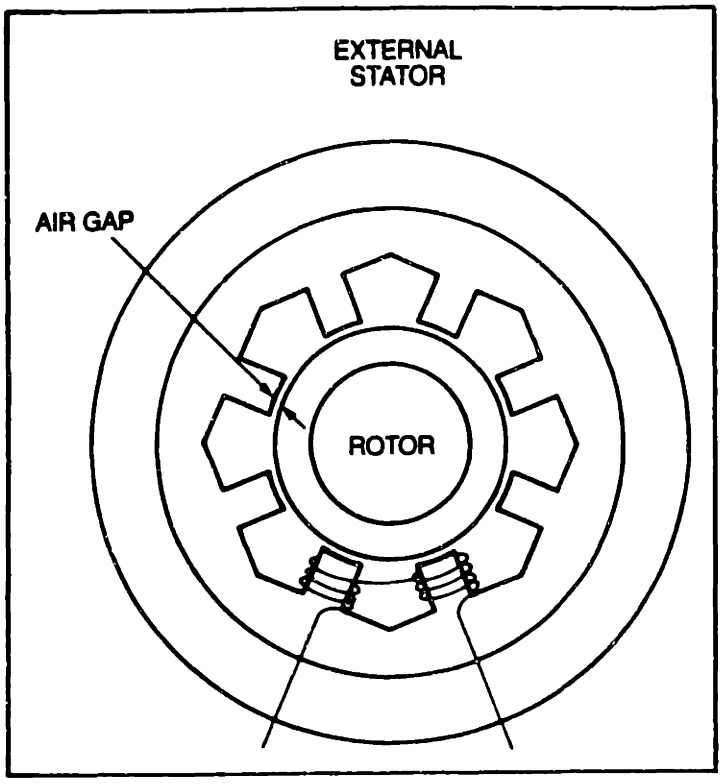

Basic diagram of a standard radial bearing.

(b)

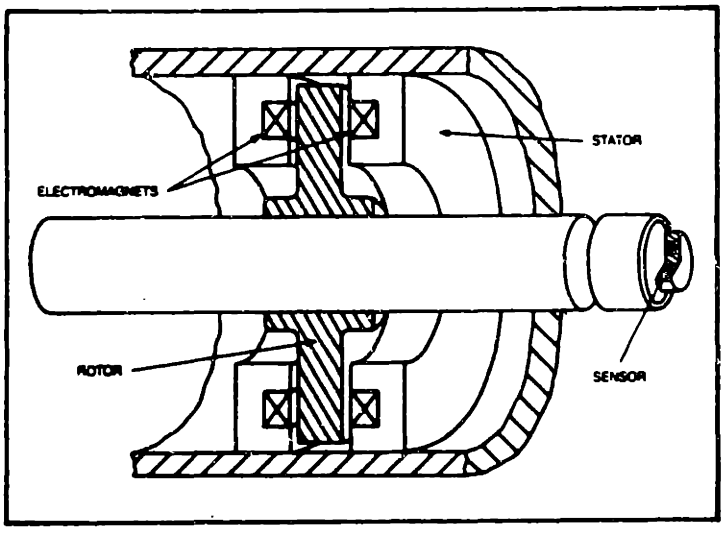

Basic diagram of an axial magnetic bearing.

Figure 4.18. Active magnetic bearings [from I2].
(a) A radial magnetic bearing.
(b) An axial magnetic bearing.

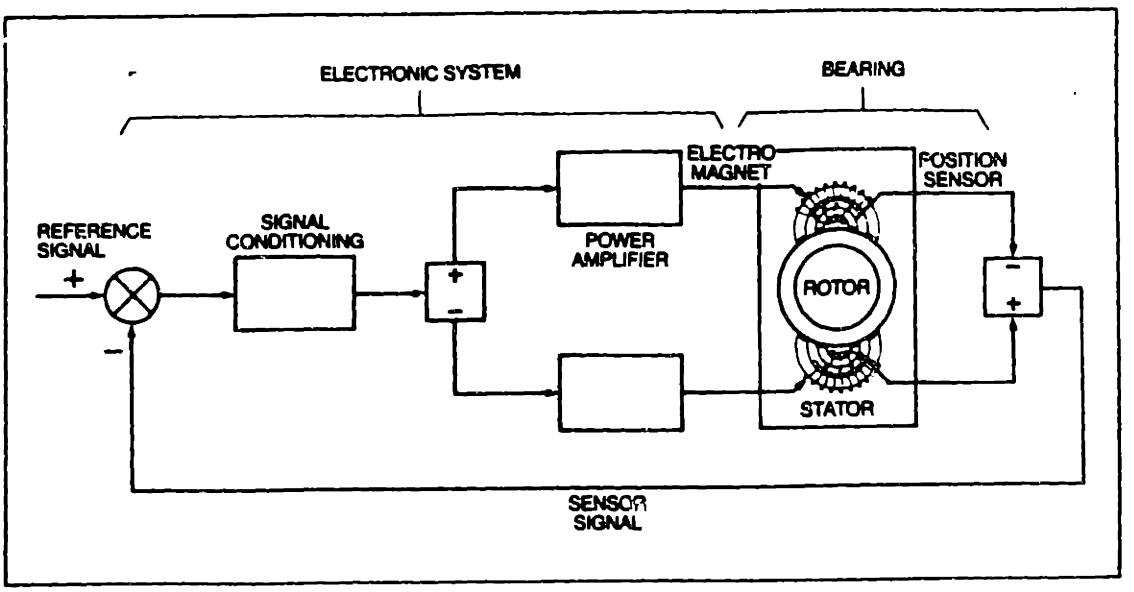

Basic diagram of control system for magnetic bearings.

Figure 4.19. An active-magnetic bearing control system [from I2].

dynamic behavior of the shaft. The output of the signal conditioner is sent to the power amplifiers. The power amplifiers amplify the control signal from the signal processor to a signal of sufficient strength for use in the bearing-stator electromagnets, thus affecting rotor position.

The ability to control shaft dynamic behavior gives active-magnetic bearings a significant advantage over hydrodynamically lubricated bearings. Conventional bearings provide very little damping [H2]. By changing the phase advance of the control circuit, active-magnetic bearings have the ability to alter their damping as necessary for the desired rotor dynamic response [H2, H3, H4]. Stiffness is controlled by gain, and can be increased 10 to 100 times by the addition of an integration term [H2, H4]. By controlling bearing dynamic behavior, it is possible to suppress shaft vibrations by 20-db [H3,H4]. This is important when operating at, or near, rotor critical speeds. When accelerometers mounted on the machine housing sense vibration, the magnetic-bearing system will increase damping to suppress vibrations [W2]. Figure 4.20 shows the dramatic effect of vibration control on a compressor rotor as it passes a critical speed.

A general feature of magnetic bearings is the ability to monitor rotor behavior continuously while in operation. Position sensors continuously monitor rotor position. The electronic control circuitry is capable of adjusting rotor behavior as desired. Whereas conventional bearings try to maintain the rotor geometric axis in the centerline of the bearing, active-magnetic bearings permit the rotor to turn about its axis of inertia, resulting in vibration-free operation due to this self-balancing effect. Complete electronic

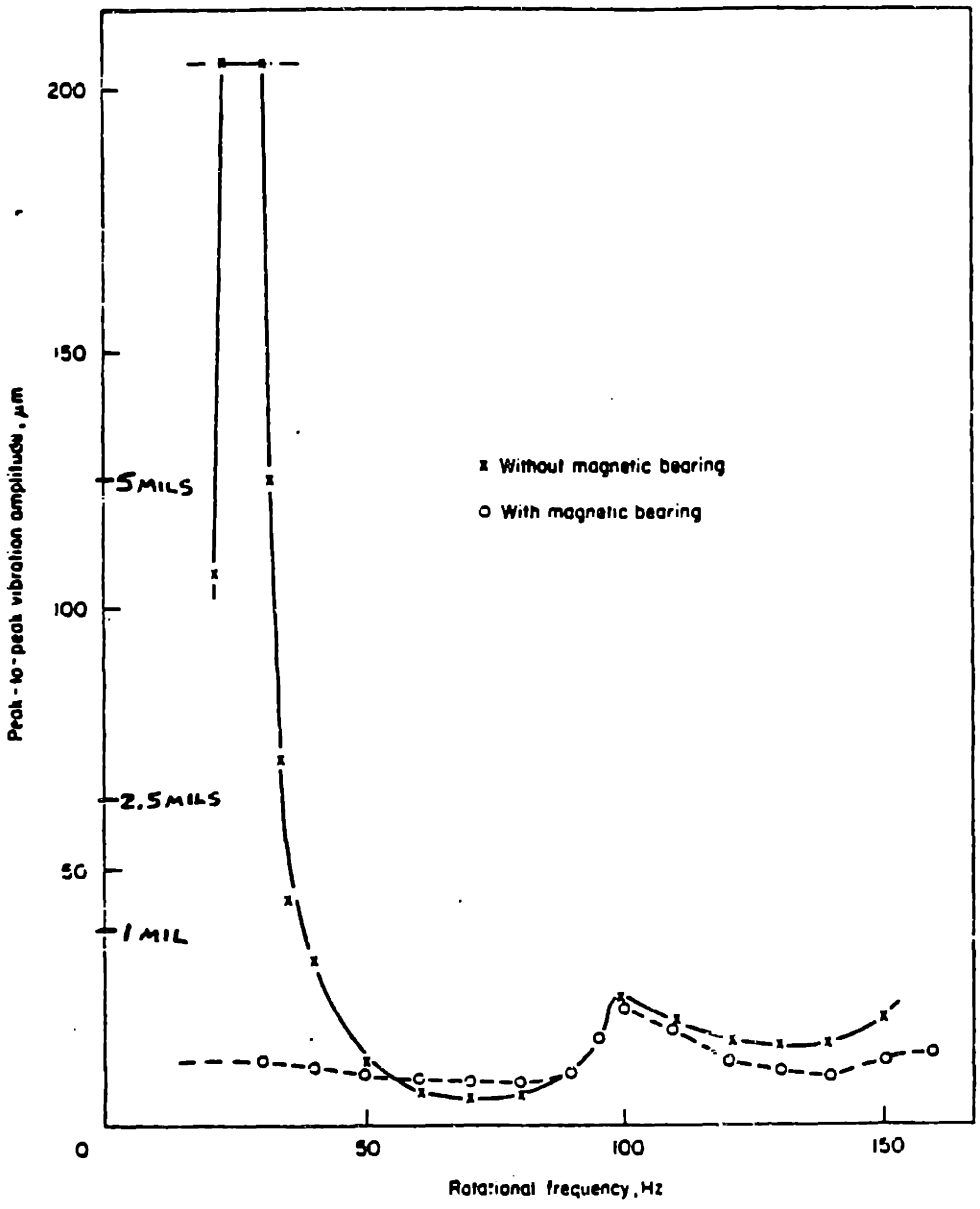

Figure 4.20. Active-magnetic-bearing suppression of critical speed deflection [from H4].

monitoring of shaft position and behavior is possible. With active magnetic bearings, some common maintenance procedures that require shutdown of fluid-lubricated bearings can be performed while the rotor is in operation. Full-speed, in-place balancing of the rotor is possible as well as continuous monitoring of bearing clearances [W2]. Shaft position is maintained very accurately, an important feature for high-performance turbomachinery. Precisions of 0.2 mils (5-μm) are common, with precisions of 2-μin (.05-μm) achieved in some special systems [H4].

4.6.3 Auxiliary Bearing.

At times when the shaft is not rotating and the magnetic bearing is shutdown, the shaft rests on an auxiliary bearing. Auxiliary bearings are generally solid or grease lubricated ball or roller bearings, or carbon rings for very small machine applications. In a helium environment, roller bearings are unsuitable, and only ball bearings may be used for the auxiliary bearing [P4]. For one large thrust-bearing application, an angular-contact-ball bearing is recommended, and is pictured in Fig. 4.21a. The auxiliary-bearing-rotor clearance is half that of the magnetic-bearing stator. A magnetic-bearing assembly is shown in Fig. 4.21b with the auxiliary bearing. The auxiliary bearings are not normally intended to support the shaft during shaft rotation. In the event of a loss of power to the magnetic-bearing system, a battery supplies sufficient power to support the shaft during rundown. Once the shaft has stopped, the auxiliary bearing can be used to support the shaft. In the event that the magnetic-bearing system fails such that magnetic suspension is not possible, the shaft runs down on the auxiliary bearing. In this

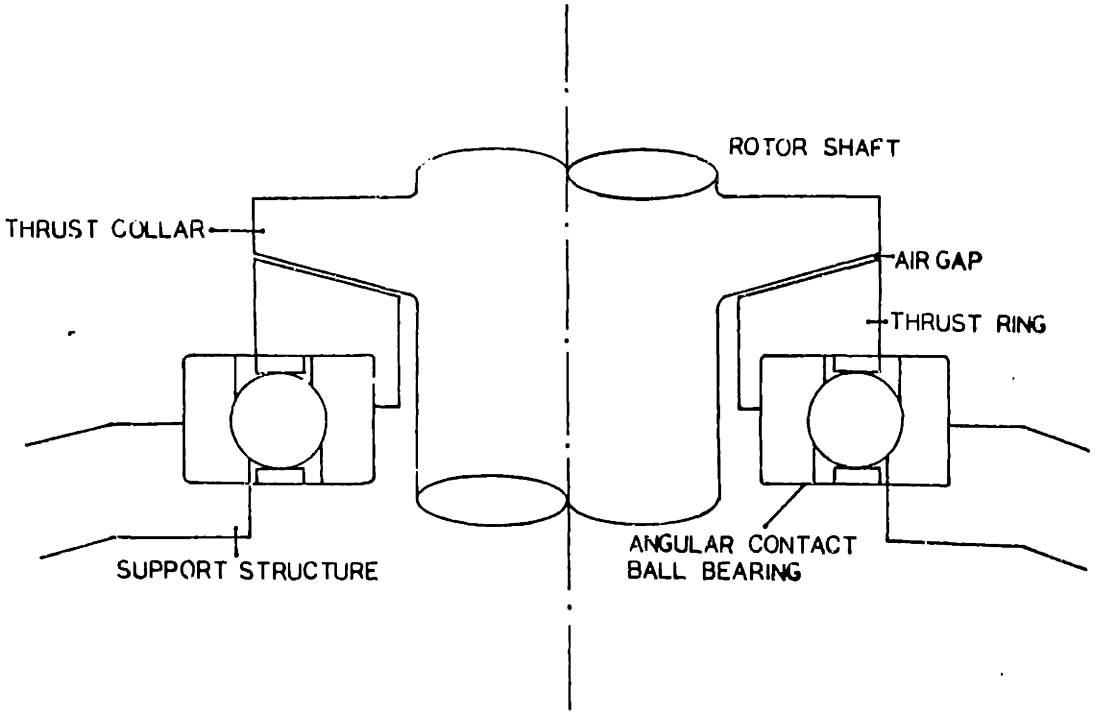

Figure 4.21a. An auxiliary bearing for a large active-magnetic thrust-bearing application [from P4].

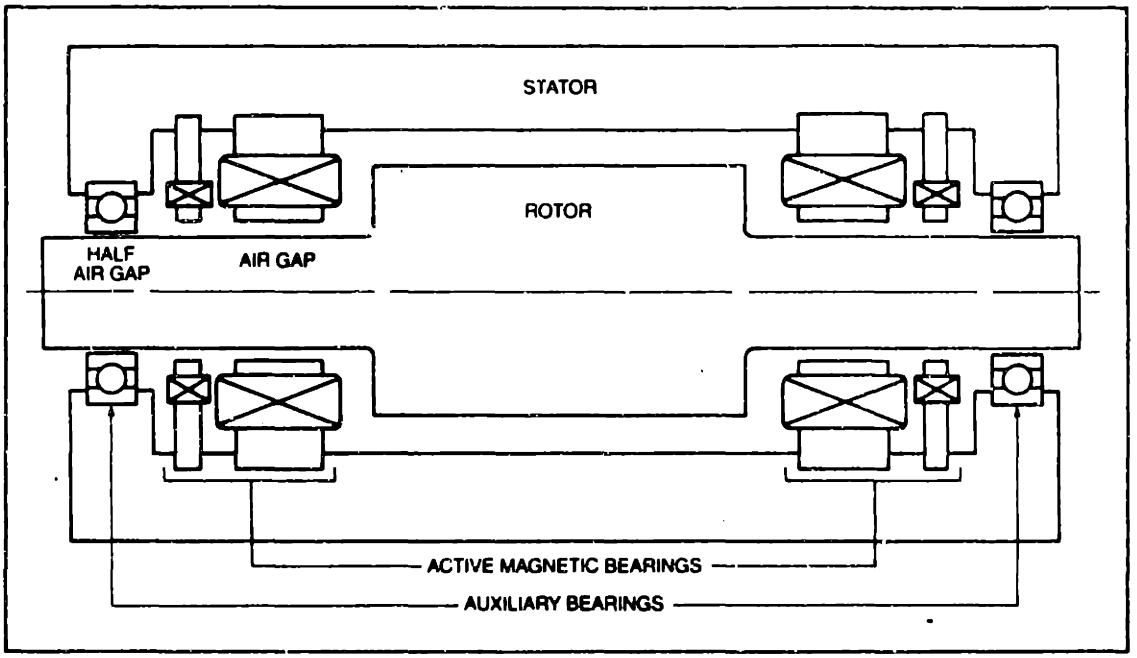

Basic arrangement of auxiliary bearings in machine with magnetic bearings.

Figure 4.21b. A magnetic-bearing assembly [from I2].

function, the auxiliary bearing is often referred to as a catcher bearing. The catcher bearing is used only for short durations during roll down, and it is not intended for normal use. Only a limited number of such rundowns are normally allowed for the catcher bearing over its lifetime.

4.6.4 Operational Applications and Limitations.

The following are some limits on the application of active magnetic bearings [H2, H3, H4, P4, W2,M26].

- Maximum Load: This depends upon the area available for the bearing. A nominal pressure of 140 psi with as high as 200 psi applies for both radial and axial bearings. This is slightly lower than oil-lubricated bearings, which have a maximum pressure typically around 250 psi [H9].

- Maximum Rotational Speed: For radial bearings, maximum surface lineal speed is 40,000-ft/min. For axial bearings, maximum lineal speed is 70,000-ft/min. These are determined by the ability of the radial-bearing rotor laminations and the axial-bearing thrust disc to withstand centrifugal forces.

- Temperature: Magnetic bearings have been used in environments ranging from -250°C to 450°C. Reliability data, however, is not available for all of these applications.

- Environment: Magnetic bearings have been used in air, vacuum, water, helium, UF_6, liquid oxygen, liquid hydrogen, and hydrocarbons. Again, reliability data is not available for all of these applications.

- Losses: Magnetic bearings have energy losses that are 10 to 100 times lower than the energy losses of fluid-lubricated bearings.

In Germany, active-magnetic bearings are used in a test-facility for high-temperature gas-cooled-reactor circulators. The bearings are subjected to temperatures up to 450°C. S2M lists the following advantages of magnetic bearings specific to the hot-helium-blower

application [P4]:

- No mechanical wear, and service lifetime expected of over 10 years.
- Compatability with a high temperature (450°C)
- Continuous electronic monitoring and control.
- High reliability due to redundancy. Multiple windings and multiple electronics cabinets.

The above list does not include some important advantages that would apply to a gas-cooled-reactor power plant, such as: elimination of moisture-ingress potential, elimination of a fluid-lubrication system that could potentially become contaminated, and elimination of several maintenance procedures that require plant shutdown and exposure of maintenance personnel to radioactivity.

4.6.5 Experience and Reliability.

Since active-magnetic bearings are a fairly new technology, there is a limited amount of experience with them. Only one company, S2M of France, presently manufactures active magnetic bearings, and markets them in the United States through their affiliate, Magnetic Bearings, Incorporated. Despite its youth, magnetic-bearing technology is growing in acceptance. Ingersoll-Rand presently offers magnetic bearings on their large turbomachinery [I2]. Table 4.3 lists several heavy-industrial applications of active-magnetic bearings manufactured by S2M, and their operating parameters. For the most part, the MGR-GT rotor dimensions and operating parameters will be within values that have been previously attained. The primary concern is the higher thrust load of the MGR-GT machinery.

Table 4.4 lists information on failure for a few of these

Table 4.3

Heavy-Industrial Applications of Active-Magnetic Bearings [P4]

Application (year)	Shaft speed (rpm)	Rotor mass (lbs)	Shaft dia. (in)	Bearing Capacity axial (lbs)	radial (lbs)	Machine power (hp)
Compressor (1980)	12,000	600	5.91	2,700	1,125	5,350
High Pressure Pump (1980)	10,000	400	6.69	2,920	90	135
Hot Helium Blower (1980)	3,600	570	7.48	695	810	27
Crusher (1981)	20,000	110	4.33	225	450	20
Compressor (1981)	20,000	660	5.91	1,575	560	410
Bearing test stand (1981)	3,300	5,070	23.60	-	11,000	70
Cryo-expander (1983)	40,000	90	3.74	1,560	165	200
Hot Helium Blower (1984)	6,000	2,428	14.10	13,245	993	7
Turbo-Blower (1984)	5,100	596	7.48	-	298	109
Turbo-Generator (1985)	3,000	16,555	21.25	8,830	8,830	6,795
Bearing test Stand (1985)	10,000	353	7.48	-	540	42
Shaft Bearings (1985)	3,000	4,415	12.20	-	3,300	54
Centrifugal Compressor (1985)	5,500	2,207	10.6	12,375	1,125	-

Table 4.4

Operating Data For
Industrial Equipment Equipped with
Active Magnetic Bearings [P4]

Machine	A	B	C	D
Printing Roll Lathes				
#1	14,900	12	no	PA
#2	18,500	8	no	PA
#3	3,800	1	no	PA
Hot Helium Blower	8,000	5	no	PA
Radial Bearing	310	0	no	

A Operating Hours

B # of Emergency Shutdowns

C Auxiliary Bearing Replaced

D Failed Component

PA = Power Amplifier

applications. From the limited data available, it appears that the component that contributes the most to failure is the power amplifier. In the early designs, the power amplifier Mean Time Between Failures (MTBF) was only about 2000 hours. Newer models offer an MBTF of the control circuit on the order of 40,000 hours (or, about five years of continous service) [H4, P4]. The remainder of the system components have demonstrated relatively trouble-free performance. In a recent report by Proto-Power Corporation to the Electric Power Research Institute on the potential application of magnetic bearings to electrically-driven-HTGR-helium circulators, the following conclusion was reached regarding the reliability potential of active-magnetic bearings [P4]:

> Based on the limited data available, it appears that the reliability of the magnetic bearings is almost solely dependent upon the reliability of the electronic control system and power amplifiers. Early magnetic bearing applications experienced a mean time between failures of only about 2000 hours due to failures of the power amplifiers. Recent applications have demonstrated improved reliability. Further developments in control circuit design which provide redundancy, fault detection, and automatic solid state switching offer the potential for high reliability. It should be possible to design active magnetic bearing components which are equivalent to other electrical power equipment and solid state control components in terms of reliability.

4.6.7. Application of Magnetic Bearings to the MGR-GT.

The performance capabilities of magnetic bearings are impressive, and the limited information on magnetic-bearing reliability appears promising. Active-magnetic bearings provide a solution to several problems that have plagued gas-cooled reactors, especially those with rotating machines within the primary-coolant circuit. The use of

active-magnetic bearings is therefore an essential ingredient in the MGR-GT design. The principal difficulty appears to be development of an auxiliary thrust bearing that can withstand the thrust loading of the MGR-GT in the event of magnetic-bearing failure, especially for a vertically configured turbomachine. In horizontal gas-turbine sets, the turbine and compressor are oriented so that their thrust loads oppose one another, reducing the required thrust-bearing size. If effort is made to orient the MGR-GT turbomachines such that their aerodynamic thrust opposes the machinery weight, the net thrust-bearing load can be substantially reduced. It is estimated that the turbine and compressor develop a net aerodynamic thrust of about 45,000-lbs (about 90,000-lbs for the turbine and 45,000-lbs for the compressor). Total weight of the rotating group is estimated at about 15,000-lbs. Net thrust while operating will therefore be about 30,000-lbs if the machinery is configured to minimize the thrust. This is the thrust that the auxiliary thrust bearing would be subjected to immediately after a sudden loss of the magnetic bearing system. The thrust load would drop as the aerodynamic thrust dropped while the machinery slowed down. Based upon the data of Table 4.3, it appears that the MGR-GT thrust load is roughly within the range of previous applications if more than one thrust bearing is used. It is expected that maintenance and accessibility requirements will make it necessary to use more than one thrust bearing.

4.7 The MGR-GT Electric Plant.

Previous sections demonstrated the need for turbomachine operation at rotational speeds much greater than 60-hz electrical generator synchronous speeds. Additionally, the need to eliminate liquid-lubricated machinery within the helium-coolant circuit makes any methods of shaft-speed reduction impossible. The MGR-GT generator must, therefore, operate at the same high speeds as the turbomachine, and produce electrical power at a frequency greater than 60-hz. Electrical frequency must then be reduced electronically to 60-hz. This section will discuss the generator and methods for electrical power conversion that are proposed for the MGR-GT.

4.7.1 Generator Design Considerations.

This section will briefly describe some important design considerations for the generator. Emphasis will be placed on understanding general effects of design parameters rather than the details of generator design. The effects discussed apply to all electrical rotating machinery, motors and generators; however, the discussion will primarily be in the context of generators. Of primary importance is the effect of raising generator rotational speed on the generator design.

4.7.1a Generator Mechanical Design Considerations.

This section will briefly outline the major mechanical-design considerations for electric generators.

4.7.1a.1 Stresses.

The generator rotor can be modelled as a rotating disk. Hence Eqs. 4.53 and 4.54 can be used to determine rotor stresses. The stresses are, therefore, proportional to the square of the surface

velocity.

$$\sigma \approx \left[\omega\ r_2\right]^2 \tag{4.72}$$

The limiting stress will correspond to a limiting surface velocity. For a fixed limiting stress:

$$r_2 \approx \left[\frac{1}{\omega}\right] \tag{4.73}$$

Thus, as rotational speed is increased, the maximum allowed rotor diameter will be reduced proportionately.

4.7.1a.2 Dynamic Behavior.

Synchronous machine designs, like turbine designs, need to consider critical speeds; however, there are some additional forces that must be considered. Cores of synchronous machines are subject to lateral vibrations due to magnetic pull. Two-pole machines are particularly affected by this (see Fig. 4.22). If the frequency of the lateral force is near a natural frequency for the rotor, severe fatigue damage could result to the machine. This effect must, therefore, be considered in the critical speed analysis.

When motorizing a synchronous machine from a commutated inverter, torsional ocillations will occur [U1]. These must not be at a frequency corresponding to a torsional natural frequency, or fatigue damage could result.

4.7.1b Generator Electrical Design Considerations.

This section will estimate the effect of changing rotor rotational speed and rotor cooling on the generator design. The scaling relationships shown here are approximate. They are not intended for detailed design. Certainly, much more analysis would be required for an actual design; however, the relationships demonstrate important trends to be considered in the actual generator design.

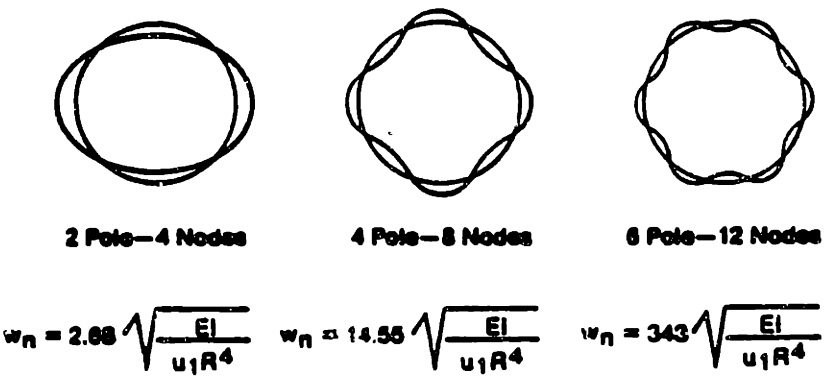

Figure 4.22. Lateral magnetic vibration of synchronous machines [from D6].

Power output from the generator is equal to

$$\bar{P} = \bar{T}\cdot\omega = \tau\cdot 2\cdot\pi\cdot r_2^2\cdot L\cdot\omega$$

$$\approx \frac{r_2 L}{g}(nI)_R(nI)_S\sin(\delta)\cdot\omega \qquad (4.74)$$

If torque angle is kept constant, since

$$B_{max} \approx \frac{nI}{g}\ , \qquad (4.75)$$

it can be shown that

$$\bar{P} \approx r_2\cdot L\cdot g\cdot B_{max,R}\cdot B_{max,S}\cdot\omega \qquad (4.76)$$

Also, from Eqs. 4.73 and 4.74,

$$\bar{P} \approx \tau\cdot r_2\cdot L \qquad (4.77)$$

τ is the surface shear stress on the surface of the generator (or motor) rotor. This can be limiting for the machine. Most often machines operate near saturation, so that B_{max} is limiting. Therefore, keeping in mind that r_2 is inversely proportional to ω because of centrifugal stresses, from Eq. 4.76

$$\bar{P} \approx L\cdot g \qquad (4.78)$$

Most generators are cooled with hydrogen or air. Hydrogen has good heat transfer characteristics, is fairly available, and has low pumping and windage losses. It is used in large utility generators. Air has poorer heat- transfer characteristics and higher pumping and windage losses, but is readily available. Air is used as the cooling medium in most smaller machines. The properties of helium are such that its heat-transfer performance will be close to that of hydrogen, with pumping losses only slightly worse.

If rotor cross-sectional geometry is kept constant, as in Fig. 4.23, the cross-sectional area of conductor will behave as the square of rotor diameter. Electrical resistance will increase with $\left[\frac{1}{r_2}\right]^2$, or

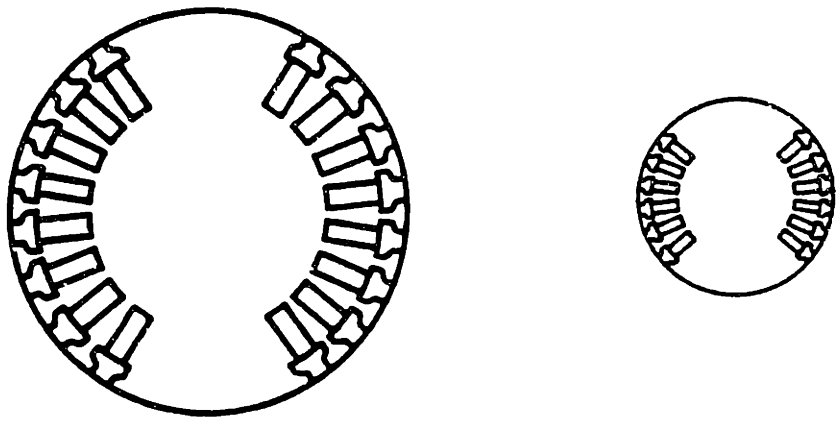

Figure 4.23. Effect of increasing rpm on geometrically similar rotors [from H9].

with ω^2. The effects of heat transfer can be scaled if the following relationships are considered:

$$Q_r = I^2 \cdot R = H \cdot A \cdot \Delta T \tag{4.79}$$

and

$$R \approx \left[\frac{1}{r_2}\right]^2 \tag{4.80}$$

and

$$A \approx r_2 \approx \frac{1}{\omega} \tag{4.81}$$

Assuming that the coolant flow in the generator is mostly turbulent and obeys the McAdams analogy [R1],

$$\frac{H \cdot D_h}{k_b} = (0.023)\left[\frac{G \cdot D_h}{\mu}\right]_b^{0.8}\left[\frac{\mu \cdot C_p}{k}\right]_b^{0.4}. \tag{4.82}$$

the following equation will result from Eqs. 4.73-4.82 if ΔT, B_{peak}, and $\bar{P}$ are kept constant:

$$\frac{L_1}{L_2} = \left[\frac{\omega_1}{\omega_2}\right]^{1.4} \cdot \left[\frac{\mu_1 \cdot C_{p2}}{\mu_2 \cdot C_{p1}}\right]^{0.2} \cdot \left[\frac{\rho_2}{\rho_1}\right]^{0.4} \cdot \left[\frac{k_2}{k_1}\right]^{0.3} \tag{4.83}$$

1 and 2 refer to two rotors that are geometrically similar in cross section, are operating at the same rotor and stator flux-density levels, use different cooling mediums, have the same rotor and fluid velocities at geometrically similar locations, and operate at different rotational speeds.

If rotor 1 circulates 300°C helium at 80 atmospheres for cooling, and rotor 2 circulates 300°C air at atmospheric pressure for cooling, then the following expression will result from Eq. 4.83.

$$\frac{L_1}{L_2} = (0.1638) \cdot \left[\frac{\omega_1}{\omega_2}\right]^{1.4} \tag{4.84}$$

Thus, for equal rotational speeds, a rotor cooled with high-pressure helium should be shorter than a geometrically similar rotor of equal power and speed that is cooled by air at atmospheric pressure. In fact, for $\frac{\omega_1}{\omega_2} < 3.6$, Eq. 4.84 predicts that $L_1 < L_2$. It is possible that the rotor will become shear-stress limited before the

length is reduced as much as this model predicts; however, the results of this model can be applied to do some rough scaling.

The reduced length of a rotor cooled with high-pressure helium results from the increased current density permitted through improved cooling. This increased current density results in the higher electrical losses of Eq. 4.79. Combining Eqs. 4.73, 4.75, 4.78, 4.79, 4.80, and 4.84, the following expression results for current losses.

$$\frac{Q_{r1}}{Q_{r2}} = \left[\frac{\omega_1}{\omega_2}\right]^2 \cdot \left[\frac{L_2}{L_1}\right]^2 = 37.3 \cdot \left[\frac{\omega_2}{\omega_1}\right]^{0.8} \tag{4.85}$$

For most conditions, the electrical losses in the rotor cooled in high-pressure helium will be much greater than the losses in the rotor cooled in atmospheric air.

To estimate the pumping losses for the coolant circulation it is again assumed that flow is largely turbulent so that:

$$\Delta P = 4 f \frac{L}{D_h} \frac{G^2}{2 \rho} \tag{4.86}$$

and

$$f = \frac{0.046}{Re^{0.2}} \tag{4.87}$$

and

$$Re = \frac{G D_h}{\mu} \tag{4.88}$$

Pumping power equals $\dot{V} \cdot \Delta P$. If rotor 1 is cooled by helium at 80-atm and rotor 2 is cooled with air at 1-atm, coolant channel length is proportional to rotor length, fluid velocities are the same, and flow cross-sectional area is proportional to r_2^2, or $\left[\frac{1}{\omega}\right]^2$, it can be shown that

$$\dot{V} \cdot \Delta P \approx \left[\frac{\mu^{0.2} \rho^{0.8}}{\omega^{0.8}}\right] \cdot L \tag{4.89}$$

$$\frac{(\text{Pumping Power})_1}{(\text{Pumping Power})_2} = 6.935 \frac{L_1}{L_2} \left[\frac{\omega_2}{\omega_1}\right]^{0.8}$$

$$= 1.136 \left[\frac{\omega_1}{\omega_2}\right]^{0.6} \tag{4.90}$$

If rotor 1 operates at 10000-rpm and rotor 2 operates at 5250-rpm, rotor 1 will have roughly 1.7 times the coolant-pumping losses of rotor 2.

Windage losses are equal to

$$\bar{P}_{WL} = \tau_{WL} \cdot 2\pi \cdot r_2^2 \cdot \omega \cdot L \tag{4.91}$$

with

$$\tau_{WL} = \mu \frac{du}{dy} \tag{4.92}$$

Since $u_1 = u_2$, $dy \approx g$, and g is inversely proportional to L (see Eq. 4.78), for rotor 1 (the 80-atm helium-cooled rotor), and rotor 2 (the 1-atm air-cooled rotor),

$$\frac{\bar{P}_{WL1}}{\bar{P}_{WL2}} = \frac{\mu_1 \cdot L_1^2 \, \omega_2}{\mu_2^2 \cdot L_2^2 \, \omega_1} = 0.0288 \left[\frac{\omega_1}{\omega_2}\right]^{1.8} \tag{4.93}$$

and the windage losses for the helium rotor at 10000-rpm are only about 9% those of the air rotor at 5250-rpm. This is largely due to the smaller surface area and larger air gap of the high-speed rotor.

4.7.2 The MGR-GT Generator.

Because utility generators supply 50 or 60-hz electrical power, and are driven by machines operating at synchronous rotational speeds, or sometimes through reduction gears, the difficulties of operating a high speed generator have not posed serious problems in past generator design. Hence, there is no experience with large, utility generators that operate at speeds greater than 3600-rpm. However, recent interest in variable-speed-drives has caused development of large, high-speed, synchronous motors, driven by variable-frequency power supplies. Since the difference between a synchronous motor and a synchronous generator is primarily the application, not the machine, the technology of variable-speed-drives may be applied directly to high-speed-generator applications.

Large variable-speed-drive systems, for power levels from a few megawatts to about 50-MW, and rotational speeds up to over 5000-rpm (for the largest), are presently available through a few manufacturers. Most systems in this power range are composed of a Load Commutated Inverter (LCI), that converts 60-hz power to high-frequency power for a high-speed, air-cooled, two-pole synchronous motor. Figure 4.24 shows the operating range for the Toshiba Super Motor Drive System. Total system efficiencies are high, over 95% for the combined motor and LCI (Fig. 4.25).

The 5250-rpm, 30-MW Toshiba Super Motor has a rotor with a diameter of 15-in and a length of 27-ft [S17]. If a 5250-rpm machine were to be cooled by high-pressure helium and operate at 10,000-rpm and the same power level, Eq. 4.84 predicts that the rotor length would be reduced to about 40% of the original length. Based upon this, a 30-MW machine with a geometrically similar rotor to the Super Motor would have a diameter of 7.9-in and a length of 11-ft. According to Eq. 4.58, its first critical speed would be increased to over 300% of the original first critical speed. This much shortening of the shaft (and increasing of critical speed) might not, in fact, occur because of rotor shear-stress limitations; however, the results show very favorable trends. Hence, it is not believed that design of such a generator will require more than a modest design effort.

Toshiba Corporation performed a preliminary design of a high-speed, 100-MW generator cooled by high-pressure helium. At a rotational speed of 8000-rpm, it had two 50-MW cores connected in tandem on the same shaft for a total machine length of about 11-meters. This is in good agreement with the results of the scaling

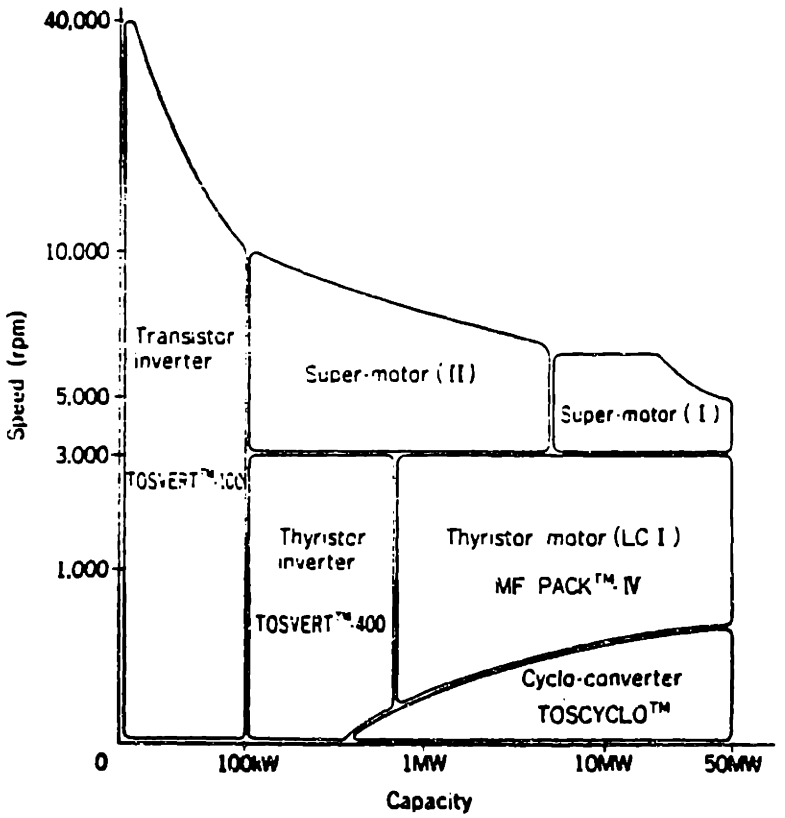

Figure 4.24. The operating range of Toshiba variable-speed-drives [from T3].

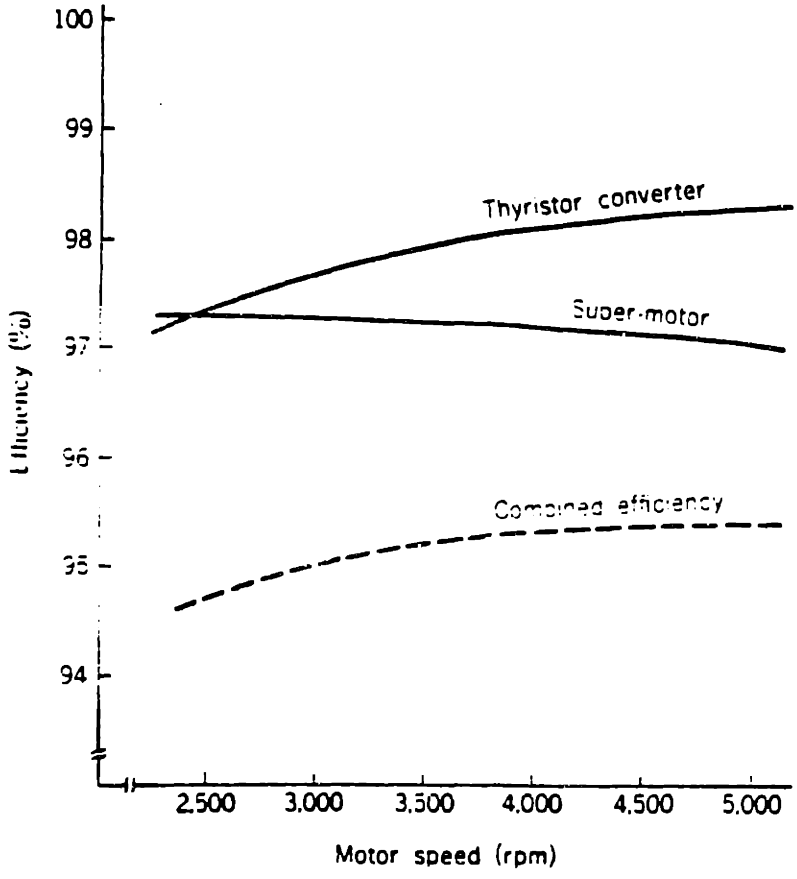

Super Motor Drive System efficiency (30,000kW-5,250rpm)

Figure 4.25. Efficiencies of Toshiba Super-Motor [from T3].

calculations in the previous paragragh. Efficiency of the machine is lower than normal, 95%. This is largely a result of higher friction losses in pumping the dense high-pressure helium. Toshiba is confident that a higher efficiency will result after a detailed design is performed [T5].

4.7.3 Frequency Conversion Methods.

Solid-state methods for conversion of electrical power of one frequency to electrical power of another frequency have been developed and widely used. The technologies that are useful for the power levels of interest generally operate by rectifying AC power from the source to DC power, and constructing AC power from the DC through solid-state switching circuits. High Voltage DC (HVDC) is used for connection of very large systems of different frequencies or for isolation of weak sections of the power grid. Four applications on the order of the size of the MGR-GT power system are listed in Table 4.5. For large synchronous motors, LCI's are normally used, and an LCI-type of system would probably be chosen for the generator of the MGR-GT.

Creating DC from an AC signal is not a difficult problem. By rectifying the AC signal and using a smoothing reactor, it is possible to generate a good DC signal. Creating a good AC signal from a DC signal is more difficult. Stepped signals can be generated and smoothed close to a sine wave with a reactor; however, the more difficult problem is dealing with the harmonics that are produced (see Fig. 4.26). The fundamental produces torque; however, the harmonics produce circulating currents and losses. The harmonics are on the order of $k \cdot p \pm 1$ ($k = 1,2,3...$, $p \equiv$ number of thyristor pulses, always a multiple of six). The fifth and seventh harmonics are of particular

Table 4.5

Installed Converter Terminals [B16]

Location	Capacity (MW)	Cost (Million $)
Mile City, Montana*	200	28
Clovis, New Mexico	200	23
Highgate, Vermont	150	19.5
Sydney, Nebraska	200	23

* This links two weak systems, and therefore requires a more expensive system.

Examples of some converter terminals installed in the United States. All are for 60 hz.- 60 hz. system isolation.

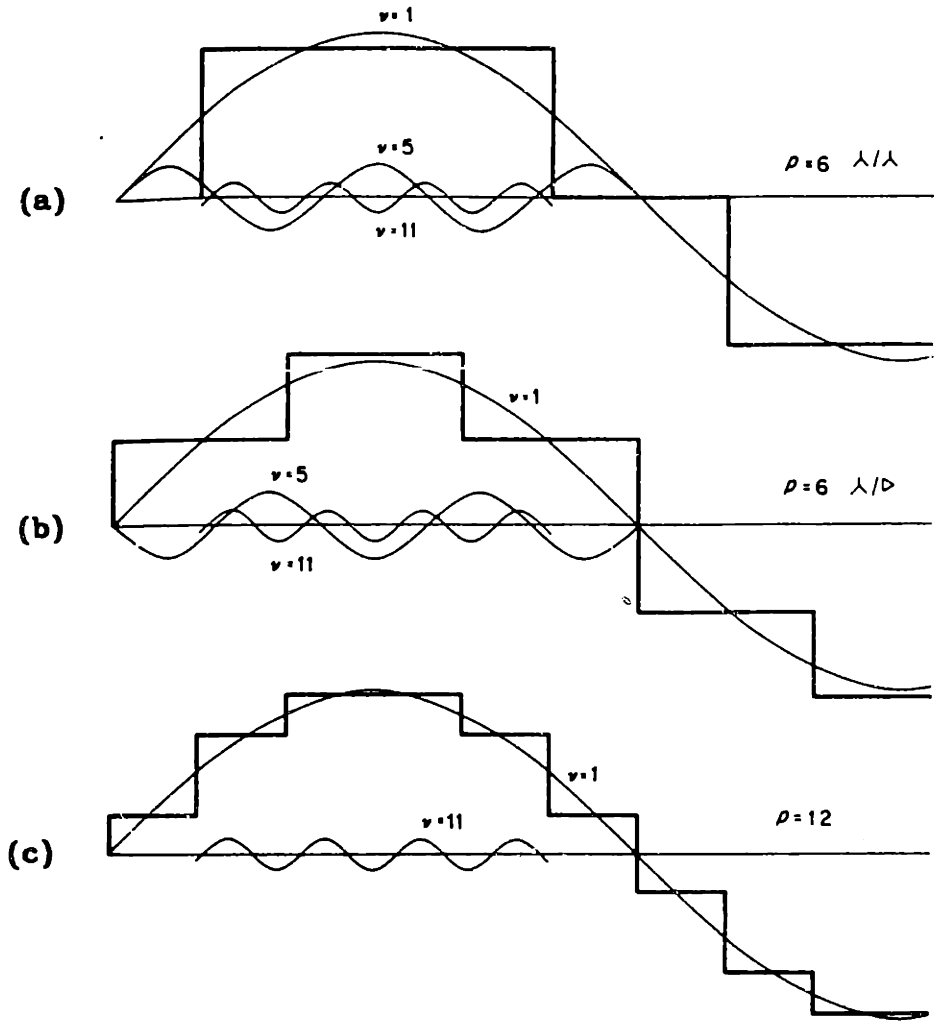

Figure 4.26. Effects of number of thyristor pulses on wave shaping and harmonics [from M23].
(a) Six-pulse Y-Y
(b) Six-pulse Y-Δ
(c) Twelve-pulse Y-Y or Δ-Δ

concern because they can induce rotor-surface currents that may damage some rotors through local heating. By increasing the number of thyristor pulses, the harmonics can be diminished. Inducing a $\frac{\pi}{6}$ phase shift by using Δ-Y transformation improves the waveshaping, but does not reduce the harmonic currents. Table 4.6 compares harmonic currents present in six-pulse and twelve-pulse inverters. The fifth and seventh harmonics are virtually eliminated in the twelve-pulse inverter. Thus, high-pulse inverters (12-pulse or higher, up to 36-pulse) are used in applications where it is important for harmonics to be minimal and waveshape good. Toshiba's proposed electrical system design for the MGR-GT uses a 24-pulse LCI for frequency conversion [T5].

4.7.3a Load Commutated Inverter.

This section will give a brief discussion of the LCI as an example of the type of technology that might provide the basis for the MGR-GT electrical system. LCI's offer variable-speed, speed-regulation, and braking capabilities for large synchronous motors. Power levels of over 40-MW are presently available with machine speeds of 5000-rpm. Smaller sized machines are capable of even higher speeds [H9,T3,U1]. Frequencies of over 400-hz are possible [W3] with developments to increase capabilities in progress [T2].

Figure 4.27 shows the basic circuit of the Toshiba MF Pack LCI. When power is being supplied to the machine (motor), the incoming AC is passed through a rectifier that, with a smoothing reactor, creates a DC signal. The DC signal is not usable in the synchronous motor and must be converted to a usable signal in the inverter. The inverter, or thyristor-commutator, is controlled by the gate logic circuit, and converts the DC to AC power, which is used to power the synchronous

Table 4.6

Converter pulses	Harmonic Order							
	5	7	11	13	17	19	23	25
6	.175	.11	.045	.029	.015	.010	.009	.008
12	.026	.016	.045	.029	.002	.001	.009	.008

Table 4.6. Typical harmonic currents present in the input current to a static power converter (per unit of fundamental current) [from U1].

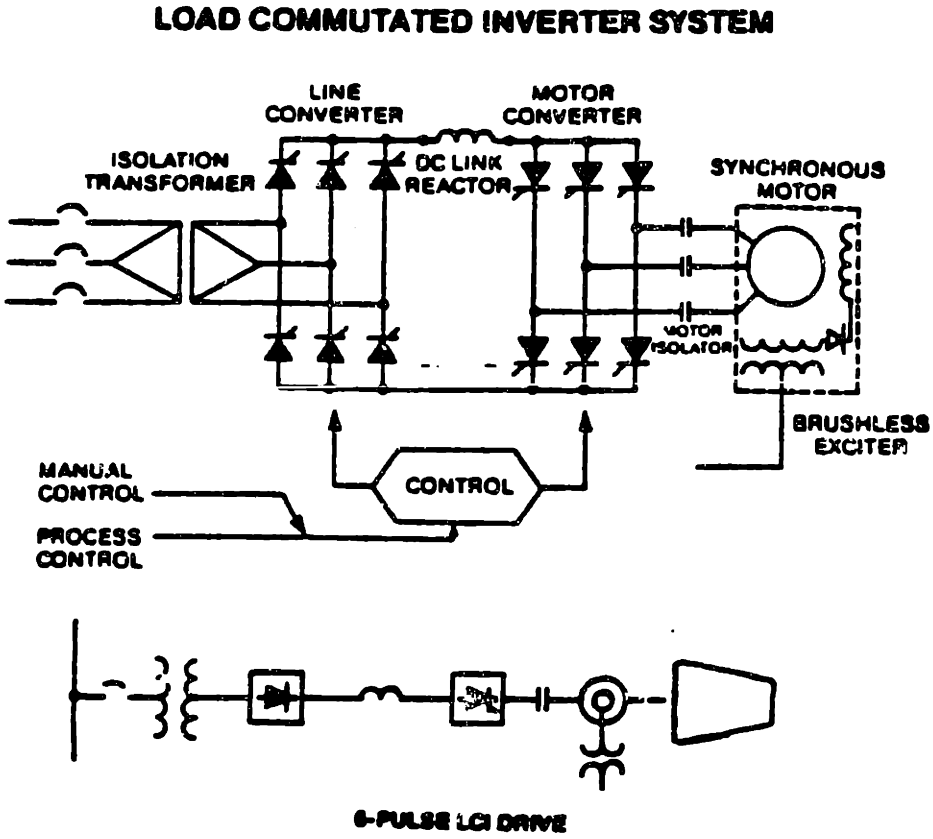

Figure 4.27. Basic circuit of an LCI [from G11].

motor. The thyristor-commutator in an LCI works by the principle of load-commutation.

The principle of load-commutation is best explained by Fig. 28. When the counter-EMF of phase u (e_u) is greater than the counter-EMF of phase v (e_v), the gate-logic circuit triggers the positive thyristor for phase v (VP) to fire. This point leads β, the control-angle of advance, from the point where e_u is equal to e_v. This establishes a short-circuit current ($e_u > e_v$) that turns off the positive thyristor of phase u (UP). Rotor rotation and gate-logic-circuit operation cause this operation to continue sequentially on each phase, so that each phase of the machine armature receives an alternating square-wave signal. The phase-phase voltage will have more of a stepped shape because of the phase shift. The machine has small differences from a normal synchronous machine that permit it to use such signals; however, it is essentially the same.

Four quadrant operation is possible with an LCI drive - the machine may be operated in forward or reverse, as a motor or a generator. By microprocessor control, acceleration and deceleration can be programmed as well as control speeds. The machine can brake, in the event of overspeed. With reactors installed in the LCI, the microprocessor can provide power-factor control, or can alter electrical harmonics as necessary. The ability to control the LCI system by microprocessor and the ability of the LCI-drive system to operate in all four quadrants introduces interesting control-system possibilities that will be addressed in Chapter Six.

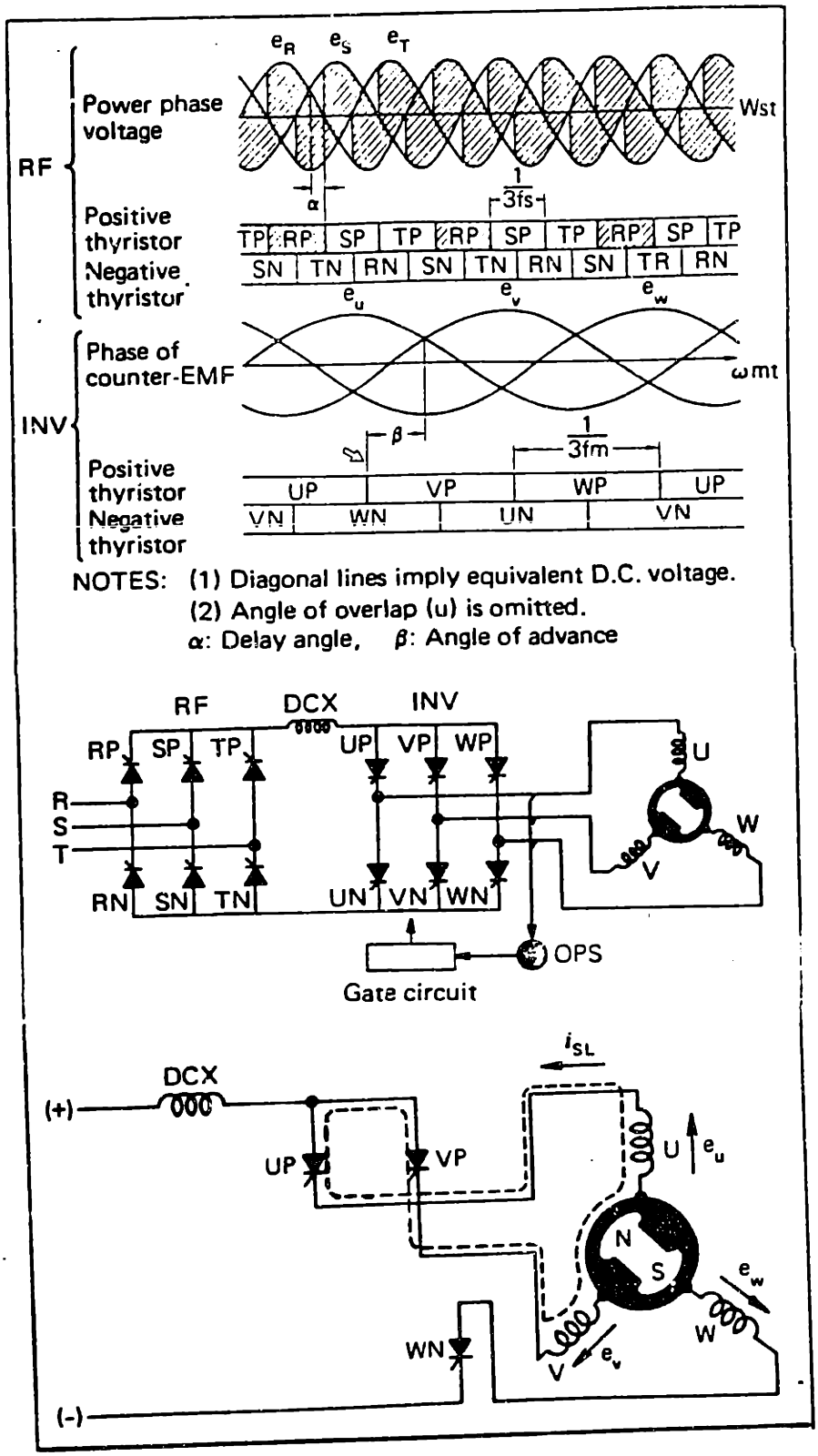

Figure 4.28 The principles of load commutation [T3].

Machinery Design Nomenclature

(except where specified in text)

Symbol	Meaning	Units
a	First constant in general SRE soln.	
A	Annulus area swept by blades	m^2
b	Blade axial chord	m
b'	Second constant in general SRE soln.	
B	Flux density	tesla
c	Blade chord	m
c^*	Distance of the furthest point from the blade cross-section neutral axis	m
C	Actual gas velocity	m/sec
C_p	Constant pressure specific heat	J/kgK
D	Diameter	m
D_t	Tip diameter	m
D_h	Hub diameter	m
e	Radius of curvature of blade convex surface downstream of throat	m
g	Acceleration of gravity	= 9.8 m/s^2
g	Generator gap width	meters
h	Specific enthalpy	J/kgK
H	Blade height	m
I	Moment of inertia (except Section 4.7)	m^4
I	Current (Section 4.7)	amperes
k	An integer	

k	Thermal conductivity	W/m^oK
L	Length (normally of rotor)	meters
$\dot{m}$	Mass flow rate	kg/sec
M	Bending moment on blade	N m
n	Number of turbomachine stages, or number of generator windings (Section 4.7)	
n_c	Compression polytropic exponent	
n_t	Turbine expansion polytropic exponent	
N	Rotational Speed	rpm
N_s	Specific Speed	
O	Throat	m
p	Number of thyristor-pulses	
P	Pressure	Pa
$\bar{P}$	Power	W
Q	Volume flow rate	m^3/sec
Q_r	Generator heat transfer	W
r	Radius	
R	Electrical resistance	ohms
Re	Reynolds' number	
Rn	Stage reaction	
s	Blade spacing	m
t	Time	sec
T	Temperature	^oK
$\bar{T}$	Torque	N m
tf	Blade-stress taper factor	
U	Blade velocity	m/sec
v	Specific volume	m^3/kg

$\dot{V}$	Volume flow rate	m^3/sec
W	Gas velocity relative to rotor blade	m/s

Greek

α	Actual angle of gas flow	deg.
β	Angle of gas flow relative to rotor blade	deg.
δ	Synchronous machine torque angle	deg.
∂	Partial derivative	
Δ	Change in parameter	
γ	Ratio of specific heats	
η_t	Turbine isentropic efficiency	
η_c	Compressor isentropic efficiency	
η_{pt}	Turbine polytropic efficiency	
η_{pc}	Compressor polytropic efficiency	
η_{ts}	Total-to-static efficiency	
η_{tt}	Total-to-total efficiency	
λ	Blade setting angle	
μ	Dynamic viscosity	kg/msec
υ	Kinematic viscosity	m^2/sec
ψ	Stage loading coefficient	
ϕ	Flow coefficient	
π	Geometric constant = 3.14159	
ρ	Density	kg/m^3
ρ_m	Metal density	kg/m^3
σ_c	Centrifugal blade stress	Pa
σ_b	Blade bending stress	Pa

τ	Shear stress	Pa
ω	Angular speed	rad/sec

Others

Θ	Hub-to-tip diameter ratio
$\approx$	Proportional tc

Superscripts

*	Base case

Subscripts

c	Referring to the compressor
m	At the mean diameter
t	Referring to the turbine
in	At the turbomachine inlet
exh	At the turbomachine exhaust
max	Maximum
o	Indicating at stagnation conditions
r	Referring to the rotor
s	Referring to the stator
st	Indicating at static conditions
x	In the axial direction
θ	In the tangential direction
0	At the turbomachine-nozzle inlet
1	At the turbomachine rotor-blade inlet, or at the rotor inner radius, or for high-speed, high-pressure-helium cooled machine
2	At the turbomachine rotor-blade exit, or at the rotor outer radius, or for 3600-rpm, air-cooled machine

CHAPTER FIVE

HEAT-EXCHANGER AND SYSTEM HYDRAULIC DESIGN

5.1 Introduction.

The Brayton-cycle analysis summarized in Chapter Two demonstrated that system performance, especially cycle thermal efficiency, is strongly affected by recuperator effectiveness, compressor-inlet temperature, and system pressure drop. Each one of these parameters is largely a function of the design of the heat exchangers in the system. It is possble, in the limit, to design a heat exchanger of near 100% effectiveness with near zero pressure drop, but this heat exchanger would be of such great size as to make it too expensive to produce and too awkward to put in a real system. It is possible, however, to design heat exchangers of high effectiveness, low specific pressure drop, and reasonable size, if novel design methods are utilized.

The following chapter discusses the design of the MGR-GT heat exchangers other than the heat source; the recuperator, and the precooler. This chapter will also discuss the system pressure drop in the ducting. A list of nomenclature used in this chapter is located at the end of the chapter.

5.2 Heat Exchangers in the MGR-GT.

The heat exchangers of interest in this chapter are only those of the power-conversion system; the recuperator, and the precooler.

5.2.1 Recuperator Design.

All previous direct-cycle designs for gas-cooled reactors have used tube-and-shell recuperators. Tube-and-shell heat exchangers, due

to their rugged construction, have traditionally been used in all applications where high pressure differences exist between heat transfer media, and where high reliability is demanded. Tube-and-shell heat exchangers offer great ease in repair compared to other heat-exchanger designs. Their heat-transfer surface area, however, is limited to the area of the tubes. For this reason, they tend to have lower heat-transfer surface area densities (hereafter referred to as surface compactness, units being m^2/m^3) than some other heat-exchanger designs.

Because of the low densities of gases, convective heat-transfer coefficients for gas heat transfer are generally lower than those of liquids. Consequently, very large surface areas are normally required in heat exchangers for gases. Heat-transfer coefficients may be improved somewhat by increasing the Reynolds number of the flow; however, the pressure drop across the heat exchanger will increase rapidly, demanding additional pumping power and a loss in efficiency. To meet design criteria, tube-and-shell, gas-to-gas heat exchangers tend to be very large because of their low surface compactness. Thus, the capital cost of a power plant using a high-effectiveness, low-pressure-drop tube-and-shell recuperator can be so high as to make such a design economically untenable.

5.2.1a The Plate-Fin Heat Exchanger.

Plate-fin heat exchangers have previously been used in gas-to-gas heat exchangers where the ruggedness and simplicity of a tube-and-shell heat exchanger were not mandatory. Plate-fin geometries generally have a much higher heat-transfer surface compactness. Figure 5.1 compares the surface compactness of tube-and-shell heat exchangers

to plate-fin heat exchangers, and shows the dramatic advantage in surface compactness, roughly an order of magnitude, that plate-fin heat exchangers have over their tube-and-shell counterparts. It is possible to manufacture a plate-fin heat exchanger that is a fraction of the size of a tube-and-shell heat exchanger of equal performance. Plate-fin heat exchangers are especially useful in equipment where size and weight are important. Aerospace systems are one example of where plate-fin heat exchangers have seen extensive application. Industrial systems can benefit from the use of plate-fin heat exchangers through improved transportability, and reduced pressure-vessel sizes. Consideration of these effects could make a plate-fin heat exchanger much more attractive than a tube-and-shell heat exchanger of equal performance.

5.2.1b Plate-Fin Heat Exchanger Construction.

Rugged and reliable plate-fin heat exchangers have been constructed in recent years as a result of advances in plate-fin heat-exchanger manufacturing methods. The need for reliable, lightweight, high-performance heat exchangers in aerospace applications has driven development of the plate-fin heat exchanger [01]. Materials and manufacturing methods have been the principal areas of advancment.

Two methods of metallic plate-fin heat-exchanger construction are shown in Fig. 5.2. In the compression-braze method of plate-fin heat-exchanger construction, high-pressure air fills the air passages while the finned sections are loaded in compression. Strongbacks are needed to hold the unit together since these units are normally used in systems that are located in a normal-atmospheric environment.

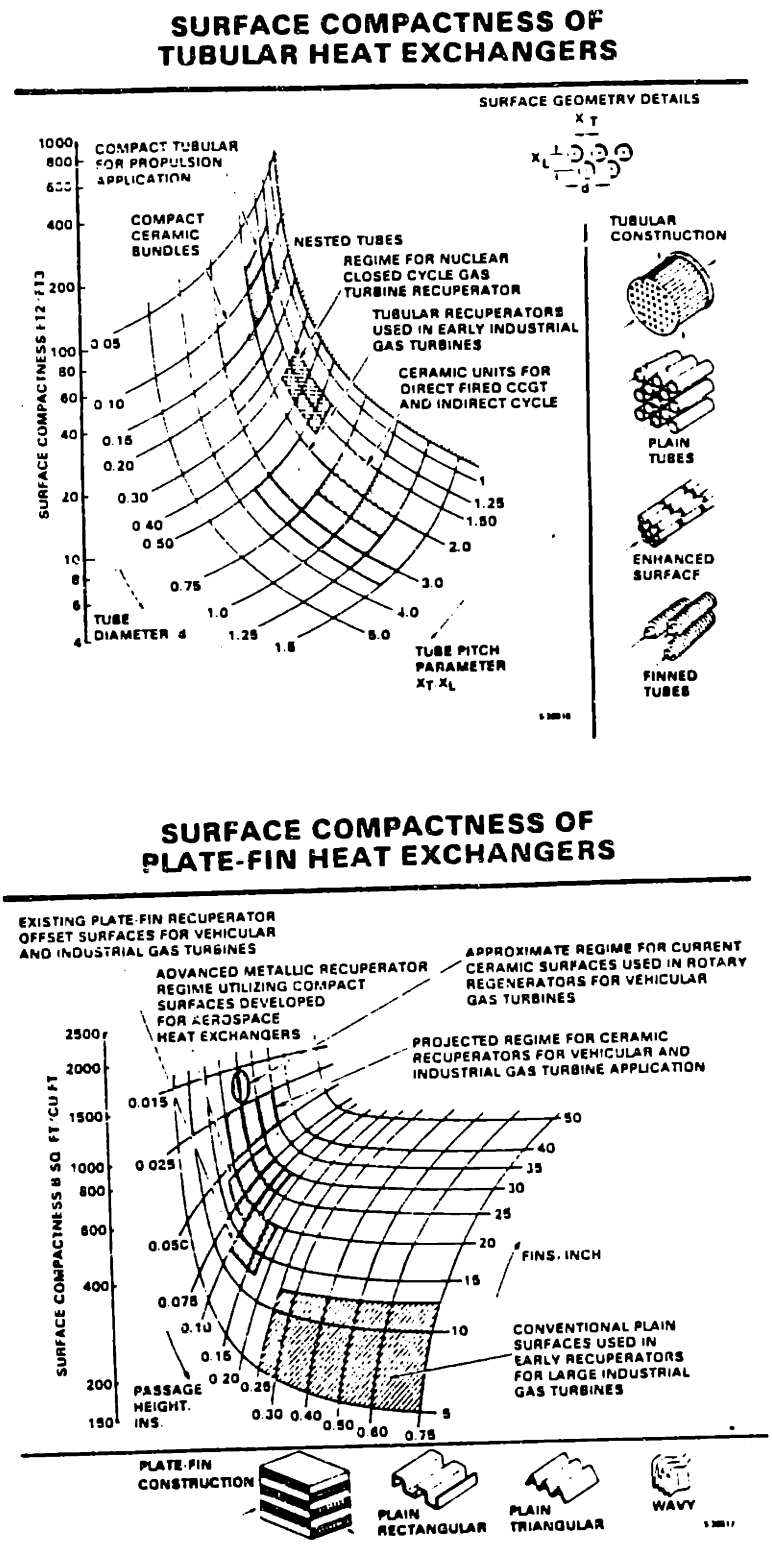

Figure 5.1. Comparison of surface compactness for tubular and plate-fin surfaces [from P3].

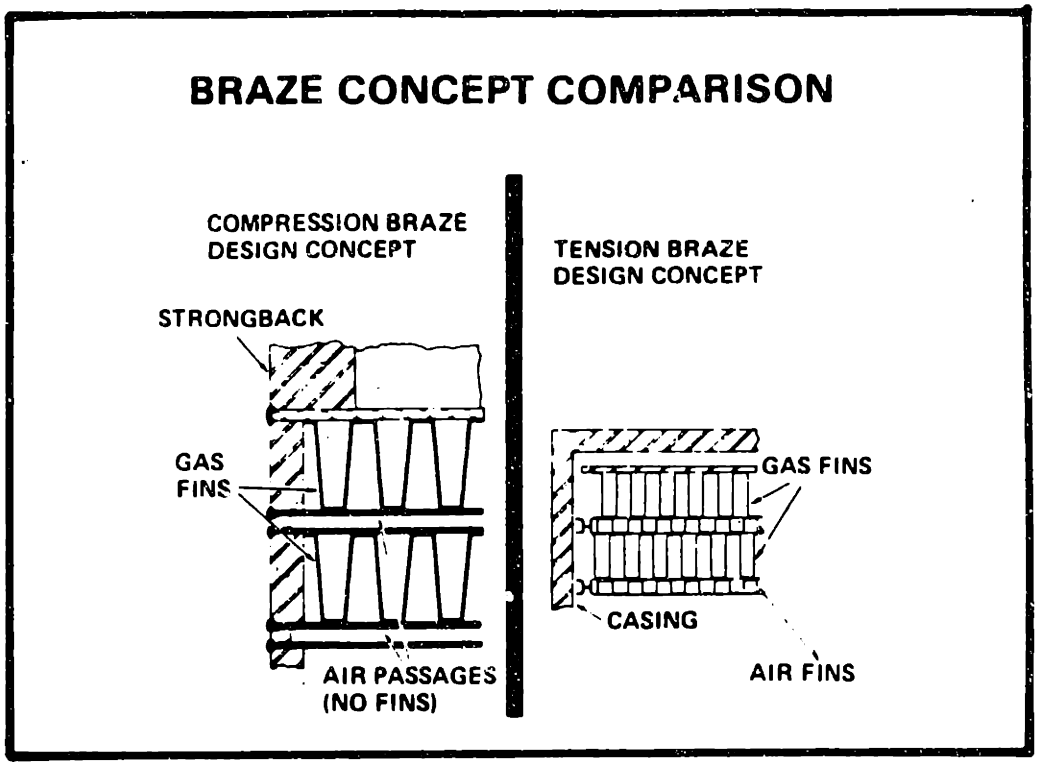

Figure 5.2. Compression-braze and tension-braze plate-fin heat-exchanger construction methods [from K2].

However, the unpredictability of creep-buckling makes tension-braze construction much more attractive than compression-braze heat-exchanger construction. Time-dependent material behavior under tension loads is well understood and predictable. The tension-braze method of plate-fin heat-exchanger manufacture has been developed in recent years by the AiResearch Manufacturing Company, and is used to build high-performance plate-fin heat exchangers for industrial and aerospace applications [K2, P2]. In the tension-braze method, the heat-exchanger core is held together by loading the fins in tension. Each fin is bonded to the plate by a nickel-alloy braze. Tension-braze construction is intended for use in systems where heat-exchanger internal pressure is equal to, or greater than, the pressure of the heat-exchanger's environment. This is the case in most aerospace applications.

5.2.1c Plate-Fin Heat Exchanger Experience and Reliability.

Many tension-braze plate-fin heat exchangers have been constructed for aerospace and industrial applications. This section will give an example of one gas-turbine-recuperator design that has demonstrated plate-fin heat-exchanger reliability and experience.

A gas-turbine-recuperator design by the AiResearch Manufacturing Company is used in 15,000-HP gas turbines. It is designed for 140,000-hr lifetime and 5,200 cycles at an operating temperature of 1100 F (593.3 C). The operating temperature of these units will be upgraded to 1200 F (648.9 C) for a new turbine design [P2]. Test results indicate that a life expectancy at nominal conditions of 500,000 hours can be expected without leakage [K2]. The results of rupture tests conducted on these heat-exchanger cores is listed below

[K2].

Room temperature burst	3,470 psig 23.9 MPa
High temperature burst at 1100 F (593 C)	2,460 psig 17.0 MPa

Experience with these units is listed in Table 5.1. They have demonstrated a high level of reliability. With over 60 units in operation, a total of over 768,000 operating hours, and over 9250 starts, all units have met or exceeded all performance guarantees. No failures have occurred [K2]. It is important to note that the units used in these gas-pipeline gas turbines were designed for operation in a corrosive environment and remote locations, where maintenance must be minimal.

5.2.1d The MGR-GT Recuperator.

An MGR-GT recuperator can be manufactured using essentially the same technology as is used in the gas-pipeline gas-turbine-recuperator design discussed in the previous section [M9]. The proposed operating temperatures and pressures of the MGR-GT recuperator are well within the capabilty of conventional heat-exchanger materials, such as 304 stainless steel [R3, M9, P5]. Therefore, using current materials and manufacturing techniques, the design of a high-performance plate-fin recuperator for the operating conditions of the MGR-GT that meets the reliability requirements of the nuclear industry is well within the present capability of high-performance heat-exchanger manufacturers [M9]. It is of equal importance to note that large-scale manufacturing of high-performance, high-reliability industrial units has been *demonstrated*.

Name and Location	Regenerator Model	Operating Experience as of January 1985	
		Hours	Starts
Pacific Gas and Electric Company			
Delevan, California	ARG282H	27,400	303
Delevan, California	ARG282H	To start first quarter 1985	
Canadian Pipeline			
Cabri, Saskatchewan	ARG361V	18,300	60
Herbert, Saskatchewan	ARG361V	14,382	144
Texas Eastern Transmission Corporation			
Danville, Kentucky	ARG280H	17,654	383
Danville, Kentucky	ARG282V	14,915	371
Athens, Ohio	ARG282V	33,358	150
Athens, Ohio	ARG282V	27,759	135
St. Francisville, Louisiana	ARG281V	25,712	101
St. Francisville, Louisiana	ARG281V	26,705	123
Clinton, Mississippi	ARG282V	16,848	96
Clinton, Mississippi	ARG282V	16,928	111
Yazoo City, Mississippi	ARG281V	18,868	216
Grantville, Pennsylvania	ARG281V	22,835	203
Grantville, Pennsylvania	ARG282V	14,897	98
Athens, Ohio	ARG282V	11,519	138
Athens, Ohio	ARG282V	16,162	83
St. Francisville, Louisiana	ARG282V	14,614	53
St. Francisville, Louisiana	ARG282V	12,431	67
Clinton, Mississippi	ARG282V	11,518	46
Owingsville, Kentucky	ARG282V	3,647	11
Owingsville, Kentucky	ARG282V	4,032	18
Gladeville, Tennessee	ARG482H	394	9
Transwestern Pipeline (Division of Texas Eastern Transmission Corporation)			
Corona, New Mexico	ARG281V	29,129	393
Chemical Plant			
Louisiana	ARG481H	31,950	62
Louisiana	ARG481H	33,278	71
El Paso Natural Gas Company			
Caprock, New Mexico	ARG281V	28,627	113
Loupp, Arizona	ARG282H	17,501	83
Gallup, New Mexico	ARG282H	15,460	105
Tennessee Gas Pipeline			
Leesville, Louisiana	ARG282H	12,671	53
Port Sulphur, Louisiana	ARG282H	13,976	30
Alexandria, Louisiana	ARG282V	5,497	68
Collinwood, Tennessee	ARG282V	17,934	121
Bay St. Louis, Mississippi	ARG281H	12,068	81
Port Sulphur, Louisiana	ARG282H	4,481	33
Hamilton, Alabama	ARG282V	3,229	98
Morehead, Kentucky	ARG282V	344	12
Columbus, Mississippi	ARG282V	11,767	72
Savannah, Tennessee	ARG282V	0	2
Texas Gas Transmission Company			
Columbia, Louisiana	ARG282V	18,245	33
Greenville, Mississippi	ARG282V	22,751	31
Slaughters, Kentucky	ARG282V	8,319	40
Lake Cormorant, Louisiana	ARG282V	15,019	25
Jeffersontown, Kentucky	ARG282V	6,780	92
Clarksdale, Mississippi	ARG282V	10,447	55
Kenton, Tennessee	ARG282V	4,366	17
Hardingsburg, Kentucky	ARG282V	3,498	44
ANR Pipeline Company			
Delhi, Louisiana	ARG282V	8,329	82
Brownville, Tennessee	ARG282V	16,910	83
Great Lakes Transmission Company			
Crystal Falls, Michigan	ARG281H	8,084	76
Philadelphia Electric			
Philadelphia, Pennsylvania	ARG286H	3,266	686
Philadelphia, Pennsylvania	ARG286H	3,266	686
Philadelphia, Pennsylvania	ARG286H	2,834	718
Philadelphia, Pennsylvania	ARG286H	2,834	718
Philadelphia, Pennsylvania	ARG286H	3,195	625
Philadelphia, Pennsylvania	ARG286H	3,195	625
Foothills Pipeline			
Playot, Saskatchewan	ARG482H	432	38
Arco-Parsons			
Prudhoe Bay, Alaska	ARG481H	8,032	79
Natural Gas Pipeline Company			
Glasco, Kansas	ARG282V	7,252	77
Independence Power and Light			
Independence, Missouri	ARG286H	59	22
Independence, Missouri	ARG286H	59	22
Trunkline Gas Company			
Eppa, Louisiana	ARG282H	To start third quarter 1985	

Table 5.1. Tension-braze gas-turbine regenerator experience [K2].

Improved surface compactness is not the only advantage of using plate-fin heat-exchanger technology for the MGR-GT recuperator. At the high turbine-outlet temperatures and high pressure differences in the MGR-GT recuperator, the design of a tubesheet for a tube-and-shell heat exchanger would be a very difficult, if not impossible, job [M24]. On the other hand, tension-brazed plate-fin heat exchangers are frequently used in high-temperature, high-pressure-difference applications [M24].

5.2.2 Precooler and Dry Cooler Design.

The designs of the precooler and dry-air cooler are not independent of one another. As discussed in the next two sections, the precooler design is largely governed by the heat-rejection method. In any case, these heat exchangers will use tubular surfaces because they interface the helium coolant and the environment. Leaks must be avoided in order to prevent water-ingress into the helium-coolant circuit, or activity-discharge to the environment. Leaks are more easily detected and repaired in tubular heat exchangers than in heat exchangers using other surfaces.

5.2.2a Precooler Design.

The precooler design is largely dependent upon whether or not dry cooling is desired. For the precoolers of both the dry-cooling and wet-cooling versions of the MGR-GT, the helium will flow outside of the tubes to minimize the pressure drop on the helium side. If an abundant supply of water is available, the precooler can be designed as a simple crossflow heat-exchanger. If dry cooling is desired, the water-outlet temperature of the precooler must be high, and a multiple-pass cross-counterflow heat exchanger must be used. In the

HTGR-GT design, dry cooling was expected to be utilized, and the heat exchanger was a multiple-pass cross-counterflow tube-and-shell heat exchanger with an annular gas flow and helically-wound tubesheets. It is pictured in Fig. 1.24. Surface enhancement was used on both sides of the tubes. The circular tubes had external, annular fins on the gas side, and internal, helically-wound fins on the water side. Water-side surface enhancement was needed in the HTGR-GT because the height of the PCRV was determined by the precooler height, and water-side surface enhancement helped to reduce the precooler height. In the MGR-GT, this problem does not exist, and water-side surface enhancement is not necessary. Thus, the dry-cooling version of the MGR-GT precooler will be of similar design as that of the HTGR-GT, with the exception that water-side surface enhancement will not be used, and gas-side surface enhancement may not be used. The MGR-GT precooler design for wet cooling will be a crossflow heat-exchanger with circular tubes; gas-side surface enhancement may be used.

5.2.2b Air-Cooler Design.

Air coolers of two types can be used in dry-cooling systems, and their names describe the method of airflow: natural draft, and forced convection. Natural-draft systems have large towers that are tailor made for the specific site. Therefore, they do not lend themselves well to modular construction. Forced-convection systems use fans to establish the airflow. They can be built and transported in modules, the number of modules being determined by the site requirements. Forced-convection dry-cooling systems are, therefore, identified as being more desirable for the MGR-GT when dry-cooling is used. Dry-cooling system sizing, however, will not be addressed in this

study.

5.3 Heat Exchanger Design.

This section will discuss the structural design and thermal sizing of the MGR-GT heat exchangers.

5.3.1 Structural Design.

The heat exchangers in the MGR-GT experience high pressure differences across their surfaces. For this reason, it is important that the structural design of these heat exchangers be considered. In this study only strip-fin plate-fin heat exchangers and tubular heat exchangers are considered. The fins of plate-fin heat exchangers provide structural support as well as heat-transfer area. Therefore, structural considerations will partly determine fin pitch and thickness. Structural considerations also affect selection of plate-thickness for plate-fin heat exchangers. For the tube-and-shell heat exchangers, no structural analysis was performed since the fins do not provide structural support and the tube thickness has negligible effect on heat-exchanger size. The following is a brief discussion of some structural design considerations for the recuperator.

In the recuperator, temperatures are such that the limitations of ASME Boiler and Pressure Vessel Code, Case N-47 apply. Therefore, the stress intensity, or double the maximum shear stress, must be kept below the stress-intensity limit.

$$S \leq S_{mt}$$

For the fin of a strip-fin or straight-fin plate-fin heat exchanger, there is only one component of primary-membrane stress.

Hence, the stress intensity equals the primary-membrane stress. It can be shown that

$$S_{fin} = \frac{(1 - p\,\delta)}{p\,\delta}\left[P_h - P_l\right] \qquad (5.1)$$

where P_h and P_l refer to the high and low pressures in the heat exchanger.

For the plate, the maximum stress-intensity can be shown to equal

$$S_{p,plate} = \frac{\left[P_h - P_l\right] b}{2\,a} \qquad (5.2)$$

For the plate, the maximum bending stress can be estimated if the part of the plate that extends between the loaded fins is treated as a cantilever beam, uniformly loaded, with both ends fixed. For this situation,

$$S_{b,plate} = \frac{\left[P_c - P_h\right]\left[\frac{1}{p}\right]^2}{2\,a^2} \qquad (5.3)$$

Equation 5.1 assumes that the fin will fail before the braze. This has been shown to be the case [K2]. The braze is generally much stronger than the fin. Using Eqs. 5.1 through 5.3, it is possible to determine plate thicknesses and allowable heat-exchanger surfaces. In all cases, the heat-exchanger surfaces of ref. K15 are used, and 304 stainless steel is the material of construction.

5.3.2 Heat Exchanger Thermal-Hydraulic Design.

For the purpose of this design study, heat-exchanger surfaces from Ref. K15 will be used because of their general acceptance and good documentation. Reference K15 recommends a heat-exchanger design approach that is visually depicted in Fig. 5.3. This design approach was used in the present study to size heat exchangers. The thermal-hydraulic analysis portion of this procedure will be stated briefly, and then described in more detail.

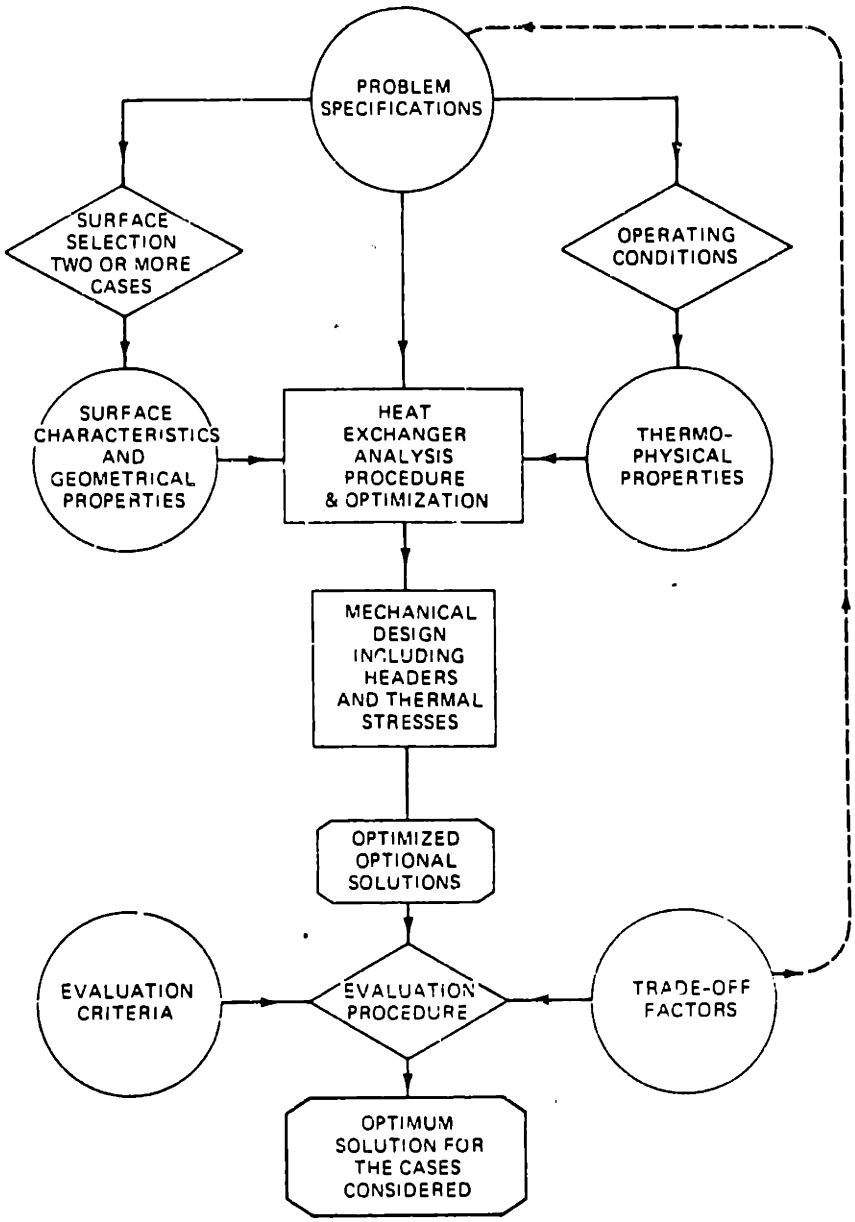

Figure 5.3. Heat exchanger design methodology [from K15].

HEAT EXCHANGER DESIGN APPROACH

1. Specify the desired heat transfer, pressure drop, heat-exchanger flow, and heat-exchanger surface.

2. Determine UA of the heat exchanger from NTU or ΔT_m.

3. Make a first estimate the fluid mass velocity.

4. Determine Reynolds number of the flow.

5. Determine the friction factor and Colburn j factor.

6. Determine h.

7. Determine fin effectiveness.

8. Determine U.

9. Determine heat exchanger size for required heat transfer from U and UA.

10. Determine pressure drop of heat exchanger.

11. If calculated pressure drop is significantly different from desired pressure drop, adjust G and repeat calculation.

12. If calculated pressure drop is acceptably close to the desired pressure drop, consider this design a candidate design.

13. Select the most desirable of the candidate designs.

1. Setting Specifications

The first step sets the specifications. For the purpose of this study, these are largely obtained by running the CYCLE program. CYCLE will specify the temperatures, pressures, and mass flow of the cycle. Precooler calculations will require the additional specifications of amount and temperature of available water.

Heat-exchanger flowpath is determined by several factors. Ratio

of heat capacities, the desired outlet temperatures, relative heat-transfer coefficients, and desired shape are a few. Probably the most important factors are the ratio of the heat-capacity rates (heat-capacity rate equals $\dot{m} \cdot C_p$) and the desired outlet temperatures of the streams. A counterflow or several-pass cross-counterflow heat exchanger will enable the temperature of each outlet stream to approach the inlet temperature of the alternate-side inlet stream if total heat-capacity rates are equal. Because the MGR-GT recuperator will have equal heat capacity on both sides, and it is desirable to have maximum heat transfer in a gas-turbine recuperator, it will be of the counterflow type.

If a precooler is used to cool gas with water that will in turn be cooled in a dry-cooling tower, a high water-outlet temperature is required. In this situation, a multiple-pass cross-counterflow heat-exchanger will be used for the precooler because the water side will normally have a much higher convective heat-transfer coefficient than the gas side, a much higher volumetric specific heat-capacity than the gas side, and a high desirable outlet-temperature. If an abundant supply of water is available, the precooler can be a crossflow heat exchanger. Forced-convection dry coolers are generally crossflow. Also, it is normally desirable from a heat transfer standpoint to have gases flow over finned tubes of tubular heat exchangers even though this may require putting the high-pressure fluid outside the tubes (as in the precooler). This has two benefits. It provides more heat-transfer surface-area for gas heat-transfer. It also reduces the pressure drop on the helium side. It will be seen that finned surfaces may not be desirable in the MGR-GT precooler.

Heat-transfer surfaces were selected from Ref. K15. Reference S7 gives guidance for a method of determining an optimum surface according to minimum volume needed for the same heat transfer and pressure drop. A low-volume heat exchanger is generally less expensive, and therefore more desirable, than a large heat exchanger. There are other factors that need to be taken into effect, such as geometry of the heat-exchanger core, and the strength and manufacturability of the surface. The geometry of the core is of importance when the heat exchanger must fit within a certain space, such as a pressure vessel or the front of a car. Wavy fin and strip fin surfaces seemed to perform the best of the surfaces examined in Ref. S7. (The results of Ref. S7 cannot be applied directly to MGR-GT heat exchangers because the calculations of Ref. S7 were performed on the basis of aluminum heat exchangers. The effect of fin efficiency will be very different for stainless-steel heat exchangers.) Strip-fin plate-fin surfaces were selected for the MGR-GT recuperator.

2. Determine UA

The Number of Transfer Units (NTU) is defined as:

$$NTU \equiv \frac{U \cdot A}{C_{min}} \tag{5.4}$$

a) For counterflow heat exchangers with $C_{min} = C_{max}$ (gas turbine recuperator, or several-pass cross-counterflow precooler with $C_{water} = C_{He}$),

$$NTU = \frac{\epsilon}{1 - \epsilon} \tag{5.5}$$

Also, for these cases,

$$\Delta T_m = T_{h1} - T_{c1} = T_{h2} - T_{c2} \tag{5.6}$$

where 1 and 2 refer to the ends of the heat exchanger.

b) For other cases, ΔT_m equals

$$\Delta T_m = \frac{(T_{h2} - T_{c2})-(T_{h1} - T_{c1})}{\ln[(T_{h2}-T_{c2})/(T_{h1} - T_{c1})]} \qquad (5.7)$$

For a crossflow heat exchanger with one side mixed, NTU can be determined from Fig. 5.4.

For all heat exchangers, effectiveness equals

$$\epsilon = \frac{\text{actual heat transfer}}{\text{maximum possible heat transfer}} \qquad (5.8)$$

With NTU and/or ΔT_m determined by one of the above methods, UA can be determined.

$$UA = NTU \times C_{min} \qquad (5.9)$$

for all heat exchangers.

For all counterflow and several-pass cross-counterflow heat exchangers,

$$UA = Q/\Delta T_m \qquad (5.10)$$

3. Selection of Mass Velocity

Reference K15 recommends that a good first estimate of mass velocity can be made by assuming that fin effectiveness is equal to one. This results in:

$$G \approx \left[\frac{j \ \Delta P \ \rho_m}{f \ NTU \ Pr^{2/3}}\right]^{1/2} \qquad (5.11)$$

Where f and j are estimated for the surface being evaluated.

It is also possible to make a first estimate of G by making a first estimate of Reynolds number. Calculations will normally require a few iterations to arrive at the correct value of G.

4. Calculation of Reynolds Number

Reynolds number is defined as:

$$Re \equiv \frac{4r_h \ G}{\mu} = \frac{D_h \ G}{\mu} \qquad (5.12)$$

5. Determine values for f and j

These are generally taken from graphs in ref. K15. For computer

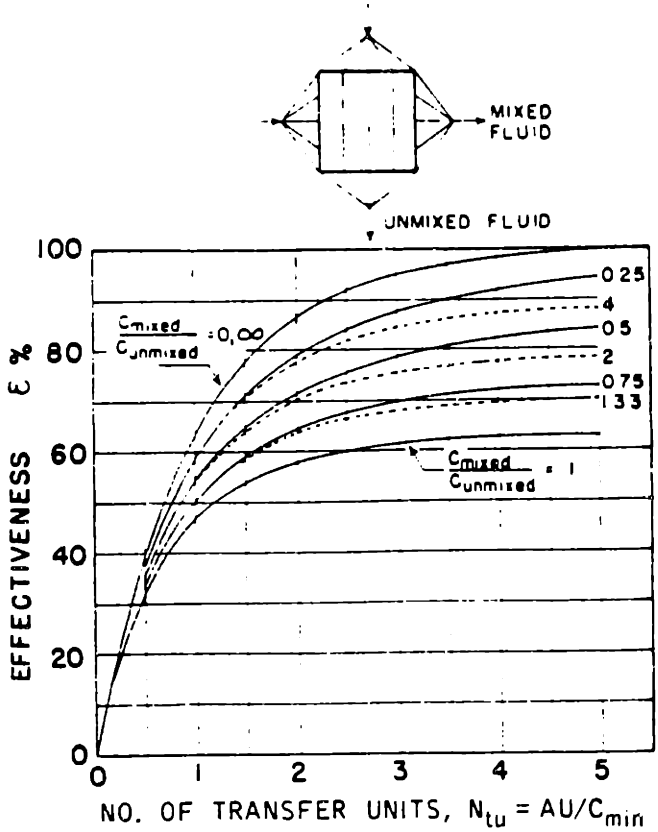

Figure 5.4. NTU and heat-exchanger effectiveness for crossflow heat exchangers with one side mixed [from K15].

programs, correlations based upon the data in ref. K15 were normally used to determine f and j.

6. Determine h

For heat-exchanger surfaces taken from ref. K15:

$$h = \frac{j\ G\ C_p}{Pr^{2/3}} \tag{5.13}$$

For flow *inside* circular cylinders, the MacAdams analogy for turbulent, convective heat-transfer coefficient was used [R2]:

$$h = \left[0.023\ k\ \frac{Pr^{0.4}}{\mu^{0.8}}\right] \frac{G^{0.8}}{D^{0.2}} \tag{5.14}$$

Water velocity was taken as about 3 m/s for the precooler and the air-cooler. Velocities much lower than this tend to result in fouling, and velocities much higher than this tend to result in excessive pumping power. Fouling effects were not considered because they generally can be neglected in liquid-to-gas heat exchangers [R2].

7. Fin Effectiveness

Only thin sheet finned surfaces were used for any finned heat exchangers in this study, as they are the most common of extended-surface heat-exchanger types. No pinned surfaces were used. For thin sheets:

$$m = \left[\frac{2\ h}{k\ \delta}\right]^{1/2} \tag{5.15}$$

$$\eta_f = \frac{\tanh(ml)}{ml} \tag{5.16}$$

This must be averaged over the finned and unfinned heat exchanger surfaces so that:

$$\eta_o = 1 - \frac{A_f}{A}(1 - \eta_f) \tag{5.17}$$

$\frac{A_f}{A}$ is given in ref. K15 as a characteristic of the individual

heat-exchanger surface.

8. Calculation of U

It is necessary to select the side of the heat exchanger which U will be based upon. Which side is selected is usually arbitrary unless one side appears clearly easier to use than the other.

For the cold side:

$$\frac{1}{U_c} = \frac{1}{\eta_{o,c} h_c} + \frac{a}{(A_w/A_c)k} + \frac{1}{\eta_{o,h} h_h (A_h/A_c)} \tag{5.18}$$

Or, for the hot side:

$$\frac{1}{U_h} = \frac{1}{\eta_{o,h} h_h} + \frac{a}{(A_w/A_h)k} + \frac{1}{\eta_{o,c} h_c (A_c/A_h)} \tag{5.19}$$

and

$$\frac{A_w}{A} \cong 1 - \frac{A_f}{A} \tag{5.20}$$

9. Determination of heat-exchanger size.

Heat-transfer surface area (for the selected side) can be determined from U and UA. Heat-exchanger volume may be determined by

$$V = \frac{A_c}{\alpha_c} = \frac{A_h}{\alpha_h} \tag{5.21}$$

Where

$$\alpha_c = \frac{b_c \beta_c}{b_c + b_h + 2a} \tag{5.22}$$

and

$$\alpha_h = \frac{b_h \beta_h}{b_h + b_c + 2a} \tag{5.23}$$

for plate fin surfaces.

Free-flow area equals

$$A_{c,c} = \frac{W_c}{G_c} \text{ , and } A_{c,h} = \frac{W_h}{G_h} \tag{5.24}$$

Total heat-exchanger-core frontal area is determined by

$$A_{fr} = \frac{A_{c,c}}{\sigma_c} = \frac{A_{c,h}}{\sigma_h} \tag{5.25}$$

For plate-fin surfaces

$$\sigma_c = \alpha_c r_{h,c} \text{ , } \sigma_h = \alpha_h r_{h,h} \tag{5.26}$$

Heat-exchanger core length can be determined simply by

$$L = \frac{V}{A_{fr}} \tag{5.27}$$

In this study, a geometry ratio, GR, has been defined as:

$$GR \equiv \frac{L}{(A_{fr})^{.5}} \tag{5.28}$$

For circular-tube heat exchangers, the number of tubes can be determined by

$$n = \frac{W\ 4}{G\ \pi\ D^2} \tag{5.29}$$

For calculations performed in this study, the fluid inside the tubes was water, and gas flows over the tubes.

L is equal to one dimension of the tubesheet in crossflow heat exchangers. The other dimension is determined by the tube pitch in that direction and the number of tube rows needed in that direction to have n total tubes. The length of the tubes was determined by the remaining dimension needed to fill the calculated volume.

For the annular, multi-pass, cross-counterflow precooler, n was determined in the same way, but a square shaped tubesheet was assumed. The length of the tubesheet sides was determined by n and the tube pitch. The number of passes was determined by L of the gas side and tubesheet dimensions.

10. Determine the Pressure Drop

Pressure drop across heat-exchanger cores was determined by the following equation from ref. K15.

$$\frac{\Delta P}{P_1} = \frac{G^2}{2\ \rho_1 P_1}\left[(K_c+1-\sigma^2)+2\left(\frac{\rho_1}{\rho_2}-1\right)+\left(f\frac{A}{A_c}\frac{\rho_1}{\rho_m}\right)-(1-\sigma^2-K_e)\frac{\rho_1}{\rho_2}\right] \tag{5.30}$$

This equation incorporates friction as well as entrance and exit

losses and fluid acceleration losses. The frictional pressure drop was typically two orders of magnitude higher than the other pressure losses. Frictional pressure drop could, therefore, be used as the entire pressure drop with negligible error. For flow normal to banks of tubes, entrance and exit effects are included in the friction factors. K_c and K_e equal zero in these cases.

For flow within circular tubes, a correlation for turbulent pressure drop was used [R2]:

$$\Delta P = \left[\frac{0.092\,\mu^{0.2}}{\rho}\right] \frac{G^{1.8}\,L}{D^{1.2}} \qquad (5.31)$$

11. Correction of G

The pressure drop calculated in the previous step is compared to the desired pressure drop within an allowable tolerance. If the desired pressure drop is higher than the calculated pressure drop, G must be increased. Similarly, if the calculated pressure drop is higher than the desired pressure drop, G must be reduced. G can be corrected using the following relationship [K15]:

$$G_{new} = G_{old} \left[\frac{\Delta P_{desired}}{\Delta P_{calculated}}\right]^{1/2} \qquad (5.32)$$

On the order of four iterations may typically be required in this method of analysis [K15].

12. Determine an Acceptable Design

Upon completion of the previous analysis, a heat- exchanger design that meets the heat transfer requirements and pressure drop requirements is obtained. This simply means that the heat exchanger can meet its heat-transfer and pressure-drop requirements.

13. Determine an Optimum Design

It is desirable to perform several iterations of the above

procedure using a variety of surfaces, pressure drops and other constraints that meet the minimum design goals of the heat exchanger. It is then possible to select the best of a number of acceptable designs. If one uses a methodical approach to selecting the constraints, this portion of the design process becomes more organized and less haphazard. Low heat-exchanger volume usually means low cost. References K15 and S7 give some guidance on surface selection.

Another concern of the heat exchanger designer is the geometry of the heat exchanger. The shape of a heat exchanger may make it more desirable than another heat exchanger of lesser volume because the shape of the smaller heat exchanger may make it inconvenient to fit the unit in the available space. For the purposes of this study it is desirable for the heat exchanger to be longer in one direction than the other directions in order to facilitate its emplacement in a pressure vessel. This will preferably be achieved with a high frontal-area, short-length design, since such units generally have higher performance than other heat exchangers of equal volume.

5.3.3 REGEN, and PRECOOL programs.

The above steps for designing a heat exchanger are iterative in nature and lend themselves well to incorporation into a computer program. These computer programs are described in Appendix C.

5.4. The MGR-GT Heat Exchangers.

This section will present the results of sizing calculations for the MGR-GT recuperator and precooler.

5.4.1 The MGR-GT Recuperator.

Thermal sizing calculations were performed for the MGR-GT

recuperator. The calculations attempted to determine the size and geometry of recuperators as a function of performance, especially specific pressure drop and heat-transfer effectiveness under the cycle conditions of Table 5.2. In this study, strip-fin plate-fin surfaces 1/8-15.2 and 1/9-24.12 of Ref. K15 were evaluated. Properties of these surfaces are listed in Appendix D.

The results of calculations are presented in Figs. 5.5 and 5.6. These figures show heat-exchanger core volume plotted against the total specific pressure drop for recuperators of different effectivenesses. Calculations showed essentially the same trends, although the magnitudes of the results are very different. An increase in heat-exchanger effectiveness results in a very rapid increase in heat exchanger volume, especially for high-effectiveness heat exchangers. Heat-exchanger volume is reduced as pressure drop is increased. Geometry ratios (GR, defined in the nomenclature section at the end of this chapter) are shown in the figures as well. Two heat exchangers with the same surface and effectiveness will be of different geometry if their pressure drops differ. Specifically, the low-pressure-drop heat exchanger will be shorter and have a larger frontal area than a heat exchanger with a higher pressure drop. As pressure drop is reduced, frontal area will tend to increase at a rate that is greater than the reduction in length, such that volume increases.

Although Figs. 5.5 and 5.6 demonstrate similar trends, the heat exchangers constructed with surface 1/9-24.12 were much smaller than heat exchangers of equal performance using surface 1/8-15.2. The large difference in volume is a result of two effects. Surface 1/9-24.12 has

Table 5.2

Cycle Parameters for Recuperator Analysis

of Figs. 5.5 and 5.6

Turbine-inlet temperature	850°C
Turbine-inlet pressure	7.8 MPa
Compressor-outlet temperature	30°C
Helium mass-flow	151.75 kg/sec
$\sum \left[\frac{\Delta P}{P}\right] - \left[\frac{\Delta P}{P}\right]_{recup}$	5%

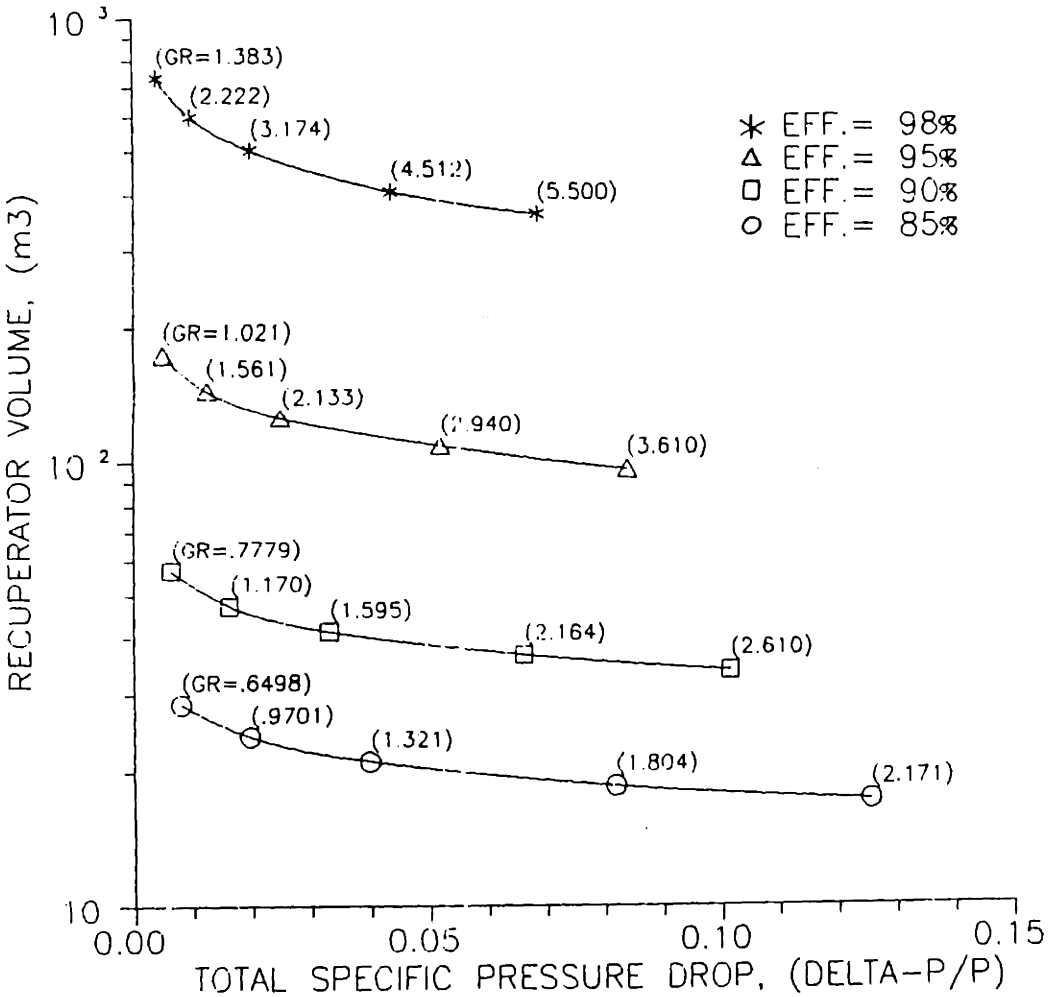

Figure 5.5. **MGR-GT recuperator-core volume for heat exchangers using strip-fin plate-fin surface 1/8-15.2 on both sides.**

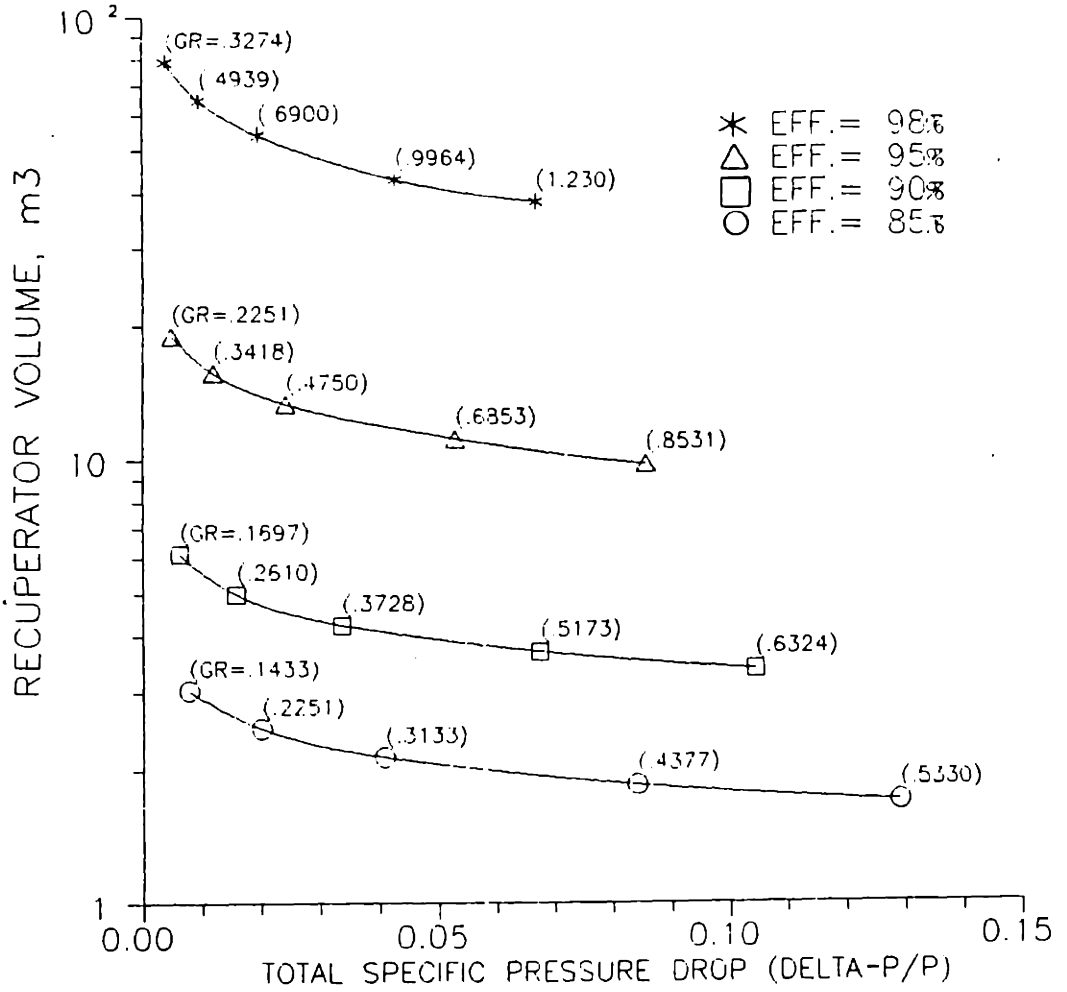

Figure 5.6. MGR-GT recuperator-core volume for heat exchangers using strip-fin plate-fin surface 1/9-24.12 on both sides.

the higher surface compactness of the two surfaces. Also, surface 1/8-15.2 had low surface efficiencies (only ≈ 25%) as opposed to much higher surface efficiencies for the shorter-finned surface 1/9-24.12 (over 60%). The low fin efficiencies result from the relatively high convective heat-transfer coefficients encountered with high-pressure helium coolant and the relatively low thermal conductivity of stainless steel (the thermal conductivity of 304 stainless steel is about 16-$W/m^{o}K$ as compared to 40-$W/m^{o}K$ for carbon steel and 250-$W/m^{o}K$ for aluminum). Although the convective heat- transfer coefficients in the MGR-GT heat exchangers are much less than those in liquid systems, they are much more than what is typical in most gas heat exchangers. Experience has shown that it is normally best to have the fins of the low-pressure side of a recuperator longer than those of the high-pressure side [P9]; however, because of the low fin efficiencies in the MGR-GT heat exchangers, it is desirable to keep the fin lengths on both sides of the recuperator much shorter than what is found in most systems.

5.4.1a Effect of Pressure on Recuperator Size.

The results of calculations for recuperators of equal heat-transfer effectiveness and specific pressure drop at different pressures are shown in Fig. 5.7. Decreased gas density at lower pressures makes it necessary to reduce mass velocity (increase frontal area) and shorten the heat-exchanger length in order to compensate for the effects of the increased fluid velocity on pressure drop. Fin efficiency is improved slightly at lower pressures. This is due to the lower convective heat-transfer coefficients that result from the reduced mass velocity. However, the improvement in fin efficiency is

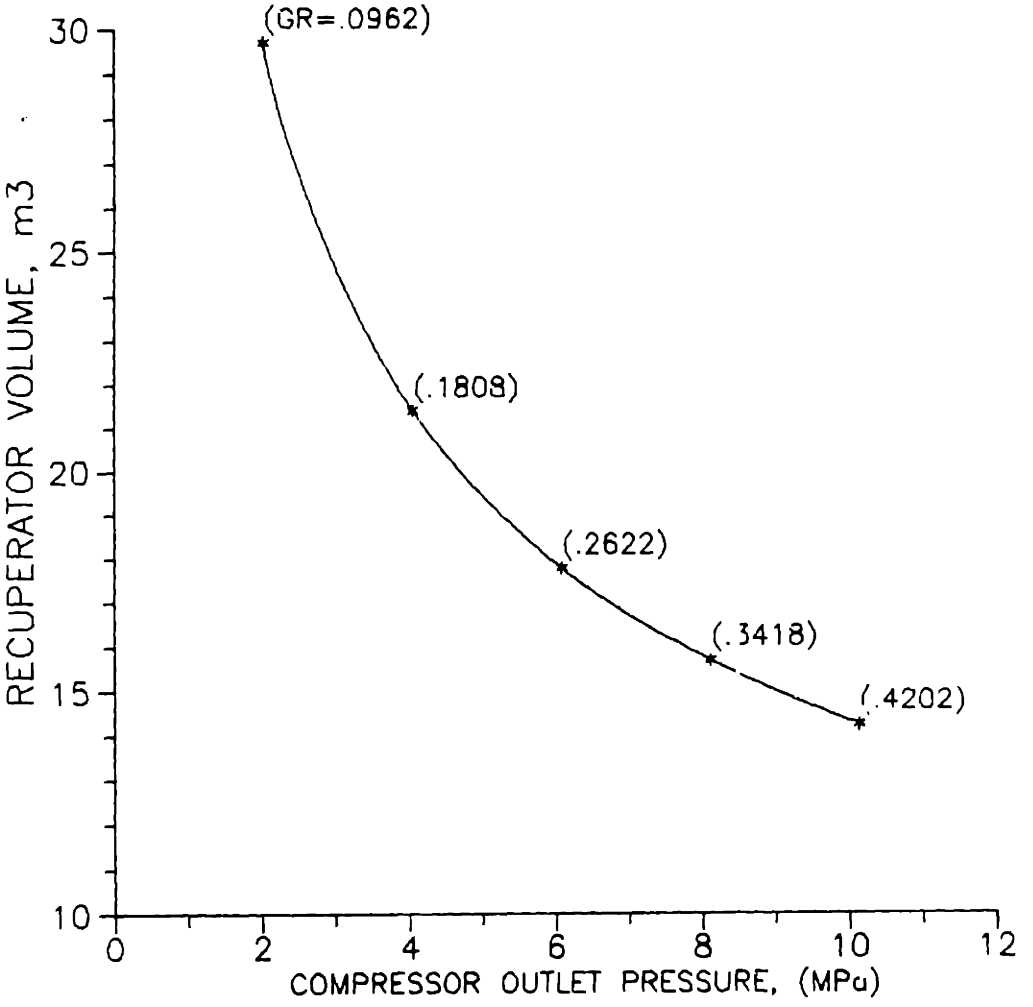

Figure 5.7. **Effect of pressure on recuperator-core size. Surfaces: sf-pf 1/9-24.12 on both sides. 95% effectiveness and $(\Delta P/P)_{recup}$ = 0.0120.**

very small. The net result is for heat-exchanger core volume to be higher at low pressures.

5.4.1b Recuperator Size for Different Power Levels.

The effects of plant power level, or recuperator heat transfer, on recuperator size and geometry were studied. Calculations show that if heat exchanger performance (effectiveness and specific pressure drop) are kept constant and mass flow is changed, thereby changing plant rated power, heat exchanger length remains constant while frontal area stays proportional to mass flow for a constant mass velocity. This is demonstrated in Fig. 5.8. Hence, the recuperator core of a plant for a 100-MWth plant could be identical to the recuperator core of a 200-MWth plant, except in the reduction of frontal area by 50%.

5.4.2 The MGR-GT Precooler.

Two configurations for the MGR-GT precooler are considered. Specifications that were maintained constant for all precooler designs evaluated in this section are listed in Table 5.3. For site locations where water supplies are not severely limited, the precooler is a crossflow heat exchanger with water flowing through the tubes (Wet Cooling). For situations where water is severely limited, a several-pass cross-counterflow heat exchanger that is liquid-coupled to a dry-cooling system will be used (Dry Cooling).

5.4.2a The MGR-GT Precooler for Wet Cooling.

Crossflow precoolers were evaluated for different water-inlet temperatures and pressure drops. Figure 5.9 shows the results of the calculations. The solid lines are for the circular finned-tube surface CF-8.72(c), and the dashed lines are for the circular-tube surface S

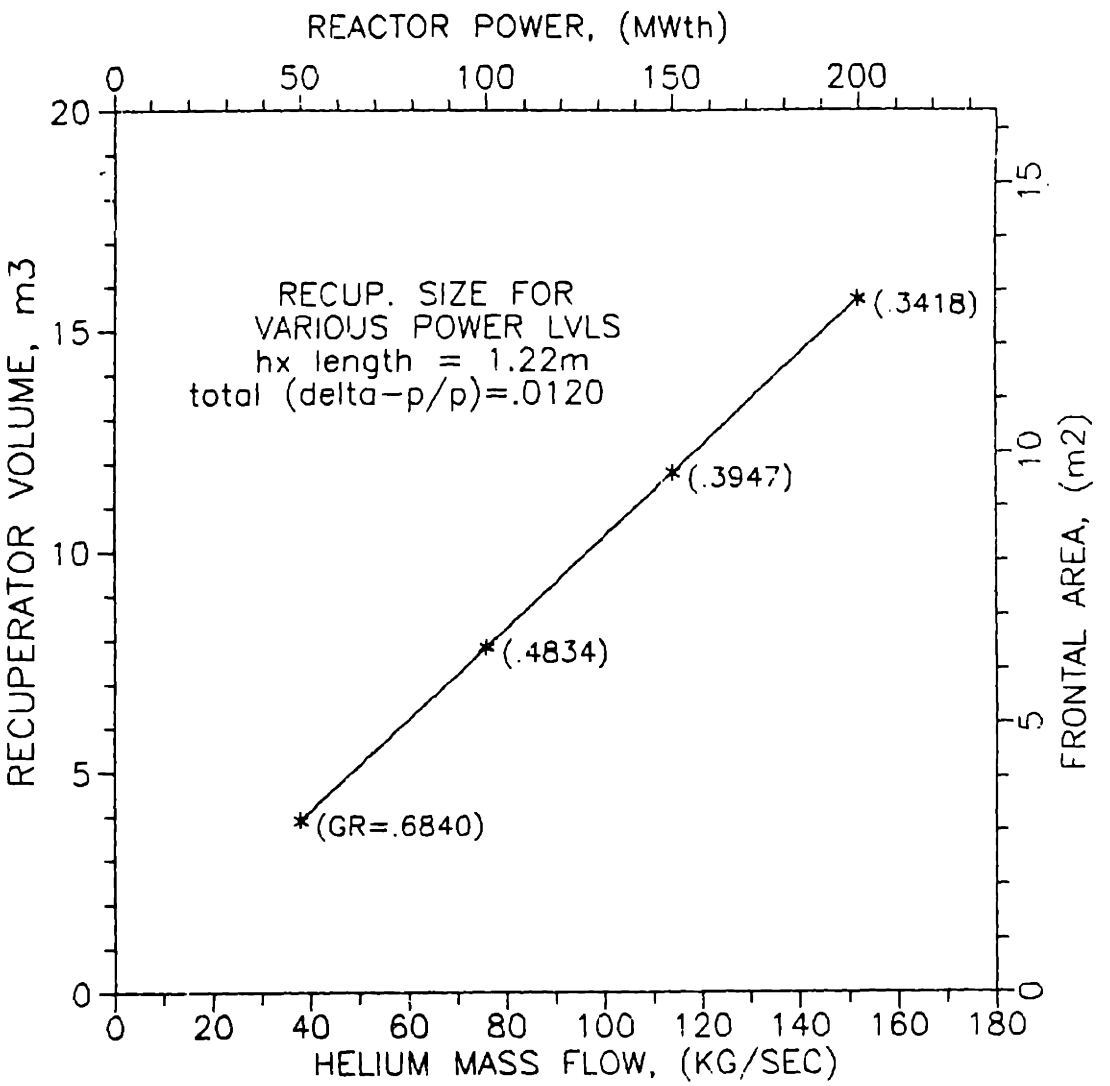

Figure 5.8. Effect of reactor thermal-power rating (helium mass flow) on sf-pf 1/9-24.12 (both sides) recuperator core with constant performance and pressure. Effectiveness = 95%, $(\Delta P/P)_{recup} = 0.0120$, and P = 4.077-MPa.

Table 5.3

Parameters for Precooler Analysis

Helium-inlet temperature	162°C
Helium-inlet pressure	4.077 MPa
Helium-outlet temperature	30°C
Helium mass-flow	151.75 kg/sec

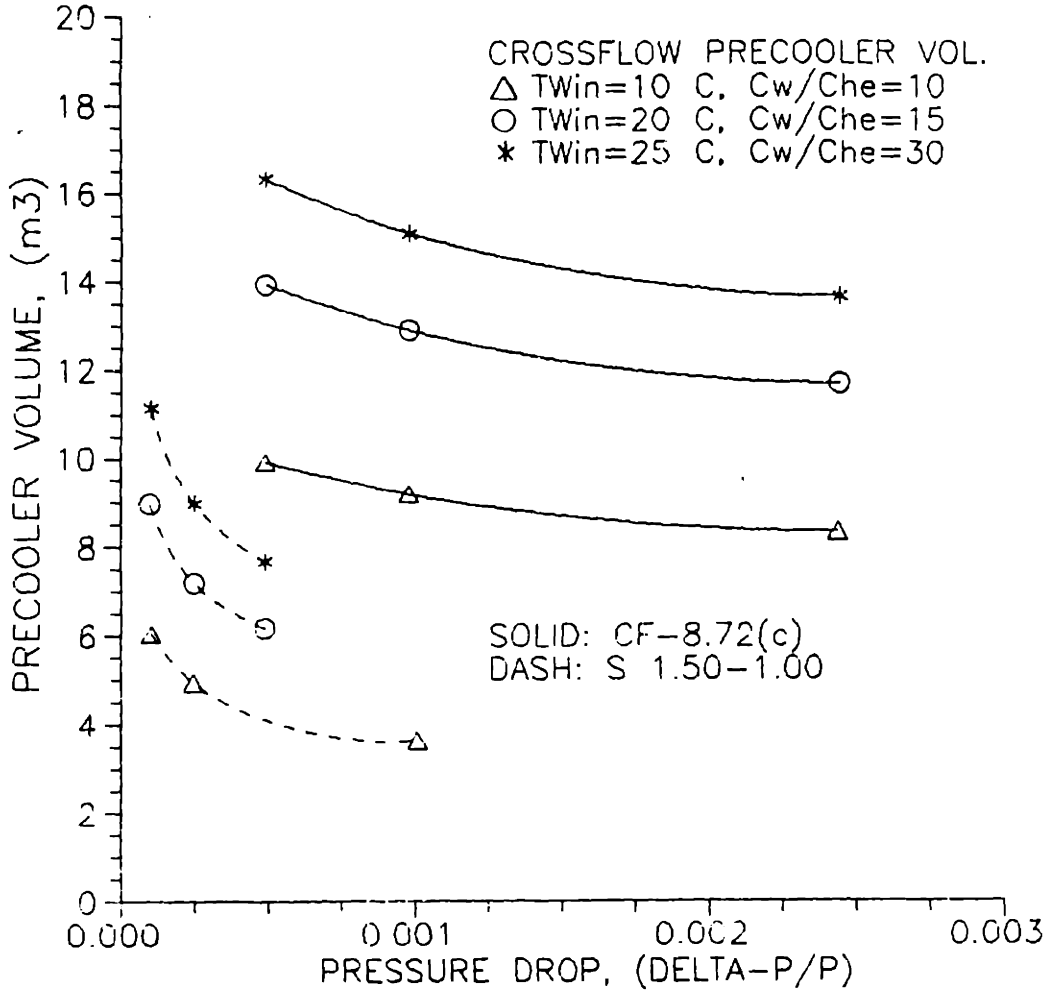

Figure 5.9. **MGR-GT precooler volumes for crossflow heat exchanger.**

1.50-1.00. Both are described in Appendix D. Appendix D also has figures that break down Fig. 5.9 by water-inlet temperature and show geometry factors (GF).

Necessary precooler volume increases rapidly as water-inlet temperature is increased. Additionally, required water flow-rate increases. Just as in the recuperator, as pressure drop is reduced, the required volume is increased since frontal area increases more rapidly than length is decreased.

Although surface CF-8.72(c) has a higher surface compactness than surface S 1.50-1.00, heat exchangers using surface CF-8.72(c) were in every case larger than heat exchangers using surface S 1.50-1.00. This is due to the low fin efficiencies encountered. Heat-transfer surface area of surface CF-8.72(c) is mostly in the fins while surface S 1.50-1.00 is unfinned, with tubes spaced much more closely together. Hence, these calculations suggest that surface enhancement may be undesirable for this heat exchanger.

The geometry ratios of these heat exchangers are generally low, especially for surface S 1.50-1.00 which has GF $\cong$ 0.06 in some cases. For this case, the heat-exchanger geometry resembles that of an automobile radiator.

Pressure drops for these heat exchangers are extremely low. Although the uppermost value of pressure drop that was evaluated was determined largely by the heat-transfer data available for the particular surface, the shape of the curves suggest that very little volume reduction can be obtained by operating at higher pressure drops than were evaluated.

5.4.2b The MGR-GT Precooler for Dry Cooling.

Results of design calculations for the MGR-GT precooler in a dry-cooling mode are presented in Fig. 5.10. In these calculations it was assumed that $C_w/C_{he} = 1.0$, so that maximum water-outlet temperature could be obtained. A high water temperature is desirable for a dry-cooling system in order to reduce the necessary dry-cooling heat-exchanger size.

The same general trends as exhibited by the crossflow precooler are exhibited here; however, the dry-cooling precooler volumes are much higher and pressure drops are much larger. Additionally, the dry-cooling precoolers tend to have higher geometry ratios (not shown).

For this heat exchanger, the use of surface S 1.50-1.00 again offers substantial volume savings when compared to surface CF-8.72(c). This is especially important because in the dry-cooling mode, the MGR-GT precooler can be very large, particularly in warmer climates where water is likely to be scarce and dry cooling desirable.

5.5 Pressure Drops in System Ducting.

This section will discuss methods for determining pressure drop in system ducting due to wall friction, bends, and sudden changes in area. Results of calculations will be reserved until Chapter Seven when the complete MGR-GT plant is evaluated.

For system ducting, pressure losses are calculated by the Darcey-Weisbach equation

$$\Delta P = f \frac{L}{d_h} \frac{G^2}{2\rho} \tag{5.34}$$

f is a function of Reynolds' number and relative surface roughness as shown in Fig. 5.11. Bends in ducting have an equivalent

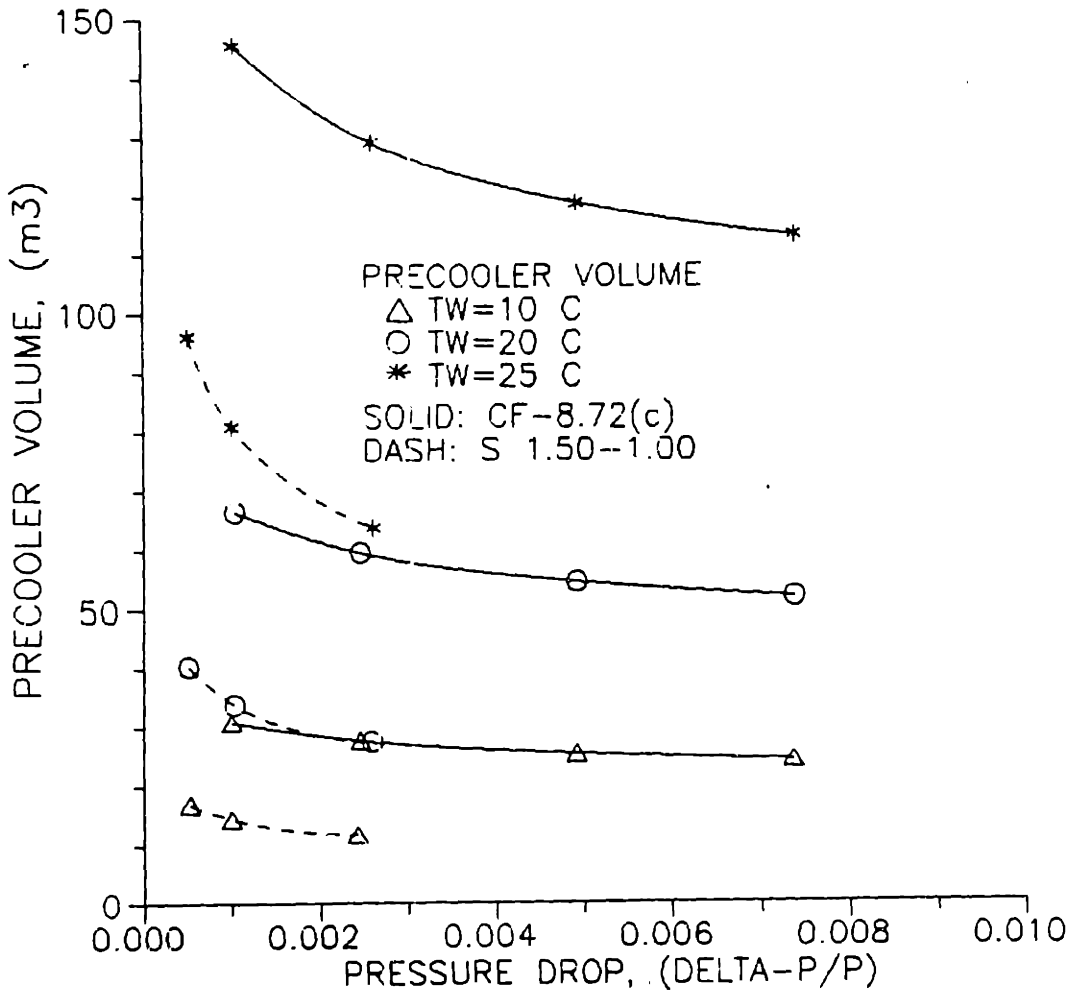

Figure 5.10. MGR-GT precooler volumes for multiple-pass cross-counterflow heat exchanger with heat-capacity rates equal on both sides.

$\frac{L}{d_h}$ which can be determined from Fig. 5.12.

For sudden expansions and contractions, pressure loss is specified as:

$$\Delta P = K \frac{G^2}{2\rho} \qquad (5.35)$$

Values for K are shown in Figs. 5.13a and 5.13b. Because sudden expansions are much more irreversible than sudden contractions, K for a contraction is much less than K for an expansion. Virtually all of the kinetic energy is lost in sudden expansions.

5.5.1 Effect of Pressure on Pressure Loss.

All of the above equations have a similar form. That is, for the same Reynolds number, the pressure losses in all components of the system are directly related to the dynamic head of the flow, $\frac{G^2}{2\rho}$. In fact, holding mass flow, duct size, and system temperatures constant; pressure losses will be inversely proportional to density, or system pressure. Specific pressure-drops will be inversely proportional to the square of pressure. This is the basis for the results of Section 3.3.3a. Hence, to maintain the same pressure drop in a system at low pressures, much larger duct sizes must be used to accomodate the higher volumetric flow. At lower pressures, the pressure losses become more significant because of the lower fluid density and higher fluid velocities.

5.6 Summary of Heat-Exchanger Design-Analysis Results.

The important results of this chapter are summarized below:

- The use of currently available compact plate-fin heat exchangers enables gas-turbine recuperators of high heat-transfer

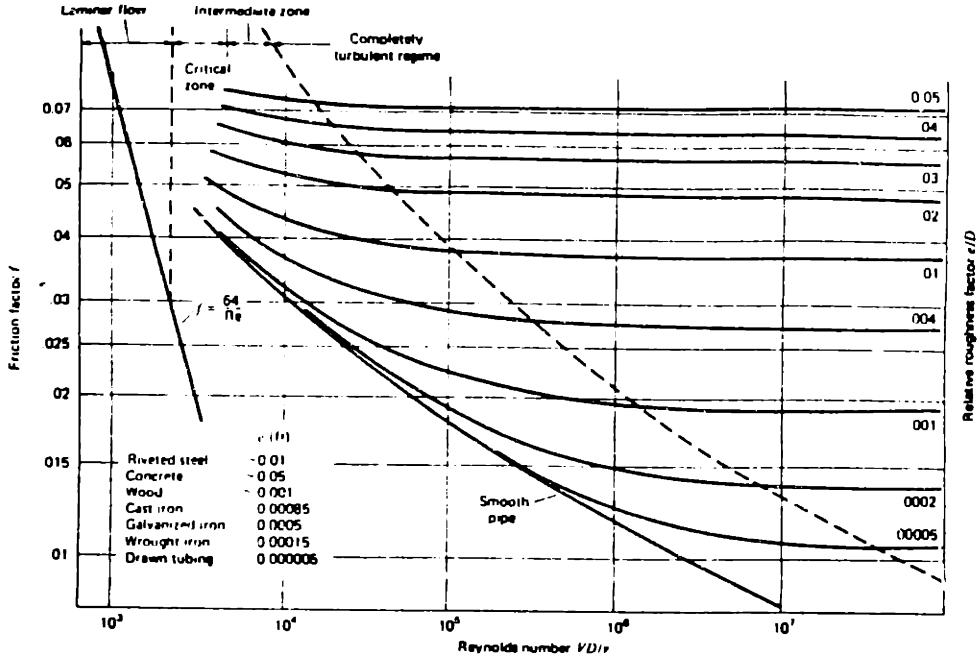

Figure 5.11. Friction factors for pipe flow [M28].

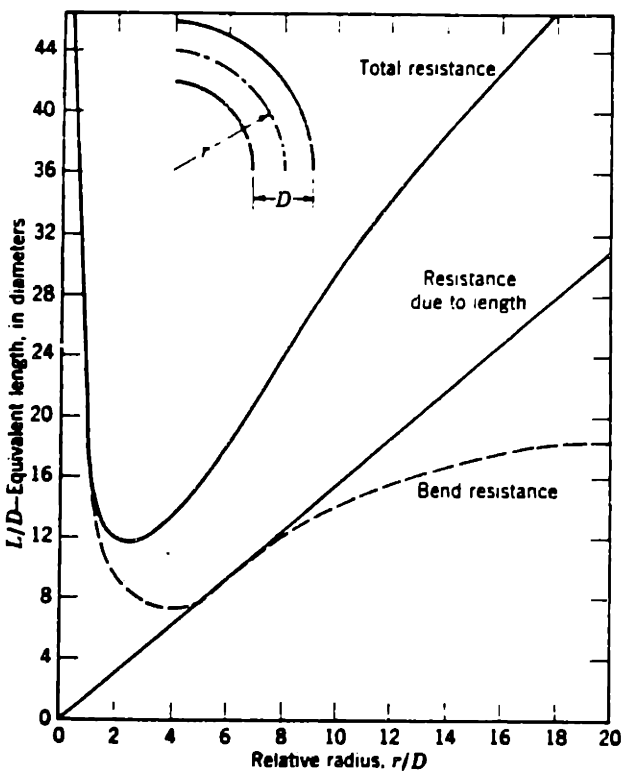

Figure 5.12. L/D ratios for bends [F9].

ENTRANCE TYPE	DIAGRAM	LOSS COEFFICIENT, K^*
Reentrant	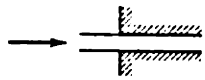	0.78
Square-edged	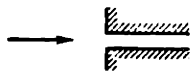	0.34
Slightly rounded	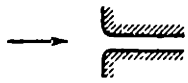	0.2–0.25
Well rounded†	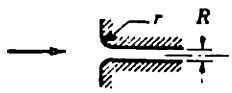	0.04

* Based on $h_L = K(\bar{V}^2/2g)$, where $\bar{V}$ is the mean velocity in the pipe
† $r/R \simeq 0.35$

Figure 5.13a. Loss coefficients (K) for sudden contractions [F9].

EXIT TYPE	DIAGRAM	LOSS COEFFICIENT, K^*
Projecting pipe	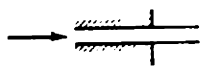	1.0
Square-edged	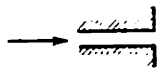	1.0
Rounded	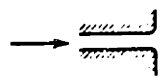	1.0

* Based on $h_L = K(\bar{V}^2/2g)$

Figure 5.13b. Loss coefficients (K) for sudden expansions [F9].

effectiveness and reasonable size to be manufactured.

- The low thermal-conductivity of stainless steel results in low fin efficiencies. For this reason, it is desirable to use plate-fin heat-exchanger surfaces with a small plate spacing. This is possible in the clean helium environment of the MGR-GT. Additionally, this effect makes the use of surface-enhancement less desirable for the precooler. In the MGR-GT, unfinned circular-tubes will be used for the precooler surface.
- Operation at a high pressure level will permit lower specific pressure drops to be achieved with smaller systems. It is desirable to operate at the maximum pressure level allowable within other limitations.

Nomenclature for Chapter Five

Symbol	Meaning	Units
A	Heat transfer area	m^2
A_c	Fluid free flow area	m^2
A_f	Finned area	m^2
A_{fr}	Heat exchanger frontal area	m^2
a	Plate thickness	m
b	Plate spacing	m
C	Total heat capacity	W/K
C_p	Constant pressure specific heat	J/kgK
D or d_h	Hydraulic diameter of tube or duct	m
G	Mass velocity, $\frac{W}{A_c}$	kg/m^2s
h	Convective-heat-transfer coefficient	W/m^2K
k	Heat conduction coefficient	W/mK
K	Sudden expansion/contraction loss coefficient	
L	Length of heat exchanger	m
n	Number of tubes	
r_h	Hydraulic radius	m
S	Stress intensity	Pa
T	Temperature	K or C
U	Heat transfer coefficient	W/m^2K
W or w	Mass flow	kg/s

Greek symbols

α	Ratio of total transfer area on one side to total volume of heat exchanger.	m^2/m^3

β	Ratio of total transfer area on one side to the volume between the plates on that side	m^2/m^3
δ	Fin thickness	m
ϵ	Heat exchanger effectiveness	
λ	Longitudinal conduction parameter	
η_f	Fin temperature effectiveness	
η_o	Total surface temperature effectiveness	
σ	Ratio of free flow area to frontal area A_c/A_f.	
μ	Viscosity	
ρ	Density	

Dimensionless Parameters

f	Friction factor	
j	Colburn convective-heat-transfer factor	
GR	Heat-exchanger geometry ratio	$\frac{L}{A_{fr}^{0.5}}$
Re	Reynolds number	$\frac{4\, r_h\, G}{\mu}$, or as specified
St	Stanton number	$\frac{h}{G\, C_p}$
Pr	Prandtl number	$\frac{\mu\, C_p}{k}$
NTU	Number of transfer units	$\frac{A\, U}{C_{min}}$

Subscripts

c	cold side
h	hot side
m	mean
max	maximum
min	minimum

p	indicating a primary-membrane stress
h1	at the high-temperature fluid inlet
h2	at the high-temperature fluid outlet
c1	at the cold-temperature fluid outlet
c2	at the cold-temperature fluid inlet

CHAPTER SIX

METHODS OF MGR-GT CONTROL

6.1 MGR-GT Control.

Chapter One discussed the fundamentals of CCGT control methods, with detailed descriptions of control systems used in previous CCGT designs. It is the intent of this chapter to discuss applicable control methods for the MGR-GT. The very high heat capacity of the graphite core permits the reactor to be treated as a constant-temperature heat source to a very good approximation for plant transients that occur on a time scale of a few minutes or less. Turbomachine response to a plant transient is many times faster than the response of reactor temperature. For example, if 20-MW of thermal energy is added evenly throughout an MGR reactor core, the average core temperature will increase at a rate of only about $2^{o}K/min$. On the other hand, calculations show that if 10-MW of power were applied to a turbo-generator about the same size and speed as that of the MGR-GT, machine speed would change at the rate of several hundred rpm per second. This effect is clearly demonstrated by the results of the plant transient analyses in Chapter One. In all situations, the reactor-outlet temperature remained relatively constant while the other components in the plant responded rapidly. Thus, the turbomachine-control system can be considered independently of reactor control. Accordingly, only turbomachine control will be discussed in this chapter; a more extended discussion of reactor control is beyond the scope of the present work.

A list of nomenclature used in this chapter can be found at the

end of the chapter.

6.2 Inventory Control.

Inventory control is a control method unique to CCGT power plants. Inventory control offers the potential for high efficiency over a broad power range. However, it requires a control vessel that may be very large, depending on the size of the plant and the power range over which it is desired to use inventory control. Inventory control also offers the ability to respond very rapidly to changes in power levels. The permissible rate of load change is determined by the size of the valves in the control system, and is limited by the economics of installing the valves and the ability of the plant to withstand rapid pressure changes. In order to limit the size of the valves, inventory control is normally used only for slow power changes.

6.2.1 Inventory Control Range and Control-Vessel Size.

Bitsch and Chabouseau [B29] determined the relationship between inventory-control power range, inventory-control-vessel volume, and total helium mass in the helium-coolant circuit for single control-vessel and multiple control-vessel arrangements. The relationships assume that the temperature of the inventory gas remains the same during the period of storage in the inventory-control vessels. Since the gas withdrawn from the helium-coolant circuit is probably cooled in a purification system before entering the inventory-control vessel, this is an acceptable assumption. In the case of one transfer tank, the lower limit of the equilibrium inventory-control power range is given by:

$$x_L = \frac{1 + M_v/M_p}{1 + y \cdot M_v/M_p} \tag{6.1}$$

The upper limit of the equilibrium inventory-control power range is

$$x_u = \frac{1 + M_v/M_p}{1 + \left[\frac{y}{r_p}\right](M_v/M_p)} \tag{6.2}$$

Figure 6.1 demonstrates this effect and Figs. 6.2 and 6.3 show the results of calculations for the 200-MWth MGR-GT. If inventory-control-vessel pressure equals the pressure of the low-pressure part of the circuit while the plant is initially at 100% power, better control range is available at the higher load ranges. If inventory-control vessel pressure is initially below this value, the equilibrium control band is narrower and lower, requiring the use of transfer compressors to return to 100% load.

Bitsch and Chaboseau also showed that if n equally sized inventory-control vessels are used in sequence such that, when reducing load from 100%, the second vessel starts filling after equilibrium is reached between the first vessel and the loop, and the third vessel starts filling when equilibrium is reached between the second vessel and the loop, etc., the total inventory-control vessel volume can be substantially reduced. Figure 6.4 demonstrates this method of inventory control. In this case,

$$x_1 = x_2 \ . \ . \ . = x_n = x = X^{\frac{1}{n}} \tag{6.3}$$

with X equal to the lower limit of the inventory-control range.

The total mass of gas in the inventory-control vessels at 100% load is equal to

$$M_T = M_p \cdot \left[\frac{1 - X}{r_p \cdot X^{\frac{1}{n}} - 1}\right] \tag{6.4}$$

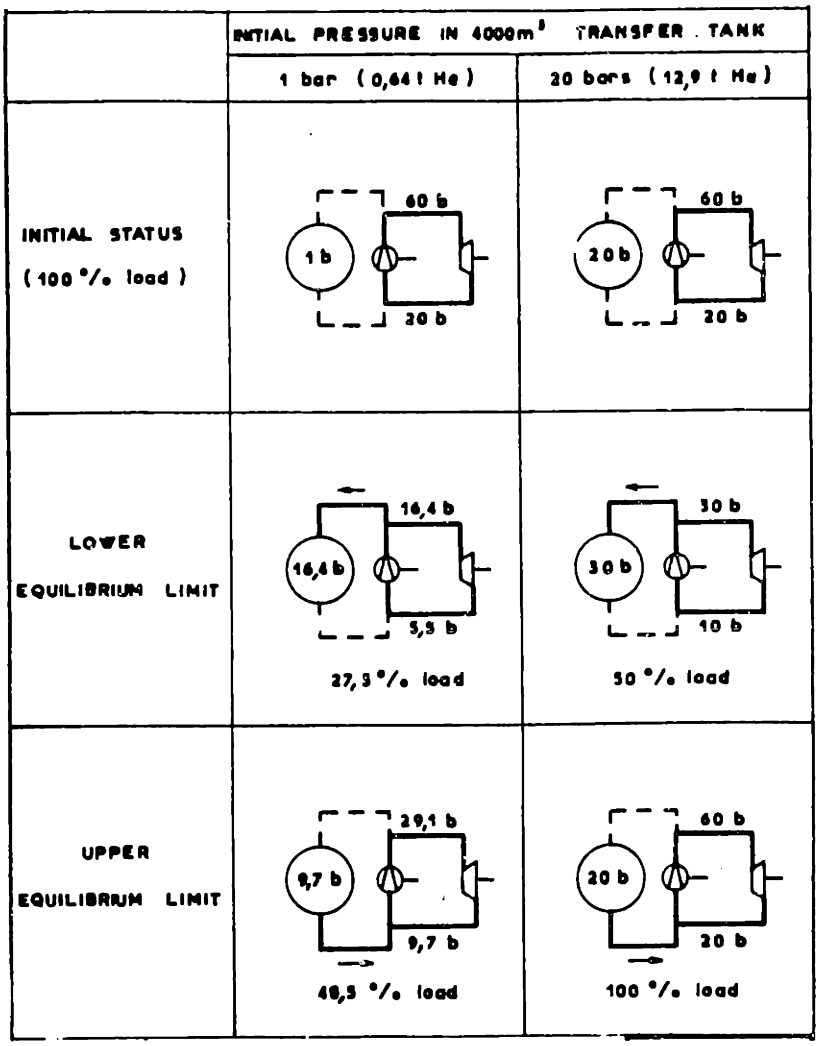

Figure 6.1. Typical examples of CCGT load control with one inventory-control vessel [from B29].

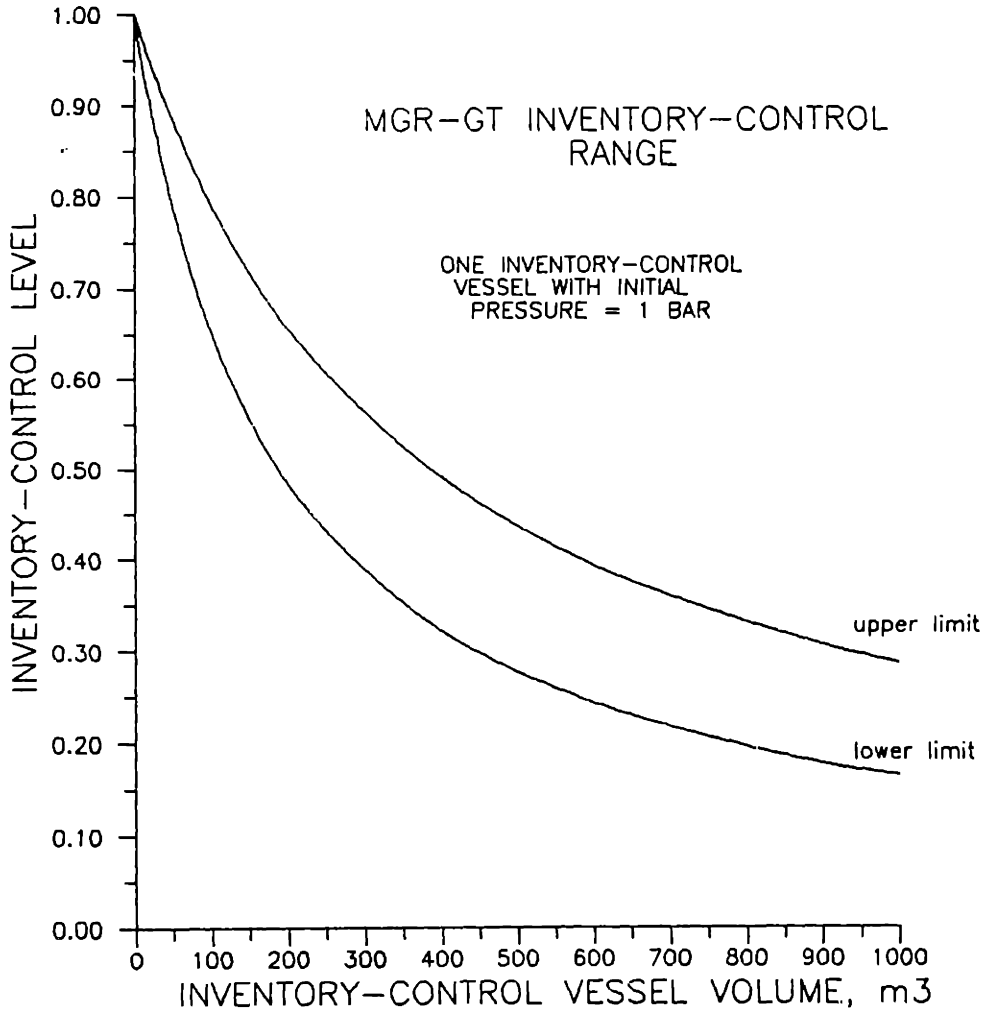

Figure 6.2. **Load range for the MGR-GT with one inventory-control vessel. Initial inventory-control vessel pressure of 1-bar.**

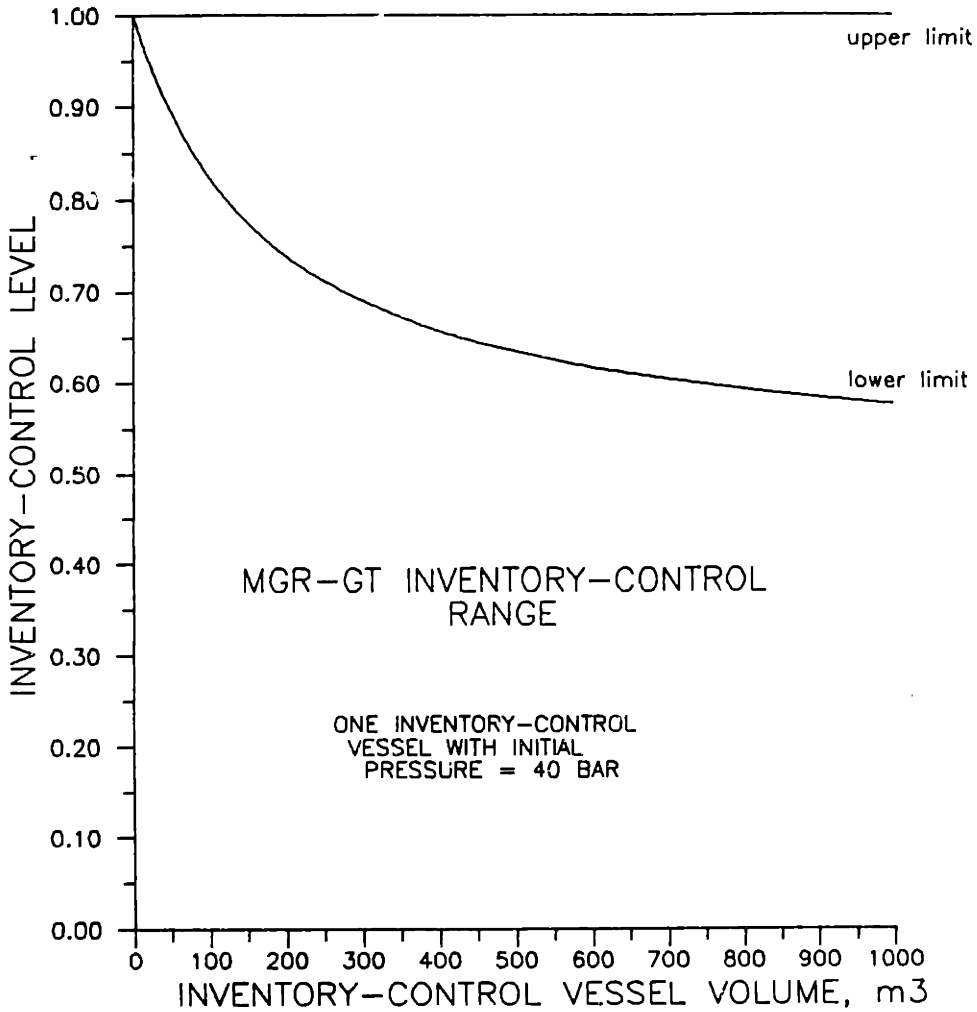

Figure 6.3. **Load range for the MGR-GT with one inventory-control vessel. Initial inventory-control vessel pressure of 40-bar.**

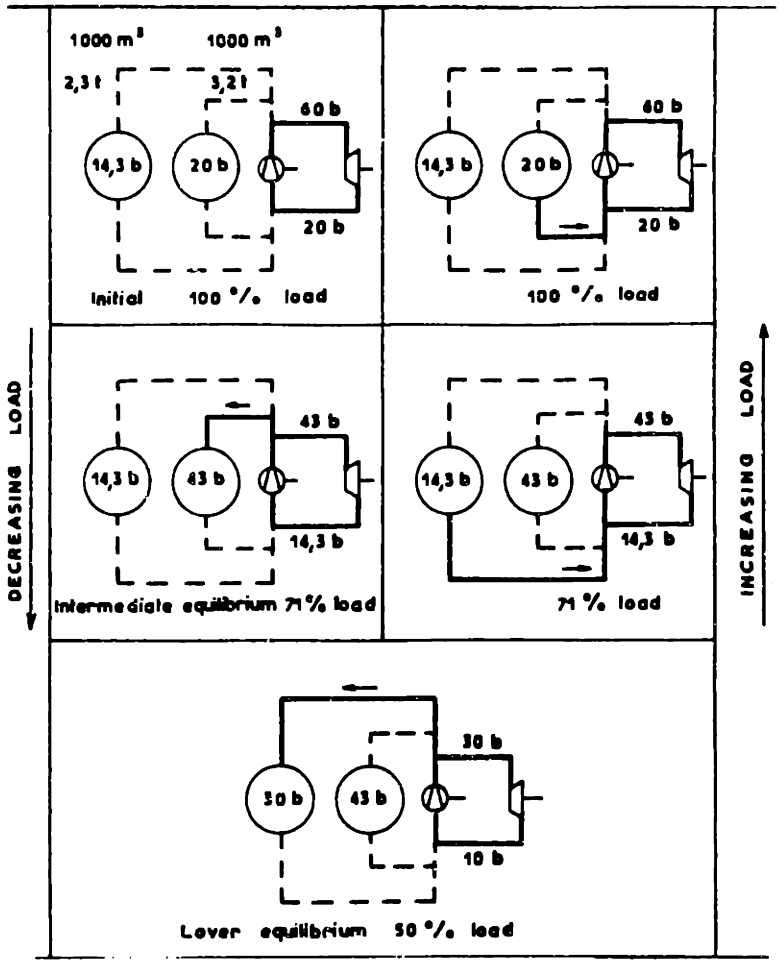

Figure 6.4. CCGT inventory control with two inventory-control vessels [from B29].

The total volume of the inventory-control vessels is equal to

$$V_T = M_p \cdot \left[\frac{R \cdot T_O}{P_{hp}}\right] \cdot r_p \cdot n \cdot \left[\frac{1 - x}{r_p \cdot x - 1}\right] \qquad (6.5)$$

For an infinite number of tanks

$$M_T = M_p \cdot \left[\frac{1 - X}{r_p - 1}\right] \qquad (6.6)$$

$$V_T = M_p \cdot \left[\frac{R \cdot T_O}{P_{hp}}\right] \left[\frac{r_p}{r_p - 1}\right] \cdot \mathrm{Log}\left[\frac{1}{X}\right] \qquad (6.7)$$

Figure 6.5 shows the results of calculations for the MGR-GT. The use of more than one inventory-control vessel significantly reduces the required total inventory-control-vessel volume. This is physically explained by considering that two vessels, each individually capable of a lower inventory-control level of 80%, will result in a lower inventory-control level of 64% when used together on the same system. Their combined volume will be much less than the volume of a single vessel capable of reducing inventory to 64%. Similar considerations apply for a system of three vessels each capable of 86% lower inventory-control level and a single vessel capable of 64% lower inventory-control level. The minimum total inventory-control vessel volume required for a desired lower inventory-control level is obtained by a very large number of very small vessels. However, Fig. 6.5 demonstrates that there is little advantage in increasing the number of inventory-control vessels beyond two or three.

6.2.2 Load Changing Rate with Inventory-Control.

The rate of inventory change is limited by the plant's ability to withstand changes in pressure, and the allowed size of the inventory-control valves. The turbomachinery is structurally capable of withstanding pressure transients much more rapid than are possible with inventory control. Similarly, the integrity of the thermal liner

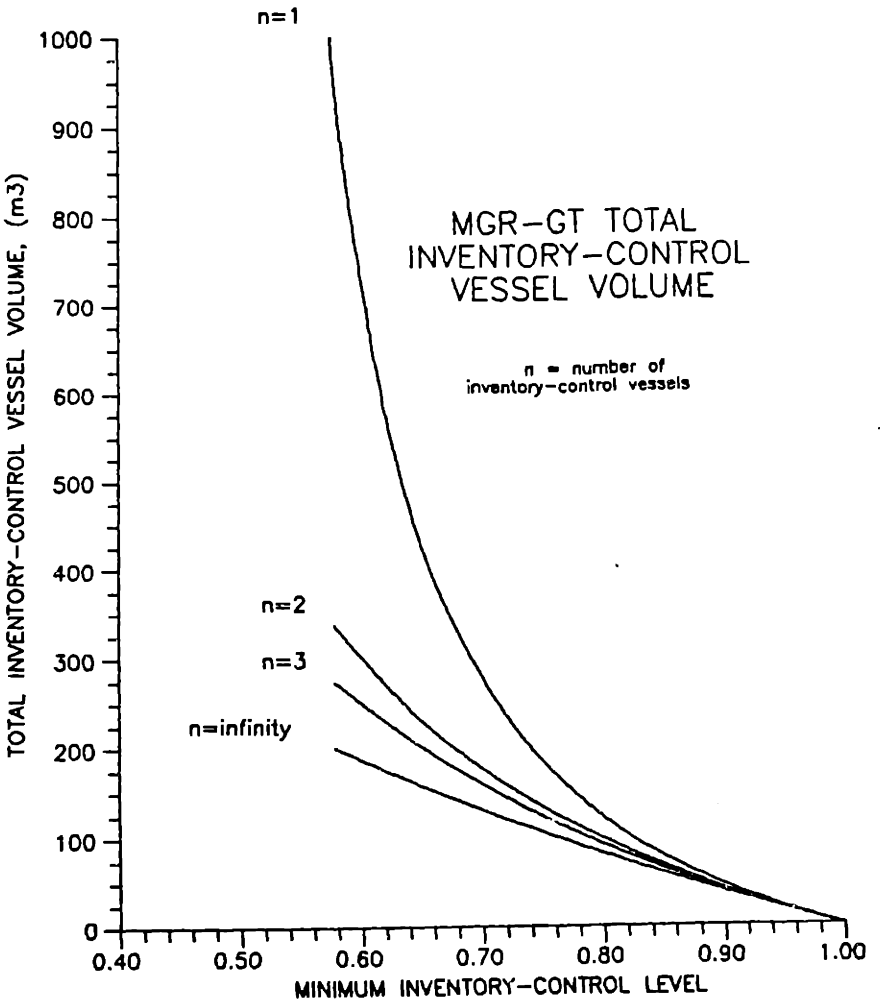

Figure 6.5. MGR-GT total inventory-control vessel volume for different numbers of equally sized inventory-control vessels.

is of concern only when considering very rapid pressure changes. The rate of pressure change anticipated for inventory control is much less severe than the rate of pressure change that a thermal liner is capable of [B22,C2,L1]. Hence, control-valve size is of primary concern when considering the limiting rate of inventory-control change.

The critical pressure ratio for helium is 0.487. If the MGR-GT inventory-control system is designed such that 100% inventory can be restored without use of transfer compressors, the ratio of the compressor-outlet pressure to the initial control-vessel pressure will be roughly equal to the cycle pressure ratio. Since cycle pressure ratios of about 2.0 are expected, choking is not expected to occur in the inventory-control ducting when inventory changing occurs. In fact, since the pressure drop occurs almost entirely across the control valve, flow rates in the ducting are sufficiently low that the effects of compressibility can be neglected to a good approximation (calculated G will be at most about 7% in error). Also, the effects of temporal inertia will be insignificant. Hence, mass flow in the ducting during inventory change can be determined by

$$G = \left[\frac{\Delta P \cdot \rho}{2 \cdot f \cdot (L/D)_{eq}}\right]^{1/2} \tag{6.8}$$

and

$$\frac{dm}{dt} = \frac{G \cdot \pi \cdot D^2}{4} \tag{6.9}$$

and

$$f = 0.046 \cdot Re^{-0.20} \tag{6.10}$$

where Eq. 6.9 gives the mass-flow rate between the helium-coolant circuit and the inventory-control vessel and Eq. 6.10 is the friction factor for smooth ducts. According to these equations, if the valve opening is kept constant, the mass-flow rate will initially start out

high and then diminish as the pressure drop is reduced.

Loop helium-mass inventory can be determined by

$$m_{he}(t=t) = m_{he}(t=0) - \int_{t=0}^{t=t}\left[\frac{dm}{dt}\right]dt \qquad (6.11)$$

Although Bitsch and Chaboseau assumed that the entire process was isothermal, because the gas in the inventory-control vessel is compressed when loop inventory is diminished, the temperature of the gas in the inventory-control vessel will increase in the absence of heat transfer to the environment or to a cooling system. The assumption of an adiabatic inventory-control vessel is believed to be a more accurate representation of the actual process. The temperature of the helium in the inventory-control vessel, in the absence of any cooling, will equal

$$T_v(t=t) = T(t=0)\cdot\left[\frac{[M_v(t=t)-M_v(t=0)]\cdot C_p + M_v(t=0)\cdot C_v}{M_v(t=t)\cdot C_v}\right] \qquad (6.12)$$

The computer program LAST1 uses the above equations to perform calculations of inventory-control transients for both adiabatic and isothermal inventory-control vessels. It is described in Appendix E.

The results of calculations for inventory-control response to an inventory reduction are shown in Figs. 6.6, and 6.7 for isothermal and adiabatic inventory-control vessels, respectively. Both show the effects of duct diameter on inventory reduction rate for initial compressor-outlet pressure of 8-MPa and initial inventory-control vessel pressure of 4-MPa. In both cases, a rate of only about 1%/minute is possible for a 5-cm dia. system, while a 20-cm dia. system enables an almost 20%/minute rate of inventory reduction. Hence, for both adiabatic and isothermal control-vessels,

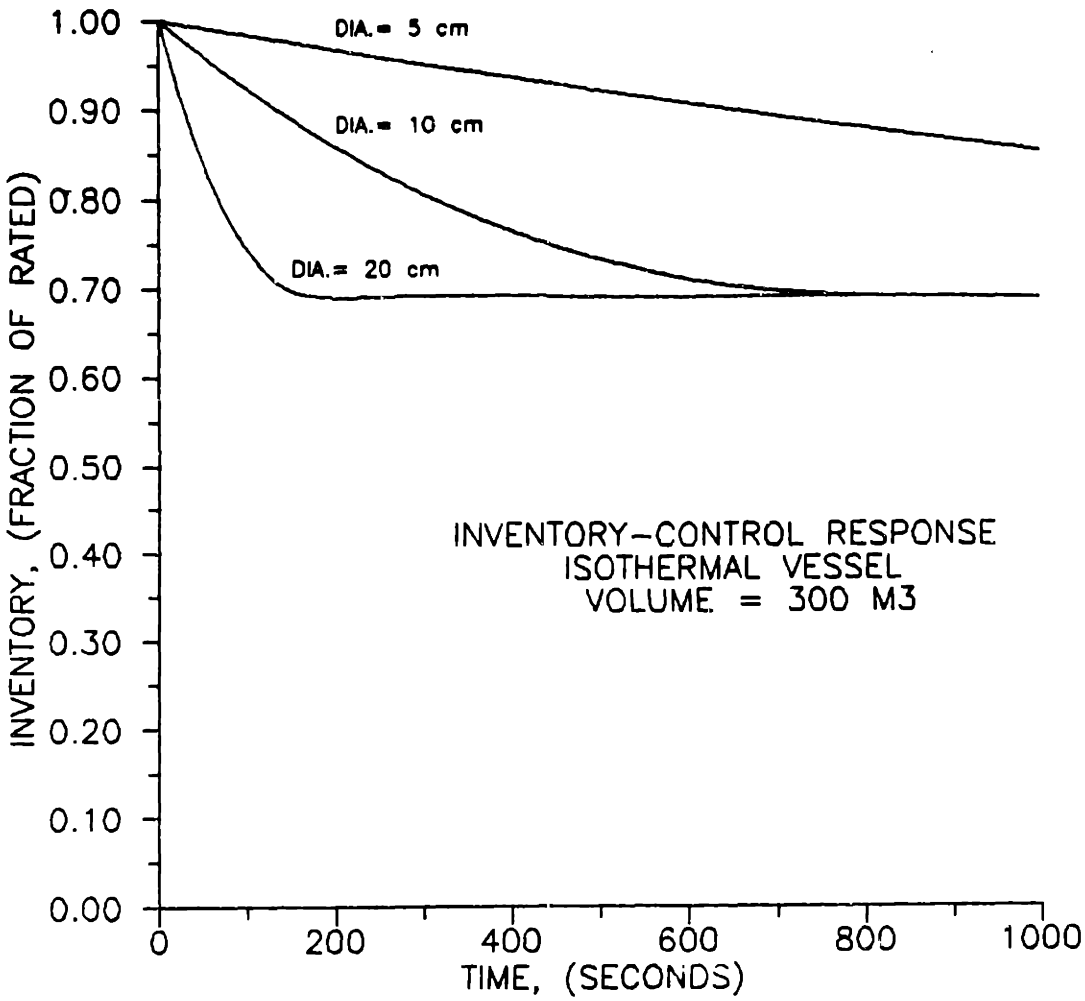

Figure 6.6. MGR-GT inventory-control response for isothermal inventory-control vessel. Initial compressor-outlet pressure = 8-MPa, initial inventory-control vessel pressure = 4-MPa.

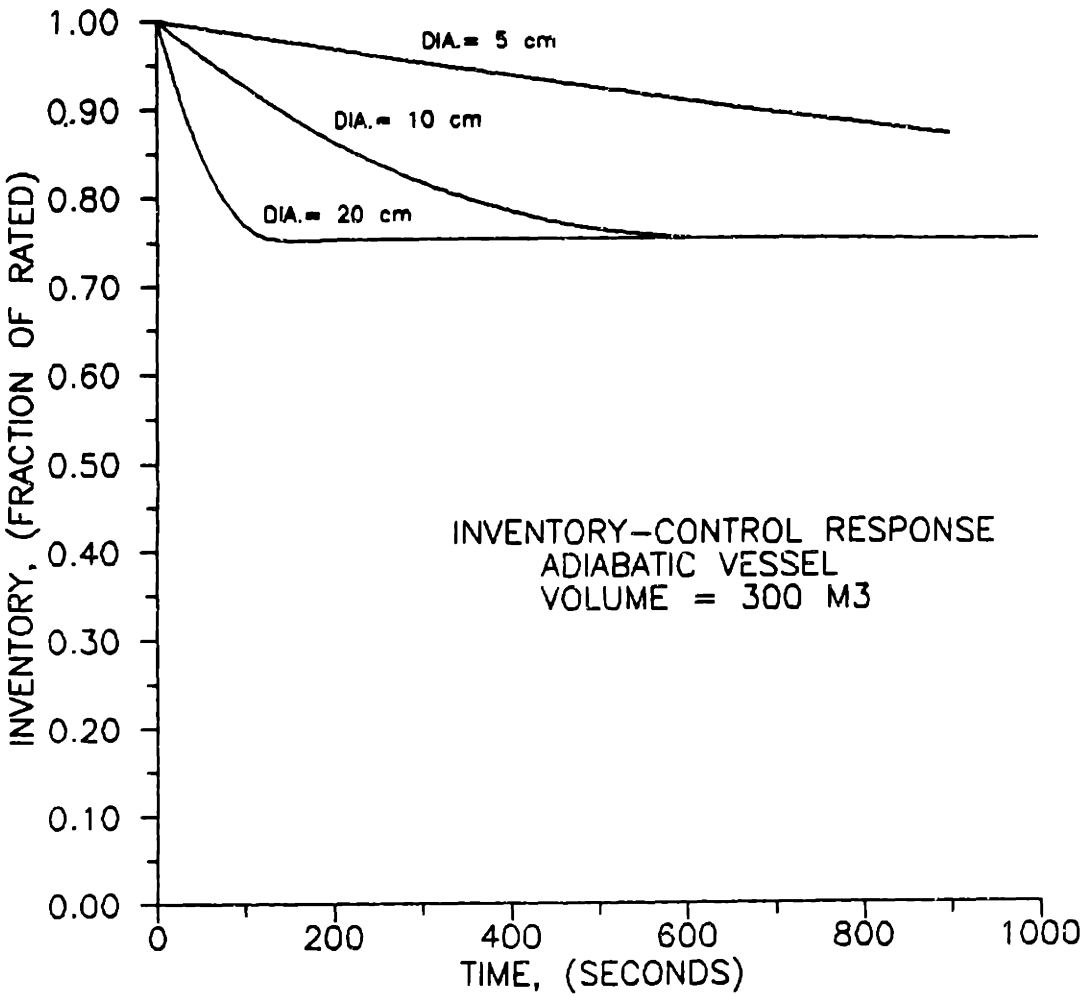

Figure 6.7. **MGR-GT inventory-control response for adiabatic inventory-control vessel. Initial compressor-outlet pressure = 8-MPa, initial inventory-control vessel pressure = 4-MPa.**

inventory-control power changes at rates sufficiently rapid for most normal power changes are possible with control valves of reasonable size.

By assuming that the inventory-control vessel is adiabatic, the lower level of inventory control is increased. This is demonstrated further in Fig. 6.8, which compares the results of calculations for an isothermal control-vessel to the results of calculations for an adiabatic control vessel. The isothermal line for a 300-m^3 inventory-control vessel coincides with the adiabatic line for a 500-m^3 inventory-control vessel. This is because

$$\frac{500\text{-}m^3}{300\text{-}m^3} = 1.67 = \frac{C_p}{C_v} \qquad (6.13)$$

In every case, under otherwise similar conditions, the adiabatic situation results in a higher minimum inventory-control level than the isothermal situation by a factor of 1.67. Another important conclusion that can be drawn from Fig. 6.8 is that the rate of inventory change is primarily a result of valve size, not of inventory-control vessel size. Inventory-control vessel size only determines the minimum inventory-control level.

6.3 MGR-GT Control During Upset and Abnormal Conditions.

This section will consider speed control of the MGR-GT turbomachine during normal operation and during periods of turbomachine overspeed, startup, and shutdown. Turbomachine speed control is simplified over previous CCGT variants due to the unique electrical system that is used on the MGR-GT.

6.3.1 MGR-GT Speed Control During Normal Operation and Turbomachine Overspeed.

The use of an electrical rectifier-inverter system (such as an

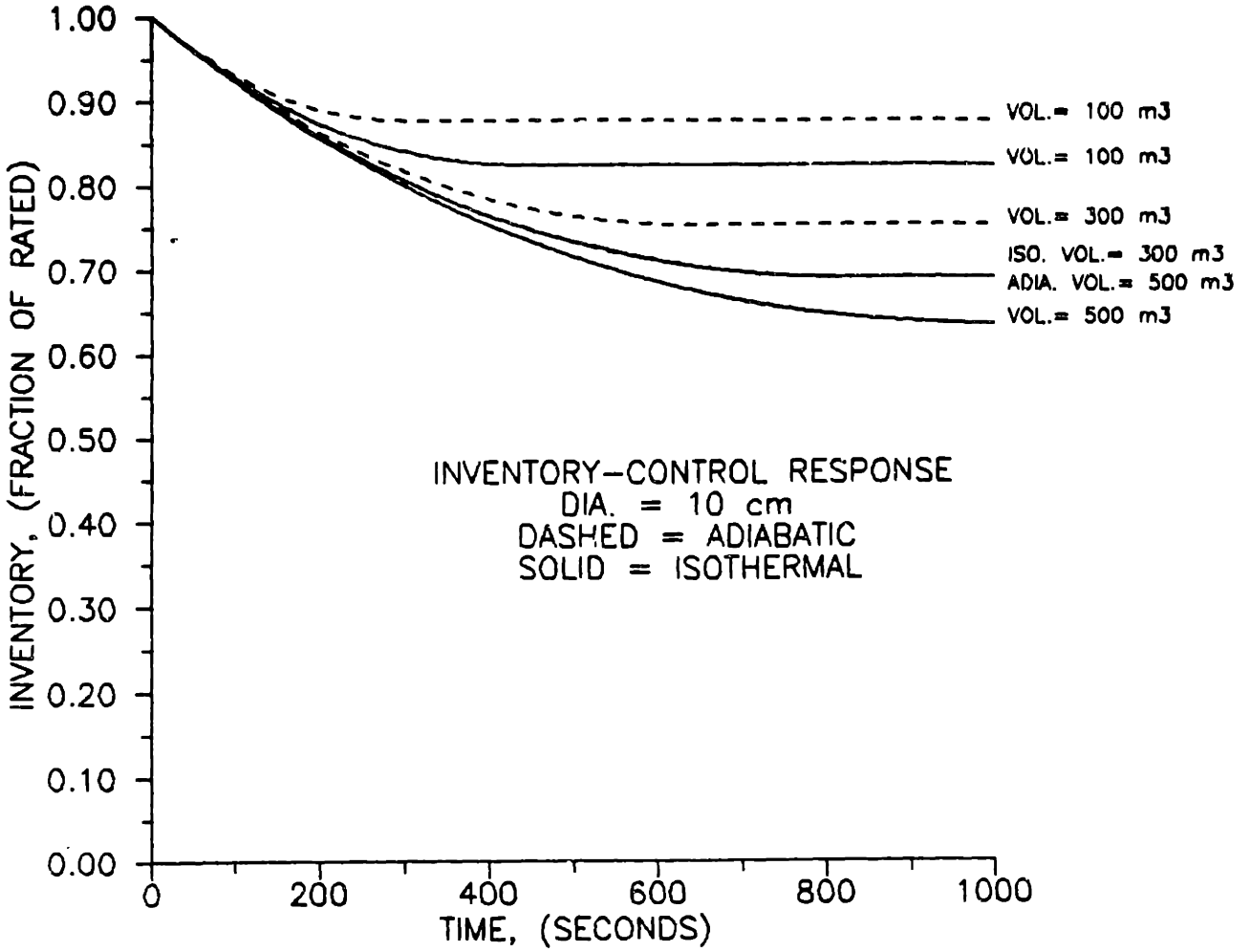

Figure 6.8. MGR-GT inventory-control response. Initial compressor-outlet pressure = 8-MPa, initial inventory-control vessel pressure = 4-MPa.

LCI), with dynamic braking capability and acceleration limiting circuits, enables accurate speed control of the MGR-GT rotating machinery during most conditions of turbomachine operation. Present industrial systems of this type have a standard speed-control accuracy of ±0.5% [T3].

Turbomachine overspeed is of primary concern in the event of a sudden loss of electrical load. In all previous COGT systems, a bypass system of control was necessary to prevent turbomachine overspeed during this accident. Chapter One discusses several of these bypass control systems. The use of rectifier-inverter circuits potentially enables use of other control methods in the event of a sudden loss of load. If the DC bus of the rectifier-inverter circuitry is connected as in Fig. 6.9 to a load resistor, it is possible to rapidly load the generator on the DC bus in the event of sudden deenergization of the AC load bus. An alternative is to rapidly connect the load resistor to the generator-output. Such a load resistor would probably take the form of a tank of electrolyte. Such large resistors are commonplace in applications where "dummy" electrical loads are needed. The advantage of this control method is that it does not require the operation of valves internal to the MGR-GT machinery module.

In the event of a shaft break between the turbine and the generator, the control system discussed in the previous paragragh would not be useful in preventing turbine overspeed. In such an accident, turbine overspeed could only be prevented with a bypass-control system. In such a control system, upon the sensing of a discrepancy between turbine rotational speed and generator rotational speed, bypass valves located between the high pressure and low

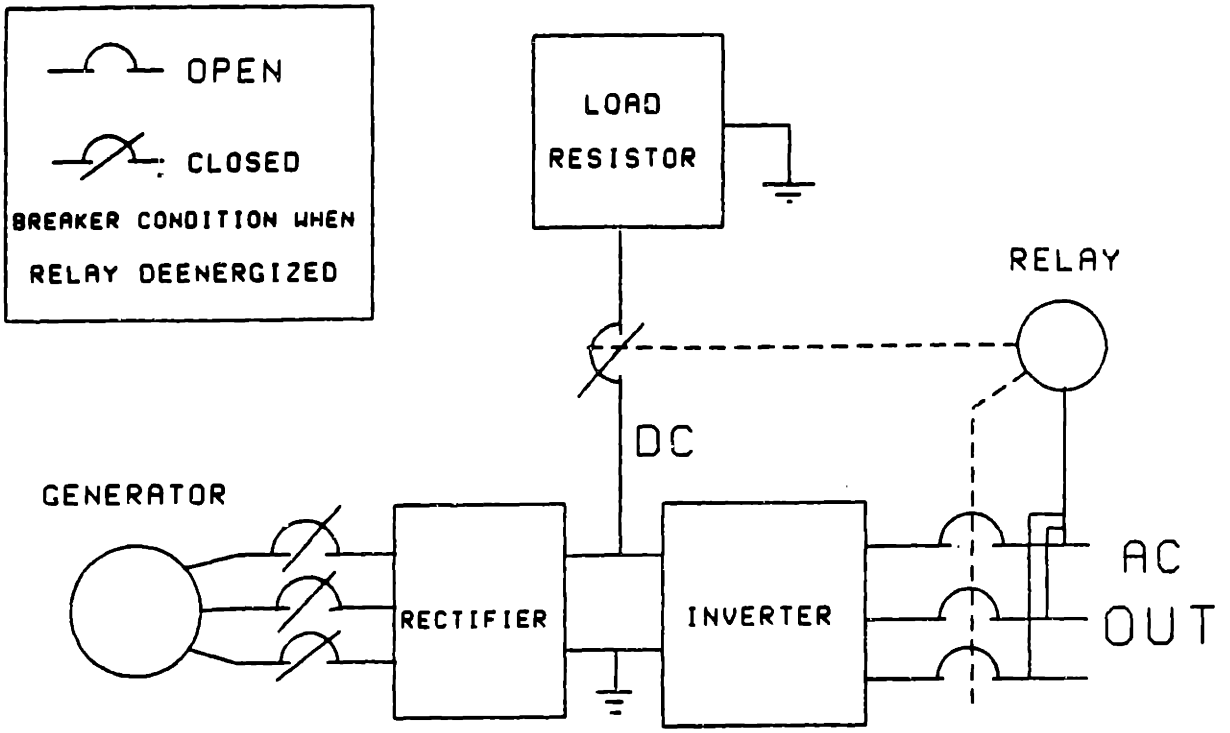

Figure 6.9. **Proposed method of turbomachine overspeed control in the event of sudden loss-of-load.**

pressure parts of the system would fully open to reduce the pressure ratio accross the turbine. The turbine would slow down under load of the compressor and windage losses. Further work could determine whether the investment-risk of a shaft break is sufficient to warrant such a control system.

6.3.2 MGR-GT Turbomachine Startup and Shutdown.

CCGT startup is normally performed using what is sometimes called a "bootstrap" method. The machinery is first motorized up to 3600-rpm to induce circulation and a pressure difference in the helium-coolant circuit. As the turbine-inlet temperature is increased by reactor heatup, the turbine will eventually get to a point where it can provide more power than the compressor absorbs. The turbomachine will then speed up to full speed. Control of turbomachine speed during startup has always been performed by control-bypass valves in CCGT systems of the past. In the MGR-GT, control-bypass valves are not needed for startup. The turbomachine speed can be controlled through the electrical system, since continuous four-quadrant operation is possible with current LCI (or similar rectifier-inverter) drive systems. Elimination of these valves would provide capital-cost savings and improved reliability.

Previous CCGT systems were shut down by unloading the turbomachine on control-bypass, and then securing the heater (ie., shutting down the reactor). The electrical system of the MGR-GT permits shutdown to proceed differently. The reactor would first be shutdown. As the reactor slowly cooled down, the power output of the turbine would diminish until turbine-inlet temperature reached a point where no net power could be produced by the turbo-generator. At this

point, the electrical system would be fully unloaded and the generator-output breaker could be opened, permitting the turbomachine to slow down on its own. Such a method of shut down could simplify design and operation of auxiliary reactor-cooling systems.

The methods for startup and shutdown that are described in the previous paragraghs have the considerable advantage of eliminating the need for continuous position control of the control-bypass valves. Although bypass valves may be needed in the event of a shaft break, these valves will operate in a safety-valve manner such that they are either fully shut (normal condition), or fully open (upset condition). Such valves are considerably easier to design than valves that offer continuous position control.

6.4 Multi-Module Control.

Since the MGR-GT may be depioyed at sites where there may be several power-system modules supplying a common power grid, multi-modular control is a topic to briefly consider. The MGR-GT electrical system allows for integration and control of several MGR-GT power systems. These systems are each capable of operating independently of one another. That is, in contrast to those systems that share a common steam-plant to obtain the necessary economy of scale, multiple MGR-GT plants have no interconnections or shared systems on the plant side of the busbar. The integrated control of a multi-module MGR-GT site is therefore vastly simplified over the steam-plant system.

Present technology permits nearly complete automation ofa single MGR-GT unit, or a large site with sveral MGR-GT units. Presently,

adjustable-speed drives are used in several process-plant applications. Each LCI-drive unit is microprocessor controlled. In applications where there are several adjustable speed drive units, integrated control is possible. Several microprocessors can be integrated into networks for control of complex systems. These systems are presently available through manufacturers of LCI systems [T4]. This technology can be directly applied to the MGR-GT, where the control of a single module, or several modules at a common site, may be necessary.

Nomenclature for Chapter Six

Symbol	Meaning	Units
C_p	Constant pressure specific heat	J/kg^oK
C_v	Constant volume specific heat	J/kg^oK
D	Hydraulic diameter	meters
f	Friction factor	
G	Mass velocity	$kg/m^2sec.$
L	Length	meters
m or M	Mass	kg
n	Number of inventory-control vessels	
P	Pressure	Pa
r_p	Pressure ratio of cycle.	
Re	Reynolds number	
ρ	Density	kg/m^3
t	Time	seconds
t	Some time after t=0	seconds
T	Temperature	^oK
T_0	Temperature of isothermal helium transfer.	^oK
V_T	Total volume of all inventory-control vessels	m^3
x	Lower level of inventory control for one vessel.	
X	Lower level of inventory control for more than one vessel.	
y	Ratio of cycle HP-pressure to initial control-vessel pressure.	

Subscripts

eq	Equivalent
hp	Of high-pressure part of cycle
L	Lower
p	Plant, or helium loop
u	Upper
v	Vessel

CHAPTER SEVEN

THE MGR-GT

7.1 The Objectives of this Chapter.

The previous chapters discussed the design considerations that went into each major system and component of the benchmark MGR-GT. In this section, the MGR-GT plant will be described with reference to specific component-design considerations and their role in determining the integrated-plant design. Plant performance will be evaluated. Issues concerning maintenance, safety, and investment-risk will be addressed, and an estimation of the cost of an MGR-GT power plant will be made. The final section of this chapter will summarize the conclusions of this study and make recommendations for future work.

7.2 The MGR-GT Configuration.

The following is a list of design objectives that were kept in mind when determining the MGR-GT plant configuration.

- System placed in a below-grade silo.
- Flowpath permitting sweeping the reactor vessel with cool helium.
- Minimum machinery-module vessel size, and no larger than the reactor vessel.
- Flowpath maintaining low pressure difference across inner tube of concentric ducts.
- Flowpath that minimizes system pressure losses.
- Vertical turbomachine configuration, allowing easy access for machine removal from below-grade silo.

- Net turbomachine thrust in a direction opposite machine to weight to minimize thrust-bearing load.
- All bearings in a low-temperature environment.
- Generator submerged in high-pressure, low-temperature helium.
- Plate-fin recuperator fins loaded in tension only.
- Easy access to heat-exchangers, especially the precooler, for inspection and maintenance.

7.2.1 The Machinery-Module Arrangement.

Since it is the objective to put the MGR-GT in a below-grade silo, a vertical machinery arrangement is desirable. The below-grade silo offers many safety benefits. Fig. 7.1 shows the general arrangement of the MGR-GT in a below-grade silo. Figure 7.2 shows the machinery-module with components labelled and flowpaths indicated. The machinery module must be kept small enough to ensure transportability for modular construction. All of the power-plant machinery and heat exchangers are contained in the machinery-module cavity. Vessels for inventory control are also contained in the machinery-module cavity.

7.2.1a Machinery.

All rotating machinery is on the same shaft. Solid couplings between each of the machines permit dissassembly. Turbomachinery is oriented to minimize the thrust load on the thrust bearings by opposing the machinery weight with the net aerodynamic thrust of the turbomachines. A thrust bearing and coupling between the generator and the turboset enable the generator to be removed without turboset removal. Access to the bearings and couplings is made possible with

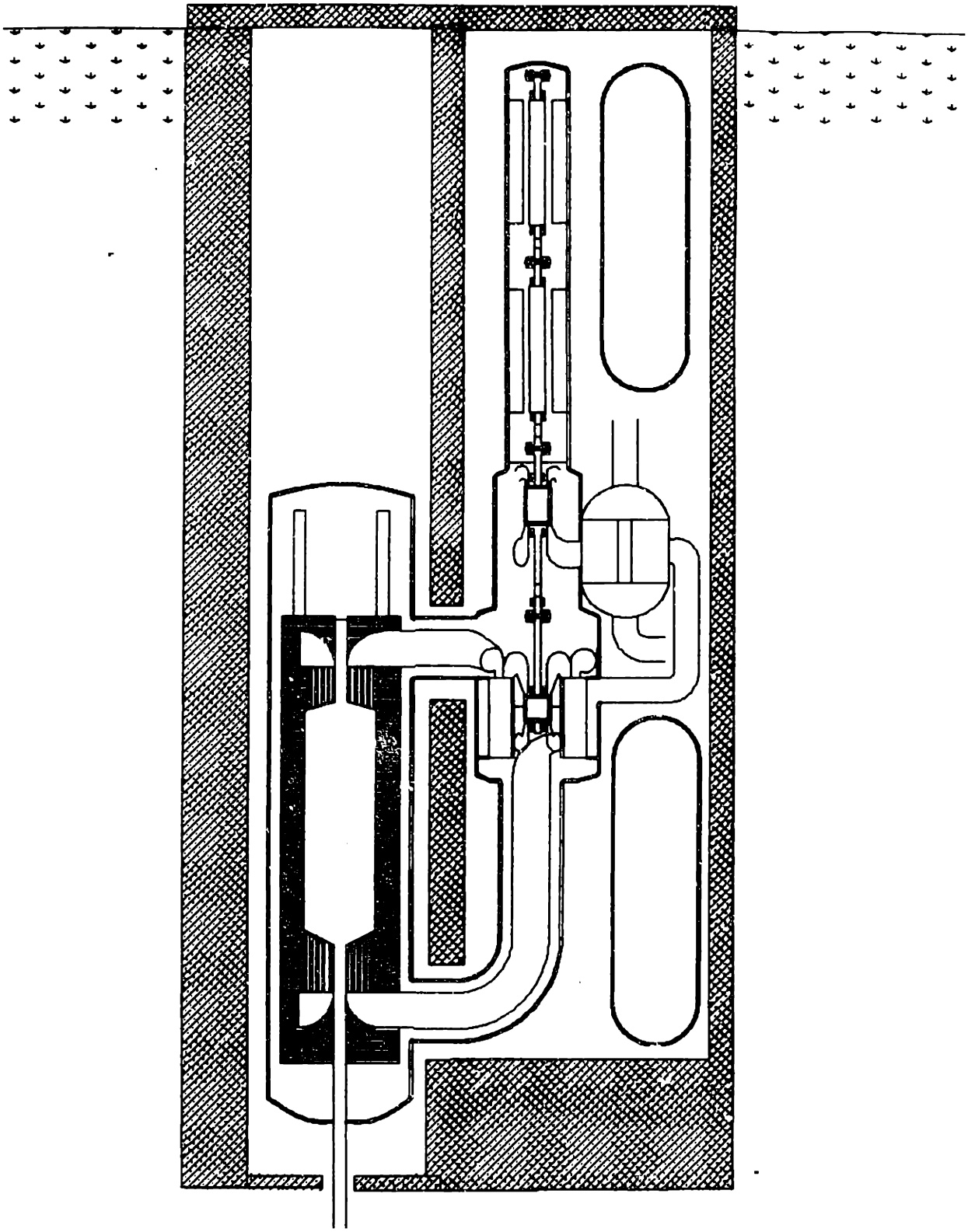

Figure 7.1. The MGR-GT in a below-grade silo.

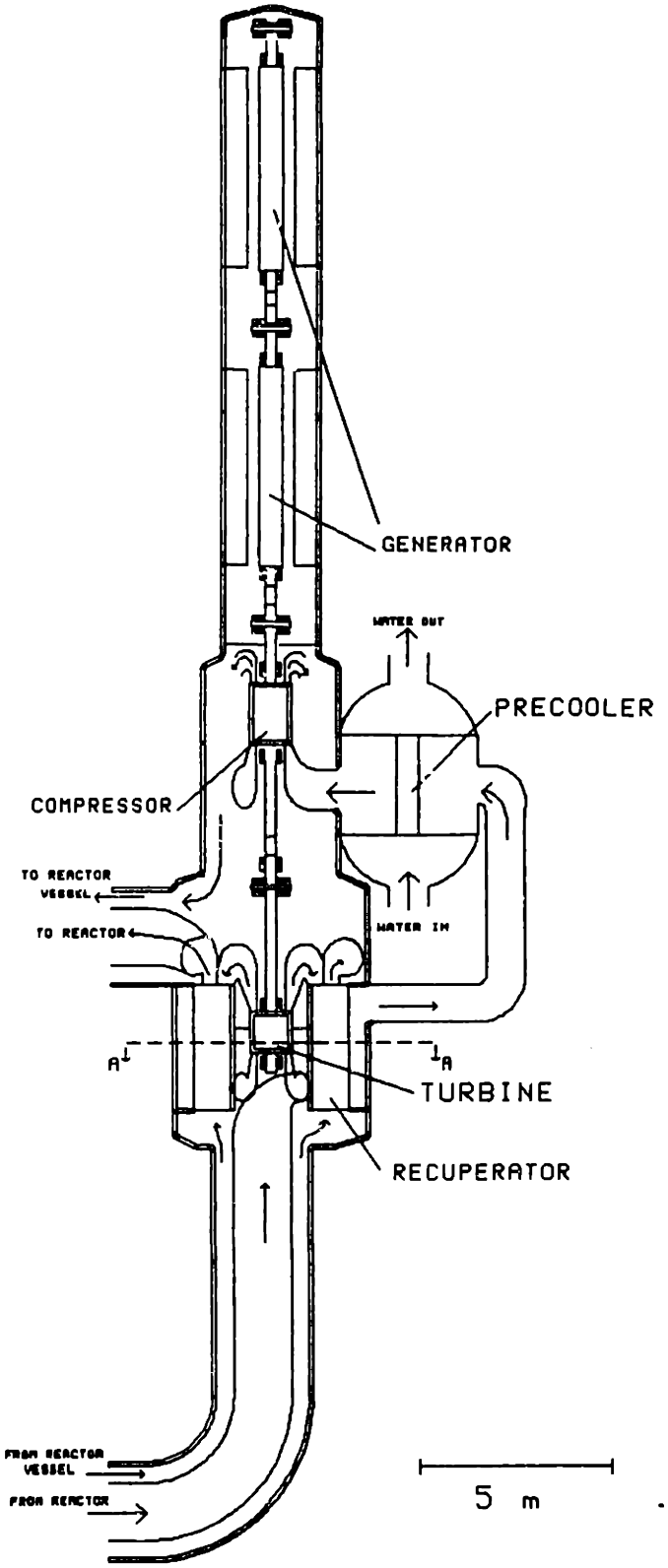

Figure 7.2. The MGR-GT machinery module.

handholes (not shown) in the vessel. The handholes are normally welded shut.

Because the generator must operate at temperatures below that of the compressor-discharge gas, a non-pressure-retaining surface is placed between the generator casing and the rest of the system. This barrier is designed to prevent circiut helium from circulating in the generator cavity. Sufficient leakage is permitted to ensure that the barrier is not exposed to a large pressure difference during plant transients.

7.2.1b Recuperator.

Placing the highly-compact plate-fin recuperator around the turbine, as in Fig. 7.3, offers two benefits. It uses space very efficiently, resulting in a machinery-module diameter of only 5-meters. It also reduces the flowpath from the turbine exhaust to the recuperator, thereby minimizing the pressure losses. The recuperator is manufactured from 304 stainless steel. Because the internal pressure of the tension-brazed plate-fin recuperator must be at least as great as the external pressure, a pressure-retaining surface is needed between the turbine casing and the recuperator. This internal pressure-vessel will be made of the same material as the reactor and machinery-module pressure vessels, SA-533 low-alloy steel, and needs to be just under an inch thick. The highest pressure difference it should experience occurs during normal operations. At other times, including upset conditions, it will have no pressure difference, or a low pressure difference, across its surface. This internal pressure vessel offers the additional advantage of reducing the required thickness of the machinery-module pressure vessel at some locations. A

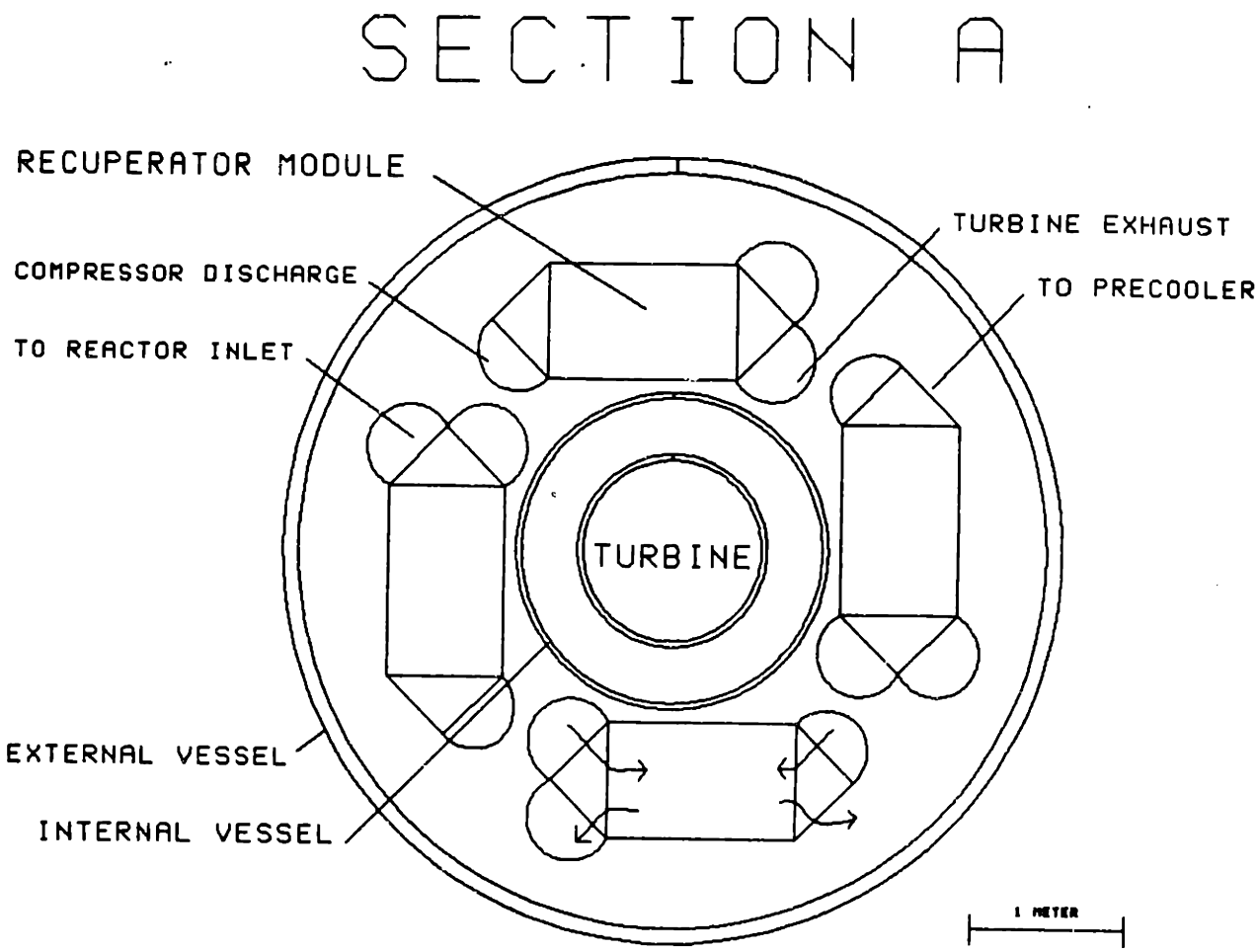

Figure 7.3. Cross-section of the MGR-GT machinery module.

surface extending between the turbine casing and the inner pressure vessel ensures that helium from the compressor discharge passes through the reactor vessel to maintain reactor pressure vessel temperature low enough to ensure metal strength. This surface experiences only a small pressure difference across its surface. Hence, it can be constructed of thin steel plate.

As shown in Fig. 7.4, the recuperator-inlet manifolds have a length equal to the height of the heat-exchanger modules. These manifolds are not of constant cross-sectional area. Manifold cross-sectional area is varied along the length of the manifold to maintain a constant pressure along the manifold length at design-rated conditions. The area change compensates for the effects of fluid momentum and friction on the manifold pressure. This assures a well-distributed flow in the high-performance recuperator when operating at design conditions. At conditions other than design, some flow maldistribution may occur, and system performance may be somewhat reduced. The MGR-GT, being a nuclear plant, will normally be base-loaded and therefore operated at design conditions.

7.2.1c Upper Recuperator Manifolds and Ducting.

Helium flows from the turbine through the recuperator LP upper manifold to the recuperator LP side (Fig. 7.5). Helium leaving the recuperator HP side flows through the HP upper manifold to the reactor-inlet concentric duct. These manifolds can be manufactured from 304 stainless steel. The inner tube of the concentric duct is manufactured from the same materials as the manifolds. A thermal liner is required in the inner duct that leads the helium from the reactor outlet to the turbine inlet. The use of carbon-carbon composite

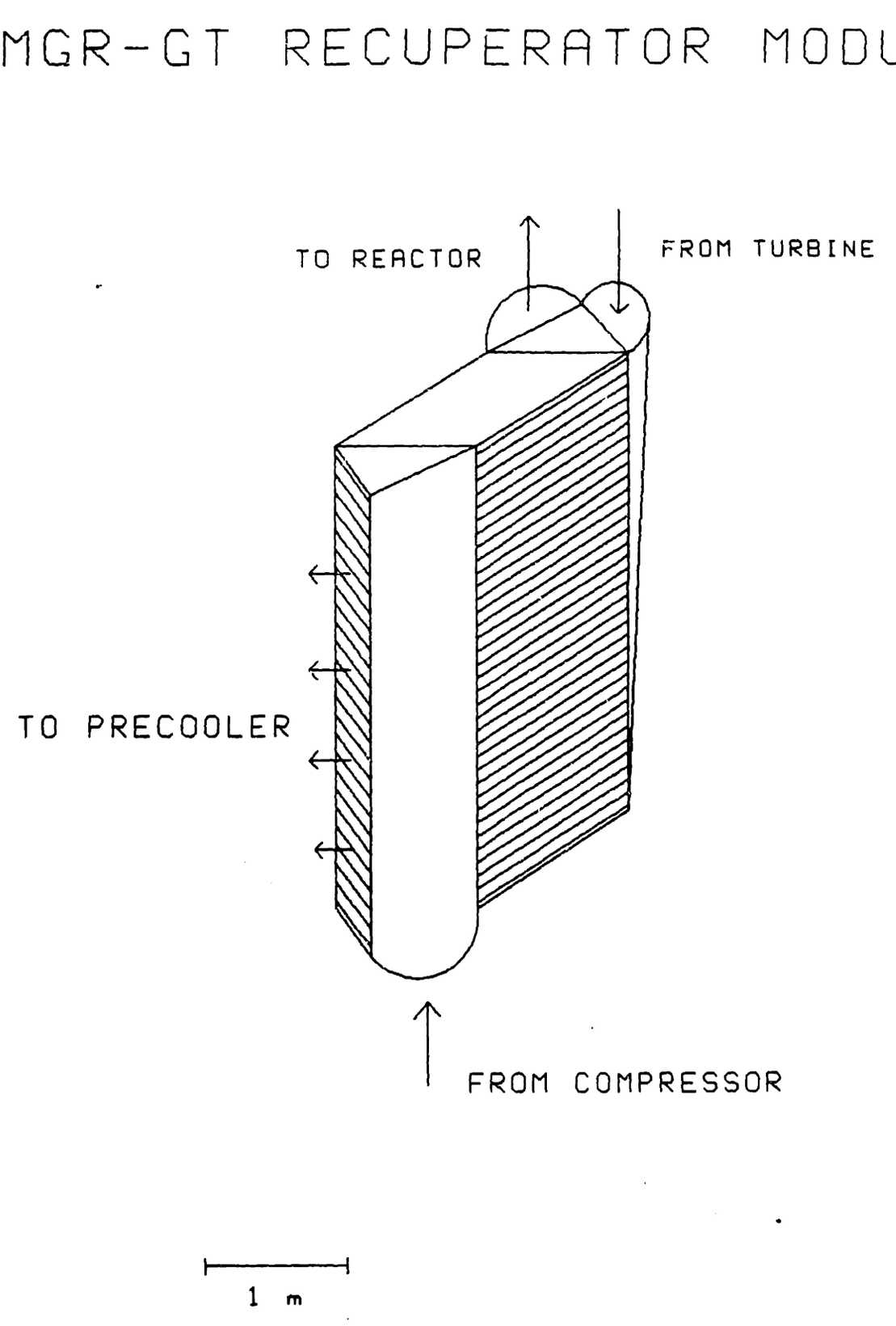

Figure 7.4. **An MGR-GT recuperator module.**

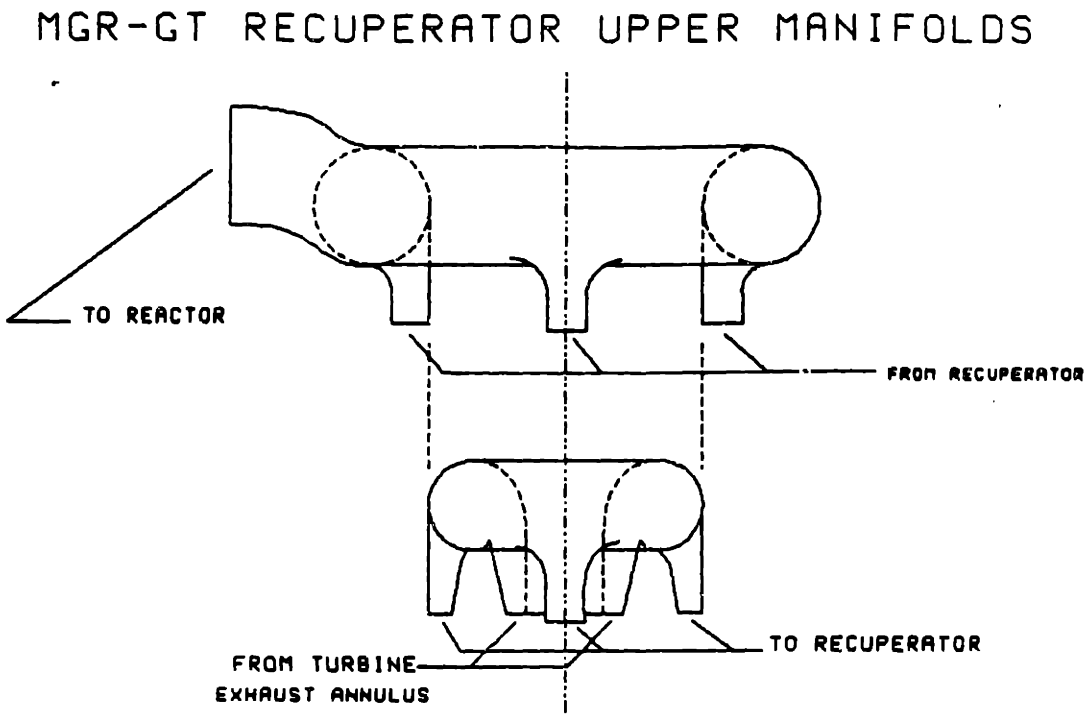

Figure 7.5. The MGR-GT recuperator upper-manifolds.

materials for the high-temperature ducting is an attractive future alternative to metal ducts with thermal liners [P8]; however, carbon-carbon composite materials are not yet design-code approved and therefore do not meet the design criteria of the MGR-GT.

7.2.1d Precooler.

The LP outlet of the recuperator sweeps the MGR-GT machinery vessel in the region of the recuperator. The helium then flows to the precooler (see Fig. 7.6), which is a simple crossflow tube-and-shell heat exchanger (for wet cooling) with an unfinned circular-tube surface manufactured from 304 stainless steel. Baffles (not shown) might be used to ensure even flow distribution in the crossflow precooler. They will not significantly affect pressure drop. The precooler for a dry-cooled system would look similar to the precooler pictured in Fig. 1.24. For both types of precoolers, water flow is upward to enhance natural circulation in the event of a loss of forced cooling-water flow. The large difference in static head between the hot-water and cold-water sides of the precooler, resulting from the below-grade arrangement, will help to maintain good natural circulation.

7.2.1e Electrical.

Toshiba Corporation provided a preliminary design for the MGR-GT electrical system based upon specifications provided by the author [T5]. The designs are shown in Figs. 7.7 and 7.8. The dimensions of the generator designed by Toshiba are in good agreement with dimensions predicted by Eq. 4.84. The electrical system consists of a two-pole, 10,000-rpm generator. A 24-pulse load-commutated inverter converts the generator output to 60-hz electrical power. Based upon

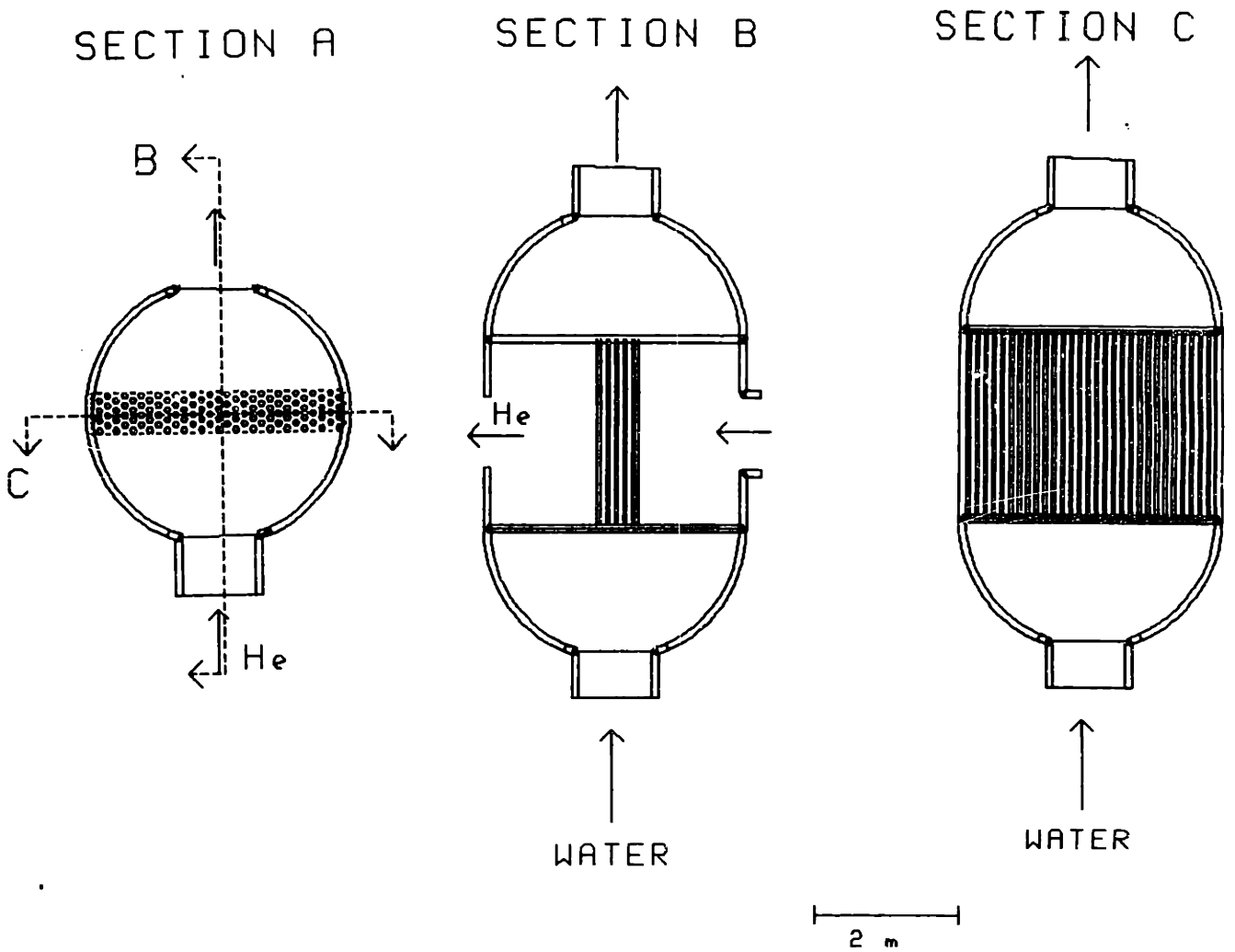

Figure 7.6. The MGR-GT precooler.

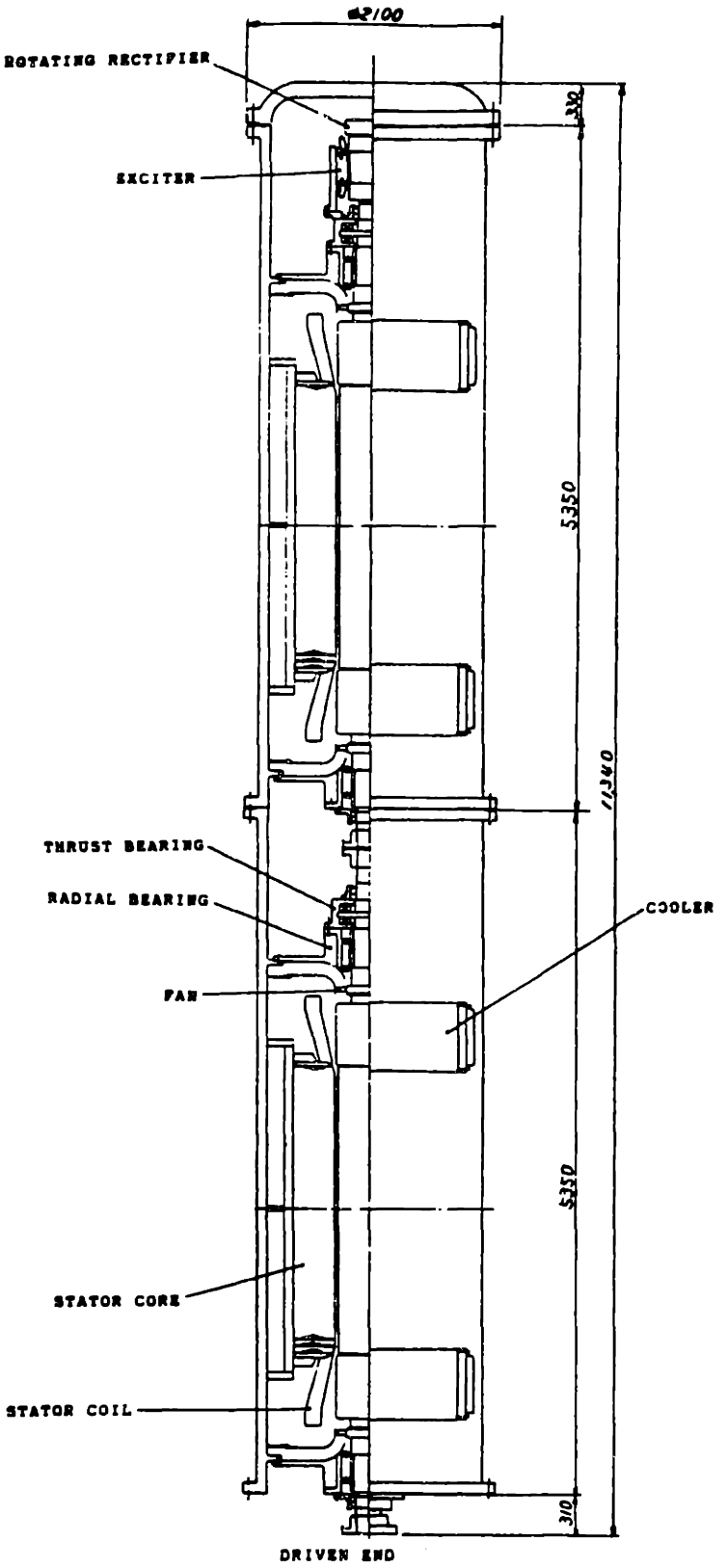

Figure 7.7. The MGR-GT generator [T5].

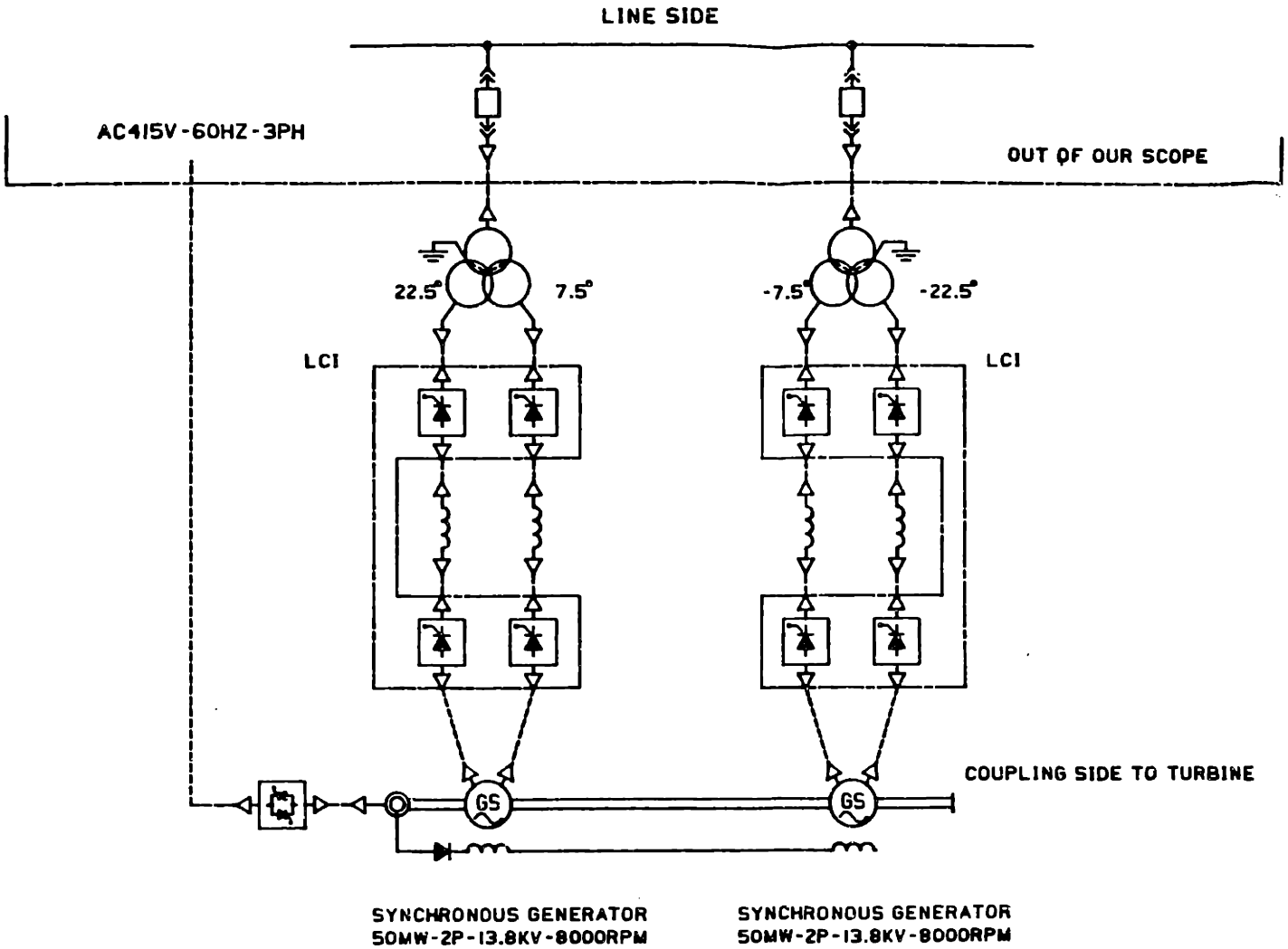

Figure 7.8. The MGR-GT electrical system [T5].

Toshiba's preliminary design, the generator is only 95% efficient, resulting in a minimum combined efficiency of 92% for the generator and LCI. This low efficiency value is largely due to the increased frictional losses incurred in pumping the high-pressure-helium coolant. Toshiba engineers are confident that the generator efficiency will be improved upon more detailed design [S20].

7.2.1f Control.

The MGR-GT inventory-control system is shown in Fig. 7.9. During normal operation, helium is circulated through the helium-purification system and returned to the generator cavity (the details of the purification system depend upon reactor-coolant chemistry requirements and are beyond the scope of this work). The non-pressure-retaining barrier of the generator cavity permits leakby of purified helium into the plant circuit. During an inventory reduction, helium from the compressor discharge passes through the purifier, through the inventory-control valves, to the inventory-control vessels. During an inventory increase, helium is passed from the inventory-control vessels, through the inventory-control valves, to the precooler inlet. Transfer compressors permit transfer of helium between inventory-control vessels and storage vessels, as necessary. The necessary inventory-control vessel size will be determined by the desired range of inventory control. Two vessels, each with volumes of 100-m^3, would permit inventory control down to about 76% inventory (power) level without the use of transfer compressors (based upon the assumption of an adiabatic inventory-control vessel). Inventory levels below 76% would require the use of transfer compressors. If four 100-m^3 inventory-control vessels are used, inventory-control down to

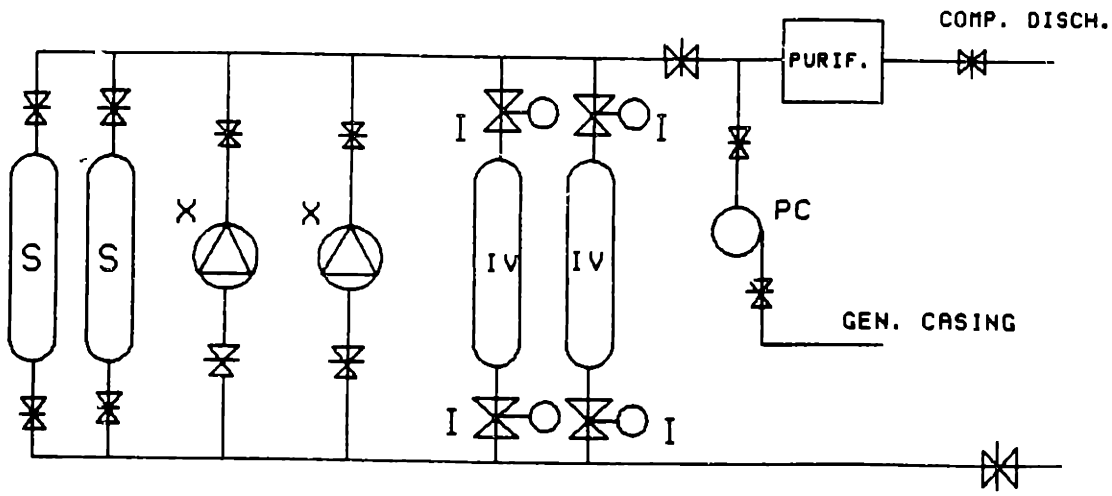

S: STORAGE VESSELS
X: TRANSFER COMPRESSORS
I: INVENTORY-CONTROL VALVES
IV: INVENTORY-CONTROL VESSELS
PC: PURIFICATION CIRCULATOR
PURIF: PURIFIER

Figure 7.9. The MGR-GT inventory-control system.

57% is possible without transfer compressors. From the analysis of Chapter Six, it is estimated that inventory-control valves with diameters of 14-cm (5.5-in) will permit inventory changes at a rate of about 10%/minute.

Turbomachine speed control can be accomplished with the electrical system during normal and upset conditions. The LCI offers speed-control accuracy better than ±0.5% during normal conditions. During system startup, the generator may be operated as a motor up to 3,600-rpm. Acceleration of the turbomachine between 3,600 and 10,000-rpm can be controlled with the generator load. After shutdown, the generator may be used to motorize the turbogroup to circulate helium for decay-heat removal. During upset conditions, such as a sudden loss of AC load, it is possible to rapidly load the generator with a dummy load to prevent overspeed.

7.2.2 Plant Ferformance.

Table 7.1 lists helium conditions at selected MGR-GT cycle locations and Table 7.2 summarizes plant parameters and system performance for the MGR-GT. The two columns in table 7.2 list minimum-expected performance and predicted performance. The difference in the two lies in the turbomachine and electrical efficiencies used. Well established methods predicted that the turbomachines would both achieve total-to-total polytropic efficiencies of over 93%. The combined effects of high Reynolds numbers, low Mach mumbers, the low molecular weight of helium, and efficient velocity triangles result in low blade-profile losses. Based upon this, a polytropic efficiency value of 91% should be considered a conservative minimum for both turbomachines. Toshiba engineers predict that the electrical system is

Table 7.1

Conditions at MGR-GT Cycle Locations

Location	Temp. (^{o}C)	Press. (MPa)
Compressor Inlet	30.0	3.99
Compressor Outlet	138.6	8.18
Reactor Inlet	583.1	8.01
Turbine Inlet	850.0	7.80
Turbine Exhaust	606.5	4.05
LP-Regenerator Outlet	165.0	4.00

Helium mass flowrate = 145.8 kg/sec

Table 7.2

MGR-GT Plant Parameters,

Equipment Sizes, and System Performance

Turbomachinery

	Turbine	Compressor
Stages	6	15
RPM	10,000	10,000
Max tip diameter	86.2-cm	73.3-cm
Bladed length	63.0-cm	130-cm
Poly. Eff. (expected)	0.931	0.937
Poly. Eff. (minimum)	0.91	0.91

Heat Exchangers

	Precooler (Crossflow)	Recuperator
Ref. K15 surface	S 1.50-1.00	SF-PF 1/9-24.12 (both sides)
Volume	5.3-m3	3.96-m3 x 4-modules
Length	56.5-cm	1.22-m
Frontal Area	3.6-m x 2.6-m	3.25-m x 1-m
Ht. X-fer Area	1,168-m2	17,933-m2 (ea. side)
$\sum \frac{\Delta P}{P}$	0.00096	0.00241 (cold side)
		0.00921 (hot side)

Pressure Losses and Efficiency

Component	$\frac{\Delta P}{P}$
Reactor	0.02560
Recuperator	0.01162
Precooler	0.00096
Turbine Exh.	0.00614
Compressor Exh.	0.00823
Ducting/Manifolds	0.00707
Total	0.05962

	minimum	expected
Cycle Thermal-Efficiency =	48.19%	50.53%
Ambient Losses =	1.22%	1.22%
Electric Plant Efficiency =	92%	95%
Cool. Wtr. Pmp. Pwr. =	0.1%	0.1%
Total System Efficiency =	43.11%	46.74%
Electric Power Output = (200-MWth MGR)	86.22-MW	93.49-MW

capable of at least 92% efficiency and they are confident that a higher figure would result upon a detailed design [S20, T5]. An efficiency close to that of their current large super-motor drive systems, about 95%, might be expected after a more detailed design.

The turbomachine-exhaust pressure losses are based upon the conservative assumption of 65% pressure recovery in the turbomachine-exhaust diffusers. Thermal losses from the reactor are accounted for in Table 7.2 also. Calculations for reactor heat-transfer losses are shown in Appendix E. The cooling-water pumping-power requirement accounts for the pumping power consumed in pumping water through the precooler and assumes a water-pump efficiency of 60%.

7.3 Maintenance Considerations.

In the design of the MGR-GT, consideration for equipment maintenance and repair was made. Maintenance and repair of nuclear components is especially difficult because equipment may become activated or may have activated species deposited on the surfaces. It is essential that equipment requiring maintenance be accessible, and have sufficiently low levels of radioactivity to permit necessary maintenance and repair procedures to be performed.

7.3.1 Plate-Out of Fission Products.

The primary cause of activation of plant components in the helium-circuit locations outside of the reactor is deposition of fission products. Present fuel technology is such that the amount of fission products that escape the fuel is very low. New, improved particle fuel will reduce the fission-product plateout by one to two

orders-of-magnitude from that of previous fuels [I3].

Investigations into fission-product deposition have identified the plant heat-transfer components as the equipment with the highest fission-product deposition rate in the primary circuit. Calculations by Iniotakis, et. al., predicted fission-product plateout on the gas circulator of a PNP-500 reactor after 30-years of operation to be about two orders of magnitude lower than plateout on the heat-exchange components [I4]. Experiments by Hanson [H11] confirmed these trends by showing that most of the fission products would deposit in the chilled region of a test loop. Therefore, the heat-exchange equipment of the MGR-GT, the recuperator and the precooler, are expected to experience higher activity levels than the turbomachinery. Also, cooled turbine-blades should experience significantly greater levels of contamination than uncooled blades. Hence, the use of turbine-blade materials TZM and IN-100 - materials that will not require blade cooling - offer maintenance as well as performance advantages for the MGR-GT because low contamination levels can be expected on the MGR-GT turbomachinery, especially in light of the high-quality particle fuel that is currently available. Fission-product plateout on the electrical generator is expected to be very low; in the MGR-GT, a non-pressure-retaining barrier prevents circuit helium from circulating freely in the generator. Purified helium is sent directly to the generator cavity from the purification system, maintaining the generator cavity at a slight overpressure so that the net flow of purified helium will be from the uncontaminated generator cavity into the fission-product contaminated helium circuit.

7.3.2 Access to Machinery.

Even though modern diagnostic techniques will reduce the need for machinery removal, it is anticipated that the turbomachine will be removed periodically for scheduled maintenance and inspection. At these times the blades could be decontaminated or discarded. Couplings on the turbomachine ducting permit removal of the turbomachinery within the machine casings from the MGR-GT machinery-module vessel. The duct couplings and seals will be of the same type as used in many aerospace applications. Virtually leakproof seals, designed to withstand temperatures as high as 2000°F and pressures up to 20 ksi, are available [A8]. They can be remotely operated to facilitate use in spaces where access is limited, and can be manufactured to diameters up to a few meters [W5].

7.3.4 Access to Heat Exchangers.

Because of poor access to complex surfaces, decontamination of the heat exchangers, especially the plate-fin recuperator, will be much more difficult than decontamination of the turbomachinery. Hence, it is essential that the heat-exchange components be designed for minimum maintenance over the lifetime of the plant. Access for inservice inspection and repair should be good, or heat exchanger removal should be possible. Although the recuperator cannot be removed without removal of the turbine and upper recuperator manifolds, once these are removed, removal of the recuperator modules is easy. Furthermore, since a recuperator leak is kept within the reactor system, repairs are not urgent, as plant performance, not safety, is affected. In the case of the precooler, it is essential that the tubesheet of this heat exchanger be easily accessible. A precooler leak can result in potential release of activity to the environment,

and will also provide the potential for moisture ingress in the event that helium pressure drops below cooling-water pressure. Locating the precooler in a separate vessel permits good accessibility for inspection and repair. The water side of the tubesheet is accessible through handholes in the heat-exchanger end bells. Therefore, tubesheet inspection is possible with little or no exposure of maintenance personnel to radioactivity.

7.4 MGR-GT Safety and Investment Risk.

This section will look at potential upset and accident conditions that might occur in the MGR-GT. Two issues must be considered in all of these scenarios: safety, and investment risk. Safety issues are those dealing with situations where there is a threat to the general public, especially through the release of radioactivity to the environment. Investment-risk issues are those dealing with situations where a significant portion of the plant may be damaged, but the safety of the general public may not be threatened. There are a number of accident scenarios that are different for the MGR-GT than for other MGR conceptual designs. This chapter will identify these scenarios, and address them in a context appropriate to the MGR-GT.

The important accidents discussed in this chapter are broadly divided into four categories: 1) Loss-of-cooling accidents, 2) Water-ingress accidents, 3) Pressure-transient accidents, and 4) Turbine-failure accidents.

7.4.1 Loss-of-Cooling Accidents.

The fundamental safety criterion of the MGR is "passive-safety". That is, in the event of an accident, the plant will always fail in a

way such that no threat is posed to the safety of the public. It has been determined that if the maximum temperature of the MGR fuel remains below 1600°C, fission-product release is sufficiently low such that there is no significant threat to the public. Thus, passive-safety requires that in no situation may fuel temperature be permitted to exceed 1600°C. For this reason, the MGR is designed in such a way that in the event of an accident that disables the normal methods of decay-heat removal, sufficient heat may be passively conducted/radiated through the reactor vessel to the environment that peak core temperatures remain below 1600°C.

Loss of cooling may be a result of a loss of forced helium circulation, or of a loss of water-flow in the precooler. The loss of forced-circulation may occur in a pressurized mode, as in a failure of the circulator, or in a depressurized mode, as in a depressurization due to a break in a pressure surface. The loss of precooler-flow could be a result of failure of a cooling-water pump.

7.4.1a Loss-of-Forced-Circulation, Depressurized Case.

In the event of a break in the pressure surface, helium will escape from the plant, and pressure will drop. Helium will not be available in sufficient amounts for circulation and heat-removal from the reactor core. The reactor after-heat will be removed by passive conduction/radiation through the pressure vessel. Calculations have shown that a 200-MWth, pebble-bed reactor operating at temperatures representative of a gas-turbine plant (reactor-inlet temperature of 600°C and reactor-outlet temperature of 850°C), will maintain peak-core temperatures below 1600°C during a depressurized cooldown (see Fig. 7.10) [I3]. The MGR-GT is, therefore, capable of operating

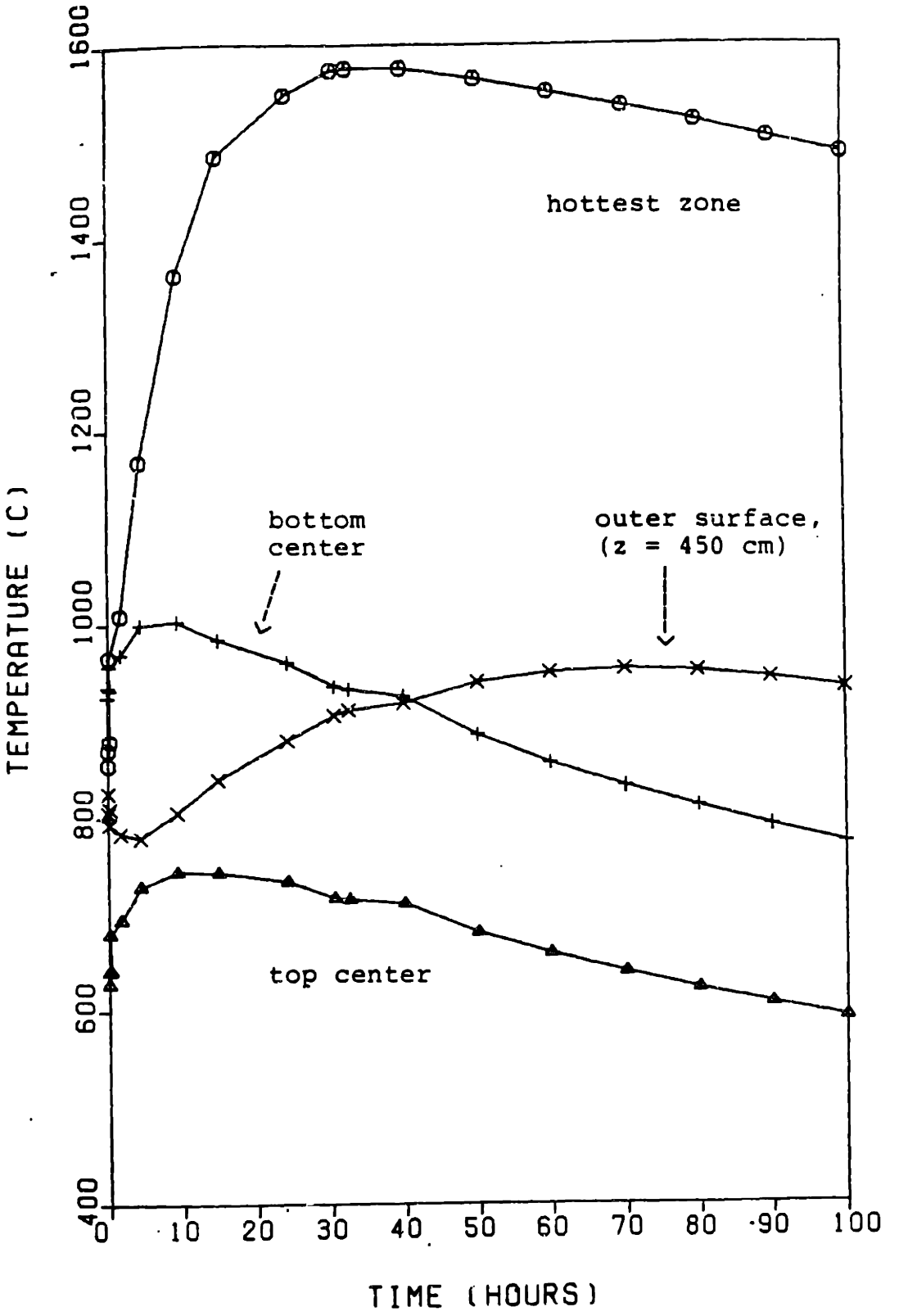

Figure 7.10. **MGR-GT core temperatures resulting from a depressurized loss of forced circulation. Calculations by Izenson [I3].**

at the elevated temperatures necessary to utilize its performance capability without risking public safety in the event of an accident.

7.4.1b Loss of Circulation, Pressurized Case.

In this accident it is assumed that it is impossible to circulate the helium coolant, although the system is at pressure. Such a case would result in the event of a failure of the rotating assembly in an MGR-GT, or the failure of the circulator in a steam-plant MGR. For the steam-plant MGR, this has been shown to be a less serious accident for the reactor core than the depressurized case. Calculations by General Electric Company on a 250-MWth pebble-bed steam-plant MGR with helium-outlet temperature of 686°C determined that a peak core-temperature of 1120°C is reached [W4]. This accident will result in slightly higher pressure-vessel temperatures than occur in the depressurized accident. In the steam-plant MGR, circulation develops, causing a flow that is in the reverse direction of the normal-operating flowpath. Helium flows up through the core, to the vessel, heating the vessel to a high temperature. Calculations by General Electric determined that pressure-vessel temperature will rise to a peak of 380°C (716°F) after 60 hours, and then decrease gradually [W4]. The temperature reached by the vessel will slightly violate the maximum permitted temperature allowed for SA-533 low-alloy steel by the current design code, 371°C (700°F). However, an extension of the temperature limit for SA-533 to 1000-1100°F is currently being evaluated and is expected to be incorporated into the ASME code soon [M30], thus permitting much higher temperatures to be reached without a design-code violation.

Furthermore, the MGR-GT flowpath is very different from that of

the steam-plant MGR, and it is uncertain if any significant natural circulation of helium will result from a pressurized loss-of-forced-circulation accident. Because the reactor vessel is normally swept by the compressor-discharge helium, the hot helium rising from the reactor will not immediately contact the reactor vessel. Any hot helium rising from the reactor will first be ducted to the recuperator, which is made of materials that can tolerate higher temperatures than the reactor-vessel materials can withstand. But, because of the sinuous flowpath and additional flow resistances of the MGR-GT, it is expected that any circulation resulting from such an accident would probably be much less than in the steam-plant MGR.

Considering the lower power rating of the MGR-GT core (200-MW versus 250-MW), the different flowpath, and lower circulation expected, it is expected that the peak vessel temperature of the MGR-GT resulting from a pressurized loss-of-forced-circulation will remain within the new design-code limits being proposed.

In any event, since there is ample time to take corrective action, it is possible to avoid helium circulation by reducing the helium-coolant inventory. The probability of a loss-of-forced-circulation accident occurring at the same time as a failure of the helium-pumpdown system on the steam-plant MGR has been shown to be so low that current policy permits neglecting the investment risk involved in this accident [M27]. In the MGR-GT, the generator has the added capability of being used as a motor for the rotating assembly to induce circulation when needed. The tandem-generator configuration and the 24-pulse LCI system (as opposed to a 6, 12, or 18-pulse system) provide inherent redundancy. It is expected that the probability of a

loss-of-forced-circulation under pressurized conditions would prove to be negligible.

7.4.1c Loss of Precooler Flow.

In the event of a failure of the precooler cooling-water system, it will be impossible for the MGR-GT to reject its waste heat. Such a transient for the HTGR-GT is shown in Fig. 7.11. It is expected that such an accident would result in a similar transient in the MGR-GT (with a few noted exceptions). Initially, compressor-inlet temperature rises as a result of the loss of cooling in the precooler. Compressor-discharge temperature will increase. The increase in the compression temperature causes a reduction in pressure ratio. The reduced pressure ratio across the turbine produces an increase in turbine-exhaust temperature. To prevent an excessive thermal transient, the attemperation-bypass valve opens and the reactor is tripped (The use of an attemperation valve - or any other bypass valve - may not be needed in the MGR-GT). The pressure ratio will continue to drop. When turbine power drops below 10%, the generators are tripped and the primary-bypass valve opens to prevent turbine overspeed (In the MGR-GT, this sequence may be different because of the unique electrical control system discussed in Chapter Six). Pressure ratio then drops at an even more rapid rate, and turbine-exhaust temperature increases rapidly. When the pressure ratio reaches 1.0, turbine-inlet and turbine-exhaust temperatures will be equal. Similarly, compressor-inlet and compressor-outlet temperatures will be equal.

After the initial plant transient is over, the reactor will continue to generate decay heat. The decay-heat generated by the

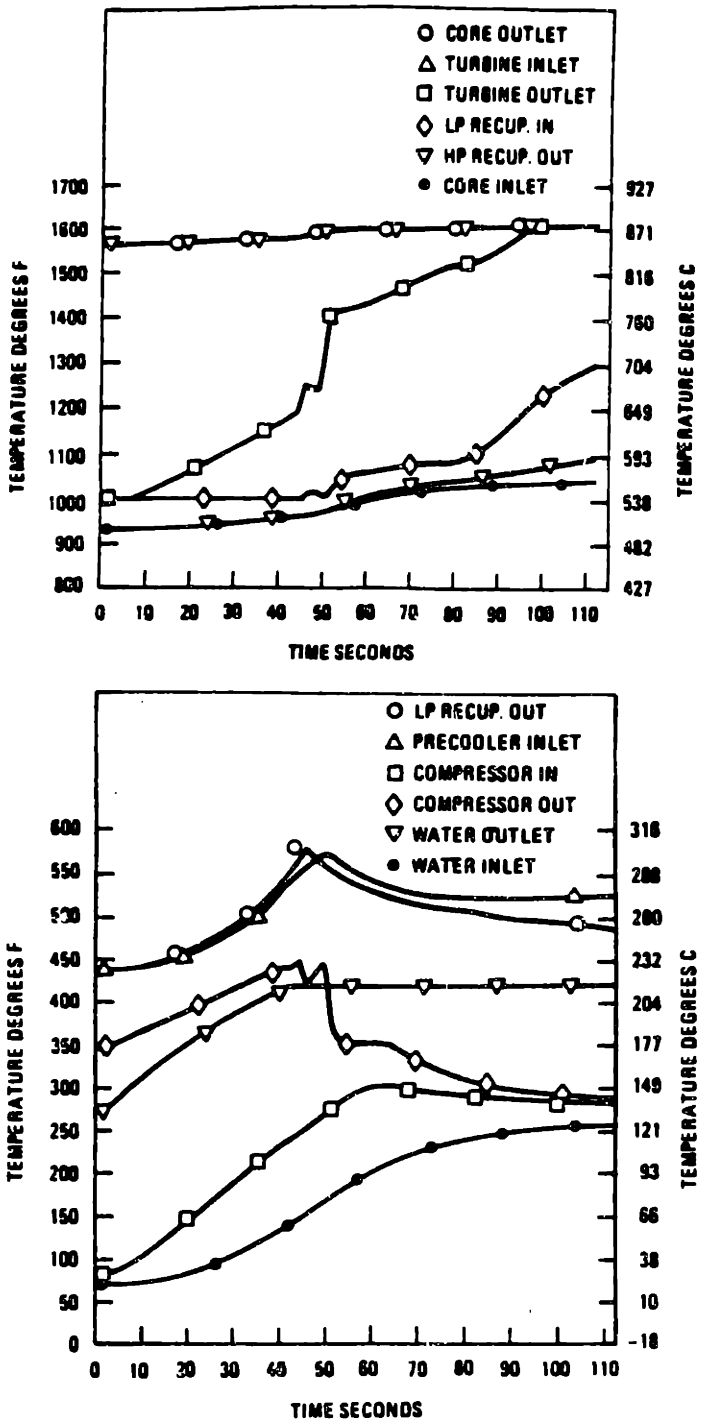

Figure 7.11. Transient resulting from a loss of precooler flow in the HTGR-GT [from D1].

reactor is normally removed by circulation of helium through the precooler. The precooler of the MGR-GT is configured to enhance natural circulation of cooling water in the event of a loss of cooling-water flow. By circulating helium coolant with the rotating assembly, it is expected that sufficient heat may be transferred to the cooling-water during such an accident that no threat to the plant will result. Without circulation of helium, the consequences of this accident after the initial transient are expected be similar to those of the pressurized loss-of-forced-circulation accident. If water is completely lost to the precooler, the precooler will not reach a temperature where failure would occur. The precooler is constructed of 304 stainless steel, which is capable of withstanding high temperatures.

7.3.2 Water Ingress.

Ingress of moisture into the helium-coolant circuit can result in serious reduction in availability, as demonstrated by the Fort St. Vrain reactor and the AVR reactor (see Section 1.2.3). Potential sources of moisture are the bearing-lubrication system and the plant heat-exchangers. In a plant using a PCRV, water may also enter the helium-coolant circuit through leaks in the thermal-liner cooling system. However, this is not of concern for the MGR because a PCRV is not used. Because the MGR-GT does not have a steam generator, this major source of moisture present in the steam-plant MGR is eliminated. By submerging the electric generator in the high-pressure helium and by using active magnetic-bearings, the other major sources of moisture ingress are eliminated. The only potential source of moisture ingress into the MGR-GT helium-circuit is the precooler. However, since the

water pressure in the precooler is maintained well below that of the helium coolant, the possibility of water ingress into the MGR-GT is extremely remote.

7.4.3 Pressure Transients.

The large pressure differences in a COGT-plant coolant circuit create the potential for large pressure transients caused by a rapid pressure equilibration. In the HTGR-GT study there was concern over the effect such a transient might have on the core structure, the integrity of the thermal-barrier system, and the ability to remove decay heat. Such a transient could result from a sudden deblading of a turbomachine or a sudden rupture of an internal pressure surface. A sudden pressure transient could also result from a rupture of an external pressure surface; however, the probability of pressure-vessel rupture is extremely low. Sudden rupture of an internal pressure surface is equally remote.

In the case of the MGR-GT, the ability to remove decay heat by conduction/radiation through the pressure vessel changes the nature of pressure-transient accidents. Rather than being a safety concern, pressure-transient accidents are investment-risk concerns for the MGR-GT. Additionally, it was found in the HTGR-GT study that design of a core structure and thermal barrier that could withstand any perceived pressure transient resulting from a sudden turbine deblading was possible [M17]. Since the pressure difference in the MGR-GT helium circuit is less than that of the HTGR-GT (this is due to a lower pressure ratio and similar peak pressures), it is expected that pressure transients will be less severe for the MGR-GT. Furthermore, while the thermal barrier of a PCRV requires a complex cooling-water

system, the thermal barrier used in the MGR-GT does not. Additionally, a PCRV must be fully lined with a thermal barrier, while a thermal barrier is needed only in the inner concentric cross-duct of the MGR-GT. Hence, the probability and the consequences of thermal-barrier failure in the MGR-GT are substantially less than in the HTGR-GT.

7.4.4 Missiles from Turbine.

The existence of high-speed rotating machinery in the vicinity of the reactor raises concern over the consequences of a turbomachine rotor failure that could throw missiles and potentially damage the reactor. A catastrophic failure of a rotating machine can be caused in several ways. Loss of blading caused by overspeed, for example, would imbalance the machine, possibly causing severe rotor vibrations that damage the rotor. Inadvertant motorization of the generator during turbine operation could also result in a catastrophic machine failure (This is unlikely for the MGR-GT electrical system, and is avoided in most electrical systems through the use of reverse-power relays in the generator-output breaker). Previous studies identified the probability of a catastrophic rotor failure as low, but not so low as to permit it to be totally disregarded [S3]. These studies, however, used data for built-up rotors. It is anticipated that a welded rotor will be used for the MGR-GT turboset. No welded-rotor failures have ever occurred. Hence, the probability of rotor failure should be evaluated in light of the appropriate rotor-construction method. In any event, the probability of such a machine failure resulting in damage to the reactor is extremely remote. The turbine is contained within a casing, two pressure-vessels, and a crushable heat exchanger. The reactor vessel and machinery module are additionally separated by a reinforced

concrete structure (see Fig. 7.1). Hence, it is inconceivable that any turbomachine failure would pose a missile hazard to the reactor. Turbomachine failure will pose only investment risk, not safety risk.

7.4.5 Seismic Considerations.

Since the MGR-GT machinery module is long and narrow, and more ducts are needed than for the side-by-side steam-plant MGR reactor-module and steam-generator, consideration of the consequences of an earthquake may be slightly more involved than for the steam-plant MGR. The MGR-GT plant may require some additional support for its structure, particularly for the generator; however, any additional support needed will be very slight since the two below-grade arrangements are so similar. Both MGR power systems are seismically much simpler than present light-water-reactor systems; hence, seismic issues are not expected to be a difficulty for the MGR-GT.

7.5 Cost Estimates for the MGR-GT.

The cost of the MGR-GT will be estimated in this section.

7.5.1 Reactor Plant.

Coxe has estimated the cost of a serial produced HTR-100 pebble-bed reactor, less helium circulators and steam generator, to be about $49-million [C8]. An additional $3-million is allowed for factory labor for a total cost of about $52-million [C8].

7.5.2 Turbomachines.

The turbomachine is certainly the most difficult component to cost-estimate, partly because of the uniqueness of the MGR-GT turbomachine, and largely because any multi-stage turbomachine is

difficult to cost-estimate. Hence, there is the potential for a large variance in cost estimates. Wilson gives some guidance for cost-estimating serial-produced industrial turbomachines [W6]. This method was used with costs updated with the Nelson Cost Index for pumps and compressors [N3, N4]. Appendix G shows calculations for this method. Total turbomachine (turbine and compressor) costs are estimated at about $2-million.

7.5.3 Generator Costs.

The cost of the unique generator and electrical system in the MGR-GT is estimated at $60/KVAR, which is based upon the costs of LCI motor drives with an extra allowance for some of the additional technology used in the MGR-GT, such as magnetic bearings [S20]. Total electrical-system cost is therefore estimated at $6-million.

7.5.4 Cost of Heat Exchangers.

Heat-exchanger costs are estimated at $8.50 per square foot of total heat-transfer surface area. This value is for stainless-steel heat-exchangers of either plate-fin or tubular design [P10]. The costs of the heat-exchanger vessels are considered in Section 7.5.5. The costs of the heat exchangers, not including the vessels, are estimated at:

Recuperator	$3.2-million
Crossflow precooler	$110-thousand

7.5.5 Pressure Vessels.

The cost of the pressure vessels was estimated on the basis of $15 per pound of steel [R8]. Vessel weights were estimated from the size and thickness of the vessel, and the density of steel. The cost of the reactor pressure-vessel is included in the reactor cost stated

in Section 7.5.1. The estimated cost of the vessels and HP-ducting for the remainder of the power-conversion system is estimated at $5.6-million. The cost of two 100-m^3 inventory-control vessels, each 10-m tall and 3.5-m in diameter, is appoximately $1.7-million. If an equivalent volume of helium storage is maintained, the total vessel costs of the plant, excluding the cost of the reactor pressure-vessel, is $9-million.

7.5.6 Total MGR-GT Costs.

The total of all MGR-GT direct costs is given below to the nearest $0.1-million:

Reactor plant	52.0
Turbomachinery	2.0
Heat Exchangers	3.3
Electrical	6.0
Vessels (excluding reactor)	9.0
Total	72.3

This corresponds to about $780/KW.

All of the above numbers are considered good estimates, with th turbomachinery cost having possibly the highest uncertainty. If actua turbomachine cost is $10-million, at least five times the estimated cost, the total direct plant cost will be $80.3-million ($860/KW). In contrast to this, the total direct costs of a two-module HTR-100 steam-cycle plant were estimated by Coxe to be $265-million, or about $133-million per module ($1325/KW). For an eight-module HTR-100 steam-cycle plant, Coxe estimated total direct costs at $119-million per module ($1190/KW). The above costs do not include on-site construction and assembly costs, which are expected to be substantially less for the MGR-GT due to its improved modularity, smaller size, and simplicity of design.

7.6 Conclusions.

Previous to this study there had been several design studies directed at the development of a nuclear gas-turbine. Although these studies produced some optimistic results, the technology assumed available during these studies was inadequate, and certain critical problem areas arose that could not be overcome. Hence, the gas-turbine variant of the gas-cooled reactor has been looked upon by some as exclusively an advanced power-generating system to be developed some time in the next century.

The results of this study prove that in light of the present technological state-of-the-art, the direct-cycle gas-turbine variant gas-cooled reactor is, in fact, a power system that can be developed in the near-term. Furthermore, the MGR-GT has design characteristics and performance capabilities that make it extremely attractive when compared to alternative power-generating systems. The following sections will briefly review some of the important features of the MGR-GT.

7.6.1 Passive Safety.

An essential feature of the Modular Gas Reactor is its ability to release sufficient afterheat by entirely passive means that fuel will never reach a temperature where significant activity levels will be released to the environment. The MGR-GT reactor has been proven to be passively safe.

7.6.2 Moisture-Ingress Concerns.

Moisture-ingress is a problem that has plagued gas-cooled reactors. By eliminating the two principal sources of

moisture-ingress, the steam-generator and liquid-lubricated bearings and seals, the potential for moisture ingress into the MGR-GT is substantially less than that of the steam Rankine-cycle MGR. This has been made possible only through the application of advanced technology that is presently-available, such as magnetic bearings and electrical power-conversion equipment.

7.6.3 Improved Modularity and Lower Cost.

Several other modular-reactor designs have been proposed that achieve modularity in the reactor, but economics require that a large steam Rankine-cycle be served by several reactor modules. The MGR-GT is the only nuclear power system that offers modularity in a "stand-alone" package. The size of the MGR is more conveniently matched to a gas-turbine. The small size of the MGR-GT is the key to its low cost and improved modularity. Direct costs for the MGR-GT are estimated as being substantially lower than those of the steam-plant MGR; this difference should become even greater once site costs are accounted for. Due to the improved modularity of the MGR-GT, it is expected that site costs for the MGR-GT will be much less than those of the steam-plant MGR. Additionally, with the MGR-GT, generating capacity may be expended in small increments without the need for a commitment to a large steam Rankine-cycle power-system.

7.6.4 High Performance.

The MGR-GT offers very high thermal efficiencies. The high efficiencies are possible using only presently-available heat-exchanger and gas-turbine technology. It has been predicted by well established methods that the MGR-GT turbomachinery is capable of very high efficiencies. Recuperators of high effectiveness and low

pressure drop can be constructed using modern compact heat-exchanger designs similar to those currently used in industry.

7.6.5 Improved Control.

The small size of the MGR-GT enables inventory control to be employed economically. It has been determined that an inventory-control system capable of responding to most normal MGR-GT power-level changes can be utilized. For control during upset and casualty conditions, the unique electrical system of the MGR-GT creates the potential for improved methods of control. Furthermore, the inherent simplicity of the gas-turbine plant makes it more amenable to completely automated computer control.

7.6.6 Shrinking of the Safety Envelope.

Unlike any other nuclear system, the entire MGR-GT power-generating system is contained within a below-grade silo. This feature shrinks and clearly defines the nuclear-safety envelope, providing clear licensing advantages.

7.6.7 Summary and Recommendations.

This study has proven that there are no technical impediments to development of the MGR-GT. In fact, this study has concluded that all necessary technologies for the development of the MGR-GT are presently available from manufacturers of the required equipment. The economic and performance advantages of the MGR-GT are clear. Further development of the MGR-GT should continue with the objective of near-term prototype construction. Topics that should be addressed follow.

7.6.7a Areas for Future Study.

The following areas are identified as issues to be addressed with

the objective of near-term MGR-GT development in mind.

- The unique electrical system of the MGR-GT offers potential for improved methods of CCGT control. These potential control methods were identified in Chapter Six. They should be evaluated in greater detail with special emphasis on integrated-control and system-dynamics of MGR-GT power systems during various plant evolutions and casualties.
- Once these new control methods are completely evaluated, integration of these control methods into a fully-automated control system design should be performed.
- The MGR-GT design proposed in this dissertation is not intended to be an optimal design, but a self-consistent benchmark design. Additional studies should be performed to determine the optimum plant conditions for most economical operation. Some consideration should be given to the following: reactor power, plant pressure, machinery rpm, heat-exchanger surfaces, turbine-inlet temperature, and plant configuration.
- The possibility of construction of a prototype MGR-GT creates a need to evaluate the neutronic and thermal-hydraulic behavior of smaller MGR's for the purpose of determining an optimal size for this prototype.
- Since the prismatic core is capable of lower pressure drops, it may be beneficial to evaluate the use of a prismatic core in a direct-Brayton cycle by performing a comparative design study.

REFERENCES AND BIBLIOGRAPHY

A1 A.S.M.E. Boiler and Pressure Vessel Code, 1986

A2 Adams, R. G. and Boenig, F. H., "The Design of Turbomachinery for the Gas Turbine (Direct Cycle) High Temperature Gas Cooled Reactor Power Plant", ASME paper 77-GT-38.

A3 Adams R. G., Boenig, F. H. and Pfeifer, G. D., "Bearing Compartment Seal Systems for Turbomachinery in Direct-Cycle HTGR Power Plants", ASME paper 78-GT-38.

A4 "An Assessment of the Interatom/KWU Modular HTGR Concept", a study performed by Gas-Cooled Reactor Associates, Southern California Edison Company, General Electric Company, Combustion Engineering, Incorporated and Bechtel Group, Incorporated for Northeast Utilities Company, September 1985.

A5 Arthur D. Little, Inc., "The Economic Viability of the Fort St. Vrain HTGR Nuclear Power Plant", Report to Public Service Company of Colorado, September 21, 1984.

A6 Adjustable Speed Drives, Directory, Manufacturers and Applications, Electric Power Research Institute, 1985.

A7 Ainley, D.G., and Matheison, G.C.R., "A Method of Performance Estimation for Axial-Floww Turbines", R & M No. 2974, Aeron. Research Comm., 1957.

A8 Aeroquip Corporation, Aerospace Engineering Bulletin, AEB 197A.

B1 Bammert, K., A General Review of Closed-Cycle Gas Turbines Using Fossil, Nuclear and Solar Energy, Verlag Karl Thiemig, Munich, 1975.

B2 Bammmert, K., Rurik, J., and Griepentrog, H., "Highlights and Future Development of Closed-Cycle Gas Turbines", ASME paper 74-GT-7.

B3 Bammert, K., "Design of a Fossil-Fired Helium Turbine Plant for Combined Power and Heat Production", Atomkernenergie, Bd. 18, 1971, Lfg. 3.

B4 Bammert, K., "Layout and Present Status of the Closed-Cycle Helium Turbine Plant Oberhausen", ASME paper 74-GT-132.

B5 Bammert, K., "Operation and Control of the 50-MW Closed-Cycle Helium Turbine Oberhausen", ASME paper 74-GT-13.

B6 Bammert, K., "Performance of High-Temperature Reactor and Helium Turbine", Kertechnik, 11.Jahrgang (1969) No. 2.

B7 Bammert, K. and Bohm, E., "Nuclear Power Plants with High Temperature Reactor and Helium Turbine", ASME paper 69-GT-43.

B8 Bammert, K. and Rehbach, J., "Gas Turbine for a Nuclear Power Plant", Atomkernenergie, Bd. 18 (1971), Lfg. 2.

B9 Bammert, K., "Emergency Cooling System for a Nuclear Power Gas Turbine", Atomkernenergie, Bd. 18 (1971), Lfg. 2.

B10 Bammert, K., "Optimal Gas Mixture for Direct Cycle Gas Turbine"

B11 Boyce, M., Gas-Turbine Engineering Handbook, Gulf Publishing Co., Houston, 1982.

B12 Bohm, E., et. al., "The 25 MW Schleswig-Holstein Nuclear Power Plant (Geesthacht II)", Kerntechnik, 11. Jahrgang (1969) No. 2.

B13 Barrett, L. E., Gunter, E. J. and Allaire, P. E., "Optimum Bearing and Support Damping for Unbalance Response and Stability of Rotating Machinery", ASME paper 77-GT-27.

B14 Bardia, A., "Dynamics and Control Modeling of the Closed-Cycle Gas Turbine (GT-HTGR) Power Plant", Fourth Power Plant Dynamics, Control and Testing Symposium, Gatlinburg, Tennessee, March 17-19, 1980.

B15 Betts, W. S. and Blevins, R. D., "The Response of a Thermal Barrier System to Acoustic Excitation in a Gas Turbine Nuclear Reactor", ASME paper 81-GT-16.

B16 Ball, Jim, General Electric Company, telephone conversation with, July 23, 1986.

B17 Balje, O. E., Turbomachines A Guide to Design, Selection and Theory, John Wiley and Sons, 1981.

B18 Bammert, K., "The Oberhausen Heat-and-Power Station with Helium Turbine", Address on the occasion of the inauguration of the Helium Turbine Power Plant of EVO, Oberhausen-Sterkrade, December 19, 1974

B19 Bechtel Group, Inc, presentation at Modular HTGR briefing for DOE/NRC interaction plan for advanced HTGR's, June 13, 1984.

B20 Bammert, K., "Operating Experiences and Measurements on Turbo Sets of CCGT-Cogeneration Plants in Germany", ASME paper 86-GT-101.

B21 Bammert, K. and Duester, G., "Experience with Fossil Fired CCGT Power Plants and its Transfer to Nuclear, Solar and Space Applications", Keynote Address 31st Annual International Gas Turbine Conference of the American Society of Mechanical Engineers, Dusseldorf, W. Germany, June 8-12, 1986.

B22 Black, W. E. and Betts, W. S., "Vibration Damage Testing of

Thermal Barrier Fibrous Blanket Insulation", Nuclear Engineering and Design, vol. 80 (1984) no. 3, August, 1984.

B23 Barbat, V. J., et. al., "Steam-Turbine-Driven Circulators for High-Temperature Gas-Cooled Reactors Part II: Development", Transactions of the ASME, Journal of Engineering for Power, April 1974.

B24 Bohm, E., et. al., "The 25 MW Schleswig-Holstein Nuclear Power Plant (Geesthacht II)", Kerntecknik, 11, Jahrgang (1969) no.2.

B25 Bertilsson, J. E. and Scarlin, B., "Integrity of Low-Pressure Steam Turbine Rotors in Stress Corrosion Environments", Brown Boveri Review, vol. 71, March/April 1984.

B26 Bertilsson, J. E., Faber, G. and Kuhnen, G., "50 Years of Welded Turbine Rotors", Brown Boveri Review, vol. 68, December 1981.

B27 Bell. F. R. and Koutz, S. L., "Gas Turbine HTGR and the Environment", Combustion, April 1973.

B28 Bammert, K., Krapp, R. and Reiter, U., "Nonsteady Operational Behavior of Single-Shaft and Two-Shaft Closed-Cycle Gas Turbines", ASME paper submitted for presentation at the Gas Turbine Conference and Products Show, London, April 9-13, 1978.

B29 Bitsch, D., Chaboseau, J., "Power Level Control of a Closed Loop Gas Turbine, By Natural Transfer of Gas Between the Loop and Auxiliary Tanks", International Conference of the British Nuclear Energy Society, London, April 8-9, 1970.

B30 Barrett, C. R., Nix, W. D. and Tetelman, A. S., The Principles of Engineering Materials, Prentice Hall, Englewood Cliffs, New Jersey, 1973.

B31 Bellis, E. A. and Inamati, S. B., "Safety Characteristics of the Modular High Temperature Gas-Cooled Reactor", ANS/ENS Conference on Thermal Reactor Safety, San Diego, February 2-6, 1986.

B32 Baumeister, T., Ed., Marks' Standard Handbook for Mechanical Engineers, Eighth Edition, McGraw-Hill, New York, 1978.

C1 Chan T., Openshaw. F. and Pfremmer D., "HTGR-GT and Electrical Load Integrated Control", ASME paper 80-WA/DSC-25.

C2 Cadwallader, G. J. and Deremer, R. K., "HTGR-GT Primary Coolant Transient Resulting from Postulated Turbine Deblading", ASME paper 81-GT-19.

C3 Calhoun, J. R., "Licencing History and Regulatory Requirements for the Turbine Generator of Bellefonte Nuclear Power Plant", American Power Conference, Chicago, April 21-23, 1980.

C4 Charmichael, A. D., notes from course 2.601J, "Thermal Power Systems", Massachusetts Institute of Technology, Spring 1986.

C5 Cook, Jack, Combustion Engineering, telephone conversation with, November 5, 1986.

C6 Craig, H.R.M., and Cox, H.J.A., "Performance Estimation of Axial Flow Turbines", Inst. Mech. Eng. Vol. 185 32/71, 1971.

C7 Crane Valve Company, "Flow of Fluids through Valves, Fittings, and Pipe", Crane Industrial Products Group, Chicago, 1957.

C8 Coxe, R.L., "Modular Gas Reactor Cost Estimation", MIT-NPI-TR-002, April 1985.

D1 Deremer, R. K., "Gas Turbine HTGR Power Plant 1978 Utility Program Report on Safety and Availability Studies", GA-A15416, June 1979.

D2 Dixon, S. L., Fluid Mechanics Thermodynamics of Turbomachinery, Pergamon Press, Oxford, 1975.

D3 Duester, G. and Zenker, P., "Operating Experience of the Oberhausen Helium Turbine Plant", 25th International Gas Turbine Conference, New Orleans, March 9-13, 1980.

D4 Dean, J. R., "Prospective Studies of HTR Gas Turbine Plant Performance", Dragon Project Technical Note, DPTN/462, July 3, 1973.

D5 Dean, R. A., "The Modular High-Temperature Gas-Cooled Reactor (MHTGR) An Opportunity For Cooperative International Energy Development", GA Technologies, February 1986.

D6 Den Hartog, J.P., Mechanical Vibrations, fourth ed. McGraw-Hill, New York, 1956.

E1 "Evaluation of Small Modular High Temperature Gas-cooled Reactors Applied to Electricity Generation", a report by Bechtel Group, Inc., Gas-Cooled Reactor Associates, GA Technologies and Hochtemperatur-Reakturbau GMBH for the Pacific Gas and Electric Company, GCRA-84-002, May 1984.

E2 EPRI report EL-3359, vol. 2 April 1984

F1 Finnie, I. and Heller, W., Creep of Engineering Materials, McGraw-Hill, New York, 1959

F2 Fenech, H., ed., Heat Transfer and Fluid Flow in Nuclear Systems, Pergamon Press, New York, 1981.

F3 Fortescue, P., "Tomorrow's Plant: Gas Turbines, Nuclear Power, Dry Cooling", Power Engineering, August 1971.

F4 Fortescue, P., "Gas Turbines and Nuclear Power", Combustion, December 1972.

F5 Frewer, H. and Keller, W., "The Modular High Temperature Reactor", Nuclear Science and Engineering, vol. 90, pp. 411-426, 1985.

F6 Frutschi, H. U., "Ensuring Stable Circuit Conditions of Direct Cycle Helium Gas Turbine System", ASME Journal of Engineering for Power, October 1974.

F7 Fraser, W. M., "A Review of Submerged Gas Circulators as Applied to Advanced Gas Cooled Reactors", Nuclear Energy, vol. 24, no. 5, 1985.

F8 Ferraro, R. J., "Advanced Power Electronic Systems for Fuel Cells, Battery Storage, and Adjustable Speed Drives (ASDs)", Overview Report based on EPRI project 1464-1 on work accomplished by United Technologies Corporation, April 1985.

F9 Fox, R.W., McDonald, A.T., Introduction to Fluid Mechanics, John Wiley and Sons, New York, 1973.

F10 Fitzgerald, A.E., Kingsley, C., Kusko, A., Electric Machinery, third edition, McGraw-Hill, New York, 1971.

G1 Gulf General Atomic, "Nuclear Gas Turbine Power Plant Preliminary Development Plan", Gulf-GA-A12161, January 1973.

G2 Gulf General Atomic, "State of the Art of HTGR Gas Turbine Technology", Gulf-GA-A12098, June 1973.

G3 Gulf General Atomic, "HTGR Gas Turbine Power Plant Control, Safety, and Maintenance Studies Phase II", Gulf-GA-A12700, August 1973.

G4 General Atomic Company, "HTGR Gas Turbine Power Plant Control and Safety Studies", GA-A12799, October 1973.

G5 General Atomic Company, "HTGR Gas Turbine Power Plant Control and Safety Studies", GA-A12865, February 1974.

G6 Gas-Cooled Reactor Associates, High Temperature Gas-Cooled Reactor Gas Turbine Application Study, December 1980.

G7 General Electric Co., GTO Induction Motor Drive, GEA-11280A.

G8 General Electric Co., Solid State Frequency Converter, GEA-11469.

G9 General Electric Co., Load Commutated Inverter, GEA:10816A.

G10 General Electric Co., Planning for Power Plant Auxiliaries, GEA 9301B, 1979.

G11 Gutzwiller, R. A. and Bitto, G. G., "Load Commutated Inverter Drives Reliability Alternatives". General Electric Co., Drive Systems Dept., Salem, VA.

G12 General Electric Co., Adjustable Speed Drive Systems, GEK-95469.

H1 Horlock, J. H., Axial Flow Compressors, Butterworths Scientific Publications, London, 1958.

H2 Haberman, H. and Brunet, M., "The Active Magnetic Bearing Enables Optimum Damping of Flexible Rotor", ASME paper 84-GT-117.

H3 Haberman, H. and Brunet, M., "The Active Magnetic Bearing Enables Optimum Control of Machine Vibrations", ASME paper 85-GT-221.

H4 Humphris, R. R., "State-of-the-Art of Magnetic Bearings in Rotor Systems", University of Virginia report no. UVA/643092/MAE84/316, July 1984.

H5 Haselbacher, H. and Eirmann, A., "Development of Helium Gas Turbine Systems in the Nuclear Field", ASME paper 74-GT-123.

H6 Holman, J. P., Heat Transfer, McGraw Hill, New York, 1976.

H7 Hosegood, S., Lockett, G. and McIver, R., "Dragon Project Engineering Studies on the Direct Cycle HTR", Dragon Project Report 711, February 1970.

H8 Hohn, A. and Rieder, A., "BBC Solution for Low-Pressure Rotors Endangered by Stress Corrosion Cracking", Brown Boveri Review, vol. 71, March/April 1984.

H9 Hickok, H. N., Leonardi, D. W. and Gutzwiller, R. A., "Gearless Adjustable High-Speed Motor Drives for Application through 60,000 HP", General Electric Co.

H10 Hannaman, G. W., Orvis, D. D. and Scarborough, J. C., "Modular Gas Reactor-Brayton Cycle Conceptual Safety Assesment", prepared for Japan Atomic Energy Research Institute by NUS Corporation, NUS-4960, November 15, 1986.

H11 Horlock, J.H., Axial Flow Turbines, Butterworths Scientific Publications, London, 1966.

I1 Izenson, M. G., Lanning, D. D., Lidsky, L. M. and Maneke, J. L., "Identification of the Safety Requirements of a New Reactor Concept: The MHTGR as an Example", MIT Nuclear Power Plant Inovation Report MIT-NPI-TR-006, 1985.

I2 Ingersoll-Rand, "I-R Now Offers Large Rotating Equipment with Revolutionary Friction-free Bearings", The Turbo Report, no. 17, January 1985.

I3 Izenson, M. G., "Effects of Fuel Particle and Reactor Core Design on Modular HTGR Source Terms", MITNPI-TR-012, October 1986.

J1 Johnson, B. M., et. al., "The Development of an Advanced Concept of Dry/Wet Cooling for Power Plants", Proceedings of the American Power Conference, vol. 43, 1981.

J2 Jakobeit, W., Pfeifer, J. and Ullrich, G., "Evaluation of High-Temperature Alloys for Helium Gas Turbines", Nuclear Technology, July, 1984.

K1 Kaburaki, H. and Lidsky, L. M., Studies of the Modular High Temperature Gas Cooled Reactor Closed Cycle Gas Turbine at the Massachusetts Institute of Technology, unpublished, 1986.

K2 Kretzinger, K., Valentino, S. and Parker, K., "Gas Turbine Regenerators", Garrett AiResearch Manufacturing Company of California technical paper 85-22130, Rev. 5, January 1985.

K3 Kacker, S. C. and Okapuu, U., "A Mean Line Prediction Method for Axial Turbine Efficiency", ASME paper 81-GT-58.

K4 Kammerzell, L. L. and Read, J. W., "HTGR-GT Systems Optimization Studies", ASME paper 80-WA/GT-3.

K5 Kosten, G. J., et. al., "Operating Experience and Performance Testing of the World's Largest Air-Cooled Condenser", Proceedings of the American Power Conference, vol. 43, 1981.

K6 Kusko, Alexander, Alexander Kusko Incorporated, telephone conversation with, June 19, 1986.

K7 Krey, G., "Bypass Control of Closed-Cycle Gas Turbines", ASME paper 78-GT-70.

K8 Kohl, W. and Brandes, S., "HTR 100 is a versatile cogeneration plant", Modern Power Systems, June 1986.

K9 Kesavan, K., et. al., "Gas Cooled Reactors for Advanced Terrestrial Applications", 21st Intersociety Energy Conversion Engineering Conference, San Diego, California, August 25-29, 1986.

K10 Katterhenry, A. A., "Gas-Turbine Nuclear Power Plants", Reactor Technology, vol. 13, no. 1, Winter 1969-1970.

K11 Kramer, H., "GCR-AGR-HTGR-development of the gas-cooled reactor concept", Kerntechnik, 14, Jahrgang (1972) no.10.

K12 Keller, C. and Schmidt, D., "Industrial Closed Cycle Gas Turbines for Conventional and Nuclear Fuels", ASME paper 67-GT-10.

K13 Keller, C., "The Origin and Development of the Closed Cycle Gas Turbine System", Escher Wyss News, vol. 39, 1966, no. 1.

K14 Keller, C., "The Use of the Closed Cycle Helium Gas Turbine in Atomic Power Plants", Escher Wyss News, vol. 39, 1966, no. 1.

K15 Kays, W. M., London, A. L., Compact Heat Exchangers, 3rd edition, McGraw Hill, New York, 1984.

K16 Keller, C and Schmidt, D., "The Helium Gas Turbine for Nuclear Power Plants", ASME paper 67-GT-10.

K17 Korakianitis, T. P., "Introduction of a Low-Pressure-Ratio, Highly-Regenerative, Advanced Brayton-Cycle Engine for Marine Propulsion and Problems of Its Integration in the Fishing Industry", MS Thesis, Department of Mechanical Engineering, Massachusetts Institute of Technology, 1985.

K18 Koch, C.C., Smith, L.H., "Loss Sources and Magnitudes in Axial-Flow Compressors", ASME paper 75-WA/GT-6.

L1 Lightner, S. and Betts, W., "The Venting Characteristics of a Fibrous Thermal Barrier System During a Rapid Depressurization Accident (Rotor Failure) in an HTGR-GT", ASME paper 81-GT-14.

L2 Lidsky, L. M., "The Reactor of the Future?", Technology Review, February/March 1984.

L3 Lester, R. K., Driscoll, M. J., Golay, M. W., Lanning, D. D. and Lidsky, L. M., "National Strategies for Nuclear Power Development", MITNPI-PA-002, March 1985.

L4 Lockett, G. and Huddle, R., "The HTR Direct Cycle: Engineering Possibilities and Material Requirements", Dragon Project Report 719 part 2, May 1970.

L5 Lieblein, S., "Loss and Stall Analysis of Compressor Cascades", ASME Trans., J. of Basic Eng., September, 1959.

M1 McDonald, C. F., "The Closed-Cycle Turbine - Present and Future Prospectives for Fossil and Nuclear Heat Sources", A.S.M.E. paper 78-GT-102.

M2 McDonald, C. F., "Turbomachinery Design Considerations for the Nuclear HTGR-GT Power Plant", A.S.M.E. transactions, Journal of Engineering for Power, vol. 103, January 1981. .

M3 Maneke, J. L., "Radiation Releases from MHTGR Confinement Buildings", Ph.D. thesis, Massachusetts Institute of Technology, 1986.

M4 McDonald, C. F. and Paget, J. A., "Maintenance Considerations in the Design of the Direct-Cycle Nuclear Gas Turbine Power Plant", ASME paper 79-GT-116.

M5 McDonald, C. F., Bass, J. C. and Amtmann, H. H., "Primary System Design Studies for Advanced Direct Cycle Nuclear Gas Turbine Plant", ASME paper 77-GT-25.

M6 McDonald, C. F., Vepa, K., "Ammonia Turbomachinery Design Considerations for the Direct Cycle Nuclear Gas Turbine Waste Heat Power Plant", ASME paper 77-GT-75.

M7 Montakhab, A., "Preliminary Design of Dry Cooling Tower for the Closed Cycle Gas Turbine HTGR", ASME paper 81-GT-20.

M8 McDonald, Colin F., GA Technologies, telephone conversation with, June 1986.

M9 McDonald, John, Garrett AiResearch Manufacturing Company, personal conversation with, June 1986.

M10 McDonald, C. F., "The Role of the Recuperator in High Performance Gas Turbine Applications", ASME paper 78-GT-46.

M11 McDonald, C. F., "Heat Exchanger Design Considerations for High-Temperature Gas-Cooled Reactor (HTGR) Plants", presented by the Heat Transfer division of the ASME for presentation at the Joint ASME/AIChE National Heat Transfer Conference, Orlando, Florida, July 27-30, 1980.

M12 Melese, G. and Katz, R., Thermal and Flow Design of Helium-Cooled Reactors, American Nuclear Society, La Grange Park, Illinois, 1984.

M13 McDonald, C. F., "Primary System Design Studies for Advanced Direct Cycle Nuclear Gas Turbine Plant", ASME paper 77-GT-25.

M14 Mock, E. A., "Closed Cycle Gas Turbine Optimization - Procedures and Examples", Lecture notes for Von Karman Institute for Fluid Dynamics lecture series "Closed-Cycle Gas Turbines", Brussels, Belgium, May 9-13, 1977.

M15 McDonald, C. F., Goodjohn, A. J. and Silady, F. A., "Small Passively Safe Modular Gas-Cooled Nuclear Power Plant with Pebble-Bed Reactor", GA Technologies Report GA-A17552, June 1984.

M16 Mohr, W. P., et. al., "Inservice Inspection of Turbine Rotors", American Power Conference, Chicago, April 21-23, 1980.

M17 McDonald, C. F., GA Technologies, personal conversation with, August 26, 1986.

M18 McDonald, John, Garrett AiResearch Manufacturing Company, personal conversation with, August 27, 1986.

M19 McDonald, C. F., Bass, J. C. and Amtmann, H. H., "Primary System Design Studies for Advanced Direct Cycle Nuclear Gas

Turbine Plant", ASME paper 77-GT-25.

M20 Marnet, C., Kruger, K. J. and Ziermann, E., "Operational Experience with the AVR Reactor", Gas Cooled Reactors Today, BNES, London, 1982.

M21 McDonald, C. F., "Exploitation of the Very High Temperature Capability of the MHTGR to Meet National Energy Needs After the Year 2000", GA-A18416, 21st IECEC Conference, San Diego, August 25-29, 1986.

M22 Mueller, Ralph, Huntington Alloys, telephone conversation with, August 18, 1986.

M23 Moltgen, G., Converter Engineering - An Introduction to Operation and Theory, Siemens Aktiengesellschaft, John Wiley and Sons, Berlin, 1984.

M24 McDonald, John, AiResearch Manufacturing Company, personal conversation with, January 29, 1987.

M25 Mellor, G.L., "The NACA 65-Series Cascade Data", Gas Turbine Laboratory Charts, MIT, Cambridge, Massachusetts, 1956.

M26 Magnetic Bearings, Incorporated, "The Active Advantage! A High Technology Answer for the Advanced Bearing Application", Magnetic Bearings, Inc., Radford, Virginia.

M27 Maneke, J., GA Technologies, conversation with, November, 1986.

M28 Moody, L.F., "Friction Factors for Pipe Flow", Trans. ASME, 66, 8, 1944.

M29 McDonald, C.F., "Performance Potential of a Future Advanced Nuclear Gas Turbine Concept", GA Technologies technical paper GA-A18576, December 1986.

M30 McDonald, C.F., GA Technologies, telephone conversation with, April 24, 1987.

N1 Nickel H. and Schubert, F., "Status of Structural Design Code for Metallic High-Temperature Gas-Cooled Reactor Components", Nuclear Technology, September 1984.

N2 Northeast Cryogenics, Inc., quotation on price of helium for industrial users, October 17, 1986.

N3 Nelson W.L., "Nelson Cost Index", Oil and Gas Journal, p. 95, March 3, 1986.

N4 Nelson, W.L., "Index Price Bases Explained", Oil and Gas Journal, pp. 59-60, December 13, 1976.

O1 O'Reilly, W. J., "A High-Effectiveness Regenerator Design

Concept", ASME paper 78-GT-78.

O2 Openshaw, F. L. and Chan, T. W., "Operational, Control and Protective System Transient Analyses of the Closed-Cycle GT-HTGR Power Plant", ASME paper 80-WA/GT-1.

O3 Openshaw, F. L., Estrine, E. and Croft, M., "Control of a Gas Turbine HTGR", ASME paper 76-GT-97.

O4 O'Keefe, W., "Developments in active magnetic bearings offer new choices for rotating equipment", Power, May 1979.

P1 Parker, K. O. and Coombs, M. G., "New Developments in Compact Heat Exchangers", Garrett AiResearch Manufacturing Company Technical Paper 79-15783, Rev. 1, July 1980.

P2 Parker, K. O., "Selection of a High-Efficiency Regenerator for Pipeline Gas Turbines", ASME paper 77-GT-39.

P3 Parker, K. O., Kindlimann, L., Coombs, M. and Kotchick, D., "Materials for High-Temperature Heat Exchangers", Garrett AiResearch Manufacturing Company of California for DARPA Workshop on High Temperature Materials for Advanced Military Engines", 79-15936 April 1979.

P4 Proto-Power Corporation, "Demonstration Testing of Compo s for Electric-Driven HTGR Helium Circulator Applications with Magnetic Bearings", RP2079-12, preliminary report prepared for Electric Power Research Institute, February 1986.

P5 Parker, Ken, Garrett AiResearch Manufacturing Company, telephone conversation with, June 1986.

P6 Page, R. and Read, D., "High Temperature Gas Cooled Reactor Development Outside the United States - A Consultants View" Combustion, June 1973.

P7 Penkalla, H., Over, H., and Schubert, F., "Constitutive Equations of Creep and Creep Rupture Behavior of Metallic Materials at Temperatures Above 800 C", Nuclear Technology, September 1984.

P8 Popp, G., Gruber, U., Boder, H., and Janssen, K., "Graphite and Carbon/Carbon Components for Hot Gas Ducts", IAEA International Working Group on Gas-Cooled Reactors, Specialists' Meeting on Heat Exchanging Components of Gas-Cooled Reactors, Dusseldorf, W. Germany, April 16-19, 1984.

P9 Parker, K., AiResearch Manufacturing Company, personal conversation with, January 29, 1987.

P10 Parker, K., AiResearch Manufacturing Company, telephone conversation with, March 20, 1987.

R1 Rohsenow, W. M., Choi, H. Y., Heat, Mass and Momentum Transfer, Prentice Hall, Englewood Cliffs, New Jersey, 1961.

R2 Rohsenow, W. M., "Heat Exchangers - Basic Methods", from Heat Exchangers Thermal-Hydraulic Fundamentals and Design, McGraw Hill, 1981.

R3 Roberts, Dave, GA Technologies, telephone conversation with, June 27, 1986.

R4 Raymond, Bob, Combustion Engineering, telephone conversation with, November 3, 1986.

R5 Reutler, H. and Lohnert, G. H., "Advantages of Going Modular in HTR's", Nuclear Engineering and Design, vol. 78, no. 2, April 1984.

R6 Roelke, R.J., 1973, Miscellaneous losses. In Turbine Design and Application, Vol. 2. Ed. by Glassman, A., SP-290. NASA. Washington, D.C., pp. 127-128.

R7 Reynolds, W.C., Thermodynamic Properties in SI, Department of Mechanical Engineering, Stanford University, Stanford, California, 1979.

R8 Raymond, Bob, Combustion Engineering Corporation, telephone conversation with, March 20, 1987.

S1 Schubert, F., et. al., "Creep Rupture Behavior of Candidate Materials for Nuclear Process Heat Applications", Nuclear Technology, August 1984.

S2 Snow, A. and Jakub, M., "Developments in Elevated Temperature Structural Design Criteria", Pressure Vessels and Piping: Design Technology - 1982 - A Decade of Progress, American Society of Mechanical Engineers, New York, 1982.

S3 Scarborough, J. C., Driscoll, M. J., Schwoerer, F., Shin, J. I. and Wolf, L., "Gas Turbine HTGR A Technology Assessment", work performed by NUS Corporation under EPRI contract no. RP900-2 GT-HTGR, NUS-3041, 1977.

S4 Schuster, J. R., Vrable D. L. and Huntsinger, J. P., "Binary Plant Cycle Studies for the Gas Turbine HTGR", ASME paper 76-GT-39.

S5 Schoene, T. W., "The HTGR Gas Turbine Plant with Dry Air Cooling", Nuclear Engineering and Design, vol. 26 (1974) 170-178.

S6 Sanchez, R. G., "Passive After Heat Removal: Sensitivity Study for Modular Pebble Bed Reactors", S.M. Thesis, Massachusetts Institute of Technology, January 1988.

S7 Soland, J. G., Mack, W. M. and Rohsenow, W. M., "Performance

Ranking of Plate-Finned Heat Exchanger Surfaces", ASME Journal of Heat Transfer, 100:3, pp 514-519, August 1978.

S8 Sawyer's Gas Turbine Engineering Handbook, Turbomachinery International Publications, Norwalk, Connecticutt, 1985.

S9 South of Scotland Electricity Board, "The AGR", presented at the 1984 GCRA annual conference, San Diego, California.

S10 Sayers, J. E., "Howden in the Nuclear Power Station Industry", Howden Journal, no. 18, October 1980.

S11 Schmidt, D., "Steam and Gas Turbine Systems-Increase of Capacity and Product Improvement", Kerntechnik 14, Jahrgang (1972) no. 10.

S12 Sarlos, G., et. al., "A Study of a High Temperature Nuclear Power Plant Incorporating a Non-Integrated Indirect Cycle Gas Turbine", ASME paper 82-GT-39.

S13 Schoene, T. W., "Bray: A Simple Computer Code for Gas Turbine Cycle Analysis", General Atomic Report GA-D12884, March 15, 1974.

S14 Scarborough, J. C., JCS Limited , correspondence with, July 1986.

S15 Shigley, J.E., Dynamic Analysis of Machines, McGraw-Hill, New York, 1961.

S16 Shigley, J.E., Mechanical Engineering Design, McGraw-Hill, New York.

S17 Saker, Richard, Toshiba International Corporation, correspondance with, January 1987.

S18 Smith, R.J., Circuits, Devices, and Systems, third edition, John Wiley and Sons, Inc., New York, 1976.

S19 Shapiro, A.H., The Dynamics and Thermodynamics of Compressible Fluid Flow, John Wiley and Sons, New York, 1953.

S20 Saker, Richard, Toshiba Corporation, personal conversation with, March 19, 1987.

T1 Thermophysical Properties of Matter, vol. 1, Thermal Conductivity, IFI Plenum Data Corporation, New York, 1970.

T2 Tanaka, H., Shizunori, M. Namiki, M., and Hirata, A., "Super Motor Drive System - Super-Highspeed, Variable-Speed Motor Drive System - ", Toshiba Review, no. 146, Winter 1983.

T3 Toshiba Corporation, "Toshiba AC Variable-Speed Drive System - MF Pack - High-Power High-Performance Load Commutated Inverter", KSP-E1416, 1985-5(2).

T4 Toshiba Corporation, "Tosmatic Prosec Series PC200", KSP-E1467, 1985-7(2).

T5 Tanaka, H., Toshiba Corporation, correspondence with, High-speed, helium-cooled electrical generator design courtesy of Toshiba Corporation, March 9, 1987. Original Toshiba design was for 8,000-rpm. 10,000-rpm design is currently being evaluated.

U1 Urano, A. S. and Appiarius, J. C., "System Benefits and Considerations When Using AC Adjustable Frequency Drives in Generating Stations", presented at the American Power Conference, Chicago, April 27-29, 1981.

V1 Valentino, S. J., "Designing Reliability into High-Effectiveness Industrial Gas Turbine Regenerators", ASME paper 79-GT-199.

V2 Van Hagen, T. H., McDonald, C. F. and Creek, R. B., "Heat Exchanger Designs for Gas Turbine HTGR Power Plant", ASME paper 79-WA/GT-2.

V3 Verfondern, K., "Experimentelle Uberprufung des Thermohydraulik-Programms THERMIX und rechnerische Analyse der transienten Temperatur- und Stromungsfelder im Corebereich des THTR Reaktors nach Ausfall der NWA", Kerforschungsanlage Julich GmbH, Institut fur Reaktorentwicklung, Interner Bericht KFA-IRE-IB-13/78, Oktober 1978.

W1 Wilson, D. G., The Design of High Efficiency Turbomachinery and Gas Turbines, .MIT Press, Cambridge, Massachusetts, 1984.

W2 Weise, D., "Active Magnetic Bearings Provide Closed Loop Servo Control for Enhanced Dynamic Response", Magnetic Bearings, Inc., Radford, Virginia.

W3 Wade, C. A., General Electric Co., Manager, AC Drives Sales and Application Engineering, correspondence with, October 1986.

W4 Wu, T., Cowan, C.L., "Core Heatup Analysis of a Small Pebble-Bed HTGR", ANS Trans., vol. 50, November 1985.

W5 Wood, Daniel, Aeroquip Corporation/Aerospace Division, telephone conversation with, September 1986.

W6 Wilson, D.G., Dunteman, N.R., "The Inverted Brayton Cycle for Waste-Heat Utilization", ASME paper 73-GT-90.

Y1 Yampolsky, J., et. al., "Steam Turbine Driven Circulators for High-Temperature Gas-Cooled Reactors Part I: Design", Transactions of the ASME, Journal of Engineering for Power, April 1974.

Z1 Zenker, P., "The Oberhausen 50MW Helium Turbine Plant", Combustion, April 1976.

Z2 Zenker, P., "Operating Experience with the Oberhausen Helium Turbine Plant", 24th International Gas Turbine Conference, San Diego, California, March 11-15, 1979.

Z3 Zenker, P., "Past Experience and future Prospects of Closed Cycle Gas Turbines", 27th International Gas Turbine Conference, London, April 18-22, 1982.

Z4 Zollinger, E. and Gregory, N., "Optimization Analysis of a CCGT Nuclear Power Plant with Application to the HHt 3000 MWth Commercial Plant (HHT-Project)", ASME paper.

APPENDIX A

THE "CYCLE" AND "INTCLD" PROGRAMS

CYCLE and INTCLD are two of several small programs that were written to aid in the design process. All of the mathematical background for the calculations performed by the programs is covered in Chapter Two. The programs calculate efficiencies for each pressure ratio and select the pressure ratio for highest efficiency as optimum. CYCLE then calculates cycle parameters for the optimum efficiency.

The programs are written in BASIC and all calculations in the present work were performed on a personal computer. The program asks the user for all input. No additional data files are needed. All output is sent to a line printer. Program listings and sample results follow.

Table A.1.
Listing of the CYCLE program

```
10 DIM E(100)
20 LET EM=0
30 LET E(RT)=0
40 PRINT "Direct Cycle Gas Turbine Efficiency Calculation "
44 PRINT "What is reactor power (MWth)?"
45 INPUT QRX
50 PRINT "Turbine Inlet Temp. (deg C)?"
60 INPUT T4
70 PRINT "turbine inlet pressure (MPa)?"
80 INPUT P4
90 PRINT "what is compressor inlet temp.(deg C)?"
100 INPUT TC
110 LET TR=(T4+273)/(TC+273)
120 PRINT "What are specific pressure losses?(Rx,Reg.hot,Reg.cold,Precooler)"
130 INPUT PRX,PRH,PRC,PPC
140 LET P=PRX+PRH+PRC+PPC
150 PRINT "What is the maximum total pressure ratio that you want calculated?"
160 INPUT RH
170 PRINT "what is the compressor polytropic efficiency?"
180 INPUT NPC
190 PRINT "What is the turbine polytropic efficiency?"
200 INPUT NPT
210 PRINT "What is the regenerator effectiveness?"
220 INPUT ER
230 LET R=2077
240 LET CP=5194
250 LPRINT "XXXXXXXXXXXXXXX DCGT MHTGR CALCULATION RESULTS XXXXXXXXXXXXXXXXX"
260 LPRINT
270 LPRINT
280 LPRINT "Turbine inlet temp=";T4
290 LPRINT "regenerator effectiveness=";ER
300 LPRINT "compr. poly. eff.=";NPC,"turb. poly. eff.=";NPT
310 LPRINT "specific pressure losses:"
320 LPRINT "       reactor=";PRX
330 LPRINT " regen. cold =";PRC
340 LPRINT " regen. hot  =";PRH
350 LPRINT "precooler    =";PPC
360 LPRINT "     total   =";P
370 LPRINT
380 LPRINT
390 LPRINT "rt","efficiency"
400 LPRINT
410 LPRINT
420 FOR RT=1 TO RH STEP .05
430 LET E1=1-(RT*(1-P))^(-R*NPT/CP)
440 LET C=RT^(R/(CP*NPC))-1
450 LET E(RT)=(E1*TR-C)/(TR*(1-ER*(1-E1))-(1+C)*(1-ER))
460 LPRINT RT,E(RT)
470 IF E(RT)<0 THEN 520
480 IF E(RT)>1 THEN 520
490 IF E(RT)<EM THEN 520
500 LET RMT=RT
510 LET EM=E(RT)
520 NEXT RT
530 LPRINT
540 LPRINT
550 LPRINT
560 LPRINT "optimum pressure ratio is=";RMT
570 LPRINT "efficiency at optimum pressure ratio =";EM
580 LET T4=T4+273
```

```
590 LET T5=T4*(RMT*(1-P))^(-R*NPT/CP)
600 LET T1=TC+273
610 LET T2=T1*(RMT^(R/(CP*NPC)))
620 LET T3=T2+ER*(T5-T2)
630 LET T6=T5-ER*(T5-T2)
640 LET P5=P4/((1-P)*RMT)
650 LET P6=P5*(1-PRH)
660 LET P1=P6*(1-PPC)
670 LET P2=RMT*P1
680 LET P3=P2*(1-PRC)
690 LPRINT "station","temp (c)","press (MPa)"
700 LPRINT "comp in:",T1-273,P1
710 LPRINT "comp out:",T2-273,P2
720 LPRINT "react in:",T3-273,P3
730 LPRINT "turb in:",T4-273,P4
740 LPRINT "turb exh:",T5-273,P5
750 LPRINT "regen out:",T6-273,P6
752 LET MH=QRX*10^6/(CP*(T4-T3))
753 LPRINT "helium mass flow=";MH;"kg/s"
754 LPRINT "net power output=";EM*QRX;"MWe"
755 LPRINT "reactor power=";QRX;"MWth"
850 LPRINT
860 LPRINT
870 LPRINT
880 LPRINT
890 LPRINT "XXXXXXXXXXXXXXXXXXXXXXXXXXXXXXXXXXXXXXXXXXXXXXXXXXXXXXXXXXXXXXXXXXXXXXX"
900 LPRINT
910 LPRINT
920 LPRINT
930 LPRINT
940 LPRINT
950 LPRINT
960 END
```

Table A.2.
Output of the CYCLE program

```
XXXXXXXXXXXXXXX DCGT MHTGR CALCULATION RESULTS XXXXXXXXXXXXXXXXX

Turbine inlet temp= 850
regenerator effectiveness= .95
compr. poly. eff.= .89      turb. poly. eff.= .91
specific pressure losses:
      reactor= .025
 regen. cold = .015
 regen. hot  = .03
precooler    = .005
     total   = .075

rt            efficiency

 1            -3.137344
 1.05         -.6386891
 1.1          -.131564
 1.15          8.370786E-02
 1.2           .2011169
 1.25          .273962
 1.3           .3228157
 1.35          .3572935
 1.4           .3824958
 1.45          .4013745
 1.5           .4157577
 1.55          .4268367
 1.599999      .4354207
 1.649999      .4420794
 1.699999      .4472236
 1.749999      .4511576
 1.799999      .4541119
 1.849999      .4562637
 1.899999      .4577512
 1.949999      .4586844
 1.999999      .4591505
 2.049999      .4592211
 2.099999      .4589546
 2.149999      .4583997
 2.199999      .457595
 2.249999      .4565756
 2.299999      .4553692
 2.349999      .4539998
 2.399999      .4524883
 2.449999      .4508519
 2.499999      .4491064


optimum pressure ratio is= 2.049999
efficiency at optimum pressure ratio = .4592211
station       temp (C)       press (MPa)
comp in:       30             3.970033
comp out:      145.3272       8.138563
react in:      593.1537       8.016483
turb in:       850            7.8
turb exh:      616.7235       4.113384
regen out:     168.8971       3.989982
```

helium mass flow= 149.9183 kg/s
net power output= 91.84422 MWe
reactor power= 200 MWth

XXXXXXXXXXXXXXXXXXXXXXXXXXXXXXXXXXXXXXXXXXXXXXXXXXXXXXXXXXXXXXXXXXXXXXX

Table A.3.
Listing of the INTCLD program

```
5 DIM E(100)
6 LET EM=0
7 LET E(R1)=0
10 PRINT "Direct Cycle Gas Turbine w/ Intercooling Efficiency"
20 PRINT "Turbine inlet temp.(deg.C)?"
30 INPUT T6
40 PRINT "What is compressor inlet temp.(deg.C)?"
50 INPUT TC
60 LET T1=(T6+273)/(TC+273)
70 PRINT "What is specific pressure loss?"
80 INPUT P
90 PRINT "What is highest pressure ratio of a single compressor";
100 PRINT "that you want calculated?"
110 INPUT RH
120 PRINT "What are compressor poly. efficiencies (first,second)?"
130 INPUT NPC1,NPC2
140 PRINT "What is turbine poly. efficiency?"
150 INPUT NPT
160 PRINT "What is recuperator effectiveness?"
170 INPUT ER
180 PRINT "Is working fluid helium (y/n)?"
210 INPUT W$
220 IF W$="y" THEN 260
230 PRINT "Input gas const. and heat cap. in J/kgK.(R,Cp)"
240 INPUT R,CP
250 GOTO 280
260 LET R=2077
270 LET CP=5194
275 LPRINT "DCGT WITH INTERCOOLING EFFICIENCY CALCULATION RESULTS"
276 LPRINT
277 LPRINT
280 LPRINT "Turbine inlet temp.=";T6
281 LPRINT "recuperator effectiveness =";ER
282 LPRINT "poly. eff.: c1=";NPC1;", c2=";NPC2;", turb.=";NPT
283 LPRINT "specific pressure loss is =";P
290 LPRINT "r1=pressure ratio of first compressor"
291 LPRINT "r2=pressure ratio of second compressor"
292 LPRINT "rt=total pressure ratio"
300 LPRINT
301 LPRINT
302 LPRINT "r1","r2","rt","efficiency"
303 LPRINT
304 LPRINT
310 FOR R1=1 TO RH STEP .05
315 LET R2=R1
316 RT=R1*R2
320 LET E1=1-(R1*R2*(1-P))^(-R*NPT/CP)
330 LET C1=R1^(R/(CP*NPC1))-1
340 LET C2=R2^(R/(CP*NPC2))-1
350 LET E(R1)=(E1*T1-C1-C2)/(T1*(1-ER*(1-E1))-(1+C2)*(1-ER))
360 LPRINT R1,R2,RT,E(R1)
370 IF E(R1)<EM THEN 420
380 LET EM=E(R1)
390 LET RM1=R1
400 LET RM2=R2
410 LET RMT=RT
420 NEXT R1
430 LPRINT
440 LPRINT
450 LPRINT
460 LPRINT "optimum pressure ratio is: r1=";RM1;", r2=";RM2;", rt=";RMT
470 LPRINT "efficiency at optimum pressure ratio is=";EM
480 LPRINT
490 LPRINT
500 LPRINT
510 END
```

Table A.4.
Output of the INTCLD program

DCGT WITH INTERCOOLING EFFICIENCY CALCULATION RESULTS

Turbine inlet temo.= 850
recuperator effectiveness = .9
poly. eff.: c1= .9 , c2= .9 , turb.= .9
specific pressure loss is = .05
r1=pressure ratio of first compressor
r2=pressure ratio of second compressor
rt=total pressure ratio

r1	r2	rt	efficiency
1	1	1	-.331229
1.05	1.05	1.1025	.0537783
1.1	1.1	1.21	.220631
1.15	1.15	1.3225	.311288
1.2	1.2	1.44	.366553
1.25	1.25	1.5625	.402548
1.3	1.3	1.69	.426921
1.35	1.35	1.8225	.443765
1.4	1.4	1.96	.455467
1.45	1.45	2.1025	.463513
1.5	1.5	2.25	.468875
1.55	1.55	2.4025	.472216
1.6	1.6	2.56	.474001
1.65	1.65	2.7225	.474568
1.7	1.7	2.89	.474168
1.75	1.75	3.0625	.47299
1.8	1.8	3.24	.471179
1.85	1.85	3.4225	.46885
1.9	1.9	3.61	.466091
1.95	1.95	3.8025	.462976
2	2	4	.459562
2.05	2.05	4.2025	.455897
2.1	2.1	4.41	.45202
2.15	2.15	4.6225	.447965
2.2	2.2	4.83999	.443757
2.25	2.25	5.06249	.439421
2.3	2.3	5.28999	.434975
2.35	2.35	5.52249	.430436
2.4	2.4	5.75999	.425818

optimum pressure ratio is: r1= 1.65 , r2= 1.65 , rt= 2.7225
efficiency at optimum pressure ratio is= .474568

APPENDIX B

THE "TURBINE" AND "COMPRES" PROGRAMS, AND EFFICIENCY ESTIMATION

B.1. Computer Programs.

TURBINE and COMPRES are simple programs that were written to aid in the turbomachine design process. The background for all calculations is covered in Chapter Four, except for some compressible flow equations that can be found in many fluid mechanics texts. The user inputs the number of stages, along with other data, and the program performs calculations based upon an equal stagnation-enthalpy drop at each stage. The compression and expansion processes are modelled as polytropic processes in the calculations. The polytropic efficiency used in the TURBINE and COMPRES programs should, therefore, be the same as those used in the CYCLE program when determining the cycle parameters, or a small error will result. Calculations are performed stage by stage, with analysis of critical flow parameters at the mean diameter, the hub, and at the blade tip. The hub and tip diameter values that are output are at the turbine-rotor inlet and the compressor-rotor outlet only of each stage. All output is sent to a line printer except for screen output that gives the user the status of stage calculations. No additional files are needed. The programs are written in BASIC and all calculations were performed on a personal computer. Program listings follow. Sample output is for the 200-MWth MGR-GT design.

Table B.1. TURBINE Turbine Design Program Listing

```
5 DIM P(100)
10 DIM A(100)
15 DIM Q(100)
20 DIM R(100)
25 DIM S(100)
30 DIM T(100)
50 PRINT "What is mass flow?"
70 INPUT M
100 PRINT "is working fluid helium?(y/n)"
110 INPUT C$
120 IF C$="y" THEN 160
130 PRINT "input R and Cp (J/kgK)"
140 INPUT R,CP
150 GOTO 180
160 LET R=2077
170 LET CP=5194
180 LET G=CP/(CP-R)
190 PRINT "input turbine inlet press.(MPa), turbine inlet temp (C), ";
200 PRINT "turbine exhaust temp.(C),turbine exhaust press (MPa)"
210 PRINT "and poly. efficiency."
220 INPUT PI,TI,TE,PE,EP
230 LET PI=PI*10^6
240 LET PE=PE*10^6
250 LET TI=TI+273
260 LET TE=TE+273
270 PRINT "input mean blade speed (m/s), rpm, blade metal density (kg/m3)";
275 PRINT ", and taper factor"
280 INPUT UM,N,RM,TF
300 PRINT "input mean dia. reaction coeff., nozzle inlet ";
310 PRINT "angle (deg), number of stages."
320 INPUT RNM,A1,S
340 LET DM=(UM*60)/(N*3.14159)
345 LET A1=A1*3.14159/180
346 LET LF=(CP*(TI-TE))/((UM^2)*S)
350 LET CTM2=(2*UM*(1-RNM)-UM*LF)/2
352 LET CTM1=UM*LF+CTM2
353 LET CX=CTM1/TAN(A1)
354 LET A2=ATN(CTM2/CX)
356 LET B1=(ATN((CTM1-UM)/CX))*180/3.14159
357 LET B2=(ATN((CTM2-UM)/CX))*180/3.14159
405 LET DTO=(TI-TE)/S
420 LPRINT
430 LPRINT
440 LPRINT "-------------------------------------------------------"
450 LPRINT
460 LPRINT "CONSTANT MEAN LINE GAS TURBINE DESIGN CALCULATION RESULTS"
470 LPRINT
480 LPRINT "turbine inlet pressure=";PI/10^6;"MPa"
490 LPRINT "turb inlet temp=";TI-273;"C"
500 LPRINT "turb exh press=";PE/10^6;"MPa"
510 LPRINT "turb exh temp=";TE-273;"C"
520 LPRINT "mean blade speed=";UM;"m/s""
530 LPRINT "rpm=";N
540 LPRINT "poly eff=";EP
550 LPRINT "blade metal density=";RM;"kg/m3"
580 LPRINT "fluid mass flow=";M;"kg/s"
590 LPRINT "nozzle inlet angle=";A1*180/3.14159
610 LET PT=M*CP*(TI-TE)/10^6
620 LPRINT "turbine power output=";PT;"MW"
630 LPRINT "mean dia=";DM;"meters"
```

```
640 LPRINT "mean reaction coef=";RNM,"mean load coef.=";LF
645 LPRINT "mean flow coef.=";CX/UM
650 LPRINT
660 LPRINT
670 LPRINT "                  ----------------"
680 LPRINT
690 LPRINT
710 LPRINT "        RESULTS OF STAGE CALCULATIONS "
720 LPRINT
730 LPRINT
750 LET ROE=PE/(R*TE)
760 LET P(S+1)=PE
770 LET T(S+1)=TE
780 LET W1=(CX^2+(CTM1-UM)^2)^.5
790 LET W2=(CX^2+(CTM2-UM)^2)^.5
800 LET C2=(CX^2+CTM2^2)^.5
810 LET C=(CX^2+CTM1^2)^.5
811 LPRINT "-----------MEAN LINE VELOCITY TRIANGLES-------------"
812 LPRINT "a1=";A1*180/3.14159;"deg","a2=";A2*180/3.14159;"deg"
813 LPRINT "b1=";B1;"deg","b2=";B2;"deg"
814 LPRINT "c1=";C;"m/s","c2=";C2;"m/s"
815 LPRINT "w1=";W1;"m/s","w2=";W2;"m/s"
816 LPRINT "u=";UM;"m/s"
817 LPRINT "-----------------------------------------------------"
818 LPRINT
819 LPRINT
820 LET B=.5*3.14159*DM^2
830 FOR I=S TO 1 STEP -1
840 LET T(I)=T(I+1)+DTO
841 LET P(I)=PE*((T(I)/TE)^(CP/(R*EP)))
842 LET T1=T(I)-((C^2)/(2*CP))
843 LET T2=T(I+1)-((C2^2)/(2*CP))
844 LET T0=T(I)-((C^2)/(2*CP))
845 LET M1=C/((G*R*T1)^.5)
846 LET M2=C2/((G*R*T2)^.5)
847 LET M0=C2/((G*R*T0)^.5)
848 LET Q(I)=P(I)*((1+(((G-1)/2)*M1^2))^(G/(1-G)))
849 LET R(I)=P(I+1)*((1+(((G-1)/2)*M2^2))^(G/(1-G)))
850 LET S(I)=P(I)*((1+(((G-1)/2)*M0^2))^(G/(1-G)))
851 LET RD1=Q(I)/(R*T1)
852 LET RD2=R(I)/(R*T2)
853 LET RD0=S(I)/(R*T0)
854 LET MR1=W1/((G*R*T1)^.5)
855 LET MR2=W2/((G*R*T2)^.5)
875 PRINT "density(";I;")=";RD1
876 PRINT "temp(";I;")=";T1,"stag temp(";I;")=";T(I)
880 LET A(I)=M/(RD1*CX)
890 LET L=((B-A(I))/(B+A(I)))^.5
910 LET DT=DM*(2/(1+L^2))^.5
920 LET DH=L*DT
930 LET CTH1=CTM1*(DM/DH)
940 LET CTH2=CTM2*(DM/DH)
950 LET CTT1=CTM1*(DM/DT)
960 LET CTT2=CTM2*(DM/DT)
970 LET UT=N*3.14159*DT/60
980 LET UH=N*3.14159*DH/60
990 LET LFT=(CTT1-CTT2)/UT
1000 LET LFH=(CTH1-CTH2)/UH
1010 LET RNH=1-((CTH1+CTH2)/(2*UH))
1020 LET RNT=1-((CTT1+CTT2)/(2*UT))
```

```
1030 LET ST=TF*1.3708*10^(-9)*RM*N^2*(DT^2-DH^2)
1040 LPRINT "------------STAGE NUMBER ";I;"----------------"
1050 LPRINT
1051 LPRINT "relative mach #'s"
1052 LPRINT "nozzle inlet: ";M2,"nozzle exit: ";M1
1053 LPRINT "rotor inlet: ";MR1,"rotor exit: ";MR2
1055 LPRINT "nozzle inlet stagnation pressure = ";P(I)/(10^6);"MPa"
1056 LPRINT "rotor exit stagnation pressure = ";P(I+1)/(10^6);"MPa"
1060 LPRINT "hub dia=";DH;"meters"
1070 LPRINT "hub reaction=";RNH
1080 LPRINT "hub load coef=";LFH
1090 LPRINT "tip dia=";DT;"meters"
1100 LPRINT "tip reaction=";RNT
1110 LPRINT "tip load coef=";LFT
1120 LPRINT "hub/tip ratio=";L
1130 LPRINT "centrifugal blade stress at the hub =";ST;"MPa=";
1135 LPRINT ST/6.895;"ksi"
1140 LPRINT
1150 LPRINT
1155 LET TH=TH+((Q(I)-R(I))*A(I))
1160 NEXT I
1180 LPRINT "axial thrust =";TH;"newtons=";TH/4.448;"lbf"
1190 LET TOR=(PT*30*10^6)/(3.14159*N)
1200 LPRINT "shaft torque=";TOR;"nm=";TOR*.68525;"ft-lbf"
1210 LPRINT
1220 LPRINT
1230 LPRINT
1240 LPRINT "XXXXXXXXXXXXXXXXXXXXXXXXXXXXXXXXXXXXXXXXXXXXXXXXXXXXX"
1260 LPRINT
1270 LPRINT
1280 LPRINT
1290 LPRINT
1300 END
```

Table B.2. TURBINE Sample Output

```
--------------------------------------------------

CONSTANT MEAN LINE GAS TURBINE DESIGN CALCULATION RESULTS

turbine inlet pressure= 7.8 MPa
turb inlet temp= 850 C
turb exh press= 4.11 MPa
turb exh temp= 616.7 C
mean blade speed= 400 m/s
rpm= 10000
poly eff= .91
blade metal density= 7800 kg/m3
fluid mass flow= 150 kg/s
nozzle inlet angle= 60
turbine power output= 181.764 MW
mean dia= .7639444 meters
mean reaction coef= .5       mean load coef.= 1.26225
mean flow coef.= .6530566

                ---------------

        RESULTS OF STAGE CALCULATIONS

------------MEAN LINE VELOCITY TRIANGLES-------------
a1= 60 deg     a2=-11.35328 deg
b1= 11.35328 deg              b2=-60 deg
c1= 522.4445 m/s              c2= 266.4363 m/s
w1= 266.4363 m/s              w2= 522.4445 m/s
u= 400 m/s
--------------------------------------------------


------------STAGE NUMBER  6 ----------------

relative mach #'s
nozzle inlet:  .1524211      nozzle exit:  .2956393
rotor inlet:  .1507702       rotor exit:  .2988766
nozzle inlet stagnation pressure =  4.622673 MPa
rotor exit stagnation pressure =  4.11 MPa
hub dia= .651443 meters
hub reaction= .3123924
hub load coef= 1.735866
tip dia= .861884 meters
tip reaction= .607178
tip load coef= .9916793
hub/tip ratio= .7558361
centrifugal blade stress at the hub = 170.2558 MPa= 24.69265 ksi


------------STAGE NUMBER  5 ----------------

relative mach #'s
nozzle inlet:  .1491715      nozzle exit:  .2894679
rotor inlet:  .1476229       rotor exit:  .2925046
nozzle inlet stagnation pressure =  5.174278 MPa
```

```
rotor exit stagnation pressure =  4.622673 MPa
hub dia= .6600425 meters
hub reaction= .3301931
hub load coef= 1.690928
tip dia= .8553163 meters
tip reaction= .6011221
tip load coef= 1.006967
hub/tip ratio= .7716941
centrifugal blade stress at the hub = 158.197 MPa= 22.94372 ksi


------------STAGE NUMBER  4 ----------------

relative mach #'s
nozzle inlet:  .1461214      nozzle exit:  .2836677
rotor inlet:  .1446649       rotor exit:  .2865238
nozzle inlet stagnation pressure =  5.766035 MPa
rotor exit stagnation pressure =  5.174278 MPa
hub dia= .6676282 meters
hub reaction= .3453274
hub load coef= 1.652721
tip dia= .8494083 meters
tip reaction= .5955541
tip load coef= 1.021024
hub/tip ratio= .785992
centrifugal blade stress at the hub = 147.4284 MPa= 21.38193 ksi


------------STAGE NUMBER  3 ----------------

relative mach #'s
nozzle inlet:  .143251       nozzle exit:  .2782027
rotor inlet:  .1418778       rotor exit:  .2808953
nozzle inlet stagnation pressure =  6.399141 MPa
rotor exit stagnation pressure =  5.766035 MPa
hub dia= .6743601 meters
hub reaction= .3583329
hub load coef= 1.619889
tip dia= .8440736 meters
tip reaction= .5904256
tip load coef= 1.033971
hub/tip ratio= .7989351
centrifugal blade stress at the hub = 137.7689 MPa= 19.98098 ksi


------------STAGE NUMBER  2 ----------------

relative mach #'s
nozzle inlet:  .1405434      nozzle exit:  .2730418
rotor inlet:  .1392459       rotor exit:  .275586
nozzle inlet stagnation pressure =  7.074782 MPa
rotor exit stagnation pressure =  6.399141 MPa
hub dia= .6803667 meters
hub reaction= .3696128
hub load coef= 1.591413
tip dia= .8392397 meters
tip reaction= .5856937
tip load coef= 1.045916
hub/tip ratio= .8106942
centrifugal blade stress at the hub = 129.0684 MPa= 18.71912 ksi
```

```
------------STAGE NUMBER  1 ----------------

relative mach #'s
nozzle inlet:  .1379837      nozzle exit:  .2681581
rotor inlet:  .1367553       rotor exit:  .2705668
nozzle inlet stagnation pressure =  7.794146 MPa
rotor exit stagnation pressure =  7.074782 MPa
hub dia= .6857525 meters
hub reaction= .3794758
hub load coef= 1.566514
tip dia= .8348446 meters
tip reaction= .5813201
tip load coef= 1.056958
hub/tip ratio= .8214133
centrifugal blade stress at the hub = 121.2014 MPa= 17.57816 ksi


axial thrust = 407580.8 newtons= 91632.38 lbf
shaft torque= 173572 nm= 118940.2 ft-lbf


XXXXXXXXXXXXXXXXXXXXXXXXXXXXXXXXXXXXXXXXXXXXXXXXXXXXXXXXXXXXXX
```

Table B.3. COMPRES Compressor Design Program Listing

```
 5 DIM P(100)
 6 DIM Q(100)
 10 DIM T(100)
 20 DIM R(100)
 30 DIM A(100)
 40 PRINT "XXXXXXXXXX AXIAL COMPRESSOR DESIGN PROGRAM XXXXXXXXXXX"
 50 PRINT "input mass flow (kg/s), inlet pressure (MPa), exit presure(MPa)";
 60 PRINT ", inlet temp (C), exit temp (C)"
 70 INPUT M,PI,PE,TI,TE
 80 LET PE=PE*10^6
 90 LET PI=PI*10^6
 100 LET TI=TI+273
 110 LET TE=TE+273
 120 PRINT "input poly eff, blade metal density (kg/m3), and taper factor "
 130 INPUT EP,RM,TF
 140 LET R=2077
 150 LET CP=5194
 160 LET G=CP/(CP-R)
 180 PRINT "input mean blade speed (m/s), rotor inlet angle (a1,deg, <0), ";
 190 PRINT "number of stages, mean reaction, rpm"
 200 INPUT UM,A1,S,RNM,N
 210 LET A1=3.14159*A1/180
 215 LET LF=CP*(TI-TE)/(S*(UM^2))
 220 LET CX=(UM*(2-2*RNM+LF))/(2*TAN(A1))
 230 LET A2=ATN(TAN(A1)-UM*LF/CX)
 240 LET CTM1=CX*TAN(A1)
 250 LET CTM2=CX*TAN(A2)
 260 LET WTM1=CTM1-UM
 270 LET WTM2=CTM2-UM
 280 LET W1=(WTM1^2+CX^2)^.5
 290 LET W2=(WTM2^2+CX^2)^.5
 300 LET HR=W2/W1
 350 LET C1=(CX^2+CTM1^2)^.5
 360 LET C2=(CX^2+CTM2^2)^.5
 365 LET HN=C1/C2
 370 LET AA=UM*(1-RNM)
 380 LET DM=(UM*60)/(N*3.14159)
 390 LET BB=DM*(CTM1-AA)
 420 LET B1=(ATN(WTM1/CX))*180/3.14159
 430 LET B2=(ATN(WTM2/CX))*180/3.14159
 440 LPRINT "XXXXXXXXX MEAN LINE COMPRESSOR VELOCITY TRIANGLES XXXXXXXXXXX"
 450 LPRINT
 460 LPRINT
 465 LPRINT "inlet temp = ";TI-273;" C","exit temp = ";TE-273;" C"
 466 LPRINT "inlet press = ";PI/10^6;" MPa","exit press = ";PE/10^6;" MPa"
 470 LPRINT "a1=";A1*180/3.14159;"deg","a2=";A2*180/3.14159;"deg"
 480 LPRINT "b1=";B1;"deg","b2=";B2;"deg"
 490 LPRINT "C1=";C1;"m/s","C2=";C2;"m/s"
 500 LPRINT "W1=";W1;"m/s","W2=";W2;"m/s"
 505 LPRINT "W2/W1 = ";HR,"C1/C2 = ";HN
 507 LPRINT "um=";UM;"m/s"
 508 LPRINT "flow coef.=";CX/UM
 510 LPRINT "load coef=";LF
 520 LPRINT "reaction =";RNM
 525 LPRINT "rpm=";N
 527 LPRINT "# of stages = ";S
 530 LPRINT
 540 LPRINT "------------------------------------------------"
 555 PRINT "s=";S
 560 LET DTO=(TE-TI)/S
```

```
580 LET P(0)=PI
590 LET T(0)=TI
600 LET B=.5*3.14159*DM^2
610 FOR I=1 TO S STEP 1
611 LET T(I)=T(I-1)+DTO
612 LET T1=T(I-1)-C1^2/(2*CP)
613 LET T2=T(I)-C2^2/(2*CP)
614 LET P(I)=PI*((T(I)/TI)^((CP*EP)/R))
615 LET M1=C1/((G*R*T1)^.5)
616 LET M2=C2/((G*R*T2)^.5)
617 LET P1=P(I-1)*((1+(((G-1)/2)*M1^2))^(G/(1-G)))
618 LET P2=P(I)*((1+(((G-1)/2)*M2^2))^(G/(1-G)))
619 LET R2=P2/(R*T2)
620 LET T3=T(I)-(C1^2/(2*CP))
621 LET M3=C1/((G*R*T3)^.5)
622 LET P3=P(I)*((1+(((G-1)/2)*M3^2))^(G/(1-G)))
623 LET R1=P1/(R*T1)
624 LET R01=P(I-1)/(R*T(I-1))
625 LET R02=P(I)/(R*T(I))
640 PRINT "dens(";I;")=";R2
650 PRINT "temp(";I;")=";T2,"stg temp(";I;")=";T(I)
660 LET A(I)=M/(R2*CX)
670 LET L=((B-A(I))/(B+A(I)))^.5
680 LET DT=DM*(2/(1+L^2))^.5
690 LET DH=DT*L
695 LET TH=TH+(P1-P2)*A(I)
700 LET ST=TF*1.3708*10^(-9)*RM*N^2*(DT^2-DH^2)
710 LET CTH1=AA-BB/DH
720 LET CTH2=AA+BB/DH
730 LET CTT1=AA-BB/DT
740 LET CTT2=AA+BB/DT
750 LET UT=N*3.14159*DT/60
760 LET UH=N*3.14159*DH/60
770 LET LFH=(CTH1-CTH2)/UH
780 LET LFT=(CTT1-CTT2)/UT
790 LET RNT=1-AA/UT
800 LET RNH=1-AA/UH
910 LPRINT
920 LPRINT
930 LPRINT "---------------- STAGE (";I;") -------------------"
940 LPRINT
945 LPRINT "stage inlet stag. press. = ";P(I-1)/(10^6);"MPa"
946 LPRINT "stage exit stag. press. = ";P(I)/(10^6);"MPa"
947 LPRINT "rotor inlet stag. dens.= ";R01;" kg/m3"
948 LPRINT "stator inlet stag. dens.= ";R02;" kg/m3"
950 LPRINT "hub dia=";DH;"meters"
960 LPRINT "hub load coef=";LFH
970 LPRINT "hub reaction=";RNH
980 LPRINT "tip dia=";DT;"meters"
990 LPRINT "tip load coef=";LFT
1000 LPRINT "tip reaction=";RNT
1010 LPRINT "hub to tip ratio=";L
1020 LPRINT "centrifugal blade stress at the hub=";ST;"MPa=";
1030 LPRINT ST/6.895;"ksi"
1040 LPRINT
1041 LPRINT "            -------"
1042 LPRINT
1043 LPRINT "rotor inlet:"
1044 LPRINT "temp. = ";T1;"K","  dens.= ";R1;"kg/m3"
1045 LPRINT "stator inlet:"
```

```
1046 LPRINT "temp. = ";T2;"K","  dens.= ";R2;"kg/m3"
1047 LPRINT
1050 LPRINT
1060 LPRINT "            --------------------"
1065 LET T(I-1)=T(I)+DTO
1070 NEXT I
1080 LET TOR=M*CP*(TE-TI)*30/(N*3.14159)
1100 LPRINT "shaft torque=";TOR;"nm"
1110 LPRINT "axial thrust=";TH;"newtons"
1120 LPRINT
1130 LPRINT "XXXXXXXXXXXXXXXXXXXXXXXXXXXXXXXXXXXXXXXXXXXXXXXXXXXXXXXXXXXXXXXXXXXXXXX"
1140 LPRINT
1150 LPRINT
1160 LPRINT
1170 LPRINT
1180 LPRINT
1190 LPRINT
1200 LPRINT
1210 GOTO 4000
4000 END
```

Table B.4. COMPRES Sample Output

```
XXXXXXXXX MEAN LINE COMPRESSOR VELOCITY TRIANGLES XXXXXXXXXXX

inlet temp =  30  C          exit temp =  145.3  C
inlet press =  3.97  MPa     exit press =  8.140001  MPa
a1= 35 deg     a2= 54.01811 deg
b1=-54.01811 deg             b2=-34.99999 deg
C1= 205.6658 m/s             C2= 286.7453 m/s
W1= 286.7453 m/s             W2= 205.6658 m/s
W2/W1 =  .7172421            C1/C2 =  .7172421
um= 350 m/s
flow coef.= .4813474
load coef=-.3259146
reaction = .5
rpm= 10000
# of stages =  15

-------------------------------------------------


---------------- STAGE ( 1 ) -------------------

stage inlet stag. press. =  3.97 MPa
stage exit stag. press. =  4.197642 MPa
rotor inlet stag. dens.=  6.308286  kg/m3
stator inlet stag. dens.=  6.504985  kg/m3
hub dia= .5968669 meters
hub load coef= .4087789
hub reaction= .4400332
tip dia= .7330787 meters
tip load coef= .2709831
tip reaction= .5440795
hub to tip ratio= .8141922
centrifugal blade stress at the hub= 96.84721 MPa= 14.04601 ksi

            -------

rotor inlet:
temp. =  298.9282 K          dens.=  6.181496 kg/m3
stator inlet:
temp. =  302.7715 K          dens.=  6.257873 kg/m3


           ------------------


---------------- STAGE ( 2 ) -------------------

stage inlet stag. press. =  4.197642 MPa
stage exit stag. press. =  4.432295 MPa
rotor inlet stag. dens.=  6.504985  kg/m3
stator inlet stag. dens.=  6.702788  kg/m3
hub dia= .5991713 meters
hub load coef= .4056406
hub reaction= .4421869
tip dia= .7311964 meters
tip load coef= .2723801
tip reaction= .5429058
hub to tip ratio= .8194397
centrifugal blade stress at the hub= 93.90026 MPa= 13.6186 ksi
```

```
          -------

rotor inlet:
temp. =  306.6148 K           dens.=  6.377464 kg/m3
stator inlet:
temp. =  310.4582 K           dens.=  6.454273 kg/m3

          -------------------


---------------- STAGE ( 3 ) -------------------

stage inlet stag. press. =  4.432295 MPa
stage exit stag. press. =  4.673994 MPa
rotor inlet stag. dens.=  6.702788  kg/m3
stator inlet stag. dens.=  6.901669  kg/m3
hub dia= .6013433 meters
hub load coef= .4027156
hub reaction= .4442016
tip dia= .7294111 meters
tip load coef= .273715
tip reaction= .541787
hub to tip ratio= .8244231
centrifugal blade stress at the hub= 91.11221 MPa= 13.21424 ksi

          -------

rotor inlet:
temp. =  314.3015 K           dens.=  6.574552 kg/m3
stator inlet:
temp. =  318.1448 K           dens.=  6.651772 kg/m3

          -------------------


---------------- STAGE ( 4 ) -------------------

stage inlet stag. press. =  4.673994 MPa
stage exit stag. press. =  4.92278 MPa
rotor inlet stag. dens.=  6.901669  kg/m3
stator inlet stag. dens.=  7.101613  kg/m3
hub dia= .6033938 meters
hub load coef= .3999832
hub reaction= .4460904
tip dia= .7277158 meters
tip load coef= .2749919
tip reaction= .5407195
hub to tip ratio= .8291614
centrifugal blade stress at the hub= 88.47086 MPa= 12.83116 ksi

          -------

rotor inlet:
temp. =  321.9882 K           dens.=  6.77273 kg/m3
stator inlet:
temp. =  325.8316 K           dens.=  6.850365 kg/m3
```

```
-------------------

---------- STAGE ( 5 ) -------------------

stage inlet stag. press. =  4.92278 MPa
stage exit stag. press. =  5.178688 MPa
rotor inlet stag. dens.=  7.101613  kg/m3
stator inlet stag. dens.=  7.302596  kg/m3
hub dia= .6053325 meters
hub load coef= .3974253
hub reaction= .4478643
tip dia= .7261039 meters
tip load coef= .2762142
tip reaction= .5397
hub to tip ratio= .833672
centrifugal blade stress at the hub= 85.96535 MPa= 12.46778 ksi

          -------

rotor inlet:
temp. =  329.6749 K           dens.=  6.971985 kg/m3
stator inlet:
temp. =  333.5182 K           dens.=  7.050021 kg/m3

          -------------------

---------- STAGE ( 6 ) -------------------

stage inlet stag. press. =  5.178688 MPa
stage exit stag. press. =  5.441756 MPa
rotor inlet stag. dens.=  7.302596  kg/m3
stator inlet stag. dens.=  7.504604  kg/m3
hub dia= .6071678 meters
hub load coef= .3950262
hub reaction= .4495334
tip dia= .7245698 meters
tip load coef= .277385
tip reaction= .5387254
hub to tip ratio= .8379701
centrifugal blade stress at the hub= 83.58585 MPa= 12.12268 ksi

          -------

rotor inlet:
temp. =  337.3615 K           dens.=  7.172292 kg/m3
stator inlet:
temp. =  341.2049 K           dens.=  7.250723 kg/m3

          -------------------

---------- STAGE ( 7 ) -------------------

stage inlet stag. press. =  5.441756 MPa
stage exit stag. press. =  5.712021 MPa
```

```
rotor inlet stag. dens.=  7.504604  kg/m3
stator inlet stag. dens.=  7.70762  kg/m3
hub dia= .6089081 meters
hub load coef= .3927715
hub reaction= .4511065
tip dia= .7231081 meters
tip load coef= .2785076
tip reaction= .537793
hub to tip ratio= .8420706
centrifugal blade stress at the hub= 81.32317 MPa= 11.79451 ksi

            -------

rotor inlet:
temp. =  345.0482 K           dens.=  7.373635 kg/m3
stator inlet:
temp. =  348.8916 K           dens.=  7.452456 kg/m3


           --------------------


---------------- STAGE ( 8 ) -------------------

stage inlet stag. press. =  5.712021 MPa
stage exit stag. press. =  5.989516 MPa
rotor inlet stag. dens.=  7.70762  kg/m3
stator inlet stag. dens.=  7.911623  kg/m3
hub dia= .6105599 meters
hub load coef= .3906492
hub reaction= .4525916
tip dia= .7217139 meters
tip load coef= .2795846
tip reaction= .5369001
hub to tip ratio= .845986
centrifugal blade stress at the hub= 79.16939 MPa= 11.48214 ksi

            -------

rotor inlet:
temp. =  352.7349 K           dens.=  7.575999 kg/m3
stator inlet:
temp. =  356.5783 K           dens.=  7.655198 kg/m3


           --------------------


---------------- STAGE ( 9 ) -------------------

stage inlet stag. press. =  5.989516 MPa
stage exit stag. press. =  6.274278 MPa
rotor inlet stag. dens.=  7.911623  kg/m3
stator inlet stag. dens.=  8.1166  kg/m3
hub dia= .6121298 meters
hub load coef= .388648
hub reaction= .4539955
tip dia= .7203828 meters
tip load coef= .2806188
tip reaction= .5360444
```

```
hub to tip ratio= .8497285
centrifugal blade stress at the hub= 77.11699 MPa= 11.18448 ksi

            -------

rotor inlet:
temp. =  360.4216 K           dens.=  7.779357 kg/m3
stator inlet:
temp. =  364.2649 K           dens.=  7.858937 kg/m3

          ------------------


---------------- STAGE ( 10 ) --------------------

stage inlet stag. press. =  6.274278 MPa
stage exit stag. press. =  6.566342 MPa
rotor inlet stag. dens.=  8.1166  kg/m3
stator inlet stag. dens.=  8.322536  kg/m3
hub dia= .6136236 meters
hub load coef= .386758
hub reaction= .4553247
tip dia= .7191109 meters
tip load coef= .2816124
tip reaction= .5352238
hub to tip ratio= .8533088
centrifugal blade stress at the hub= 75.15921 MPa= 10.90054 ksi

            -------

rotor inlet:
temp. =  368.1082 K           dens.=  7.983705 kg/m3
stator inlet:
temp. =  371.9516 K           dens.=  8.063651 kg/m3

          ------------------


---------------- STAGE ( 11 ) --------------------

stage inlet stag. press. =  6.566342 MPa
stage exit stag. press. =  6.865737 MPa
rotor inlet stag. dens.=  8.322536  kg/m3
stator inlet stag. dens.=  8.529411  kg/m3
hub dia= .6150465 meters
hub load coef= .3849706
hub reaction= .4565848
tip dia= .7178941 meters
tip load coef= .2825678
tip reaction= .534436
hub to tip ratio= .8567371
centrifugal blade stress at the hub= 73.28981 MPa= 10.62942 ksi

            -------

rotor inlet:
temp. =  375.7949 K           dens.=  8.189016 kg/m3
stator inlet:
```

```
temp. =  379.6383 K           dens.=  8.26933 kg/m3

          ------------------


---------------- STAGE ( 12 ) -------------------

stage inlet stag. press. =  6.865737 MPa
stage exit stag. press. =  7.172501 MPa
rotor inlet stag. dens.=  8.529411  kg/m3
stator inlet stag. dens.=  8.737216  kg/m3
hub dia= .6164035 meters
hub load coef= .3832774
hub reaction= .4577811
tip dia= .7167294 meters
tip load coef= .2834869
tip reaction= .5336795
hub to tip ratio= .8600227
centrifugal blade stress at the hub= 71.50315 MPa= 10.37029 ksi

            -------

rotor inlet:
temp. =  383.4816 K           dens.=  8.395278 kg/m3
stator inlet:
temp. =  387.325 K            dens.=  8.475953 kg/m3


          ------------------


---------------- STAGE ( 13 ) -------------------

stage inlet stag. press. =  7.172501 MPa
stage exit stag. press. =  7.486665 MPa
rotor inlet stag. dens.=  8.737216  kg/m3
stator inlet stag. dens.=  8.945935  kg/m3
hub dia= .6176987 meters
hub load coef= .3816718
hub reaction= .458918
tip dia= .7156134 meters
tip load coef= .2843718
tip reaction= .5329522
hub to tip ratio= .8631738
centrifugal blade stress at the hub= 69.79404 MPa= 10.12241 ksi

            -------

rotor inlet:
temp. =  391.1683 K           dens.=  8.602482 kg/m3
stator inlet:
temp. =  395.0116 K           dens.=  8.683509 kg/m3


          ------------------


---------------- STAGE ( 14 ) -------------------
```

```
stage inlet stag. press. =  7.486665 MPa
stage exit stag. press. =  7.808261 MPa
rotor inlet stag. dens.=  8.945935  kg/m3
stator inlet stag. dens.=  9.155554  kg/m3
hub dia= .6189363 meters
hub load coef= .3801471
hub reaction= .4599999
tip dia= .7145433 meters
tip load coef= .2852242
tip reaction= .5322528
hub to tip ratio= .8661983
centrifugal blade stress at the hub= 68.15775 MPa= 9.885099 ksi

            -------

rotor inlet:
temp. =  398.8549 K           dens.=  8.810608 kg/m3
stator inlet:
temp. =  402.6983 K           dens.=  8.891981 kg/m3


          -------------------


---------------- STAGE ( 15 ) -------------------

stage inlet stag. press. =  7.808261 MPa
stage exit stag. press. =  8.137323 MPa
rotor inlet stag. dens.=  9.155554  kg/m3
stator inlet stag. dens.=  9.366062  kg/m3
hub dia= .6201198 meters
hub load coef= .3786973
hub reaction= .4610305
tip dia= .7135165 meters
tip load coef= .2860457
tip reaction= .5315796
hub to tip ratio= .8691037
centrifugal blade stress at the hub= 66.58975 MPa= 9.657687 ksi

            -------

rotor inlet:
temp. =  406.5416 K           dens.=  9.019642 kg/m3
stator inlet:
temp. =  410.385 K            dens.=  9.101359 kg/m3


          -------------------
shaft torque= 85781.62 nm
axial thrust=-207842.9 newtons

XXXXXXXXXXXXXXXXXXXXXXXXXXXXXXXXXXXXXXXXXXXXXXXXXXXXXXXXXXXXXXXX
```

B.2 Turbine Efficiency Estimation.

The method of Craig and Cox, as discussed in refs. C6 and W1, is used to estimate the turbine efficiency for the 200-MWth MGR-GT turbine.

Assume 60 blades per nozzle and blade row (this will result in blade-aspect ratios ranging from about 1.9 to about 2.7).

$$s = 0.040 \text{ m}$$

$$\left.\frac{b}{s}\right]_{opt} = 0.9664 \quad \text{(from Eq. 4.31)}$$

$$b = 0.0387 \text{ m}$$

Therefore, if the gap between blade rows is about 35% blade axial chord, total bladed length of a six-stage machine is about 0.630 meters.

Calculating the blade-backbone length [W1],

$$\frac{b_c}{c} = 0.0096(\alpha_{in}-\alpha_{out})/\sin(0.55(\alpha_{in}-\alpha_{out})) = 1.0828$$

From Fig. B.1,

$$\lambda = 50^{o}$$

$$\cos(\lambda) = \frac{b}{c} = 0.6428$$

Therefore,

$$b_c = 0.0651 \text{ m}$$

(The blade-backbone length is what is used for "b" in Figs. B.2 through B.7.)

$$\left[1 - \frac{\cos|\alpha_{out}|}{\cos|\alpha_{in}|}\right] = 0.49$$

From Fig. B.2,

$$CR = 1.6$$

From Fig. B.3,

$$C_L^x = 12.5$$

Therefore,

$$C_L^x \cdot \left[\frac{s}{b_c}\right] = 7.67$$

From Fig. B.4,

$$X_p \cdot \left[\frac{s}{b_c}\right] \sin\beta = 0.9\ \%$$

Therefore, $X_p = 1.69\ \%$

Assume $\tau_{te}/s \cong 0.05$

From Fig.B.5,

$$X_{p,inc} = 0.00020, \qquad \frac{X_{p,te}}{X_p} = 1.19$$

For $\frac{s}{e} \cong 0.5$, $\quad O = 0.0202$ m (Eq. 4.32)

Reynolds numbers and effects on turbine-loss parameters are listed in Table B.5.

Rotor group 1 losses equal [C6]:

$$\frac{1}{2} \sum \left[\left(N_p \left[\frac{X_{p,te}}{X_p} \cdot X_p + X_{p,inc}\right] + X_{sec}\right) W_2^2\right]$$

Stator losses are the same as above, except substitute C_1 for W_2.

Total group 1 losses = 46.898 m^2/s^2

$$\eta_t = \eta_2 \cdot \left[\frac{\text{Turbine Work}}{\text{Turbine Work} + \text{Grp. 1 Losses}}\right]$$

$$= 0.9627 \cdot \eta_2$$

η_2 accounts for tip-clearance losses and can be obtained from Fig. B.8.

Since the MGR-GT turbine will normally go through a heat-up procedure that is slow when compared to those of combustion turbines, we can design for a low clearance. Magnetic bearings offer accurate rotor-position control, which will tend to allow for small clearances as well. Hence, a 1% clearance should be possible.

For a 1% tip clearance, $\eta_t = 0.9387$, or $\eta_{pt} = 0.9307$.

These results are expected to be within an accuracy of ±1.25% [C6].

The high turbine efficiency is largely a result of the high Reynolds numbers of the flow and the low molecular weight of helium (density for a given pressure is ≈1/7 that of air.).

Table B.5

Reynolds Number Effects on Turbine Losses

Stage	$Re_o/10^5$	N_p (Fig. B.6)	$\frac{H}{b}$	X_{sec}(Fig. B.7)
1N	6.89	.66	1.9	1.9 %
1R	6.77	.66	1.9	1.9
2N	6.65	.67	2.1	1.6
2R	6.51	.67	2.1	1.6
3N	6.41	.67	2.2	1.5
3R	6.22	.68	2.2	1.5
4N	6.14	.68	2.3	1.4
4R	6.00	.68	2.3	1.4
5N	5.89	.69	2.5	1.3
5R	5.74	.69	2.5	1.3
6N	5.67	.69	2.7	1.2
6R	5.49	.70	2.7	1.2

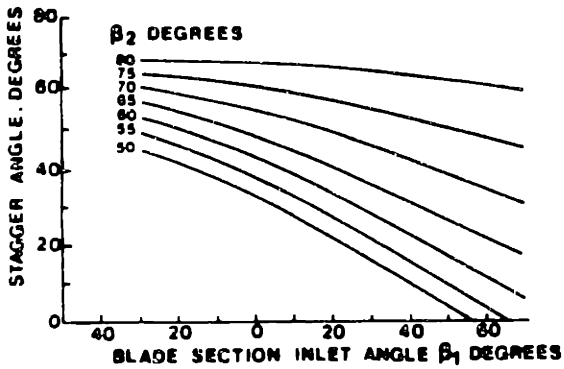

Figure B.1. Stagger angle for typical turbine blade sections [from K3].

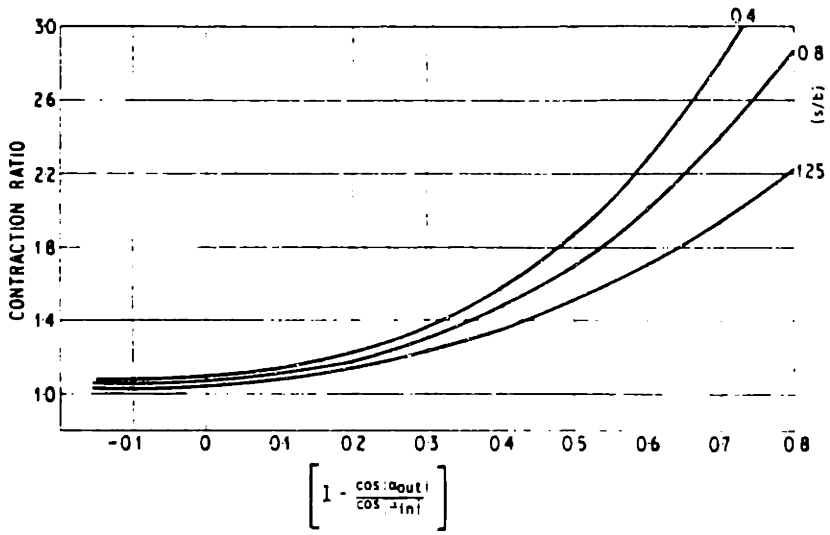

Figure B.2. Contraction ratios for average profiles [from C6].

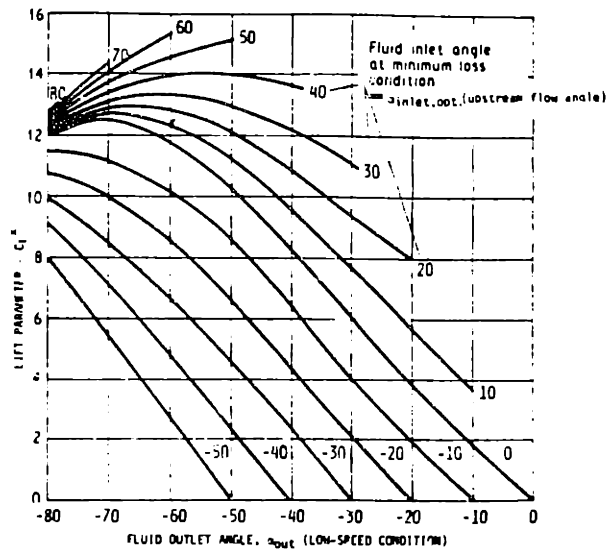

Figure B.3. Lift parameter versus flow angles [from C6].

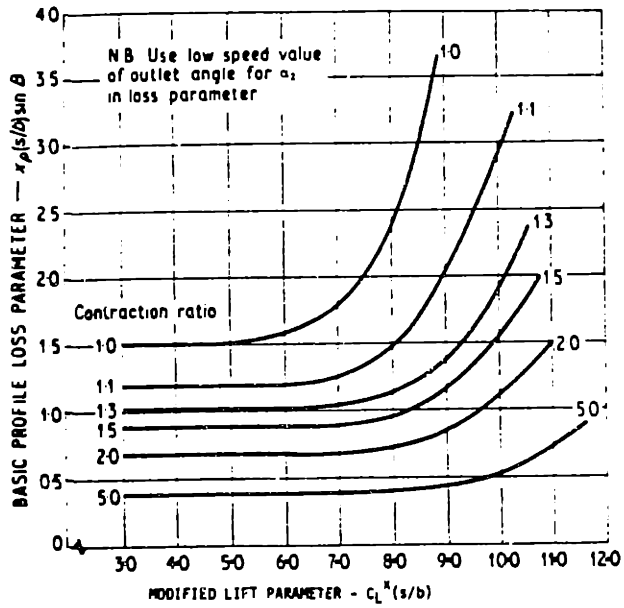

Figure B.4. Basic profile loss [from C6].

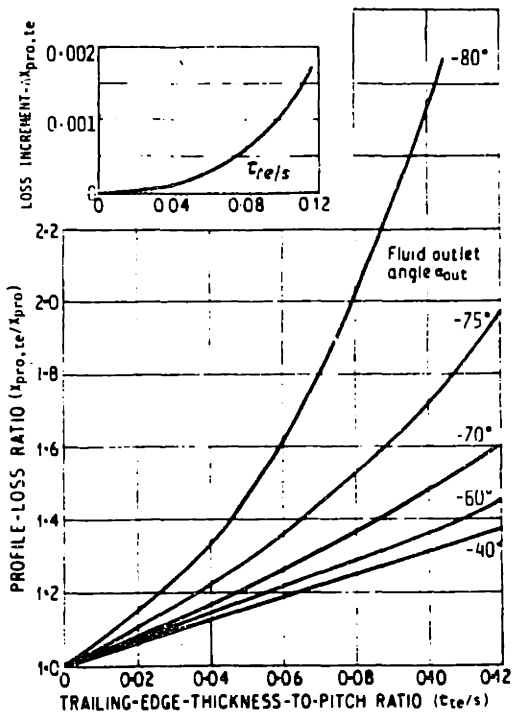

Figure B.5. Trailing-edge-thickness loss [from C6].

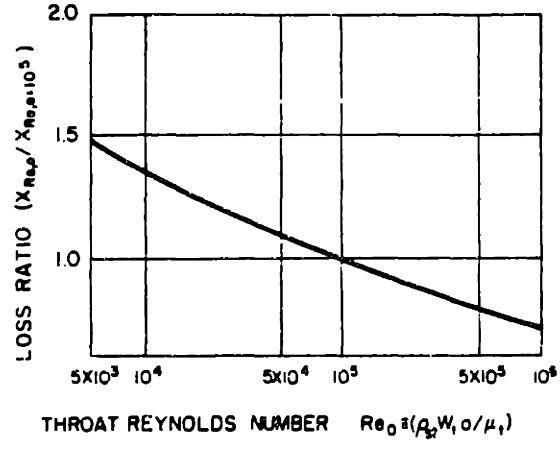

Figure B.6. Effect of Reynolds number on profile losses [from C6].

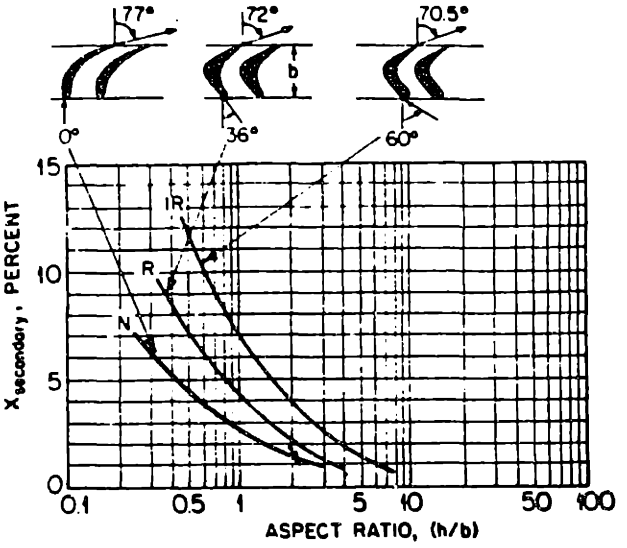

Figure B.7. Secondary-flow and annulus losses. [from Forster's discussion of Craig and Cox (C6)].

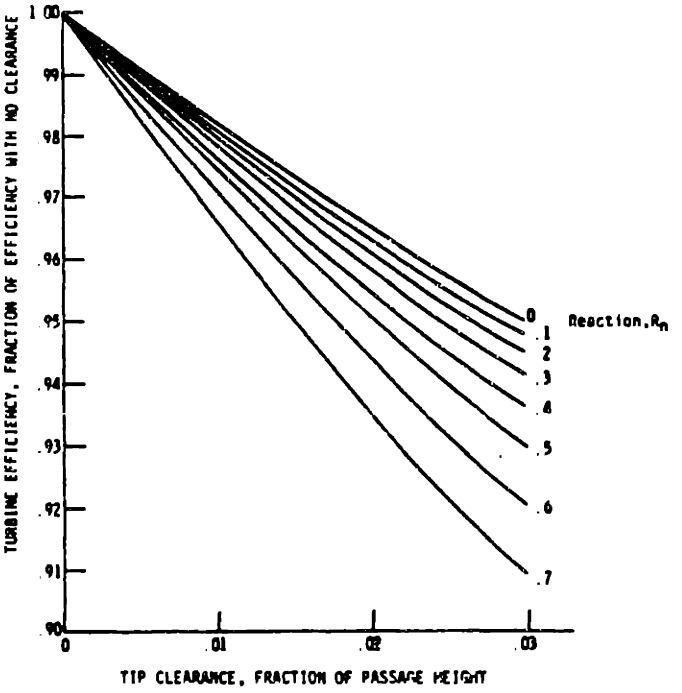

Figure B.8. Tip-clearance correlation for unshrouded blades. [from R6].

B.3 Compressor Efficiency Calculations.

NACA 65-(12)10 blades at a setting angle of 42^{o} and solidity of 1.0 were selected for both moving and stationary compressor-blade rows. Choosing 50 blades per blade row (this will result in an aspect ratio of about 2.0),

$$s = c = 0.0420 \text{ m}$$

$$b = 0.0312 \text{ m}$$

Therefore, total bladed length, allowing for an axial gap between blade rows of 35% of the axial chord, and a set of inlet guide vanes, is about 1.30 m.

Koch and Smith give this correlation for equivalent diffusion ratio [K18]:

$$D_{eq} = \frac{W_1}{W_2}\left[1+0.7688\left[\frac{t_{max}}{c}\right]+0.6024\Gamma\right]\left[(\sin\alpha_1 - 0.2445\sigma\Gamma)^2 + \left[\frac{\cos\alpha_1}{1-[0.4458\sigma(t_{max}/c)/\cos((\alpha_1+\alpha_2)/2)][1-[1-(A_{a2}/A_{a1})]/3]}\right]^2\right]^{1/2}$$

where

$$\Gamma = \frac{r_1'W_{\theta 1}' - r_2'W_{\theta 2}'}{\sigma W_1'}$$

$$r' = \frac{r}{r_m}$$

and

$$W' = \frac{W}{U_m}$$

The contraction ratio for this compressor is very close to one, or

$$A_{a2}/A_{a1} \cong 1.0$$

Therefore,

$$D_{eq} = 1.7017$$

at the mean diameter.

Boundary-layer momentum thickness can be correlated to D_{eq} by [W1]:

$$\left[\frac{\theta_2}{c}\right] = 0.00138\ e^{1.1127\ D_{eq}} + 0.0025$$

$\left[\frac{\theta_2}{c}\right]$ is corrected for Reynolds number with Fig. B.9.

Trailing-edge boundary-layer shape factor equals [W1]

$$H_{te} = 1.26 + 0.795\ (D_{eq} - 1)^{1.681}$$

Because Mach numbers are very low, and streamtube- contraction ratio is very close to one, it is not necessary to make these corrections.

Chord Reynolds numbers are listed in Table B.6.

Profile losses are given by:

$$\frac{\Delta p_{o,pro}}{[\rho_{o1} W_1^2/2]} = 2\left[\frac{\theta_2}{c}\right]\frac{\sigma}{\cos\alpha_2}\left[\frac{\cos\alpha_1}{\cos\alpha_2}\right]^2\left[\frac{2}{3-(1/H_{te})}\right]$$
$$\left[1 - \left[\frac{\theta_2}{c}\right]\frac{\sigma H_{te}}{\cos\alpha_2}\right]^3$$

Table B.7 lists the stage-profile losses.

$$\sum\left[\frac{\Delta P_o}{P_o}\right]_{pro} = 0.01486$$

Not accounting yet for end-wall losses, isentropic free-stream efficiency is equal to

$$\eta_{c,fs} = \frac{r_p^{(R/C_p)} - 1}{\left[r_p + \sum\left[\frac{\Delta P_o}{P_{o1}}\right]_{pro}\right]^{(R/C_p)} - 1}$$
$$= 0.988$$

This may seem high for free-stream efficiency. It is due to the high Reynolds numbers, and the low density of helium relative to air at the same pressure.

$\frac{(\Delta P/q)}{(\Delta P/q)_{max}}$ can be estimated from [W1]

$$\frac{(\Delta p/q)}{(\Delta p/q)_{max}} = \frac{1 - \left[\frac{\cos\alpha_1}{\cos\alpha_2}\right]^2}{1 - \left[\frac{\cos\alpha_1}{\cos\alpha_2}\right]^2_{stall}}$$

Table B.6

Compressor Reynolds Numbers

Stage	$Re_c/10^6$	Stage	$Re_c/10^6$
1R	3.75	1S	3.76
2R	3.80	2S	3.82
3R	3.86	3S	3.87
4R	3.91	4S	3.92
5R	3.96	5S	3.97
6R	4.01	6S	4.02
7R	4.06	7S	4.07
8R	4.11	8S	4.12
9R	4.15	9S	4.16
10R	4.20	10S	4.21
11R	4.24	11S	4.25
12R	4.29	12S	4.30
13R	4.33	13S	4.34
14R	4.37	14S	4.38
15R	4.42	15S	4.43

Table B.7

Compressor-Stage Profile Losses $\left[\frac{\Delta P}{P_{o1}}\right]_{pro}$

Stage	Loss x 10^4	Stage	Loss x 10^4
1R	6.00	1S	5.85
2R	5.87	2S	5.71
3R	5.73	3S	5.57
4R	5.59	4S	5.44
5R	5.46	5S	5.32
6R	5.34	6S	5.20
7R	5.22	7S	5.09
8R	5.11	8S	4.98
9R	5.00	9S	4.88
10R	4.90	10S	4.78
11R	4.80	11S	4.69
12R	4.71	12S	4.60
13R	4.62	13S	4.52
14R	4.54	14S	4.44
15R	4.46	15S	4.35

During normal operations

$$\alpha_1 = 54^o$$

$$\alpha_2 = 35^o$$

From Fig. B.10, at positive stall

$$\alpha_1 = 59^o$$

$$\alpha_2 = 37^o$$

Therefore, $$\frac{(\Delta P/q)}{(\Delta P/q)_{max}} = 0.83$$

Assuming a rotor-radial-gap of 1-mm, from Fig. B.11,

$$\frac{2\,\bar{\delta}^*}{g} = \frac{2\,\bar{\delta}^*}{s\cos\lambda} \cong 0.20$$

From Fig. B.12, $$\frac{2\,\bar{\delta}^*}{(2\,\bar{\delta}^*)_{\text{Fig. B.11}}} = 0.98$$

and $$2\,\bar{\delta}^* = 0.00612$$

From Fig. B.13, $$\frac{2\,\bar{v}}{2\,\bar{\delta}^*} = 0.48$$

Compressor-stage efficiency equals

$$\eta_c = \eta_{c,fs}\left[\frac{1 - (2\bar{\delta}^*/\bar{g})(\overline{g/h})}{1 - (2\bar{v}/2\bar{\delta}^*)(2\bar{\delta}^*/\bar{g})(\overline{g/h})}\right]$$

We will take the average height of all of the compressor stages as an approximation. With contraction ratios so close to one, very little error will result from this approximation.

$$\bar{h} = .0563 \text{ m}$$

$$\eta_c = (0.988)(0.940)$$

$$\eta_c = 0.929$$

Hence, end-wall losses contribute the most to compressor losses, which is what is expected.

Compressor polytropic efficiency is equal to

$$\eta_{p,c} = 0.937$$

Like the turbine efficiency, the high compressor efficiency

results from the high Reynolds numbers of the flow and the low molecular weight of helium.

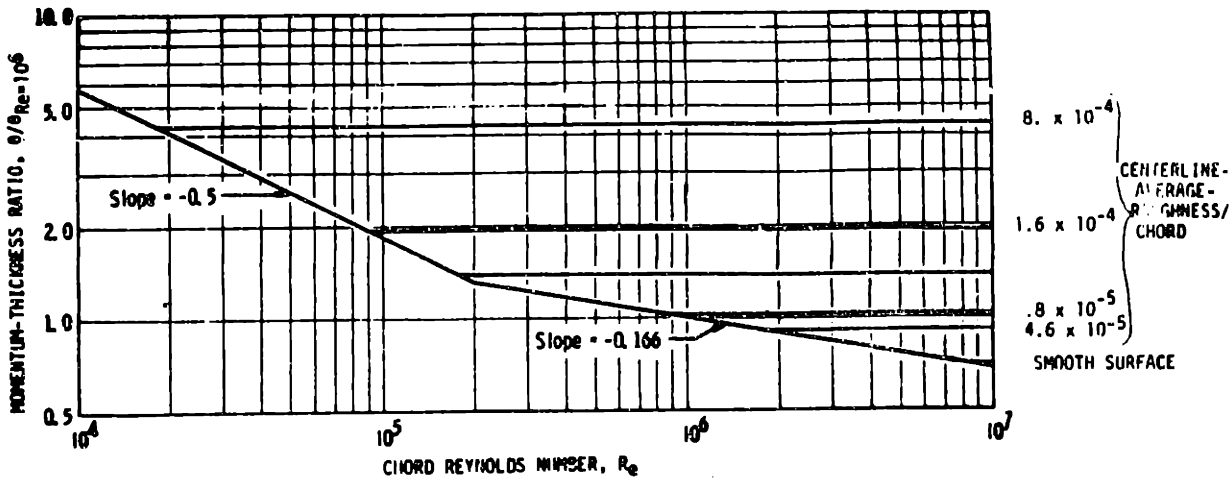

Figure B.9. Reynolds number correction for momentum-thickness ratio [from K18].

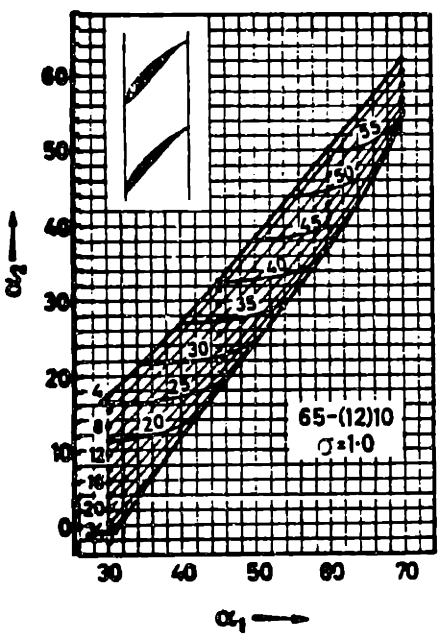

Figure B.10

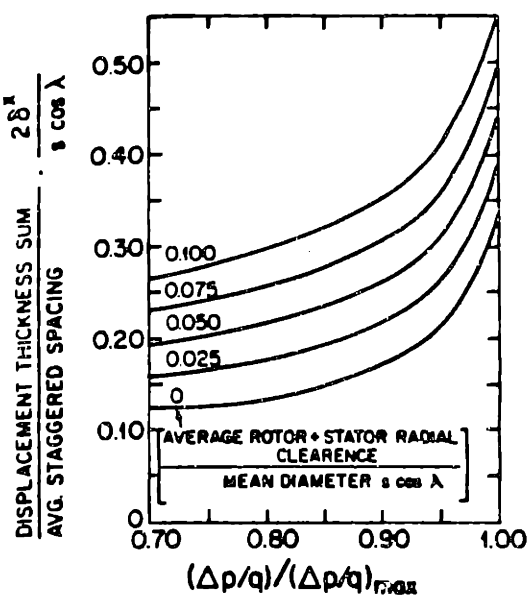

Figure B.11

Figure B.10. NACA Mellor chart for NACA blades 65-(12)10, σ=1.0 [from M25].

Figure B.11. Radial-clearance multiplier for end-wall-loss correction [from K18].

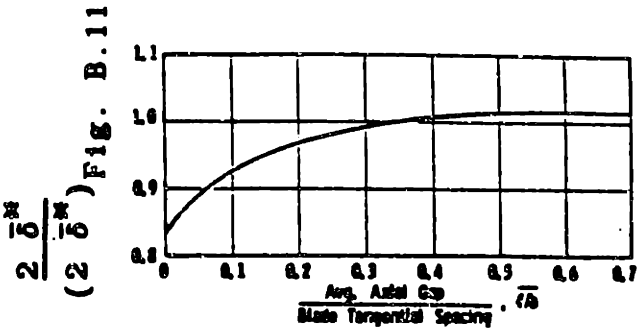

Figure B.12. Axial-gap multiplier for end-wall-loss correction [from K18].

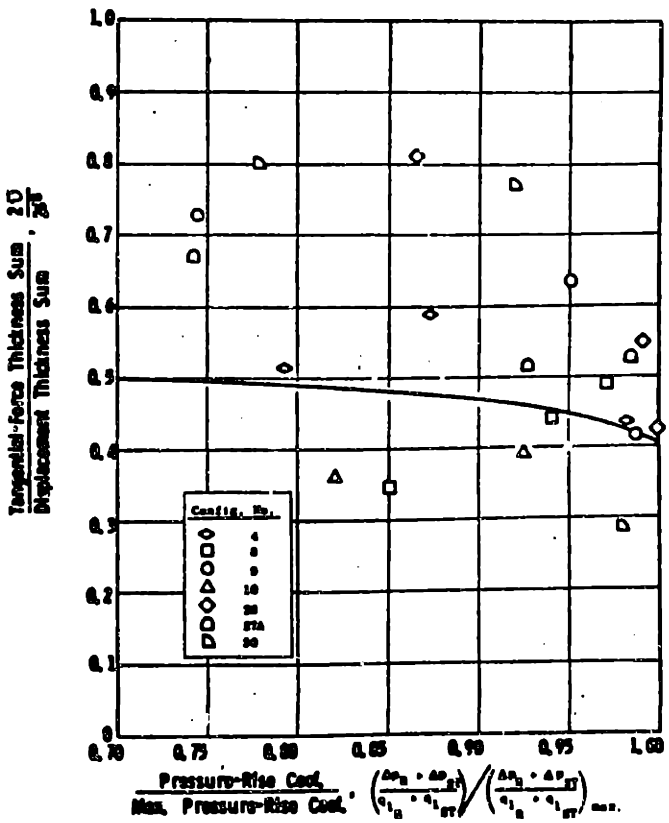

Figure B.13. Tangential-force-thickness multiplier for end-wall-loss correction [from K18].

APPENDIX C

THE "REGEN" AND "PRECOOL" PROGRAMS

REGEN and PRECOOL are simple programs written to aid in the heat exchanger design process. REGEN performs calculations for the gas turbine recuperator, and PRECOOL performs design calculations for the precooler in either a crossflow or a multiple-pass cross-counterflow configuration. The calculation methods are discussed in Chapter Five.

Both REGEN and PRECOOL were written in BASIC. Calculations were performed on a personal computer equipped with a line printer. The program asks the user for all input data except for surface specification, which is incorporated into the code. All output is in hard copy to the line printer, except for screen output that gives the user the status of iterations. No additional files are necessary for use. Listings and sample output follow.

Table C.1.

Listing of REGEN Computer Program

```
10 PRINT "MGR-GT RECUPERATOR DESIGN PROGRAM"
20 PRINT
30 PRINT "           REGEN"
40 PRINT
50 REM xxxxxxxxxxxxxxx DATA FOR SURFACES xxxxxxxxxxxxxxx
60 REM b=plate spacing
70 REM l-=fin thickness (1/2 of b)
80 REM r-=Hydraulic radius
90 REM del-=fin thickness
100 REM bb-= total heat transfer area/volume between plates
110 REM afa-=fin area/total heat transfer area
115 REM pit=fin pitch
120 REM t5=turbine exhaust temp
130 REM t6=regenerator hot side outlet temp
140 REM t2=compressor outlet temp
150 REM t3=regenerator cold side exit temp
152 REM j=j1*re^(-j2)
155 REM f=f1*re^(-f2)
160 REM XXXXXXXXXXX HOT SIDE DATA XXXXXXXXXXXX
170 LET H$="strip-fin plate-fin 1/9-24.12"
180 LET BH=.00191
190 LET LH=BH/2
200 LET RH=.001209/4
210 LET DELH=.000102
220 LET BBH=2830
222 LET AFAH=.665
230 LET PITH=950
232 LET FH1=.522
233 LET FH2=.335
234 LET JH1=.132
235 LET JH2=.347
240 REM XXXXXXXXXXX COLD SIDE DATA XXXXXXXXXXX
250 LET C$="strip-fin plate-fin 1/9 24.12"
260 LET BC=.00191
270 LET LC=BC/2
280 LET RC=.001209/4
290 LET DELC=.000102
300 LET BBC=2830
302 LET AFAC=.665
310 LET PITC=950
312 LET FC1=.522
313 LET FC2=.335
314 LET JC1=.132
315 LET JC2=.347
319 REM -------- HEAT EXCHANGER CONSTRUCTION --------
320 REM a=plate thickness
330 LET A=.0005
340 REM km=metal thermal conductivity (W/mC)
350 LET KM=16
355 REM ------------------------------------
360 PRINT "input mass flow (kg/s)"
370 INPUT W
380 PRINT "input T2,T3,T5,T6 (C)"
390 INPUT T2,T3,T5,T6
392 LET T2=T2+273
393 LET T3=T3+273
394 LET T5=T5+273
395 LET T6=T6+273
400 PRINT "input P2 (MPa), and (delta P)/P2"
410 INPUT P2,PC
```

```
420 LET P2=P2*(10^6)
430 PRINT "input P5 (MPa)"
440 INPUT P5
450 LET P5=P5*(10^6)
460 LET CP=5193
470 LET R=2077
480 LET PR=.666
490 LET E=(T5-T6)/(T5-T2)
500 LET RHO5=P5/(R*T5)
505 LET RHO6=P5/(R*T6)
510 LET RHO2=P2/(R*T2)
515 LET RHO3=P2/(R*T3)
520 LET KE=.28
530 LET KC=.5
540 LET NTU=E/(1-E)
550 LET JC=.015
560 LET JH=.015
570 LET FC=.07
580 LET FH=.07
590 LET TC=(T2+T3)/2
600 LET TH=(T5+T6)/2
610 LET RHOC=P2/(R*TC)
620 LET RHOH=P5/(R*TH)
630 LET VISC=(.036*TC+10.7)*10^(-6)
640 LET VISH=(.036*TH+10.7)*10^(-6)
650 LET DPC=P2*PC
660 LET ALFAC=BC*BBC/(BC+BH+2*A)
670 LET ALFAH=BH*BBH/(BC+BH+2*A)
680 LET SIGC=ALFAC*RC
690 LET SIGH=ALFAH*RH
700 LET GC=((JC*DPC*RHOC)/(FC*NTU*PR^(2/3)))^.5
710 REM xxxxxxxxxxxx LOOP WILL START HERE xxxxxxxxxxxxxxxxx
714 LET I=I+1
715 PRINT "I=";I
720 LET GH=SIGC*GC/SIGH
730 LET REC=GC*4*RC/VISC
740 LET REH=GH*4*RH/VISH
750 LET JC=JC1*(REC^(-JC2))
760 LET FC=FC1*(REC^(-FC2))
770 LET JH=JH1*(REH^(-JH2))
780 LET FH=FH1*(REH^(-FH2))
850 LET HC=JC*CP*GC/PR^(2/3)
860 LET HH=JH*CP*GH/PR^(2/3)
870 LET MC=(2*HC/(KM*DELC))^.5
880 LET MH=(2*HH/(KM*DELH))^.5
890 LET MLC=MC*LC
900 LET MLH=MH*LH
910 LET NFC=((EXP(MLC)-EXP(-MLC))/(EXP(MLC)+EXP(-MLC)))/MLC
920 LET NFH=((EXP(MLH)-EXP(-MLH))/(EXP(MLH)+EXP(-MLH)))/MLH
930 LET NOC=1-AFAC*(1-NFC)
940 LET NOH=1-AFAH*(1-NFH)
943 PRINT "cold side fin eff.=";NFC
944 PRINT "cold side avg. fin eff.=";NOC
945 PRINT "hot side avg. eff.=";NFH
946 PRINT "hot side avg. fin eff.=";NOH
950 LET AWAC=(1-AFAC)
960 LET AWAH=(1-AFAH)
970 LET UC=1/(1/(NOC*HC)+A/(AWAC*KM)+ALFAC/(ALFAH*NOH*HH))
980 LET Q=W*CP*(T3-T2)
990 LET UAC=Q/(T6-T2)
```

```
1000 LET AC=UAC/UC
1010 LET VOL=AC/ALFAC
1020 LET AH=VOL*ALFAH
1030 LET ACC=W/GC
1040 LET ACH=W/GH
1050 LET AFR=ACC/SIGC
1060 LET L=VOL/AFR
1070 LET PCC1=(GC^2/(2*P2*RHO2))
1080 LET PCC2=(KC+1-SIGC^2)
1090 LET PCC3=2*(T3/T2-1)
1100 LET PCC4=FC*AC*RHO2/(ACC*RHOC)
1110 LET PCC5=(1-SIGC^2-KE)*(T3/T2)
1120 LET PCC=PCC1*(PCC2+PCC3+PCC4-PCC5)
1130 IF ABS((PCC-PC)/PC)<.05 THEN 1160
1135 PRINT "pc=";PC,"pcc=";PCC
1140 LET GC=GC*(PC/PCC)^.5
1150 GOTO 710
1160 LET PH1=GH^2/(2*P5*RHO5)
1170 LET PH2=(KC+1-SIGH^2)
1180 LET PH3=2*(T6/T5-1)
1190 LET PH4=FH*AH*RHO5/(ACH*RHOH)
1200 LET PH5=(1-SIGH^2-KE)*(T6/T5)
1210 LET PH=PH1*(PH2+PH3+PH4-PH5)
1215 LET PTOT=PC+PH
1220 LPRINT "XXXXXXXXXX HEAT EXCHANGER DESIGN RESULTS XXXXXXXXXX"
1221 LPRINT
1222 LPRINT
1223 LPRINT
1230 LPRINT "hot side surface: ";H$
1240 LPRINT "cold side surface: ";C$
1250 LPRINT "T5=";T5-273;"C","T6=";T6-273;"C"
1260 LPRINT "T2=";T2-273;"C","T3=";T3-273;"C"
1265 LPRINT "P2=";P2/10^6;"MPa","P5=";P5/10^6;"MPa"
1270 LPRINT "heat exchanger effectiveness=";E
1280 LPRINT "material thermal conductivity=";KM;"W/mK"
1290 LPRINT "plate thickness=";A;"m"
1300 LPRINT
1310 LPRINT "             --------------"
1320 LPRINT
1330 LPRINT "heat exchanger volume=";VOL;"m3"
1340 LPRINT "total frontal area=";AFR;"m2"
1350 LPRINT "heat exchanger length=";L;"m"
1355 LPRINT "geometry ratio = "L/(AFR^.5)
1360 LPRINT "cold side specific pressure drop=";PCC
1370 LPRINT "hot side specific pressure drop= ";PH
1371 LPRINT "total specific pressure drop = ";PTOT
1373 LPRINT "cold side fin eff.=";NFC
1374 LPRINT "cold side avg. surface eff.=";NOC
1375 LPRINT "hot side fin eff.=";NFH
1376 LPRINT "hot side avg. surface eff.=";NOH
1380 LET AK=AFR-(ACC+ACH)
1390 LET LA=(KM*AK)/(L*W*CP)
1400 LPRINT "longitudinal conduction parameters:"
1410 LPRINT "    Ak=";AK
1420 LPRINT " lambda=";LA
1470 LPRINT
1490 LPRINT
1500 LPRINT "XXXXXXXXXXXXXXXXXXXXXXXXXXXXXXXXXXXXXXXXXXXXX"
1510 LPRINT
1520 LPRINT
```

```
1530 LPRINT
1540 LPRINT
1550 LPRINT
1560 END
```

Table C.2.
Output of REGEN

```
XXXXXXXXXX HEAT EXCHANGER DESIGN RESULTS XXXXXXXXXXX


hot side surface: strip-fin plate-fin 1/9-24.12
cold side surface: strip-fin plate-fin 1/9 24.12
T5= 625.5 C    T6= 157.95 C
T2= 133.34 C   T3= 600.9 C
P2= 8.11 MPa   P5= 4.226 MPa
heat exchanger effectiveness= .9499959
material thermal conductivity= 16 W/mK
plate thickness= .0005 m

              --------------

heat exchanger volume= 15.96576 m3
total frontal area= 13.05701 m2
heat exchanger length= 1.222773 m
geometry ratio =  .3383952
cold side specific pressure drop= 2.406942E-03
hot side specific pressure drop=  9.216774E-03
total specific pressure drop =  1.171677E-02
cold side fin eff.= .5455891
cold side avg. surface eff.= .6978168
hot side fin eff.= .5436791
hot side avg. surface eff.= .6965466
longitudinal conduction parameters:
     Ak= 4.205591
 lambda= 6.85446E-05


XXXXXXXXXXXXXXXXXXXXXXXXXXXXXXXXXXXXXXXXXXXXXXXX
```

Table C.3.
Listing of PRECOOL Computer Program

```
10 PRINT "PRECOOLER DESIGN PROGRAM"
20 REM HT XFER DATA IN FORM OF F OR J = A*RE^-B
30 LET S$="CF-8.72 (C)"
40 REM ----------HT EXCHANGER DATA -----------
50 LET OD=.01067
60 LET DF=.02187
70 LET FP=343
80 LET RH=.004425/4
90 LET DEL=.00048
100 LET SIGMA=.494
110 LET AFA=.876
115 LET ALFA=446
120 LET DT=.02032
130 LET WT=.024765
140 LET J1=.222
150 LET J2=.402
160 LET F1=.29
170 LET F2=.246
180 LET LF=(DF-OD)/2
190 REM -----------HT EXCHANGER CONSTRUCTION --------
200 LET ID=.95*OD
210 LET KM=16
220 LET PIE=3.14159
230 LET E=2.71828
240 REM --------- DATA INPUT --------------
250 PRINT "INPUT MASS FLOW OF HELIUM (KG/S)"
260 INPUT MH
270 PRINT "INPUT INLET PRESSURE OF HELIUM (MPa)"
280 INPUT P6
290 LET P6=P6*10^6
300 PRINT "INPUT HELIUM INLET TEMPERATURE (C)"
310 INPUT T6
320 LET T6=T6+273
330 PRINT "INPUT HELIUM OUTLET TEMPERATURE TO COMPRESSOR (C)"
340 INPUT T1
350 LET T1=T1+273
354 LET CPH=5193
355 LET Q=MH*CPH*(T6-T1)
360 PRINT "INPUT HELIUM SPECIFIC PRESSURE DROP"
370 INPUT DP
380 PRINT "INPUT WATER VELOCITY (M/S)"
390 INPUT VW
400 LET GW=VW*980
410 PRINT "INPUT WATER INLET TEMPERATURE (C)"
420 INPUT TWI
430 LET TWI=TWI+273
440 PRINT "IS THIS A CROSS-COUNTERFLOW (1), OR CROSSFLOW (2) HT X-CHNGR ?"
450 INPUT TYPE
460 IF TYPE=1 THEN 530
470 PRINT "CW/CH MUST BE GREATER THAN ";(T6-T1)/(T1-TWI)
480 PRINT "INPUT CW/CH"
490 INPUT CWCH
500 LET TWO=((T6-T1)/CWCH)+TWI
510 LET TM=((T6-TWO)-(T1-TWI))/LOG((T6-TWO)/(T1-TWI))
512 PRINT "EFFECTIVENESS = ";(T6-T1)/(T6-TWI)
515 PRINT "INPUT NTU"
517 INPUT NTU
518 LET UA=NTU*MH*CPH
520 GOTO 600
530 PRINT "INPUT CW/CH (=OR>1)"
```

```
540 INPUT CWCH
550 LET TWO=((T6-T1)/CWCH)+TWI
560 IF CWCH=1 THEN 590
570 LET TM=((T6-TWO)-(T1-TWI))/LOG((T6-TWO)/(T1-TWI))
572 LET UA=Q/TM
575 LET NTU=UA/(MH*CPH)
580 GOTO 600
590 LET TM=T1-TWI
592 LET UA=Q/TM
595 LET NTU=UA/(MH*CPH)
600 LET CPW=4189
610 LET PRH=.668
620 LET CPH=5193
630 LET R=2077
640 PRINT "AVG WATER TEMP IS";((TWO+TWI)/2)-273;"C"
650 PRINT "INPUT VISCOSITY(10^-5 PaS), PRANDTL NO., AND THERMAL ";
660 PRIHT "CONDUCTIVITY (W/mK)"
670 INPUT VISW,PRW,KW
680 LET VISW=VISW*(10^(-5))
690 LET TAV=(T1+T6)/2
695 LET DENSH=P6/(R*TAV)
700 LET VISH=(6.7+.044*TAV)*10^(-6)
720 LET GH=((.006*P6*DP*DENSH)/(.02*NTU*.7631))^.5
730 REM -------------START LOOP HERE-------------
740 LET REH=(GH*4*RH)/VISH
750 LET FH=F1*(REH^(-F2))
760 LET JH=J1*(REH^(-J2))
770 LET HH=(JH*GH*CPH)/(PRH^(2/3))
775 PRINT "Hhe = ";HH;"W/m2K","Ghe = ";GH;"KG/m2s"
776 PRINT "Re he = ";REH,"JH = ";JH
780 LET HW=(.023*KW*(PRW^.4)*(GW^.8))/((VISW^.8)*(ID^.2))
785 PRINT "HW = ";HW
790 LET M=((2*HH)/(KM*DEL))^.5
800 LET ML=M*LF
810 LET NF=((EXP(ML)-EXP(-ML))/(EXP(ML)+EXP(-ML)))/ML
830 LET NOF=1-AFA*(1-NF)
840 LET A=(OD-ID)/2
850 LET AWA=1-AFA
860 LET U=1/((1/(HH*NOF))+(A/(KM*AWA))+(1/(HW*AWA)))
865 PRINT "FIN EFF.=";NF,"U = ";U
880 LET AH=UA/U
885 PRINT "Q= ";Q
890 LET VOL=AH/ALFA
900 LET AC=MH/GH
910 LET AFR=AC/SIGMA
920 LET L=VOL/AFR
940 LET DELP=(FH*AH*(GH^2))/(2*P6*AC*DENSH)
950 IF ABS((DELP-DP)/DP)<.05 THEN 990
960 LET GH=GH*((DP/DELP)^.5)
970 GOTO 740
980 REM -----------END OF LOOP--------------
990 LET MW=MH*CPH*CWCH/CPW
1000 LET NT=INT(4*MW/(GW*PIE*(ID^2))+.5)
1010 LPRINT "PRECOOLER DESIGN PROGRAM"
1020 LPRINT
1030 LPRINT "HELIUM TEMPS:"
1040 LPRINT "INLET = ";T6-273;"C","OUTLET = ";T1-273;"C"
1050 LPRINT "HELIUM INLET PRESS.= ";P6/(10^6);"MPa"
1060 LPRINT "HELIUM MASS-FLOW = ";MH;"KG/S"
1070 LPRINT "WATER INLET TEMP = ";TWI-273;"C","OUTLET TEMP = ";TWO-273;"C"
```

```
1080 LPRINT "HEAT EXCHANGER SURFACE: ";S$
1090 LPRINT "RATIO OF HEAT CAPACITIES, (Cw/Ch) = ";CWCH
1100 IF TYPE=2 THEN 1130
1110 LPRINT "CROSS-COUNTERFLOW HEAT EXCHANGER"
1120 GOTO 1140
1130 LPRINT "CROSSFLOW HEAT EXCHANGER"
1140 LPRINT "------------------------------"
1150 LPRINT
1160 LPRINT
1170 LPRINT "--------- RESULTS OF CALCULATIONS ------------"
1180 IF TYPE=1 THEN 1400
1190 LET ND=INT((L/DT)+.5)
1200 LET NW=INT((NT/ND)+.5)
1210 LET W=NW*WT
1220 LET LT=AFR/W
1230 LPRINT "CROSSFLOW HEAT EXCHANGER DIMENSIONS"
1240 LPRINT "VOL= ";VOL;"m3"
1250 LPRINT "--------TUBESHEET--------"
1260 LPRINT "# OF TUBES = ";NT
1270 LPRINT "WIDTH =";W;"m"
1280 LPRINT "DEPTH = ";L;"m"
1290 LPRINT "TUBE LENGTH = ";LT;"m"
1300 LPRINT "--------- GAS FLOW ---------"
1310 LPRINT "PRESSURE DROP = ";DELP
1320 LPRINT "LENGTH = ";L;"m"
1330 LPRINT "FRONTAL AREA = ";AFR;"m2"
1335 LPRINT "GEOMETRY RATIO = ";L/(AFR^.5)
1340 LPRINT "EFFECTIVENESS = ";(T6-T1)/(T6-TWI)
1350 LPRINT "------------------------------------------------------------"
1360 LPRINT
1370 LPRINT
1380 LPRINT
1390 GOTO 2000
1400 LET W=(NT*DT*WT)^.5
1410 LET NP=INT((L/W)+.5)
1480 REM ------------ OUTPUT ------------
1490 LPRINT "CROSS-COUNTERFLOW HEAT EXCHANGER"
1500 LPRINT "VOLUME = ";VOL;"m3"
1510 LPRINT "LENGTH = ";L;"m"
1520 LPRINT "FRONTAL AREA = ";AFR;"m2"
1525 LPRINT "GEOMETRY RATIO = ";L/(AFR^.5)
1530 LPRINT "PRESSURE DROP = ";DELP
1540 LPRINT "NO. OF TUBES = ";NT
1550 LPRINT "NO. OF PASSES = ";NP
1560 LPRINT "SQUARE TUBE SHEET DIMENSION PER SIDE = ";W;"m"
1565 FOR NL=1 TO 6 STEP 1
1570 LET DO(NL)=((4*AFR/PIE)+((NL^2)*(W^2)))/(2*NL*W)
1575 LET DI(NL)=DO(NL)-(NL*W)
1580 LPRINT "FOR ";NL;" LOOP(S)"
1585 LPRINT "PRECOOLER OUTER DIA. = ";DO(NL);"m"
1590 LPRINT "PRECOOLER INNER DIA. = ";DI(NL);"m"
1595 LPRINT
1600 NEXT NL
1610 LPRINT "EFFECTIVENESS = ";(T6-T1)/(T6-TWI)
1620 LPRINT "------------------------------------------"
1630 LPRINT
1640 LPRINT
1650 LPRINT
1660 LPRINT
1670 GOTO 2000
```

```
2000 END
```

Table C.4.
Output of PRECOOL for Crossflow Precooler

```
PRECOOLER DESIGN PROGRAM

HELIUM TEMPS:
INLET =  161.9 C              OUTLET =  30 C
HELIUM INLET PRESS.=  4.055 MPa
HELIUM MASS-FLOW =  150.7 KG/S
WATER INLET TEMP =  20 C     OUTLET TEMP =  28.79334 C
HEAT EXCHANGER SURFACE: S 1.50-1.00
RATIO OF HEAT CAPACITIES, (Cw/Ch) =  15
CROSSFLOW HEAT EXCHANGER
--------------------------------


--------- RESULTS OF CALCULATIONS ------------
CROSSFLOW HEAT EXCHANGER DIMENSIONS
VOL=  5.303019 m3
--------TUBESHEET--------
# OF TUBES =  14822
WIDTH = 3.58679 m
DEPTH =  .5648861 m
TUBE LENGTH =  2.617317 m
--------- GAS FLOW ---------
PRESSURE DROP =  9.604492E-04
LENGTH =  .5648861 m
FRONTAL AREA =  9.387767 m2
GEOMETRY RATIO =  .1843655
EFFECTIVENESS =  .9295278
-------------------------------------------------------------
```

Table C.5.

Output of PRECOOL for

Multi-Pass Cross-Counterflow Precooler

```
PRECOOLER DESIGN PROGRAM

HELIUM TEMPS:
INLET =  162.01 C            OUTLET =  30 C
HELIUM INLET PRESS.=  4.077 MPa
HELIUM MASS-FLOW =  151.75 KG/S
WATER INLET TEMP =  20 C     OUTLET TEMP =  152.01 C
HEAT EXCHANGER SURFACE: CF-8.72 (C)
RATIO OF HEAT CAPACITIES, (Cw/Ch) =  1
CROSS-COUNTERFLOW HEAT EXCHANGER
--------------------------------


--------- RESULTS OF CALCULATIONS ----------
CROSS-COUNTERFLOW HEAT EXCHANGER
VOLUME =  54.64608 m3
LENGTH =  6.081005 m
FRONTAL AREA =  8.986357 m2
GEOMETRY RATIO =  2.02854
PRESSURE DROP =  4.930027E-03
NO. OF TUBES =  793
NO. OF PASSES =  10
SQUARE TUBE SHEET DIMENSION PER SIDE =  .6317098 m
FOR  1  LOOP(S)
PRECOOLER OUTER DIA. =  9.372066 m
PRECOOLER INNER DIA. =  8.740356 m

FOR  2  LOOP(S)
PRECOOLER OUTER DIA. =  5.159816 m
PRECOOLER INNER DIA. =  3.896396 m

FOR  3  LOOP(S)
PRECOOLER OUTER DIA. =  3.966302 m
PRECOOLER INNER DIA. =  2.071172 m

FOR  4  LOOP(S)
PRECOOLER OUTER DIA. =  3.527473 m
PRECOOLER INNER DIA. =  1.000633 m

FOR  5  LOOP(S)
PRECOOLER OUTER DIA. =  3.390517 m
PRECOOLER INNER DIA. =  .2319679 m

FOR  6  LOOP(S)
PRECOOLER OUTER DIA. =  3.404498 m
PRECOOLER INNER DIA. =  -.3857608 m

EFFECTIVENESS =  .9295824
-----------------------------------------
```

APPENDIX D

HEAT EXCHANGER SURFACE DATA

AND CROSSFLOW PRECOOLER CALCULATIONS

This appendix provides the geometry, friction, and heat-transfer data on each surface used in the heat exchanger analyses of Chapter Five.

D.1. Strip-fin plate-fin surface 1/8-15.2

Correlations determined from f and j data of Fig. D.1.

Re > 1200: $$f = 0.207\ Re^{-0.167} \quad (D.1)$$

Re < 1200: $$f = 4.70\ Re^{-0.609} \quad (D.2)$$

All Re: $$j = 0.071\ Re^{-0.243} \quad (D.3)$$

Plate thickness of this surface was selected as 2-mm.

D.2. Strip-fin plate-fin surface 1/9-24.12.

Correlations determined from f and j data of Fig. D.2:

$$f = 0.522\ Re^{-0.335} \quad (D.4)$$

$$j = 0.132\ Re^{-0.347} \quad (D.5)$$

For calculations with this surface the plate-thickness was selected at: $a = 0.5$ mm

D.3. Circular-tube surface S 1.50-1.00.

Correlations determined from f and j data of Fig. D.3.

$$f = 0.384\ Re^{-0.221} \quad (D.6)$$

$$j = 0.299\ Re^{-0.399} \quad (D.7)$$

D.4. Circular-finned-tube surface CF-8.72(c).

Correlations determined from f and j data of Fig. D.4:

$$f = 0.290\ Re^{-0.246} \quad (D.8)$$

$$j = 0.222\ Re^{-0.402} \quad (D.9)$$

Strip-fin plate-fin surface 1/8-15.2.

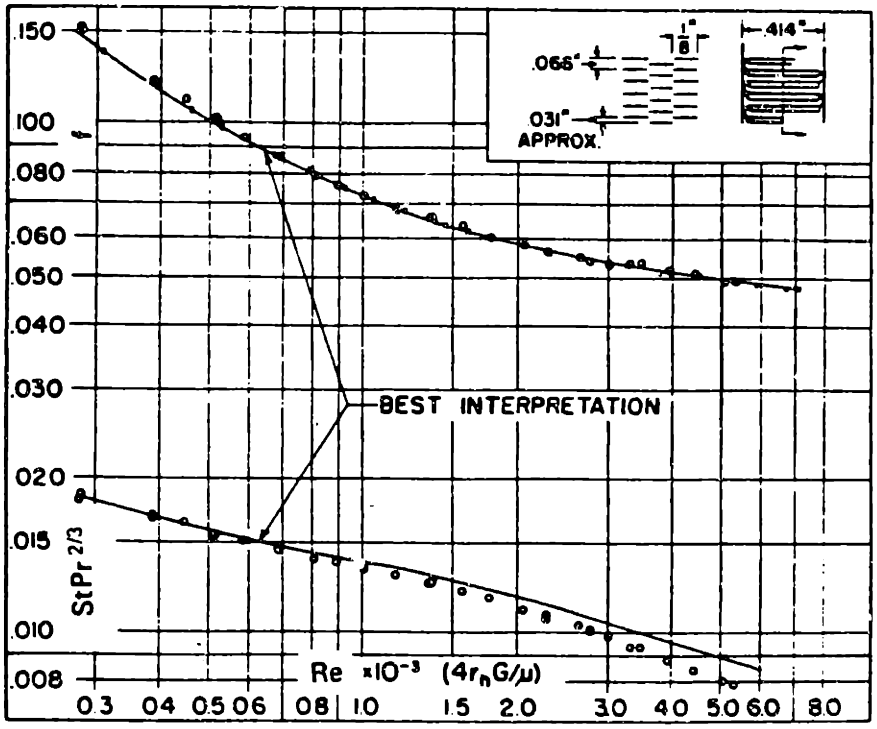

Fin pitch = 15.2 per in = 598 per m

Plate spacing, b = 0.414 in = 10.5 x 10^{-3}m

Fin length = 0.125 in = 3.18 x 10^{-3}m

Fins staggered symmetrically

Flow passage hydraulic diameter, $4r_h$ = 0.00868 ft = 2.647 x 10^{-3}m

Fin metal thickness = 0.006 in, aluminum = 0.152 x 10^{-3}m

Total heat transfer area/volume between plates, β = 417 ft^2/ft^3 = 1368 m^2/m^3

Fin area/total area = 0.873

Note: Fin leading and trailing edges slightly scarfed from fin-cutting operation. Friction factors may be lower with clean fins.

Figure D.1. Strip-fin plate-fin surface 1/8-15.2 [from K15].

Fig. 10-59 Strip-fin plate-fin surface 1/9-24.12.

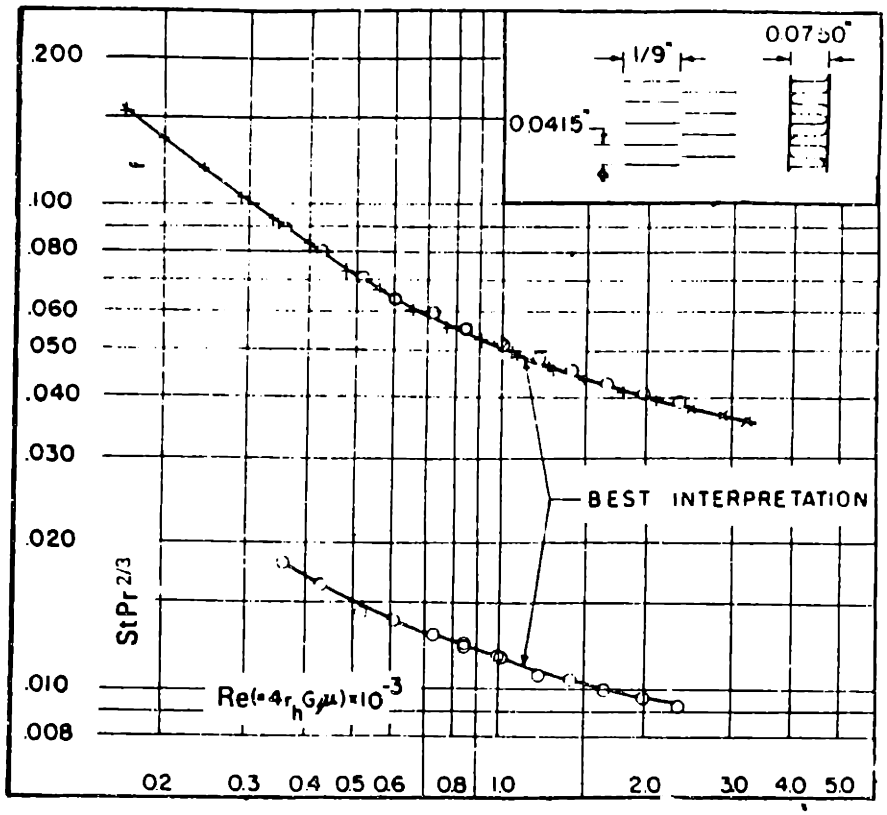

Fin pitch = 24.12 per in = 950 per m

Plate spacing, b = 0.075 in = 1.91 x 10^{-3} m

Fin length = 0.111 in = 2.8 x 10^{-3} m

Flow passage hydraulic diameter, $4r_h$ = 0.003966 ft = 1.209 x 10^{-3} m

Fin metal thickness = 0.004 in = 0.102 x 10^{-3} m

Total heat transfer area/volume between plates, β = 862.7 ft^2/ft^3 = 2,830 m^2/m^3

✱ Fin area/total area = 0.857

✱ **Correct value for fin-area/total-area is 0.665 [L6].**

Figure D.2. Strip-fin plate-fin surface 1/9-24.12 [from K15].

S 1.50-1.00.

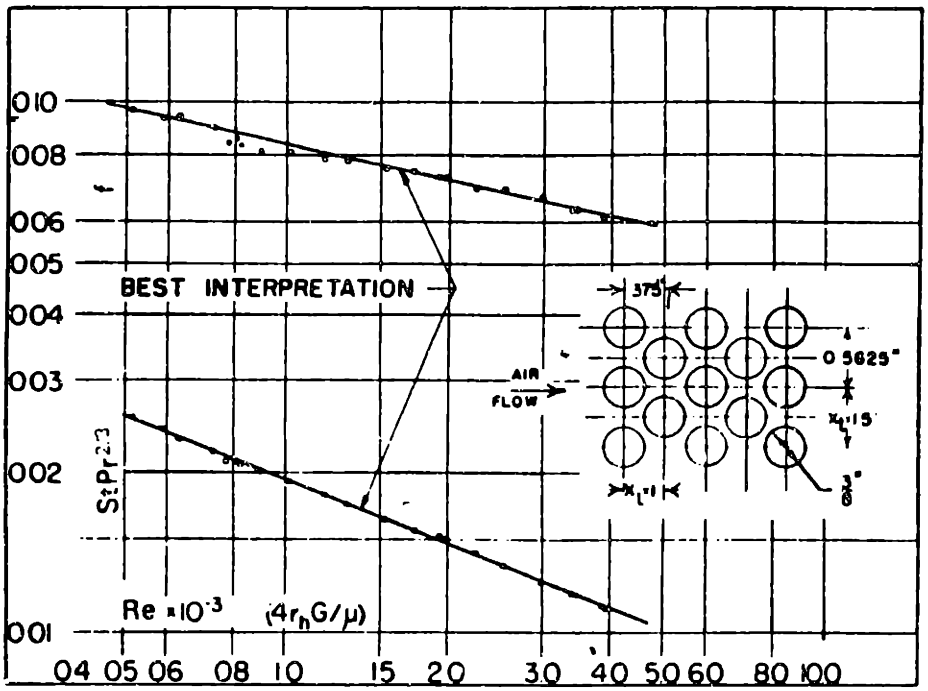

Tube outside diameter = 0.375 in = 9.525×10^{-3} m

Hydraulic diameter, $4r_h$ = 0.0196 ft = 6.071×10^{-3} m

Free-flow area/frontal area, σ = 0.333

Heat transfer area/total volume, α = 67.1 ft^2/ft^3 = 220.144 m^2/m^3

Note: Minimum free-flow area is in spaces transverse to flow.

Figure D.3. Circular-tube surface S 1.50-1.00 [from K15].

Finned circular tubes, surface CF-8.72(c).

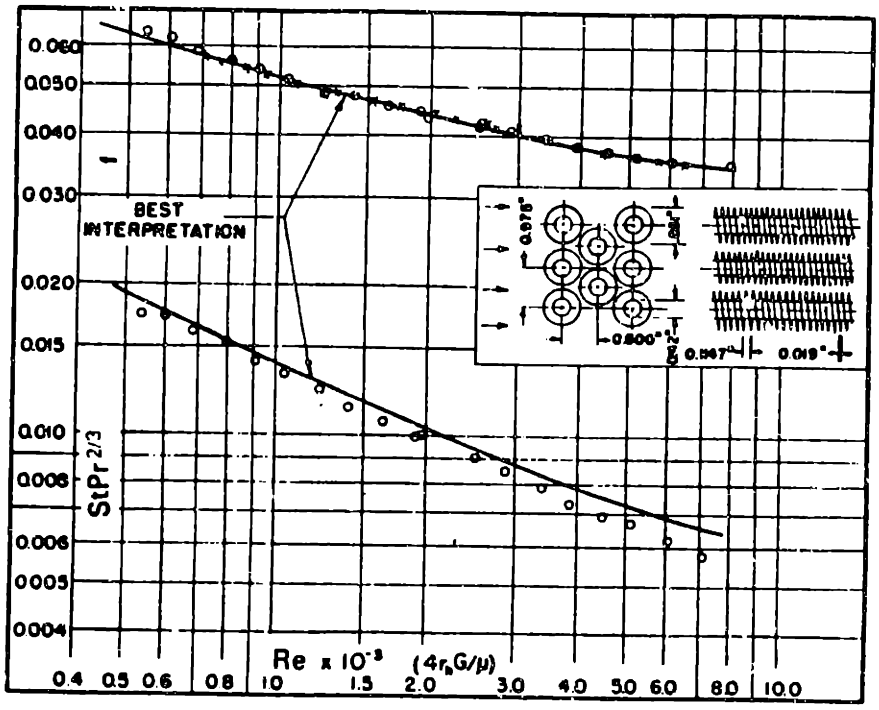

Tube outside diameter = 0.42 in = 10.67×10^{-3} m

Fin pitch = 8.72 per in = 343 per m

Flow passage hydraulic diameter, $4r_h$ = 0.01452 ft = 4.425×10^{-3} m

Fin thickness (average) † = 0.019 in, copper = 0.48×10^{-3} m

Free-flow area/frontal area, σ = 0.494

Heat transfer area/total volume, α = 136 ft^2/ft^3 = 446 m^2/m^3

Fin area/total area = 0.876

†Fins slightly tapered.

Figure D.4. Finned-circular-tube surface CF-8.72(c) [from K15].

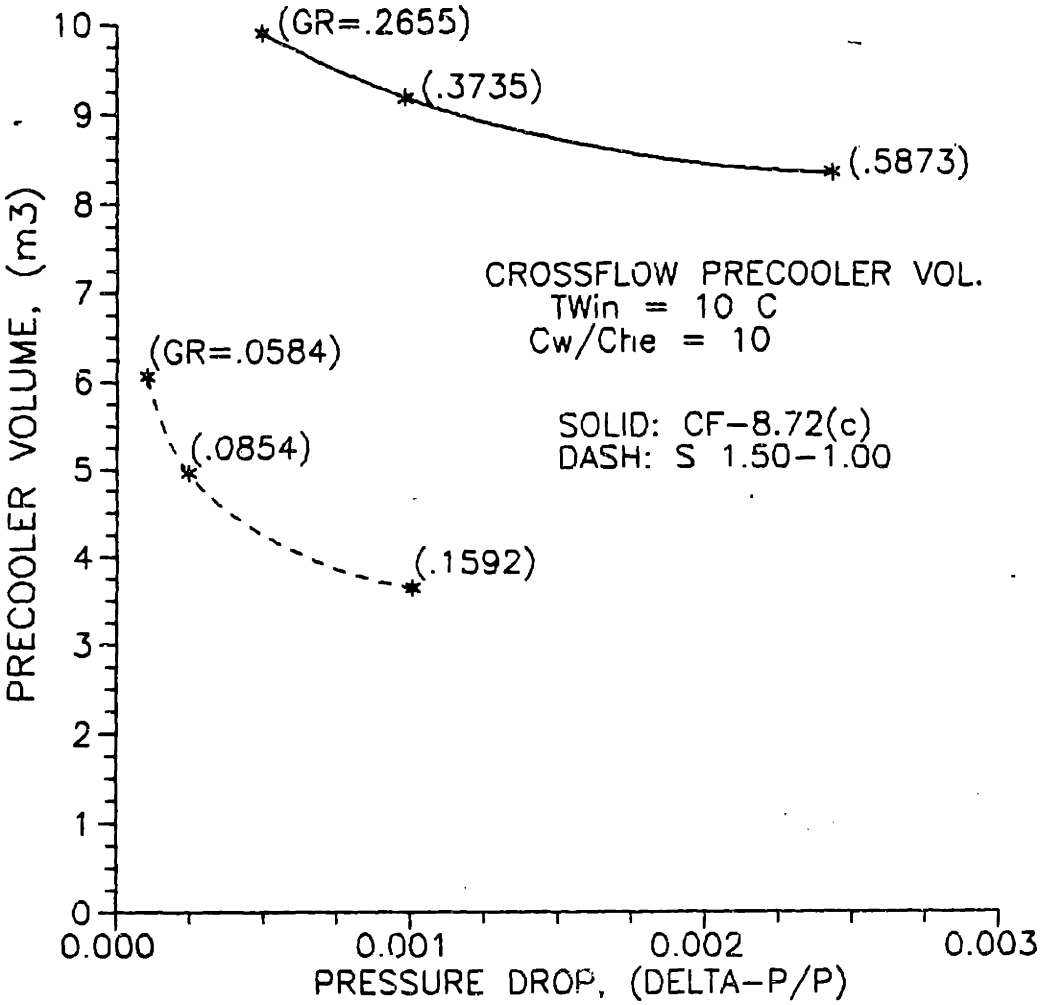

Figure D.5. Calculated crossflow precooler volume for water-inlet temperature at 10 C.

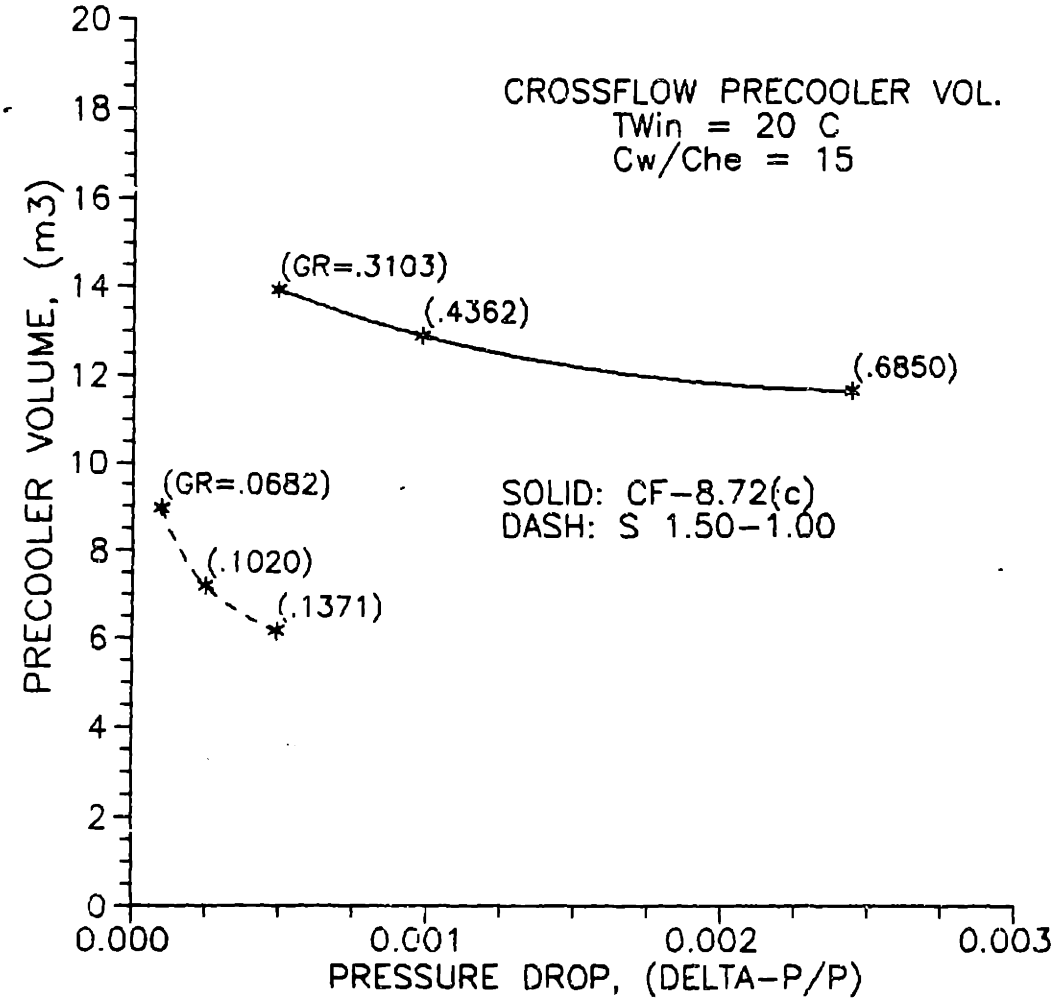

Figure D.6. **Calculated crossflow precoolerr volume for water-inlet temperature at 20 C.**

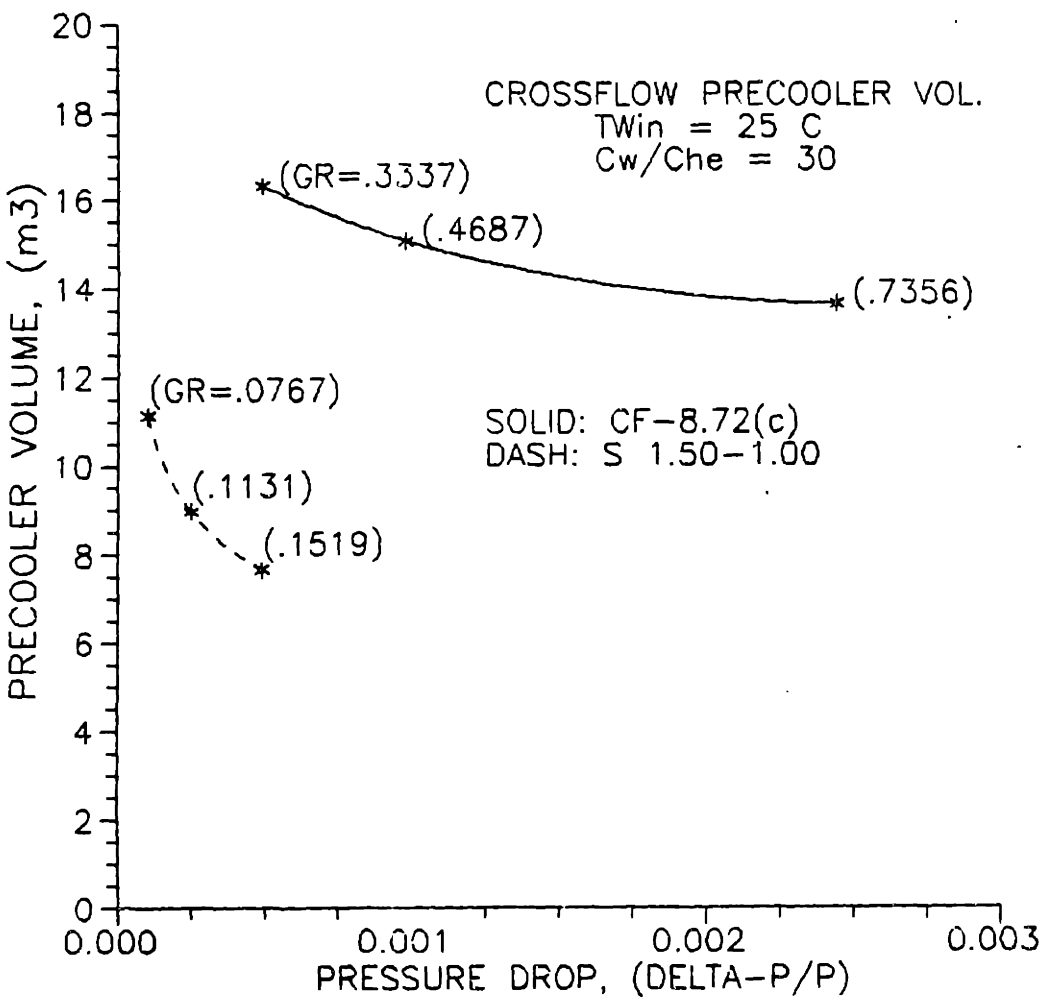

Figure D.7. Calculated crossflow precooler volume for water-inlet temperature at 25 C.

APPENDIX E

"LAST1" INVENTORY-CONTROL TRANSIENT COMPUTER MODEL

LAST1 is a small computer program that was written in BASIC for use on a personal computer. No files are needed to run LAST1. Output is sent directly to a line printer. LAST1 models the transient resulting from a reduction in inventory. A picture of the general model is shown in Fig. E.1. The helium travels isothermally along the length of a duct with a globe valve. A globe valve was selected because a gate valve would not be able to open under the high pressure differences initially across the valve. Reference C7 recommends $(L/D)_{eq} = 350$ for a fully open globe valve. The total duct length is assumed to be 10-meters long. Hence, most of the pressure drop is across the valve, except for very small diameter ducts. It is assumed that the inventory-control valve fully opens at time t=0. Initial compressor discharge pressure is assumed to equal 8-MPa, and initial inventory-control vessel pressure is assumed to equal 4-MPa for all cases. Initial helium-coolant circuit inventory is assumed to equal 2350-kg. These conditions are roughly what is expected in the MGR-GT. The inventory-control vessel may be treated as adiabatic or isothermal.

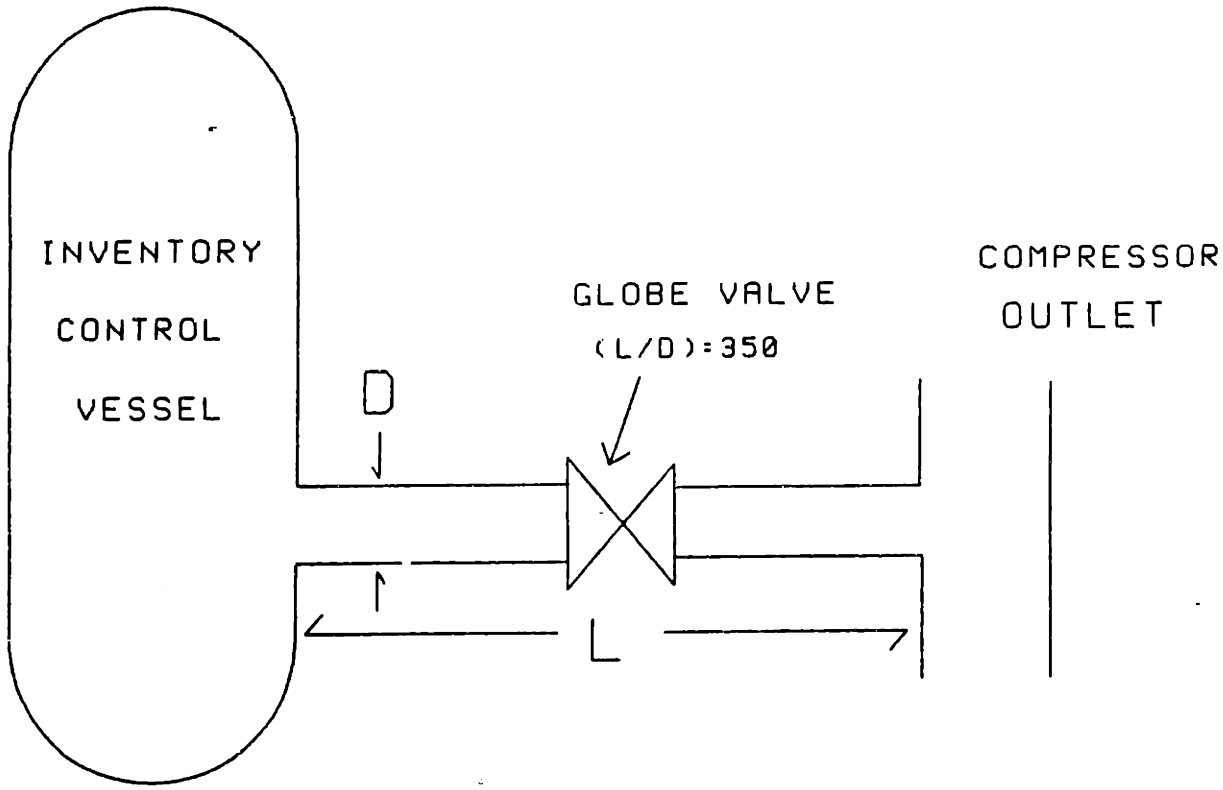

Figure E.1. **The inventory-control system modelled in LAST1.**

Table E.1. LAST1 Computer Program Listing

```
10 PRINT "INVENTORY CONTROL PROGRAM"
20 PRINT "LAST ONE!"
30 REM "INPUT INITIAL HELIUM MASS IN COOLANT CIRCUIT (KG)"
40 LET M0=2350
42 PRINT "WILL THE CONTROL-VESSEL BE ISOTHERMAL (1), OR ADIABATIC (2)?"
43 INPUT HX
50 PRINT "INPUT CONTROL-VESSEL VOLUME (m3)"
60 INPUT V
70 REM "INPUT INITIAL COMPRESSOR-OUTLET PRESSURE (MPa)"
80 LET P0=8
90 LET P0=P0*10^6
92 REM "INPUT INITIAL CONTROL-VESSEL PRESSURE (MPa)"
93 LET PV0=4
94 LET PV0=PV0*10^6
100 REM "INPUT TEMP. OF HELIUM BEING TRANSFERED (DEG. K)"
110 LET TEMP=300
115 LET VIS=19.9*(10^6)
120 PRINT "INPUT DUCT DIAMETER (METERS)"
130 INPUT D
140 REM "INPUT EQUIVALENT (L/D)"
150 LET LD=350+(10/D)
160 REM "INPUT FRICTION FACTOR"
170 LET F=.002
180 PRINT "INPUT TIME STEP (SECONDS)"
190 INPUT DT
192 PRINT "INPUT FINAL TIME (SECONDS)"
193 INPUT TF
195 PRINT "HOW MANY TIME STEPS BETWEEN PRINTING?"
196 INPUT PS
200 LET R=2077
205 LET CP=5193
206 LET CV=CP-R
210 LET MV0=(PV0*V)/(R*TEMP)
220 LET PIE=3.14159
230 LET A=PIE*(D^2)/4
240 LET P=P0
250 LET PV=PV0
260 LET T=0
270 LET M=M0
275 LET MV=MV0
280 LPRINT "SEC","INV","LP. PRESS.","CV PRESS."
290 FOR T=0 TO TF STEP DT
295 IF I/PS=INT(I/PS) THEN 300
296 GOTO 310
300 LPRINT T,(M/M0),P,PV
310 LET DENS=(P+PV)/(2*R*TEMP)
315 IF (P-PV)<10 THEN 440
320 LET G=(((P-PV)*DENS)/(2*F*LD))^.5
330 LET RE=G*D/VIS
340 LET F2=.046/(RE^.2)
350 IF ABS((F-F2)/F)<.05 THEN 380
360 LET F=F2
370 GOTO 320
380 LET DMDT=G*A
390 LET M=M-(DMDT*DT)
400 LET MV=MV+(DMDT*DT)
410 LET P=(M/M0)*P0
411 IF HX=1 THEN 419
412 LET TV=TEMP*(((MV0*CV)+(MV-MV0)*CP)/(MV*CV))
413 GOTO 420
```

```
419 LET TV=TEMP
420 LET PV=R*TV*MV/V
425 LET I=I+1
430 NEXT T
440 END
```

Table E.2. LAST1 Computer Program Output

SEC	INV	LP. PRESS.	CV PRESS.
0	1	8000000	4000000
10	.9628617	7702893	4181269
20	.9282394	7425916	4350259
30	.8960909	7168727	4507173
40	.8670157	6936125	4649087
50	.8402987	6722390	4779490
60	.8160033	6528027	4898075
70	.79426	6354080	5004202
80	.7746544	6197235	5099896
90	.7574735	6059788	5183755
100	.7423193	5938554	5257722
110	.7293338	5834671	5321102
120	.7183392	5746714	5374766
130	.7092639	5674111	5419063
140	.7020405	5616324	5454319
150	.696578	5572624	5480981
160	.6927549	5542039	5499641
170	.6904606	5523685	5510838
180	.689514	5516112	5515458

APPENDIX F

CALCULATION OF LOSSES FROM REACTOR VESSEL AND REFLECTOR HEAT TRANSFER

This section will evaluate the losses from the transfer of heat to the compressor-discharge helium that sweeps the reactor vessel and the losses from the transfer of heat through the vessel to the environment.

Q_r = heat transfer through the reflector

Q_h = heat transfered to the helium

Q_v = heat transferred through the pressure vessel

Figure F.1 is a cross-section of the reactor, reflector and vessel. Mean core height is 9.43-m. One-dimensional heat-transfer in the radial direction will be assumed.

By the First Law of Thermodynamics:

$$Q_r = Q_v + Q_h \tag{F.1}$$

also:

$$Q_r = (T_i - T_o)/R_{total} \tag{F.2}$$

For radial conduction in a cylinder:

$$R = \frac{\ln(r_o/r_i)}{2\,\pi\,k\,L} \tag{F.3}$$

For convective heat transfer:

$$R = 1/(h \cdot A) \tag{F.4}$$

with

$$h = Nu \cdot \frac{k}{d} \tag{F.5}$$

Treating the flow in the annular region between the core barrel and the pressure vessel as flow between two infinite parallel plates, Nu can be estimated to be 350 from Fig. 6.9 of Ref. K15.

Izenson's calculations determined that the average T_i is 762°C [I3].

Using $T_o = 135^{\circ}C$

$k_{reflector} \cong 40\text{-W/m}^{\circ}K$

$k_{carbon\ brick} \cong 60\text{-W/m}^{\circ}K$

$k_{304\text{-SS}} \cong 16\text{-W/m}^{\circ}K$

and assuming a contact resistance at the interface between the carbon brick and the core barrel equal to the equivalent of $5\cdot(10)^{-4}$-m of helium, it is determined that

$$Q_r = 2.44\text{-MW}$$

From the equation for radiation heat transfer,

$$Q_v = \epsilon\cdot\sigma\cdot A\cdot(T_v^4 - T_e^4) \qquad (F.6)$$

Assuming $T_v \cong 135^{\circ}C$

and $T_e \cong 40^{\circ}C$

and $\epsilon \cong 0.80$,

it is found that $Q_v \cong 0.14\text{-MW}$

From Eq. F.1 $Q_h \cong 2.30\text{-MW}$

The helium will be heated up almost 3°C. This will cause recuperator-outlet temperature to the precooler to be raised by this amount. Additional heat will be rejected in the precooler equal to Q_h.

Total heat-transfer losses will equal the amount lost through helium heating (Q_h) plus the heat lost through the vessel (Q_v). Hence, Q_r will be the total losses from this effect and will account for a net efficiency penalty of 1.22% from the cycle efficiency.

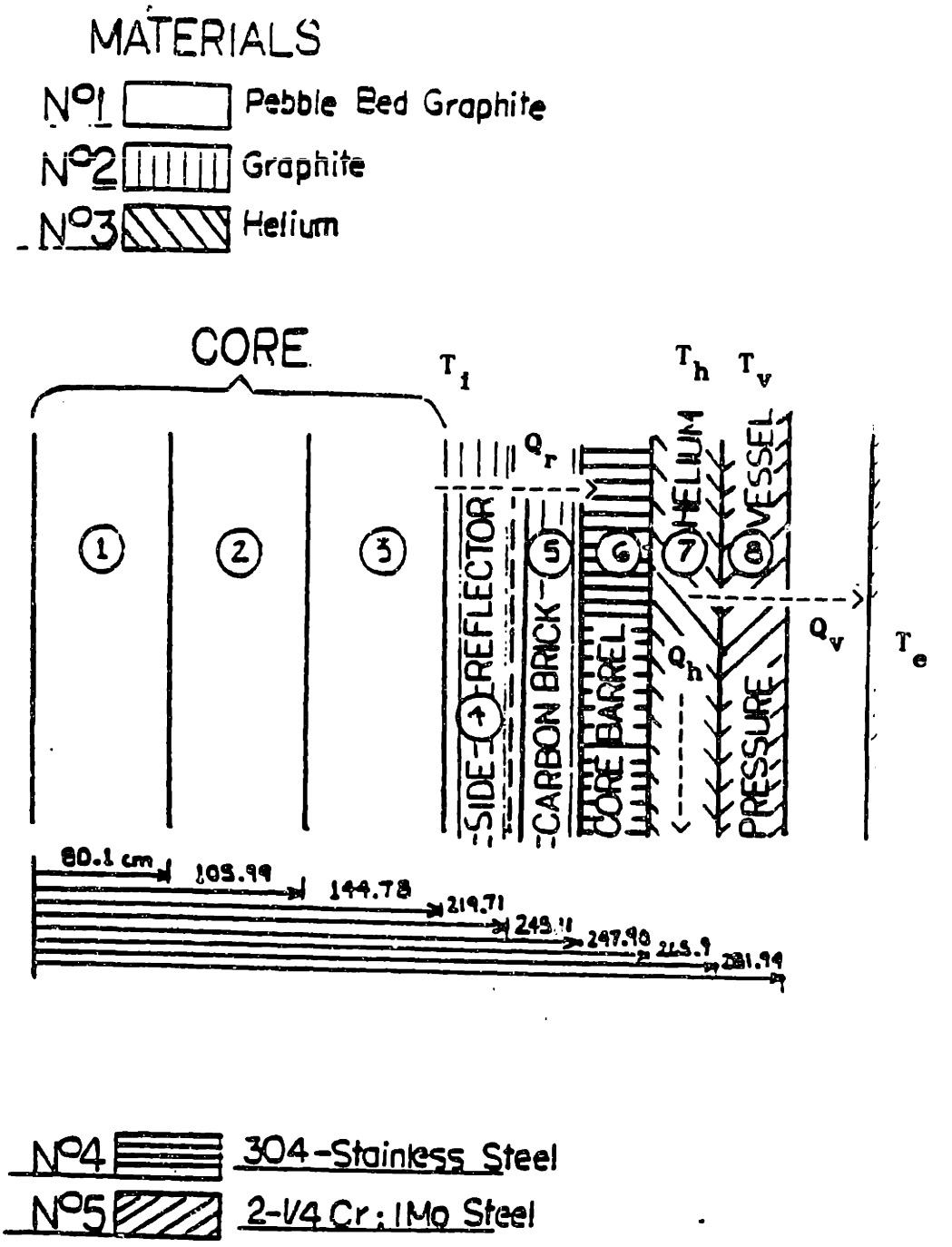

Figure F.1. Cross section of the MGR, including the reactor, the reflector, the core barrel, and the pressure-vessel [S6].

APPENDIX G

G.1 Turbomachine Cost Calculation.

Turbomachine costs are estimated by a method given in Ref. W6. The resulting costs are corrected for inflation with the Nelson Cost Index for pumps and compressors. Turbine and compressor base costs can be determined from Figs. G.1 and G.2. These costs are then adjusted with cost multiplying factors (CMF) given in Figs. G.3 - G.6.

G.2 Turbine Cost Estimation.

From Appendix B, turbine-inlet annulus area is equal to 1.94-ft^2. Extrapolating Fig. G.1, the base turbine cost in 1970 dollars is about $40,000. Correcting this for inflation with a factor of about 3, the base cost is $120,000 in 1985 dollars.

Figure G.3 gives CMF = 1.0.

Figure G.4 gives CMF = 4.5.

Figure G.5 gives CMF = 1.0.

Figure G.6 gives CMF = 2.25.

The cost of the turbine is estimated as $1.215-million.

G.3 Compressor Cost Estimation.

Compressor-inlet volume flow is roughly 51,000-cfm. From Fig. G.2, this results in a base cost of $50,000 (1970 dollars). Correcting for inflation, the base cost is about $150,000.

Figure G.3 gives a CMF of about 1.0.

Figure G.5 gives a CMF of 1.0.

Rather than correcting for pressure ratio as in Ref. W6, Fig. G.6 will be used to adjust for the number of stages. Because the MGR-GT uses a helium turbomachine, using the pressure-ratio correction in Ref. W6 would probably result in an underestimation of the cost.

Extrapolating Fig. G.6 results in CMF $\cong$ 5.0.

Total compressor cost is expected to be about $750,000.

Total cost of both turbomachines will be about $2-million.

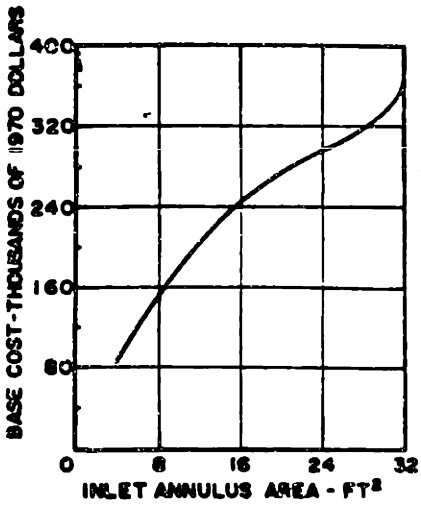

Figure G.1.
Base cost of turbine [from W6].

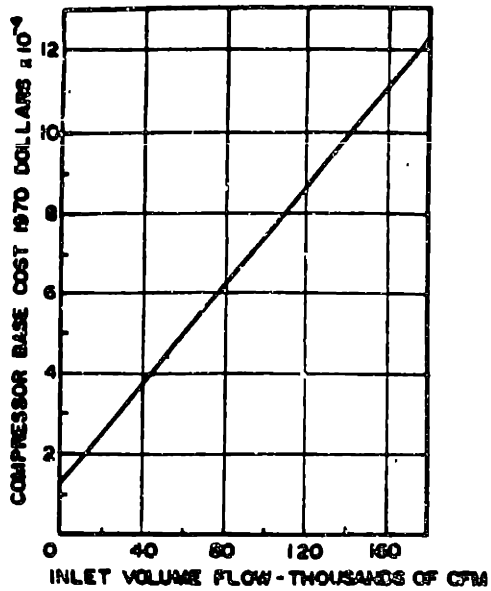

Figure G.2.
Base cost of compressor [from W6].

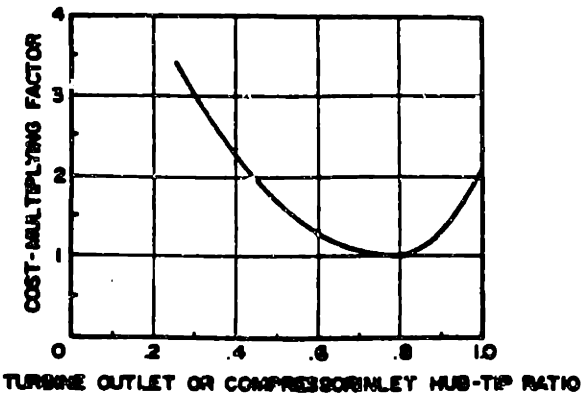

Figure G.3.

Cost-multiplying factor for hub/tip ratio [from W6].

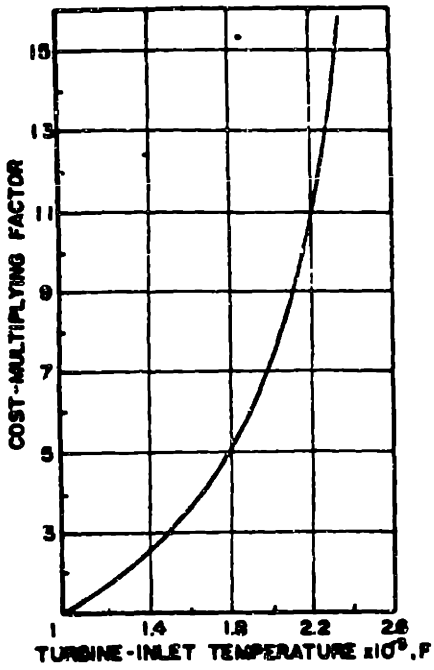

Figure G.4.

Cost-multiplying factor for turbine-inlet temperature [from W6].

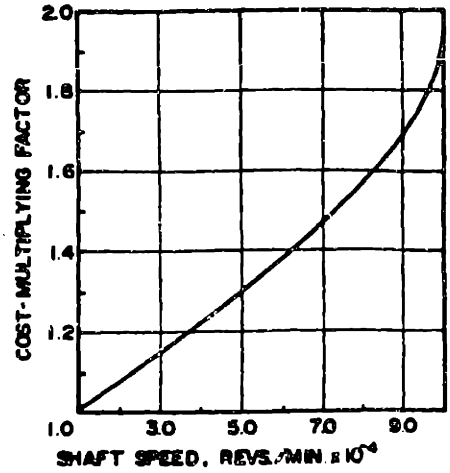

Figure G.5.

Cost-multiplying factor for shaft speed [from W6].

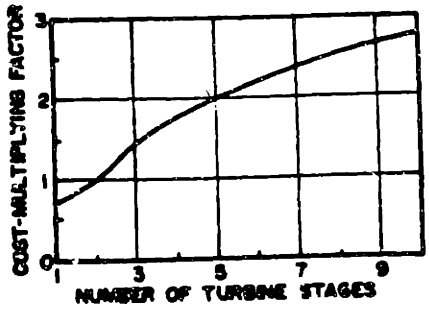

Figure G.6.

Cost-multiplying factor for number of stages [from W6].